SHATIS 22

PROCEEDINGS OF 6th INTERNATIONAL CONFERENCE ON STRUCTURAL HEALTH ASSESSMENT OF TIMBER STRUCTURES

7th – 9th September 2022, Prague

Editors
Jiří Kunecký
Hana Hasníková

Proceedings of the SHATIS 2022 – 6th International Conference on Structural Health Assessment of Timber Structures

7th – 9th September 2022, Prague, Czechia

International Conference on Structural Health Assessment of Timber Structures

Editors
Jiří Kunecký & Hana Hasníková
Institute of Theoretical and Applied Mechanics of the Czech Academy of Sciences

Proceedings of SHATIS 2022

Edited by Jiří Kunecký & Hana Hasníková

Institute of Theoretical and Applied Mechanics

ISBN 978-80-86246-54-3
DOI: 10.21495/54-3

ORGANIZING INSTITUTIONS

Institute of Theoretical and Applied Mechanics,

Czech Academy of Sciences, v.v.i.

University Centre for Energy Efficient Buildings,

Czech Technical University in Prague

in collaboration/with support of

National Heritage Institute (NPÚ)

National Technical Museum (NTM)

Czech Society for Mechanics (ČSM)

SCIENTIFIC COMMITTEE

Bohumil Kasal (WKI Fraunhofer / TU Braunschweig, Germany)

Philipp Dietsch (Karlsruhe Institute of Technology (KIT), Germany)

Gerhard Schickhofer (Graz University of Technology, Austria)

Thierry Descamps (University of Mons, Belgium)

Thomas Tannert (University of Northern British Columbia, Canada)

Tomaž Pazlar (Slovenian National Building and Civil Eng. Institute, Slovenia)

Francisco Arriaga Martitegui (Technical University of Madrid, Spain)

Maria Adelaide Parisi (Politecnico di Milano, Italy)

Jorge M. Branco (University of Minho, Portugal)

Lina Nunes (LNEC, Portugal)

Petr Kuklík (Czech Technical University in Prague, Czechia)

Miloš Drdácký (Institute of Theoretical and Applied Mechanics, Czechia)

Andreea Dutu (Tech. Univ. of Civil Eng. of Bucharest, Romania)

Gi Young Jeong (Chonnam National University, South Korea)

Georg Hochreiner (TU Wien, Austria)

Jerzy Jasieńko (Wroclaw University of Technology, Poland)

Ivan Giongo (University of Trento, Italy)

Maurizio Piazza (University of Trento, Italy)

Jose Saporiti Machado (National Laboratory for Civil Engineering, Portugal)

Ronald Anthony (Anthony & Associates, USA)

Thomas Bader (Linnaeus University Växjö, Sweden)

Richard Harris (University of Bath, Britain)

Xiaobin SONG (Tong<i University, China)

Beatrice Faggiano (University of Naples “Federico II”, Italy)

ORGANIZING COMMITTEE

Jiří Kunecký (ITAM, chairman of the conference)

Hana Hasníková (ITAM)

Martin Hataj (UCEEB CTU)

ACKNOWLEDGEMENT

The conference would be not possible without help and advices from ITAM, among others especially our director Stanislav Pospíšil, Cyril Fischer for sharing the skills in event organization, Kateřina Kulawiecová for help with the proceedings, Karel Juliš for webmastering, Jan Válek for valuable advices, Marek Eisler for proof reading, Dita Frankeová for overall support, Barbora Přechová for help with organization of the event, Jaroslava Musilová for help in accounting, Zlatuše Burianová for help with financial issues, Květuše Gregorová for accounting, the whole organizing committee, from UCEEB CTU to Jan Jochman and all the students helping in the conference.

Special thank goes to our families for their patience and support.

TABLE OF CONTENTS

BASIS OF TIMBER STRUCTURAL DESIGN

TIMBER PROPERTIES

MONITORING AND SURVEY OF TIMBER STRUCTURES

STRUCTURAL INTERVENTIONS

CASE STUDIES - RESEARCH & PRACTICE

BASIS OF TIMBER STRUCTURAL DESIGN

SHATIS 22

6th International Conference on Structural
Health Assessment of Timber Structures
7-9 September 2022, Prague

SEISMIC ASSESSMENT OF TIMBER DIAPHRAGMS ACCORDING TO THE NEW DRAFT OF EN1998-3

Ivan GIONGO[1], Ermes RIZZI[1], and Maurizio PIAZZA[1]

[1] University of Trento, Italy, Department of Civil, Environmental and Mechanical Engineering

ABSTRACT

The paper reports on the procedure for the seismic assessment of timber diaphragms that has been introduced in the new draft of EN1998-3. The procedure covers the knowledge gap that is currently existing in the European standards and that is of special relevance in earthquake-prone countries such as Italy. The critical analysis of the new provisions is preceded by a brief summary on the standard background, with reference to the highest recognized codes in the field at the international level. Case-study buildings are then selected and analysed to better illustrate the various steps of the procedure and to assess the impact of the new provisions when applied to real scenarios.

KEYWORDS: Timber diaphragms, Seismic assessment, Eurocodes

INTRODUCTION

The importance of an accurate assessment of the in-plane diaphragm behaviour of timber floors when evaluating the seismic response of existing buildings is well-known. The dramatic earthquake events that in the last few decades hit many countries of the world have shown numerous examples of building collapses where the failure was favoured by the inadequacy of the diaphragms [1]. Additionally, past earthquakes proved that some popular retrofit strategies, such as replacing original wood floors with new concrete floors, were erroneous

Over the years, growing awareness of the role of timber floor diaphragms has produced standard codes with targeted procedures for assessing the in-plane diaphragm response (e.g., [2] and [3]). A discussion on current international code framework concerning timber diaphragms can be found in [4] where the background of [2] and [3] is analysed in detail. The new approach included in Chapter 10 of the new draft of EN1998-3 [5], which represents the latest addition to the timber diaphragm codes, makes a step forward by having its roots firmly in [2] and [3] while taking advantage of a decade-long research conducted at the University of Trento (Italy) in collaboration with the University of Auckland (NZ).

THE NEW PROVISIONS

The provisions in [5] address the seismic assessment of original timber floors and also provide recommendations for retrofitted diaphragms (Figure 1). The European countries most prone to earthquakes dangerous to buildings are those in the South, where timber diaphragms are typically found inside masonry buildings and are commonly made of solid timber joists spaced at approximately 0.5-0.7 m and covered by a layer of timber floorboards (2-3 cm thick) nailed perpendicularly to the joists. Among the retrofit solutions shown in Figure 1, those that see the use of timber-based products combine material compatibility, reversibility, and light weight (a, b, e, f) with remarkable mechanical performance in-plane (a, b, e, f) and out-of-plane (e, f).

The seismic action on the diaphragm is determined by assuming a parabolic inertia force distribution as in [2]. The total inertia force acting on the diaphragm (F_a [kN], see equation (a)) is the product of the diaphragm tributary mass (m_{ap} [kg]) and the diaphragm spectral acceleration (S_d [m/s^2]), reduced by the behaviour factor (q_{ap}), which for timber diaphragms is assumed to be equal to 1.5. The acceleration value depends directly on the period of the diaphragm oscillating in-plane (T_{ap} [s]), which is obtained

by adopting the common shear beam analogy and applying the Rayleigh quotient as recommended by [6] and experimentally validated by [7] (equation (b)).
The diaphragm displacement demand (Δ_d [m]), measured with reference to the mid-span, is obtained according to equation (c) where μ_d is the ductility factor depending on q_{ap}, as per the relation proposed by [8]; L_a [m] is the distance between diaphragm lateral supports; B [m] is the diaphragm width in the direction parallel to the seismic action; and $G_{d0,eff}$ [kN/m] is the effective value of the diaphragm equivalent shear stiffness. $G_{d0,eff}$ is obtained (see equation (d)) by modifying the diaphragm equivalent shear stiffness (G_{d0} [kN/m]) to take into account: 1) the knowledge level and the condition rating of the diaphragm (φ factor); 2) the stiffness contribution from the walls loaded out-of-plane (α_m, see [9] for further details); 3) the stiffness reduction due to possible diaphragm openings (A_n/A).

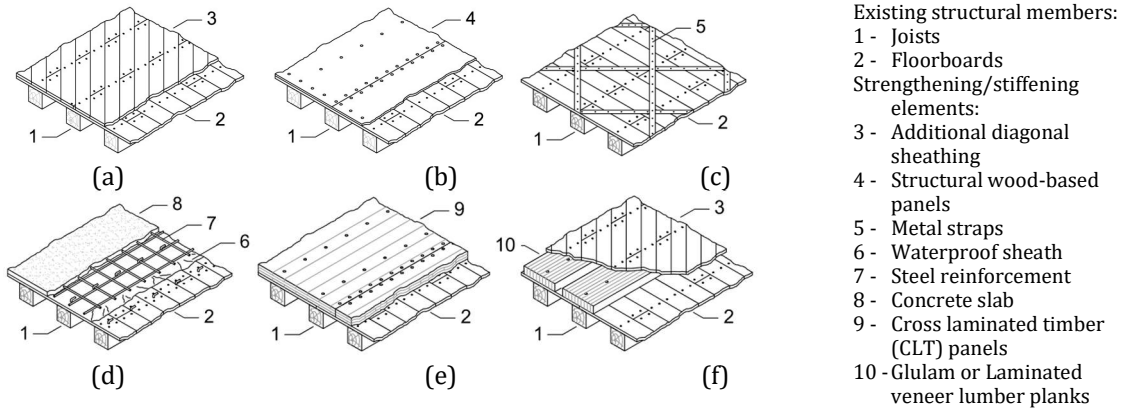

Figure 1: Retrofit: a) additional diagonal sheathing; b) structural wood-based panels; c) metal straps; d) concrete slab; e) CLT/LVL panels; f) timber planks and additional diagonal sheathing (adapted from [5])

Reference values of the diaphragm equivalent shear stiffness are provided (see Table 1) for the diaphragm type most representative of the existing building stock in earthquake prone countries (i.e., single straight sheathing) before and after the application of the timber-based retrofit solutions shown in Figure 1. Such values were derived starting from the experimental and numerical evidence collected over the years and included in publications such as [7], [9]-[13]. The stiffness values are larger in case of diaphragms with squat joists (SQ), characterized by a height over width ratio smaller than 2, loaded in the direction perpendicular to the joists.

$$F_a = \frac{S_d g m_{ap}}{q_{ap}} \quad \text{(a)} \qquad T_{ap} = 0{,}7\sqrt{\frac{m_{ap} g L_a}{10^3\, G_{d0,eff}\, B}} \quad \text{(b)}$$

$$\Delta_d = 0{,}00125 \mu_d S_d(T_{ap}) \frac{L_a\, m_{ap}}{B G_{d0,eff}} \quad \text{(c)} \qquad G_{d0,eff} = \varphi \alpha_m \frac{A_n}{A} G_{d0} \quad \text{(d)}$$

*Table 1: Equivalent shear stiffness values G_{d0} [kN/m]**

	No retrofit	Type of retrofit (Figure 1) (a)	(b)	(e)	(f)**
Single straight sheathing	150	3000	1800	3000	3000
Single straight sheathing (SQ joists) ***	400	3600	2400	4100	3800

* Given values can be considered as reference values.
** This retrofit strategy, that is mainly intended for improving diaphragm out-of-plane performance, requires squat joists (SQ) in order to be effective.
*** When the diaphragm is loaded in the direction perpendicular to the joists.

Table 2: Acceptance criteria in terms of unit shear strength v_R [kN/m]

	No retrofit	Type of retrofit (Figure 1) (a)	(b)	(e)	(f)
Parallel to joists	3	30	25	40	30
Perpendicular to joists	5*	45	25	45	40

* In case of SQ joists, diaphragm shear strength in the direction perpendicular to the joists, can be significantly higher than the $v_{R,k}$ value reported in the table.

Table 3: Acceptance criteria for horizontal diaphragms in terms of drift ratios d_r [%]

	No retrofit	Type of diaphragm (Figure 1)			
		(a)	(b)	(e)	(f)
Near Collapse (NC)	6,0	2,1	1,6	1,5	2,1
Significant Damage (SD)	4,0	1,5	1,2	1,1	1,5
Damage Limitation (DL)	2,5	0,8	0,7	0,6	0,8

Diaphragm verifications consist of checking that the diaphragm strength and deformation capacity are not exceeded by demand. The characteristic values of the unit shear strength (v_R [kN/m]) given in Table 2 represent the maximum shear force that the diaphragm can transfer to the lateral walls without the diaphragm showing any structural damage. To ensure safety, the design value of the unit shear strength ($v_{Rd} = \varphi v_R k_{mod}/\gamma_R$; $\gamma_R = 1$; for k_{mod} see [14]) needs to be checked against the unit shear load ($v_{Ed} = 2F_a/B$). Diaphragm deformation demand is evaluated in terms of drift ratio ($d_r = 2\Delta_d/L_a$) which is then compared with the limits provided in Table 3.

RESULTS AND DISCUSSION

Different case study buildings were selected to investigate possible critical points in the application of the code procedure to realistic full-size structures characterized by multi-bay diaphragms. Building geometry was designed to maximise the impact of key structural aspects, such as eccentricity between the centre of mass and the centre of stiffness, and strength imbalance between different walls. The predictions obtained from [5] were in fact compared with those from finite element model simulations. For the sake of brevity, here are reported the results of case study building A, whose plan geometry is visible in Figure 2(on the right). Figure 2 also shows (on the left) the finite element model of the building, created as a reference for the above-mentioned comparison. The building is a two-storey building with 30 cm thick walls made of stone masonry and straight sheathed timber floors. The first floor diaphragm is located at 2.7 m from the ground (floor load = 2.19 kN/m²) while the second is at 5.4 m (floor load = 1.32 kN/m²). Due to the wall layout, the floors consist of multiple floor-bays characterized by different orientation of the joists (see Figure 2 on the right).

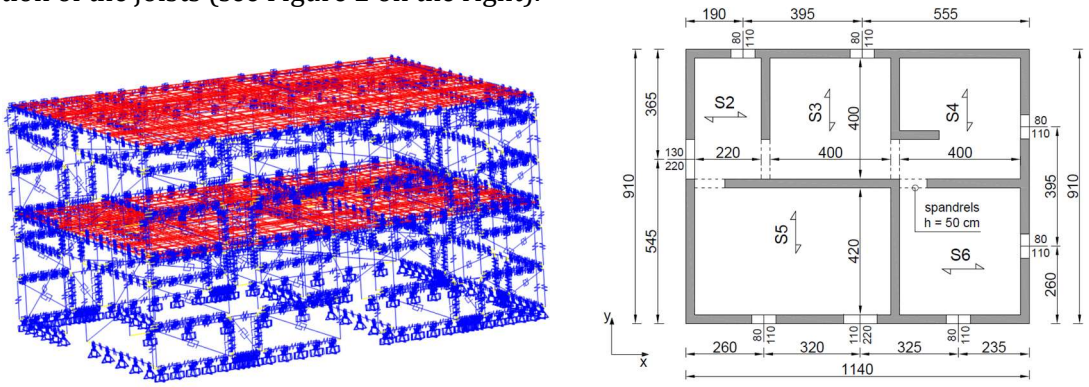

Figure 2: Case-study building A –Finite Element model (left); Building plan geometry (right)

The interaction between floor bays aligned in the direction parallel to the seismic loading (e.g., S6 and S4 when the inertia forces are parallel to the y direction) was accounted for by referring to equivalent diaphragms obtained by averaging the shear stiffness of the interacting bays under the equal deformation assumption. The equivalent diaphragms are shown in Figure 3 where the reader can see that they are different depending on the seismic loading direction. The values of the equivalent shear stiffness of the equivalent diaphragms are given in Table 4. Both perimeter and internal walls that are oriented perpendicular to the seismic force add to the tributary mass of the equivalent diaphragms (see, for example, the purple walls within the floor footprint of equivalent diaphragm S_A in Figure 3).

Walls oriented parallel to the seismic force are treated as full restraints for the in-plane deformation of the floors, provided that such walls have sufficient strength and stiffness. Tentatively, any wall with a length of at least 25% of the total width of the equivalent diaphragm was considered capable of providing effective restraint. For this reason, when defining the equivalent diaphragms for the earthquake acting in the x direction, the short wall on wall-line "B" was not considered an effective restraint and consequently diaphragm S_B spans from wall-line "A" to wall-line "C".

Table 4: Details of the equivalent diaphragms

Seismic force direction	Equivalent diaph.	Floor bay	Orientation*	$G_{d,0}$ - floor bay *[kN/m]*	*B [m]*	$G_{d,0}$ – equiv. diaph. *[kN/m]*
x	S_A	S_5	90	400	6.65	304
		S_6	0	150	4.15	
	S_B	S_2	0	150	2.35	346
		S_3	90	400	4.30	
		S_4	90	400	4.15	
y	S_C	S_2	90	400	4.15	272
		S_5	0	150	4.35	
	S_D	S_3	0	150	4.15	150
		S_5	0	150	4.35	
	S_E	S_4	0	150	4.15	278
		S_6	90	400	4.35	

* Joist orientation: 0 – parallel to the seismic load; 90 – perpendicular to the seismic load

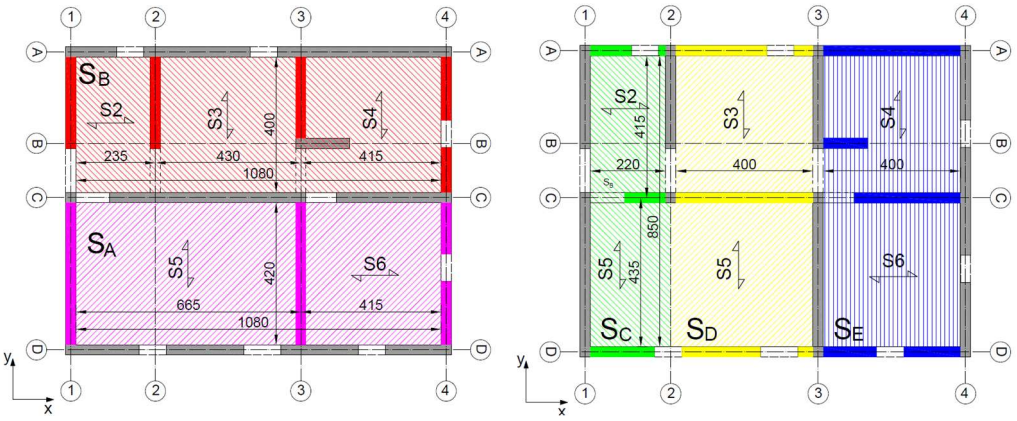

Figure 3: Equivalent floor diaphragms for checks related to earthquake action in the x (left) and y (right) directions.

In the example reported here, the spectral acceleration (S_d) was determined referring to the formula for the seismic coefficient (S_d/g, g = acceleration of gravity) applicable to non-structural elements, which is present in the current version of EN1998-1 [15]. The building construction site was assumed to be in the municipality of Ferla (IT) with an expected peak ground acceleration of 0.28 g for a return period of 475 years. The natural period of the building (T_1) was calculated as 0.177s. Table 5 shows the total seismic force on the equivalent diaphragms (F_a) and the midspan displacement (Δ_d), together with the effective equivalent shear stiffness determined assuming φ = 0.75 (health condition assessment: "*D2-Fair*"). The tributary mass, the diaphragm period (T_{ap}) and the geometric parameters (L_a and B) of the equivalent diaphragms are also reported in the table. The Δ_d values were compared with the maximum deformations measured from nonlinear static analyses performed on the finite element model shown in Figure 2. The masonry walls were simulated using sets of nonlinear link elements that create macro-elements exhibiting a behaviour similar to that described in [16]. The floor diaphragms were modelled using bidimensional shell elements according to the approach reported in [10] where the shell stiffness has been calibrated on the results of nonlinear dynamic analyses performed on refined models that reproduce every component of the floor (e.g., joists, floorboards and fasteners).

From the comparison with the modelling results, it emerges that the analytical procedure largely underestimated the deformation of the floor area occupied by S_C and S_D diaphragms due to the translational constraint along the y direction provided by the wall-line "2". The numeric simulations, in fact, showed the failure of wall-line "2" prior to the reaching of the performance point. Having observed that, the strength of wall-line "2" was checked against the shear force transferred to it by diaphragms S_C and S_D, corresponding to 50% of the inertia force (F_a) calculated for the two diaphragms according to [5]. Consistently with the modelling results, the calculated shear force exceeded the wall nominal capacity and therefore it was decided to consider wall-line "2" as incapable of providing an effective restraint to the diaphragm deformation, similarly to what done for wall-line "B". Such assumption meant the replacement of equivalent diaphragms S_C and S_D with diaphragm S_F (Figure 4). The seismic demand calculated for diaphragm S_F is given in Table 6. The midspan displacements obtained for diaphragm S_F adequately match the outcome of the model for that area of the floor, showing a small yet inevitable

overestimation of the deformation due to the model experiencing a partial effectiveness of the aforementioned restraint even after the maximum capacity of wall-line "2" was exceeded.

Table 5: Seismic demand and related parameters

Fl. level		L_a *[m]*	B *[m]*	$G_{d0,eff}$ *[kN/m]*	m_{ap} [kg]	T_{ap} [s]	F_a [kN]	Δ_d *[mm]*
1	S_A	4.2	10.8	233	32005	0.507	60.46	30.19
	S_B	4.0	10.8	264	30526	0.454	57.67	24.22
	S_C	2.2	8.5	206	13339	0.284	70.53	26.52
	S_D	4.0	8.5	118	26693	0.715	50.43	60.05
	S_E	4.0	8.5	214	29164	0.555	55.10	36.20
2	S_A	4.2	10.8	230	17725	0.379	70.53	35.58
	S_B	4.0	10.8	261	17116	0.341	88.11	37.31
	S_C	2.2	8.5	205	7219	0.209	72.39	27.33
	S_D	4.0	8.5	115	14751	0.538	27.87	33.99
	S_E	4.0	8.5	211	15830	0.412	50.20	33.42

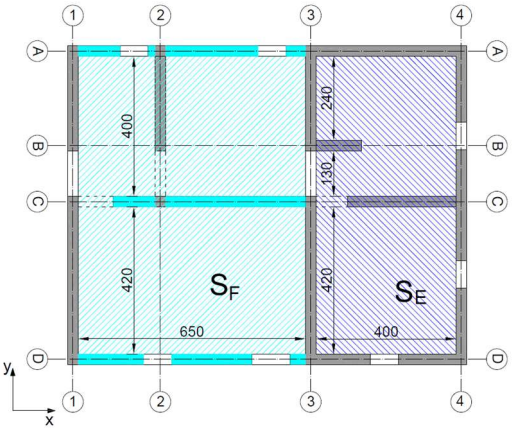

Figure 4: Equivalent floor diaphragms for checks in the y direction with wall-line "2" ineffective.

Table 6: Seismic demand and related parameters for floor S_F

L_a *[m]*	B *[m]*	$G_{d,0}$ *[kN/m]*	Floor level	$G_{d,eff}$ *[kN/m]*	m_a [kg]	T_a [s]	F_a [kN]	Δ_d *[mm]*
6.50	8.50	193	1	160	40591	0.966	76.69	109.68
			2	152	22355	0.734	42.23	63.34

Table 7: Deformation limit checks - floor level 1

		As-B	Retrofit type - Figure 1			
			(a)	(b)	(e)	(f)
Floor level	Floor ID	$dr/dr_{,cap}$	$dr/dr_{,cap}$	$dr/dr_{,cap}$	$dr/dr_{,cap}$	$dr/dr_{,cap}$
1	S_A	0.36	0.28	0.57	0.34	0.27
	S_B	0.30	0.25	0.52	0.30	0.24
	S_E	0.45	0.34	0.68	0.42	0.33
	S_F	0.84	0.46	0.69	0.62	0.46

Table 8: Diaphragm force limitation check (v_{Ed}/ v_{Rd}) - floor level 1

		As-B	Retrofit type - Figure 1			
			(a)	(b)	(e)	(f)
Direction	Floor ID	v_{Ed}/ v_{Rd}	v_{Ed}/ v_{Rd}	v_{Ed}/ v_{Rd}	v_{Ed}/ v_{Rd}	v_{Ed}/ v_{Rd}
x	S2	0.52	0.32	0.37	0.21	0.30
	S3	0.82	0.25	0.50	0.25	0.29
	S4	0.82	0.25	0.50	0.25	0.29
	S5	0.98	0.28	0.55	0.29	0.32
	S6	0.61	0.35	0.41	0.24	0.34
y	S2	**1.50**	0.42	0.56	0.43	0.48
	S3	**2.49**	0.63	0.56	0.49	0.64
	S4	0.78	0.42	0.49	0.29	0.41
	S5	**1.56**	0.59	0.50	0.43	0.58
	S6	**1.24**	0.34	0.65	0.35	0.39

The procedure used to determine the parameters of Table 5 and Table 6, previously described, was then extended to include new scenarios where the original floors had been retrofitted with the timber-based techniques shown in Figure 1. Once the demand was determined, the safety checks were performed, and the results are shown in Table 7 and Table 8 concerning the deformation and force limitation, respectively. The earthquake action in the *y* direction proved to be the most severe condition for the building, with most diaphragm bays in the as-built configuration (As-B, straight sheathing) exceeding their strength even though the drift capacity appeared always to be sufficient, thanks to the flexibility and deformation resources of this type of diaphragms. It is worth reminding that, unlike [3], the deformation limits given by [5] (Table 3) depend exclusively on the diaphragm performance that can

exceed that of the face-loaded walls. Therefore, the compatibility of the diaphragm deformation capacity with first-mode collapse mechanisms of perimeter walls has to be verified case by case.
All the diaphragm retrofits investigated have shown a far better performance than the minimum required by the seismicity of the selected construction site. This tendency was also observed in other case studies analysed by the authors that have not been reported herein for the sake of brevity.

CONCLUSION

The new approach for seismic assessment and retrofitting of timber diaphragms included in the new draft of EN 1998-3 was presented and discussed. The approach was proof-tested on selected case studies; the results were then compared to simulations obtained from finite element modelling. The outcome of the safety checks performed on the case-study buildings confirmed the tendency often observed by post-earthquake surveys and research studies, that straight-sheathed diaphragms may be inadequate to face high seismic demands. The analysis results also showed that the adoption of light and reversible timber-to-timber retrofit strategies can produce a marked increase in the level of safety capable of meeting even the strongest demands.

ACKNOWLEDGEMENTS

The research was carried out within the framework of the 2022-2024 ReLUIS-DPC network. The authors wish to thank former student Arianna Brunelli for the help with the modelling.

REFERENCES

[1] Penna, A., P. Morandi, M. Rota, C. F. Manzini, F. da Porto, and G. Magenes. 2013. “Performance of masonry buildings during the Emilia 2012 earthquake.” Bull. Earthquake Eng. 12 (5): 2255–2273.

[2] ASCE (American Society of Civil Engineers) (2017). “Seismic Evaluation and Retrofit of Existing Buildings”. Reston, VA: ASCE. United States of America.

[3] NZSEE (New Zealand Society for Earthquake Engineering) (2017). “Assessment and improvement of the structural performance of buildings in earthquakes”. NZSEE 2017. Wellington, New Zealand.

[4] Giongo I., Schiro G., Tomasi R., Dizhur D., Ingham J., 2015, “Seismic assessment procedures for flexible timber diaphragms”, ISBN 978-3-319-39492-3. DOI: 10.1007/978-3-319-39492-3_22

[5] CEN (European Committee for Standardization) (2021). “Earthquake resistance design of structures – Part 3: Assessment and retrofitting of buildings”. prEN1998-3:2021. Brussels, BE.

[6] Wilson, A., Quenneville, P., and Ingham, J. (2013). “Natural period and seismic idealization of flexible timber diaphragms.” Earthquake Spectra, 29(3), 1003–1019.

[7] Giongo, I., D. Dizhur, R. Tomasi, and J. M. Ingham. 2014. “Field testing of flexible timber diaphragms in an existing vintage URM building.” J. Struct. Eng. 141 (1).

[8] Newmark, N. M., and Hall, W. J. (1982). “Earthquake spectra and design.” Earth System Dynamics.

[9] Giongo I., Wilson A., et al. (2014). “Detailed seismic assessment and improvement procedure for vintage flexible timber diaphragms”, NZSEE Bulletin, vol.47, pp. 97-118.

[10] Rizzi E., Capovilla M., Giongo I., Piazza M., 2017, “Numerical study on the in-plane behaviour of existing timber diaphragms strengthened with diagonal sheathing”. SHATIS’17, Instanbul, Turkey.

[11] Giongo I. ,Rizzi E., Ingham J., Dizhur D., 2018, “Numerical modelling strategies for the in-plane behavior of straight sheathed timber diaphragms”, J. Struct. Eng., vol. 144, No.10.

[12] Rizzi E., Capovilla M., Piazza M., Giongo I. (2019). “In-plane behaviour of timber diaphragms retrofitted with CLT panels”. RILEM Bookseries. DOI:10.1007/978-3-319-99441-3_173.

[13] Rizzi E., Giongo I., Ingham J., Dizhur D. (2020). "Testing and Modeling In-Plane Behavior of Retrofitted Timber Diaphragms", J. Struct. Eng., v. 2020, vol. 146, n. Issue 2 (2020).

[14] CEN (European Committee for Standardization) (2021). “Design of timber structures – Common rules and rules for buildings – Part 1-1: General”. prEN1995-1-1:2021. Brussels, BE.

[15] CEN (European Committee for Standardization) (2004). “Design of structures for earthquake resistance – Part 1: General rules, seismic actions and rules for buildings”. EN1998-1:2004. BE.

[16] Caliò, I., Pantò, B. (2014). “A macro-element modelling approach of Infilled Frame Structures”. Comput. Struct. vol.143, pp. 91-107, http://dx.doi.org/10.1016/j.compstruc.2014.07.008.

ILLUSTRATION OF THE BOND BEHAVIOUR OF WOOD SCREWS USING EXTENSION MODEL

Professor Dr.-Ing. Mazen AYOUBI[1]

[1] Chair of Building Materials, Frankfurt University of Applied Sciences, Frankfurt am Main, Germany

ABSTRACT

Self-tapping wood screws are important fasteners for timber-to-timber or timber-to-steel-connections as well as for compression reinforcement of beams. Furthermore, the use of self-tapping screws with continuous threads to reinforce timbers and glue-laminated elements represents an effective, simple and economic method. For these joints and reinforcing methods, the decisive property is the load-bearing capacity, which is determined by the bonding mechanisms between the screw thread and the wood. The analysis of the bond behaviour and the load transfer between screws and wood depending on the angle to the grain enables the safe and efficient design of wood screws.

The load distribution in glue-laminated timber elements, being reinforced using self-tapping screws with continuous threads has been measured with a non-destructive measuring procedure (3D image correlation system) and analysed in over 84 tests, whereby the stress analysis considers the long embedment length of the screws. The experimental investigations are comprised of over 160 pull-out tests with long embedment length tests, which cover different angles to the grain and various screw diameters.

The extension of the modelling for the stress distribution concerning the rotation angle to the screw axis is investigated experimentally using coloured crack patterns. The use of the model for design is shown on the parameter flank angle. Improved models of the bond behaviour can be used by manufacturers to optimize the screw geometry as well as to enable of a safe and economic design approach. Timber engineering thus benefits from withdrawal capacities as well as higher reliability of the screw joint. This paper aims to examine the models of the bond behaviour of wood screws from the point of view of design. As a result, requirements on load-bearing models for the design are shown and a model extension depending on the relationship between the thread design of the screws and the load-bearing capacity is presented.

KEYWORDS: wood screws, bond behavior fasteners, anchorage length, load-bearing capacity, stress distribution

INTRODUCATION

Self-tapping wood screws with continuous threads are nowadays used beyond their common application in the joining of timber elements and, as fasteners, in timber-to-timber connections, to strengthen and increase the load-carrying capacity of beam supports, as well as to act against the tensile stresses perpendicular to the grain in notched beam supports. Furthermore, self-tapping screws can be utilized to reinforce curved beams or beams with holes. Regarding these new fields of application, the reinforcing and joining of timbers with screws represents an effective, simple and economic method [1]. Modern self-tapping screws with continuous threads (figure 1), available in nominal diameters up to 14 mm and lengths of more than 1500 mm, have many advantages in comparison to traditional standardized screws, which are partially threaded and need pre-drilled pilot holes for the installation in timber elements. The continuous threading of the screws allows a consistency in the bond, the interaction between screws and wood, and enables the usage of these screws for reinforcing and joining of timber elements in a mechanism similar to the reinforcing of concrete with steel [1-3].

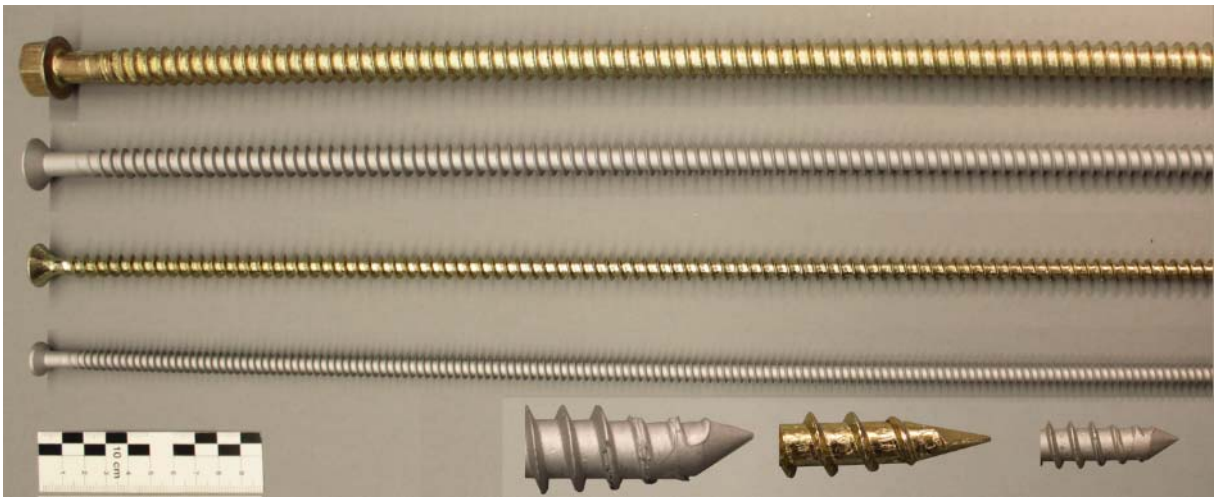

Figure 1: Self-tapping screws continuously-threaded and threaded rods of different sizes, down right details of the different screw tips.

The description of the bond behaviour between the screws and the surrounding wood is essential for the development and evaluation of design methods for reinforced structures with self-tapping screws. However, the nature of wood being an anisotropic material with a high grade of inhomogeneity makes the analytic and numeric description of the bond behaviour of the screws more challenging. In this context, the geometry of the screws, the angle between screw axis and grain (α), the lateral pressure, timber density and the diameter of the screws as well as the penetration depth in the wood are the most important parameters [1].

3D DIGITAL IMAGE CORRELATION SYSTEM

Digital image correlation system (DIC) is a non-contact, nondestructive method to measure displacements and strains. DIC is as Surface Strain Measurement techniques, which has been developed and used to measure deformations and strains of materials under various loading regimes with sub-pixel accuracy since the 1980's [2]. It allows the determination of displacements of the points on the surface of the formed specimens by comparing successive images acquired during a test and cross correlating the gray intensity patterns of the direct neighbourhood of the points (or the reference areas) [3]. In addition, out of plane displacements may be accurately measured if two cameras are arranged in front of the same specimen area at an angle so that the displacements are captured at the same time instants [3]. DIC software detects image displacements in pixels and converts them into physical

displacements involving a calibration process. An accurate calibration of the imaging system prior to the measurement is a crucial point for ensuring the reliability of the measured data, as calibration uncertainties show up as systematic error in the measurement results [4].

APPLICATION ON TIMBER ELEMENTS

Digital image correlation system (DIC) being non-destructive testing procedure can be used on timber elements to evaluate the specimens' properties without causing damage or having an influence on the material behaviour during testing. These systems give a detailed visualization of the strain distribution in the timber surface and enable to obtain and quantify the strain results in any orientation required. Furthermore, the monitoring of the loading process and the stress distribution in timber elements with suitable non-destructive testing procedures enables a better understanding of the load transfer mechanisms in wood being an anisotropic material with high grade of inhomogeneity.
ARAMIS is a non-contact and material-independent measuring system based on digital image correlation (DIC). It offers a stable solution for full-field and point-based analyses of test objects of just a few millimetres up to structural components of several meters in size [5]. It uses image correlation based on the tracking of a random speckle pattern instead of the conventional grid system. Therefore, prior to testing, a speckle pattern has to be generated by applying white and black paint on the specimens. For the quality of the analysis it is benefiting to have a wide gradient the gray shades [6], which is difficult to realize given the relatively wide measurement field.

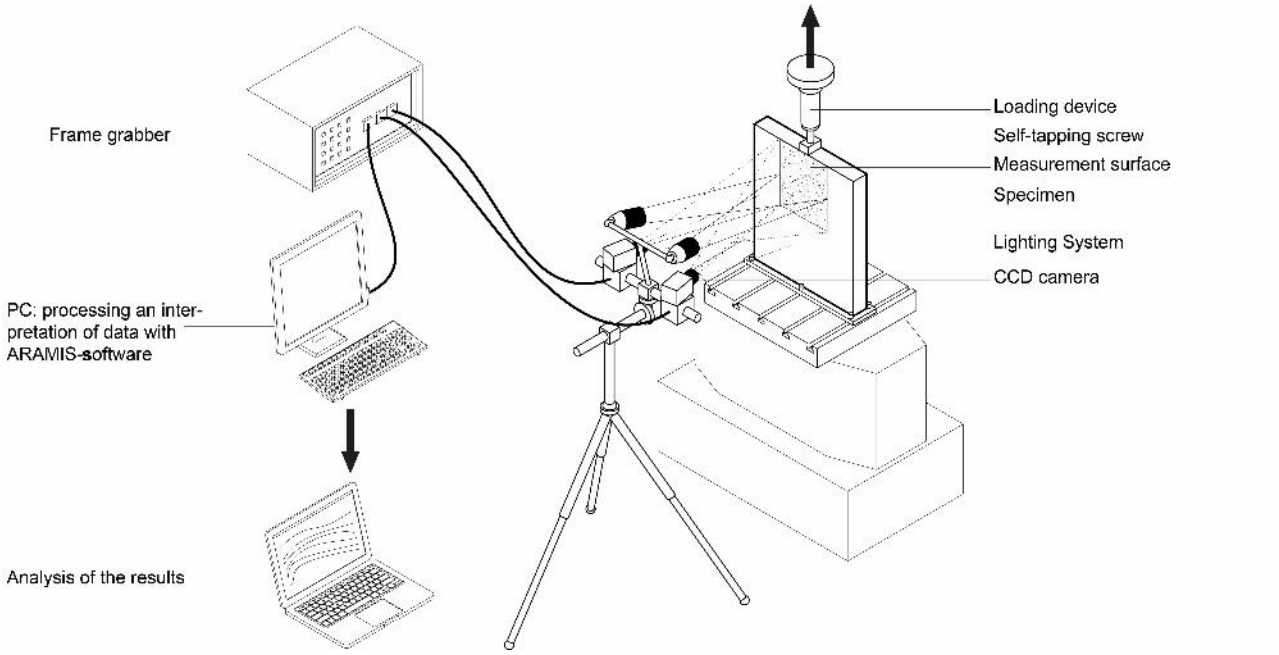

Figure 2: Schematic diagram illustrating the utilized 3D ARAMIS measurement system for the glulam specimen [7].

The ARAMIS system [5] is composed of three components, including two CCD (charge coupled device) cameras, computer and software. The cameras are arranged in front of the specimens and aligned to their surface, which frames the area of analysis. Through the capture of the displacements at the same instants of time stereoscopic information is provided, so that out of plane displacements can be measured accurately. To assure the stability, necessary for the precision of the measurements, the cameras are fixed on a tripod. Grayscale images (12-bits resolution converted into 8-bits resolution) are captured real-time through a frame grabber (figure 2) and processed by a computer with ARAMIS Software [5]. There are many factors that play a critical role with regard to the precision of the measurements on the surface of timber elements, such as the speckle pattern, calibration and the lighting circumstances [6].

LOAD DISTRIBUTION TESTS USING 3D IMAGE CORRELATION SYSTEM

The force transfer along the anchorage length of the self-tapping screws being used as reinforcement in glue-laminated timber elements has been analysed with load distribution tests based on the results of the pull-out tests (s. [8]). The monitoring of the loading process and the stress distribution along the embedded length of self-tapping screws in timber elements aims at seeking a better understanding of the load transfer mechanisms between the surrounding wood areas and the screws, which are elementary for the analytical approach of the force transfer along the screw's anchorage length. For the determination of the specimens' deformation and strain distribution, an optical three-dimensional image correlation system (ARAMIS) [5] has been employed. The measured strain distributions in the load transmission zone are used in the modelling the bond between the screws and the timber [9]. The test takes into account the size effect of the screws [10].

MEASUREMENT FIELD UP TO 500 X 600 MM

Different angles to the grain were tested with the optimized measuring device based on the results of the parametric study, where the whole surface of the specimen was measured with the ARAMIS system. The specimens have a thickness of about five times the nominal diameter of the used screws, so that it is still possible to measure the deformations on the whole area. The optimized configurations were used on measurement fields of 500 x 600 mm with different parameters of the load distribution test to verify the load transfers mechanisms of the screws, as well as to determine the load distribution and the anchorage length of the screws. The testing program takes up this enquiry and sets out the parameters such as screw diameters, the angle to the timber, the load type and the screw combinations concretely. Figure 3 exemplarily identifies the surface displacement in the vertical direction at traction of 35 kN and screw installed centric to the specimen with a nominal diameter of 12 mm.

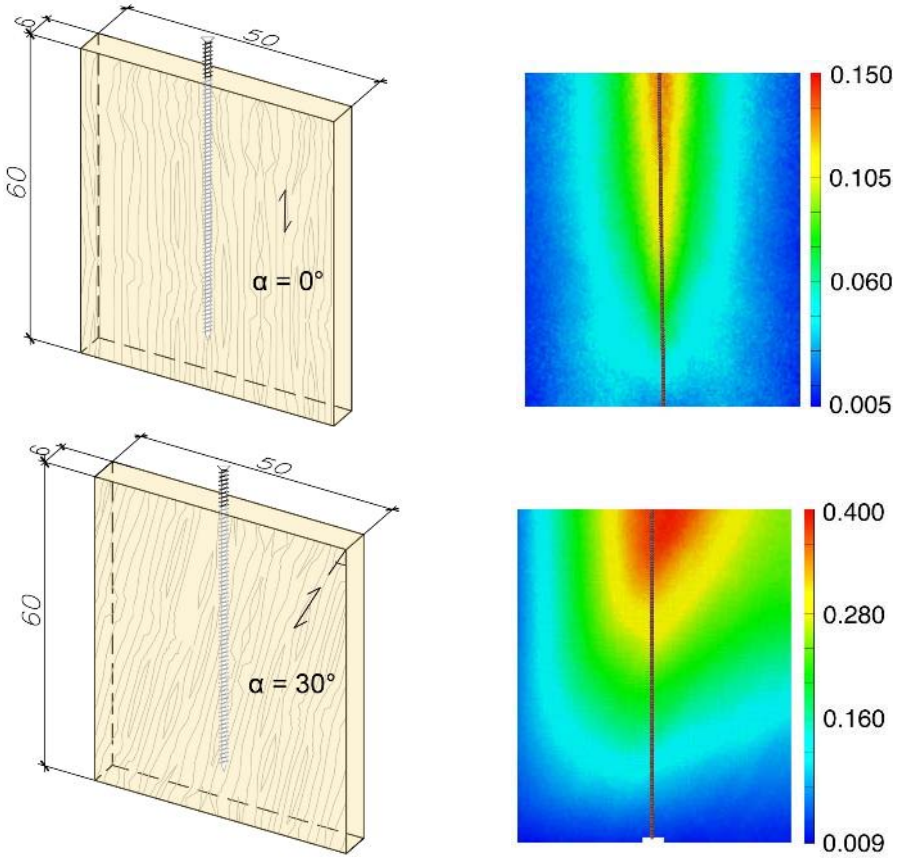

Figure 3: Visualization of displacement in the vertical direction in mm at traction 35 kN from ARAMIS software analytical model.

In the experimental investigations (load distribution tests), the specimen was fixed on a stainless steel plate on the unloaded end to ensure the same boundary condition at the edge of the specimen. To ensure the measurement accuracy of the employed image correlation system for every specimen, additional electro-mechanical transducers (LVDTs) were fixed on each screw at the point of screw insertion to measure the screw slip at the loaded end (figure 4, b) and figure 5, b)). Moreover, a system that ensures the same loading on each screw at the first loading step for the test with three screws was installed. The utilized system consists of load cells, spherical calottes from hard metal and a load distribution plate as well as adjustable screw mechanisms (see figure 4, a) and figure 5, b)).

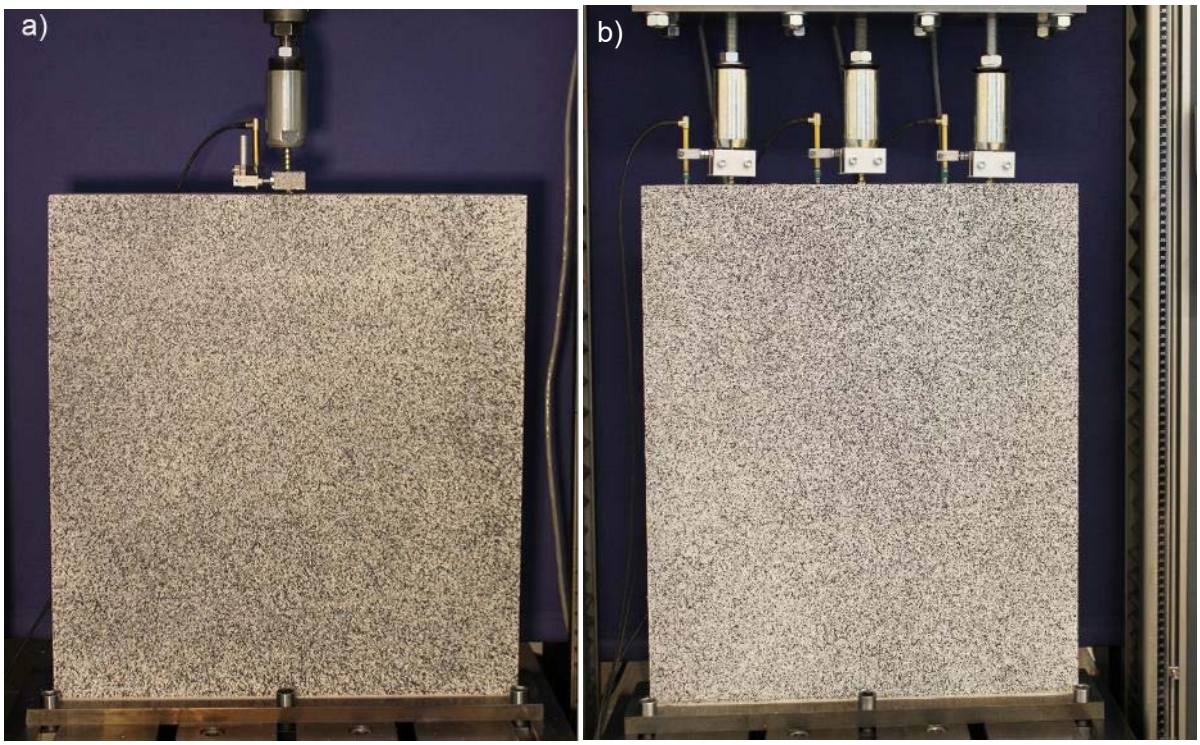

Figure 4: Load distribution test of specimen under tension loads: a) representation of the whole specimen with one centric screw, b) representation of the whole specimen with three screws.

The full-field data obtained from the 3D image correlation system (ARAMIS) shows the real local deformation and strain variation, as well as the locations of maxima and minima for different angles between the screw and the grain (α). Figure 5 illustrates the gradient of the vertical displacements of the specimens for two different angles (30°, figure 5, a and 60°, figure 5, b). These are critical information for model iteration, and for the model validation, as well as for the determination of the anchorage length and the load distribution angle along the anchorage length of the screws. Figure 6 gives a comparison of the load distribution zone with different angles to the grain for screw combination with a nominal diameter of (d = 12 mm). In this illustration the distribution of the gradually vertical displacement for one screw parallel to the grains determined with ARAMIS system (figure 6, a)) is compared with theses with three screws (figure 6, b)). Herewith the screw combination with three centric and symmetrically installed screws was employed to investigate the influences of the neighbouring screws. The system gives a detailed visualization of the strain distribution in the glulam surface and enables to obtain and quantify the strain results in any orientation required. Based on the results, it can be concluded that the method is a promising tool to investigate the bond behaviour and load distribution of self-tapping screws in glue-laminated timber elements. The results signify that the systematic relative errors are still smaller than 0.04 of the maximum strain. Thus, a sufficient accuracy with regard to the determination of stress distribution with the optical 3D field measuring system (ARAMIS) on timber elements up to 500 x 600 mm has been confirmed.

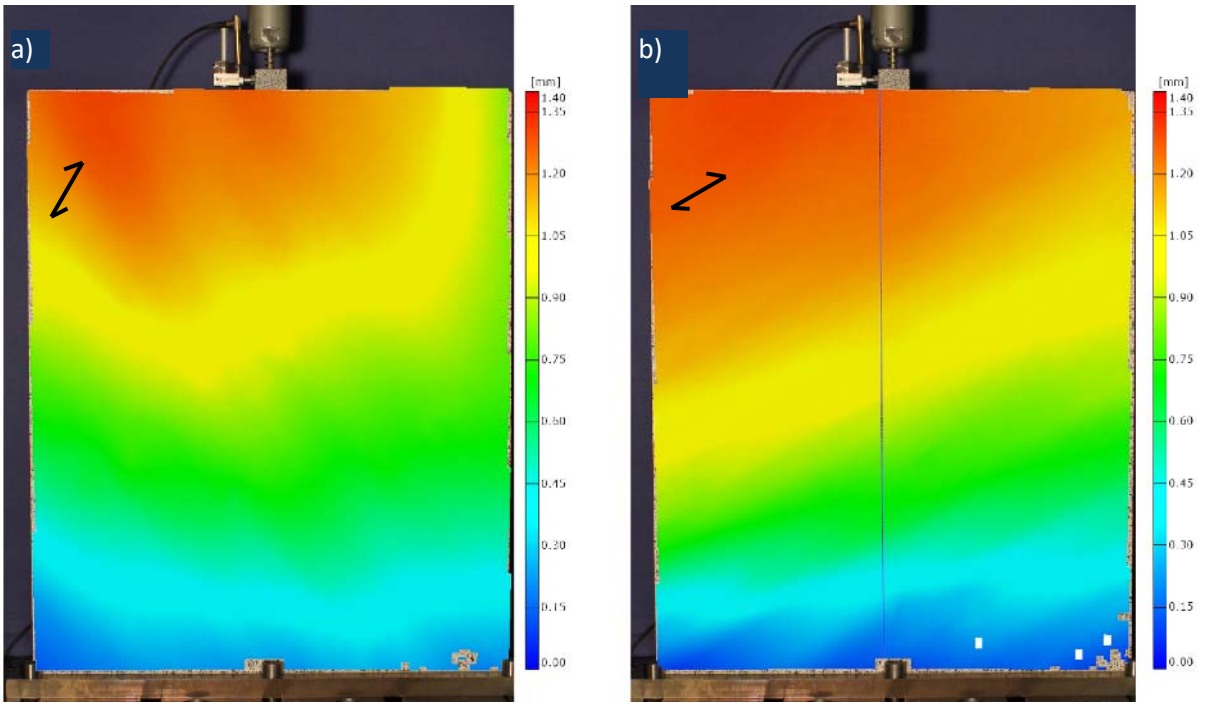

Figure 5: Gradient of the wood displacements of the load distribution tests of specimens with one screw (d= 12 mm) under tension loads at: a) tension load of 52,6 kN and angle to the grain of 30°, b) tension load of 20,4 kN and angle to the grain of 60°.

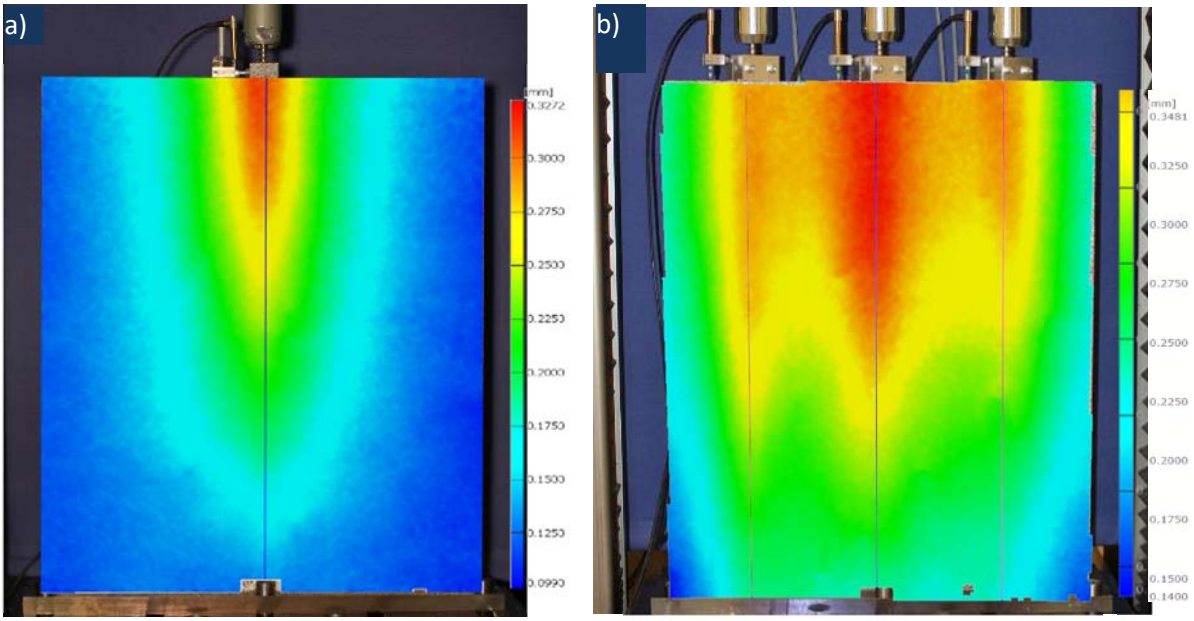

Figure 6: Gradient of the wood displacements parallel to the screws of the load distribution tests of specimens under tension loads with screws (d=12 mm) parallel to the grain (α=0) with: a) one screw under tension load of 49,5 kN, b) three screws installed symmetrically under arithmetic mean tension load of 49,1 kN.

The investigating and evaluating the strains and displacements of the wood surface of the test specimens, enable the determination of the load transfer and anchorage length of the screws. The load distribution angles of the screws (γ) were detected based on the test results obtained from the 3D image correlation system with different angles to the grain (s. figure 5 and 6) and screw combinations as well as load types. The load distribution angles (γ) angles are between 5°, when screwing in parallel to the grain direction and up to 60°, when screwing in perpendicular to the grain direction. The results of the load distribution tests are essential for the providing comprehensive information about the load distribution angles of the screw in the timber (γ) in combination with the different parameters such as:

Angles between the screw insertion and the grain (α), axis load types (tension and compression) and screw combinations. Furthermore, for a better interpretation of the results, the displacements out of the measuring plane were explicitly analysed; this was particularly relevant for the specimens with compressive loading Such information was only possible thanks to the application of optical 3D field measuring system.

MODELS FOR THE BOND BEHAVIOR OF WOOD SCREWS

For the design of wood screws, being an economic and effective method of reinforcing glue-laminated timber elements and fasteners for timber-to-timber or timber-to-steel-connections, there is a lack of suitable models that describe the relationship between the thread design and the load-bearing capacity. Depending on the result of the experimental investigations the models of the bond behaviour of wood screws has been examined from the point of view of design. As a result, a model extension has been suggested [11]. The extension to the stress distribution concerning the rotation angle to the screw axis is investigated experimentally by Hölz et al. [11] using coloured crack patterns. The use of the model for design is shown on the parameter flank angle. Improved models of the bond behaviour can be used by manufacturers to optimize the screw geometry as well as to enable of a safe and economic design approach. Timber engineering thus benefits from withdrawal capacities as well as higher reliability of the screw joint [11].

THEORETICAL MODELS

The load-bearing capacity for wood screws can be explained with bonding mechanisms. Three different bonding mechanisms can be distinguished in the contact area between thread of the screw and wood [7, 12]:

- Adhesive and positive locking of the screw thread with the wood matrix: The shallowly inclined spiral thread of a screw, locked by self-locking, causes resistance due to the form-fit of the thread with the intervening cell walls of the wood matrix.
- Shear bond due to the mechanical interlock between the thread and the wood: It is caused by the shearing of the matrix components located in the thread interstices and the adjacent wood cells, which are stressed to shear.
- Friction bond: It is caused by the slightest displacement between the contact surfaces of the separated matrix components in the interface between the cylindrical thread outer surfaces and the wood matrix.

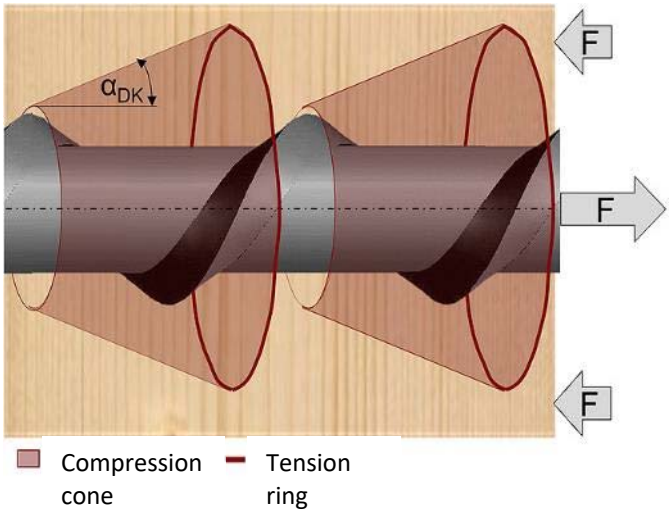

Figure 7: Compression cone-tension ring model on a wood screw connection, from [11]; shown are the resulting compression cones under the angle α_{DK} as well as the tension rings [7, 11]

The activation of the different mechanisms is associated with the relative displacement of the screws against the surrounding wood. Further loading of the screw causes the adhesion to be overcome,

resulting in relative displacements, which in turn cause the shear bond stresses. The bond stresses along the anchorage length are not constant, they reach their peak value in the area of force application and decrease until the end of force application according to a non-linear function.
Under axial load, the wood screw supports itself against the wood via the thread flanks. This force support occurs at an angle α_{DK} to the flanks, creating so called pressure cones. The resulting state of stress also creates ring stresses, called tension rings, to ensure the balance of forces. When the wood strength is exceeded, these stresses cause cracks to initiate and widen [7, 11] (s. figure 7). From a mechanical point of view, the maximum values of the achieved bond stresses as well as the degradation process depend on the bond quality and the bond mechanisms during force transmission. In the anisotropic, inhomogeneous material wood, these are largely influenced by the angle between the screw and the wood fibre direction (α), but also by the matrix properties (s. figure 5 and 6) [13].

MODEL EXTENSIONS

In order to represent the stress distribution depending on the angle of rotation around the screw axis, the compression cones are not circular cone-shaped and the tension rings are not circular, but represented by an elliptical helix shape for screw-in angles greater than 0° [11]. The semi-axes a and b of the load propagation are therefore of different lengths. For an adaptation to a fibre-parallel screwing-in, the half-axes can be chosen to be the same size in order to represent a circular load propagation. The semi-axes are dependent on the running variable t for the anchorage length, whereby non-linear relationships can be represented. The pressure cones and tension rings can thus be mapped according to the stress distribution depending on the anchorage length. This model extension with the corresponding stress distribution is shown in Figure 7 [11].

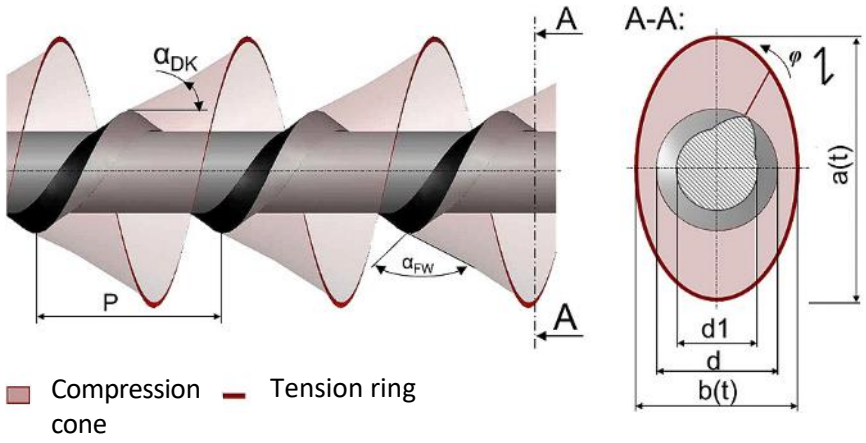

Figure 8: Extension of the compression cone-tension ring model with an angle α_{DK} and elliptical helix (a ≠ b) as a function of screw-in depth (a(t) and b(t)); compression cones under the angle α_{DK}; shown are the screw parameters outer diameter d, inner diameter d1, flank angle α_{FW} and pitch P, from [11].

The parameters of the semi-axes a(t) and b(t) as well as the angle α_{DK} of the composite load-bearing model have to be determined experimentally in further investigations in order to adapt the model to the boundary conditions of the wood screw connection.

CONCLUSION

The use of self-tapping screws with continuous threads to reinforce timbers and glue-laminated elements represents an effective, simple and economic method. Wood screws are important fasteners for timber-to-timber or timber-to-steel-connections as well as for compression reinforcement of beams. For these joints and reinforcing methods, the decisive property is the load-bearing capacity, which is determined by the bonding mechanisms between the screw thread and the wood. The analysis of the bond behaviour and the load transfer between screws and wood depending on the angle to the grain enables the safe and efficient design of wood screws. Non-destructive testing procedures allow the

evaluation of the specimens' properties without causing damage or having an influence on the material behaviour during testing. The monitoring of the loading process and the stress distribution in timber elements with suitable non-destructive testing procedures enables a better understanding of the load transfer mechanisms in wood being an anisotropic material with high grade of inhomogeneity. The extension of the modelling for the stress distribution concerning the rotation angle to the screw axis is investigated. Improved models of the bond behaviour can be used by manufacturers to optimize the screw geometry as well as to enable of a safe and economic design approach. Timber engineering thus benefits from withdrawal capacities as well as higher reliability of the screw joint.

REFERENCES

[1] Ayoubi, M.; Trautz, M.: Bond Behaviour of Self-Tapping Screws being used as Reinforcement in Glue-Laminated Timber Elements. In: SHATIS' 15, the 3nd International Conference on Structural Health Assessment of Timber Structures, Proceedings of the International Conference on Structural Health Assessment of Timber Structures, ISSN 0860-2395, ISBN 978-83-7125-255-6, September 9-11, 2015, Wroclaw, Poland, pp. 859-871.

[2] Muszyński, L.; Lagana, R.; Shaler, S.M.: An optical method for characterization of basic hygro-mechanical properties of solid wood in tension. In: Proceedings of the 8th International IUFRO Wood Drying Conference, Brasov, Romania, August 24–29, 2003. pp. 77–82.

[3] Lopez-Anido, R.; El-Chiti, F.; Muszynski, L.; Dagher, H.; Thompson, L.; Hess, P.: Composite material testing using a 3-D digital image correlation system. In: American Composites Manufacturers Association, COMPOSITES 2004, October 6-8, Tampa, Florida USA.

[4] Siebert, T. Becker, K. Spiltthof, I. Neumann, R. Krupka, Error Estimations in Digital Image Correlation Technique, Applied Mechanics and Materials, Vols. 7-8, 2007, 265-270.

[5] ARAMIS: User manual-software, GOM – Optical Measuring Technologies, Braunschweig.

[6] Vogelsberg, A. H.: Zur Eigenspannungsermittlung in Holz. PhD-Thesis, RWTH-Aachen University, ISBN: 978-3-8440-0594-3, 2011.

[7] Ayoubi, M.: Zum Verbundverhalten von Vollgewindeschrauben mit großen Einbindelängen beim Einsatz als Bewehrung in Brettschichtholzbauteilen, PhD Thesis, RWTH Aachen University, 2014.

[8] Ayoubi, M.: Non-Destructive Testing Procedure for Determining Stress Distribution in with Self-Tapping Screws Reinforced Glue-Laminated Timber Elements. In: SHATiS'19, 5th International Conference on Structural Health Assessment of Timber Structures, Proceedings of the International Conference on Structural Health Assessment of Timber Structures SHATiS'2019, ISBN: 978-989-54496-2-0, Guimarães, Portugal, September 25-27, 2019, pp. 526-536.

[9] Ayoubi, M.; Trautz, M.: Determination of the Stress Distribution in Timber Elements reinforced with Self-Tapping Screws using an Optical Metrology System. In: *Proceedings of the 2nd International Conference on Structural Health Assessment of Timber Structures (SHATIS 13)*, September 4-6, 2013, Trento, Italy, Editors: Maurizio Piazza and Mariapaola Riggio.

[10] Ayoubi, M.; Rößler, G.; Trautz, M.; Raupach, M.: Experimental and Numerical Investigation of Bond between Glue-laminated Timber Elements and Self-Tapping Screws. In: 13 proceedings of the IASS 2013 Symposium, Wrocław, Poland, 23-27 September 2013, ed. Jan B. Obrębski and Romuald Tarczewski; International Association for Shell and Spatial Structures, Wrocław, Poland, 23-27 September 2013.

[11] Hölz, K.; Ayoubi, M.; Gwosch, T.; Matthiesen, S.: Theoretische Modelle zum Verbundtragverhalten von Holzschrauben für die Schraubengestaltung. In: Bautechnik (Zeitschrift für den gesamten Ingenieurbau), Volume 98, Issue 14, S. 86-94, 2021. DOI:10.1002/bate.202100003, https://onlinelibrary.wiley.com/doi/abs/10.1002/bate.202100003

[12] Ayoubi, M.; Trautz, M.: Bond behaviour of self-tapping screws being used as reinforcement in glue-laminated timber elements. Part 1: experimental investigations on self-tapping screws with continuous threads and long embedment length being used as reinforcement in glue-laminated timber elements. Bautechnik 92(11):790–799. https://doi.org/10.1002/bate.201400098

[13] Ayoubi M (2016) Bond behaviour of self-tapping screws being used as reinforcement in glue-laminated timber elements. Part 2: analytical and numerical investigations as well bond model derivation for the calculation of anchorage length. Bautechnik 93(11):817–827. https://doi.org/10.1002/bate.201500086

Thermo-mechanical response of Steel-Timber Composite structures exposed to fire

Matias GODOY[1], Juan C. PINA[1], Sergio J. YANEZ[1], Carlos F. GUZMAN[1], and Erick I. SAAVEDRA FLORES[1]

[1] University of Santiago of Chile (USACH), Faculty of Engineering, Civil Engineering Department, Chile

ABSTRACT

Despite the environmental benefits of timber as a building material, the response of timber structures under a fire scenario remains a consistent concern. To address this issue, here the thermo-mechanical response of Steel-Timber Composite (STC) floors i.e., Cross-Laminated Timber (CLT) slabs and steel beams, exposed to fire is investigated. A one way coupled Computational Fluid Dynamics (CFD) and Finite Element Method (FEM) approach was employed. The software Fire Dynamics Simulator (FDS) was used for the CFD fire analyses and ANSYS for the FEM transient heat transfer and thermo-mechanical analyses. FDS was used to model a 30-minute fire in a small apartment. The outcome of this analysis was the temperature distribution on the SCT slab exposed surface. This information was then used as input for the coupled thermo-mechanical analyses carried out in ANSYS. The latter enabled to assess the thermal and structural performance of the SCT slab when subjected to a fire scenario.

KEYWORDS: Steel-Timber Composite, Thermo-mechanical Response, Fire Structure Interaction, Coupled Fire-Structural Analyses

INTRODUCTION

The renewable nature of wood has led to an increased in the use of timber as a building material. This trend has been further enhanced by the potential of timber as a lower carbon footprint alternative to concrete and steel [1-3]. Thus, it is important that timber is regarded as a viable construction alternative not only for housing, or low-rise buildings, but also for mid- and high-rise buildings. Nevertheless, the latter could be hindered by the lack of knowledge on the performance of timber structures under fire scenarios. Recently, with the aim to reduce fire associated risks a proposal to cut down the maximum height of wood-framed buildings from six to four storeys was issued by the UK government [3]. Measures such as the one previously mentioned pose a real threat to the expansion of the use of timber as a building material. To address this issue is important to investigate the performance of timber structures subjected to fire. Here the thermo-mechanical response of STC floors, composed of CLT slabs and steel beams, exposed to fire is investigated. To this end, a one way coupled CFD-FEM approach was used to investigate the complex fire-structure interaction [4].

METHODOLOGY

First, the fire scenario is simulated using the CFD software Fire Dynamic Simulator (FDS) [5]. From these analyses the evolution of the temperature distribution on the SCT slab surface is obtained. These results are then used as input for transient heat transfer analyses in the FEM software ANSYS [6]. The outcome of the latter is the temperature distribution over time on the entire structure. This is then used as input for the transient thermo-mechanical analyses. For all the thermal and mechanical analyses carried out

temperature dependent properties were used. To transfer the information from the CFD software to ANSYS, the Adiabatic Surface Temperature concept proposed by Wickström et al. [7] was employed.

RESULTS

Figure 1 shows the results from the transient heat transfer analysis on the CLT slab. After 30 minutes of fire exposure the temperature on the bottom side of the CLT slab reached 1000 ºC while on the topside it remained close to 20 ºC. Furthermore, on the lower 25 mm of the slab temperatures above 300 ºC were registered. Thus, it is assumed that wood in that region has already burned and become char.

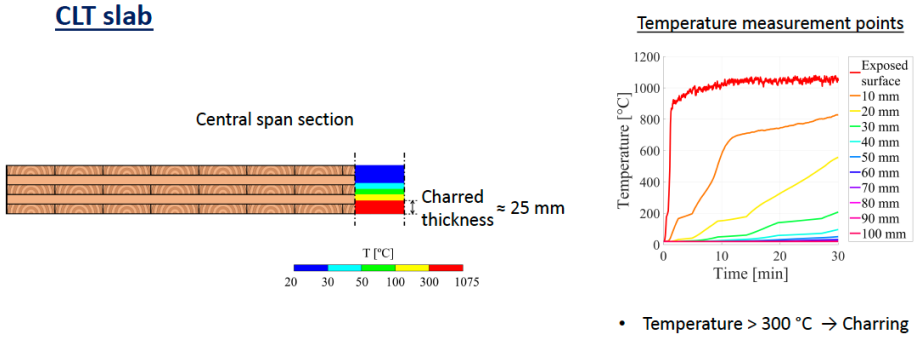

Figure 1: Temperature distribution on the CLT slab after 30 minutes of fire exposure.

The influence of the fire exposure on the structural performance of the SCT structure is presented in Figure 2. Because of charring, the lower 25 mm of the CLT slab cease to contribute to the floor structural performance. This leads to an increase on the stresses measured on the CLT slab. Furthermore, due to temperature induced steel softening large mid span vertical displacements registered. Also, local buckling and damage is observed at the steel beam end supports.

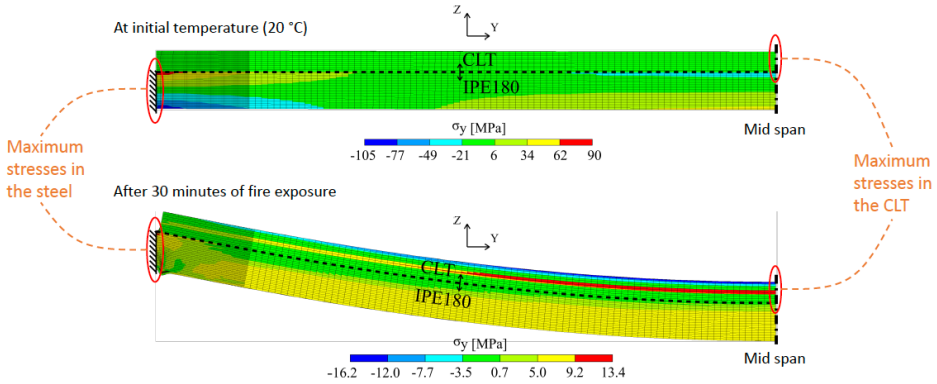

Figure 2: Stress distribution on the SCT floor before and after 30 minutes of fire exposure, side view.

CONCLUSION

A one way coupled CFD-FEM methodology was implemented to study the response of SCT structures exposed to fire. After 30 minutes of fire exposure the CLT slabs presented a 25 mm thick charred layer and compression failure on topside of the slab. The steel beams showed local buckling and fracture in the regions adjacent to the end supports.

REFERENCES

[1] S. Riffat, R. Powell, D. Aydin, Future cities and environmental sustainability, Future Cities and Environment, 2(1):1-23, 2016.

[2] H.R. Lu, A.E. Hanandeh, B.P. Gilbert, A comparative life cycle study of alternative materials for Australian multi-storey apartment building frame constructions: Environmental and economic perspective, Journal of Cleaner Production, 166:458-473, 2017.

[3] R. Moore, Do you want beautiful, sustainable and safe tall buildings? Use wood. The Guardian, 2020. https://www.theguardian.com/commentisfree/2020/jun/06/want-beautiful-sustainable-andsafe-buildings-use-wood, 2020, accessed 10.03.2021.

[4] J. C. G. Silva, A. Landesmann, and F. L. B. Ribeiro. Fire-thermomechanical interface model for performance-based analysis of structures exposed to fire. Fire Safety Journal, 83:66–78, 2016.

[5] K. McGrattan, S. Hostikka, R. McDermott, J. Floyd, C. Weinschenk, and K. Overholt. NIST Special Publication 1019, Sixth Edition. Fire Dynamics Simulator, User's Guide. National Institute of Standards and Technology (NIST), Gaithersburg, Maryland, USA, 2013.

[6] ANSYS. Parametric Design Language Guide. Release 19.0 R1. ANSYS Inc, Canonsburg, PA 15317, USA, 2019.

[7] U. Wickström, D. Duthinh, and K. McGrattan. Adiabatic surface temperature for calculating heat transfer to fire exposed structures. In Proceedings of the 11th International Interflam Conference, London, England, September 3-5, 2007, 2:943-953.

CREEP OF OAK DOWEL: VARIOUS LOADING AND ENVIRONMENTAL CONDITIONS

H. HASNÍKOVÁ[1], J. KUNECKÝ[1], M. HATAJ[2]

[1] Institute of Theoretical and Applied Mechanics, Czech Academy of Sciences, v.v.i., Prosecká 76, Praha 9, Czech Republic

[2] University Centre for Energy Efficient Buildings CTU in Prague, Třinecká 1024. 273 43 Buštěhrad, Czech Republic

ABSTRACT

For research of timber joints, the crucial role in force distribution inside the joint is played by distribution and variability of stiffness of the dowels. Not only the instant stiffness, but the one that we can encounter after some longer period. Also, this value and its statistical distribution is influenced by many other factors, however, humidity and temperature are in timber (oak) dowels of utmost importance. In the work results of a creep experiment made using a special testing rig is presented. It has been found, that biggest changes in creep behavior are in case if very humid conditions are present, and, also, that cycling the temperature in high humidity conditions can produce about 104% of the original instantaneous displacement. The result is not surprising, however, new insights are made thanks to relatively high number of samples and ability to produce some statistics. Another outcome is relation of dowel stiffness in time to the level of applied stress, which is quantified in the article.

KEYWORDS: oak dowel, creep, humidity.

INTRODUCTION

The work is in continual development and actually it is already second article in the SHATIS conference to have the same theme [1]. The authors consider the theme to be relatively interesting, because nonlinearity present in timber joints play a significant role in their mechanical response. If one thinks about the load distribution inside a joint only in linear way (linear stiffness), the results are valid only when small forces act on the dowels. In any statically indeterminate problem (e.g. more dowels in one timber joint) we face the same problem – force distribution. If the creep influence is a question of few percent points, nobody would care. However, if we show creep of dowels can reach more than 100% of the instantaneous displacement, one doubts about force redistribution reliability at all.
Since much information about the testing rig and test configuration can be read in the first article [2], we go more in depth here with just mentioning a few basic stuff about the research.
The whole research was focused on testing of oak dowel from many points of view. The reason was to bring light to design of all-wooden joints, especially the half lap joints, which are loaded very complex way and are sometimes used in historic cultural heritage sites. First, bearing capacity when loaded along the grain [3] has been conducted and statistics was used to evaluate the result. Second, bearing capacity perpendicular to grain and in an angle to grain has been made, including statistics. Third, research has

been conducted on non-linear behavior of oak dowels. This work describes the last mentioned work package, with a short comparison to distribution of oak dowels in linear part of loading along the grain.

METHODS

For testing of nonlinear behavior a special testing machine has been constructed, which allows for testing in different climates using salt solutions and dead weight (load), no energy input is needed and the testing can be really made long-term. The testing rig is shown in Fig. 1 along with the specimen which consists of four dowels loaded in series, allowing for testing of multiple dowels in one experiment.

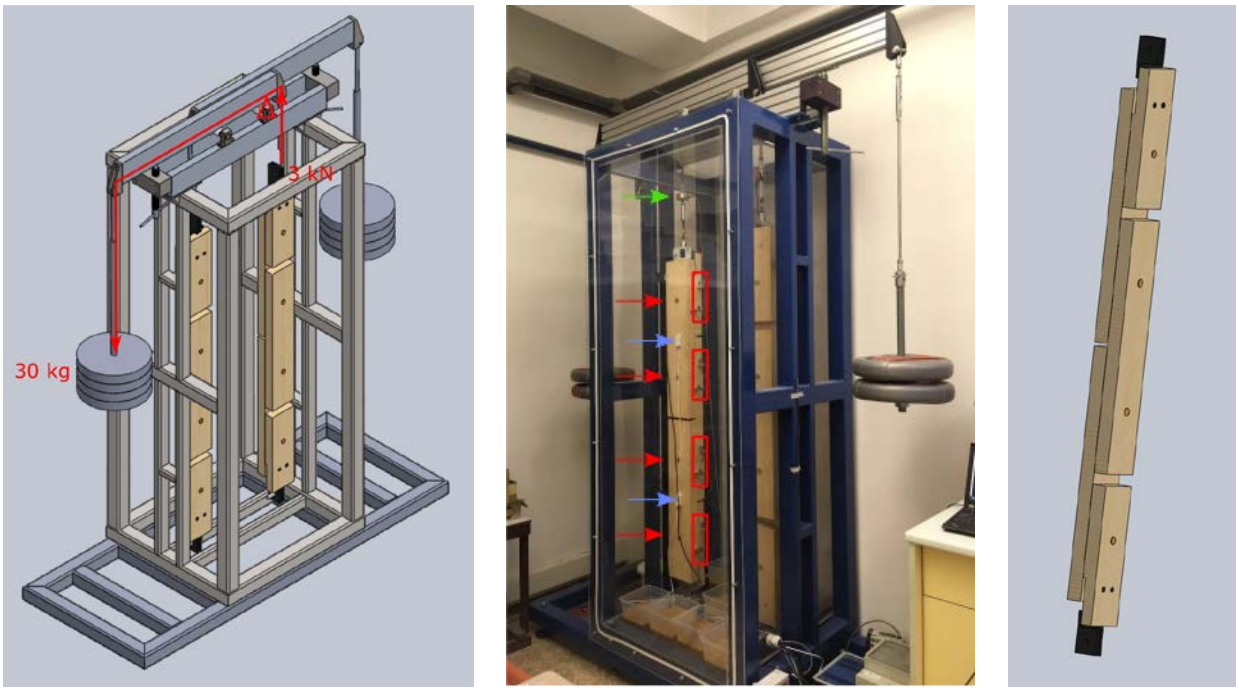

Figure 1: Testing rig and a sample of a chain of samples to test more dowels in series. Please note in the middle the arrows which show points where displacement was measured

Dowels of diameter 24 mm made of English Oak were tested. The members (connected with the dowels and forming the chain) were made of Norway Spruce. During the experiment moisture content of the members was measured using MoistureGuard [4], air humidity and temperature inside the climate chamber were recorded using standard lab thermo-hygrometer by Comet [5]. All the members in which the dowels are inserted, are oriented along the grain. Few solutions of different salts were used to simulate the right conditions. The environment state was monitored for the whole time of the testing by two independent devices. A was the first one; can be found in Figure 2 marked by a violet arrow. An innovative system for continuous monitoring of moisture and humidity Moisture Guard [8] was used as a major source of the data. The dead load applied using gym weight of 30 and 15 kg. Along with other weights of the machine parts it yielded 3.3 kN and 1.9 kN respectively, the values were recorded using a force cell inserted into the chain. For more details, please look into [1].

In this article we will focus on determination of role of load applied to the chain, since it looks from the results as the very crucial influence. Nevertheless, it should be noted that other important quantities are dowel diameter, moisture content of the dowel, humidity, temperature and history of them along with dowel and member's density. Because such a complexity is limiting any reasonable outcome of the article, we decided to include to the research only the experiments, which differ significantly only in one quantity. The dowels chosen for this paper have properties shown in Tab. 1. Both groups, A and B, have nearly similar properties. Testing temperature was moving around the point 21 ° C.

Table 1: Dowel series used in the comparison

Group	Subgroup number	Load applied [kN]	# of samples	Mean dowel density [kg.m^{-3}]	Mean moisture content [% abs.]	Mean relative humidity [%]
A	3	1,9	8	740	13,7	75
	4	1,9	8	746	14,1	75
	13	1,9	8	721	14,7	81
Mean				***735***	***14,2***	***77***
B	6	3,3	8	729	15,0	79
	7	3,3	8	742	15,5	80
	9	3,3	8	776	17,0	80
Mean				***754***	***15,8***	***79***

RESULTS

Because creep is a never ending process, we chose first 600 hours to be the most important period. This is expressed in the results as u_{creep}. Instantaneous displacement u_{inst} was read using automatic processing, it was the first value after the biggest change (application of load took place in one data point). The instantaneous stiffness is computed as $k_{inst}=F_{applied}/u_{inst}$. The results are summarized in Tab. 2.

Table 2: Results of the creep loading of dowels in absolute numbers

Group	Subgroup number	Load applied [kN]	# of samples	u_{inst} [mm]	k_{inst} [kN/mm]	u_{creep} [mm]	U_{creep}/u_{inst} [%]
A	3	3,3	8	0,79	4,18	0,81	103
	4	3,3	8	0,44	7,52	0,54	124
	13	3,3	8	0,82	4,04	0,77	94
Mean				***0,68***	***5,25***	***0,71***	***104***
B	6	1,9	8	0,40	4,73	0,32	80
	7	1,9	8	0,36	5,34	0,46	130
	9	1,9	8	0,28	6,71	0,21	75
Mean				***0,35***	***5,60***	***0,33***	***96***

It can be concluded, that the initial stiffness in group A and B is nearly the same in average. Another interesting output can be the relative important amount of creep reaching 104% of the instantaneous displacement. What is interesting is the comparison of k_{inst}, which shows nearly the same behavior in both groups. Nevertheless, it should be compared and explained in context of stiffness distribution taken from [3], because such a stiffness was measured from the slope when tested and reaches mean values of 1,7 kN/mm. Such a high value what we obtained here (around 5,5 kN/mm) lies somewhere by the quantile values. When comparing u_{creep} of the two groups it is visible that in group A it is highly nonlinear and that the creep stiffness is a function of applied load, thus being not usable in a linear computation.

DISCUSSION

Of course, the data are not robust enough, the subgroup 4 behaves very differently than the others, and if we exclude it, we get even bigger difference, in such a relatively modest loading (3 kN represents the design value), which can be met in the construction. If it is so, we are not any more in some theoretical area when considering creep as an important player in load distribution in a joint.

GROUP A **GROUP B**

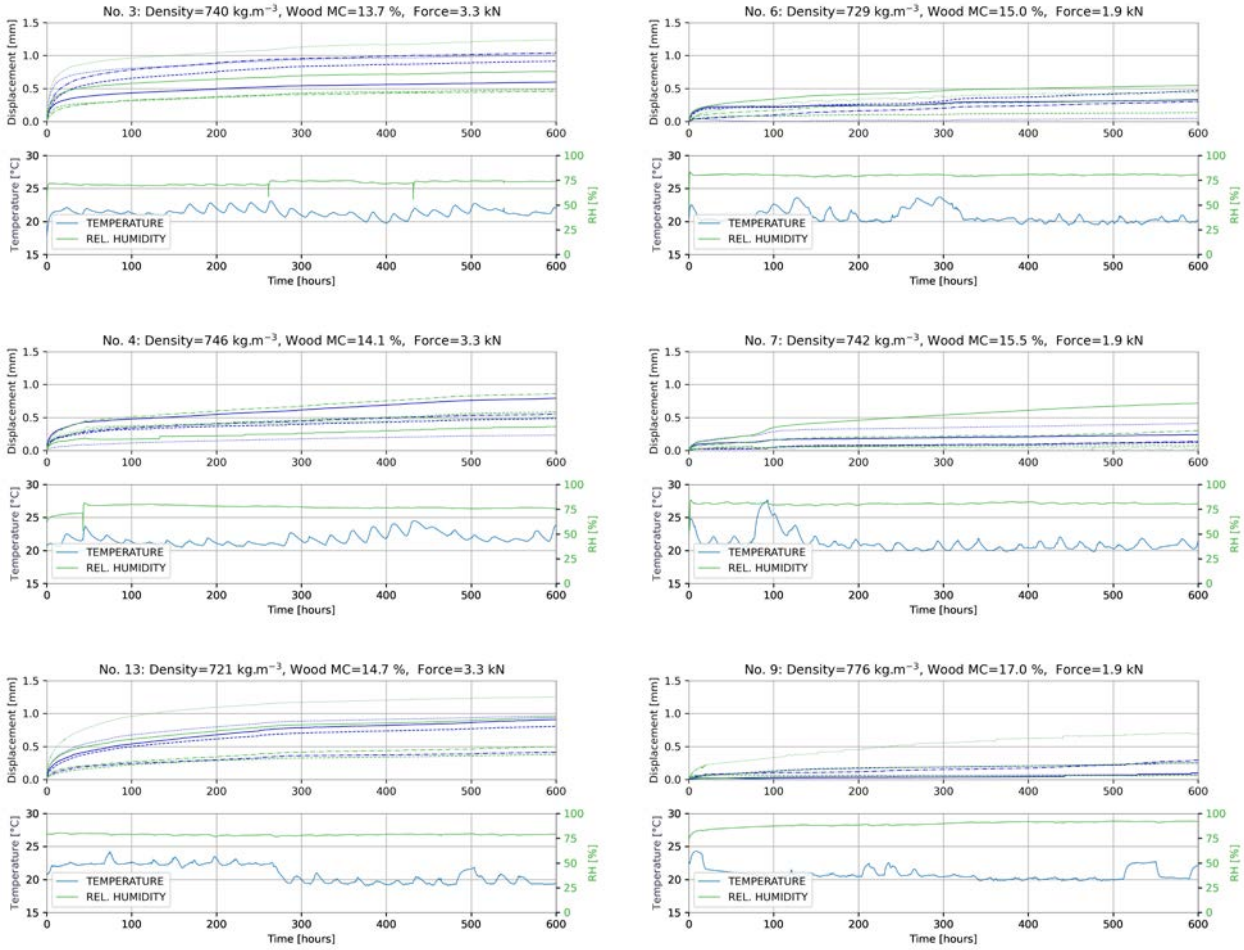

Figure 2: Creep part (without initial displacement) of dowels from both groups

Another problem is of course relative sensitivity to changes in temperature, which can be seen in Fig. 3. Such an influence will be present much stronger in e.g. roof structures, where temperature change is not only in ten degrees as shown in the picture.

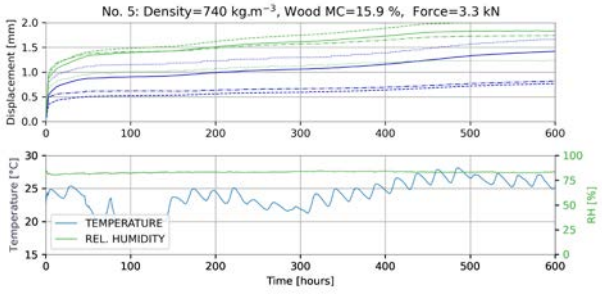

Figure 3: Temperature influence in secondary creep

CONCLUSION

Paper shows a comparison of two groups of oak dowels when loaded using different magnitude of force. It is shown, that the behavior in elastic linear instantaneous part is similar, however, in creep they differ and if we filter a bit the results, the creep differs relatively importantly.

ACKNOWLEDGEMENT

The research was financially supported by the Technology Agency of the Czech Republic – ZETA Programme, project *TJ01000412 Oak fastener in timber structures: materials for normative anchorage*.

REFERENCES

[1] Hasníková, H., Kunecký, J., Hataj, M., Milch, J., Kloiber, M. Creep of moisturized oak dowels under tensile loading. Proceedings of the International conference on structural health assessment of timber structures, SHATiS'2019. Guimarães: Universidade do Minho, 2019 - (Branco, J.; Poletti, E.; Sousa, H.), s. 428-436. ISBN 978-989-54496-2-0.

[2] Hataj, M., Tyrová, M., Hasníková, H., Kunecký, J., Milch, J., Suchomelová, P. Experimental and numerical investigation of oak dowel. Proceedings of the International conference on structural health assessment of timber structures, SHATiS'2019. Guimarães: Universidade do Minho, 2019 - (Branco, J.; Poletti, E.; Sousa, H.), s. 418-427. ISBN 978-989-54496-2-0.

[3] Hasníková, Hana - Kunecký, Jiří - Hataj, M. - Tyrová, M. - Milch, J. - Suchomelová, P. Oak fastener in timber structures: materials for normative anchorage. Praha: Technologická agentura ČR, 2019. 54 s.

[4] Moisture Guard System, Online. https://www.moistureguard.cz. Accessed 20.6.2022.

[5] Comet Data Loggers, Online. https://www.cometsystem.com/products/data-loggers, Accessed 20.6.2022.

Experimental study on fire resistance of damaged beam-column mortise-tenon joints

Zhang Yu[1], Song Xiaobin[1]

[1] Department of Structure Engineering, Tongji University

ABSTRACT

In order to study fire resistance of damaged beam-column mortise-tenon joints, six mortise-tenon joints were made, including three undamaged joints and three joints with different damage forms. One of the undamaged joints was loaded at ambient temperature to obtain the ultimate bearing capacity, and the remaining five joints were subjected to the ISO 834 standard fire condition under 30% load level. The influence of damage on fire resistance of mortise-tenon joints were analysed. The bearing capacity test at ambient temperature showed that, when the load arrived 13.66kN, the load-displacement curve dropped suddenly due to cracking at the tenon where the cross-section varied. The fire resistance tests showed that, the displacement of the beam end of the undamaged mortise-tenon joints increased suddenly at about 54 min, but the load still can be carried by the shallower part of the tenon after cracking at the tenon. Compared with the undamaged mortise-tenon joints, the displacement of beam end of joints with wood decay or crack increased more quickly in fire. However, the influence of looseness was less obvious. In addition, as the displacement increased, gaps in the joints increased, and the influence of gap increase on heat transfer cannot be ignored.

KEYWORDS: mortise-tenon joint, damage, bearing capacity, fire resistance.

INTRODUCTION

Fire is one of the most frequently encountered disaster to buildings. The safety of timber structures in fire is a problem that must be faced. Different from concrete or steel, wood is combustible. High temperature can not only degrade the mechanical properties of wood, but also can ignite wood, which aggravates the persistence and spread of fire. Compared with beam and column members, the cross-section of wood components in mortise-tenon joints are smaller and the joints may more easily lose bearing capacity in fire. It is necessary to study fire resistance of mortise-tenon joints.

Scholars at home and abroad have done a lot of work on fire resistance of commonly used joints of modern timber structures, such as wood-wood-wood (WWW) nailed connection joints[1], WWW bolted connection joints[2], wood-steel-wood (WSW) bolted connection joints[3]and so on. However, studies on the fire performance of mortise-tenon joints are very limited. Zhang et al.[4] carried out fire tests on dovetail mortise-tenon joints and post-beam timber frames with dovetail joints. Chen et al.[5] compared fire resistance of one-way straight and through mortise-tenon timber joints. Ancient timber structures usually have been in service for a long time, and it is common that different forms of damage occurred in mortise-tenon joints. However, there has been yet no relevant study on fire resistance of damaged mortise-tenon joints.

In view of this context, this paper reports the results of fire resistance tests of mortise-tenon joints with different damage forms, to provide technical reference for fire design and fire performance enhancement of traditional Chinese timber structures.

EXPERIMENTAL PROGRAM AND PARAMETERS

Specimen Design

According to the regulations of mortise-tenon joints in Ma's *Chinese Ancient Building Timber Construction Technology*[6], six full-scale mortise-tenon joints were designed and manufactured, among three undamaged specimens and three damaged specimens (looseness, crack and decay). Except for the cross-section dimensions of members, the length of the beam and column is designed to fit the size of the horizontal fire test furnace. The geometric dimensions of the undamaged tenon-mortise joint are shown in Figure 1. The length of the column is 1900mm and the diameter is 260mm. The length of beam is 700mm and the cross-section dimension is 210mm×260mm.The differences between damaged and undamaged specimens are mainly in the tenons, and the other geometry is the same.

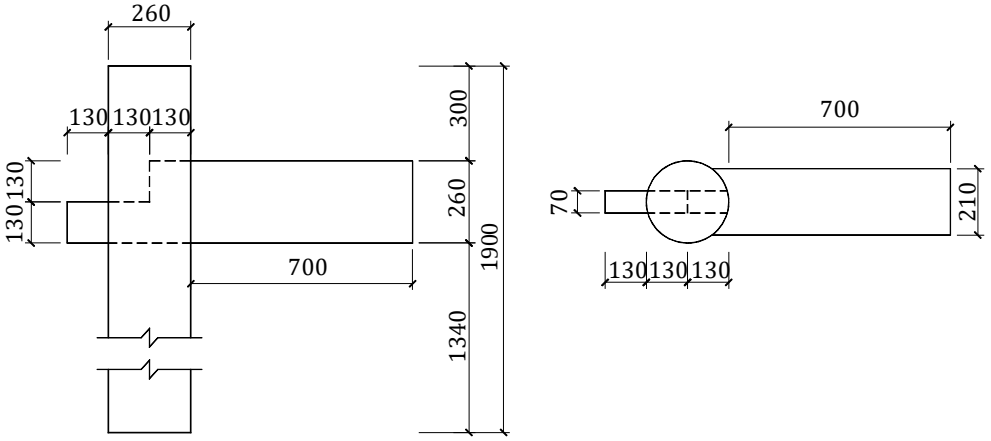

Figure 1: Geometry of undamaged specimens

One undamaged specimen was loaded at ambient temperature to obtain the ultimate bearing capacity. The remaining five joints were subjected to the ISO 834 standard fire condition under 30% load level. In the fire test of SH-1, the nail tied with the wire of displacement meter was pulled out from the beam member. The SH-1 specimen was redone. The number of specimens is shown in Table 1.

Table 1: Statistics of specimen

Number	The form of damage	Fire condition	Load level	Experiment type
SW-1	undamaged	ambient	-	bearing capacity test
SH-1	undamaged	ISO 834	30%	fire resistance test
SH-1-1	undamaged	ISO 834	30%	fire resistance test
SH-2	looseness	ISO 834	30%	fire resistance test
SH-3	decay	ISO 834	30%	fire resistance test
SH-4	crack	ISO 834	30%	fire resistance test

Note: the load level is the ratio of the applied load to the ultimate load of SW-1.

SH-2 specimen simulates the looseness of mortise-tenon joint by reducing the height of the tenon. According to the investigation of He[7], the height being reduced was taken as 10mm. Referring to experiment conducted by Xie et al.[8], the decay of wood is simulated by drilling holes on the surface of wood. For specimen SH-3, the diameter of the hole is 5mm, and the depth and spacing is 10mm and 8mm, respectively. In specimen SH-3, there is a crack at the tenon where the cross-section varied. The widest part of the crack is about 3mm and the length is about 75mm. Photos of specimens see Figure 2.

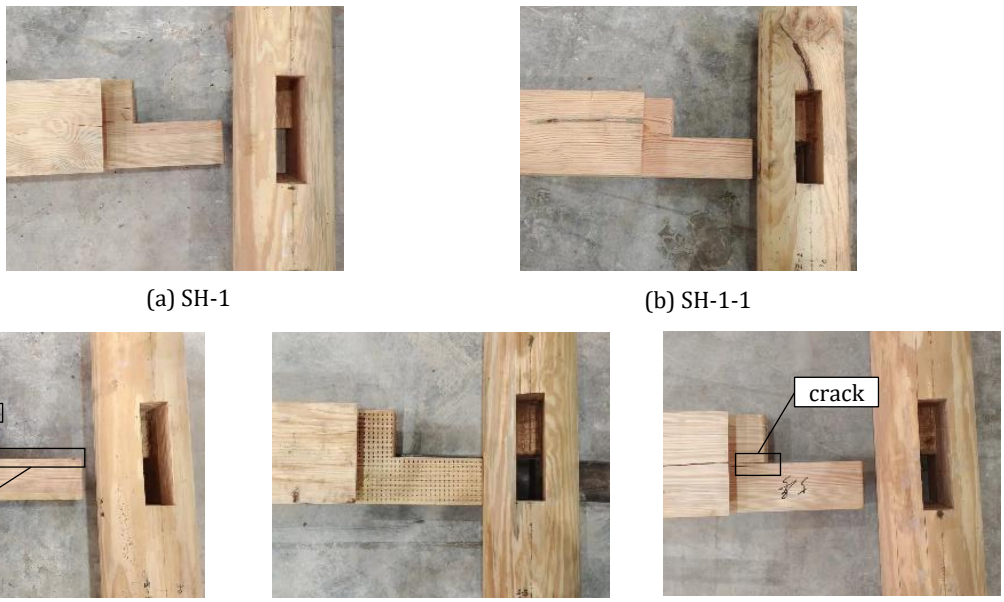

(a) SH-1 (b) SH-1-1

(c) SH-2 (d) SH-2 (e) SH-2

Figure 2: Photos of undamaged specimens

Material Properties

The mortise-tenon joints were all made of Southern pine, which is commonly used in traditional timber structures. According to the relevant test standards, the mechanical properties of wood were measured. The measured density and moisture content is 517.6 kg/m3 and 18.8%, respectively. The measured compressive strength and modulus of elasticity parallel to grain are 32.62MPa and 10740MPa, respectively. The measured flexural strength and modulus of elasticity are 101.51MPa and 11991MPa, respectively.

Experimental Setup

The bearing capacity test was conducted in the timber structure laboratory, Tongji University. Referring to the existing joint loading programme[9], the column member was placed horizontally and the beam member was placed vertically. The load on the column was taken as 50 kN and kept constant. The beam end was loaded by the electro-hydraulic servo actuator placed horizontally until the joint fails. The test setup is shown in Figure 3.

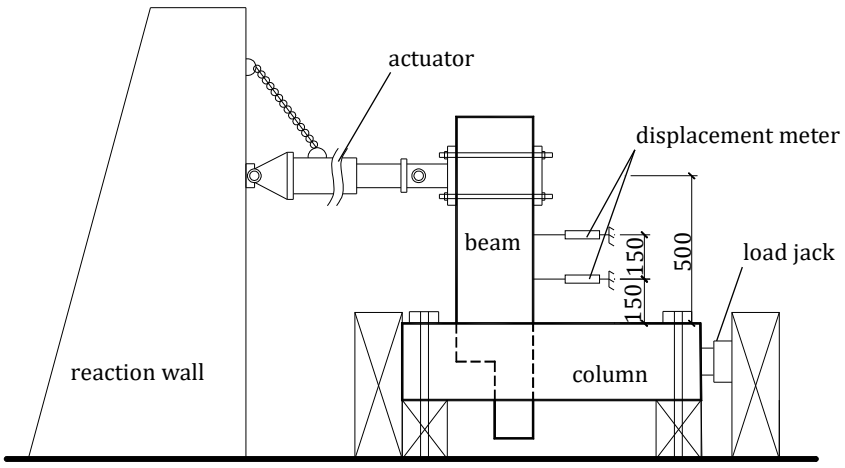

Figure 3: Setup of bearing capacity test

The fire tests were conducted in the horizontal fire test furnace in Shanghai Jianke Technical Assessment of Construction Co., Ltd. The mortise-tenon joints were placed vertically in the furnace, with one column end inserted into the prefabricated concrete base in the bottom of the furnace, and the other end loaded by the load jack. The columns were exposed to fire in four sides, and the beams were exposed to fire in three-sides. Only the connection region was allowed to be exposed to fire, while the other regions were wrapped with fireproof wool. Figure 4 shows the test setup.

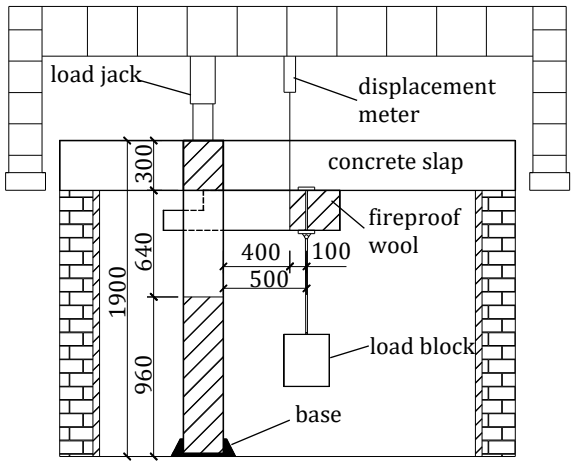

Figure 4: Setup of fire tests

The vertical load on the column was taken as 50kN. Then the load at the beam end was applied by a concrete block, weighting 409 kg. Then the test was started with the furnace temperature increasing according to ISO 834 standard fire curve. During the fire resistance test, the load applied on the columns were kept constant through adjusting oil pump of load jacks. The fire was stopped at the failure of the specimens or the block dropping on the bottom of furnace.

Measurement Arrangement

In the fire tests, the displacement meter was used to record the downward movement of the beam at a distance of 400mm from the column. In order to monitor temperature variations, thermocouples were arranged in timber members at different distance from the surface. The arrangement of thermocouples in beams is shown in Figure 5. The depth and distance from the beam bottom are shown in table 2.

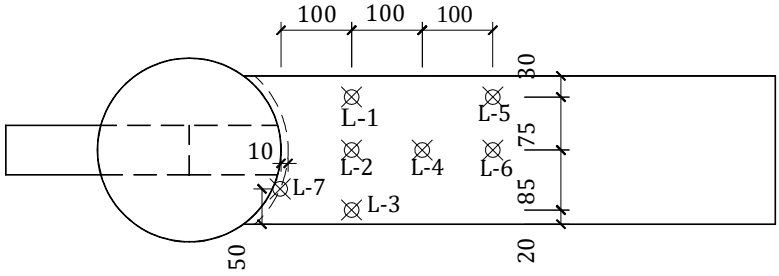

Figure 5: The arrangement of thermocouples

Table 2: The depth of thermocouples

Number	L-1	L-2	L-3	L-4	L-5	L-6	L-7
Drilling depth (mm)	240	200	240	220	230	230	50
Distance from bottom (mm)	20	60	20	40	30	30	-

RESULTS

Bearing Capacity Test

At the initial stage of loading, there was a slight squeezing sound. As the loading continuing, the pull-out amount of the tenon increased continuously. When approaching the failure load, the joint made a regular "gege" sound. When loaded to 13.66kN, the joint made a loud noise and the test was terminated. When SW-1 failed, the tenon was pulled put obviously and a full-length crack occurred at the tenon where the cross section varied. The failure morphology is shown in Figure 6.

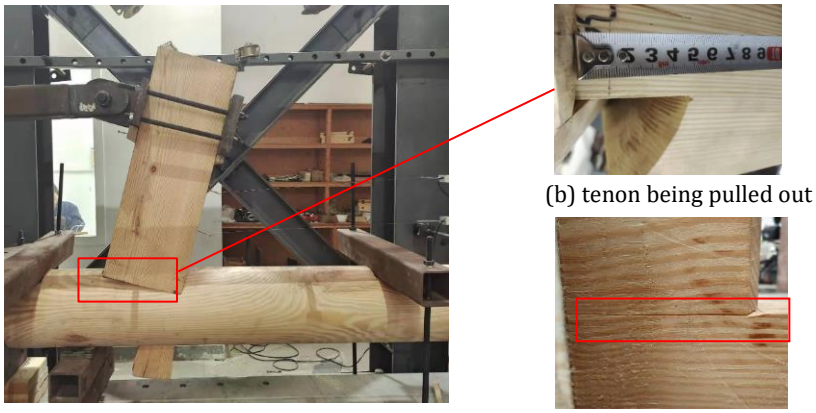

(a) failure of SW-1

(b) tenon being pulled out

(c) crack at the tenon

Figure 6: Failure morphology of SW-1

The moment-rotation curve is shown in Figure 7. Due to the manufacture error, there was a certain gap between the tenon and the mortise. Therefore, the initial stiffness of joint was very low. As the rotation angle increased to about 0.01 rad, the mortise and mortise began to squeeze, and the bending moment increased rapidly with the increase of the rotation angle, which was close to a linear change. As the increase of rotation angle, the increase of bending moment became slower. When the bending moment reaches 8.6kN·m, the bearing capacity decreased suddenly.

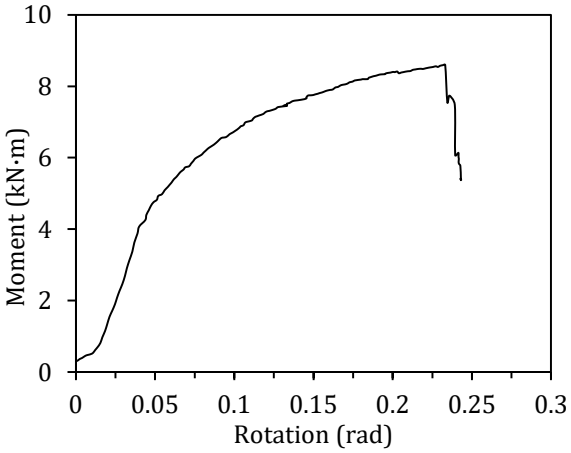

Figure 7: Moment-rotation curve

Fire Resistance Test

During the fire test, some white smoke kept coming out from the furnace, but no flame was found. The downward displacement of beam end increased with the time. When a sudden increase of displacement occurred or the load block dropped on the bottom of the furnace, the test was terminated. Then the burning specimens were extinguished by water and taken away from the furnace. The photos of specimens after fire are shown in Fig 8.

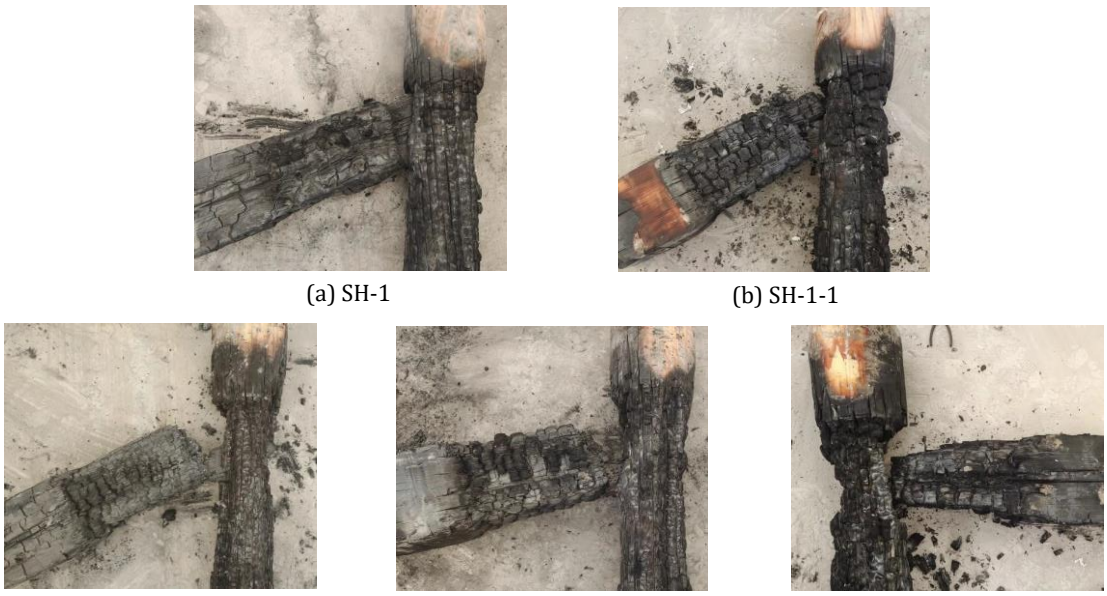

(a) SH-1 (b) SH-1-1

(c) SH-2 (d) SH-3 (e) SH-4

Figure 8: Photos of specimens after fire

It can be seen that both beams and columns suffered serious charring, and all the outside parts of tenons were fully charred. During the fire test, the tenon was pulled out continuously, and the upper parts of tenons were exposed to fire and charred to different degrees. The upper part of tenons of SH-2~SH-4 were fully charred and broke into pieces, while the upper tenons of SH-1 and SH-1-1 were slightly charred.

The displacement-time curve is shown in Figure 9. For specimen SH-1, SH-1-1 and SH-4, the tests stopped due to the sudden increase of displacement. The failure of specimen SH-4 was due to the fracture of tenon at the root, while the sudden increase of displacement of specimen SH-1 and SH-1-1 were due to cracking at the tenon where the cross section varied and the load still can be carried by the shallower part of the tenon. For specimen SH-2 and SH-3, the test was stopped because the load block dropped on the bottom of furnace. When the tests stopped, cracking had occurred at the tenon where the cross-section varied. Compared with the undamaged mortise-tenon joint, the displacement of the beam end of joints with decay or crack in tenon increased more quickly in fire. However, the influence of looseness is less obvious. In addition, as the displacement increased, gaps in the joints increased, and the influence of gap increase on heat transfer cannot be ignored.

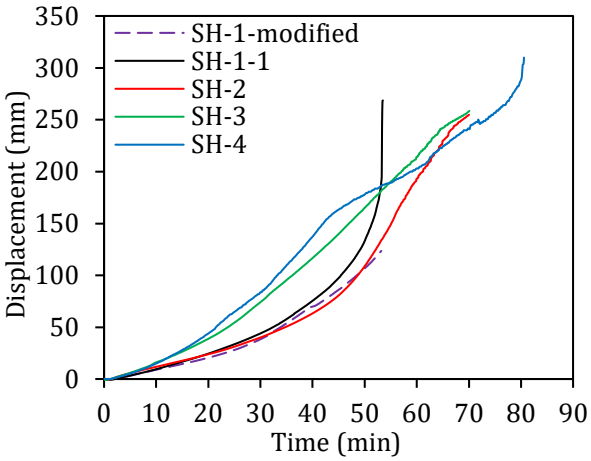

Figure 9: Displacement-time curve

Four cross-sections (C-1, C-2, C-3 and C-4) on the beam and column members were selected to measure the dimensions of residual cross-sections and calculate the charring rate. The locations of measured cross-sections are shown in Fig 10. And the residual cross-sections of SH-1-1 are shown in Fig 11.

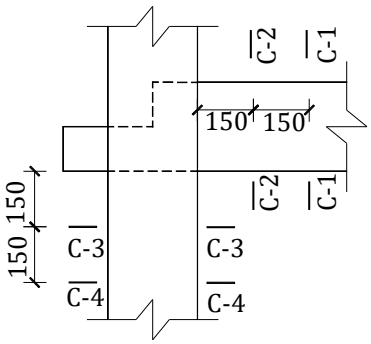

Figure 10: Locations of measured cross-sections

(a) C-1 (b) C-2 (c) C-3 (d) C-4

Figure 11: The residual cross-sections of SH-1-1

The measured dimensions of residual cross-sections are shown in Table 3. β_H and β_W represent the charring rate of beam along the height direction and width direction, respectively. While β_D represents the charring rate of column along the diameter direction.

Table 3: Measured dimensions of residual cross-sections and charring rate

Number	Location	Test time (min)	Initial dimension (mm)		Residual dimension (mm)		Charring rate (mm/min)	
			Height	Width /Diameter	Height	Width /Diameter	β_H	β_W/ β_D
SH-1	Beam	55	260	209	222	139.8	0.69	0.63
	Column		-	259	-	187.5	-	0.65
SH-1-1	Beam	61	258	208	217	129.2	0.67	0.65
	Column		-	260	-	177	-	0.68
SH-2	Beam	77.75	260	212	206	120.3	0.69	0.59
	Column		-	262	-	162.6	-	0.64
SH-3	Beam	70	259	211	212	122.2	0.67	0.63
	Column			259	-	167.7	-	0.65
SH-4	Beam	80.75	262	209	178	103	1.04	0.66
	Column		-	261	-	147.7	-	0.70

The variations of temperature of different specimens are similar. Specimen SH-1is taken as an example to analyse. Figure 12 illustrates the measured temperature of specimen SH-1 in the whole test. After the test started, the temperature of each measuring point increased in varying degrees. It is observed that each measuring point had a temperature lag at 100 ℃, which is caused by the evaporation of water in wood. When the measuring point is at the same distance from the bottom of beam, the closer it is to the side surface, the faster the temperature increases. The temperature of L-1 and L-6 increase more slowly than L-3 and L-5 respectively. When the measuring point is at the same distance from the side surface, the closer it is to the bottom, the faster the temperature increases. On the vertical central axis of the beam section, the temperature increase rate is L-6 > L-4 > L-2. At the same time, it is noted that the

temperature lag of L-1 is longer L-5. This is probably because the wood is not completely dry and the moisture content of the inner parts is larger than the outside, or it may be because some water vapor enters the inner wood after the moisture of the outer wood evaporates.

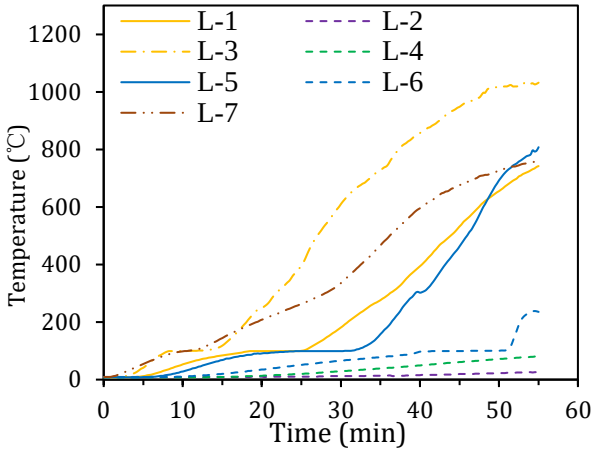

Figure 12: Temperature-time curve

DISSGUSSION

(1) In the bearing capacity test, SW-1 failed with an ultimate rotation of 0.23rad, showing a good deformation ability. Mortise-tenon joint bears the external bending moment by the extrusion of mortise and tenon. The tenon is mainly compressed perpendicularly to the grain, while the mortise is mainly compressed parallel to the grain. The low yield strength and elastic modulus in compression perpendicular to grain may be the main reason for the good deformation ability.

(2) In fire resistance test, the fire resistance limit of SH-4 seemed much longer than SH-1 and SH-1-1. The sudden increase of displacement of specimen SH-4 was due to the fracture of tenon at the root, and specimen SH-4 lost bearing capacity completely. However, for specimen SH-1 and SH-1-1, the load still can be carried by the shallower part of the tenon when the test was terminated. If the test of SH-1 and SH-1-1 was continued, the fire resistance limit and failure mode may be similar to SH-4.

(3) The shape of the residual cross-section is irregular, which may be caused by the defects of wood. However, the residual cross-section of the beam is basically U-shaped, and the residual cross-section of the column is basically circular. And it can be noticed that, the charring rate along the height direction and diameter direction is greater than that along the width direction.

CONCLUSION

(1) The mortise-tenon failed due to cracking at the tenon where the cross-section varied and showed a large failure displacement and good ductility.

(2) The fire resistance limit of undamaged mortise-tenon was about 54min. Compared with the undamaged mortise-tenon joint, the displacement of the beam end of joints with wood decay or crack at the tenon increased more quickly in fire. However, the influence of looseness was less obvious.

(3) Due to the defects of wood, the residual cross-section is irregular. And the charring rate along the height and diameter directions is greater than that along the width direction. As the rotation of beam increased, gaps in the joints increased, and the influence of gap increase on heat transfer cannot be ignored.

(4) Temperature increased with the increase of fire exposure time. The closer the thermocouples to the surface exposed to fire, the higher their temperature was.

REFERENCES

[1] J. Norén, Load‐bearing Capacity of Nailed Joints Exposed to Fire. Fire and Materials 20 (1996) 133-143.
[2] Poliana, Dias, De, Moraes, João, Paulo, C., Rodrigues, Nadia, and Diana, Behavior of bolted timber joints subjected to high temperatures. European Journal of Wood & Wood Products (2012).
[3] L. Peng, G. Hadjisophocleus, J. Mehaffey, and M. Mohammad, Predicting the fire resistance of wood--steel--wood timber connections. Fire technology 47 (2011) 1101--1119.
[4] J. Zhang, Y. Wang, L. Li, and Q. Xu, Thermo-mechanical behaviour of dovetail timber joints under fire exposure. Fire Safety Journal 107 (2019) 75--88.
[5] Chen, L.Z., Wang, X. and Han, C.Q, Experimental study on fire endurance of one-way straight and through mortise-tenon timber joints, Building Structure 51 (2021) 98-102+119.
[6] Ma, B.J, Chinese Ancient Building Timber Construction Technology, Beijing: Science and Technology Press (2003).
[7] He, J.X, Study on mechanical properties of key joints and column frame in traditional timber structure, Doctor of Philosophy Dissertation, Beijing Jiaotong University, China (2019).
[8] Xie, Q.F., Zheng, P.J. and Xiang, W, Experimental study on seismic behavior of damaged straight mortise-tenon joints of ancient timber building, Journal of Building Structures 35 (2014) 143-150.
[9] Wang, M.Q., Song, X.B. and Gu, X.L, Study on rotational behavior of bolted glulam beam-to-column connections with slotted-in steel plates, Journal of Building Structures 35 (2014) 141-150.

EXPERIMENTAL PERFORMANCE OF SCREWS FOR COMPOSITE TIMBER-CONCRETE USING PUSH-OUT TESTS

Sergio J. YANEZ[1], Juan Carlos PINA[1], Eduardo PÉREZ[1], Carlos F. GUZMÁN[1] and Erick I. SAAVEDRA FLORES[1]

[1] *University of Santiago of Chile (USACH), Faculty of Engineering, Civil Engineering Department, Chile*

ABSTRACT

In this paper, a parametric mechanical characterization of typical timber to concrete connections is experimentally performed using push-out tests. To this end, different types of connectors were tested in different arrangements and number, to study the mechanical response at the system interface. Here, the slip force curve is statically obtained for a continuous loading increment until failure. Additionally, recommendations regarding constructive care are provided. The tests used radiata pine wood of dimensions of 5 x 5 inches, G30 concrete and 6 mm lag screws. The number of connectors varied from 1 to 4. Three different arrangements were analysed: (1) screws placed at 90 ° with threads embedded in the timber element; (2) screws placed at 90 ° with 1 cm of threads embedded in the concrete; (3) lag screw at 45°. Group effect and screw inclination was study and a comparison with international standard was performed. The series of specimens with 4 connectors (spacing of 10 cm from each other), did not show a significant variation in resistance, based on linear extrapolation from single screw resistance. Inclined screws showed an increase in resistance and rigidity due to induced tensile stress. Differences up to 150% in the estimation of the slip modulus were found when compared with the formulation of Eurocode 5.

KEYWORDS: Timber-concrete composite, push-out test, stiffness

INTRODUCTION

Composite concrete-wood systems or TCC (Timber Concrete Composite), are complex to analyze due to its highly variable behavior that depends on the connection characteristics. This connection can be described to be fully bonded when estimating service loading conditions. However, slip at the connection interface is almost inevitable. Therefore, estimating the load-slip curve is essential to accurately predict the overall structural performance. Consequently, the importance in the analysis of different connectors is of paramount importance when design composite structures using local materials or when design codes do not cover specific connections features.

Design codes estimate the stiffness resistance of the connection as the relation between the applied load and the slip. However, no specific code exist that considers the composite concrete-timber behavior. Usually, designers have adopted different expressions to obtain this parameter [1]. Therefore, the TCC systems relies on expressions that are not intended to characterize the connection performance in this type of systems. It is even more urgent to establish this parameter as timber and composite timber-concrete building are a sustainable solution for climate emergency regions.

METHODOLOGY

Radiata pine wood with a controlled humidity of 12% - 15% was used to construct the timber element. Structural classification was performed according to the Chilean standard NCh1207 as G1. The concrete slabs used in the experimental tasks was cast in-situ according to NCh1017. The compressive strength of the concrete specimens was G30, typically used in TCC building [2]. The connection between the concrete slab and the timber element was obtained by placing ¼ x 5" screws (see Figure 1). The number of connectors was modified from 1 to 4 connectors, with and without threads in the shear plane. Moreover, one set of samples with 1 connector was modified to test the screws at 45°. The loading protocol consisted of loading up to the 40% of the expected capacity, unloading, and ultimately reaching the ultimate capacity of the system according to EN 26891.

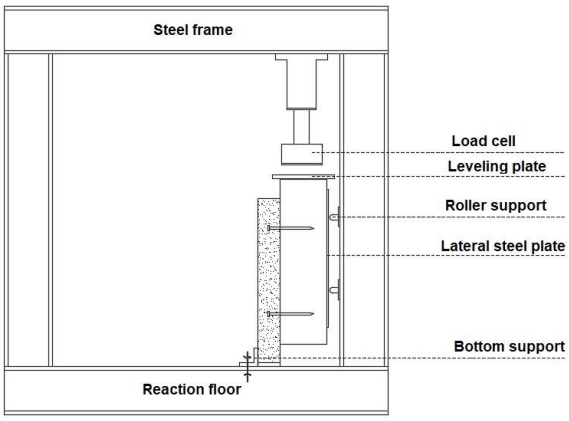

Figure 1: Experimental setup configuration

RESULTS

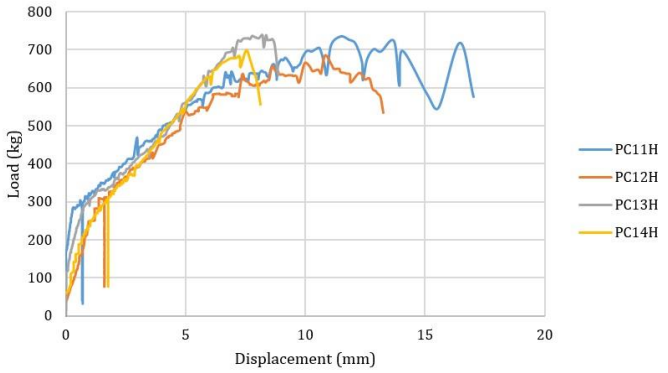

Sample	Ks (kg/mm)	K5 (kg/mm)	K50 (kg/mm)	K40 (kg/mm)
PC11H	375.1	399.5	154.0	367.8
PC12H	155.8	410.2	146.6	197.7
PC13H	251.5	518.4	132.9	251.5
PC14H	152.6	442.6	126.3	156.2

Figure 2: Experimental results and stiffness parameters.

CONCLUSION

The failure mode in most of the cases were wood crushing, followed by shearing of the connector. No evident failure was observed in the concrete slab. Differences up to 150% in the estimation of the slip modulus were found when compared with the Eurocode 5. Slip modulus using the secant method at 50% of the maximum resistance shows to be lower than the calculation according to EN 26891.

REFERENCES

[1] A. Ceccotti, "Composite concrete-timber structures," *Prog. Struct. Eng. Mater.*, vol. 4, no. 3, pp. 264–275, 2002, doi: 10.1002/pse.126.

[2] J. N. Rodrigues, A. M. P. G. Dias, and P. Providência, "Timber-Concrete Composite Bridges: State-of-the-Art Review," *BioResources*, vol. 8, no. 4, Art. no. 4, Nov. 2013.

THE EFFECT OF AN INTERLAYER ON DOWELLED CONNECTIONS IN TIMBER LIGHTWEIGHT CONCRETE COMPOSITE SYSTEMS

Elif APPAVURAVTHER[1], Bram VANDOREN[1], and Jose HENRIQUES[1]

[1] Hasselt University, Belgium

ABSTRACT

The use of lightweight concrete (LWC) with timber structures is an efficient solution for renovation and, with current high strength LWC, it is also an option for new constructions. In this paper, dowelled connections for timber concrete composite systems are experimentally investigated. Often, when renovating an existing building and implementing a composite solution, but also in new constructions, wood based panels are used between the concrete layer and timber beams. In the current literature it is known that the interlayer causes reduction in strength and stiffness. In this work, the effect of an interlayer and the improvement of the connection using an adhesive are experimentally investigated with the use of lightweight concrete. In addition to these two parameters, two different fasteners, screws and ribbed rods, are also considered. This work indicates that, with the use of an adhesive, the negative effect of an interlayer can be mitigated.

KEYWORDS: timber lightweight concrete composites, shear dowel type connections, adhesively bonded connections, effect of interlayer

INTRODUCTION

The use of timber lightweight concrete composites (TLCC) is an increasing trend with various research projects and several examples in the world [1, 2]. Dowelled connections are still the most popular and simple solutions for both renovations and new constructions. Besides renovation of timber buildings, these connections can be easily replaced which will extend the life of the timber joists. For renovation purposes, the use of lightweight concrete is a better solution than using a non-structural mortar screed [3] as it contributes to the structural integrity of the floor while adding a lower weight, which can be often more appropriate for existing structures. The rehabilitation of timber floor with lightweight concrete requires a performant connection that can guarantee an efficient a composite action between these two materials.

The use of dowel connections are the most common solutions for shear connections to mobilize the composite action in timber-concrete composite members. They are the most commonly studied connections due to their optimal strength, stiffness and ductility along with a variety of choices and easy access [4-7]. In addition, in the current EN 1995-1-1, the strength models based on the Johansen/ European yield models leads to a good estimation [8, 9]. In design, the target is to obtain the most optimized solution by using a lower number of screws and obtaining highest strength and stiffness possible. Dowel connections are also a good solution for renovations. In existing structures, there is a floor system, which can serve as a permanent formwork and be referred as an interlayer. However, the interlayer leads to lower mechanical performance due to the gap layer they cause between the concrete

and the timber layer. Even though in numerous experimental work, it has been concluded that the use of an interlayer is significant, in cases such as rehabilitation or wet solutions (casting concrete layer on site), the use of an interlayer cannot be neglected. Use of adhesively bonded connections leads to a much stiffer behaviour and this solution may mitigate the effect of an interlayer [10].
In this paper, the effect of an adhesive and an interlayer on screw and ribbed rod dowelled connections are investigated by means of experimental tests. Throughout the experimental program, lightweight concrete is used. During the design of the specimens EN 1995-1-1 is used [9]. The results show that by introducing an adhesive layer, negative effects of an interlayer can be improved.

MATERIALS AND METHODS

The experimental tests within this work considered symmetrical push-out tests on dowelled connections for TLCC. An overview and dimensions of the specimens with an interlayer are given in Figure 1. For the specimens without an interlayer, the only difference is the embedment length in the concrete is smaller as the size of the interlayer.
Glulam with strength class of GL 24 h and lightweight concrete with a strength class of LC 20/22 is used. Two different types of connectors are used; i) fully threaded Wurth screws [11] and ii) S500 ribbed rods. Both of the dowels have an outer diameter of 8 mm. In all series, the embedment length of the dowel connector in the timber is 110 mm. The embedment length is 50 mm for the series without and interlayer and 32 mm for the series with an interlayer.
Three different parameters are investigated; i) effect of dowel type (screw vs. ribbed rod), ii) effect of the adhesive between the dowel and the timber (epoxy acrylate-based Sika Anchorfix-3030 [12]) and iii) effect of an interlayer (18 mm OSB-3 from Norbord). Test specimens are labelled as dowel type (S – screw or R – rod), existence of adhesive (NG – no adhesive or G – adhesive is present) and existence of an interlayer (NI – no interlayer or I – interlayer is present). Test specimen properties are presented in Table 1. The test specimens are designed by provisions given in EN 1995-1-1 [9].

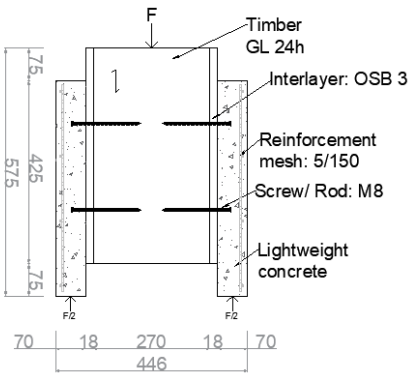

Figure 1: Test specimen with all members and dimensions

Table 1 Test specimen properties

Experiment ID	Concrete type & strength	Concrete thickness	Dowel type	Embedment length	Glue	Interlayer
S-NG-NI	LC 20/22	70 mm	Screw	110 mm	No	-
S-NG-I						-
S-G-I						Yes
R-G-NI			Rod		Yes	-
R-G-I						Yes

RESULTS

Each series had five replicas. In Figure 2 the average force slip curve for each series is presented. F_1 is a load level where initial failure occurred which is identified as the stiffness degradation in the force slip curve. At this load level, yielding of the dowel by formation of a plastic hinge occurred. After this load level, F_1, plastic hinge occurred, leading to a significant deformation with small increase of strength. After this load level, only shear loading is no longer represented. In series S-NG-NI and S-NG-I, a second stiffness degradation is observed due to the strain hardening of the screw. After this load, the maximum load capacity, Fmax, is reached by all specimens as the pull-out strength in the concrete is reached.

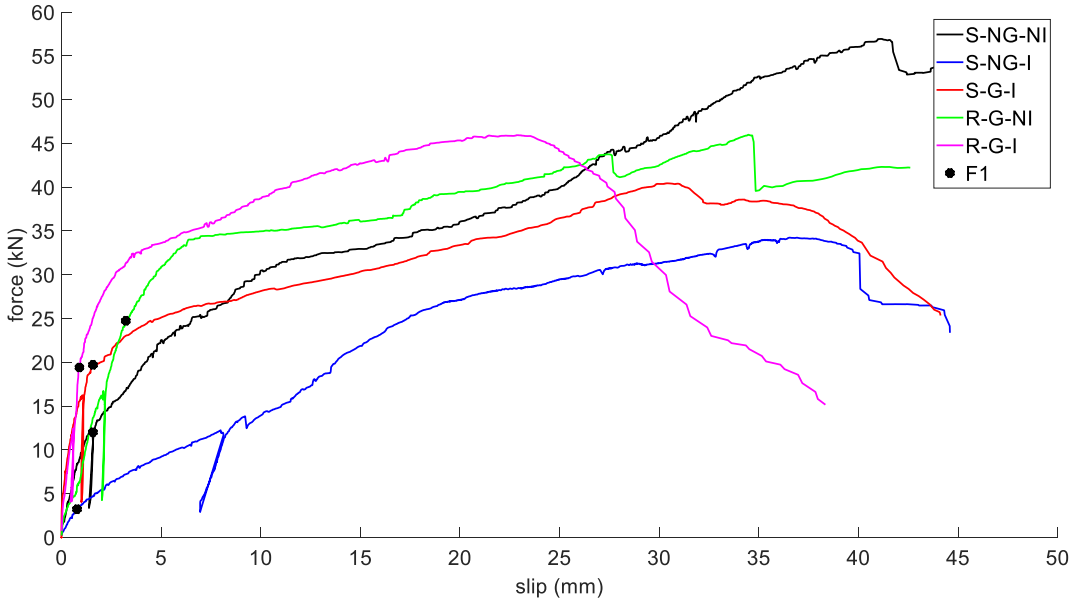

Figure 2 Average force-slip curve of all series

The mean results from the shear tests are presented in Table 2. Two different load levels are identified and the patterns were very similar for all five series. At initial damage, reduction in the stiffness is caused due to the plastic hinge formation of the connector. At the maximum load capacity, F_{max}, failure occurs due to the connector reaching its withdrawal strength in the concrete. Stiffness, K_{ser}, is calculated using EN 26891 [13]. The ultimate slip, v_u, is the slip corresponding to the 80% of F_{max} after the F_{max}. From *Table 2*, following observations can be made;

- The stiffest and the strongest series is R-G-NI.

- The use of an adhesive layer had a positive impact in the initial failure load, F_1 and stiffness, K_{ser}.
- The negative effect of an interlayer on load capacity and stiffness are removed by introducing an adhesive layer (S-NG-I vs S-G-I)
- Same initial damage and failure mode is observed.
- There is a similarity between the maximum load carrying capacity in all series (37 – 49 kN)
- There is a same order between the ultimate slip in all series (32 – 39 mm)

Table 2: Test results

Specimen ID	F_1 (kN)	F_{max} (kN)	K_{ser} (kN/mm)	v_u (mm)	Initial damage mode (F_1)	Failure mode (F_{max})
S-NG-NI	11.24	42.87	8.52	37.42	Plastic hinge formation	Withdrawal strength at the concrete is reached
S-NG-I	3.19	37.08	1.59	39.53		
S-G-I	17.14	40.46	15.13	38.60		
R-G-NI	22.14	49.48	11.86	39.02		
R-G-I	19.07	42.69	15.55	32.54		

EFFECT OF TESTING VARIABLES ON MECHANICAL PROPERTIES

In this experimental campaign, three different parameters are investigated. The effect on strength, stiffness and ultimate slip are hereafter discussed.

i) Effect of the dowel type (screw vs. ribbed rod) – series S-G-I and R-G-I are compared. In both connectors, an outer diameter of 8 mm is used, however, the inner diameter and the tensile strength of the connector varied. Changing the connector from screw to rod lead to an increase of 11% and 5% in F_1 and F_{max}, respectively. In terms of stiffness however, only an increase of 3% is observed. As the adhesive layer caused a stiff connector between the dowel and the timber, such behaviour in the elastic range is expected. There was a 15% reduction in the ultimate slip, which reflects the post-elastic behaviour difference between the two connectors (F_1 vs F_{max}).

ii) Effect of the adhesive between the dowel and the timber – series S-NG-I and S-G-I are compared. By introducing an adhesive layer for the series with the use of screws and an interlayer, a 438% increase in F_1 and 9% increase in F_{max} is recorded. The quadruple increase in the initial damage load is expected as the adhesive reinforced the screw, timber and the interlayer to work as a single connection. The consistency in the F_{max} is also expected as in both cases the maximum load capacity is by the pull-out strength at the concrete layer. In both series, the mechanical properties were the same (embedment length of the screws in the concrete and the concrete strength). The stiffness was increased by an 850% with the introduction of an adhesive, due to the stiff layer. In term of ultimate slip, only 2% reduction is recorded.

iii) Effect of an interlayer – in this comparison, two separate comparisons are made for the screw connectors (S-NG-NI vs S-NG-I) and rod connectors (R-G-NI vs R-G-I).

   a. For screw connectors, introducing an interlayer (without an adhesive) lead to a decrease of 71% and 17% in the $F1$ and F_{max}. In terms of stiffness, 81% reduction is observed. As

the interlayer acts as a gap layer, this is an expected behaviour and in agreement with the literature [14]. In terms of ultimate slip, a 5% increase is observed which can be neglected.

b. For rod connectors, introduction of an interlayer lead to a reduction of 14% in F_1 and F_{max}. Even though there was an adhesive layer which connected the rod connection to the interlayer, such decrease is acceptable since the interlayer changes the force transfer mechanism. In the stiffness, an increase of 31% is recorded, this proves that the adhesive stiffens the connection significantly. A 16% decrease is observed in ultimate slip. The maximum load capacity is reached by the pull-out strength of the concrete, which was smaller for the series with an interlayer (as the embedment length is smaller) therefore the ultimate slip is affected from this.

CONCLUSION

In this paper, dowelled connections within TLCC with the effect of an interlayer, adhesive and fastener type are experimentally investigated. Lightweight concrete is used throughout the entire experimental program as the target of these connections is for renovation reasons. In this experimental campaign, glulam is used for the timber layer due to its easy access.

Introducing an interlayer caused significant reduction in stiffness and in load capacity. Introducing an adhesive layer between the screw and the interlayer compensates the negative effect/impact of an interlayer. With this solution, renovation of existing timber buildings will be possible without a high loss in strength and stiffness capacity of the dowel connectors.

The use of an adhesive has a positive impact on the strength and the stiffness. Even though an adhesive increases execution sensitivity of the connector and the cost of the execution, for special projects, it may be considered.

The use of a rod rather than a screw (in specimens with adhesive and an interlayer) lead to a slightly better strength and stiffness, however, the ultimate slip is limited.

The results in this paper gives a good indication of dowel connections that can be used for renovation purposes. Nevertheless, further research is still necessary to evaluate the impact of used/old timber on the mechanical performance of the investigated connections.

REFERENCES

[1] ARUP. (2019) Rethinking Timber Buildings.

[2] E. Appavuravther, B. Vandoren, and J. Henriques, "Behaviour of screw connections in timber-concrete composites using low strength lightweight concrete," *Construction and Building Materials,* vol. 283, 2021.

[3] S. Carvalho, T. Panzera, A. Christoforo, J. Fiorelli, F. Lahr, and R. Freire, "Epoxy mortar timber beam upgrading," *International Wood Products Journal,* 2017.

[4] M. Van der Linden, "Timber-Concrete Composite Floor Systems," PhD Dissertation, Technical University of Delft, Delft, The Netherlands, 1999.

[5] A. Dias, "Mechanical behaviour of timber-concrete joints," PhD, TU Delft, Delft, Netherlands, 2005.

[6] L. Jorge, "Timber-concrete structures using lightweight aggregate concrete / Estruturas mistas madeira-betão com a utilização de betões de agregados leves [In Portuguese] " Ph. D., University of Coimbra, Coimbra, Portugal, 2005.

[7] COST, *Design of timber-concrete composite structures - A state-of-the-art report by COST Action FP1402 / WG 4*. Shaker Verlag Aachen, 2018.

[8] K. Johansen, "Theory of timber connections," *International association of bridge and structural engineering,* vol. 9, pp. 249-262, 1949.

[9] *EN 1995-1-1 - Design of timber structures - Part 1-1: General rules and rules for buildings,* E. C. f. Standardization, 2004.
[10] G. Tlustochowicz, E. Serrano, and R. Steiger, "State-of-the-art review on timber connections with glued-in steel rods," *Materials and Structures,* 2011.
[11] ETA-13/0029, "Self-tapping screws for use in wood-concrete slab kits," ed. ETA-Denmark A/S, 2017.
[12] Sika, "Product Data Sheet Sika Anchorfix - 3030," ed: Sika.
[13] *EN 26891 - Timber Structures - Joints Made with Mechanical Fasteners - General Principles for the Determination of Strength and Deformation Characteristics*, 1991.
[14] L. Jorge, S. Lopes, and H. Cruz, "Interlayer Influence on Timber-LWAC Composite Structures with Screw Connections," (in English), *Journal of Structural Engineering-Asce,* Article vol. 137, no. 5, pp. 618-624, MAY 2011 2011.

Experimental study on seismic performance of partially damaged masonry-timber mixed structures

Xiaobin Song[1], Xingjie Chen[1]

[1] Department of Structural Engineering, Tongji University, Shanghai 200092, China

ABSTRACT

In Shanghai, there are a large number of masonry-timber mixed structures that have been in service for nearly 100 years and carry various forms of damages due to natural and human induced hazards. Investigation shows there is difference between the impact of the different forms of damage on the seismic performance of the masonry-timber mixed structures. In order to explore such impact, six full-scale timber frame walls with brick masonry infilled were made, including two walls with no damage, two walls with column foot decay, one wall with dry shrinkage in mortise-tenon beam-column joints and one wall with horizontal crack in the masonry infill. Through reversed cyclic loading tests, the failure characteristics, load-displacement hysteretic curves and skeleton curves of the wall specimens were analysed. The test results show that the main failure mode of brick filled timber frame walls is diagonal crashing of infilled wall and compression failure of the mortise-tenon joints. The hysteretic curves show obvious pinching effect. More specifically, the decay of column foot has little effect on the seismic performance of the wall; the shrinkage of joints reduces the initial stiffness of the wall, and the horizontal crack in the masonry leads to premature separation of the masonry and affects the stiffness and peak load of the wall.

KEYWORDS: brick masonry infilled walls, seismic performance, different damages

1 Introduction

Masonry-timber mixed structure is one of the main forms of traditional building structures in China, among which wood frame with bricks infill is commonly used as lateral load carrying components. The timber beams and columns are the primary framing members, and the masonry infill wall is mostly used for thermal insulation and separation (Figure 1). According to earthquake disaster surveys, masonry-timber mixed structure is prone to be damaged under earthquake actions, however, structural collapse is rare [1][2], which implies good seismic performance. The good seismic performance mainly lies in the composite action between the timber frame and the masonry infill wall. The timber frame resists horizontal load and absorbs seismic energy through plastic deformation and friction of mortise-tenon joints and floating column feet [3]. The masonry infill wall, on the other hand, can add to the lateral stiffness and bearing capacity of the timber frame.

Some scholars have carried out research on the seismic performance of this kind of structures. Xu et al.[4] compared low cyclic reversed seismic performance of typical mortise-tenon jointed wood frames with and without brick masonry infill. The test results showed that the infilled mortise-tenon joint wood frame had higher lateral load carrying capacity and better stiffness and energy dissipation capacity. Qu et al. [5] also carried out in-plane quasi-static loading tests on six full-scale Chuan-dou timber frames infilled with masonry walls. The test results showed that the masonry infills provided the most lateral

resistance of the frames, whereas the timber frames maintained the integrity of the wall frames under large lateral drifts.

Figure 1: Masonry-timber mixed structure

In Shanghai, there are a number of masonry-timber mixed structures that have been in service for more than less than 100 years. Under natural and human induced hazards, these structures show different kinds of damage, such as column foot decay, dry shrinkage in mortise-tenon beam-column joints and horizontal crack in the masonry infill (Figure 2). These damage can affect the seismic performance of the entire structures. Therefore, it is necessary to quantify the impact of different damage on the seismic performance of the mixed structures. This paper presents the results on six full-scale timber framed walls with brick masonry infill to explore the influence of different damage on seismic performance of masonry-timber mixed structures through reversed cyclic loading tests.

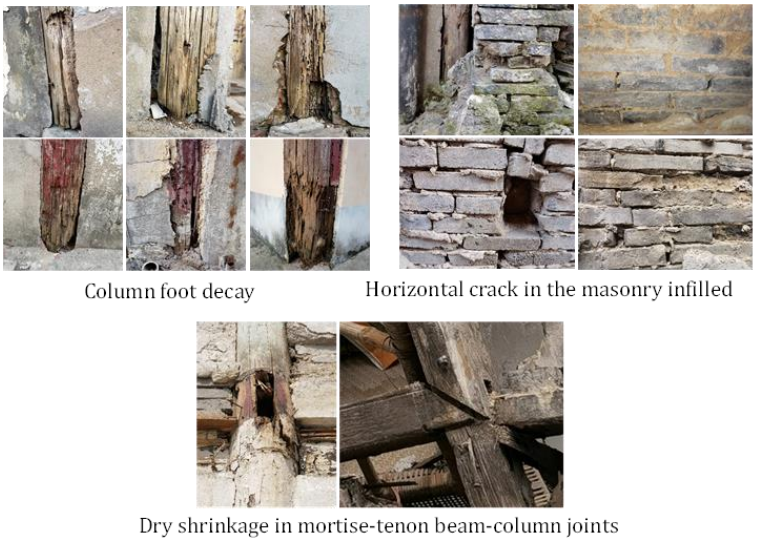

Figure 2: Different kinds of damage of masonry-timber mixed structures

2 Experimental programe

2.1 Specimens

As is shown in Table 1 and Figure 3, six full-scale timber frame walls with brick masonry infill were made, including two walls with no damage (F1a&F1b), two walls with column foot decay (F2a&F2b), one wall with dry shrinkage in mortise-tenon beam-column joints (F3) and one wall with horizontal crack in the masonry infill (F4). All specimens had the same height of H = 2500 mm and the same wide of L=1950mm. The diameter of the timber columns is 200 mm, and the section size of the rectangular timber beam is 120 (width) ×200 mm^2. The columns and the beams were connected through straight

tenon joints (Figure 4), with tenon of 60 mm in width, 200 mm in height and 100 mm in length. The columns rest freely on independent stone base, known as the floating support (Figure 4).

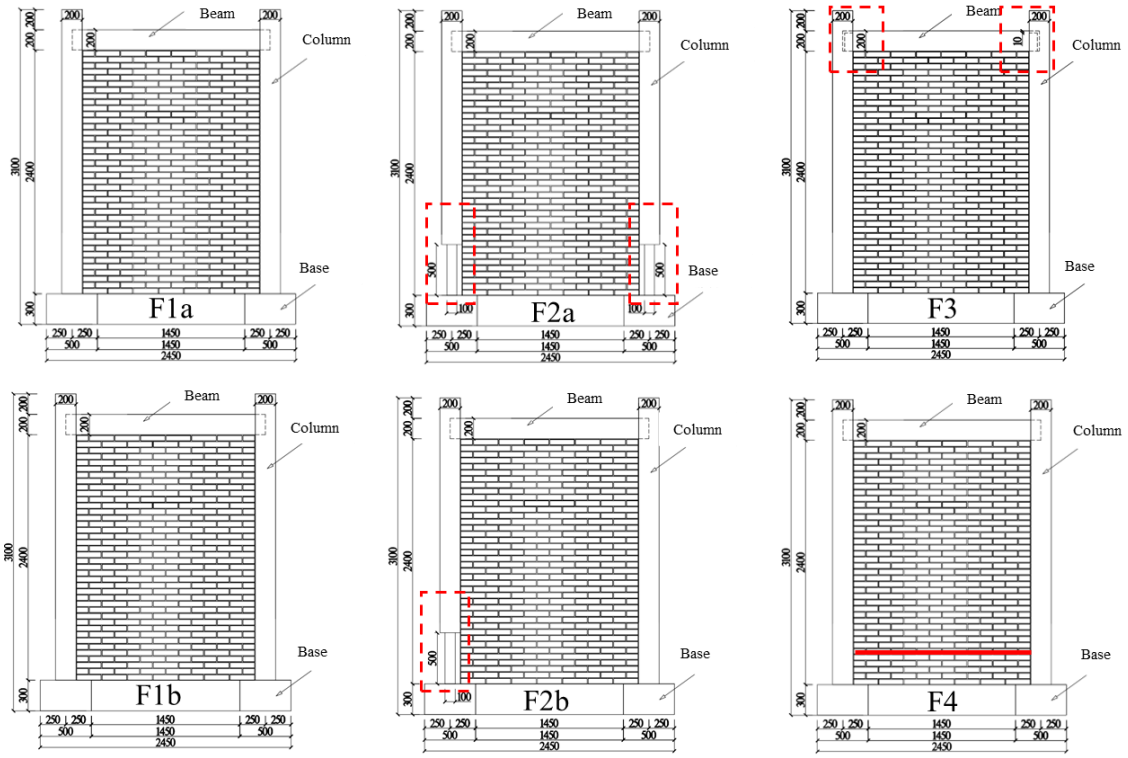

Figure 3: Dimension of six test walls

Table 1: Detailed introduction of each test piece

Walls ID	Size (height × wide ×thick)/mm	Damage condition
F1a	2500×1950×120	No damage
F1b	2500×1950×120	No damage
F2a	2500×1950×120	The column feet on both sides are reduced with a diameter of 100 mm over a height of 500 mm.
F2b	2500×1950×120	The column foot on one side is reduced with a diameter of 100 mm over a height of 500 mm.
F3	2500×1950×120	The height of the straight tenon is reduced by 10mm.
F4	2500×1950×120	A preset horizontal crack in the masonry at 300 mm away from th bottom.

The top of the columns extends 200 mm out of the timber beam to connect with the loading jack for application of the vertical load. The masonry infills were made of stretcher bond 230 × 110 × 50 mm burnt (sintered) clay bricks. The mortar was of M2.5 grade (nominal compression strength no less of 2.5 MPa), and the bricks were of MU10 grade (nominal compression strength no less of 10 MPa), as specified in *Chinese Code for Design of Masonry Structures*. From standard material property tests [6-9], the parallel to grain compression strength of the timber (Douglas Fir) used in this study was 32.9 MPa, the bending modulus of elasticity of the timber was 10876 MPa. the tested compression strength of the bricks was 12.4 MPa, and the tested cubic compression strength and the shear strength of the mortar were 4.82 MPa and 0.20 MPa, respectively.

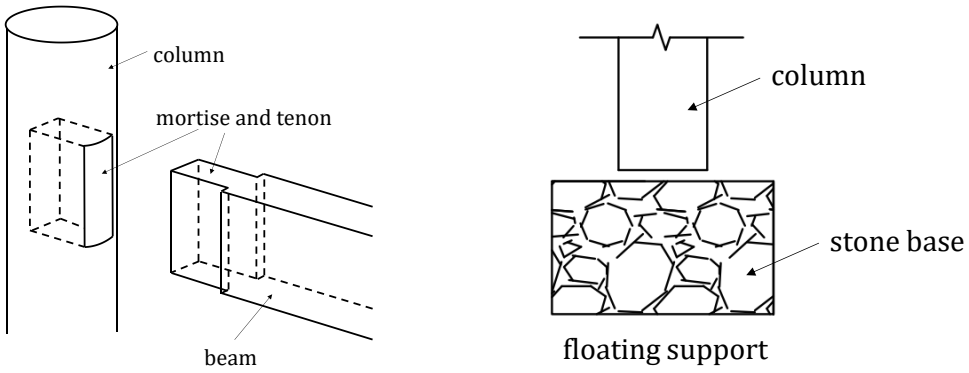

Figure 4: Straight tenon joints and floating support

2.2 Test setup and measuring scheme

The concrete foundation was fixed on the ground with steel bolts. Two vertical loads of 50 kN, determined from the typical traditional timber structures in Shanghai, were applied by two loading jacks on the top of the two columns. The setup of the specimens and the arrangement of the vertical loading jack and the hydraulic actuator (max loading capacity of 200 kN and a displacement range of ±250 mm) for lateral loading are shown in Figure 5.

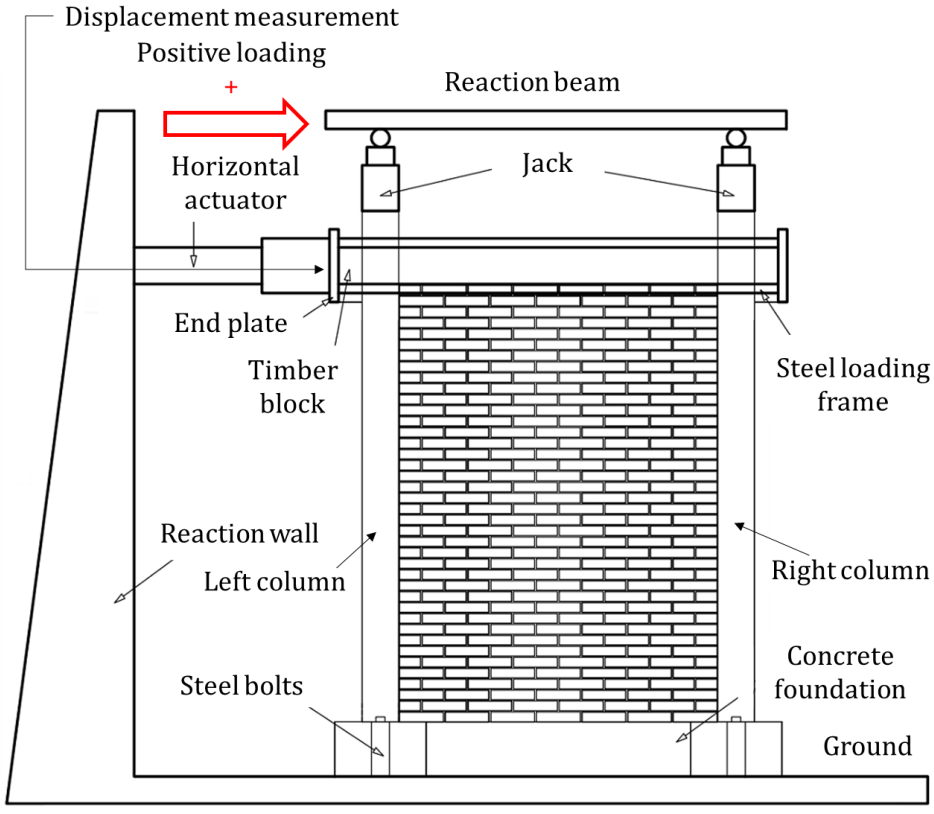

Figure 5: Test setup and measuring scheme

The lateral loading was applied to the timber frames in displacement control by the hydraulic actuator. The actuator was connected to the timber frame through a steel loading cage and two timber cushion blocks. To quantify the strength and stiffness degradation incurred by repeated loading, the CUREE loading protocol [10] was adopted, as shown in Figure 6. According to previous research on comparable frames [11], the reference displacement Δ was taken as 40 mm.

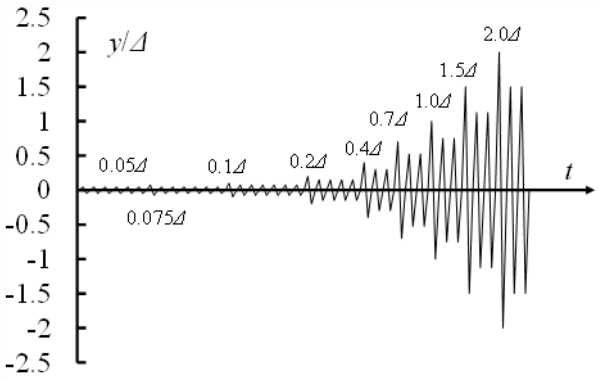

Figure 6: Cyclic displacement loading based on CUREE protocol [10]

3 Results

3.1 Test phenomena and primary damage modes

For specimen F1a（Figure 7）， when loaded to + 8mm, the first horizontal crack appeared between the first brick and the second brick at the bottom of the lower left corner of the brick wall. When the displacement reached 16 mm, the crack penetrated with width of the wall. When the displacement was increased to 40 mm, more cracks appeared on the surface of the corner bricks under compression. The left column foot was raised by about 10 mm, and the column was separated from the brick wall by about 6 mm. When the displacement reached 60 mm, horizontal and vertical cracks joined together in the lower left corner. Noticeable out-of-plane deformation was observed. The loading was terminated as a significant drop of the applied load was observed.

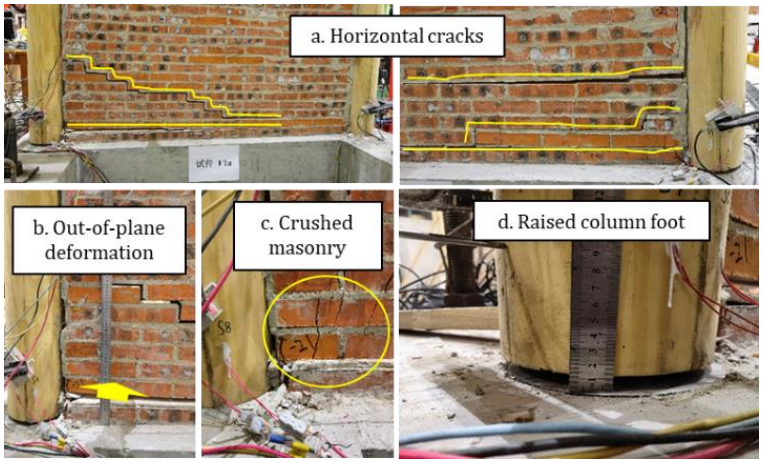

Figure 7: Experimental phenomena of the wall without damage (*specimen F1a*)

For specimen F1b (Figure 8), its failure mode was similar to F1a. It was mainly reflected in the crack through the bottom of the infilled wall, and the corner masonry crushed under compression. The timber frame obviously separated from the infilled wall, and the mortise-tenon joints were pull-out and damaged.

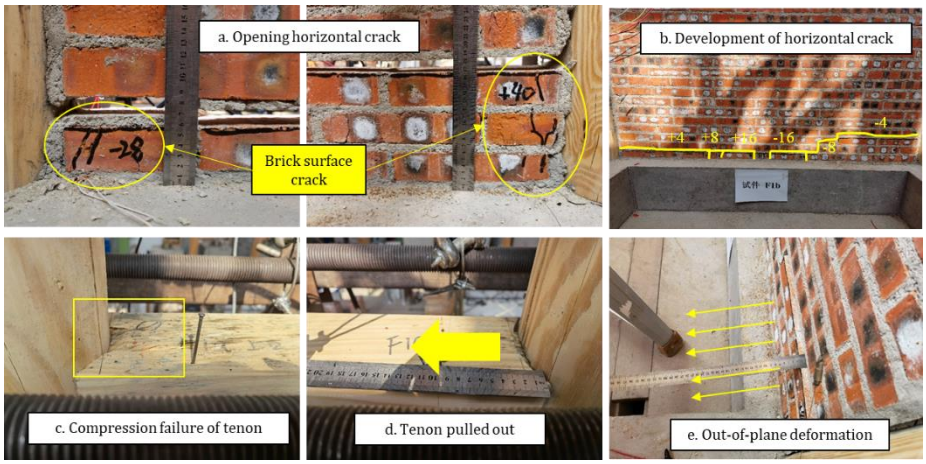

Figure 8: Experimental phenomena of the wall without damage (*specimen F1b*)

For specimen F2a (Figure 9), the first crack also appeared at the bottom of the infilled wall during ±8mm displacement level. The mortise-tenon joint was severely deformed when the displacement reached + 28mm. Reversed loading to - 28mm, the right timber column foot moved 15mm out of the plane. The masonry in the lower right corner was completely crushed during the loading cycle of +40mm. When the load reached - 60mm, the decayed column foot (with reduced cross-section diameter) exhibited bending failure, and the bearing capacity of the frame specimen dropped ever since.

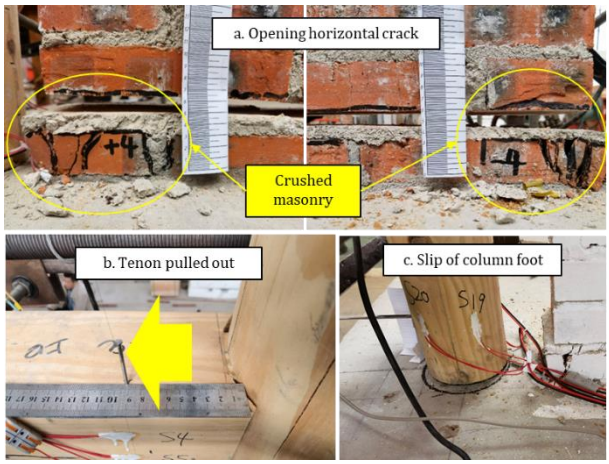

Figure 9: Experimental phenomena of the wall with columm foot decay (*specimen F2a*)

For specimen F2b（Figure 10）, its failure mode is similar to F2a.

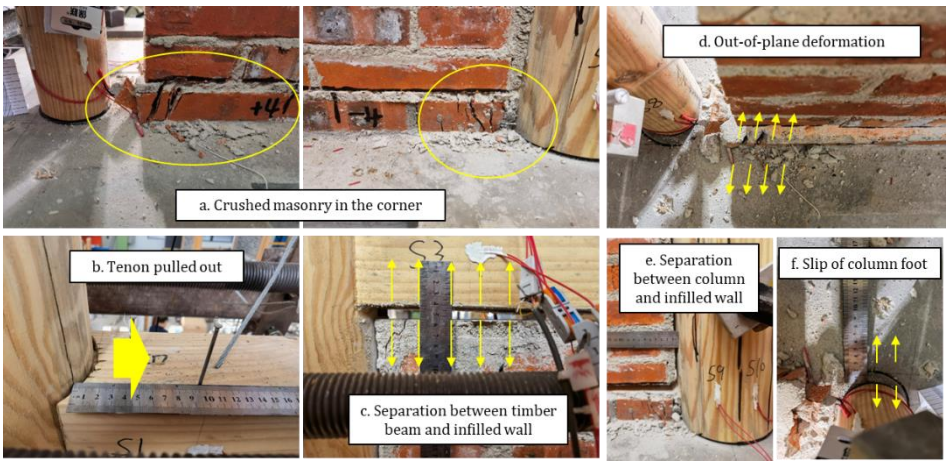

Figure 10: Experimental phenomena of the wall with columm foot decay (*specimen F2b*)

For specimen F3 (Figure 11), similar to the previous specimens, a crack appeared through the bottom of the brick wall in the early stage of the loading. The bottom of the timber beam was separated from the brick wall. The mortise-tenon joints showed noticeable pull-out and slippage during the early loading stage. When loaded to +60mm, the wall showed large out-of-plane displacement. The timber column was completely separated from the brick wall.

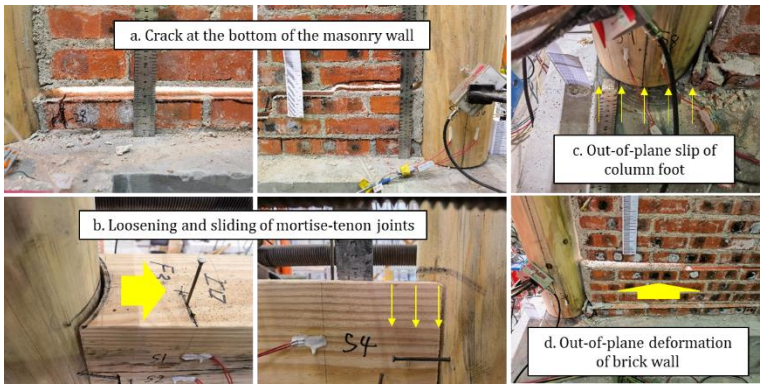

Figure 11: Experimental phenomena of the wall with dry shrinkage in joints (*specimen F*3)

For specimen F4 (Figure 12), horizontal cracks still appeared at the bottom of the infilled wall at the beginning of the loading. With the increase of the load level, more cracks appeared in the masonry near the preset horizontal crack and propagated rapidly and continuously. Finally, the frame wall was deemed as damaged by the crushed masonry and mortise-tenon joints.

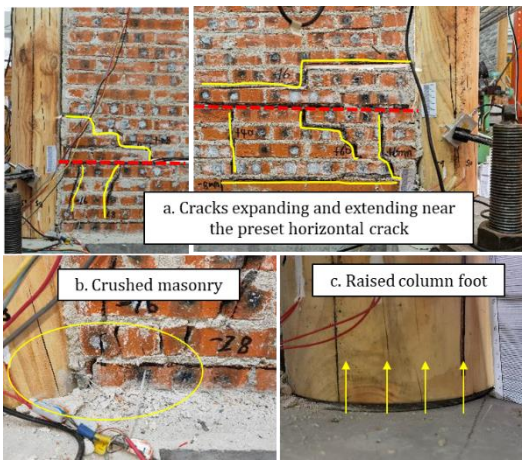

Figure 12: Experimental phenomena of the wall with horizontal crack in the masonry infill (*specimen F*4)

3.2 Load-displacement hysteretic curves

The load-displacement hysteretic curves of the six specimens are shown in the Figure 13. The shapes of the hysteretic curves of the six specimens were similar, all of which showed strong nonlinearity and pinching effect. There are two reasons for the pinching phenomenon. Firstly, the brick masonry slipped and dislocated near the cracks. The friction between the cracks led the bricks with residual deformation at unloading. Secondly, the mortise and tenon joints did not restore from the pulling-out damage with reduced stiffness.

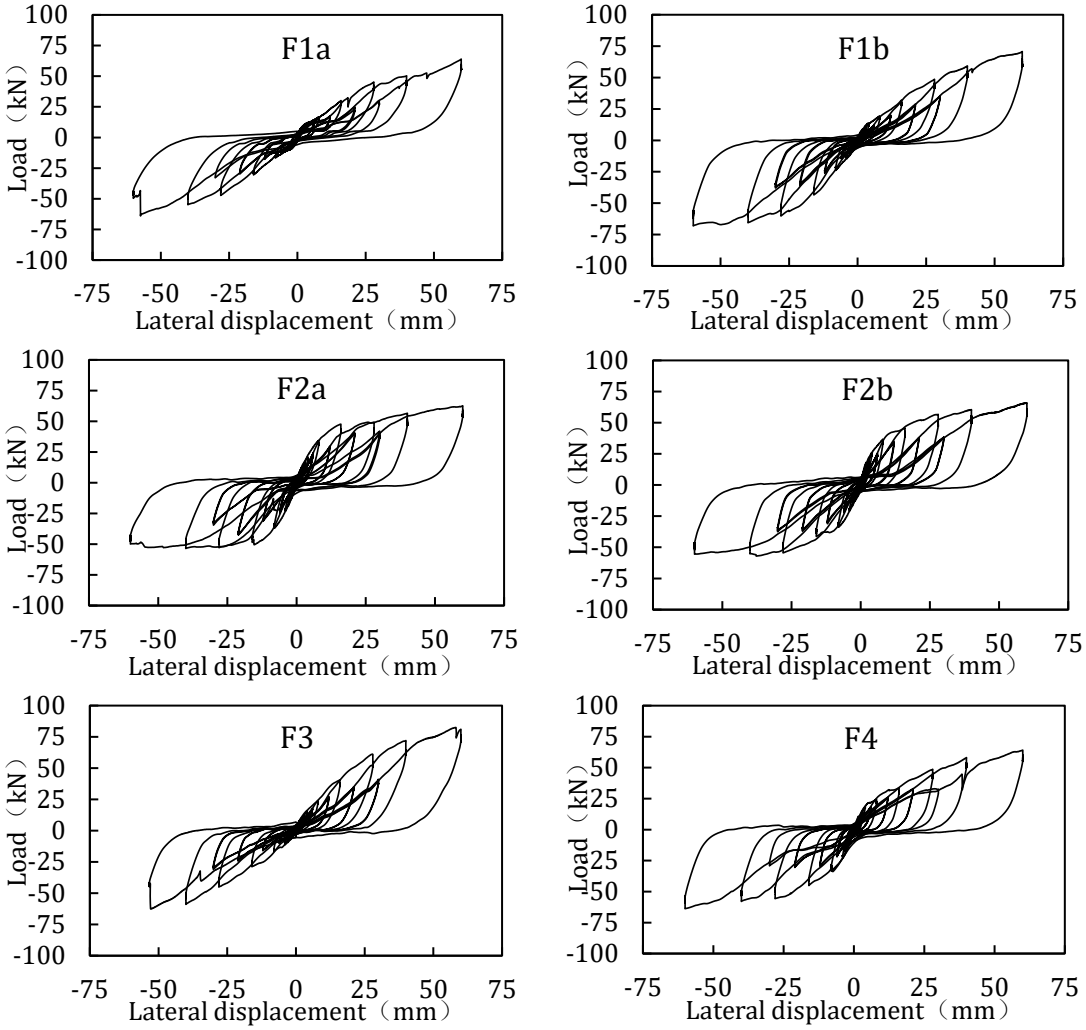

Figure13: Load-displacement hysteric curves of the tested walls

3.3 Load-displacement skeleton curve

The load displacement skeleton curves of the frame specimens can be obtained by connecting the peak points of each primary cycle of the load displacement hysteretic curves of the specimens. The results are shown in Figure 14.

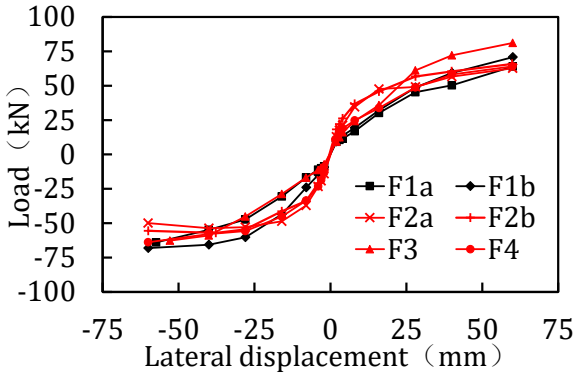

Figure 14: Load-displacement skeleton curves of the tested walls

Comparing the skeleton curves, it can be found that the skeleton curves showed similar trend, and all can be divided into three stages: the elastic stage, the yield stage and the failure stage. In the elastic stage, the load-displacement curve is linear elastic. There is no obvious crack in the brick wall and the timber frame shows no residual deformation. The slope of the skeleton curve in this stage is defined as the initial stiffness of the specimen. With the increase of the loading, the frame enters the yield stage

and the slope decreases due to the development of cracks and the plastic deformation of the mortise-tenon joints. The load-displacement curve become nonlinear. In the failure stage, the infill wall shows oblique compression failure, and the mortise-tenon joints are pulled out. At further lateral displacement, the corresponding load ceases to increase or starts to drop, implying the ultimate capacity of the wall.

4 Conclusion

This paper investigates the seismic performance of partially damaged masonry-timber mixed structures in China. Six wall specimens with different kinds of damage were tested by cyclic loading. The failure patterns and the load-displacement hysteretic curves of the wall specimens with different damage were discussed. It was found that the failure of the timber frame walls with brick masonry infill was triggered by the diagonal crushing of the masonry, pulling-out of the mortise-tenon joints and out-of-plane bulging deformation. The hysteretic curves show noticeable pinching effect. The decay of column foot had little effect on the performance of the wall; the shrinkage of joints reduced the initial stiffness of the wall, and the horizontal crack in the masonry led to premature separation of the masonry and impaired the stiffness and the peak load of the framed wall.

References

[1] Vieux-Champagne F, Sieffert Y, Grange S, Polastri A, Ceccotti A, Daudeville L. Experimental analysis of seismic resistance of timber-framed structures with stones and earth infill. Eng Struct 2014;69:102–15.

[2] Qu Z, Dutu A, Zhong J, Sun J. Seismic Damage to Masonry-Infilled Timber Houses in the 2013 M7.0 Lushan, China, Earthquake. Earthq Spectra 2015;31(3):1859–74.

[3] Xue J , Xu D , Qi L . Experimental seismic response of a column-and-tie wooden structure[J]. Advances in Structural Engineering, 2019, 22(8):136943321982864.

[4] Xu Q , Liu Q , Zhang F , et al. Experimental research on seismic performance of mortise-tenon joint wood frame with brick masonry infilled wall[J]. Building Structure, 2015.

[5] Qu Z, Fu X, Kishiki S, et al. Behavior of masonry infilled Chuandou timber frames subjected to in-plane cyclic loading[J]. Engineering Structures. 2020, 211: 110449.

[6] JGJ/T70 -2009 Standard for test method of performance on building mortar. Beijing: China 469 Architecture & Building Press.

[7] GB/T2542-2012 Test methods for wall bricks. Beijing: Standards Press of China

[8] GB/T 1936.2_2009 Method for determination of the modulus of elasticity in static bending of wood. Beijing: Standards Press of China.

[9] GB/T 1935-2009 Method of testing in compressive strength parallel to grain of wood. Beijing: 474 Standards Press of China.

[10] Krawinkler H, Parisi F, Ibarra L F, et al. Development of a testing protocol for wood frame structures[J]. 2001.

[11] Emile Crassac. Experimental study of the lateral performance of typical Chinese mortise-tenon connected timber frames[D]. Shanghai: Tongji University, 2016.

MODELLING THE HYSTERETIC BEHAVIOUR OF CONNECTIONS IN CROSS-LAMINATED TIMBER STRUCTURES

Rodrigo Tapia[1], Erick I. SAAVEDRA FLORES[1], Sergio J. YANEZ[1], Juan Carlos PINA[1] and Carlos F. GUZMÁN[1]

[1] *University of Santiago of Chile (USACH), Faculty of Engineering, Civil Engineering Department, Chile*

ABSTRACT

Cross-laminated timber (CLT) is a relatively new construction building system based on structural panels made of several layers of boards stacked crosswise and glued together on their faces [1]. As CLT panels are light-weight structural elements with high stiffness and strength to bending, compression and shear, they are an economically competitive building system when compared to traditional options and therefore, are a suitable candidate for some applications which currently use concrete, masonry and steel. Given the numerous advantages of building with timber, an increasing number of multi-story CLT buildings is sprouting around the world. In this work we investigate the hysteretic behaviour of CLT connections by means of a finite element modelling strategy. The mechanical response of connections is described with several unidimensional modelling devices along three orthogonal axes. The modelling process includes important features, such as, stiffness and strength degradation as a function of the hysteresis loops, among others. At a preliminary development stage, the proposed finite element model has shown promising results. This is part of an ongoing research.

KEYWORDS: Hysteresis, Connections, Cross-laminated timber, Finite Elements

INTRODUCTION

CLT is a relatively new construction building system. It was developed in Austria and Germany in the 1990s as a product that could take advantage of the amount of wood wasted in timber processing factories. Among its advantages, we can find its ability to self-protect against fire, its high strength-to-weight ratio and its fast and efficient on-site installation [2]. Although CLT presents several advantages as a construction material, its technology is much younger than concrete or steel. In fact, due to the complexity of wood mechanics, many timber design rules are still based on an empirical background, resulting in conservative design procedures [3].

Under cyclic loads, CLT shear walls behave rigidly. Here, the main contribution to energy dissipation comes from the ductile behaviour of steel-timber connections, which prevent potential mechanisms of brittle failure. Several research works have been carried out in order to capture numerically the response of metal connectors in the context of timber structures. A popular modelling approach consists of describing the connections by means of an array of non-linear unidimensional modelling devices, such as, springs, slides, hooks and gaps, among others. In general, the arrangement of multiple non-linear springs captures properly the hysteretic behaviour, stiffness degradation and failure of steel-timber connections with low requirement of computing resources. Therefore, this modelling approach is adopted in the present study.

PRELIMINARY RESULTS

In this section we present preliminary results of our computational simulations for experimental tests carried out on connections subjected to cyclic loads. The connections investigated here correspond to angle brackets and hold-downs. A displacement-controlled cyclic loading protocol was applied according to [4].

In order to enhance further the accuracy of the numerical predictions made by the proposed model, we adopt a standard GA-based optimisation scheme. A summary with different weighted errors for the dissipated energies for connectors subjected to in-plane shear and vertical tension/compression loads is presented in Table 1 [5].

Type of connection	Type of load	Cycle 1	Cycle 2	Cycle 3	Cycle 6	Cycle 9
Angle bracket	In-plane shear load	0.43%	0.24%	1.51%	1.7%	0.33%
Hold down	Vertical load	0.09%	0.69%	1.77%	3.22%	4.78%

Table 1: Weighted errors between dissipated energies

CONCLUSIONS

A non-linear finite element model was proposed to investigate the hysteretic response of CLT connections subjected to cyclic loads. Numerical predictions have shown promising results, revealing the potential predictive capabilities of the proposed model.

ACKNOWLEDGEMENTS

E.I. Saavedra Flores acknowledges the support from the Chilean National Agency for Research and Development (ANID), research grant FONDECYT REGULAR No. 1211767.

REFERENCES

[1] E.I. Saavedra Flores, R.M. Ajaj, I. Dayyani and Y. Chandra: Multi-scale model updating for the mechanical properties of cross-laminated timber. Computers and Structures, 177 (2016), 83-90.

[2] E. I. Saavedra Flores, K. Saavedra, J. Hinojosa, Y. Chandra, R. Das, Multi-scale modelling of rolling shear failure in cross-laminated timber structures by homogenisation and cohesive zone models 81 219–232. doi:10.1016/j.ijsolstr.2015.11.027

[3] E.I. Saavedra Flores, I. Dayyani, R. Ajaj, R. Castro-Triguero, F. DiazDelaO, R. Das and P. González, (2015), Analysis of cross-laminated timber by computational homogenisation and experimental validation, Composite Structures 121(0), 386 – 394.

[4] EN 12512:2003, Timber structures - test methods - cyclic testing of joints made with mechanical fasteners. European standard.

[5] R. Tapia, E.I. Saavedra Flores, J.C. Pina, S.J. Yanez and C.F. Guzmán, Non-linear finite element model for cross-laminated timber building connections subjected to cyclic loads. *In Preparation*.

TIMBER PROPERTIES

IN SITU SCREW WITHDRAWAL TEST FOR THE QUANTIFICATION OF ANOBIID INFESTATION OF STRUCTURAL TIMBER ELEMENTS

D. F. Lima[1], J. M. Branco[1], J. L. Parracha[2,3] and L. Nunes[3]

[1] Civil Engineering Department, University of Minho, ISISE, 4800-058, Guimarães, Portugal

[2] CERIS, Instituto Superior Técnico, University of Lisbon, 1049-001, Lisbon, Portugal

[3] LNEC - National Laboratory for Civil Engineering, 1700-066, Lisbon, Portugal

ABSTRACT

Timber degradation is frequently caused by insects, namely wood boring beetles. The assessment of the structural soundness of the remaining timber is, however, a difficult task. In a previous study, a correlation among screw withdrawal force and mass loss was established, thus allowing quantification of the residual strength of anobiid infested timber. However, the method was initially developed in laboratory and its use for in situ applications is not yet validated. In this paper, we extend the experimental work using a portable device to measure the *in situ* screw withdrawal resistance of timber elements degraded by anobiids. Screw withdrawal tests were performed on sound and artificially damaged timber samples using two different types of equipment (universal testing machine – lab environment; portable device – *in situ* application). Screw withdrawal resistance was correlated with both density (original and residual) and mass loss and the results obtained using the two types of equipment were compared. Results show the viability of using the portable device for the *in situ* assessment of timber elements degraded by anobiids.

KEYWORDS: Timber structures, anobiid infestation, screw withdrawal, damage assessment.

INTRODUCTION

Timber is known as one of the oldest construction materials and has been widely used in the construction industry over the centuries. However, knowledge about the biological degradation processes and their impact on timber structures remains a key challenge towards the preservation of existing buildings.

Wood is susceptible to biological degradation, which is frequently caused by fungi and insects. While fungal decay tends to be localized and linked to moisture sources, insect degradation often leads to a general deterioration of the timber structure [1]. Considering insect infestations in temperate countries, subterranean termites and old house borers stand out for their ability to cause damage to structures shortening their service life. Anobiids may also play a major role in the deterioration problems though the assessment of the structural soundness of the remaining timber is a difficult task and timber elements are often removed and replaced without real need.

For an adequate intervention plan, it is necessary to correctly assess the level of degradation and its effects on the behavior of the structure. Therefore, it is urgent to fill the gaps in the existing bibliography and current normative references about the biological degradation of wooden structures in existing buildings to serve as the basis for more accurate and reliable decision-making by engineers and architects.

Usually, the *in situ* assessment of the level of degradation of a timber element caused by anobiids is performed initially by visual inspection, analyzing the quantity and dispersion of the exit holes on the surface of the wood. However, previous studies demonstrated that surface exit holes are not a good indicator for the estimation of the level of degradation, and the internal galleries in the element tend to be higher than indicated by visual inspection [1]. Thus, methods to assess that level of degradation through screw withdrawal tests were developed [1, 2]. In [1], the method was established by performing tests on sound and degraded specimens, correlating the results with the residual compressive strength. Moreover, the method proposed by [2] is based on the correlation between screw withdrawal resistance and the density loss caused by anobiid infestation. However, these methods were developed in the laboratory and their use for *in situ* applications is not yet validated.

This work aims to validate the use of a portable device equipment initially developed to perform pull-off tests on mortars for the *in situ* quantification of the level of anobiid degradation of structural timber elements by comparing results with those obtained in the laboratory. For this, screw withdrawal tests were performed on both sound and artificially degraded specimens (with two different levels of degradation). The tests were carried out using a portable device equipment (*in situ* application) and a universal testing machine (laboratory equipment). Then, the test results were correlated with the original density, the residual density, and the mass loss caused by insect degradation. Finally, the viability of using the portable device was assessed by comparing the *in situ* and lab results.

MATERIALS AND METHODS

Prior to the tests, the specimens (*Pinus sylvestris* L.) were stored in a climatic chamber at a constant temperature of 20 ± 1°C and relative humidity of 60 ± 5%. The recommendations of the standards NP EN 13183 [3] and NP 616 [4] were followed to determine the moisture content and the density, respectively. The dimensions of the specimens were (160 x 100 x 100) mm^3.

Screw withdrawal tests in the direction perpendicular to the grain were conducted following the recommendations of EN 1382 [5] on sound and artificially degraded Scots pine samples. The nominal diameter of the screw used in this study was 6 mm and a penetration of 20 mm was also adopted. No distinction was made between radial and tangential directions since no relevant differences were found in the results obtained by [1].

The simulation of degradation was performed by manual drilling in the direction perpendicular to the grain in two densities, 1.67 holes/cm^2 (DL-I) and 4,00 holes/cm^2 (DL-II). The dimension of the perforated galleries was 2mm in diameter over the entire length of the specimen (100mm) since anobiids circular galleries range between 1 and 3 mm in diameter [6]. The quantification of the artificial degradation was carried out by measuring the mass of the specimen before and after drilling the galleries, thus obtaining the mass loss.

Two sets of twelve replicates were tested: the first was tested on the Laboratory Equipment (Lloyd LR50KPlus), and the second set was tested with the Portable Device Equipment (MATEST Digital pull-off tester E142-01) (Figure 1). 84 screw withdrawal tests were conducted on 24 specimens: 36 using the Laboratory Equipment and 48 using the Portable Device Equipment. The average results obtained for each specimen were adopted as the screw withdrawal resistance.

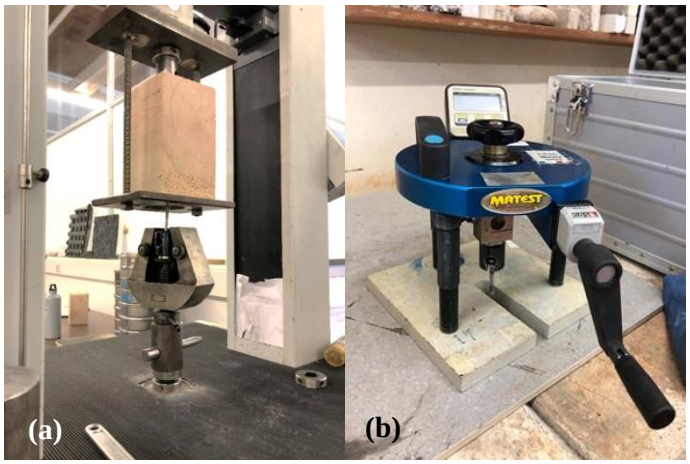

Figure 1: Screw withdrawal test equipment. (a) Laboratory Equipment (LE); (b) Portable Device Equipment (PE).

Screw withdrawal resistance was obtained by Equation 1 [5].

$$f = \frac{F_{max}}{d_i \times l_p} \quad (1)$$

in which F_{max} is the value of the maximum force of the test, l_p the penetration depth of the screw into the wooden element, and d_i is the inner diameter of the screw.

Table 1 presents the nomenclature, the number of tests, the equipment, and the level of degradation adopted for the experimental campaign.

Table 1: Summary of the distribution of the specimens into the different degradation levels and equipment for the screw withdrawal tests.

Nomenclature	Number of specimens	Number of tests	Equipment	Degradation Level (holes/cm^2)
SW_LE_REF	4	12	Laboratory	-
SW_LE_DL-I	4	12	Laboratory	1.67
SW_LE_DL-II	4	12	Laboratory	4.00
SW_PE_REF	4	16	Portable	-
SW_PE_DL-I	4	16	Portable	1.67
SW_PE_DL-II	4	16	Portable	4.00

SW – Screw Withdrawal; REF – Reference (sound specimens); DL-I – Degradation level I; DL-II – Degradation level II; LE – Laboratory Equipment; PE – Portable Device Equipment.

RESULTS AND DISCUSSION

Table 2 presents the results obtained considering the simulation of the degradation, the original density (corrected for a 12% moisture content), the residual density (corrected for a 12% moisture content), and the screw withdrawal tests.

Table 2: Results obtained in the simulation of the degradation and the screw withdrawal tests.

Group	SW_LE_REF			SW_LE_DL-I			SW_LE_DL-II		
	$\bar{X}$	σ	C.V.	$\bar{X}$	σ	C.V.	$\bar{X}$	σ	C.V.
Nº	4			4			4		
ML [%]	0	0	0%	3.0	0.1	3.3%	6.8	0.3	4.4%
$\rho_{12,ori}$ **[kg/m³]**	549	24	4.4%	564	30	5.3%	543	25	4.6%
$\rho_{12,res}$ **[kg/m³]**	549	24	4.5%	547	30	5.4%	506	25	5.0%
f **[MPa]**	32.9	3.7	11.2%	31.2	3.1	9.9%	26.1	1.6	6.1%
Group	**SW_PE_REF**			**SW_PE_DL-I**			**SW_PE_DL-II**		
	$\bar{X}$	σ	C.V.	$\bar{X}$	σ	C.V.	$\bar{X}$	σ	C.V.
Nº	4			4			4		
ML [%]	0	0	0%	3.1	0.2	6.5%	6.6	0.3	4.5%
$\rho_{12,ori}$ **[kg/m³]**	563	32	5.7%	551	19	3.4%	549	27	4.9%
$\rho_{12,res}$ **[kg/m³]**	563	32	5.6%	533	19	3.5%	513	26	5.0%
f **[MPa]**	39.1	2.9	7.4%	36.5	3.1	8.5%	34.5	3.4	9.9%

$\bar{X}$ – Average; σ – Standard Deviation; C.V. – Coefficient of variation; ML – Mass Loss; $\rho_{12,ori}$ – Original density for a 12% moisture content; $\rho_{12,res}$ – Residual density for a 12% moisture content; f – Screw withdrawal resistance.

Additionally, it was verified that the distribution of the results fits the normal distribution through the Shapiro-Wilk test, showing the possibility of the analysis from linear regressions. Correlations between the screw withdrawal resistance and both the density (residual and original) and the mass loss are presented in Figure 2.

As expected, results show that the higher the degradation level, the lower the screw withdrawal resistance, regardless of the equipment used. When comparing the results of the two equipment, it is possible to observe that screw withdrawal resistance is higher when using a portable device even though a similar trend is observed (Figure 2), which is a strong indication of the feasibility of using the portable equipment *in situ* to estimate the residual density and the mass loss of the degraded elements, as proposed in [1] and [2]. Table 3 presents the Pearson correlation coefficients obtained considering the screw withdrawal resistance and the other parameters. The correlation line of Table 3 exposes the correlation values, and the p(uncorr.) line presents the probabilities that the parameters are uncorrelated.

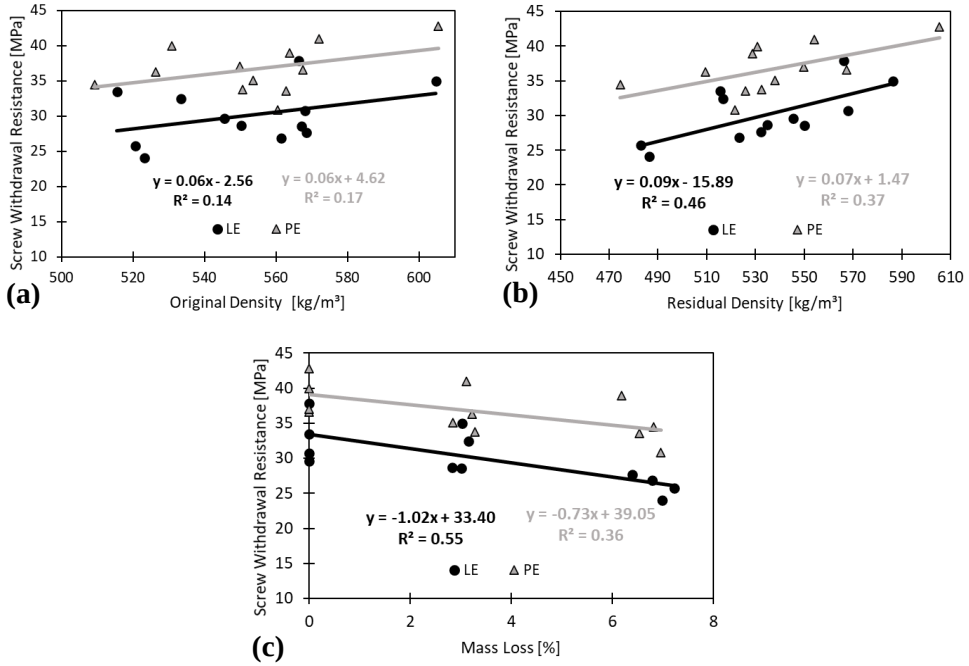

Figure 2: Correlations between screw withdrawal resistance and original density (a), screw withdrawal resistance and residual density (b) and screw withdrawal resistance and mass loss (c).

Table 3:Pearson's correlation coefficient between screw withdrawal resistance, density (original and residual) and mass loss

		$\rho_{12,ori}$	$\rho_{12,res}$	ML
LE	**Correlation**	0.38	0.67	-0.74
	p(uncorr.)	0.221	0.016	0.006
PE	**Correlation**	0.41	0.61	-0.59
	p(uncorr.)	0.182	0.037	0.042

Table 3 shows a low correlation among screw withdrawal resistance and the original density (r=0.38 and r=0.41), a medium correlation among screw withdrawal resistance and the residual density (r=0.67 and r=0.61), and medium correlation among screw withdrawal resistance and the loss of mass (r=-0.74 and r=-0.59). Moreover Table 3 also shows that the only parameter that did not present values within the 95% confidence interval (p(uncorr.) greater than 0.05) was the original density.

When comparing the results obtained by the two sets of tests, it can be observed that the regression lines in Figure 2(a) are almost parallel since the ratio between their slopes is close to the unit (0.98). On the other hand, the regression lines observed in Figures 2(b) and 2(c) are not parallel (i.e., the ratio between their slopes is far from the unit).

It is important to emphasize that these tests were performed on only 12 specimens per set, which is a relatively low number, and, in these cases, each specimen has a high influence on the correlation coefficient and the slope of the linear regression line. Therefore, it is necessary to extend the experimental campaign and performing a larger number of measurements.

CONCLUSION

When comparing the results of the screw withdrawal tests performed with the laboratory and portable equipment the feasibility of using the later for *in situ* tests was demonstrated. However, to obtain reliable results for estimating residual density and level of degradation, it will be necessary to calibrate the portable device to obtain a more reliable correction factor for the *in situ* measurements.

ACKNOWLEDGMENTS

This work was supported by national funds through FCT – Fundação para a Ciência e a Tecnologia within the scope of the Timquake project (POCI-01-0145-FEDER-032031) and through a Ph.D. scholarship (PRT/BD/152833/2021) conceded to the first author by MIT Portugal Program.

REFERENCES

[1] Gilfillan, J.R. & Gilbert, S.G. Development of a technique to measure the residual strength of woodworm infested timber. Construction and. Building Materials. 15 (7) (2001) 381-338.

[2] Parracha, J.L., Pereira, M.F.C., Maurício, A., Machado, J.S., Faria, P. & Nunes, L. A semi-destructive assessment method to estimate the residual strength of maritime pine structural elements degraded by anobiids, Materials and Structures 52 (54) (2019). https://doi.org/10.1617/s11527-019-1354-9.

[3] NP 13183:2013. Teor de água de um provete de madeira serrada. Parte 1: Determinação pelo método da secagem, IPQ, Monte da Caparica (2013).

[4] NP 616:1973. Madeiras. Definição da massa volúmica, Norma Portuguesa, IGPAI, Lisbon (1973).

[5] EN 1382:2000, Timber structures—Test methods: Withdrawal capacity of timber fasteners. European Committee for Standardization, Brussels (2000).

[6] Cruz, H., Jones, D. & Nunes, L. Wood. In Materials for Construction and Civil Engineering. Springer International Publishing. (2015) (557-583). https://doi.org/10.1007/978-3-319- 08236-3_12.

IN SITU ASSESSMENT OF MECHANICAL PROPERTIES OF TIMBER USING THE DRILLING RESISTANCE METHOD

D. MARRANZINI, G. IOVANE, F. COZZOLINO, R. LANDOLFO and B. FAGGIANO

Dept. of Structures for Engineering and Architecture, University of Naples Federico II, 21, Via Claudio, 80125, Naples, Italy

ABSTRACT

The assessment of the structural performances of existing timber structures and eventually the design of any strengthening intervention require the diagnosis and a reliable mechanical identification of timber members, possibly through on-site inspections. Nowadays visual strength-grading is the only method regulated by the Code through which professionals can address this issue. However, being a superficial analysis, it has some limitations. Thus, non-destructive techniques (NDT) result to be advantageous supporting tools. Specifically the paper focuses on the application of the drilling resistance technique. Based on a statistical regression law matching the experimental data acquired from literature, a method for the determination of the mechanical properties of timber is proposed, providing a satisfactory approximation on the safe side.

KEYWORDS: Timber on-site assessment, mechanical identification, visual inspection, non-destructive techniques, drilling resistance method.

INTRODUCTION

In order to assess the safety of old structures and preserve the original essence as much as possible, *in situ* inspection and evaluation of actual mechanical properties represent a first fundamental step towards diagnosis, structural analysis and design of possible retrofit interventions. With regards to timber structures, two alternative and complementary approaches are visual strength-grading (VSG) and non-destructive tests (NDT). The first approach (VSG) consists in evaluating the macroscopic characteristics of timber, in order to assign to it an established strength class, according to codes (in Italy UNI11119 [1]; UNI 11035-1[2]; UNI 11035-2[3]; in Europe EN338: 2016[4]). In fact the mechanical properties of timber are affected by defects such as knots, cracks, ring shakes, section bevels, grain orientation. However, given the limits of this approach, non-destructive techniques (NDT) are frequently used in professional practice and research fields, in order to acquire more details about the members conditions, taking into account also the internal ones. Although the main difficulty of the surveyor is the lack of standardised references with regards to both test set-up and protocols, the NDT are frequently used on-site mainly as a support tool to collect information, principally about the state of conservation and the mechanical properties of timber members.
NDT methods can be grouped in different categories, like probing, acoustic, vibration techniques [5].
The probing methods are mainly used to estimate the density of timber. Needle penetration, drilling resistance method and screw withdrawal belong to this group [6]. Currently also the core drilling is widely used for the density estimation, especially for the existing timber [7].

Acoustic methods are based on the propagation of stress waves through material in order to estimate the timber member stiffness. Generally two types of waves are used: sonic stress waves for frequencies within the audible range and ultrasonic stress waves at frequencies above 20 kHz [8]. Acoustic methods are based on the time-of-flight measurements, from which the dynamic modulus of elasticity (MOE_{dyn}) can be estimated. MOE_{dyn} is strictly correlated to the static Modulus of elasticity of timber (MOE) [9, 10]. Vibrations methods are based on natural frequency of timber, since frequency is directly related to the stiffness of timber member. Natural frequency data are measured after inducing vibration by hammer impact through commercial devices, therefore MOE_{dyn} is determined in order to predict the MOE.
Others NDT techniques are widely used for the diagnosis of timber structures. Acoustic tomography, widely spread in the forest field, is also applied in structural application for detecting internal timber defects (knots, checks, etc.) and damage (decay, cracks, etc.) [8]. Also digital radioscopy is a useful technique for identifying an array of internal, hidden problems in timber members likes decay and insect attacks [11].

THE DRILLING RESISTANCE METHOD

Main features

Among the probing methods, drilling resistance method (DRM) is a widespread technique for timber investigations. It is based on the resistance offered by the material to advance of a small diameter drill bit (Fig. 1a). This tool is considered a quasi-non-destructive method, since the size of the hole in the specimen after testing does not have any weakening effects. The speed and rotation of the drill bit are constant and the turning moment, required to maintain constant the drilling speed, is the drilling resistance. Measurements are represented by a graphic profile characterized by two variables: drilling penetration (cm) and drilling resistance (%), the latter is a dimensionless parameter also called "amplitude" (A) or "resistance measure" (RM). Zones characterized by a lower drilling resistance are associated to a lower wood density (Fig. 1b).

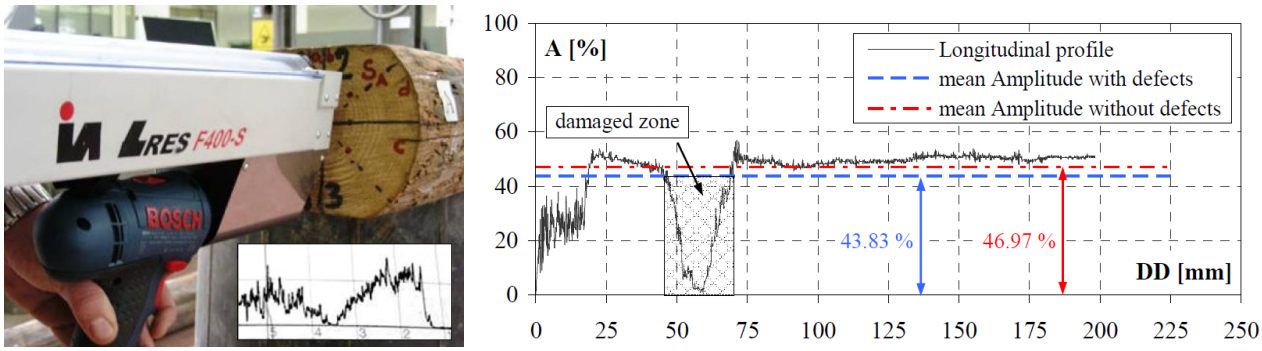

Figure 1: a) Longitudinal drilling measurement (L) on a structural dimension (S) timber specimen; b) Evaluation of A_m evidencing the presence of timber defects

The main application of DRM in the diagnostic field concerns the detection and localization of the internal damage and discontinuities in timber elements, highlighted by voids and drop trend in the graphic profile provided by the DRM. Thanks to this feature DRM is largely used in technical community for estimating the resistant cross section reduced by damaged zone and voids, as well as for identifying the geometry of the cross section of timber members. With this goal some authors have recently applied DRM in combination with the laser scanner [12]. Furthermore, DRM has been also lately applied in the field of post fire assessment, for estimating the residual cross section of members damaged by fire [13]. In addition to the aforementioned applications, DRM can be used for the prediction of the mechanical properties of timber, thanks to statistical correlations among the mean DRM output parameter (A_m) and the mechanical parameters obtained from destructive tests (DT). Several studies established relationships between A_m and timber mechanical properties, with different approximation, depending

on the test set-up and timber species. In particular, the resistance graph is influenced by the tool's settings (speed of rotation and sensitivity), the angle and direction of drilling (longitudinal or transversal), moisture content and timber species [14]. The A_m evaluation reveals defects, as knots (very high resistance to drilling) and damaged zones (low resistance to drilling) located along the direction of penetration (Fig. 1.b). Both linear and multiple regressions are used in the estimation of timber mechanical properties [15]. Specifically, linear regression seems to be more reliable for the assessment of timber density and compression strength [16-23].

Mechanical properties identification of Chestnut *(Castanea sativa Mill.)* timber through DRM

Among the timber species tested [14], several studies involve Chestnut timber *(Castanea sativa Mill.)*. Thus a review of the state of art concerning the DRM application for the mechanical identification of Chestnut is presented. As for studies carried out on other wood species, the correlations between A_m and wood density are the most consistent. The reliability of the regression fit is assessed by the coefficient of determination (R^2), with $0 \leq R^2 \leq 1$: high values indicate a strong relationship between the variables involved. The main specimen features of the experimental campaigns carried out are provided hereafter:

- Specimen dimension: structural dimension (S), small dimension (SS) and defect free (DF) specimens; this is a key parameter strictly related to the presence of wood defects;
- Direction of drilling: drilling tests are performed both in longitudinal (L) and transversal (T) directions; considering that DR on site measures can be generally done in the transverse direction;
- Number of specimens: it can influences the statistical dispersion of the variables;
- Age of timber: it is a relevant parameter since it is related to the presence of timber defects. In fact generally ancient timber members (Old wood, OW) show a greater quantity of defects respect to timber members recently placed on market (New wood, NW), which are strength graded.

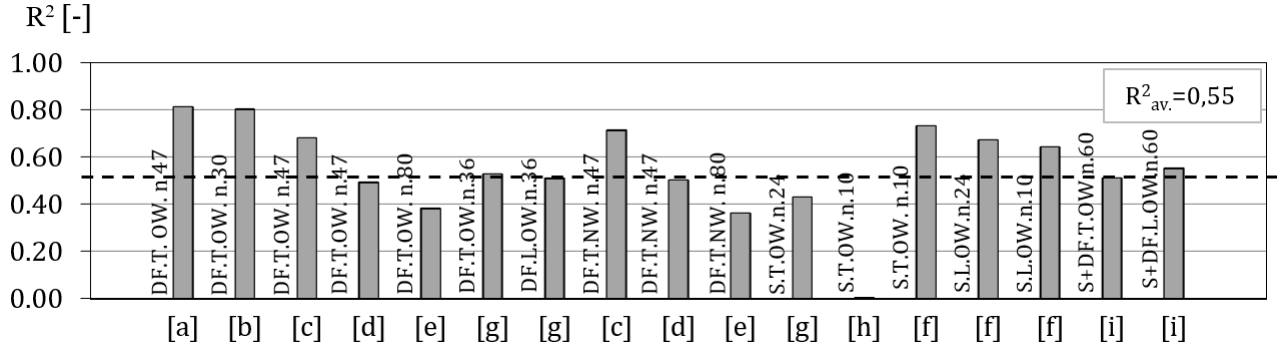

Figure 2: Correlations between A_m and density for Chestnut timber; [a]Feio et al. 2007; [b] Acuna et al. 2011; [c] Feio et al. 2005; [d] Feio et al 2007; [e] Lourenco et al. 2007; [f] Faggiano et al. 2009; [g] Faggiano et al. 2010; [h] Riggio and Piazza 2008; [i] Faggiano et al. 2011.

From the data review a general dispersion of the results is apparent, due to the natural inhomogeneity of wood. Figure 2 collects the coefficient of determinations R^2 for several experimental campaigns, for different size of the samples (n. 10, 24, 30, 36, 47, 60, 80), size of specimen (DF, S), direction of drilling (L, T), age of timber (OW, NW). The average value of R^2_{av} achieved is about 0.55.

THE SIMPLE CORRECTIVE METHOD

With reference to the wood density, the regression law defined by the correlation of NDT and DT parameters, provides a so called "theoretical density" (ρ_t), which is affected by approximations as respect to the actual density (ρ_s) measured in laboratory through the specimens weighting. With the aim of reducing the uncertainty, an adjustment method for the estimation of wood density has been already

proposed by Faggiano et al. [22]. The method is based on the definition of a correction coefficient $C_{adj,\rho}$, thus obtaining a design density value (ρ_d), as it follows:

$$\boldsymbol{\rho_d = \frac{\rho_t}{C_{adj,\rho}}} \qquad \text{where} \qquad \boldsymbol{C_{adj,\rho} = \frac{\rho_t}{\rho_s}}$$

$C_{adj,\rho}$ is evaluated for every examined specimen. In Figures 3a and b the ρ_t/ρ_s (= $C_{adj,\rho}$) and ρ_d/ρ_s ratios are drawn. It can be noted that by applying the coefficient $C_{adj,\rho}$ the ρ_d value obtained is always smaller than the experimental density ρ_s, for the sake of safety, considering that as far as the density is large, the mechanical properties of timber are better.

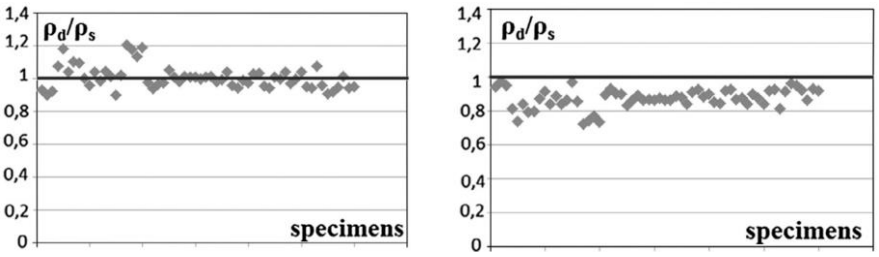

Figure 3: a) Theoretical over experimental [22] and b) Design over experimental density ratios [22].

A further enhancement of the procedure can be the determination of a single value of $C_{adj,\rho}$ ($\geq \mathbf{1}$) for the whole sample. It can be assumed as equal to the 95th percentile of the ρ_t/ρ_s distribution, namely $C_{adj,\rho,95}$. Once ρ_t/ρ_s is calculated for each specimens, the value equal to the 95th percentile is fixed as the $C_{adj,\rho,95}$. In this way, just in the 5% of the cases the design density will be lower than the experimental value.

THE APPLICATION OF THE PROPOSED METHOD

The proposed method has been applied to the data obtained from the aforementioned experimental campaigns, selecting those having the same features (sample dimension, drilling direction, etc.), in particular related to specimens of ancient wood (OW), tested in transversal direction (T). The campaigns are the following ones: a) Feio et al. [17], Lourenço et al. [19], Faggiano et al. [20] for DF specimens (Fig. 4a), with R^2 values respectively equal to 0.81, 0.35 and 0.53; b) Faggiano et al. [15, 16] for S specimens (Fig. 3b), with R^2 values respectively equal to 0.45 and 0.43.

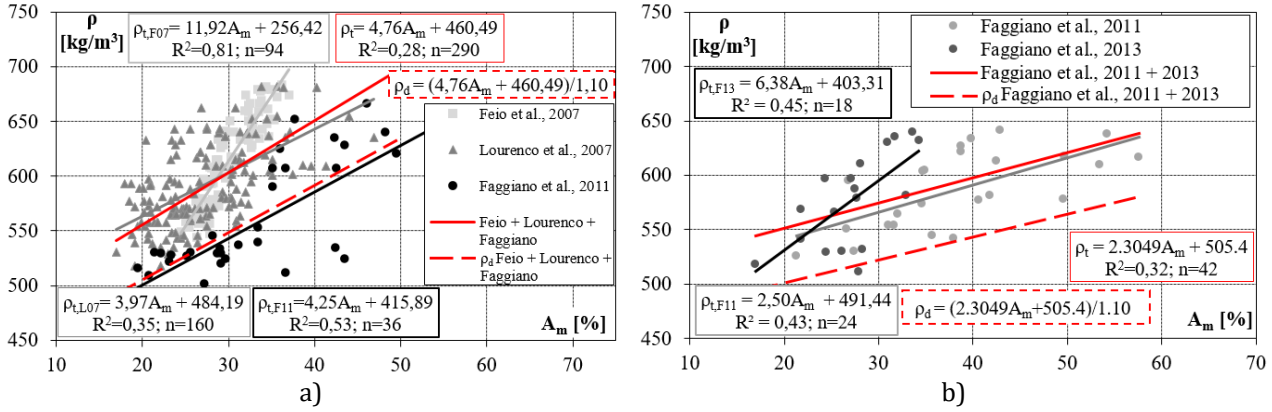

Figure 4: Correlation between transversal A_m and density for Chestnut timber: a) DF [19, 17, 20] and b) S [15, 16] dimensions.

In Figure 4 further to the experimental data for each campaign considered and the corresponding regression laws obtained, a new linear regression law (ρ_t) has been determined considering the whole data of all the campaigns, corresponding to a number of 290 and 42 specimens, for the samples a) and b) respectively, obtaining R^2 equal to 0.28 and 0.32, respectively.

In Table 1 the coefficients $C_{adj,\rho,95}$ are reported for the two aforementioned samples. In both cases $C_{adj,\rho,95}$ equal to 1.10 has been found.
Then in Figure 4 the regression laws adjusted (ρ_d) through the coefficient $C_{adj,\rho,95,}$ are also drawn, evidencing the efficacy of the method applied.

Table 1: Evaluation of $C_{adj,\rho,95}$ coefficient for Chestnut: a) DF [19, 17, 20]; b) S [15, 16] dimensions.

	a) Lourenço + Feio + Faggiano R^2=0,28				*b) Faggiano 2011 + 2013* R^2=0,32			
	ρ_s	A_m	ρ_t	$C_{adj,\rho,95} = \rho_t/\rho_s$	ρ_s	A_m	ρ_t	$C_{adj,\rho,95} = \rho_t/\rho_s$
	[kg/m³]	[%]	[kg/m³]	[-]	[kg/m³]	[%]	[kg/m³]	[-]
Max	636,8	53,2	692,6	1,27	641,7	57,6	637,9	1,11
Min	484,0	16,9	547,6	0,89	511,8	17,0	544,5	0,91
Media	533,6	28,7	594,7	1,00	583,1	33,7	582,9	1,00
95th	573,2	38,1	632,3	**1,10**	637,9	53,2	627,9	**1,10**
SD	24,5	5,8	23,3	0,07	38,8	9,5	21,8	0,06
CV	5%	20%	4%	6%	7%	28%	4%	6%

CONCLUSION

The paper focuses on the drilling resistance technique for the mechanical identification of timber members. A literature review of the DRM application for the mechanical identification of Chestnut timber is presented, evidencing the main features of the test campaigns, such as specimen size, drilling direction, number of specimens and age of timber. With regards to the studies on the correlation between transversal A_m and timber density, homogenous experimental campaigns have been collected. Thus new correlations based on linear regression have been determined. In order to reduce the uncertainties in the NDT density evaluation, a correction of the correlation has been applied, through the $C_{adj,\rho,95}$ adjustment coefficient, which allows the estimation of the density of Chestnut timber in the sake of safety. New experimental tests should be conducted in order to validate the procedure.

ACKNOWLEDGEMENT

The research project DPC-ReLUIS 2022-2024 – Contribution to standards for timber structures is acknowledged**.**

REFERENCES

[1] UNI 11035-1: 2010 Structural timber, Visual strength grading for structural timbers, Part 1: Terminology and measurements of features.

[2] UNI 11035-2: 2010 Structural timber, Visual strength grading for structural timbers, Part 2: Visual strength grading rules and characteristics values for structural timber population.

[3] UNI 11119: 2004 Cultural heritage, Wooden artefacts, Load-bearing structures-On site inspections for the diagnosis of timber members.

[4] EN 338 (2003) Structural timber–strength classes. Comité Européen de Normalisation CEN.

[5] Llana, D., Íñiguez-González, G., M. Esteban, E. Hermoso, F. Arriaga, Timber moisture content adjustment factors for non-destructive testing (NDT): acoustic, vibration and probing techniques. Holzforschung, 74 (2020) 817-827.

[6] T. Tannert, R.W. Anthony, B. Kasal, M. Kloiber, M. Piazza, M. Riggio, F. Rinn, R. Widmann, N. Yamaguchi, In situ assessment of structural timber using semi-destructive techniques, Mater. Struct. Constr. 47 (2014) 767–785.

[7] R. Martínez, J. Calvo, F. Arriaga, I. Bobadilla, In situ density estimation of timber pieces by drilling residue analysis, Eur. J. Wood Wood Prod. 76 (2018) 509–515.

[8] U. Dackermann, K. Crews, B. Kasal, J. Li, M. Riggio, F. Rinn, T. Tannert, In situ assessment of structural timber using stress-wave measurements, Mater. Struct. Constr. 47 (2014) 787–803.

[9] T. Nowak, K. Hamrol-Bielecka, J. Jasienko, Non-destructive testing of wood – correlation of ultrasonic and stress wave test results in glued laminated timber members, Ann. Warsaw Univ. Life Sci. – SGGW. For. Wood Technol. 92 (2015) 317–324.

[10] F. Arriaga, C. Osuna-Sequera, I. Bobadilla, M. Esteban, Prediction of the mechanical properties of timber members in existing structures using the dynamic modulus of elasticity and visual grading parameters, Constr. Build. Mater. 322 (2022) 126512.

[11] M. Riggio, R.W. Anthony, F. Augelli, B. Kasal, T. Lechner, W. Muller, T. Tannert, In situ assessment of structural timber using non-destructive techniques, Mater. Struct. Constr. 47 (2014) 749–766.

[12] M. Cabaleiro, C. Suñer, H.S. Sousa, J.M. Branco, Combination of laser scanner and drilling resistance tests to measure geometry change for structural assessment of timber beams exposed to fire, J. Build. Eng. 40 (2021).

[13] D. Marranzini, G. Iovane, B. Faggiano, Methodology for the assessment of timber structures exposed to fire through NDT. In: 7th International Conference on Applications of structural fire engineering, Ljubljana, Slovenia (2021) 242-247.

[14] T.P. Nowak, J. Jasieńko, K. Hamrol-Bielecka, In situ assessment of structural timber using the resistance drilling method – Evaluation of usefulness, Constr. Build. Mater. 102 (2016) 403–415.

[15] B. Faggiano, M.R. Grippa, A. Marzo, F.M. Mazzolani, Experimental study for non-destructive mechanical evaluation of ancient chestnut timber, J. Civ. Struct. Heal. Monit. 1 (2011) 103–112.

[16] B. Faggiano, M.R. Grippa, B. Calderoni, Non-destructive tests and bending tests on chestnut structural timber, Adv. Mater. Res. 778 (2013) 167–174.

[17] A.O. Feio, P.B. Lourenço, J.S. Machado, Non-Destructive evaluation of the mechanical behavior of chestnut wood in tension and compression parallel to grain, Int. J. Archit. Herit. 1 (2007) 272–292.

[18] L. Acuña, L.A. Basterra, M.M. Casado, G. López, G. Ramón-Cueto, E. Relea, C. Martínez, A. González, Aplicación Del Resistógrafo a La Obtención De La Densidad Y La Diferenciación De Especies De Madera, Mater. Constr. 61 (2011) 451–464.

[19] P.B. Lourenço, A.O. Feio, J.S. Machado, Chestnut wood in compression perpendicular to the grain: Non-destructive correlations for test results in new and old wood, Constr. Build. Mater. 21 (2007) 1617–1627.

[20] B. Faggiano, F.M. Mazzolani, Combined non-destructive and destructive tests for the mechanical characterization of old structural timber elements, In: 3rd International Conference on Advances in Experimental Structural Engineering, San Francisco, California, USA (2009).

[21] M. Piazza, M. Riggio, Visual strength-grading and NDT of timber in traditional structures. J Build Apprais 3, (2008) 267–296.

[22] B. Faggiano, A. Marzo, A method for the determination of the timber density through the statistical assessment of ND transverse measurements aimed at in situ mechanical identification of existing timber structures, Constr. Build. Mater. 101 (2015) 1235–1240.

[23] A.O. Feio, P.B. Lourenço, J.S. Machado, Parallel to the grain beahviour and NDT correlations for chestnut wood *(Castanea sativa Mill.),* in: C. Modena, P.B. Lourenço, P. Roca (Eds.), Proceedings of the IVth Int. Seminar on Structural Analysis of Historical Constructions, Padova, Italy, 10-13 November, 2004, Taylor & Francis Group, London (2005), 369-375

Strength grading of timber in historic structures – methodology and practical application

G. Linke[1/2], W. Rug[2/3], and H. Pasternak[1]

[1] BTU Brandenburg University of Technology, Cottbus/Germany

[2] VHÖB Laboratory for timber construction and ecological building technology, Eberswalde/Germany

[3] HNEE University of Sustainable Development, Eberswalde/Germany

ABSTRACT

The retrofitting and redevelopment of existing structures is of great economic and social importance. A comprehensive assessment of the building's condition is an absolute prerequisite for professional interventions in existing load-bearing structures that do not damage the substance. The assessment of the existing load-bearing capacity is an essential part. The combination of visual and non-/semi-destructive testing methods has proven to be a promising approach. Basic requirements are already included in the drafts of international codes. However, concrete specifications for practical implementation are still missing. This paper presents a method for in situ strength grading. In addition to the basic methodological approach and definite specifications for its implementation, the practical application is presented using the example of tests in the laboratory and in situ.

KEYWORDS: historic timber structures, strength grading, ultrasonic time-of-flight measurement

INTRODUCTION – CURRENT STANDARDS FOR THE ASSESSMENT OF EXISTING TIMBER STRUCTURES

The redevelopment, preservation and future use of existing structures is of increasing economic, ecological and social importance. In order to ensure professional, substance-careful and economic interventions in existing constructions, a comprehensive assessment of the building condition is required. In the recent past, the latter has increasingly become the focus of research and standardization. For example, Italy, Switzerland and Austria published national codes for the assessment of existing structures - especially timber structures - in the period 2004-2013 (see [1]).
In 2015, the Joint Research Centre of the European Union published a first draft of a unified guideline for the assessment of existing structures, which is in line with the regulations of the Eurocodes (see [1, 2]). At the same time, the COST action IE0601 "WoodCultHer" developed a guideline for the assessment of the structural condition of historic timber structures (see [3]). The basic requirements of both guidelines have since been transferred into European standards (see [4, 5]). The essential procedure includes not only the assessment of the structural geometry, the present loads and influences and any possible damage, but also the determination of the existing material quality. However, the currently available international codes [4, 5] only specify general requirements. The material quality should usually be determined using the strength grading methods developed for new timber.

However the strict application of these methods is usually not possible in-situ (see [6]). In practice, therefore, in-situ strength grading is rarely carried out and then only visually and to a limited extent. Usually, the material capacity is only estimated and static calculations are carried out assuming an average load-bearing capacity. A reliable assessment of the material quality is thus not possible. Therefore, alternative approaches are necessary. The combination of a visual examination and non-destructive/semi-destructive testing methods is currently the general consensus (see [4, 5, 7]). However, concrete specifications for the application of an in-situ strength grading are still not available in the existing regulations.

METHODOLOGY FOR THE IN-SITU STRENGTH GRADING

From 2017 to 2021, a systematic study on the strength grading of timber members in existing structures was carried out at BTU/Cottbus, Germany in cooperation with HNEE & VHÖB/Eberswalde, Germany (see [8]). The aim was to develop a methodology for in situ strength grading based on the combined use of visual grading and selected NDTs/SDTs. For this purpose, approximately 900 specimen made from new spruce, pine and oak timber were examined in comparative material tests. These tests included the following test methods (for a detailed description of the applied methods see [9]).

- visual grading according to DIN 4074-1/-5 [10, 11],
- ultrasonic time-of-flight measurement with the Sylvatest Trio measuring device,
- determination of density on cuboid specimen, core drill samples and with the penetration depth method (test device: “wood pecker wood test hammer”)
- and destructive bending tests according to EN 408 [12].

On this basis, two methods for in situ strength grading have been investigated. The first approach was a grading procedure based on the ultrasonic time-of-flight measurement with limiting values for the grading criterion “ultrasonic velocity” (see [8, 9]). The sorting yield showed a significant improvement compared to visual sorting - especially in the strength classes C30/D30 according to EN 338 [13] and higher. However, the accordance between the estimation of the material quality and the load-bearing capacity determined in destructive tests was still comparatively low. The reason for this is, on the one hand, the relatively low correlation between the ultrasonic velocity and the strength and stiffness properties. On the other hand, the ultrasonic pulse time-of-flight measurement does not include the effects of relevant features that influence the load-bearing capacity - such as knots, slope of grain and cracks. From this it can be concluded that ultrasonic time-of-flight measurement is suitable in principle for strength grading, but should not be used alone.

As an alternative approach, the applicability of so-called grading parameters was investigated. These grading parameters are already used for the machine grading of new construction timber. However, the applicable European standards currently only take into account the natural frequency and the density (see [14]). Furthermore, the investigations by the authors have shown that the direct inclusion of the essential visually measurable growth characteristics is necessary for an accurate estimation of the material quality. Therefore, based on the results of the comparative material tests, grading parameters were derived using a multi-variate regression model.

This model enabled the simultaneous evaluation of the measurement results of several non- and semi-destructive test methods. Specifically, the visually measurable growth characteristics like knots, slope of grain and cracks as well as the measurement results of the ultrasonic time-of-flight measurement, the density calculated from the penetration depth and determined on drill core samples were included in the analysis. With regard to the ultrasonic time-of-flight measurement, the transmitted electrical stress

as an indicator for the signal attenuation and the dynamic modulus of elasticity were taken into account in addition to the measured ultrasonic velocity. The bending strength and the static modulus of elasticity served as target values.

In order to take the particularities of existing structures and the possible implementation of adjusted analysis methods into account the regression model was set up as a multi-level system (see Figure 1). The extent of the measurements and examinations to be carried out on-site depends on the state of preservation of the components or constructions, their degree of stress and importance for the entire structure, as well as on the conservation value. In general, less extensive investigations are required for subordinate structural components. The main structure and critical components, on the other hand, require a more detailed investigation. This offers the possibility to precisely plan and carry out the necessary investigations in situ. Depending on the extent of the knowledge gained from the strength grading, various adjustments of the verification methods can be made (see [15]).

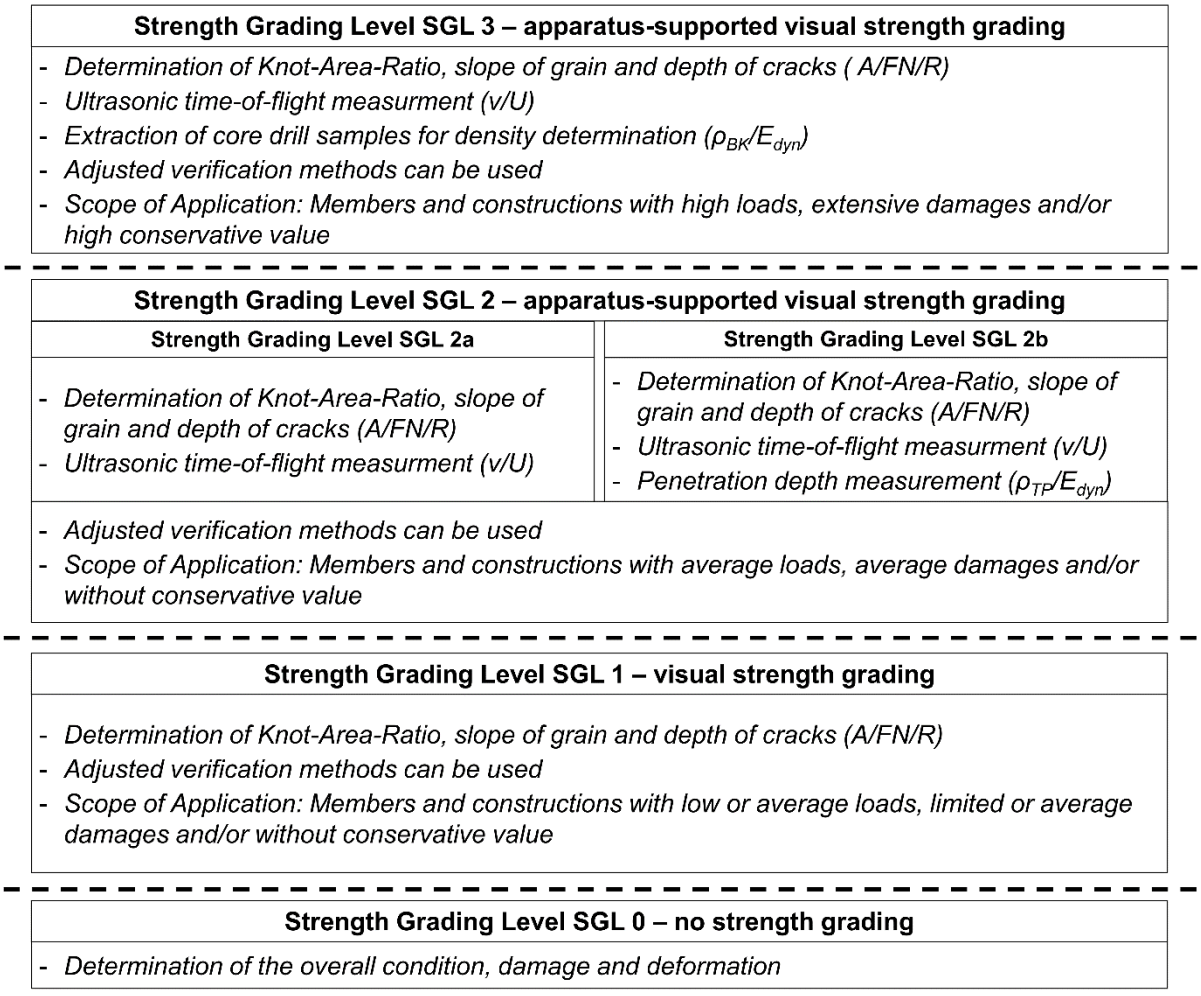

Figure 1: Schematic depiction of the methodology for in situ strength grading

RESULTS

The application of the in situ strength grading methodology to the sample material made from new construction timber showed that the material quality can be reliably estimated. The accordance between the assignment to the strength classes according to EN 338 [13] based on the developed grading method as well as based on the destructive bending tests was (86 ... 96) %.

In addition to the investigations described above, the strength grading methodology was applied in comparative material test on sample material from historical, partially deconstructed timber structures (see [16, 17] and Figures 2 & 3). In the course of this, it was determined that minor adjustments to the methodology are necessary with regard to the consideration of the load-bearing capacity-reducing growth and component characteristics.

Figure 2: Fichtenberg Oberschule, Berlin/Germany – left: exterior view; right: view on the historic roof construktion

Figure 3: Castle Friedenstein, Gotha/Germany – left: aerial view; right: view on the examined ceiling construction

The tests carried out on historic timber components showed that, regardless of the size of the features, their position in the component is also decisive for the load-bearing capacity. Knots, smaller defects, limited organic damage and superficial indentations and notches caused premature failure even if they were relatively small, provided they were located in the loaded area. If these circumstances are not taken into account, the agreement between the estimated and test-determined material quality is only (64 ... 79) %. About (10 ... 30) % of the components were overestimated.

In order to eliminate this deficit, the accuracy of the strength grading methodology was adjusted by means of correction factors. The use of a global factor in the range of k_{IP} = (0.80...0.95) resulted in a reduction of the overestimation to approx. (0 ... 23) %. At the same time the proportion of underestimated samples increased to approx. (5 ... 79) %. This does not represent an improvement in the accuracy and reliability of the results. Using a correction factor k_{vis} = (0.85...0.90) related to the individual case resulted in an overestimation of (7 ... 10) %. The agreement between the estimated and test-determined material quality was (78...85) %. This is acceptable from an engineering point of view. The application of the factor k_{vis} is recommended for components that have local weak points (i.e. predetermined breaking points) that are not included in the calculation of the grading parameter due to their characteristics or size. This is necessary, for example, in the case of knot accumulations, strong crack formation and unfavourable fibre inclinations in the tensile area - especially in the highly stressed

component sections, knots and knot accumulations in the area of load introduction, local cross-section weakenings (e.g. cuts/cervicals/etc.), and superficial damage to the edge fibres (e.g. axe notches).

Overall, the application of the proposed grading methodology represents a significant improvement compared to an exclusively visual grading. The examined sample material taken from historic timber structures was underestimated by (61 ... 69) % with regard to its material quality by an exclusively visual grading. Only (23 ... 28) % were assigned to the same strength class as on the basis of the destructive bending tests. This can result in considerable load-bearing capacity deficits, which in practice can lead to an unrealistic evaluation of the construction and thus to unprofessional, less substance-careful and uneconomical interventions in the existing constructions. This deficit can be significantly reduced by applying the proposed methodology for in situ strength grading. In the investigated constructions, reserves in the range of (17 ... 67) % related to the characteristic bending strength and (7 ... 27) % with regard to the mean value of the modulus of elasticity were found. The application of the proposed grading methodology is thus a significant improvement over the current practice in the assessment of present material quality in existing timber structures.

CONCLUSION

The study shows that the method for in situ strength grading derived from tests on new structural timber is suitable for the practical application. This conclusion is confirmed by the laboratory tests on wooden components from historical constructions. The existing uncertainties were considerably reduced with the help of additional safety factors, which take the influence of individual growth and structural characteristics on the fracture behaviour into account. The remaining uncertainties are acceptable from an engineering point of view. This is especially the case under consideration of the load-bearing reserves that can be determined and used in the assessment of the structural stability and for the planning of redevelopment measures.
However, the results also show that the grading process requires expertise in the load-bearing and fracture behaviour of timber members in order to evaluate the measurable parameters according to their structural position.
The results of the presented study are currently used to draft the framework for an application guideline. The implementation of the proposed method into the currently existing standards for the assessment of existing timber structures [4, 5] as part of a detailed on-site survey is possible.

ACKNOWLEDGEMENT

This research has been funded by private donations and supported by commitment of engineers of the Laboratory for timber construction and ecological building technology. Furthermore, the authors want to thank the Thuringian Palaces and Gardens Foundation, the Engineering offices Dr. Krämer and Trabert & Associates as well as the Senate Department for Urban Development and Housing of the City of Berlin for their support.

REFERENCES

[1] M. Loebjinski, G. Linke, W. Rug, H. Pasternak, Evaluation of existing timber structures – Current standards for the assessment and evaluation in Germany and Europe, in: J. M. Branco, H. M. Sousa, E. Poletti (eds.) Proceedings of the 5th International Conference on Structural Health Assessment of Timber Structures SHATIS, Guimaraes, Portugal, 25-27th September (2019) 884-893

[2] S. Dimova, A. Pinto, P. Luechinger, S. Denton (eds.), New European Technical Rules for the Assessment and Retrofitting of Existing Structures – Policy Framework, Existing Regulations and Standards, Prospect for CEN Guidance, Publications Office of the European Union, 2015.

[3] H. Cruz, D. Yeomans, E. Tsakanika, N. Macchioni, A. Jorrissen, M. Touza, M. Mannucci, P. Lorenço, Guidelines for the on-site assessment of historic timber structures, in: International Journal of Architectural Heritage: Conservation, Analysis and Restoration, Volume 9 (2015), Issue 3, 277-289

[4] CEN/TS 17440 (2020), Assessment and retrofitting of existing structures

[5] EN 17121 (2019), Conservation of cultural heritage – Historic timber structrues – Guidelines for the on-site assessment of load-bearing timber structures

[6] K. Lißner, W. Rug, Holzbausanierung beim Bauen im Bestand, 2nd ed., VDI Springer, Berlin, 2018

[7] J. Machado, M. Riggio, T. Descamps (eds.), State of the Art Report – Combined use of NDT/SDT methods for the assessment of structural timber members; Université de Mons, 2015

[8] G. Linke, W. Rug, H. Pasternak, Strength grading of structural timber in existing structures with the ultrasonic time-of-flight measurement, in: J. M. Branco, H. M. Sousa, E. Poletti (eds.), Proceedings of the 5th International Conference on Structural Health Assessment of Timber Structures SHATIS, Guimaraes, Portugal, 25-27th September (2019) 589-598

[9] G. Linke, W. Rug, H. Pasternak, Strength grading of structural timber in existing structures – Study on the Apparatus Supported Grading with the ultrasonic time-of-flight measurement, in: I. Vayas, F. M. Mazzolani (eds.), Proceedings of PROHITEC 2021 Protection of Historical Constructions, Athens, Greece, 25-27th October (2021) 3-19

[10] DIN 4074-1 (2012), Strength grading of wood – Part 1: Coniferous sawn timber

[11] DIN 4074-5 (2008), Strength grading of wood – Part 5: Sawn hard wood

[12] EN 408 (2012) – Timber structures – Structural timber and glued laminated timber – Determination of some physical and mechanical properties

[13] EN 338 (2016) – Structural timber – Strength classes

[14] EN 14081-2 (2018) – Timber structures – Strength grading structural timber with rectangular cross section – Part 2: Machine grading; additional requirements for type testing

[15] M. Loebjinski, W. Rug, H. Pasternak, Redevelopment of a wooden roof construction under preservation order, in: J. M. Branco, H. M. Sousa, E. Poletti (eds.), Proceedings of the 5th International Conference on Structural Health Assessment of Timber Structures SHATIS, Guimaraes, Portugal, 25-27th September (2019) 912-921

[16] G. Linke, W. Rug, H. Pasternak, In-situ-Festigkeitssortierung von Holzbauteilen in bestehenden Konstruktionen – eine Fallstudie, in: U. Kuhlmann, et al. (eds.), 9. Doktorandenkolloquium Holzbau Forschung + Praxis, Stuttgart, Germany, 10-11th March (2022) 139-146

[17] N. Luxor, G. Linke, H. Pasternak, New procedure for timber in heritage buildings – the case study of Castle Friedenstein, Gotha (Germany), in: 20th International Forum on World Heritage and Ecological Transition, Naples/Capri, Italy, 8-10th September (2022)

Microstructural analysis of the wood cell wall under radial compression

Carlos Ulloa[1], Carlos F. Guzmán[1], Juan Carlos Pina[1], Erick I. Saavedra Flores[1] and Sergio J. Yanez[1]

[1]University of Santiago of Chile (USACH), Faculty of Engineering, Civil Engineering Department, Chile.

ABSTRACT

The behavior of wood when is subjected to radial compression is characteristic of regular honeycomb structures and four stages can be distinguished: elastic response, elastic micro-buckling, plateau stage and densification. Hence the wood cell collapse is a gradual process. However, significant non-linearities such as large deformations, cell wall micro-buckling, and internal self-contacts require high accuracy from the computational models. In this work, a numerical model is developed to study the behavior of wood cell walls subjected to radial compression under quasi-static implicit analysis. The model consists of a regular honeycomb structure confined in a box subjected to in-plane compression, with different number of cells. The model parameters (contact and solution options) are adjusted, and the efficiency of the model is studied. This model is validated with numerical results obtained from the literature. Finally, using the previous procedure, the microstructural behavior of Chilean radiata pine wood subjected to radial compression is studied using an idealized regular geometry, with geometric parameters and elastic mechanical properties of *early*- and *late*-wood obtained from literature.

KEYWORDS: Wood cell, radial compression, nonlinear analysis, microstructural wood

INTRODUCTION

The advantages of wood as a structural material have made possible to improve certain structures, mainly due to its outstanding axial stiffness-to-weight and strength-to-weight ratios, which are comparable with that of the strongest steels [1]. The combined high porosity and exceptional mechanical properties of wood appear to have their basis in its micro-structural features [2]. Despite these features and due to the mechanical complexity of wood, many timber design rules are still based on an empirical background [3]. The most common cause of failure is related to structural design [4], which can be attributed to material failure, environmental effects or structural integrity [5]. In dowel type of connections, it is challenging to describe the stress transfer given the reduction of the wood cross section, the eccentricities of the connections, the anisotropic behavior of wood and the existence of a post-elastic behavior in the direction perpendicular to the grain (radial direction)[4]. Therefore, the improvement of the design standards is strongly related to the understanding of ductile/brittle behavior of wood when it is subjected to significant stresses. In particular, three regions can be identified when softwood is compressed in the radial direction, as shown in Figure 1. The elastic region, characterized by a linear and reversible process until the yield point is reached, related to the instant where cell wall collapses. After the yield point, a *plateau* region appears due a progressive failure of *early*-wood cell rows that continues until all the *early*-wood cells and the weak cells in the transition zone, between *early*- and *late*-wood, have collapsed. Finally, the densification region is characterized by a sharp increase of the stress after all *tracheids* are completely buckled, collapsed and folded. Yielding is of particular interest for engineers as marks the departure from linear-elastic constitutive equations. In order to characterize this point, both anatomical features and physical properties at the mesoscale must be considered. In stretch dominated situations, the yield in the force-deformation curve is reached in

the instant of first cell wall buckling [6]- determined the yield point from the critical Euler buckling load of the first wood cell behind the annual ring border. In [7], the authors showed that the characterization of the yield point depends more on its cell wall thickness and radial width of the cell wall than on density. More evidence regarding yielding at the microstructural level is given by Scanning Electron Microscopy (SEM) measurements for different wood specimens. For instance, [8] observed, for coniferous wood specimens (*Chamaecyparis obtusa*, *Cryptomeria japonica* and *Pinus thunbergii*), that the failure occurs in the first rows of earlywood *tracheids*. [9] observed, for softwood (*Picea glauce* and *Pinus banksiana*), that the first collapse occurs at a location with minimum cell-wall thickness and density. To simulate the mechanical behavior through numerical models, the use of phenomenological equations requires adjusting the material parameters through a fit of the experimental data, as described in [10]. In contrast, microstructural modeling depends on the definition of the boundary conditions and a reasonable estimation of the geometric and mechanical parameters of the microstructure, which can be obtained from SEM images [11], multiscale modeling [12], or study the influence of the mechanical and geometric parameters in the microstructural response [13]. In summary, both types of models can describe the behavior of wood subjected to radial/transverse compression. Due to the existence of geometric and mechanical parameters of timber at different length scales and, in turn, the absence of micro-experimental results when subjected to radial compression, the main focus of this work is the development of a numerical tool capable to describe the latter. Specifically, the goal is to study the behavior of the microstructure of wood subjected to radial compression for *early*- and *late*-wood configurations, using computational simulations.

METHODOLOGY

The irregular hexagonal shaped-tubes cells of the microstructure of soft-wood allows the idealization of the geometry as a regular honeycomb structure. In this way, hexagonal lattices can exhibit a complex behavior depending upon their mechanical and geometric properties, which can be bending- or stretch-dominated, as shown in Figure 1.

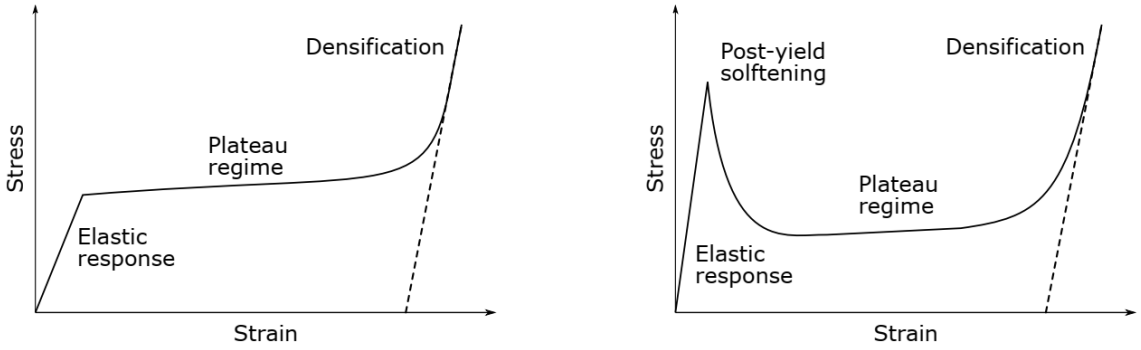

Figure 1: Behavior of honeycomb lattice subjected to in-plane compression. Adapted from [14].

The methodology and the numerical simulations developed by [15] are taken as a reference to develop the numerical model of hexagonal lattice with different configuration of number of cells. These configurations are subjected to in-plane compression, except for single cell case. To determine the number of cells necessary to obtain a representative behavior of the microstructure of softwood, it is necessary to simulate an increasing number of cells until the behavior corresponds to the desired experimental observations [10]. The commercial finite element software ANSYS [16] has been used to perform the numerical simulations. Plane-stress theory is considered through a quadratic plane element PLANE183 to model the honeycomb configuration. Also, the effect of large deflections is considered in the analysis using the NLGEOM option. For the bifurcation problem, the arc length method allows to find the fundamental modes of deformation [15].

Validation

Two cases are considered for validation: the behavior of regular lattice structures confined in a box [15] and the behavior of the microstructure of wood subjected to radial compression [12]. The material model used in this numerical validation corresponds to an adaptation of the Ogden hyperelastic model [15], which can be written as follows,

$$W = \sum_{i=1}^{N} \frac{\mu_i}{\alpha_i} \left(\bar{\lambda}_1^{\alpha_1} + \bar{\lambda}_2^{\alpha_2} + \bar{\lambda}_3^{\alpha_3} - 3 \right) + \sum_{k=1}^{N} \frac{1}{d_k} (J-1)^{2k}$$

where $\bar{\lambda}_i$ $(i = 1, 2, 3)$ represents the deviatoric principal stretches, μ_i and d_k are material constants related with shear modulus and bulk modulus, respectively. α_i is a material parameter and J is the determinant of the deformation gradient tensor. The hyperelastic material parameters used in the modeling are $N = 2$, $\mu_1 = \mu_2 = 100$ GPa and $\alpha_1 = \alpha_2 = 1.3$. The number of nodes, elements and the normalized compute time with respect to 5-cell model for each case is presented in Table 1.

Table 1: Number of nodes, elements and normalized computing for each case.

Case	Number of nodes	Number of elements	Normalized time
1 cell	1 344	384	0.55
5 cells	5 324	1 536	1.00
39 cells	32 154	9 398	2.24
105 cells	81 224	23 728	10.51

For the case of one cell in Figure 2a, it is possible to observe a clear nonlinear evolution up to the point of internal self-contact, where the stiffness of the model increases abruptly. For the case of 5 and 39 cells, the results obtained are presented in Figure 2b and Figure 2c, where a linear response can be observed in the first level of deformation due to the elastic deformation of the horizontal cell wall until reaching a drop due to stiffness failure given by a buckling effect (post-yield softening), as shown in the Figure 2. This drop decreased as the number of cells increased [15]. The plateau stage corresponds when all cells wall buckle and continues in compression until the internal self-contact begins, normal reaction increases sharply. Compared to Figure 1, the behavior of these two configurations can be assumed to be a stretch-dominant behavior. For the case of 105 cells in Figure 2d, it can be observed that similar to the two previous cases, there is a linear response in the first level of deformation, but a smooth transition between the elastic and plateau zones, *i.e.*, the post-yield softening is minimal for this configuration.

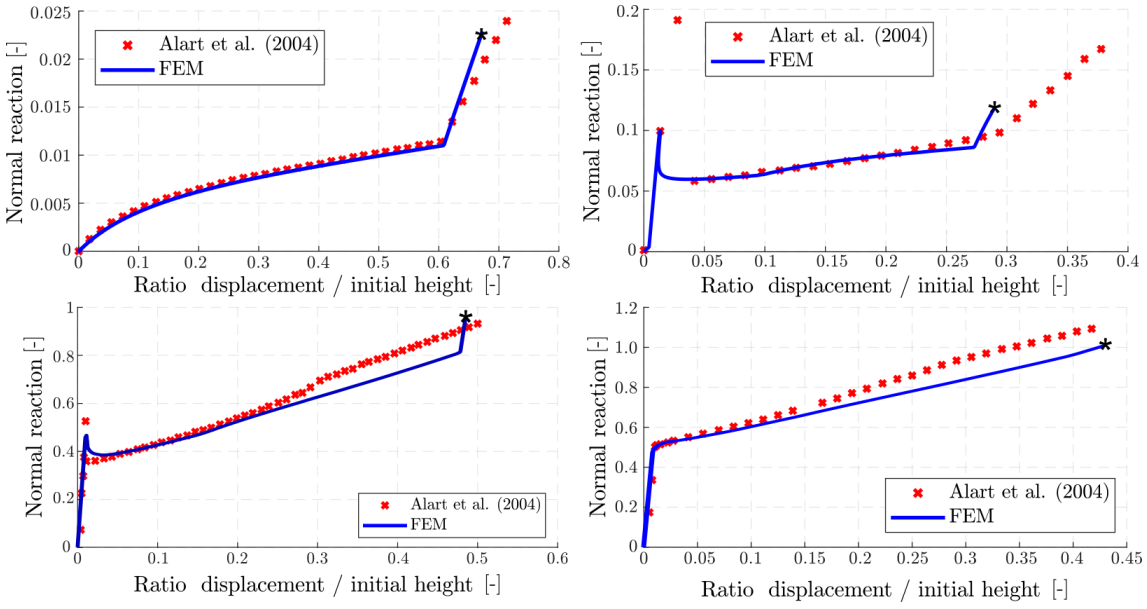

Figure 2: Reaction force versus compression ratio for different configurations.

In general, except for the post self-contact point, the model presents a similar response to that simulated by [15], where the main differences are found in the existence of increase of stiffness in the plateau region due to friction between the box and the cell wall. Then, the microstructural model simulates the stretch or bending dominated behaviors of the lattice structures. In addition, the smooth transition between the elastic and plateau zone previously observed can help to study the behavior of softwood subjected to radial compression and avoid the post-yield effect.

[12] developed a finite element model in ABAQUS using the solid C3D8R element with reduced integration. The regular hexagonal honeycomb lattice confined in a box, to represent the continuity of the microstructure of softwood along the *radial* and *tangential* directions, has a unit element size length equal to 23.094 µm and thickness equal to 5 µm. The total number of nodes and elements considered is 114 099 and 33 356, respectively. A linear isotropic material is considered, with a Young's modulus, density and Poisson's ratio equals to $E = 5.84$ GPa, $\rho = 1490$ kg/m^3 and $\nu = 0.4$, respectively. Unlike the solid model considered by [12], plane-strain hypothesis is considered in the model. The solution parameters considered are similar than the previous validation.

The results obtained are presented and compared with [12] in Figure 3a and Figure 3b, where the elastic and plateau zone can be clearly identified. The elastic stiffness obtained in the model is equal to 89.23 MPa, while the elastic stiffness obtained from [12] is equal to 82.10 MPa (15.6% difference). This difference can be attributed to the presence of shear bands deformation in the original model, which are not captured in the current model at the same level of deformation. As shown in Figure 3a, the transition between the elastic to plateau zone is smooth, i.e. there is no post-yield softening. Likewise, the curve in the plateau zone does not present oscillations, as can be seen in the curve of [12]. The presence of these oscillations is probably due to the convergence of the explicit model under a constant rate displacement. The current model does not converge at 40% approximately of the compression ratio due to the non-linearity of the problem, specifically, when the internal self-contact occurs, as shown in Figure 3b.

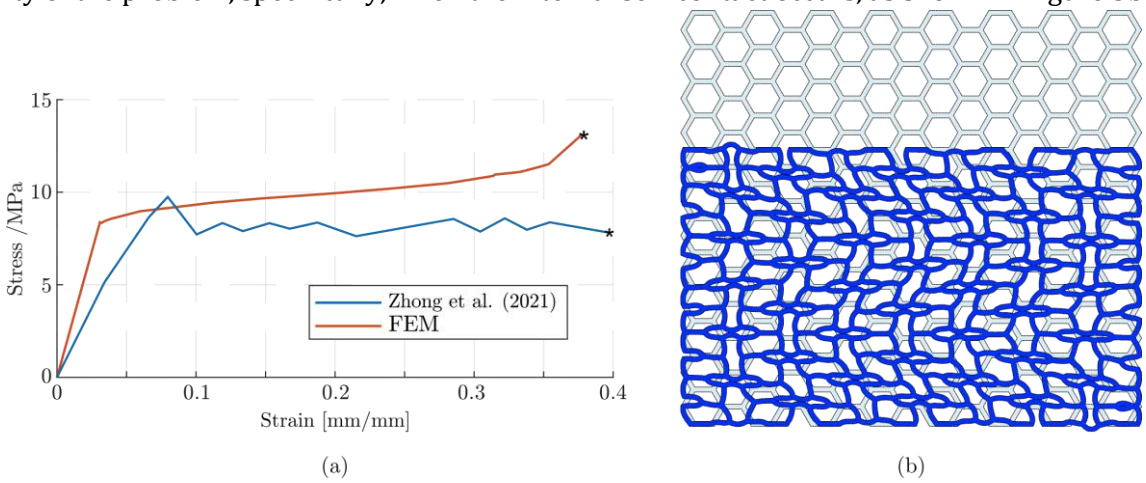

Figure 3: (a) Stress versus strain ratio of the lattice structure (b) maximum deformation at the star (*) point.

Radiata pine cell-wall analysis

The idealized softwood microstructure has been modeled using plane-strain theory with linear elastic material, where the mechanical parameters for *early*- and *late*-wood are obtained from an homogenization methodology described in [17]. Thus, the mechanical properties of the cell wall are defined as $E = 8.27$ GPa, $\nu = 0.4$, $\rho = 446.2$ kg/m^3. In the same way, the geometrical parameters of microstructure of radiata pine for *early*-wood are 40 μm, 30 μm and 4.3 μm for radial, tangential and cell wall thickness dimensions, and for *late*-wood the radial, tangential and cell wall thickness dimensions are 31 μm, 25 μm and 8 μm, respectively. These values are obtained taken the weakest and strongest parameters to model the *early*- and *late*-wood, respectively.

The numerical model considers a configuration of 8×12 cells (173 cells in total) for both cases confined in a box with imposed displacement at top of the mode. It is expected that for a sufficiently large model,

the post-yield softening may not be appreciated in the response. The solution parameters are the same as the other models. The number of total nodes and elements for both cases are similar 130 884 and 38 272, respectively.

The stress-compression ratio graph and deformed model are presented in Figure 4, where a small elastic and a plateau zone can be distinguished for both models. The response of *early*-wood is weaker than *late*-wood, as supposed before due to the geometrical parameters (and consequently, the density) considered of each model. Also, the transition between elastic to plateau zones is smooth, then, according to Figure 1, both numerical results respond to a bending-dominated behavior, which is expected for microstructure of wood under radial compression behavior based on experimental observations [20].

In addition, a higher level of deformation is captured in the *early*-wood model compared to *late*-wood model. This is due to its lower stiffness, which produces a lower level of stress and lateral pressure in the contact defined between external cell walls and the defined boundary box.

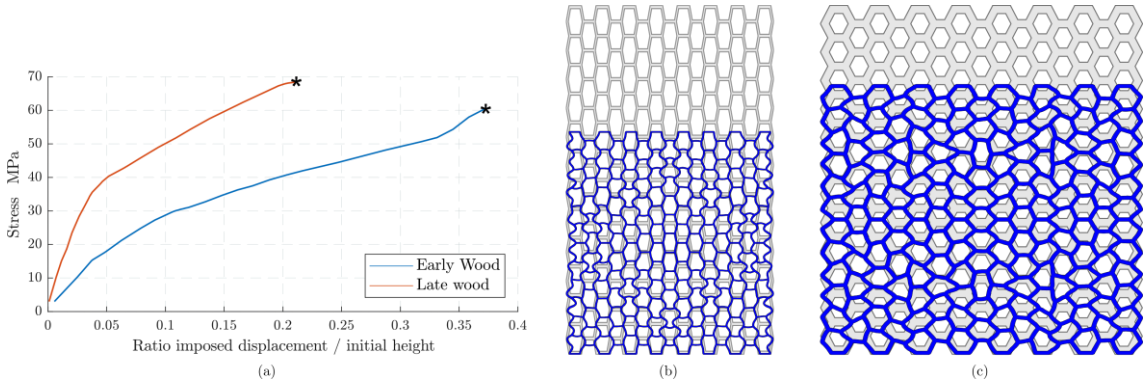

Figure 4: (a) Stress versus compression ratio results for numerical model of radiata pine microstructure. And maximum deformation for (b) early-wood and (c) late-wood.

Conclusions and perspectives

A numerical model of a regular honeycomb structure has been developed to simulate the behavior of the microstructure of radiata pine under radial compression, which is achieved through a methodological validation of the behavior of hexagonal lattices subjected to in-plane compression and a numerical validation of the microstructure of softwood. In the case of methodological validation, the numerical model can obtain stretch- or bending-dominated behavior satisfactorily, in addition to reaching high levels of deformation until the densification zone. In the same fashion, a numerical validation for the behavior of wood under low load levels has been carried out, obtaining a qualitatively good approximation of the elastic and plateau region. However, considering the geometry of radiata pine for *early*- and *late*-wood, the model presents difficulties to achieve high levels of deformations, mainly due to the high internal stiffness and convergence problems of the implicit analysis. This can be seen in the levels of deformation reached in *early*-wood compared to *late*-wood. Further work will focus on incorporating options available in ANSYS that will allow handle local instabilities, as well as the inclusion of the mechanical properties of the different wood layers, to study their influence on the macroscopic response.

Acknowledgements

C.F. Guzmán acknowledges the financial support from the Chilean National Agency for Research and Development (ANID), Fondecyt research project No. 11200638.

REFERENCES

[1] M. F. Ashby, L. J. Gibson, U. Wegst, and R. Olive, “The mechanical properties of natural materials. I. Material property charts,” *Proc. R. Soc. Lond. Ser. Math. Phys. Sci.*, vol. 450, no. 1938, pp. 123–140, Jul. 1995, doi: 10.1098/rspa.1995.0075.

[2] Q. Deng, S. Li, and Y. Chen, “Mechanical properties and failure mechanism of wood cell wall layers,” *Comput. Mater. Sci.*, vol. 62, pp. 221–226, Sep. 2012, doi: 10.1016/j.commatsci.2012.05.050.

[3] E. I. S. Flores, K. Saavedra, J. Hinojosa, Y. Chandra, and R. Das, “Multi-scale modelling of rolling shear failure in cross-laminated timber structures by homogenisation and cohesive zone models,” *Int. J. Solids Struct.*, vol. 81, pp. 219–232, Mar. 2016, doi: 10.1016/j.ijsolstr.2015.11.027.

[4] V. Karagiannis, C. Málaga-Chuquitaype, and A. Y. Elghazouli, “Modified foundation modelling of dowel embedment in glulam connections,” *Constr. Build. Mater.*, vol. 102, pp. 1168–1179, Jan. 2016, doi: 10.1016/j.conbuildmat.2015.09.021.

[5] J. A. J. Huber, M. Ekevad, U. A. Girhammar, and S. Berg, “Structural robustness and timber buildings – a review,” *Wood Mater. Sci. Eng.*, vol. 14, no. 2, pp. 107–128, Mar. 2019, doi: 10.1080/17480272.2018.1446052.

[6] U. Müller, W. Gindl, and A. Teischinger, “Effects of cell anatomy on the plastic and elastic behaviour of different wood species loaded perpendicular to grain,” *IAWA J.*, vol. 24, no. 2, pp. 117–128, Jan. 2003, doi: 10.1163/22941932-90000325.

[7] L. J. Gibson and M. F. Ashby, *Cellular Solids: Structure and Properties*, 2nd ed. Cambridge: Cambridge University Press, 1997. doi: 10.1017/CBO9781139878326.

[8] K. Ando and H. Onda, “Mechanism for deformation of wood as a honeycomb structure I: Effect of anatomy on the initial deformation process during radial compression,” *J. Wood Sci.*, vol. 45, no. 2, pp. 120–126, Apr. 1999, doi: 10.1007/BF01192328.

[9] T. Tabarsa and Y. H. Chui, “Stress-Strain Response of Wood Under Radial Compression. Part I. Test Method and Influences of Cellular Properties,” *Wood Fiber Sci.*, vol. 32, no. 2, Art. no. 2, 2000.

[10] C. Huang, Y. Chui, M. Gong, and F. Chana, “Mechanical behaviour of wood compressed in radial direction: Part II. Influence of temperature and moisture content,” *J. Bioresour. Bioprod.*, vol. 5, no. 4, pp. 266–275, Nov. 2020, doi: 10.1016/j.jobab.2020.10.005.

[11] Y. E. Aimene and J. A. Nairn, “Simulation of transverse wood compression using a large-deformation, hyperelastic–plastic material model,” *Wood Sci. Technol.*, vol. 49, no. 1, pp. 21–39, Jan. 2015, doi: 10.1007/s00226-014-0676-6.

[12] W. Zhong, Z. Zhang, X. Chen, Q. Wei, G. Chen, and X. Huang, “Multi-scale finite element simulation on large deformation behavior of wood under axial and transverse compression conditions,” *Acta Mech. Sin.*, Jul. 2021, doi: 10.1007/s10409-021-01112-z.

[13] A. Da Silva and S. Kyriakides, “Compressive response and failure of balsa wood,” *Int. J. Solids Struct.*, vol. 44, no. 25–26, pp. 8685–8717, 2007, doi: 10.1016/j.ijsolstr.2007.07.003.

[14] F. Ongaro, “Estimation of the effective properties of two-dimensional cellular materials: a review,” *Theor. Appl. Mech. Lett.*, vol. 8, no. 4, pp. 209–230, Jul. 2018, doi: 10.1016/j.taml.2018.04.010.

[15] P. Alart, M. Barboteu, and J. Gril, “A numerical modelling of non linear 2D-frictional multicontact problems: application to post-buckling in cellular media,” *Comput. Mech.*, vol. 34, no. 4, pp. 298–309, Sep. 2004, doi: 10.1007/s00466-004-0574-0.

[16] ANSYS Inc, *ANSYS Parametric Design Language Guide. Release 2021 R2*. Canonsburg, PA, 15317, 2021. [Online]. Available: http://www.ansys.com

[17] E. I. Saavedra Flores, R. M. Ajaj, I. Dayyani, Y. Chandra, and R. Das, “Multi-scale model updating for the mechanical properties of cross-laminated timber,” *Comput. Struct.*, vol. 177, pp. 83–90, Dec. 2016, doi: 10.1016/j.compstruc.2016.08.009.

EXPERIMENTAL CHARACTERIZATION OF BEECH THROUGH TENSILE AND BENDING TESTS

Carlos Martins[1,2], Cláudio Ferreira[1], Vanesa Baño[3] and Alfredo Dias[1,2]

[1] SerQ – Forest Innovation and Competences Center, Sertã, Portugal,

[2] University of Coimbra, ISISE, Department of Civil Engineering, Coimbra, Portugal

[3] CESEFOR Foundation, Soria, Spain

ABSTRACT

The use of hardwood species is increasing significantly through all over the world, mostly due to the demand for engineered wood products such as glulam and Cross Laminated Timber (CLT). However, and despite the demand and the present knowledge about the mechanical properties of boards under bending stresses, the trend of assessing timber mechanical properties at industrial level is by tensile tests. In Spain, Beech wood (*Fagus sylvatica* L.) is visually graded in the sawmills under aesthetic requirements in two qualities, first and second. First quality is mainly used for furniture, being the second one used for charcoal and fuel wood. The present paper aims to access the mechanical properties from second quality Beech wood from Spain to be used for structural applications, (e.g. glulam). A non-destructive characterization was performed based on longitudinal vibration method followed by tensile and bending tests which were performed to determine modulus of elasticity, 12100 MPa in tension and 13200 MPa in bending, tensile strength 63.5 MPa and bending strength 61.5 MPa (mean values). Linear regression analysis was performed between properties. Despite the aesthetical issues, second quality of Beech wood from Spain could be clearly considered for structural purposes.

KEYWORDS: Beech, Tension strength, Bending strength, Modulus of elasticity, Machine grading

INTRODUCTION

The increasing demand of wood for construction sector is facing new trends, namely the use of hardwoods. Beech is one of the most important and widespread hardwood species in Europe, also being present in Iberian Peninsula, specifically in Northern Spain [1]. A large number of applications are well established, being the use for furniture the main application for beech sawn wood of first quality in Spain. The potential of using it for structural products such as glulam [2] and CLT [3] has been demonstrated in Central Europe. In Spain, two "quality grades" are available being the 2nd quality a low added value raw material, defined by a darker reddish colour.

The use of non-destructive tools for grading structural sawn-wood has been widely used for softwoods and recently also for hardwoods and could be a solution to increase the use of 2nd quality of Spanish beech for structural applications. Several techniques are commercially available with different configurations and ways of achieving the indicative property named dynamic modulus of elasticity (E_{dyn}). Recent studies as the one carried by Kovryga et al. [4] focused on the accuracy of ultrasound wave

propagation (US) and longitudinal stress wave (LSW) to predict the mechanical properties of several hardwoods (European beech, European ash, European oak and maple) in bending and tension.
The prediction accuracy of static modulus of elasticity is higher than strength, where correlation coefficients for bending could vary between 0.4 and 0.6 [5], [6] whereas for tension strength are below 0.50 [4].
The present study aims to provide relevant information regarding the mechanical properties of beech from Spanish origin (2nd quality) throughout the use of LSW method. Thus, an undervalued raw-material can be easily selected for other applications such as glulam.

METHODOLOGY

Sample and non-destructive characterization

A total sample of 640 boards from 2nd quality of beech species was provided by Ademan to SerQ (Portugal) and Cesefor (Spain) within the scope of Eguralt project. Mid of the sample was stored at SerQ laboratory and mid at the Cesefor facilities for the assessment of dimensions. Thickness and width were measured at mid-length and both ends whereas moisture content was recorded by electrical moisture meter at mid-length and 0.6 m from both ends according to EN 13183-2 [7]. Also the length and weight were measured. This data was considered as input for the non-destructive characterization of each board, being adopted longitudinal vibration method to access the frequency and dynamic modulus of elasticity (E_{dyn}). Each board was simply supported avoiding external vibrations through the use of a neoprene sheet between support and specimens and MTG device was used. The device only requires access to one end of the element to be tested (both stress wave activator and detector are located at the same device). The device commutes with laptop software through Bluetooth interface.
The tensile sample (46 boards) had a cross section of 30 mm x 121 mm x 2814 mm (mean values) (thickness x width x length) and the bending sample of 30 mm x 120 mm x 2811 mm (mean values). Density had a mean value and standard deviation of 675±32.6 kg/m^3 for tensile sample and of 708±31.5 kg/m^3 for bending sample. A mean value of 12687 MPa (varying between 8491 MPa and 17131 MPa) was recorded for dynamic modulus of elasticity for tensile and of 13551 MPa (varying between 9335 MPa and 17430 MPa) for bending. After non-destructive tests a set of 46 boards in SerQ and 40 boards in Cesefor were selected for tensile and bending tests, respectively, based on the distribution of E_{dyn} values of the entire sample.

Mechanical tests

Tension tests

Tension tests of structural elements followed EN 408 (Figure 1), namely a clear test length of 9 times the larger cross-sectional dimension. The length of machine grips was 500 mm at each end. To fulfil these requirements each board was cut and non-destructive tests were applied to final length previously to static tests. For modulus of elasticity in tension parallel to grain ($E_{t,0}$) determination, the deformation over a length of 5 times the width was measured and two linear transducers of 25 mm maximum capacity were used, one per each side of the board (Figure 1), Tension strength parallel to grain ($f_{t,0}$) was determined considering that the load was applied with a constant loading-head movement in order to achieve maximum load within 300±120 s.
After each failure test, the failure mode was recorded and the moisture content of each board was determined following the so called oven-dry method, following the EN 13183-1 [8] through a sample free of defects and full cross-section. 56% of the failures were longitudinal, 26% were transversal and 22% were mixed failures. From the full sample, 22% of the failures were conditioned by the presence of knots. Table 1 summarizes the results from tension tests.

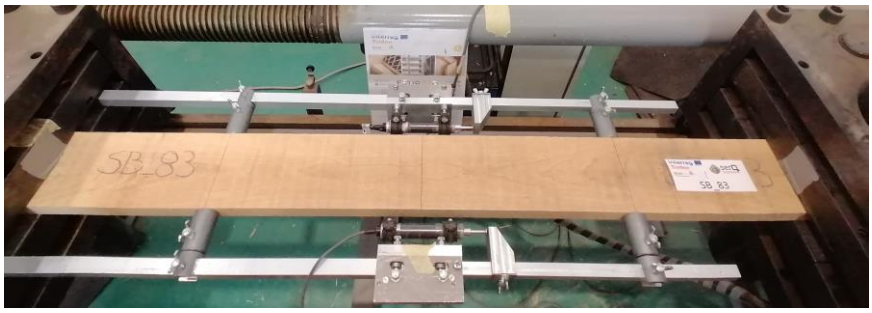

Figure 1: Layout of tensile test in SerQ from beech board

Bending tests

4-point bending tests of structural elements were made according to EN 408 (Figure 2). The span of the boards was 18 times the larger cross-sectional dimension and the load was applied over 6 times the larger cross-sectional dimension. For global modulus of elasticity in bending ($E_{m,0}$) determination, the global deformation over a length of 18h was measured using a linear transducers of 50 mm maximum capacity, (Figure 2). Bending strength (f_m) was determined considering that the load was applied with a constant loading-head movement to achieve maximum load within 300±120 s. In addition, non-destructive tests, using an accelerometer, were applied to the total length of the boards previously to static tests to measure the longitudinal natural frequency (Figure 3). As in the case of tensile tests, after each failure test, the failure mode was recorded, and the moisture content of each board was determined following the so called oven-dry method through a sample free of defects and full cross-section. 15% of the failures occurred by a knot. Table 2 summarizes the results from bending tests.

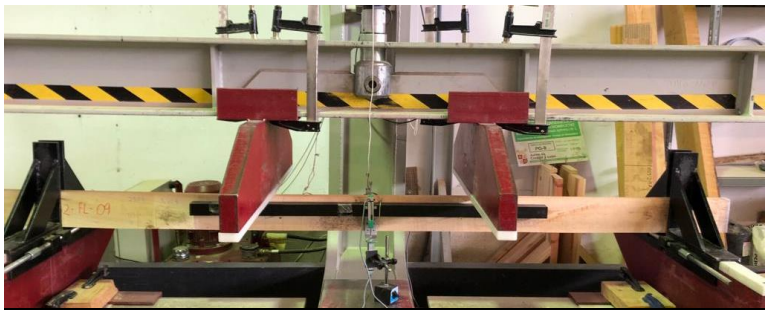

Figure 2: Layout of bending test in Cesefor from beech board

Figure 3: Layout of non-destructive testing to measure the longitudinal natural frequency

RESULTS

Mechanical properties from bending and tension tests

Table 1 gather the values obtained for the entire set of tests performed within the sample from tension characterization, namely: density from a piece free of defects (ρ); moisture content (w); dynamic modulus of elasticity with its test length (E_{dyn}); static modulus of elasticity in tension parallel to grain ($E_{t,0}$) and tension strength ($f_{t,0}$). Based on EN 384 [9] adjustments to the values from density and static modulus of elasticity were performed for a moisture content of 12% ($\rho_{12\%}$ and $E_{t,0\_12\%}$, respectively).

Also the tension strength was adjusted to a reference width of 150 mm ($f_{t,0\_adj}$). Adjusted values are also presented in Table 1.

Table 1: Non-destructive, physical and mechanical properties (46 tension tests)

Property	ρ **(kg/m³)**	W **(%)**	E_{dyn} **(MPa)**	$E_{t,0}$ **(MPa)**	$f_{t,0}$ **(MPa)**	$\rho_{12\%}$ **(kg/m³)**	$E_{12\%}$ **(MPa)**	f_{t_adj} **(MPa)**
Average	671	15.4	12687	12776	66.3	660	13199	63.5
Minimum	613	14.4	8491	7327	20.7	603	7580	19.8
Maximum	770	16.9	17131	17862	115.9	758	18510	111.1
COV (%)	5.3	3.6	18.2	21.7	39.2	5.2	21.5	39.2

Results from bending tests are listed at Table 2, namely: density from a piece free of defects (ρ); moisture content (w); dynamic modulus of elasticity (E_{dyn}); static modulus of elasticity in bending parallel to grain ($E_{m,0}$) and bending strength ($f_{m,0}$). Adjustments to the values from density and static modulus of elasticity were performed for a moisture content of 12% ($\rho_{12\%}$ and $E_{m,0\_12\%}$, respectively). Also the bending strength was adjusted to a reference depth of 150 mm ($f_{m,0\_adj}$). Adjusted values are also presented in Table 2.

Table 2: Non-destructive, physical and mechanical properties (38 bending tests)

Property	ρ **(kg/m³)**	W **(%)**	E_{dyn} **(MPa)**	$E_{m,0}$ **(MPa)**	$f_{m,0}$ **(MPa)**	$\rho_{12\%}$ **(kg/m³)**	$E_{12\%}$ **(MPa)**	f_{m_adj} **(MPa)**
Average	694	15.9	13551	11666	64.3	680	12113	61.5
Minimum	624	14.8	9335	7166	25.7	612	7477	24.6
Maximum	783	17.3	17430	14999	97.4	766	15572	92.2
COV (%)	5.3	3.8	14.1	16.1	27.3	5.2	15.8	27.3

Results (mean values) from bending tests of 2nd quality Spanish beech showed lower properties when compared with European beech [4], between 5% (E_{dyn}) and 17% ($E_{12\%}$). For tension tests the trend was similar except for tension strength where the present study had a mean value 32% higher. It is also possible to state that the results from the present study are similar to other hardwoods like ash, maple and oak, especially for bending. For tension, static modulus of elasticity values was lower, but higher if tension strength is considered. Chestnut is also a hardwood which has been considered for structural applications. Aicher et al. [10] reported 12500 MPa as mean value for static modulus of elasticity in tension and a similar value (12300 MPa) was reported by Vega et al. [11] as mean value static modulus of elasticity in bending for Spanish chestnut.

A species to be used for structural applications requires the knowledge about the mean values of stiffness and density as well as characteristic values of strength and density. EN 14358 [12] presents a parametric calculation for initial type testing for characteristic properties determination, which was considered both for tension and bending tests. Regarding tension tests, characteristic values of 597 kg/m³ and 25.2 MPa were calculated for density and tension strength respectively. Similar value of characteristic density was obtained for bending sample (615 kg/m³) whereas for bending strength the characteristic value was 32.1% higher (33.4 MPa). Results from the present study showed that beech had higher mechanical properties than chestnut, namely 13% higher in tension strength [10] (characteristic value of 22.3 MPa) and 19% higher in bending strength [11] (characteristic value of 28 MPa).

Assignment of strength class

According to EN 338 [13] a population may be assigned to a strength class based on the determined values of density, modulus of elasticity and strength. For softwoods, the standard defines both bending and tension strength classes whereas for hardwoods tension strength classes are not yet defined. Thus, based on bending sample a D30 class could be assigned (defined by bending strength), lower class when compared to strength class defined in EN 1912 [14] for German beech (D35 and D40). However, if compared with other European hardwoods, the same strength class from Spanish beech (2nd quality) was obtained in relation to oak and maple, both D30 [14] and higher strength class than chestnut from Italy (D24) [14] and from Spain (D24) [11].

In terms of tensile strength classes, a proposal was presented by Kovryga et al. [4] for medium-dense hardwoods (e.g. beech and ash), named DT-classes (D - Deciduous and T - Tension), based on an extended campaign of tensile and bending tests. Regarding that proposal, the sample analysed in the present study could be assigned to a DT25 class where the characteristic tensile strength was the conditioning property.

Prediction of mechanical properties using longitudinal vibration method

A single linear regression analysis was performed to establish correlations between mechanical properties and non-destructive properties both for tension tests and bending. As referred in the literature for temperate hardwoods, density did not present a significant correlation (highest value was 0.38) with both mechanical properties (modulus of elasticity and strength) both for bending and tension. On the other hand, the longitudinal vibration method used provided strong correlations with static modulus of elasticity, 0.87 for bending sample and 0.93 for tension sample, higher than those reported by Kovryga et al. [4] (0.70 for bending and 0.85 for tension). Regarding the strength prediction correlation coefficients (E_{dyn}) were lower as traditionally mentioned in literature, but similar to other studies, being in the present study higher in tension sample (r = 0.66) compared to bending sample (r = 0.39). Despite the fact that the use of static modulus of elasticity to predict strength provide slightly higher correlation coefficients (r = 0.73 for tension and r = 0.45 for bending), the associated costs to testing and time consuming are significant, reason why non-destructive tests are a strong solution for grading.

CONCLUSION

The present paper aimed to characterize beech species from 2nd quality with origin in Spain forests, currently not used for structural purposes, in order to show its potential to be used as structural raw material for load bearing engineered wood products. Longitudinal vibration method was considered to predict the mechanical properties both in tension and bending. It was observed a strong correlation between dynamic modulus of elasticity and static modulus of elasticity (0.87 and 0.93 for bending and tension, respectively). Bending tests sample had mean values of 680 kg/m^3, 12100 MPa and 61.5 MPa (density, modulus of elasticity and bending strength, respectively), whereas mean values of tension sample were 660 kg/m^3, 13200 MPa and 63.5 MPa (density, modulus of elasticity and bending strength, respectively). Based on EN 338 a strength class assignment to D30 could be considered, as defined for oak and maple and higher than chestnut (D24). In terms of tension, it is not possible to assign a strength class, however based on a proposal for medium-dense hardwoods, the results fits with a DT25 class, with mean values similar to most common temperate hardwoods in Europe, like ash, birch and maple.

ACKNOWLEDGMENTS

This work was partially financed by FCT/MCTES through national funds (PIDDAC) under the R&D unit Institute for Sustainability and Innovation in Structural Engineering (ISISE), under reference UIDB/04029/2020 and Interreg Sudoe Programm (FEDER funds) through EGURALT project, under reference SOE4/P1/E1115.

REFERENCES

[1] Houston Durrant, T., de Rigo, D., Caudullo, G., 2016. *Fagus sylvatica* and other beeches in Europe: distribution, habitat, usage and threats. In: San-Miguel-Ayanz, J. de Rigo, D., Caudullo, G., Houston Durrant, T., Mauri, A. (Eds.), European Atlas of Forest Tree Species. Publ. Off. EU, Luxembourg

[2] Schmidt, M., Glos, P., Wegener, G., 2010. Gluing of European beech wood for load bearing timber structures. European Journal of Wood and Wood Products. 68 (1): 43-57.

[3] Aicher, S., Hirsch, M., Christian, Z., 2016. Hybrid cross-laminated timber plates with beech wood cross-layers. Construction and Building Materials. 124: 1007-1018.

[4] Kovryga, A., P. Stapel, and J.-W. van de Kuilen, Tensile strength classes for hardwoods, in International Network on Timber Engineering Research Proceedings, R. Görlacher, Editor. 2016, KIT Scientific Publishing: Graz, Austria. p. 97-113.

[5] Nocetti, M., M. Brunetti, and M. Bacher, Efficiency of the machine grading of chestnut structural timber: prediction of strength classes by dry and wet measurements. Materials and Structures, 2016. 49(11): p. 4439-4450.

[6] Ravenshorst, G.J.P., Species independent strength grading of structural timber, in Structural Engineering - Civil Engineering and Geosciences. 2015, TU Delft: Deflt, The Netherlands.

[7] CEN, EN 13183-2 - Moisture content of a piece of sawn timber - Part 2: Estimation by Electrical Resistance Method. 2002: Brussels.

[8] CEN, EN 13183-1 - Moisture content of a piece of sawn timber - Part 1: Determination by oven dry method. 2002: Brussels.

[9] CEN, EN 384 - Structural timber - Determination of characteristic values of mechanical properties and density. 2010: Brussels.

[10] Aicher, S., Z. Christian, and G. Dill-Langer, Hardwood Glulams - Emerging Timber products of superior mechanical properties, in 13th World Conference on Timber Engineering (WCTE 2014). 2014: Quebec, Canada.

[11] Vega, A., et al., Proposal for visual grading criteria of structural timber of sweet chestnut from Spain. European Journal of Wood and Wood Products, 2013. 71: p. 529-532.

[12] CEN, EN 14358 - Timber structures - Calculation and verification of characteristic values. 2016: Brussels.

[13] CEN, EN 338 - Structural timber - Strength classes. 2016: Brussels.

[14] CEN, EN 1912 - Structural timber - Strength classes - Assignment of visual grades and species. 2012: Brussels.

COMPARISON OF MECHANICAL PROPERTIES OF WOOD DETERMINED BY LOCAL GENTLY DESTRUCTIVE TESTS AND FULLY DESTRUCTIVE TESTS ON BUILDING ELEMENTS

M. DRDÁCKÝ[1], **M. KLOIBER**[1], **M. R. VALLUZZI**[2] and **F. CASARIN**[3]

[1] Institute of Theoretical and Applied Mechanics of the Czech Academy of Sciences, Prague, Czech Republic

[2] University of Padova, Department of Cultural Heritage, Padova, Italy

[3] Expin s.r.l., Noventa Padovana, Padova, Italy

ABSTRACT

Demolition or repair of historic buildings is a valuable source of test materials for testing non-destructive and gently destructive methods for estimating the mechanical properties of built-in wood. The article uses the results of one such opportunity, when it was possible to study the mechanical properties of wood obtained by local measurements on a larger sample of historic and new wooden beams and compare them with the properties calculated from destructive tests of structural elements. Thirty-one wood elements (nineteen recovered from disassembled buildings and twelve new) were subjected to considerately destructive local tests using a loading mini-jack method. In this method, a small loading jack is inserted into a precisely drilled hole and a load test of the wood in compression along the fibers is performed on a part of the hole wall while measuring the achieved deformation under load. Red and white firs, and pine species constituted the recovered elements; red fir and larch the new ones. Destructive tests (in bending and compression) were also carried out on ten recovered and six new elements, and results were correlated with those of considerately destructive tests. Comparison of the assessed mechanical properties shows reasonably good correlation and promising conclusions for practical applications.

KEYWORDS: considerately destructive tests, mini-jack method, destructive tests, assessment of mechanical characteristics of wood, historic timber

INTRODUCTION

Determining the mechanical properties of embedded wood has attracted the attention of researchers for several decades. The achieved results are typically used in estimating the safety of the structure, in recalculating its load-bearing capacity for new functions with changing loads as well as in assessing the resistance to exceptional loads. Non-destructive (NDT) and gently destructive (SDT) tests, or tests of entire structural elements extracted from the structure, are used to determine or estimate mechanical properties. The NDT methods assess mechanical characteristics non-directly taking advantage of a response of the material or elements to an excitation or loads, which correlates with the mechanical characteristics. Naturally, the engineers prefer direct touching the materials or structures. Therefore, the methods which provide as close as possible material data are of ever rising interest. Testing of material characteristics on small specimens of wood extracted from existing structures has been largely published mainly by Kasal et al. [1], [2], [3]. However, the testing on cores started almost forty years ago. For example, Schwab et al. [4] studied correlation coefficient between the compressive strength of 10-mm cores and standard 20x20x60 mm specimens. He found that the coefficient varied in the interval

of 0.77–0.96, depending on the species. Lexa and Tokosová also tested the drilled cores [5] as well as later Rug [6] who measured on the 15-mm diameter cores the compressive strength of old and new timber loaded in the direction parallel to fibers. He observed almost perfect correlation between the core compressive strength and strength of standard 20x20x30 mm specimens. The application of tension micro specimens gives even better results because of a very high similarity to the standard tension test procedures [7]. Therefore, the character of mechanical characteristics determined from testing of small specimens is similar to the data from laboratory tests on standard clear wood specimens and they can be treated in similar way for the redesign purpose [8].

From the practical application point of view, the correlation between the pointwise NDT or SDT data acquired from the existing structures and the data from destructive tests of structural elements are of a great interest. Recently, this research has been developed mainly in connection with the protection of historic timber structures and it has brought a number of interesting findings. Both NDT and SDT methods provide highly localized data, and their structural application logically calls for harmonization with the timber classification, which takes into account visual grading. Nevertheless, Loebjinski et al. [9] showed that visual grading underestimates load-bearing capacity of existing timber elements. He destructively tested 19 old pine and oak timber pieces from an historical building (15th and 16th century) after visual grading according to the German standard DIN 4074-1 [10], and their strength was classified according to the European standard EN 1912 [11]. Recently, Arriaga et al. [12] studied possibilities of application of visual grading according to modern European standards. They concluded that currents standards are not applicable to elements of existing timber structures because of their rather high severity which typically ends with rejection of about 50% of the investigated structural elements. Only specific documents or standards as the Italian UNI 11119 [13] are prepared to assess historical timber elements in a realistic way and can help to estimate their remaining load-bearing capacity.

There are only few testing campaigns combining NDT or SDT investigations on historic structural elements with their destructive tests described in literature. Except of the already mentioned work [12] the authors tested 19 elements of recovered wood (made of red or white fir and pine species) and 12 elements of new wood (red fir and larch). This test campaign was carried out by two sets of instrumentation available to the laboratories of the authors of this article and two teams (henceforth referred to as UNIPD and ITAM, standing for University of Padova and Institute of Theoretical and Applied Mechanics of Prague, respectively) using independent test procedures. The results of the non-direct NDT and SDT methods have been published in [14], the results of the direct SDT measurement are presented in this paper.

MATERIALS AND METHODOLOGY

The availability of recovered material from demolition and reconstruction of several buildings in the vicinity of Padua provided a significant set of structural timber elements on which comparative tests of the mechanical characteristics obtained by the destruction of entire building elements could be carried out with their estimates calculated from the data provided by selected methods of ND testing. The nineteen recovered timber elements were completed with a set of twelve new elements. The destructive tests were carried out on selected elements and included ten red fir (R-RF) recovered elements with six new specimens of red fir (N-RF) and larch (N-L) species. All elements were visually inspected and classified according to (UNI 11119:2004) [15]. The mechanically tested R elements were degraded by knots, fissures, slope of grain and biotic decay, therefore they featured I or II grades or not classified (n.c.). Table 1 shows the characteristics of the investigated elements, including the dimensions of the destructively tested specimens in bending or compression.

Table 1. Characteristics of the investigated elements [14]

Element	Cross section (mm^2)	Length (mm)	Density (kg/m^3)	Classification	Bending test (length) (mm)	Compression test (length) (mm)
R-RF_2	175x160	4600	442	II grade	3330	870
R-RF_3	220x152	4500	406	I grade	4500	
R-RF_5	250x220	4980	492	I grade	4980	
R-RF_7	258x214	4230	392	I grade		1310
R-RF_9	234x215	4030	-	I grade		1290
R-RF_10	199x158	4680	416	n.c.	3780	770
R-RF_11	194x125	4530	423	I grade	3690	710
R-RF_12	214x175	4670	359	II grade		1030
R-RF_13	201x135	4660	478	I grade	3820	780
R-RF_14	220x178	4510	323	II grade	4510	
N-RF_1	160x160	5075	362	C24	3040	960
N-RF_2	160x160	5090	424	C24	3040	960
N-RF_3	160x160	5085	428	C24	3040	960
N-L_1	160x160	5090	532	C22	3040	960
N-L_2	160x160	5090	670	C22	3040	960
N-L_3	160x160	5085	606	C22	3040	960

Standard destructive tests were performed according to [16] on specimens which were either cut from the recovered elements to obtain one specimen for bending and one for compression tests (cross sections remained unaltered) or left unchanged. The four-point bending tests were applied to three R-RF full-length elements and four R-RF and six N reduced-length ones (three N-RF and three N-L). Compression tests were applied to seven R-RF specimens and the three N-RF and N-L as above. The set-up for bending tests included a hydraulic jack with load cell (max load of 300 kN) and 6 LVDT transducers (measurement range of +/- 20, 50 and 100 mm) to measure displacements. Compression tests were carried out in a hydraulic loading frame with max load capacity of 1000 kN and two LVDTs (measurement range of +/- 100 mm) were applied for displacement measurements. The attained strengths are presented in the Table 2.

For the gentle local destructive tests the method of direct mini-jack loading along fibers was applied (Drdácký & Kloiber [17]). The method requires preparing a precise radial hole of 12 mm in diameter, into which a small jack is inserted in given depths. The device measures the conventional strength and the deformability of the wood by pushing mechanical jaws into the hole surfaces, Fig. 1. On the tested elements two boreholes were made on each end with drilling in a purely radial direction. The depth of the borehole was at least 70 mm, which allowed measurements to be made in two jaws positions spanning two layers: 1 layer (5-25 mm), 2 layer (35-55 mm). The standard design of the device allows to measure in two more layers: 3 layer (65-85 mm), 4 layer (95-115 mm). Here the measurements in the third and fourth layers were not applied. During the measurement, a mini press is inserted into the radial hole to a depth fixed by a cylindrical sleeve. The imprints in the wood after the jaws have been pushed out are visible in (Fig. 1), and the spacing between the individual layers of the measurement across the element is also visible in this figure. Mechanical response was measured in 64 positions on 16 investigated structural elements.

The mechanical properties are then determined from the measured data recorded in the form of a working diagram where the force acting when pulling the rod is presented against the displacement of the jaws, (Fig. 1). The x-axis shows the displacement when pushing the jaws and the y-axis shows the force required to push the jaws. Ultimate load is determined from the intersection of the lines that formed the tangents to the elastic and plastic parts of the working diagram.

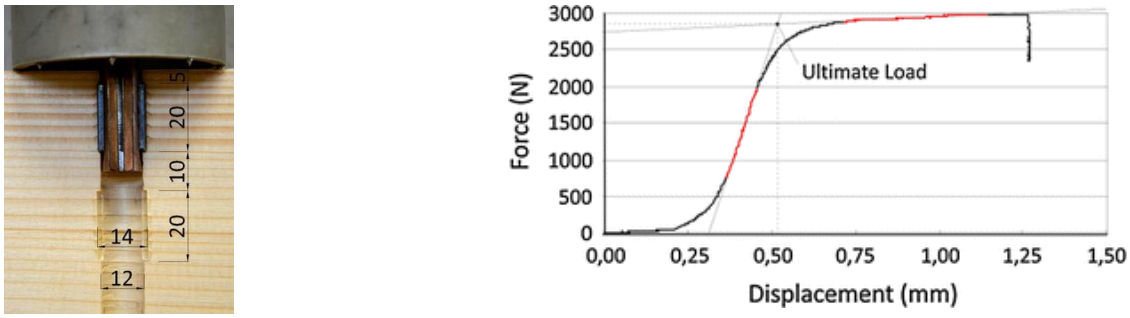

Figure 1: Mini-jack in the borehole (left), typical force-displacement diagram recorded during the test.

RESULTS

From the force-displacement diagram and the known contact area of the rounded jaws of 5x20 mm² the corresponding conventional compressive strengths CS_c along fibers were calculated, (see Table 2). Conventional compressive strength was determined from the ratio of the ultimate load and the area of the jaws pushed. The modulus of elasticity cannot be calculated directly from the force-displacement diagram, however, the modulus of deformation (MOD) can be determined from the slope of the straight part of the force and displacement record. An approximate conversion of the CS_c and MOD values to the standard mechanical properties (f_{cc}, E_{cc}) is then possible exploiting equations determined for different spruce wood moisture and described in literature [18], [19] (Table 2). The conversion takes into account moisture content of the tested wood. Figure 2 presents examples of correlation of compressive strength f_c (x-axis) and f_{cc} (y-axis) as well as E_c (x-axis) against MOD (y-axis).

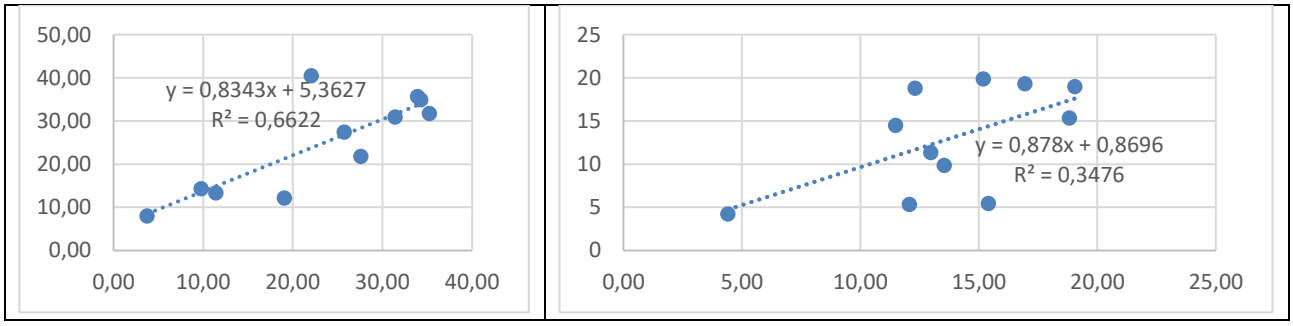

Figure 2. Correlation of compressive strength in MPa (left) and E_c against MOD in GPa (right).

Table 2. Mechanical characteristics determined by the destructive [14] and the gently destructive tests.

Element	f_b (MPa)	E_b (GPa)	f_c (MPa)	E_c (GPa)	CS_c (MPa)	MOD (MPa)	f_{cc} (MPa)	E_{cc} (MPa)
R-RF_2	34,76	7,46	25,73	13,54	44,23	9876,21	27,47	4160,11
R-RF_3	25,65	5,55			41,81	10486,57	25,87	4560,42
R-RF_5	25,65	5,55						
R-RF_7			3,76	3,22	14,75		8,03	
R-RF_9			3,76	3,22				
R-RF_10	8,60	5,17	11,42	15,40	22,81	5456,23	13,34	1261,27
R-RF_11	8,91	4,35	9,78	12,06	24,37	5361,58	14,37	1199,19
R-RF_12			19,05	4,40	21,00	4220,50	12,15	450,82
R-RF_13	23,94	7,02	22,08	16,94	63,99	19333,17	40,50	10362,46
R-RF_14	11,13	3,07			42,39	9215,67	26,26	3726,90
N-RF_1	51,48	7,24	33,92	18,82	56,69	15349,96	35,69	7750,07
N-RF_2	53,61	8,60	35,24	19,05	50,78	18995,51	31,79	10141,00
N-RF_3	37,77	8,05	34,29	15,19	55,56	19892,77	34,95	10729,47
N-L_1	36,63	5,18	27,59	12,97	35,73	11356,96	21,86	5131,26
N-L_2	44,90	6,28	31,42	12,31	49,55	18829,12	30,98	10031,88
N-L_3	41,76	6,48	26,48	11,48	46,03	14496,56	28,66	7485,50

CONCLUSION

The results demonstrate a very good correlation of the compressive strengths determined from the tests of structural elements and the compressive strengths calculated using data acquired with the gentle local destructive tests by the mini-jack method (SDT). The exceptional strength deviations apparent in the Fig. 2 relate to the recovered beams R-RF_12 and R-RF_13. The first one exhibited rather dense material damage, which even prevented to perform bending tests of the element. Therefore, the very local SDT compressive loading in the layers near the surface is influenced with the damaged structure of wood which is less impacting the test of the larger size elements extracted from the sufficiently good parts of the beam. On the other hand, the latter beam which is better graded has a sound wood structure of very good quality which results in a higher estimate of the timber strength based on the SDT test. The exceptional quality of the wood is here demonstrated by the fact that the compressive strength is almost equal to the bending strength. When the above disturbing results are removed from the correlation study the coefficient of determination R^2 reaches in our case the value of 0,936. Unevenly distributed material quality inside the recovered beams causes a higher scatter of deformation characteristics. The data in the Table 2 further show that formula suggested in the literature for the conversion of the SDT acquired deformability data needs corrections in case of the recovered or built-in timber. This will request more experimental studies.

ACKNOWLEDGEMENTS

The authors would like to thank Bozza s.r.l. for the availability of the testing material and space for experimental tests; J. Hrivnák, F.P. Marchesini and L. Scancelli are acknowledged for their support in the experimental campaign and data processing. This research was partially funded by the Italian project Corewood POR FESR Veneto 2014-2020 and supported by the ITAM institutional project RVO 68378297 – Strategie AV21.

REFERENCES

[1] Kasal, B. Semi-destructive method for in-situ evaluation of compressive strength of wood structural members. Forest Products Journal, 2003, 53 (11/12): 55–58

[2] Kasal, B., Drdácký, M., Jirovský, I. Semi-destructive methods for evaluation of timber structures. Transactions on the Built Environment Vol. 66, 2003, WIT Press, www.witpress.com, ISSN 1743-3509

[3] Kasal, B., Tannert, T. (eds.): In Situ Assessment of Structural Timber. (State of the Art Report of the RILEM Technical Committee 215-AST). RILEM 2010, Springer Dordrecht Heidelberg London New York, DOI 10.1007/978-94-007-0560-9, ISBN 978-94-007-0559-3

[4] Schwab, E., Wasshau, A., Willetneier, H.: Bohrkerne zur Beurteilung der Festigkeit hölzerner Rammpfähle. Bauen mit Holz 1982: (9): 566–570.

[5] Lexa, J., Tokosova, M.: Evaluation of allowable stresses based on small specimens. State Forest Products Research Laboratory, Bratislava, Slovakia. Research Report 9/SHI 1983. In Slovak.

[6] Rug, W.: Festigkeit von Altholz. Bauen mit Holz 1989: 10(89): 696–699.

[7] Kasal, B., Anthony, R. W..: Advances in in-situ evaluation of timber structures. Prog. Struct. Engng. Mater. 2004; 6: 94–103 (DOI: 10.1002/pse.170)

[8] Drdácký, M., Kasal, B.: Testing historic materials for redesign purposes. Proceedings of the 10th International conference on "Structural analysis of historic construction – Anamnesis, diagnosis,

therapy, controls", SAHC 2016, K. Van Balen and E. Verstrynge (eds.), CRC Press - Balkema, Taylor & Francis Group, Leiden, pp. 585-591

[9] Loebjinski, M., Linke, G., Rug, W., Pasternak, H.: Redevelopment of a wooden roof construction under preservation order, in: Proceedings of the 5th International Conference on Structural Health Assessment of Timber Structures, 2019, pp. 912–921.

[10] German standard DIN 4074-1. Sortierung von Holz nach der Tragfähigkeit,- Teil 1: Nadelschnittholz. Deutsche Institut für Normung (2012) Germany.

[11] European standard EN 1912. Structural timber. Strength classes. Assignment of visual grades and species. European Committee for Standardization (CEN), Brussels, Belgium, (2012/AC:2013).

[12] Arriaga, F., Osuna-Sequera, C., Bobadilla, I., Esteban, M.: Prediction of the mechanical properties of timber members in existing structures using the dynamic modulus of elasticity and visual grading parameters. Construction and Building Materials 322 (2022) 126512

[13] Italian standard UNI 11119. Cultural heritage–wooden artefacts–load-bearing structures. On-site inspections for the diagnosis of timber members (English version, original in Italian). Ente Nazionale Italiano di Unificazione (Italian Organization for Standardization, UNI), Italy, (2004).

[14] Valluzzi, M.R., Drdácký, M., Kloiber, M., Casarin, F.: Comparative evaluation of investigation testing methods in timber elements considering moisture content. International Journal of Architectural Heritage (submitted)

[15] Valluzzi, M. R., Casarin, F., Scancelli, L., Drdacky, M., Kloiber, M., Hrivnak, J. 2021. Influence of moisture content on the application of ND and MD tests to various species of timber elements. In Proceedings of the 12th International Conference on Structural Analysis of Historical Constructions SAHC 2021, Barcelona (Spain), 29 Sept-1 Oct 2021; P. Roca, L. Pelà and C. Molins (eds.); pp.639-650. Doi: 10.23967/sahc.2021.13

[16] EN 408:2010+A1:2012. Timber structures - Structural timber and glued laminated timber - Determination of some physical and mechanical properties.

[17] Drdácký M, Kloiber M (2013) In-situ compression stress-deformation measurements along the timber depth profile. In: Advanced Materials Research 778: Trans Tech Publications, Switzerland. pp 209–216

[18] Kloiber, M., Tippner, J., Kunecký, J., Sebera, V., Milch, J., Hrivnák, J.: Analysis of Mini-jack technique for *in situ* measurement of strength. In: 3rd International Conference on Timber Bridges, 2017, Skellefteå, Sweden. ISSN: 0284-5172, 6 pp.

[19] Kloiber, M., Drdácký, M., Tippner, J., Hrivnák, J.: Conventional compressive strength parallel to the grain and mechanical resistance of wood against pin penetration and microdrilling established by in-situ semidestructive devices. In: Materials and Structures, 48(10): 2015, Netherlands. ISSN: 1359-5997, pp. 3217–3229.

CHANGES IN VIBRO-ACOUSTIC PROPERTIES OF GREEN BEECH WOOD DUE TO KRETZSCHMARIA DEUSTA

Patrik NOP[1], Valentino CRISTINI[1]

[1] Department of Wood Science and Technology, Mendel University in Brno, 613 00 Czech Republic

ABSTRACT

Dynamic modulus of elasticity (MOED) and vibrational damping are the main parameters defining the vibro-acoustic properties of the material and can be used as important indicators in selecting a suitable wood for structures and also in the health assessment of timber constructions. Parameters are determined using a non-destructive frequency resonance technique. Degradation caused by wood-decaying fungi significantly affects observed parameters. The study presents dynamic bending properties of artificially inoculated samples with soft-rot fungus *Kretzschmaria deusta*, and their correlation to the static bending modulus of rupture (MOR) which was evaluated by standard mechanical test on small samples of beech wood (*Fagus sylvatica* L.). Data comparison with intact specimens and a relationship between mechanical properties and mass loss are also included. Presented results can be used to improve vibro-acoustic non-destructive timber assessment.

KEYWORDS: Non-destructive testing, Wood-decaying fungi, Modulus of elasticity, Vibrational damping, Vibro-acoustic properties

INTRODUCTION

Wood-decaying fungi cause the breakdown of components of the wood cell wall (lignin, cellulose and hemicellulose) which may lead to a decrease in mechanical properties [1]. The degree of wood degradation is often assessed according to mass reduction. Nevertheless, strength reduction can occur considerably sooner than weight loss [2]. However, changes in physical-mechanical properties cannot be generalized. It depends on the wood and fungus species, rot type, but on the incubation time as well [3]. A reliable method for assessing the change in physico-mechanical properties of wood caused by fungal degradation is provided by non-destructive techniques (NDT) [4]. It was demonstrated that enzymatic activity of the white-rot fungus *Physisporinus (P) vitreus* on spruce wood can reduce the density relatively more than stiffness [5]. It was presented as a modification improving the acoustic properties of wood for stringed musical instruments, but overall these parameters (and with them the velocity of sound propagation) were slightly reduced. Other studies with *P. vitreus* [6, 7] reported changes in vibro-acoustic parameters, which were evident mostly on the vibrational damping. Using the frequency resonance method, the vibrational mode shapes (longitudinal, transverse, torsional) are exciting, sensed and analyzed. From the frequency of the vibration of the first mode of each shape, dynamic moduli of elasticity (longitudinal, bending) and dynamic shear modulus (torsion) were calculated [8]. The damping coefficient (tan δ) manifests an amplitude attenuation of these vibrations [9]. According to the current state of the arts, changes of MOED and tan δ of green wood caused by fungal degradation are insufficiently explored. A detailed description of the abovementioned relationships can lead to an improvement of non-destructive methods used for timber health assessment.

METHODOLOGY

Special orthotropic samples (7×7×100 mm) of European beech (*Fagus sylvatica* L.) intact sapwood were crafted from fresh (two weeks after felling) timber. After obtaining oven-dry weight (moisture content = 0%), samples were acclimatized to moisture content of 60% (± 10%), and sterilised. To consider the influence of drying, climatization, and sterilisation process on dynamic properties (MOED and tan δ), specimens were tested in every stage of the process. The culture of soft-rot fungus Kretzschmaria deusta used for specimens' degradation was obtained from the wood of a mature standing beech tree and cultivated for one month on beech wooden blocks before the experiment to stimulate its enzymatic activity. Kolle culture flasks (400 ml) were filled with 70 ml of sterile malt extract agar medium (5%) and inoculated with a *K. deusta*. After 2 weeks of incubation at 22 °C and 70% relative humidity, when the mycelium completely covered the flask surface, samples were inserted and laid on the radial face. After 12 weeks of fungal exposure, dynamic and also static tests were carried out on samples (cleaned of superficial mycelium). To determine dynamic parameters, the frequency resonance technique of free-free-flexural vibration was used. Specimens were supported by foam pads at the nodes of the first bending mode (22.4% and 77.6% of length). Oscillations of longitudinal-tangential and longitudinal-radial bending mode shapes (B_{LT} and B_{LR}) were excited by a small hammer, sensed using vibrometer PDV-100 (Polytec, Inc., Germany), and recorded using dynamic signal acquisition module DEWE-41-T-DSA with DEWESoft (DEWETRON, Inc., USA) at sampling frequency 20 kHz. The measured signal of vibrations was decomposed into an amplitude-frequency domain using the Fast Fourier Transform (FFT) processed using MATLAB® (The MathWorks, Inc., USA). Frequencies of first bending modes were used for the MOED calculation, using an equation (1).

$$MOED = \left(\frac{2f}{2.25\pi}\right)^2 \frac{ml^2}{I} \quad [\text{Pa}] \tag{1}$$

Where f = frequency, m = sample mass, l = sample length, and I = moment of inertia [8].
The vibrational damping was determined from the amplitude (a) decrease in consecutive oscillations per period as the logarithmic decrement of damping (LDD) [10].

$$LDD = \ln \frac{a_n}{a_{n+1}} \tag{2}$$

Using the LDD, the damping coeficient tan δ is calculated [11].

$$\tan \delta = \frac{LDD}{\pi} \tag{3}$$

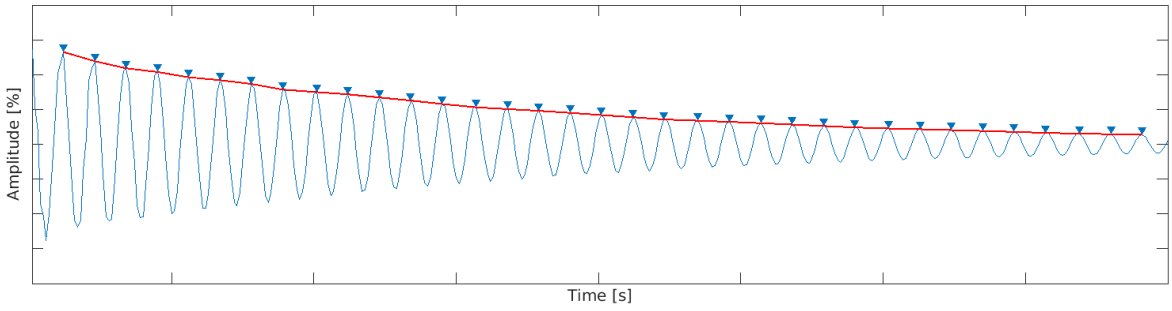

Figure 1: Damped oscillation, which decreasing amplitudes are used to calculate the LDD.

To determine MOR, static three-point bending tests were carried out on a universal testing machine (ZWICK® Z050, 50 kN). Bending stress in the tangential direction (σ_b) was calculated according to the equation (4).

$$\sigma_b = \frac{3Fl_o}{2bh^2} \quad [\text{Pa}] \tag{4}$$

Were F = applied force, l_o = distance between supports, and b, h = the base and the hight of the specimen's cross section. Modulus of rupture (MOR) was calculated as the bending stress at the highest applied force (F_{max}). For the analysis, only specimens with a statistically comparable moisture content before and after inoculation were chosen. Of the 108 samples measured, 60 samples were analysed.

Measured data was statistically processed in MATLAB, using the Kruskal-Wallis test with a multiple comparison.

RESULTS

Dynamic measurements during the inoculation process (drying, climatization, sterilisation) did not show any statistically relevant difference ($p < 0.01$). All changes in material properties were caused only by *K. deusta.* Mass loss of specimens was an average of 30%. For MOED and tan δ, a statistically relevant difference was proven ($p < 0.05$) between intact and degraded samples. Figure 2A shows an increased data variation after specimens' degradation. Due to degradation, the median of $MOED_{BLT}$ decreased by 65% and $MOED_{BLT}$ decreased by 61%. A relevant correlation coefficient between $MOED_{BLT}$ and MOR was proven ($r = 0.84$). After degradation, the median of damping coefficients raised over 288 % ($\tan \delta_{BLT}$) and 279 % ($\tan \delta_{BLR}$). Figure 2B compares the decrease of amplitudes of bending vibrations over the same time period. A conclusive relationship between tan δ and any other observed parameter wasn't found.

Table 1: Median values of measured data

	Intact	Degraded
$MOED_{BLT}$ [MPa]	11 462.6	4 062.3
$MOED_{BLR}$ [MPa]	11 861.3	4 640.7
MOR_{BLT} [MPa]	63.4	28.3
$\tan \delta_{BLT}$	0.0231	0.0899
$\tan \delta_{BLR}$	0.0227	0.0861

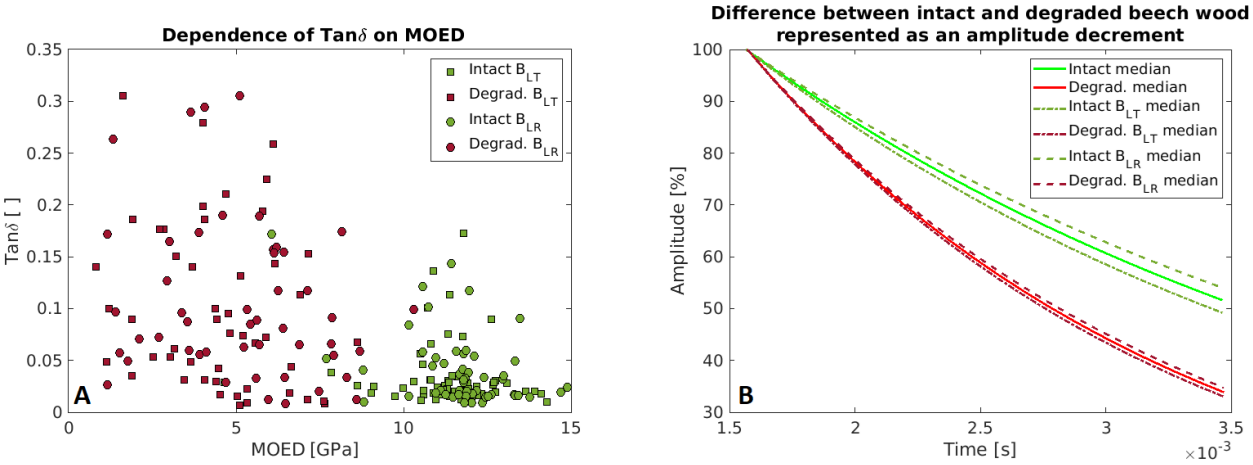

Figure 2: Comparison between MOED and tan δ for longitudinal-tangential and longitudinal-radial bendings (A), comparison of vibrational damping between intact and degraded specimens (B)

CONCLUSION

Degradation of European beech wood cell components caused by the wood-decaying fungus *Kretzschmaria deusta* led to a decrease of dynamic bending moduli of elasticity and an increase of the vibrational damping. These parameters obtained through non-destructive frequency resonance method can serve as indicators for timber health assesment.

ACKNOWLEDGEMENTS

This outcome was supported by the Internal Grant Schemes of Mendel University in Brno, registration no.: CZ.02.2.69/0.0/0.0/19_073/0016670, funded by the ESF.

REFERENCES

[1] Malakani M, Khademieslam H, Hosseinihashemi SK, Zeinaly F (2014) Influence of fungal decay on chemi-mechanical properties of beech wood (Fagus orientalis). Cellul Chem Technol 48:97–103

[2] Witomski P, Olek W, Bonarski JT (2016) Changes in strength of Scots pine wood (Pinus silvestris L.) decayed by brown rot (Coniophora puteana) and white rot (Trametes versicolor). Constr Build Mater 102:162–166. https://doi.org/10.1016/j.conbuildmat.2015.10.109

[3] Spycher, M. (2008). The Application of Wood Decay Fungi to Improve the Acoustic Properties of Resonance Wood for Violins, Ph.D. Thesis, Albert Ludwig University of Freiburg, Freiburg, Germany.

[4] Niemz P, Mannes D (2012) Non-destructive testing of wood and wood-based materials. J Cult Herit 13:S26–S34. https://doi.org/10.1016/j.culher.2012.04.001

[5] Schwarze, F. W. M. R., Spycher, M., & Fink, S. (2008). Superior wood for violins - Wood decay fungi as a substitute for cold climate. New Phytologist, 179(4), 1095–1104. https://doi.org/10.1111/j.1469-8137.2008.02524.x

[6] Danihelová, A., Spišiak, D., Reinprecht, L., Gergel, T., Vidholdov, Z., & Ondrejka, V. (2019). Acoustic properties of Norway spruce wood modified with staining fungus (Sydowia polyspora). BioResources, 14(2), 3432–3444. https://doi.org/10.15376/biores.14.2.3432-3444

[7] Gilani, M. S., Neuenschwander, J., Heeb, M., Furrer, R., Sanabria, S. J., Stoel, B. C., & Schwarze, F. W. M. R. (2016). Influence of incubation time on the vibration and mechanic properties of mycowood. Holzforschung, 70(6), 557–565. https://doi.org/10.1515/hf-2015-0128

[8] Bucur, V. (1995). Acoustics of Wood (1st ed.). CRC Press.https://doi.org/10.1201/9780203710128

[9] Brémaud I, Minato K, Langbour P, Thibaut B (2010) Physico-chemical indicators of inter-specific variability in vibration damping of wood. Ann For Sci 67:707–707. https://doi.org/10.1051/forest/2010032

[10] Salamak, M. (2007). Vibration damping identification maximizing adjustment to viscous model in civil structures. In Archives of Civil Engineering (Vol. 53, Issue 3). https://www.researchgate.net/publication/256472270

[11] Baar, J., Tippner, J., & Gryc, V. (2016). Wood anatomy and acoustic properties of selected tropical hardwoods. IAWA Journal, 37(1), 69–83. https://doi.org/10.1163/22941932-20160121

Relationships of vibroacoustic properties of oak timber at different scales

Jan Zlámal[1], Patrik Nop[1], Valentino Cristini[1], Jan Tippner[1]

[1] Mendel University in Brno, Faculty of Forestry and Wood Technology

ABSTRACT

Applying the frequency resonant method (FRM) to assessment and grading timber and rough lumber in-situ could help identify the quality of wood. However, timber grading by FRM is limited by the complex geometry of logs. Grading of lumber can use squared geometry, but the lumber dimensions and shape change in several steps during the wood processing. Therefore, the dynamic properties in phases of processing can be varied. The presented study provides an analysis of the scale effect on the possibility of estimating the dynamic modulus of elasticity (MOED) of final lumber based on FRM. Experimental measurements by FRM were performed on oak (*Quercus robur* L.) logs and lumbers. The three 4 meters long logs were measured on the ground, and with supports in nodal points too. The same setup with supports was used for lumber in different phases of the sawmill process (rough lumber with bark, 2m rough lumber, edged lumber and final lumber). The results show a significant relationship of dynamic properties between logs/lumber with different scales, although the MOED value in the edged/final lumber increased. The effect of supports in the nodal points for FRM was found.

KEYWORDS: Non-destructive assessment, wood quality grading, size effect, dynamic modulus of elasticity

INTRODUCTION

Non-destructive testing methods based on vibroacoustic principles are used for wood properties evaluation [1],[2]. Many studies [3],[4],[5] have proved the relationship between sound propagation and wood mechanical properties. The strong correlation between MOED and static modulus of elasticity (MOE) in bending and longitudinal direction has been proved [6],[7]. As one of the vibroacoustic methods, FRM is based on the measurement of natural frequencies and knowledge of the mode shapes of the vibrating beam [8]. There are longitudinal, flexural and torsional mode shapes that could be compared with static responses in tension, bending and torsion. Many factors such as microscopic structure, moisture content (MC), density, wood defect and sample dimensions can influence the static and dynamic properties of wood [9],[1],[10]. However, there is no well-described influence of the last-mentioned factor (dimensions). Regarding the static load, the Weibull distribution is most often used for the scaling effect. This describes that as the volume increases, the load resistance decreases due to the increasing probability of defects. Hoffmeyer et al.,[11] remain that the application of this theory to wood bending testing is not entirely accurate. He mentions the results of Madsen & Tomoi, [12] and others who perceive the thickness of the tested samples to be more decisive than the volume. Bohannan [13] states that the depth-to-length ratio (span/depth ratio) of the specimen is critical in bending loading. So, it depends on which specific dimensions are changed and influence the wood's response to loading. Although there is a body of literature on the scaling effect, most research has been conducted on softwood [14]. In his study focused on clear oak samples the decreasing of strength with increasing dimensions was confirmed. Non-destructive testing using FRM showed an indirect effect of sample size on MOED, however, corelation between the samples groups show a significant relationship. [15]. Rais

et al. [16] and Straže et al. [17]used this method to assess greenwood long logs. Their results show that it is possible to use this method for *in-situ* evaluation of wood for structural timber.

The aim of this study was to determine whether the vibroacoustic properties of wood change during wood processing. The study was focused mainly on describing the relationship of MOED in the bending (MOED_B) or longitudinal direction (MOED_L) between logs and lumber with different dimensions. Since for some specimens the bending or longitudinal resonance frequency may not be easily detectable, another goal of the work is to describe the mutual relationship between MOED_B and MOED_L. From the relationships found, it would thus be possible to determine the MOED_B from the MOED_L on different lumber scales. Results could bring improvement for in-situ wood assessment for structure use.

METHODOLOGY

Three 4 meters long logs of oak wood (*Quercus robur* L.) and lumber with four different scales were tested by FRM in University Sawmill Enterprise in Olomučany. The logs had similar diameters and did not contain any visible defects, knots, curves, bumbles or rot. There was used laser vibrometer Polytec PDV100, and two KS94B-10 accelerometers for the registered longitudinal and flexural vibrations. The data from those devices were captured by DEWETRON-41-T-DSA (sampling frequency 20kHz) and processed by MATLAB R2021a software. Frequency spectra for every 48 measurements were analysed by FFT. The spectrum for logs and fibre is illustrated in Fig. 3 and 4. From resonant frequencies, MOED_B and MOED_L were calculated using equations (1) and (2). For statistical data analysis, STATISTICA and MATLAB R2021a software were used.

$$\mathrm{MOED\_B} = \left(\frac{2f}{2.5\pi}\right)^2 \cdot \left(\frac{ml^3}{I}\right) \qquad (1)$$

$$\mathrm{MOED\_L} = 4\rho f^2 l^2 \qquad (2)$$

f is the frequency of the first transverse mode shape (1) or longitudinal shape (2), m = sample mass, l is the sample length, and I is the moment of inertia.

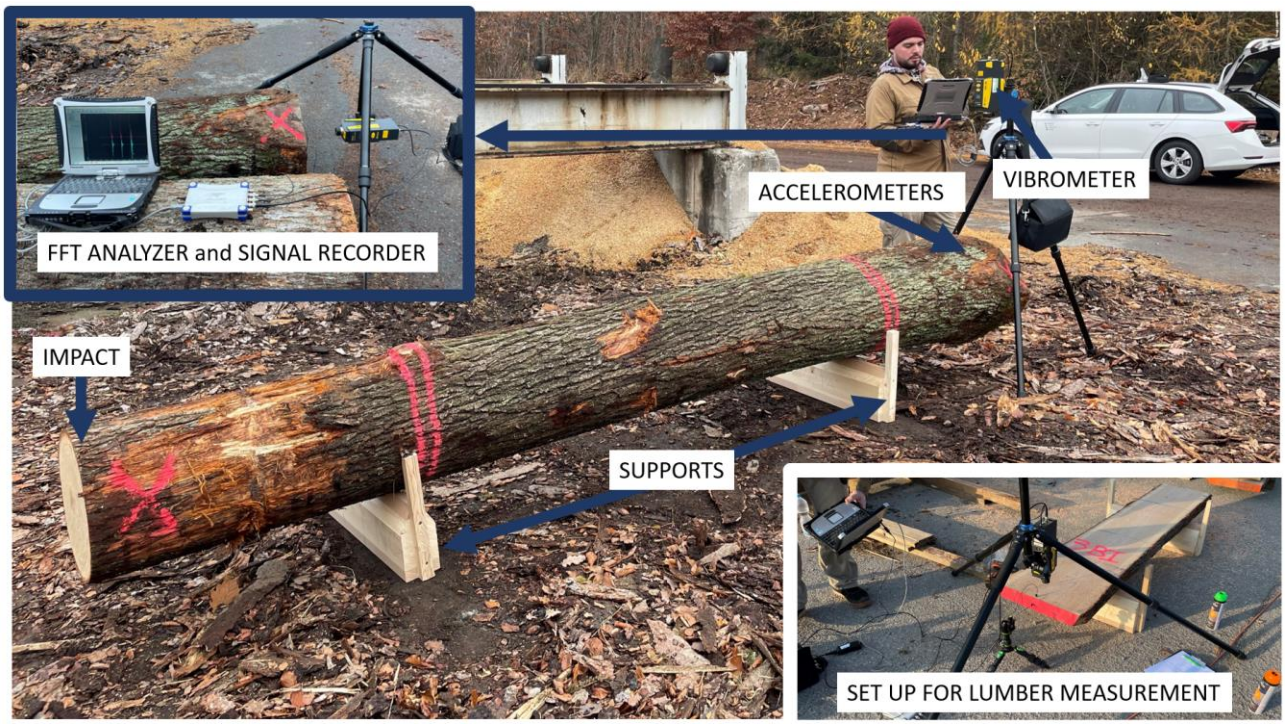

Figure 1, *In-situ measurement set up. FRM measurement of logs and lumber with support in nodal point.*

The first measurement was performed on logs placed on the ground (Fig.2 A): Afterwards, specimens were positioned on supports at the nodal point (22.4% of the length from each side) (Fig.2 B). Those supports increase the ability to clearly record the first bending resonance mode. The length of logs was 4,1m the diameters were 0,42; 0,54; 0,47 m. From all logs were cut two 80 mm thick roughn non-debark lumber (Fig. 2 C), where the length was the same as the logs and right width was 20mm less than log dimension. For MC and density assessment, small samples were cut from the middle of lumber (Fig. 2 G). For MC and density, 100 mm width stripes were cut immediately after sawmill processing, hermetically stored in plastic bags and transported to the laboratory in Útěchov. Each stripe was divided into 7 specimens and measured. A picture of rough lumber with calibration plates was taken to determine surface area and width.

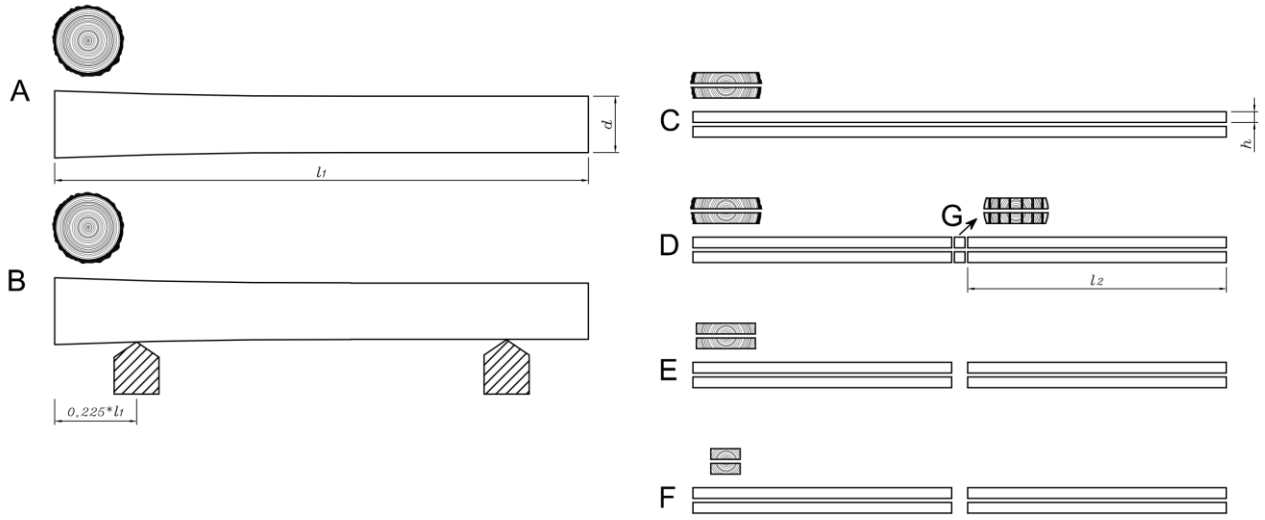

Figure 2, *Scheme of measured specimens. A) log B) log on supports C) Rough lumber D)Rough lumber-half-length E) Edged lumber F) Final lumber G) Specimens for MC and density analysis; l1 = 4,1m, l2 = 2m, d =*0,42; 0,54; 0,47m*, h = 0,08m,*

After the removal of samples for MC, two meters long lumber became (Fig. 2 D). This lumber after measurement by FRM continued to the edging. The edging consisted of two phases, wanes with bark were cut out in the first phase (Fig.2 E) and the final dimension of lumber (Fig. 2 F), was processed in the second phase. The width-to-length ratio of final lumber was the same as on 4 meters long rough lumber. FRM was performed on the lumber after each processing phase (Fig.2 C, D, E, F) in the same setup of supports (0,225*l). Six groups of samples were thus measured. The result of MOED_B and MOED_L were analysed between each group of samples to determine the relationship of scale change. The relationship between MOED_L and MOED_B of different sample groups was analysed for the possibility of property prediction. Density and MC were obtained from the samples cut from the middle of lumber immediately after the sawmill cut. Because of simple geometry, the density for group of final lumber the density was measured from lumber dimensions and weight.

RESULTS

The mean density of 42 samples and 12 lumber is 1065 kg*m^{-3} with 5% variability. Moisture content was 69% with 6% variability. After FFT the frequencies spectrum showed significant peaks of first resonant frequency for all samples and groups in longitudinal vibration. In the case of bending vibration, the importance of the supports at the nodal points was proved as significant (Group A vs. Group B). In Figure 3 is shown a significant first bending resonant frequency on log placed on a supports. For log lying on the ground was hard to find the peak of the first bending resonant frequency and verify it.. Figure 4. shows the frequency spectrum with well readable 1. bending resonance frequency which is similar for all lumber with a length of 2 m.

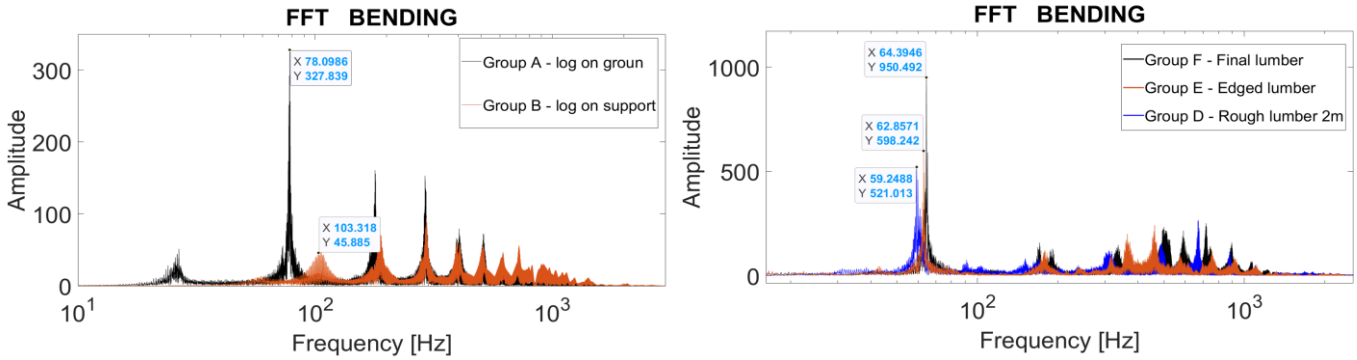

Figure 3, *Spectrum of frequencies where the marked peaks are first bending resonant frequency. after FFT for bending testing. Group A (orange spectrum) is from FRM on a log on the ground, and group B (black spectrum) is from the same log with support on a nodal point.*

Figure 4, *Spectrum of frequencies on 2 meters long lumber with different widths. The naming of the groups corresponds to fig. 2*

The results of ANOVA shows a difference in MOED_L between the lumber from group E/F and other groups (Fig. 5a), these two groups had squared cross-sections without wanes and bark. Despite this difference, high correlations (R= 0.85-0.95) were found between individual groups of samples. Based on these correlations, the simple linear prediction models were created. The relationships for group F (raw lumber) and group C,D (rough lumber) are shown in fig. 4 b), c)

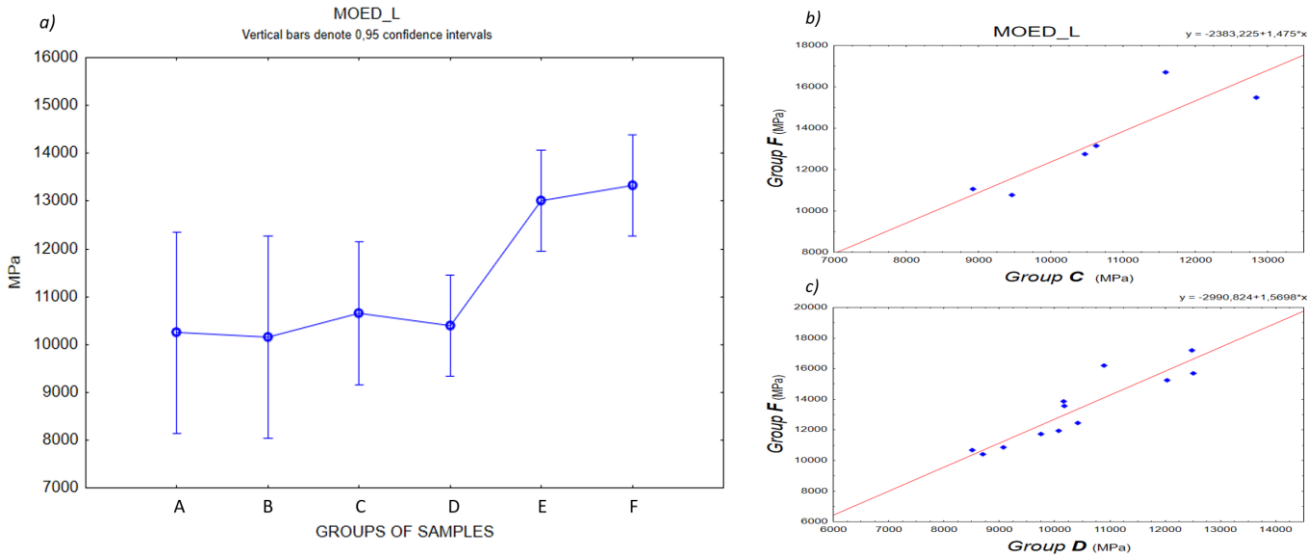

Figure 5 ***a),*** *Results of analysis of variance of MOED_L values of all groups of samples;* ***b)*** *dependence of MOED_L between Rough lumber 4m long (group C) and Final lumber (group F) with a linear regression function;* ***c)*** *dependence of MOED_L between Rough lumber 2m long (group C) and Final lumber (group F) with a linear regression function.*

Analysis of variance of MOED_B shows differences between groups of samples with different cross-section. These results partly proved the results of [14] and [15] when the MOED_B increases with decreased volume. Comparable volume have only groups A and B. Groups C/D have different lengths but similar cross-sections, the groups E/F have the same length, a similar shape of cross-section but different widths. In Fig. 6 b), c) the dependence of MOED_B between lumber groups F and C, D can be seen. Linear regression explains 77% and 83% of these cases.

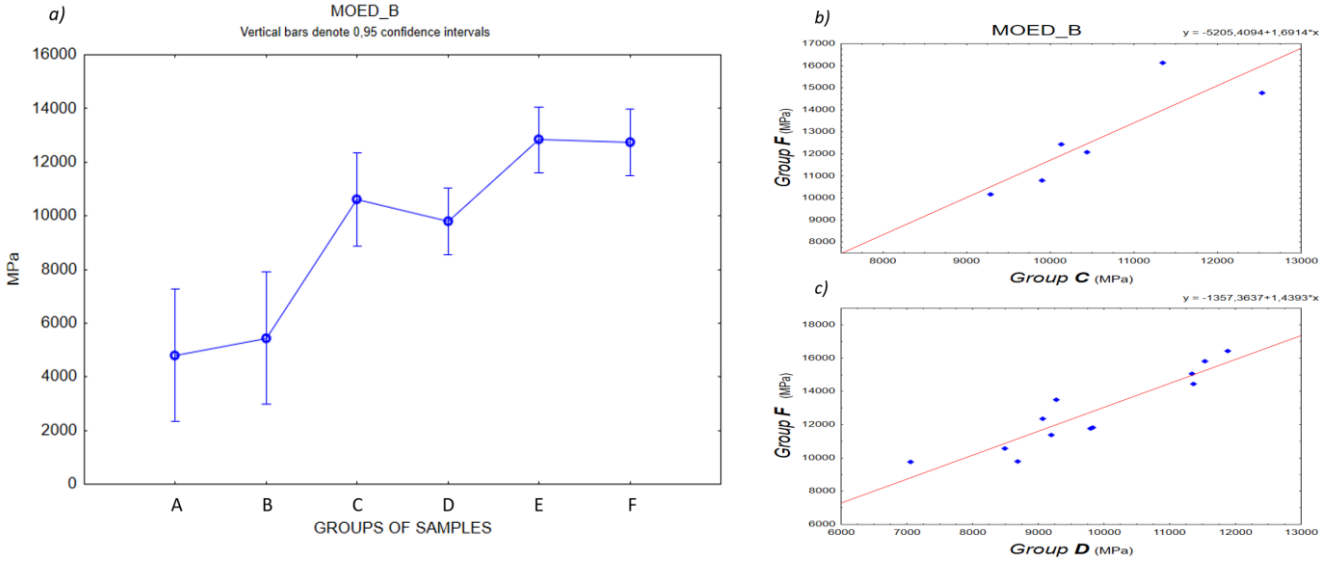

Figure 6 ***a),*** *Results of analysis of variance of MOED_B values of all groups of samples;* ***b)*** *dependence of MOED_B between Rough lumber 4m long (group C) and Final lumber (group F) with a linear regression function;* ***c)*** *dependence of MOED_B between Rough lumber 2m long (group C) and Final lumber (group F) with a linear regression function.*

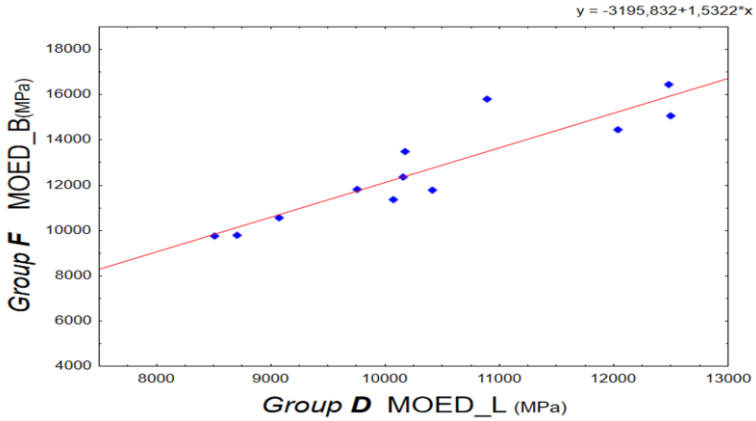

Figure 7, *Dependence of MOED_L of Rough lumber 2m long (group C) and MOED_B of Final lumber (group F) with a linear regression function.*

Analysis of the relationship between MOED_L and MOED_B demonstrated a significant relationship between these values across sample groups. A very strong correlation Spearman R=0,91 was between groups D and F. In fig. 7 can be seen the dependence between these groups when the regression equation explains 83% of the values. It has been shown that it is possible to predict MOED_B for raw lumber from longitudinal vibrations of rough lumber.

CONCLUSION

The oak green wood was measured by FRM during the sawmill processing. There were measured 4m long logs, rough timber and squared timber.
The supports placed in the nodal points are significant for determining 1st bending frequency. ANOVA results confirmed the impact of a scale on MOED_B with the change of the cross-section, where the values increased if the cross-section decreases. For MOED_L the differences in the scale effect were confirmed only between edged/final lumber and other groups.
However, the correlation analysis showed a strong relationship between groups of samples for MOED_L (Spearman R = 0,7-0,9) and MOED_B (Spearman R = 0,6 - 0,9). Relationships were described by linear regression models with satisfactory close relationships (R^2 = 0,77-0,91).
The results also showed a strong relationship between MOED_L and MOED_B, so it is possible to predict the MOED_B of the final lumber from the MOED_L of rough lumber. Results could be used to improve the in-situ evaluation of structural timber.

REFERENCES

[1] Bucur, V., 1995. *Acoustic of wood.* CRC Press, New York.
[2] Ross, J.R., Brashaw, K.B., Wang, X., White, H.R., and Pellerin, F.R., 2004. Wood and timber condition assessment manual. *Forest Products Society, Madison, 93* p.
[3] Haines, D.W., Leban, J.M., and Herbe, C., 1996. Determination of Young's modulus for spruce, fir and isotropic materials by the resonance flexure method with comparisons to static flexure and other dynamic methods. *Wood Science and Technology, 30* (4), 253–265.
[4] Halabe, U.B., Bidigalu, G.M., GangaRao, H.V.S., and Ross, R.J., 1997. Nondestructive evaluation of green wood using stress wave and transverse vibration techniques. *Materials Evaluation, 55* (9), 1013–1018.
[5] Wang, S.Y., Lin, C.J., and Chiu, C.M., 2003. The adjusted dynamic modulus of elasticity above the fiber saturation point in Taiwanian plantation wood by ultrasonic-wave measurement. *Holzforschung, 57* (5), 574–552.
[6] Ravenshorst, G.J.P., van de Kuilen, J.W.G., Brunetti, M., and Crivellaro, A., 2008. Species independent machine stress grading of hardwoods. Proceedings 10th world conference timber engineering (pp. 158–165).
[7] Liu, Z., Liu, Y., Yu, H., and Juan, J., 2006. Measurement of the dynamic modulus of elasticity of wood panels. *Frontiers of Forestry in China, 1* (4), 245–430.
[8] Unterwieser, H. and Schickhofer, G., 2011. Influence of moisture content of wood sound velocity and dynamic MOE of natural frequency and ultrasound runtime measurement. *European Journal of Wood Products, 69* (2), 171–181.
[9] Baar, J., Tippner, J., and Gryc, V., 2012. The influence of wood density on longitudinal wave velocity determined by the ultrasound method in comparison to the resonance longitudinal method. *European Journal of Wood and Wood Products, 70* (5), 767–769.
[10] Mishiro, A., 1996. Effect of density on ultrasound velocity in wood. *Mokuzai Gakkaishi, 42*,
[11] Hoffmeyer, P., Damkilde, L., & Pedersen, T. N. (2000). Structural timber and glulam in compression perpendicular to grain. In Originalarbeiten á Originals Holz als Roh-und Werkstoff (Vol. 58). Springer-Verlag.
[12]Madsen, B., & Tomoi, M. (1991). Size effects occurring in defect-free spruce-pine-fir bending specimens (Vol. 18). www.nrcresearchpress.com
[13] Bohannan. (1966). EFFECT OF SIZE ON BENDING STRENGTH OF WOOD MEMBERS.
[14]Schlotzhauer, P., Nelis, P. A., Bollmus, S., Gellerich, A., Militz, H., & Seim, W. (2017). Effect of size and geometry on strength values and MOE of selected hardwood species. In Wood Material Science and

Engineering (Vol. 12, Issue 3, pp. 149–157). Taylor and Francis Ltd. https://doi.org/10.1080/17480272.2015.1073175
[15] Ilic, J., 2003. Dynamic MOE of 55 species using small wood beams. Holz als Roh-und Werkstoff, 61(3), 167-172.
[16] Rais, A., Pretzsch, H., & van de Kuilen, J. W. G., 2014. Roundwood pre-grading with longitudinal acoustic waves for production of structural boards. European Journal of Wood and Wood Products, 72 (1), 87-98.
[17] Straže, A., Novak, K., & Čufar, K. (2022). Quality and Price of Spruce Logs, Determined Conventionally and by Dendrochronological and NDE Techniques. Forests, 13(5), 729. https://doi.org/10.3390/f13050729

MONITORING AND SURVEY OF TIMBER STRUCTURES

EVALUATION OF THE LOAD-BEARING CAPACITY OF AN EXISTING TIMBER STRUCTURE BY A STEPWISE PROCEDURE – CASE STUDY

Maria Loebjinski[1], Gunter Linke[2/3], Wolfgang Rug[3/4], Hartmut Pasternak[2]

[1] Technical University of Braunschweig / Germany

[2] Brandenburg University of Technology, Cottbus/ Germany

[3] Laboratory for timber construction and ecological building technology, Eberswalde/Germany

[4] University of Sustainable Development, Eberswalde/Germany

ABSTRACT

The investigation and the evaluation of existing structures form central and challenging tasks in the work of every architect and structural engineer. At state, codes and standards lack of specific rules and recommendations to be applied on the specific task of the evaluation of existing timber structures. Object of this case study is the listed and protected structure of an aisled house in North East Germany; to be more specific its historic roof structure. The structure has been investigated in a detailed survey in situ including an improved strength grading of the timber members supported by technical devices. For the evaluation of the load-bearing capacity of the structure, a stepwise evaluation procedure including updated information from the survey into a modified semi-probabilistic verification is applied. The developed strength grading and the stepwise evaluation procedure for a modified semi-probabilistic evaluation have been developed in former research work. The application of these developed methods and proposals for structuring the investigation process are demonstrated for the case study presented.

KEYWORDS: case study, strength grading supported by technical devices, modified semi-probabilistic evaluation, stepwise evaluation procedure

INTRODUCTION

The construction of the investigated structure (see Figure 1) dates to 1786. The building was part of a farmstead originally laid out as a four-sided courtyard. It is a so-called aisled house, which originally combined living quarters and stables. Aisled houses are a typical 15th-19th century building style in the Brandenburg region. They developed from the Lower Saxon hall house and are characterised by their gable facing the street and the corridor running lengthwise through the ground floor. In the front part was usually one large room which was used as a living, working, dining and sleeping area. The rear part was used as a stable. The so-called "black kitchen" - an open-hearth kitchen - was usually located in the middle of the building. The attic served as storage for bedding and fodder. In the 19th-20th centuries, the construction was converted into a purely residential building. In the 1970s and 1990s, extensive repair work was carried out on the gable walls and the roof cladding. The remaining wooden construction is largely unchanged to this day.

The surveyed roof construction is a collar beam roof with a double standing stool. The structure consists of a total of 13 trusses, which are formed from two rafters , a collar beam and a ceiling beam. The trusses

are supported and braced on a double standing stool. These consist of an upper frame as well as three struts with head bands and occasional riser bands between the ceiling beams and columns. The gable trusses are half-timbered. The roof structure was made entirely of pine wood. The components come from several older buildings, which can be seen in the great variability of the component cross-sections as well as the numerous recesses in the component surfaces. The latter include notches for piles and mortises with no visible current use.
The building was listed as a "well-preserved example of a two-storey mid-floor house in the March of Brandenburg". Due to extensive damage caused by wood-destroying organisms, significant deformations and the resulting impairment of the load-bearing capacity of the roof structure, the permission for its redevelopment under monument law was requested. Therefore, a comprehensive assessment of the building's condition was necessary.

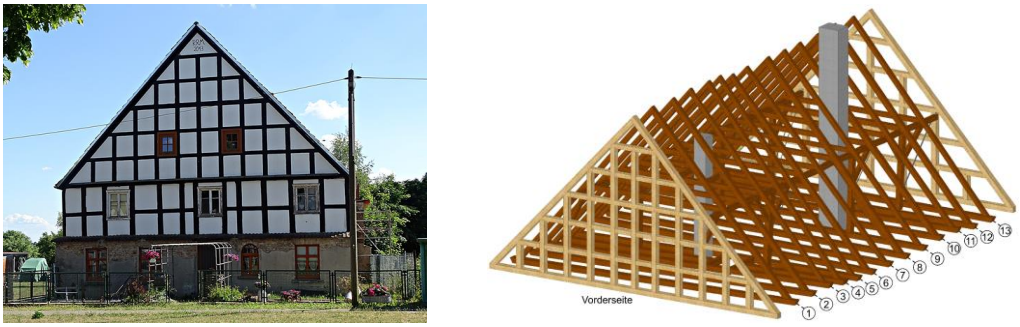

Figure 1: Exterior view of the aisled house (left) and isometric view on the roof construction (right)

METHODOLOGY

The evaluation of the load-bearing capacity of an existing structure differs fundamentally from the design of a new structure. An existing structure already exists in tangible form, so that load and material parameters can be updated by a qualified investigation in situ. What is more, the relative costs of a comparatively small increase of safety reached by technical measures are a lot higher compared to a change in the design process of a new structure, see e.g. [1–3]. Thus, the optimisation problem that in its general nature characterises all tasks of design, has to be analysed in another context.
For the structure described above, a detailed investigation in situ has been carried out including an in-situ strength grading of the timber. The basic procedure is described in [4]. The on-site applied test methods included the visual detection and measuring of knots, slope of grain and cracks, non-destructive ultrasonic time-of-flight measurements and the extraction of core drill samples to determine the density. Further characteristics such as wane, organic damage and deformations were documented. Their consideration in strength grading is not required (see [4]), but these features must be recorded for the assessment of load-bearing capacity and the planning of redevelopment measures. The levels of detail of the in-situ strength grading procedure are summarised in Table 1.

Table 1: Strength grading levels (SGL) and grading criteria

SGL	SGL 1	SGL 2	SGL 3
Grading criteria	knots/slope of grain/cracks	SGL 1 + ultrasonic velocity/transferred voltage	SGL 1 + dynamic MOE/ density

This case study presents the application of a stepwise evaluation procedure suggested for the evaluation of existing timber structures [5]. An evaluation procedure should match the current design rules that have been approved in practice and provide options for its enrichment. The more information is available, the more complex the evaluation format can get. Thus, the first step in the proposed framework is the evaluation in Knowledge Level 1 (KL 1), embracing current practice, i.e. a general investigation in situ to exclude major structural damages that may lead to serious stability concerns, and a semi-probabilistic evaluation applying safety elements from current design codes. Various

concerns may lead to the need for a more detailed evaluation of a structure including updated load and material parameters. Reasons might be changes of loads, increased consequences of failure, the (heritage) value of a structures and therefore the interest in its preservation and of course economic constraints that have to be evaluated in the special case. This update of information should be used in the semi-probabilistic evaluation format, that is widely applied in practice. For this purpose, a KL 2 comprising of a subdivision into three sub-levels is suggested. The application of level three formats, i.e. probabilistic methods, requires an experienced engineer and reliable information on probabilistic models (KL 3). The proposal is illustrated in Figure 1 and Table 2. Requirements for the application of level KL 2a format are given in Table 3. To combine grading and evaluation, the described levels for the design check (KL) and the strength grading procedure need to be combined, see Table 4.

Table 2: Summary of proposal for a stepwise evaluation procedure for existing timber structures [5]

Design check format	***Level of detail of the investigation in situ***		
semi-probabilistic <u>without</u> update - *KL 1*	**visual strength grading in situ**		
	Partial Safety Factors according to EN 1990, EN 1995-1-1, EN 1995-1-1/NA		
semi-probabilistic <u>with</u> update - *KL 2* *The requirements for the application of modified PSF have to be considered (Table 3)*	***KL 2a)***	***KL 2b)***	***KL 2c)***
	visual strength grading in situ optimisation of γ_M considering load and stress: $\gamma_{M,opt}$	**strength grading in situ supported by tech. devices** update of γ_M based on measured properties: $\gamma_{M,up}$	
	update of permanent actions: $\gamma_{G,up} = 1.20$ *(unfav.), variable loads:* $\gamma_Q = 1.50$		
	***strength grade** from visual grading and if needed supported by technical devices*	***strength grade** from grading supported by tech. devices (nd/sd)*	***strength grade** from grading supported by tech. devices (nd/sd)*
	$\gamma_{M,opt}$ *depending on the stress (calibration results for selected limit states see [5])*	$\gamma_{M,up} = \gamma_{M,opt}$ *depending on the stress (see [5])* *<u>Future work</u>:* $\gamma_{M,up}$ *depending on strength grading devices applied*	$\gamma_{M,up}$ *based on measured reference property determined in situ*
Probabilistic - *KL 3*	**visual strength grading in situ**	**strength grading in situ supported by technical devices/ update of material properties**	
	probabilistic evaluation applying 2nd or 3rd order probabilistic methods	*probabilistic evaluation applying 2nd or 3rd order probabilistic methods, update / improvement of the resistance model based on test results*	

Table 3: Requirements for the application of modified PSF in Knowledge Level (KL) 2a [5]

Requirements for the application of modified PSF for the evaluation of existing timber structures in (KL) 2a
The structure has been designed for a minimum service life of 50 years
The structure has been used as intended for a minimum period of 5 years
The structure is free of major damages*
Permanent loads, residential/office live loads, snow and/ or wind loads have to be considered
The load ratio of permanent loads to total loads is $LA_G \geq 0{,}5$
Geometric parameters and permanent loads are updated by a detailed investigation in situ
The minimum sample size to update material properties is $n_{min} = 5$
If an updated cov of the material strength is used to apply updated PSF other than given (see [5]) a conversion factor to consider a limited sample size for n < 30 has to be considered
* Note that here major structural damages that significantly affect the structural behaviour are addressed. Deterioration and deformations have to be considered in the structural evaluation

Table 4: Knowledge Level and corresponding Strength Grading Level

Complexity of evaluation format		**Level of Detail of investigation in situ**
Knowledge Level (KL)		**Strength Grading Level (SGL)**
KL 1		SGL 1
KL 2	KL 2a	SGL 1
	KL 2b	SGL 2, SGL 3
	KL 2c	SGL 2, SGL 3 + measuring result of reference properties
KL 3		(SGL 1), SGL 2, SGL 3

RESULTS

Knowledge Level 1

The investigation revealed serious deformations and misalignments of the structural members. For a first evaluation, the axis with the most unfavourable vertical deformation of the collar beam and without horizontal stabilisation of the same has been modelled. Loads where: self-weight of the roof structure and the timber floor, snow and wind load on the roof structure. Symmetrical and asymmetrical loading has been considered. Live load on the timber floor has not been considered as the upper storey is not in use. In a first step, the strength parameters for the timber members have been taken from EN 336:2016-07 based on visual grading (SGL1, KL1). Exemplary results for symmetric loads are given in Figure 2.

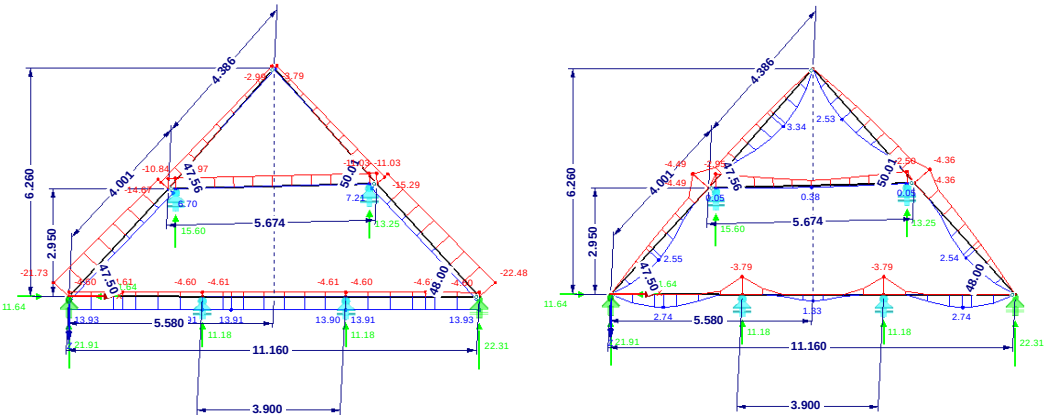

Figure 2: Exemplary modelling results in KL 1 for a truss; left: normal forces, right; bending moment

The dominating limit states are buckling for the rafters and the collar beam and bending + tension for the floor beams. The misalignment of the collar beam led to additional shear stresses. What is more, a head plate and struts have been modelled. The misalignment of the struts caused additional horizontal forces in the abutment and thus normal forces the head plates.

Knowledge Level 2

As a lot of members had to be rejected in the visual strength grading procedure, an in-situ strength grading supported by technical means has been performed in SGL 2 and SGL 3. The results are shown in Figure 3 in comparison to the grading yield of a solemnly visual grading. The figures show that the grading yield improved significantly by the application of the in-situ strength grading procedure. Thus, the visual grading is not sufficient for an accurate estimation of the load-bearing capacity of timber. The accuracy and reliability of the grading process was significantly enhanced by the additional application of non- and semi-destructive test methods. To analyse the influence on the structural behaviour of the selected part of the structure, it has been modelled in KL 2b. This means in detail: γ_G has been updated (γ_G = 1.20 instead of γ_G = 1.35) as due to the investigation dead loads can be determined more detailed. What is more, strength grades have been updated as determined in SGL 3.

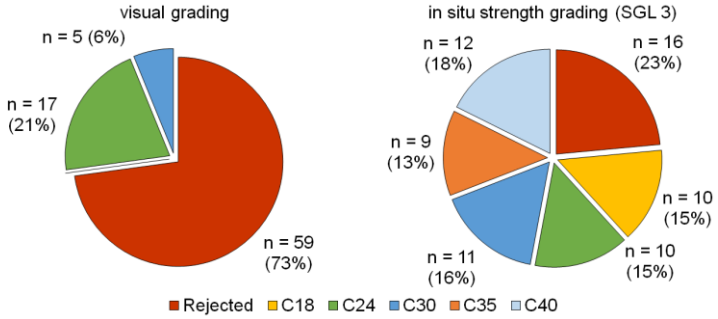

Figure 3: Grading yield of the stringent visual grading according to DIN 4074-1 (left) and the in-situ strength grading (SGL3, right)

Summary of verification results

The results are summarised in Table 5. In SGL 2b, γ_G and strength classes have been updated. Here no update of γ_M could be applied, as for the dominating limit states (buckling and shear) no calibration has been performed yet [5]. What is more, the head plate P01 is subjected to bending and tension. This is caused by the misalignment of the struts in longitudinal direction. Studies in [5] indicate that from a statistical point of view tension stresses caused by variable loads are very unfavourable due to the high variability or the parameters. What is more, the strength class of the member is low. Thus, a reduction of the cov would not be justified and no modification of γ_M can be recommended for this case study.

Table 5: Summary of verification of truss no. 03, head plates P01 & P02 and struts ST01 & ST02, selected limit states

Member	Limit State	KL 1			KL 2b[1]		
		Strength class (SGL 1)	γ_M	η	Strength class (SGL 3)	γ_M	η
Rafter S03	Buckling	C24	1.3	0.31<1	C40	1.3	0.19<1
Rafter S16	Buckling	C30	1.3	0.42<1	C40	1.3	0.30<1
Collar beam KB03	Shear	Rejected[2] (cracks)	1.3	0.59<1	C35	1.3	0.60<1
Floor beam D03	Bending & tension	C30	1.3	0.37<1	C30	1.3	0.33<1
Strut ST01	Buckling	C24	1.3	0.30<1	C30	1.3	0.23<1
Strut ST02	Buckling	C18	1.3	0.71<1	C24	1.3	0.54<1
Strut ST03	Buckling	C24	1.3	0.62<1	C40	1.3	0.40<1
Head plate P01	Bending & tension	Rejected[2] (cracks)	1.3	1.50>1	C18	1.3	1.12>1
	Bending & compression		1.3	1.29>1		1.3	0,97<1
	Bending		1.3	1.28>1		1.3	0,97<1
	Buckling		1,3	1,38>1		1.3	1,04~1
	Lat. tors. buckling		1.3	1,79>1		1.3	1,04~1
Head plate P02	Buckling	C24	1.3	0.61<1	C24	1.3	0.59<1
		γ_G = 1.35; γ_Q = 1.5			$\gamma_{G,up}$ = 1.20; γ_Q = 1.5		

[1] A verification in KL 2a is not necessary as it has been decided to perform an in-situ strength grading
[2] A remaining load-bearing capacity of C14 has been assumed

Further considerations

According to the verification based on Eurocode 5, the load-bearing capacity for this historic structure could be verified for all members but the head plate P01. The critical location here was the negative moment above the head brace combined with tension from the misalignment of the strut. However, according to its long service life of 236 years, the structure has been proven to withstand certain load values that have already been existent during its lifetime. By evaluating regional snow and wind load data, a lower bound for the structure's resistance could be concluded. Due to lack of data, this approach can be followed by considering the characteristic loads from design codes, as they are based on a middle return period of 50 years. Due to the long service life of this structure, it can be assumed that the design loads have been existent at least once. The characteristic internal forces following from the modal value of the snow and wind load in a reference period of 50 years and from the mean value of the permanent loads are given in Table 6.

Table 6: Summary of internal forces for head plate P01

	Permanent action	Snow load	Wind load	Σ
Normal force N [kN]	5.46	6.59	14.20	26.25
Tension stress σ_t [N/mm^2]	0.20	0,24	0,52	**0.96**
Bending moment M [kNm]	-1.90	-2.30	-4.96	9.89
Bending stress σ_m [N/mm^2]	2.18	2.64	5.69	**10.51**

The strength values for the bending and tension strength of strength class C18 are taken from *EN 338:2016-07* [6], cov's are taken from *JCSS Probabilistic Model Code* [7]. The statistical model is then established applying the forces resulting from the characteristic loads as a lower bound applying a 3-parametric lognormal distribution (Table 7).

Table 7: Summary of parameters for the 3-parametric lognormal distribution including a lower bound for P01

	V_{fi}	$f_{k,i}$	$\sigma_{u,i}$	m_i	m_u	$f_{k,i}$	$f_{d,i}$
Bending strength	0,25	18	0,246	27.77	3.294	28.51	21.93
Tension strength	0,30	10	0,293	16.88	2.783	10.96	8.43
$\sigma_{t,d}/f_{d,t} + \sigma_{m,d}/f_{d,m} = 1.23/8.43 + 13.46/21.93 = 0{,}76 < 1$							

CONCLUSION

The results of this case study show that by a strength grading in-situ the estimation of the quality of the timber members in the structure could be improved. What is more, it can be seen that a solely visual strength grading does not sufficiently reflect the material quality, a holistic evaluation is necessary. The evaluation of the load-bearing behaviour within the stepwise procedure indicates that by an increased effort in determination of material parameters and improved evaluation can be reached. By including the loading history, the estimation of the load-bearing can be improved.
However, the dominating concerns for the structure at hand are deformations due to a lack of stabilising elements and insufficient fixing of the connections in position. A detailed investigation of the connections is part of further work. What is more, a concept for the restoration of the structure to prevent further deformations is necessary. This includes the securing of some of the collar beams and the struts to prevent them from failure from lateral torsional buckling and buckling respectively. The calibration of partial safety factors for these limit states is also left to further, planned work.

Acknowledgements

This research has been funded by private donations and supported by commitment of engineers of the *Expert Office for Timber and Glued Laminated Timber Constructions Prof. W. Rug*.

REFERENCES

[1] R. Steenbergen, M. Sýkora, D. Diamantidis, M. Holický, and T. Vrouwenvelder, "Economic and human safety reliability levels for existing structures," *Structural Concrete*, vol. 16, no. 3, pp. 323–332, 2015, doi: 10.1002/suco.201500022.

[2] D. Diamantidis, M. Holický, and M. Sýkora, "Target Reliability Levels Based on Societal, Economic and Environmental Consequences of Structural Failure," in *Conference Proceedings, 12th International Conference on Structural Safety and Reliability (ICOSSAR)*, Vienna: TU-Verlag, 2017, pp. 644–653.

[3] T. Vrouwenvelder, "Developments towards full probabilistic design codes," *Structural Safety*, vol. 24, pp. 417–432, 2002.

[4] G. Linke, W. Rug, and H. Pasternak, "Strength grading of timber in historic structures – methodology and practical application," in *6th International Conference on Structural Health Assessment of Timber Structures (SHATiS)*, 2022.

[5] M. Loebjinski, *Bewertung der Tragfähigkeit von Holzkonstruktionen beim Bauen im Bestand: Ein Beitrag zur substanzschonenden Erhaltung von bestehenden Gebäuden*. Dissertation, Schriftenreihe Stahlbau, Band 19. Brandenburgische Technische Universität, Cottbus, 2021. [Online]. Available: https://nbn-resolving.org/urn:nbn:de:kobv:co1-opus4-55934

[6] *Structural Timber - Strength classes*, DIN EN 338:2016-07, CEN, Berlin, Jul. 2016.

[7] JCSS, "Probabilistic Model Code: Part 3 - Resistance Models," Joint Committee on Structural Safety, 2006. Accessed: Mar. 8 2016. [Online]. Available: http://www.jcss.byg.dtu.dk/

AN IDEAL MODEL FOR PREVENTING THE LOSS OF HISTORIC TIMBER STRUCTURES

Rick K. Collins[1], Nicole M. Collins[2]

[1] Trillium Dell

[2] Firmitas

ABSTRACT

This paper discusses the significant impact an Integral Planning Model (IPM) can have on the restoration and preservation of historic timber structures, reliably creating a more cost effective, historically, and environmentally sustainable option of repair to historic structures.

It illustrates the process through two case studies of very different, historically significant, restorations of timber roof trusses. The first project, located in Connecticut, USA, is known as the "Coventry Church Roof". This traditional timber frame was built in 1849 and is comprised of white oak and white ash trusses spanning 14.6m (48'). The second project discussed in this paper is known as the "Chautauqua Roof." It is the 1903 isogonal Chautauqua Auditorium Building, in Illinois USA, spanning 45.7m (150').

This paper reviews the totality of the restoration process from conception to completion, beginning with the motivations and perspective of the owners and their communities. We show how this alternative model brings a diverse, qualified team together, led by a subject matter expert to make initial evaluations and studies; a process that happened prior to, and most importantly, directed, the selection of a specialized engineering and/or architecture firm.

This approach was the key that allowed for the preservation of significant historic structures in the care of lightly funded organizations/owners.

KEYWORDS: at-risk, preservation, timber trusses, planning, case-studies

INTRODUCTION

Realistically, only a small number of historic buildings ever benefit from the intensive preservation planning and documentation that large endowments and reliable funding afford. We have observed, through our work, that the loss of culturally significant timber structures is highest in areas where stressors such as declining economic health, insufficient political will, lack of legal protections, unrest, depopulation, or an absence of cultural interest exist. The American Midwest is locked in such a struggling preservation climate. We speak specifically of our primary geographical operations area, an area of about 1.8 million square kilometers/~700,000 square miles (encompassing the states of Illinois, Iowa, Wisconsin, Minnesota, Michigan, Indiana, Missouri, as well as the 4 plains states). This situation is one that affects rural and urban environments alike with universal challenges that are shared globally.

At the crux is the question: *"How do we save more locally significant structures and provide them with the benefits of sophisticated, sustainable, historically sensitive planning?"*

Experientially, over the last twenty-seven years, we have developed and successfully practiced an alternative Integral Planning Model (IPM) that does this effectively. IPM is neither a new, nor radical method or business model. It parallels other human centric, interdisciplinary approaches to designing and engineering solutions that are mindful and efficacious in the long term (1, 2, 3). Though also similar to construction project delivery methods like Integrated Project Delivery (IPD) (4). thus far, we have not found a model specifically described, tested, or sustainably implemented in real-world scenarios in our region as it relates to historic preservation and structural timber.

This paper discusses the definition, role, and involvement of a Subject Matter Expert (SME) and the significant impact an Integral Planning Model (IPM) can have on the restoration and preservation of historic timber structure; reliably creating a more cost effective, historically, and environmentally sustainable option of repair to underfunded and often vernacular historic structures.

METHODOLOGY

The Integral Planning Model (IPM) is designed to save structures of any scale that are stewarded by stakeholders with lower visibility and/or lower budgets. In such cases some initial work is done pro bono, either free of charge or with very basic fees to cover hard costs like transportation and materials. The sliding-scale fee structure may be based on the stakeholder's financial situation, the level of urgency in the project, and/or the availability of a Subject Matter Expert (SME) to lead the initial assessment and communications. Often, these stakeholders have very few resources, may require basic education about their structure, as well as preliminary information to help them gauge feasibility, generate interest in the project, or develop their first budget. Therefore, the first phase often also involves creating an outline or sketch using parameters determined during the SME's initial assessment/discovery that the project may ultimately follow in the continuing stages of planning development.

IPM mitigates stakeholder challenges to preservation. Some of the most common obstacles include:

1. Education
    a. Awareness of the historic significance or embodied wealth/value
    b. General interest/local values
    c. Broken cultural bonds
    d. Long-term impacts and sustainability of materials and methods choices

2. Organizational
    a. Knowledge of potential funding resources
    b. Understanding basic construction processes
    c. Knowledge of standard project sequencing
    d. Identification and definition of what/who is a competent and qualified tradesperson or building professional

3. Resources
    a. Fiscal limits, or starting with no funding/self-funding
    b. Limited or no access to public or governmental support
    c. Availability of qualified trades and building professionals

Team Formation: IPM depends on a strong collaborative multi-disciplinary team that has the capacity and versatility to consider much more than specialized individual consultants are able; thereby increasing efficiency and dramatically reducing overall project costs incurred by the stakeholder.

In our model, IPM most often begins with a qualified Subject Matter Expert (SME) who builds a customized team based on their developing assessment of a project's needs (it is also common for the SME to participate as a collaborator or member of a stakeholder-built team). An SME is a team leader who represents and forwards the stakeholders' interests, as well as the long-term interests of the building and its place in the historical timeline. An SME is competent and qualified in both the planning and execution of the work itself. They have a wide range of practical building science knowledge, project management, practical building experience, good oral and written communication abilities, team building skills, and the authority from the stakeholder to make important decisions and critical recommendations.

An SME is likely to have the following qualifications and credentials at a minimum:

1. Experience
    a. More than 15 years of "on-the-job" trade experience
    b. Well-versed in the orchestration, coordination and guiding of the building process
    c. Comfort and skill in interacting with stakeholders, trades, and other building professionals
    d. The ability to identify and select team members that complement the scenario

2. Education
    a. Significant leadership training and accomplishments in the field of work relating to the trade of the project
    b. 4-year university degree or similar (i.e. military experience, leadership, organizational, and project management training)
    c. Working knowledge of a wide breadth of other building disciplines and trades

Primarily, the Team the SME guides must have the ability to assess whole building health – i.e. building envelope, basic structural engineering concepts, general preservation principles, and implications of the use of modern and traditional building methods, and materials. Secondly, they must be able to process current parameters, including those regarding greater concerns and community context, and stakeholders' goals in the short and long terms. Lastly, they must consider wider historical contexts and ideate likely future challenges and parameters the building itself may face based on patterns and principles of preservation.

The team is composed of chosen individuals that complement and enhance the SME's skill set as well as those of others that may already be involved. They provide specialized support in any of the items listed above. Team members can be documentarians, engineers, architects, project managers, marketing strategists, trades people, technical experts, drafters, financial planners, researchers, artists, or preservationists, among others.

A sequence of 4 steps is completed when following IPM:

1. Initial Assessment– Establish groundwork to fully understand the context through initial evaluations. The work done during this phase is most often pro bono (not highly monetarily compensated, if at all), however, it directly affects the stakeholders' efforts to secure funding and build broader sustainable support– thus opening opportunities to save a building. It's often

critical to do an initial assessment with an SME who has integral knowledge of these buildings prior to the involvement of an engineering and/or architecture firm. This initial discovery phase with the SME is critical in determining the path forward for the building and its restoration.

2. Information and Context– Through the practice of active listening and observation the team identifies the stakeholder's needs and concerns. Anecdotal or archival information may also be gathered at this point. The team educates the stakeholders as needed about the structure itself, and standard building processes or procedures. They may share generalized potential solutions and rudimentary budgets that are based on experiences and past projects, similar in scope. The trust and rapport built, along with the context that is discovered, play a critical role in a project's advancement from idea to fruition. Initial information gathering and context discovery is led by the qualified SME as these broad interactions are guided, building the foundations of a solution that will work for the stakeholders and community long term.

3. Discovery and Support– If the project is evaluated favorably, and the owner accepts, deeper information sharing, education and engenderment are facilitated. The creation of early budgets based on several solutions, while identifying optimal solutions first, are shared with the owners. These budgets are shared prior to bid document creation, final scope writing, or the involvement of building professionals (architectural & engineering firms). Stakeholders may then determine the feasibility of the project based on several possible and realistic solutions. To facilitate greater clarity with budget work and potential solutions, the Team may share standard details, drawings & sketches, methods & materials, good work practices, and details of previous similar projects. Stakeholders often use the information shared by the team to create content, build external or internal support, fundraise, seek grants or private funding.

4. Formal Assessment and Consultation– Ideally, the multi-disciplinary team is now formally engaged by the stakeholder or the SME to perform work that determines and balances the needs and considers an aggregate of all of the information at hand. Additional work at this time may or may not include the review and enhancement, or the commencement of, the following practices and techniques: thorough documentation of the project, observations of current conditions and environment, additional site consultations/visits, scanning, drawings, testing, suggestions for phased/prioritized repairs, materials and methodologies, completed budgeting and scope development, speaking at public meetings, writing articles and collaborating with others engaged by the stakeholder. The team has a guiding hand in everything from engineering to recommending materials and methodologies that will be performed not only in the shop restoration work but also the field work. The team utilizes their collective experience, standard details for common scenarios, documented common practices, methods, and risk analyses to provide the best possible outcome for the structure.

RESULTS

In our work with IPM over the course of almost three decades (which has affected thousands of historic structures) buildings were saved from demolition and, for many, the engineering performance of the building was increased beyond the original design while maintaining the maximum possible historic fabric. These projects time and again are completed within budget, and on time. They continue to be maintained by the stakeholders and have built more significance, and more presence and value within their communities.

In the two case studies being presented to illustrate the usefulness of IPM, we found it more cost effective and environmentally sustainable to repair these historic structures using this planning method. The outcomes once again proved: engineered, historically sensitive repairs versus demolition or other destructive/invasive options. The cultural impacts of saving these buildings were overwhelmingly positive and enriching for the local community and their economies.

The two projects introduced below will be presented as "real world" examples at the conference. Their details will be illustrated in greater detail in the slide presentation.

CASE STUDY 1: Coventry Church Roof - private building, managed by GC

Situation: Demolition threat was imminent

Figure 1: Coventry Church – demolition threat was imminent despite the stakeholder's desire for repair.

OVERVIEW

We were contacted by an engineer that had been engaged by the church owners to review truss failure. We assessed history and work completed to date before joining an existing team that had been engaged by the stakeholder. Our team took on leadership of the project, and collaborated by working with other building professionals already appointed by the stakeholders, and by directly engaging with representatives of the church congregation's building stewardship committee. The project was later put out to bid for a General Contractor (GC), and our firm was awarded the structural reconstruction work. Prior to the involvement of an SME, the team gathered by the stakeholder was on a path to advise demolition due to misconceptions, lack of knowledge/experience, and subsequent predictions of spiraling high costs. This all, despite the desire of the congregation to preserve and restore.

DISCUSSION

The IPM model puts a solid team in place to mitigate potential historic fabric losses in circumstances such as these by:

1. Utilizing Networks: By judiciously adding collaborators at key times, defining best practice early on, and finalizing scope and plan after a broad review, the stakeholders were able to make more informed decisions without investing much of their limited resources. With support and resources in place, there was time for further development and finalizing pre-project planning before the work commenced, reducing cost in implementation as well.

2. Right-Fit Collaborations: the selection of craftspeople, and additional building professionals while weighing whole project health and total budget was ultimately made by the SME. Training needs were identified and implemented as needed for all team members. In this example a local crew with the training, knowledge and proficiency to work with specialized equipment, given the dynamics of the situation and specialized repairs needed, were not available.

When we follow up with stakeholders after the project is complete, we gather empirical data that records the experience of the people directly involved and the cultural impacts of the building restoration on the community. Recording this information through interviewing, social media, images and web research builds a body of work which our team uses to strengthen the case for future restorations.

Figure 2: Repair Work Underway – following methodology determined by IPM.

CASE STUDY 2: Chautauqua Auditorium Building- public building, managed by owner (city government)

Situation: Demolition was imminent

Figure 3: Chautauqua Auditorium Building – restored and in active use by the public.

OVERVIEW

The preservation of this building and fruition of the project took years of pro bono presentations and by integral collaboration with a small group of stakeholders interested in preservation. Initially, our work was to make the case for preservation vs. razing with a very minimal budget, very few grants, some public support, vocal and vehement opposition. There was a split in the community and city council on whether to invest in saving or remove. The building ultimately was saved by a relatively narrow margin of public and council votes.

We used preliminary information gathering, which included preliminary value engineering, drawings, density and moisture testing, and the assessment to assist in building a proposal and case for reuse and revitalization. The SME met and presented on behalf of the client at various city council meetings, and with news media. Our team also crafted statements, historical and technical summaries and signage to educate, inform, excite, and engender.

Initial budgetary and political constraints made scanning the building, completed drawings, and thorough scope planning not possible prior to realizing a project budget and submission to the public. Basic decisions were made, specifications were defined for known areas, assumptions were made for unknown areas. Various repair scenarios were considered, wood density testing was undertaken, and a preliminary engineering review was made. Project documentation and excellent communication with thorough oversight of the team performing the work, quick field decision making allowed greater flexibility and lower cost. There were no changes required to the scope, very little “red tape”, or federal or state governmental oversight on this project due to the lack of funding and interest on their parts. Historically sensitive, best practice guidelines were followed, making a historically appropriate and sensitive repair.

DISCUSSION

The selection of right-fit craftspeople was made, training needs identified and implemented. The selection of right-fit craftspeople, and other professionals was made by the SME, the training needs identified and implemented for all team members. In this case finding a local crew with the training and proficiency work with specialized equipment and specialized repairs was impossible. The budgetary constraints allowed flexibility, but the direct relationship with the stakeholder allowed for good choices to be made in a timely manner.

We studied the cultural impact of the building restoration on the community by gathering empirical data. Recording this information through interviewing, monitoring social media, and web research builds a body of work which strengthens the case for future restorations.

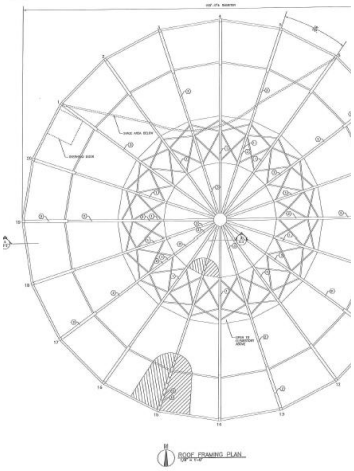

Figure 2: Case Study #2 – Chautauqua Auditorium during initial evaluations

CONCLUSION

Papers should be submitted electronically by using the conference website and registration system (a new submission type is available). The authors of the papers will be contacted after review to finish the whole process and after this step the final version will be submitted (until July 10). Expected formats of the final submission will be both PDF and a M$ Word .docx file (for the case we need some corrections). If somebody uses other word processing software, please contact us via mail, we can find a solution.

ACRONYMS

SME: Subject Matter Expert

IPM: Integral Planning Model

GC: General Contractor

DEFINITIONS

Building Envelope:

The component that separates the exterior environment of the building from the interior. It's the shell and maybe the structure of the building, and as such, it is a key consideration when constructing. It affects the ventilation, climate, energy consumption and protection of occupants and interiors.

Stakeholder:

Individuals, organizations, or other groups of people that own a structure, or have been directly appointed/engaged by the owner as responsible for the stewardship of their structure. Those stakeholders can be building professionals (i.e. architects, engineers, general contractors etc.) or committees, caretakers, maintenance directors, family members or anyone else given the power to make critical decisions for a building.

REFERENCES

[1] Creative Engineering - Promoting Innovation by Thinking Differently, John E. Arnold, edited by William J. Clancey, Copyright © 2016 John E. Arnold, Jr. https://stacks.stanford.edu/file/druid:jb100vs5745/Creative%20Engineering%20-%20John%20E.%20Arnold.pdf, accessed 1.5.2022.

[2] IDEO, Human Centered Design Toolkit, 2nd Edition http://d1r3w4d5z5a88i.cloudfront.net/assets/to olkit/IDEO.org_HCD_ToolKit_English-5fef2, accessed 4.5.2022.

[3] Human-Building Interaction (HBI): A User-Centered Approach to Energy Efficiency Innovations Lester Shen, Ph.D., Megan Hoye, Carl Nelson, and Jennifer Edwards, Center for Energy and Environment https://www.aceee.org/files/proceedings/2016/data/papers/8_714.pdf, accessed 1.5.2022.

[4] The American Institute of Architects, Integrated Project Delivery: A Guide, 2007 version 1 https://info.aia.org/siteobjects/files/ipd_guide_2007.pdf., accessed 1.5.2022.

HBIM for the conservation and the diagnosis of timber structures: Salone dei Cinquecento in Palazzo Vecchio, Florence (Italy)

A. Gasparotti[1], A. L. Ciuffreda[3], S. Longo[2], N. Macchioni[4], C. Riminesi[2], M. Tanganelli[1]

[1] Department of Architecture (DiDA), University of Florence, Florence, Italy

[2] Institute of Heritage Science, National Research Council (CNR-ISPC), Sesto Fiorentino (FI), Italy

[3] Department of Earth Sciences (DST), University of Florence, Florence, Italy

[4] Institute of Bioeconomy, National Research Council (CNR-IBE), Sesto Fiorentino (FI), Italy

ABSTRACT

In this study the timber structures of the Salone dei Cinquecento inside Palazzo Vecchio in Florence were investigated. A multidisciplinary approach using HBIM modeling to integrate data from historical research, diagnostic data obtained by rebound Hammer test, Evanescend Field Dielectrometry (EFD), IR thermography and ultrasound investigations, and geometric data obtained by digital survey. A single database, containing all the data collected from the various techniques involved was obtained. In this paper, a methodology for preventive conservation and monitoring of cultural heritage monuments will be shown. The HBIM approach to existing heritage, allows easy query of data and therefore an incentive to safeguard cultural heritage assets.

KEYWORDS: digital heritage; wooden architecture; non-destructive diagnostic techniques; preventive conservation

INTRODUCTION

Nowadays, HBIM (Heritage or Historic Building Information Modelling) is becoming a leader methodology for historical buildings conservation. The possibility of having a single database of information, containing data from the various disciplines that are involved in the cultural heritage monuments conservation, is a precious methodology for monitoring and preventive conservation [1, 2]. The first use of the acronym occurred in 2009 in the article by Maurice Murphy [1] which describes the creation of a database of parametric elements part of historical heritage where they were associated with information on construction techniques and materials.

The potential of HBIM approach, is that all information concerning the entire life of a historical building (often located in different archives) could potentially be incorporated into a single model [2, 3]. This allows advantages such as the transition from paper to digital information, the availability of information, and avoids the loss of documents in the transition from one professional to another. BIM was created as tool for the new construction and is consolidated for this type of process; different is for HBIM which is currently under study.

BIM software facilitates the modelling of serialized elements, making this phase agree with today's approach to new construction. In the built heritage, however, there are no identical elements, bringing some problems during the modelling phase. An interesting example can be found in the work of M. Diaz

and S.M. Holzer on the Basilica of Saint Anthony in Padua [4] or that of R. Brumana et al. On the Basilica of Collemaggio in L'Aquila [5]. Another theme being studied is the transition from the point clouds, to three-dimensional parametric elements.
Added to this, is the problem of the diversity of information available on individual objects, to be included in the models neatly and understandably. For this reason, it is essential to design an efficient strategy for modelling and for the organization of the data to be entered in the database [6]. Therefore, the purpose of this study is the creation of an informative model describing the state of panelled ceiling and the timber roof of the "Salone dei Cinquecento" in Palazzo Vecchio in Florence, Italy.
Hidden from view, it is a wooden structural system of historical and cultural importance, whose construction and transformation takes place between the centuries from the XV to the XIX [7, 8]. The authors of the interventions are among the most illustrious of the various periods. The theme of wood is very much present in the roof, from a structural [9] and historical-cultural point of view: with the observation of trusses, we can note the construction techniques of the various centuries in which they were performed [10-12].
The study focused initially on the knowledge of the health status of the material, following the indications in the legislation [13] (with the aim of obtaining the information to be included in the information model); at the later stage we moved on to the construction and implementation of the model. The obtained product is an easily interrogatable database, with the function of a single collector of data.

MATERIALS

In this study, a structural investigation of the timber structures that support the painted roof of the "Salone dei Cinquecento" in Palazzo Vecchio in Florence is reported. The structure is composed by 25 trusses of silver fir (*Abies sp*.) and ulm (*Ulmus sp*.) from the sixteenth and nineteenth centuries [3] and other subsets formed by timber elements connecting the stage and the frames to the supporting system (Figure1,2).

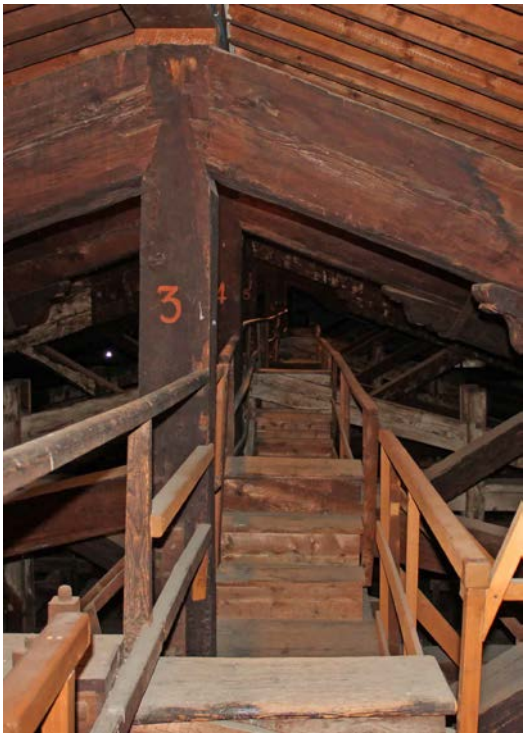

Figure 1: Interior view of the timber roof.

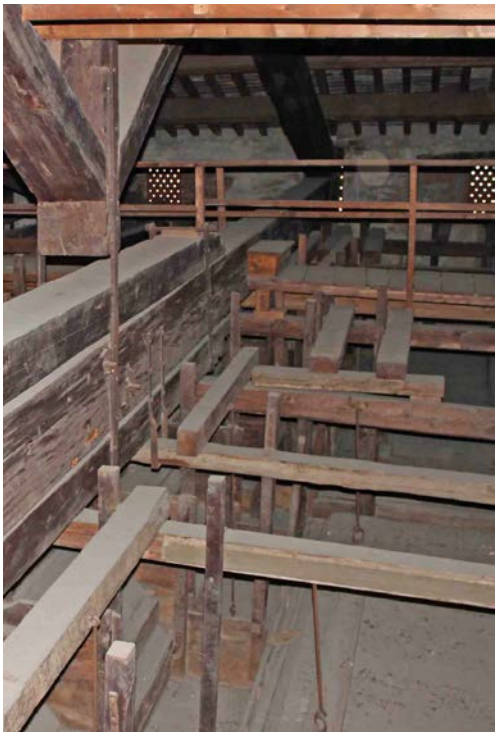

Figure 2: Anchoring system of the coffered ceiling.

The events concerning the "Sala", take place mainly in three centuries: XV, XVI and XIX. The first building of the hall dedicated to the meetings of the "Gran Consiglio" dates back to the end of the XV century,

commissioned by Girolamo Savonarola [14]. The designer was Simone del Pollaiolo, known as "Il Cronaca", who designed a truss roof (consisting of a king post and two minors) to support both the coffered and the roof [7] (figure 3a). The hall remained so composed until the modifications of Vasari in the middle of XVI century: considered "nana e con poco sfogo" the architect decided to raise the ceiling of 12 "braccia fiorentine" (about 7 meters) making substantial changes to the structural system. The new trusses had a different conformation from those of Cronaca, wich were dismantled and reused in the shorter parts of the trusses of the XVI century. Again, the new 12 elements supported both the coffered and the roof [7] (figure 3b). This caused a strong weakening of trusses that was noticed in XIX century: the weight they supported was too high. With the interventions of the engineer Martelli and the architect Giraldi [8], were then inserted other 13 Palladian trusses to which the coffered, freeing the XVI century trusses from the burden (figure 3c). All the information found during the historical research, will be inserted inside the informative model.

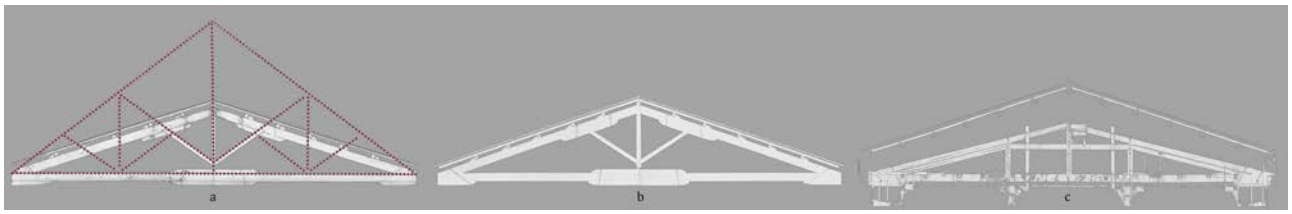

Figure 3: (a) XV century truss; (b) XVI century truss; (c) XIX century truss.

METHODOLOGY

Visual investigation was followed by diagnostic tests performed by rebound Hammer test, Evanescent Field Dielectrometry (EFD), IR thermography and ultrasonic. Rebound investigation ("Woodtester", a rebound hammer calibrated for wood elements, with whose correlation curves it's possible to obtain mechanical characteristics of the wood [17] [18]) was performed to obtain the flexural strength and the flexural modulus of elasticity. EFD analysis were carried out by SUSI instrument to determine Moisture Content (MC) and salts content (salinity index, SI) inside the material [19]. IR thermography was performed for the investigation of the presence of water infiltration from the roof, for this aim the IR images were acquired before and after rainy days [20]. While, the ultrasonic tests were performed to assess the homogeneity of the material [20]. The modelling of the structure was carried out using BIM software based on the point clouds generated by the 3D laser scanner survey. All data obtained with scientific investigations were uploaded on the HBIM model and a descriptive picture of the state of conservation of the timber structure was obtained. The final step involved the elaboration of the analytical model generated in the BIM software (Straus7) to highlight structural environment.

RESULTS AND DISCUSSION

The diagnostic campaign has shown that the timber examined are in a good state of conservation and no differences occur between elements having the same function and belonging to the same wood species (*Abies* sp. and *Ulmus* sp.). In particular, the collected data from SUSI technique have MC % values varies from a minimum of 1,02% to a maximum of 1,82% for Ulm; for white fir (top chord) the values vary between a minimum of 1,08% to a maximum of 1,65%. The variations are consistent and show the same trend. For the same type of wood were not identified large differences between elements compared. For this reason, it can be said that the state of conservation is constant.
With the data processing of the rebound test, the Flexural modulus of elasticity (E_m) and the Flexural strength (f_m) were calculated. The max. and min. values for each type of wood can be read in Table 1.

The IR Thermography were performed on the supports of the trusses before and after the rain. No active infiltrations of rainwater were identified. Finally, with ultrasonic, no gaps were identified within the investigated areas.

Table 1: Max and min values of E_m and f_m for Abies and Ulmus.

Type of wood	**E_m**	**f_m**
	[MPa]	**[MPa]**
Abies sp. (max)	10887	47
Abies sp. (min)	10082	43
Ulmus sp. (max)	9673	66
Ulmus sp. (min)	8393	60

As concern HBIM modelling, the geometric information came from the point clouds obtained from the survey campaign carried out in 2019 (relating to the internal and external parts of Palazzo Vecchio). In the structural environment, all the wooden elements present have been modelled (figure 4) giving priority to section changes and structural joints between parts.

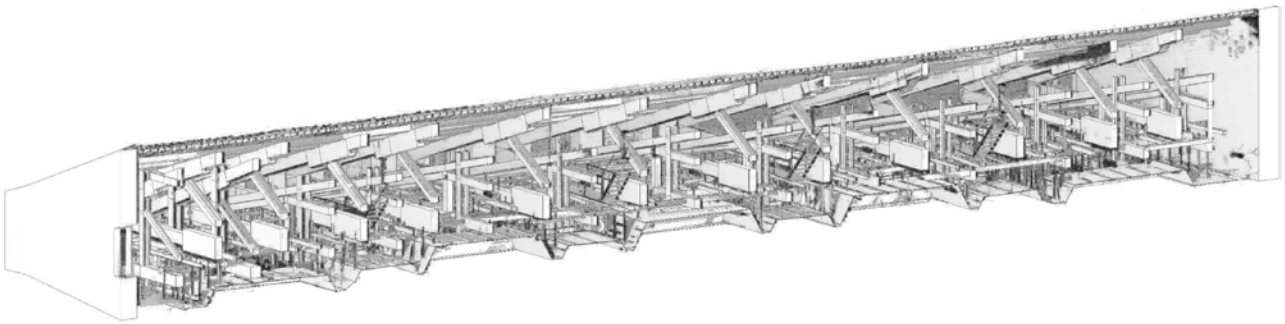

Figure 4: Axonometric section of the roof and support system modelling in structural environment of Autodesk Revit with the point clouds.

For the model, it was necessary to study first the arrangement of the elements present in the roof, because of the seemingly chaotic arrangement. The following subgroups were found: XVI century trusses, XIX century trusses, coffered support anchorage system to the bottom chord of the XIX century trusses, support system of the walkways that allow the inspection of the roof, wooden elements of the cover package.

The software automatically creates an analytical model representing the axes of the elements. They are associated with some information such as the size of section. In the architectural environment, trusses have been shaped part by part (through the creation of parametrized objects) as they are in reality. With the study of XIX century treatises carried out previously, it was possible to reconstruct the internal conformation of the nodes.

After parametric modelling the data obtained from the research is entered in the architectural environment, text, material, URL and image parameters have been created corresponding to each element. In this way, by selecting an element, you are able to have information such as the type of truss, the period of implementation, any assumptions applicable to the element, etc. With the URL parameters were linked the visual mapping files and photographs of the degradation, having a complete picture of the state of health of the element.

The insertion of the data collected during the instrumental diagnostics, has happened with the creation of objects positioned in the area where the tests were carried out. They contain URL parameters with the files summarizing the various tests, in which you have the predisposition for the insertion of monitoring data (figure 5). A symbology was created for each test and applied to the object in the exact location at which the measurements were made. The symbology highlights the analytical data derived from the processing of the tests.

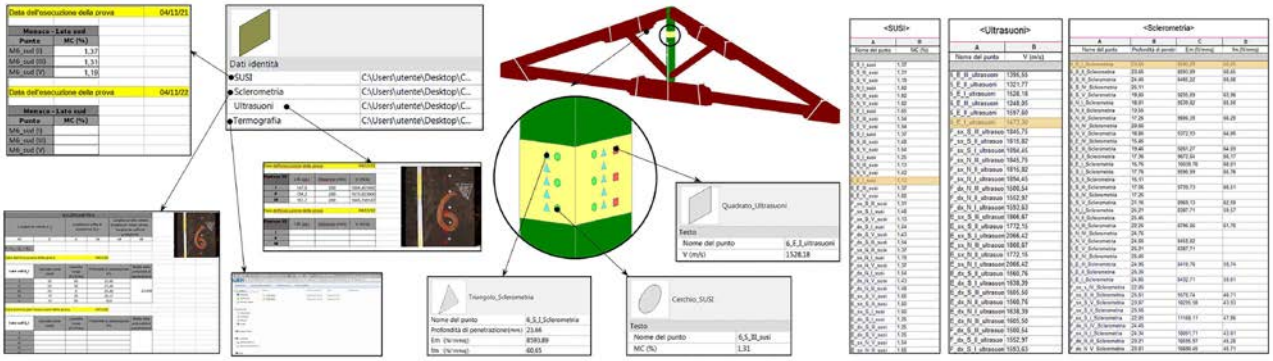

Figure 5: Integration of diagnostic data into the architectural model.

Finally, the data sheets were created, grouping all the parameters of the same type and providing a complete picture of the various tests. They also allow to identify the parameter within the project.
The analytical model was exported in the .dxf format and imported in Straus7 software (FEM). After the analysis in the FEM software is defined the principal geometrical and mechanical characteristic, the principal result is the deformations and stress states of the structures. The results was then reinserted into the structural model in Autodesk Revit, by creating an object (associated with a URL parameter), applied to line of trusses identifiable through a pre-set view.

CONCLUSION

The preservation of the existing heritage is of fundamental importance in Italy, for the concentration of buildings of historical and artistic importance. By applying the HBIM approach to a structure such as the timber roof of "Salone dei Cinquecento", we contribute to the process of digitalization, and to its safeguarding and protection: having an object containing data related to the structure, allows to have constantly available a complete descriptive picture of the element.
The model also allows the transition from paper to digital information, avoiding its loss or replication.
Another advantage is the possibility of creating monitoring plans, which can be easily integrated into the HBIM model, when properly composed.
With the structural analysis performed, another potential of the approach was demonstrated, highlighting interoperability with other software.
Finally, the interoperability between the HBIM model and other software is ensured by export in .IFC format. It is an open and neutral extension [21], readable by most software used in the construction industry. This allows access to the model even by those who do not own authoring software.
The process applied has made it possible to create a data storage tool that can be integrated over time. The database created is not limited to research, but can be developed with the inclusion of data from future research and monitoring.

REFERENCES

[1] M. Murphy, E. McGovern, S. Pavia, Historic Building Information Modelling (HBIM), in Structural Survey 27 (4) – 2009, p. 311-327

[2] M. Coli, A. Ciuffreda, T. Donigaglia, Informative models for the cultural heritage buildings: applications and case histories, in Patrimonio in divenire conoscere valorizzare abitare, Matera 23-26 Ottobre 2019, a cura di A. Conte e A. Guida, ReUSO Matera, Gangemi Editore, pp. 421-432

[3] Coli, M; Ciuffreda, A.L.; Micheloni, M. An Informative Content 3d Model for the Hall Holding the Resurrection of Christ by Piero della Francesca Mural Painting at Sansepolcro, Italy. Int. Arch. Photogramm Remote Sens. Spat. Inf. Sci. 2019, 2, 435-442

[4] M. Diaz, S. M. Holzer, The facade's dome of the st. Anthony's Basilica in Padua, in International archives of the photogrammetry, remote sensing and spatial information sciences, Milano 8-10 Maggio 2019, GEORES 2019 – 2nd International Conference of Geomatics and Restoration, Vol. XLII/W11, p. 481-487

[5] R. Brumana, S. Della Torre, M. Previtali, L. Barazzetti, L. Cantini, D. Oreni, F, Banfi, Generative HBIM modelling to embody complexity (LOD LOG LOA LOI): surveying, preservation, site intervention – the Basilica di Collemaggio (L'Aquila), in Applied Geomatics, 2018, Vol 10 (4), p. 545-367

[6] A. Santoni, R. Martìn-Talaverano, R. Quattrini, J. I. Murillo-Fragero, Hbim approach to implement the historical and constructive knowledge. The case of the real collegiate of San Isidoro (Leon, Spain), in Virtual Archeology Review 12 (24) - 2021, pp. 49-65

[7] U. Muccini, Il Salone dei Cinquecento in palazzo Vecchio, Firenze, Le Lettere, 1990

[8] G.Tampone, Conservation of historic wooden structures: proceedings of the International conference Florence, Firenze 22-27 Febbraio 2005, Firenze, Collegio degli ingegneri della Toscana 2005

[9] G. Giordano, Tecnica delle costruzioni in legno, Milano, Ulrico Hoepli Editore, 199

[10] G. Breymann, Costruzioni in legno in "Trattato generale di costruzioni civili: con cenni speciali intorno alle costruzioni grandiose", Francesco Vallardi editore, Milano, 1884

[11] N. Cavalieri San-Bartolo, Istituzioni di architettura statica e idraulica, Napoli, R. Petrarca editore, 1868

[12] L. Mazzocchi, Trattato su le costruzioni in legno compilato dall'ingegnere Luigi Mazzocchi, Milano, Antonio Vallardi editore, 1879

[13] Ente Italiano di Normazione, 2019, Conservazione del patrimonio culturale - Strutture storiche in legno - Linee guida per la valutazione in situ di strutture in legno portanti (UNI EN 17121:2019)

[14] Aa. Vv., Palazzo Vecchio, Officina di opere e di ingegni, a cura di C. Francini, Firenze, Silvana, Milano, De lettera editore, 2002

[15] Ente Italiano di Normazione, 2004, Beni culturali - Manufatti lignei - Strutture portanti degli edifici - Ispezione in situ per la diagnosi degli elementi in opera (UNI 11119:2004)

[16] Ente Italiano di Normazione, 2004, Beni culturali - Manufatti lignei - Terminologia del degradamento del legno (UNI 11130:2004)

[17] J. F. V. Vincent, M. N. Sahinkaya, W. O'Shea, A woodpecker hammer, in ARCHIVE proceedings of the Institution of Mechanical Engineers Part C Journal of Mechanical Engineering Science 1989-1996 (vols 203-2010), 221 (10), 2007, pp. 1141-1147

[18] Woodtester Novatest, User manual, 2019, Ancona

[19] R. Olmi, C. Riminesi, Study of water mass transfer dynamics in frescoes by dielectric spectroscopy in Nuovo Cimento della Società Italiana di Fisica C, 31(3) - 2008, pp. 389 - 402

[20] M. Riggio, N. Macchioni, C. Riminesi, Structural health assessment of historical timber structures combining non-destructive techniques: The roof of Giotto's bell tower in Florence in Structural Control and Health Monitoring, 24(7) – 2017, Article number e1935

[21] G. Froch, W. Gachter, A. Tautschnig, G. Specht, Merkmalserver im Open-BIM-Prozess, in Die Bautechnik 96 (4) – 2019, pp. 338-347

SHATIS 22

6th International Conference on Structural
Health Assessment of Timber Structures
7-9 September 2022, Prague

STRUCTURAL ASSESSMENT OF HISTORIC TIMBER ROOFS BY IMPROVED AUTOMATION OF POINT CLOUD PROCESSING

T. ÖZKAN[1,2], N. PFEIFER[2], G. HOCHREINER[3], G. STHYLER-AYDIN[1,4], U. HERBIG[1] ,M. DÖRING-WILLIAMS[1]

[1] Institute of History of Art, Building Archaeology and Restoration, Technische Universität Wien, Karlsplatz 13/E251, 1040 Vienna, Austria - (taskin.oezkan, gudrun.styhler, doering-williams, ulrike.herbig)@tuwien.ac.at

[2] Research Unit of Photogrammetry, Department of Geodesy and Geoinformation, Technische Universität Wien, Wiedner Hauptstraße 8/E120, 1040 Vienna, Austria - norbert.pfeifer@tuwien.ac.at

[3] Institute of Mechanics of Materials and Structures (IMWS), Technische Universität Wien, Karlsplatz 13/202, 1040 Vienna, Austria - georg.hochreiner@tuwien.ac.at

[4] Österreichisches Archäologisches Institut,Österreichische Akademie der Wissenschaften (ÖAW), Franz Klein-Gasse 1, 1010 Vienna, Austria - gudrun.styhler-aydin@oeaw.ac.at

ABSTRACT

Dense point clouds are suitable data sources for monitoring the current state of roof structures. In this study, an automated 3D model of the roof structure is generated by fitting cuboids to detected adjacent planar beam faces. Data driven occlusions like shadow effects on the point cloud, solid obstacles in front of the beams or deformations on the beams may cause incompleteness of the generated model. Structural assessment of the roof structure is only possible after modeling and interlocking all beams. To generate a complete model, an interval analysis-based beam search workflow is developed. Within the workflow, repetitive beams are classified based on position and orientation of the beam axes. The distances between neighboring beams in a repetitive beam class are used to locate the missing beams. Additionally, partly modeled beams are extended to the full size referring to the extends of all beams in the corresponding class. The developed workflow is examined on the beams, which are connected to the plane of the roof tiles. The results show that all missing beams and joints are detected for the processed data. The developed workflow fills the gap between automated modeling and structural assessment through generating a fully interlocked model.

KEYWORDS: 3D reconstruction, point cloud processing, timber roof structures

1. INTRODUCTION

Documentation stages of historic timber roof structures including surveying on site, 3D parametric modeling of individual beams, detection and identification of the joints, are challenging preliminary studies before a structural assessment analysis. While, traditional survey method consisting of measuring with tapes and documenting on paper brings intensive labor on site, total station or laser scanner based surveying can replace the big part of the effort during surveying.

TLS (Terrestrial Laser Scanners), surveying devices based on LIDAR (Light Detection And Ranging) technology, can measure, highly-precise, millions of 3D points on the object surfaces within several seconds [1]. In comparison to a total station, TLS is an expensive device, but it produces much more detailed information (point cloud) related to the scanned region in a short period of time. SfM (Structure from Motion) is an alternative low-cost way of point cloud generation through multiple images [2]. However, as this method is based on images, it is highly affected by the light conditions of the study area. A point cloud, the product of TLS, is a representation of scanned objects through a large amount of 3D point coordinates as well as attributes like color, intensity, echo-width etc. Point clouds have to be turned into useful models for the different specialists (architects, engineers, restorers, etc.) involved in the project [3].

The structural analysis depends highly on how close the as-built model is to the real situation, including various aspects of input parameters (geometry, materials and joint relationship) [4]. The parametric modeling of beam frame systems or indoor objects through segmentation of point clouds has been studied in many works [3, 5, 6, 7, 8]. However, a large number of the beams can be modeled by the automated approaches that are presented in [5, 6, 8], but the automated models are still incomplete in terms of number of structural elements or beam dimensions because of lack of information during point cloud acquisition or based on processing-driven data-loss.

This study addresses the refinement of point cloud-based automated timber roof structure models through its repetitive characteristics to generate structural assessment-ready data.

2. MATERIALS AND METHODS

2.1 Point Cloud of the Investigated Roof Structure

The roof structure of St. Michael, a medieval church in the city center of Vienna, is investigated to apply the developed methods of this study. In perspective of dimensions, the length of the roof structure along the longitudinal axis above nave and chancel is around 65 m, the extend of the latitudinal axis above the transept is 32 m, height is near to 10.5 m and the span length of the vertical slice of the repetitive sections is nearly 11.5 m [8]. While the distance between neighbor rafters is approximately 70 cm, the roof structure consists of around 1 m to 10 m long timber beams with the width of 10 cm to 25 cm.

The roof structure was scanned using Riegl VZ-2000i TLS device [9]. To cover as many as possible surfaces inside the roof structure, scanning was made from 241 different positions [8]. After registration of the point clouds from different scan positions to a superior coordinate system, 3D point cloud representation of the entire roof structure was acquired with more than 600 million points. Scanning on site and registration of the point clouds were finalized in 3 days.

2.2 Methods

2.2.1 Overview

The proposed workflow (in Figure 1) takes the registered point cloud of the roof structure as input data. The first step is modeling of individual beams within an automated approach like [5, 6, 8]. In the next step, beams are classified to sub-sets by means of position, dimension and orientation. During refinement of the model (step 3), creating, extending or merging operations are applied guided by repetitive beam order. After detection of the joints for the refined model, the possibility of extending the beams around expected joint locations is considered. The final product, are fully interlocked parametric beams (defined as cuboids) and the joints are exported to a STEP [10] file to be an input for the structural assessment.

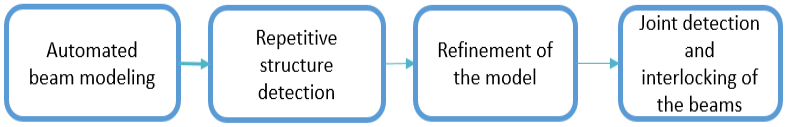

Figure 1: Processing workflow

2.2.2 Automated Beam Modeling

A set of methods were used in a developed workflow to generate cuboid models of the straight or slightly-bending beams within the roof structures made of timber beams with rectangular cross-section [8]. In this study, we follow the workflow that explained in [8] to generate a set of cuboids directly out of the point cloud. While a registered point cloud is the input of this approach, a point cloud of the roof cover and beams represented by cuboids are the outputs.

2.2.3 Repetitive Structure Detection

Repetition of the similar beams in the roof structure can give the positional information about missing, extendable or mergeable elements in the automated model. To evaluate the methods in this study, we focused on the beams which are connected to the roof tiles.

Output data of the previous step is not only a set of cuboids, but also a point cloud that corresponds to the cover of the roof [8]. Both these data are inputs of the automated repetitive beam clustering (Figure 2).

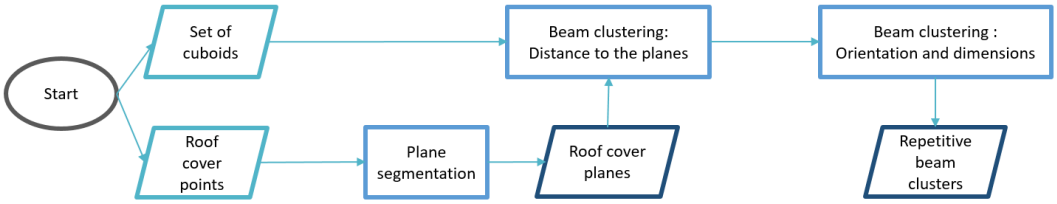

Figure 2: Flowchart of beam clustering

Within the process (Figure 2), the roof cover point cloud is segmented into large planar groups by adapting the RANSAC [11] algorithm. Then, beams are assigned to the corresponding planes using a beam to plane distance threshold.

Clustering is made with the k-means [12] algorithm in order to separate the most parallel beam groups within each beam cluster (which refers to the planes).

2.2.4 Refinement of the Automated Model

Registered point cloud, a set of parallel beams and a plane that fits well to those beams allow us to analyze the repetition in the structure. As the beams are stored as cuboids after the automated modeling, 3D line segments are easily extracted out of longitudinal axes of the cuboids. To apply the computations in 2D space, 3D line segments are projected to the corresponding planes (Figure 3).

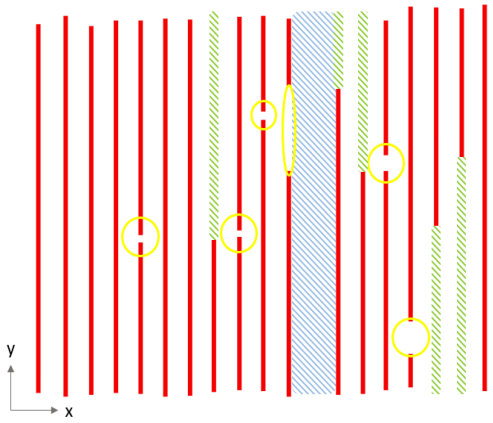

Figure 3: 2D projection of the beam axes (red), mergeable beams (in yellow circular regions), missing beam search region (blue pattern) and extendable beam region (green pattern)

A generalized interval distance (d_inter) between two lines within a set of line segments as shown in Figure 3 (vertical red lines) can be calculated thresholding the histogram of the sequential distances along the x axis. After estimation of the interval distance, the following possibilities can be formulated:

a. Missing beams:
$d\_(i,j) > d\_inter$ (1)

b. Mergeable beams:
$d\_(i,j) < w\_max$ (2)

c. Extendable beams:
$|P\_Start - P\_Bottom| > d\_max$ OR $|P\_End - P\_Top| > d\_exten$ (3)

Within the equations (1-3), $d\_(i,j)$ is the horizontal distance between two neighbor beams, w_max is maximum beam width inside the structure, P_Start and P_End are beginning and end points of a beam, P_Bottom and P_Top are projection of all P_Start and P_End to the horizontal line segment of the minimum bounding rectangle (MBR) of the beam group. d_extend is a thresholding value (e.g. 10cm) that controls extending of a beam.

As a next stage of the process, mergeable beams are merged to a single beam, if orientation and the dimensions are fitting well to each other. To create a new beam around missing beam search region or extending a beam along extendable beam region, registered point cloud is used as an additional input. Within these regions, a cuboid search is performed in order to clarify if there are scanning points that are corresponding to the beam faces.

2.2.5 Joint Detection and Interlocking of the Beams

In the previous step, the automated model is refined against process-driven loss and modified or newly added cuboids are still based on the registered point cloud. To detect data-driven loss (caused by shadows effect, irregular point density etc.) on the refined model, beams that are full-extend modeled and corresponding joints can guide the process to find out missing joints and un-interlocked beams.

Joints are located around the intersection of the beams and stored as line segments that represent the shortest connections between interlocking beams.

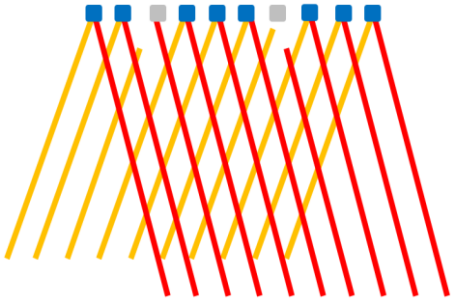

Figure 4: Joint detection: detected (blue) and expected (gray) joint locations, interlocked (orange and red) beam groups

Figure 4 shows that beams from the orange group are interlocked to the beams from the red group around the top of the roof. Missing joints and its member beams can be extracted out of this information. Then, as a last refinement process on the model, these beams are extended to each other and corresponding joints are added to the model. All the parametrically modeled beams (cuboids) and the joints are exported to STEP format to fulfill the structural analysis.

3. RESULTS

For the studied roof structure, automated beam modeling, first step of the workflow shown in Figure 1, was resulted in 1084 beams within 3 hours [8]. At the end of rest of the workflow, an .stp file including beams which are connected to the roof tiles and joints as line segment connectors between intersecting beams, the result product of the study, was generated within 8 minutes using a computer with AMD Ryzen 7 (8 x 3.70 GHz) processor.

Figure 5 (d), the result of Section 2.2.3, visually shows that a repetitive structure can be extracted out of an automated model and its roof cover point cloud.

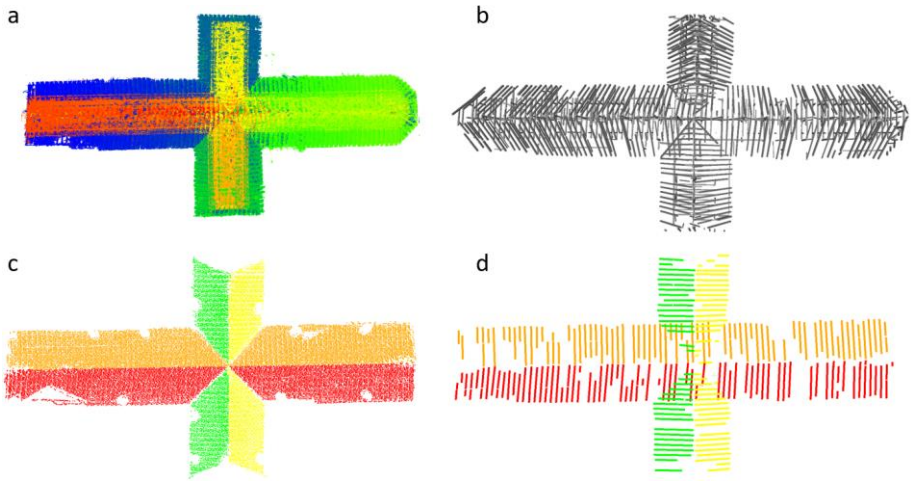

*Figure 5: Registered point cloud colorized by the scanning time-stamp of the TLS (**a**), automated roof structure model as a set of cuboids (**b**), Planar segmentation of the large roof tiles (**c**), 4 repetitive parallel beam groups that are corresponding to the plane segments (orange, red, green and yellow)*

Within the 4 sets of beams, 274 beams exist (Table 1). 55 joints can be extracted out of all those beams.

Table 1: Number of the beams in the refined model

Beam Group	Nr. of Beams	Create	Extend	Merge	
				Before	After
Group 1 (Orange)	84	10	34	26	13
Group 2 (Red)	95	12	25	50	24
Group 3 (Yellow)	51	3	7	18	9
Group 4 (Green)	44	8	15	18	9
Total	274	33	81	112	55

While the number of automatically detected joints after application of the method (Section 2.2.4) increased to 270, the next step (Section 2.2.5) resulted in 305 joints. Figure 6 shows all modeled beams and the joints stored in an .stp file are imported to DLUBAL RSTAB [13], a software that contains structural assessment analysis tools.

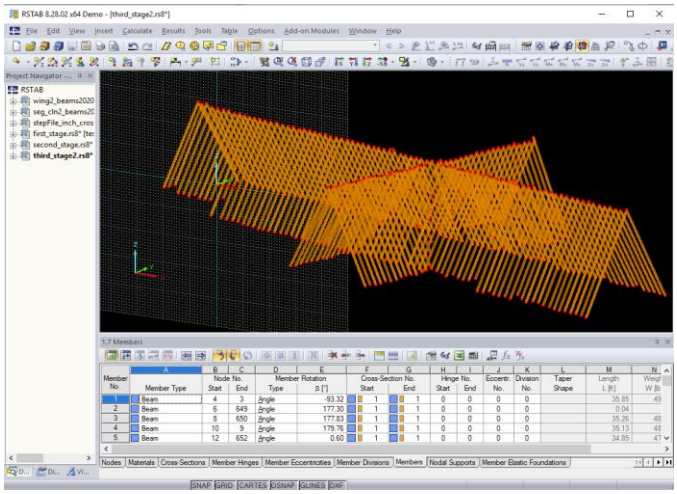

Figure 6: Result model on RSTAB 8 software

CONCLUSION

The results show that the proposed method is feasible to fulfill the incomplete structural elements through the repetitive structure of the roof construction. Together with extended and additionally

created beams within the workflow resulted in detection of all missing joints and a fully-interlocked model.
As the method was applied on a limited number of beams from an automated model, the solution should be improved to cover the entire beam structure. Deformed geometry still has to be converted into the original stressless geometry from the time of machining for structural analysis. Therefore the identification of master geometries is very important.

REFERENCES

[1] Vosselman, G.; Maas, H.G. Airborne and Terrestrial Laser Scanning; Whittles Publishing: Dunbeath, Scotland, **2010**.

[2] Schönberger, J L.; Jan-Michael F. Structure-from-Motion Revisited, 2016 IEEE Conference on Computer Vision and Pattern Recognition - CVPR **2016**, 4104-4113.

[3] Barazzetti L. Parametric as-built model generation of complex shapes from point clouds, Advanced Engineering Informatics, **2016**, 30, 298-311, ISSN 1474-0346.

[4] Yang, X.; Koehl, M.; Grussenmeyer, P. Automating Parametric Modelling From Reality-Based Data by Revit Api Development, Latest Developments in Reality-Based 3D Surveying and Modelling, MDPI, **2018**, 978-3-03842-685-1-14.

[5] Pöchtrager, M.; Styhler-Aydin, G.; Döring-Williams, M.; Pfeifer, N. Digital reconstruction of historic roof structures: Developing a workflow for a highly automated analysis. Virtual Archaeol. Rev. **2018**, 9, 21–33.

[6] Murtiyoso, A.; Grussenmeyer, P. Virtual Disassembling of Historical Edifices: Experiments and Assessments of an Automatic Approach for Classifying Multi-Scalar Point Clouds into Architectural Elements. Sensors **2020**, 20, 2161.

[7] Truong-Hong, L.; Lindenbergh, R. Extracting structural components of concrete buildings from laser scanning point clouds from construction sites, Advanced Engineering Informatics, **2022**, 51,101490, ISSN 1474-0346.

[8] Özkan, T.; Pfeifer, N.; Styhler-Aydın, G.; Hochreiner, G.; Herbig, U.; Döring-Williams, M. Historic Timber Roof Structure Reconstruction through Automated Analysis of Point Clouds. J. Imaging, **2022**, 8, 10.

[9] Riegl VZ-2000i Terrestrial Laser Scanner, http://www.riegl.com/nc/products/terrestrial-scanning/produktdetail/product/scanner/58, accessed 16.05.2022.

[10] STEP, Industrial Automation Systems and Integration—Product Data Representation and Exchange. (Version ISO 10303-21:2016), https://www.loc.gov/preservation/digital/formats/fdd/fdd000448.shtml, accessed 16.05.2022.

[11] Fischler, M.A.; Bolles, R.C. Random sample consensus: A paradigm for model fitting with applications to image analysis and automated cartography. Commun. ACM **1981**, 24, 381–395.

[12] MacQueen, J. B. Some Methods for classification and Analysis of Multivariate Observations, Proceedings of 5th Berkeley Symposium on Mathematical Statistics and Probability, University of California Press., **1967**, 1, 281–297.

[13] DLUBAL RSTAB Software, https://www.dlubal.com/en/products/rstab-beam-structures/what-is-rstab, accessed 26.05.2022.

A SURVEY FORM FOR THE STRUCTURAL HEALTH ASSESSMENT OF TIMBER CONSTRUCTIONS

B. FAGGIANO[1], M. NICOLELLA[2], G. IOVANE[1], and D. MARRANZINI[1]

[1] Dept. of Structures for Engineering and Architecture, [2] Dept. of Civil, Building, Environmental Engineering, University of Naples Federico II, 80, P.le Tecchio, 80125, Naples, Italy

ABSTRACT

Despite timber is one of the oldest building materials, it is vulnerable to environmental degradation actions. Thus, the design of timber structures should integrate the aspects related to the structural performances together with those related to durability. The vulnerability against decay actions can be mitigated through several design choices, having different impact on durability performances. Nevertheless monitoring and maintenance play a fundamental role.
Therefore, given the importance of durability issues in the design and maintenance of timber structures, a new survey form for the structural health assessment is proposed. The outline is articulated for addressing structural typology, decay identification and possible interventions. The survey form is validated on a sample of simple existing structures, demonstrating the reliability and effectiveness of the evaluation.

KEYWORDS: Timber structures durability, on-site assessment, survey form, visual inspection, structural health assessment.

INTRODUCTION

Timber has numerous attributes that make it an attractive building material. Especially in the last decades timber-based products with high performances have been developed and spread. However, one of the weakest points of timber can be the durability, if it is exposed to environmental agents, since the service life of the structure can be drastically reduced.
Durability of timber is influenced by several factors like environmental conditions, wood species and protective treatments. Generally, it can be evaluated by comparing demand and capacity. The most common durability related actions, which can mine the structural bearing capability, are fungi and insect attacks. They induce a biological decay [1] with consequences varying from the degradation of the mechanical properties to the cross-section size reduction of the structural member due to the loss of integrity, furthermore the effect can be localized or diffused. Besides each timber species has a different behaviour against the durability related actions, a scale is reported in EN 350 [2]. When the timber durability is not adequate, protective treatments can be used, in order to reduce the vulnerability of the structure. Nowadays various types of treatments are spread. Traditional one consists on the superficial or deep application of simple products that reduce the absorption of water, as well as biocide products. Also those inducing thermal and chemical modifications of timber are efficient, they increasing the resistance to biodegradation [2, 3]. Currently, the influence of these treatments on the mechanical proprieties of timber is object of extensive research [4]. The selection of timber species and treatments

is regulated by Codes [5, 6, 7, 8, 9]. Other fundamental factors that impacts on durability are the design choices, dealing with construction details, the appropriate on site storage of timber, the scheduled maintenance of the structure. Nevertheless, structural health monitoring and maintenance are certainly the most effective actions, especially for historic timber structures [10], as they are more vulnerable to decay. Scheduled maintenance is reliable when, through structural health monitoring, the pathologies of deterioration are promptly recognized and interventions are taken. Visual inspection and measuring survey are fundamental steps of structural health monitoring. Therefore, an indispensable and base tool for the inspection of timber structures is the survey form, either hardcopy or digital document that allows the collection of all the necessary information. With regards to timber structures, many templates for inspection and diagnosis are spread in literature, they differ in scope (damage, vulnerability, conservation assessment) and level of investigation (preliminary, general, detailed). Concerning the damage assessment, templates are proposed by Toratti [11] and Serafini et al. [12], the latter specifically devoted to the failure prevention of heritage timber roofs. For the vulnerability assessment on a territorial scale, a survey form is provided by Riggio et al. [13]. Many authors suggested a multi-purpose inspection template, for guiding the expert in the collection and interpretation of data [14]. It is worth noticing that most of the aforementioned templates were conceived in digital form, in order to easily create consistent database for subsequent analyses [13, 15].

In this paper a new survey form for the structural health assessment (SHA) of timber (T) structures is proposed. The form has been conceived for the identification of the structural types focusing on the aspects related to the seismic vulnerability, in the framework of the Italian project DPC–ReLUIS 2019-2021, for the development of activities related to the seismic prevention and protection of built heritage. Durability issues concerning timber structures have been further included for extending the structural vulnerability assessment also against the environmental actions. Accordingly, the causes of decay can be recognized. Finally, the indication of the corresponding best fitting interventions is given. The purpose of the survey form is twofold: 1) to provide an operational tool for the structural health assessment of timber structures through a guided descriptive procedure, which could be used even by not specifically expert technicians; 2) to provide a support tool for the estimation of the seismic vulnerability through quick level methods taking into account also the durability of the timber structures. The SHA-T survey form has been applied and validated on a sample of simple existing timber structures in order to evaluate the reliability and effectiveness of the proposal.

THE DRAFT PROPOSAL OF A SHA-T SURVEY FORM

The SHA-T form, inspired by the Cartis form [15], was specifically conceived for the existing timber structures characterized by large-span. Then, it has been modified and integrated, in order to involve a wider range of timber structural types, making it applicable also to the historical structures and ordinary timber structures, at the same time, taking into account durability aspects.

The framework is conceived through a top-down approach, going from the localization and description of the building to the structural member characterization. The template is articulated in three main parts, corresponding to the following issues: building identification, timber decay detection, treatments/interventions. It is divided in seven sections (Table 1), synthetically described hereafter.

Table 1: Outline of the SHA-T survey form

Building Identification	A	Identification of municipality and building
	B	Identification of the building constructive technology and typology
	C	Description of the building
Timber decay detection	D	Characterization of the structural members
	E	Decay effects identification
	F	Decay typology
Interventions and treatments	G	Possible interventions and treatments

Section A collects general information related to either the municipality where the building is located, or the surveyor and the building.
Section B deals with the characterization of the building construction (Fig. 1): materials of each structural systems, structural type, floor in plane stiffness, bracing system, roof structure and foundations .
Section C allows the description of the main aspects of the overall building (Fig. 3): main geometrical features, age and use of the building.
Section D should be filled for a single structural member, whose state of degradation is characterized in the subsequent section (Fig. 3): type, material and timber species of the member, as well as year of construction, environmental temperature, hazard (EN 335-1) and durability (EN 350-2) classes.
Section E reports the distinctive aspects that allow the recognition of timber decay typology on the basis of the scientific literature (Fig. 4): timber colour, consistency, cracks, holes and cavities, extent of damage, existing treatments, moisture contents.
Section F allows the identification of the timber decay, if biological or abiotic, and then the specific fungus or insects attack on the basis of the decay effects described in the previous section, through a manual of use based on the scientific literature ([16, 17]; Fig. 4).
Section G lists possible curative interventions and treatments, selected as function of the recognized timber decay (Fig. 4).

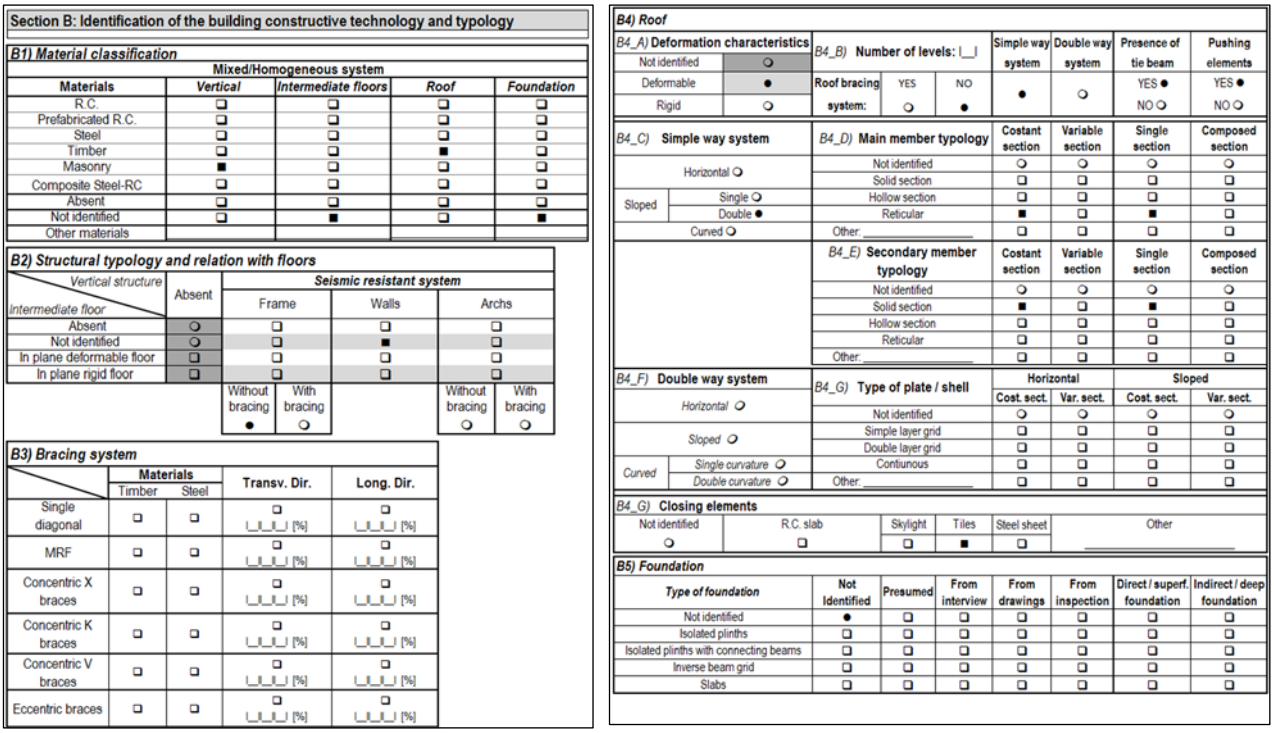

Figure 1: SHA-T survey form: Section B "Identification of municipality and building".

APPLICATION TO CASE STUDIES

The survey form is tested on four simple case studies located in different municipalities of the Southern Italy. They are selected for the sake of representativeness of recurrent types of constructions, structural types and decay, in order to verify the reliability and versatility of the survey form.
Below the application of the SHA-T survey form is presented for the case study of Palazzo Caracciolo (Fig. 2), an historical building placed in the centre of Naples (Figs. 1-4). The assessment is carried out through visual inspection, filling on site the survey forms. The information about the municipality where the building is located and the identification of the surveyor are reported in section A. It has masonry walls as vertical structural system, with the roof characterized by ancient timber trusses (section B; Fig.

1). The intermediate floors and foundation haven't been identified since they were not investigated. The roof is a simple way system with secondary beams supported by main trusses, the roof structure is in-plane deformable, without bracing system, the presence of pushing elements and tie beam are recognized. Structural members have a single section. The closing elements are tiles. The building has 4 stories, with average interstory height ranging between 3.5-5m. It has a destination of use for public utility activities (section C; Fig. 3).

a) *b)*

Figure 2: a) Palazzo Caracciolo (Naples); b) The study trusses

The decay analysis (sections D-G; Figs. 3-4) concerns the two struts and tie belonging to the timber truss placed at the roof level. Both of them are made of solid timber, however the timber species have not been recognized, so that the durability class could not be assigned to the members. The year of construction is before the 1950. The hazard class has been successively identified, being the members exposed to occasional humidity.

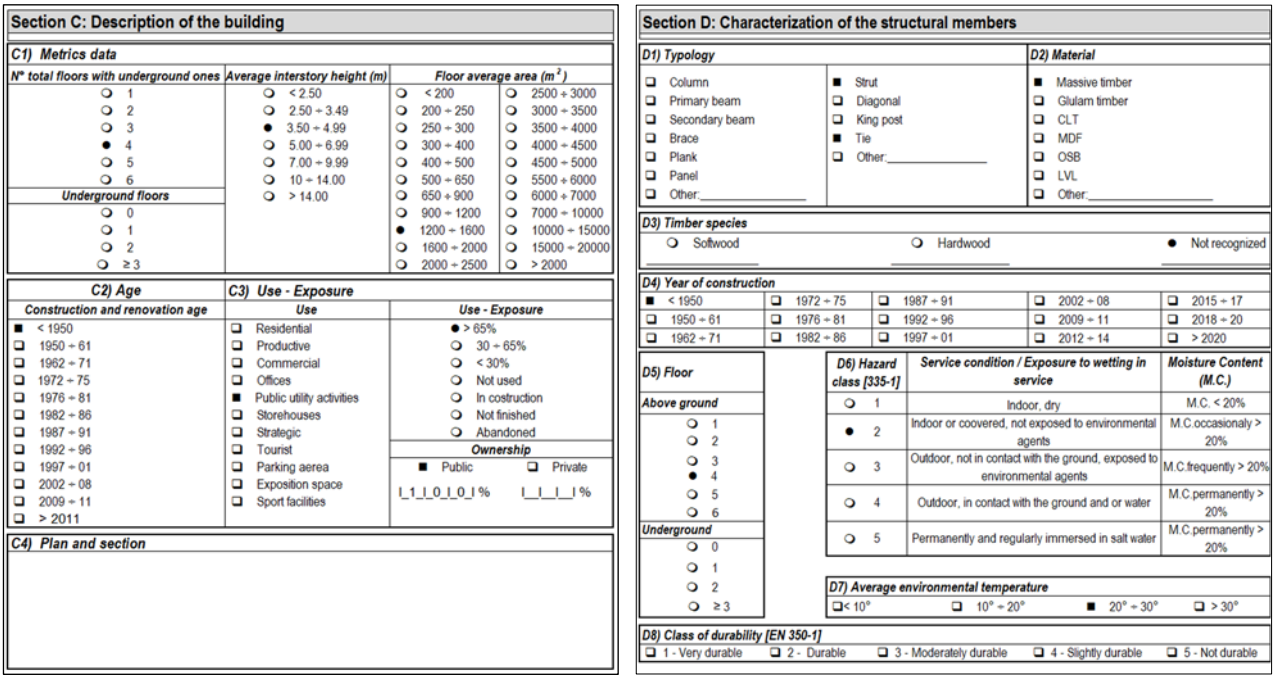

Section C: Description of the building

C1) Metrics data

N° total floors with underground ones	Average interstory height (m)	Floor average area (m²)	
○ 1	○ < 2.50	○ < 200	○ 2500 ÷ 3000
○ 2	○ 2.50 ÷ 3.49	○ 200 ÷ 250	○ 3000 ÷ 3500
○ 3	● 3.50 ÷ 4.99	○ 250 ÷ 300	○ 3500 ÷ 4000
● 4	○ 5.00 ÷ 6.99	○ 300 ÷ 400	○ 4000 ÷ 4500
○ 5	○ 7.00 ÷ 9.99	○ 400 ÷ 500	○ 4500 ÷ 5000
○ 6	○ 10 ÷ 14.00	○ 500 ÷ 650	○ 5500 ÷ 6000
Underground floors	○ > 14.00	○ 650 ÷ 900	○ 6000 ÷ 7000
○ 0		○ 900 ÷ 1200	○ 7000 ÷ 10000
○ 1		● 1200 ÷ 1600	○ 10000 ÷ 15000
○ 2		○ 1600 ÷ 2000	○ 15000 ÷ 20000
○ ≥ 3		○ 2000 ÷ 2500	○ > 2000

C2) Age	C3) Use - Exposure	
Construction and renovation age	Use	Use - Exposure
■ < 1950	❑ Residential	● > 65%
❑ 1950 ÷ 61	❑ Productive	○ 30 ÷ 65%
❑ 1962 ÷ 71	❑ Commercial	○ < 30%
❑ 1972 ÷ 75	❑ Offices	○ Not used
❑ 1976 ÷ 81	■ Public utility activities	○ In costruction
❑ 1982 ÷ 86	❑ Storehouses	○ Not finished
❑ 1987 ÷ 91	❑ Strategic	○ Abandoned
❑ 1992 ÷ 96	❑ Tourist	**Ownership**
❑ 1997 ÷ 01	❑ Parking aerea	■ Public ❑ Private
❑ 2002 ÷ 08	❑ Exposition space	I_1_I_0_I_0_I % I_I_I_I %
❑ 2009 ÷ 11	❑ Sport facilities	
❑ > 2011		

C4) Plan and section

Section D: Characterization of the structural members

D1) Typology

❑ Column	■ Strut	■ Massive timber
❑ Primary beam	❑ Diagonal	❑ Glulam timber
❑ Secondary beam	❑ King post	❑ CLT
❑ Brace	■ Tie	❑ MDF
❑ Plank	❑ Other:_____	❑ OSB
❑ Panel		❑ LVL
❑ Other:_____		❑ Other:_____

D2) Material

D3) Timber species

○ Softwood ○ Hardwood ● Not recognized

D4) Year of construction

■ < 1950	❑ 1972 ÷ 75	❑ 1987 ÷ 91	❑ 2002 ÷ 08	❑ 2015 ÷ 17
❑ 1950 ÷ 61	❑ 1976 ÷ 81	❑ 1992 ÷ 96	❑ 2009 ÷ 11	❑ 2018 ÷ 20
❑ 1962 ÷ 71	❑ 1982 ÷ 86	❑ 1997 ÷ 01	❑ 2012 ÷ 14	❑ > 2020

D5) Floor

Above ground	Underground
○ 1	○ 0
○ 2	○ 1
○ 3	○ 2
● 4	○ ≥ 3
○ 5	
○ 6	

D6) Hazard class [335-1]	Service condition / Exposure to wetting in service	Moisture Content (M.C.)
○ 1	Indoor, dry	M.C. < 20%
● 2	Indoor or coovered, not exposed to environmental agents	M.C.occasionaly > 20%
○ 3	Outdoor, not in contact with the ground, exposed to environmental agents	M.C.frequently > 20%
○ 4	Outdoor, in contact with the ground and or water	M.C.permanently > 20%
○ 5	Permanently and regularly immersed in salt water	M.C.permanently > 20%

D7) Average environmental temperature

❑ < 10° ❑ 10° ÷ 20° ■ 20° ÷ 30° ❑ > 30°

D8) Class of durability [EN 350-1]

❑ 1 - Very durable ❑ 2 - Durable ❑ 3 - Moderately durable ❑ 4 - Slightly durable ❑ 5 - Not durable

Figure 3: SHA-T survey form: Sections C and D

Both investigated members showed the same damage (section E; Fig. 4), consisting in the widespread presence of oval shape holes, as well as superficial deterioration (stripes and exfoliations). The decay effects are extended on the whole structural member. Finally, the decay type has been recognized (section F; Fig. 4) as caused by *Cerambycidea* and *Anobium* (Coleoptera). Indeed the insect attack is due to the presence of sapwood inside the timber members. Possible interventions and treatments are indicated (section G; Fig. 4): firstly the superficial cleaning of the members and subsequently the application of treatments. If the case, for the most damaged parts of the member the realization of timber prostheses could be required, although it is a more invasive intervention.

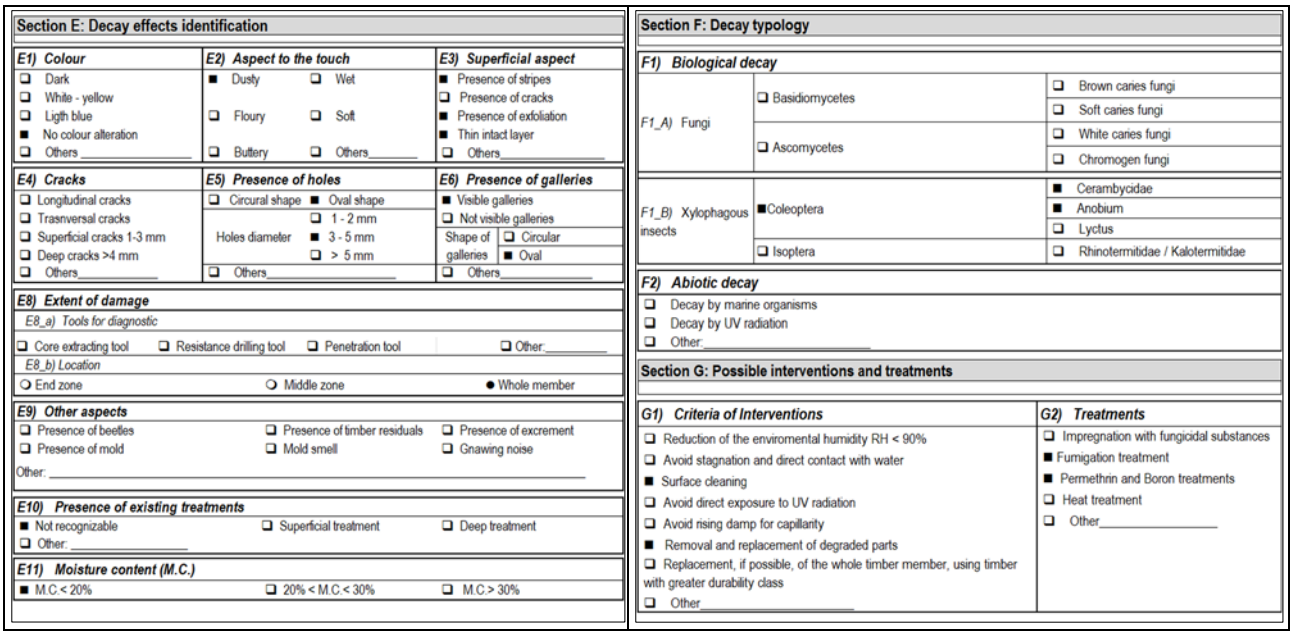

Figure 4: SHA-T survey form: Sections E, F and G

CONCLUSIVE REMARKS

The survey form presented for the structural health assessment allows for a comprehensive building description, structural typology characterization and timber decay assessment. The layout of the form makes it quick and easy to fill out, furthermore the assessment required only visual inspection and the use of simple survey tools. Non-destructive tests can be used if specific issues should be identified. The form appears to be a useful operational tool for the professional community, as guideline in the assessment of structural health conditions of existing timber structures, as well as for creating databases on one hand of timber structural types, on the other hand of recurrent decay effects and causes. It is also worth noticing that the proposed survey form is a support tool for the vulnerability estimation of existing timber building using quick level methods.

The survey form has been applied and validated on four case studies, having positive feedback on the effectiveness of the form framework. More applications are needed in order to include any additional structural types. At the same time supplementary information could be added for including the decay effects and typologies spread in specific environmental condition. In the end possible future developments consist in the digitalization of the form in order to create a web-app that can be easily used via device and that can store the forms in a shared database.

ACKNOWLEDGEMENT

The research project DPC–ReLUIS 2022-2024, both WP13 – Contribution to standards for timber structures and WP2 – Inventory of existing buildings and structural types, as well as the contribution by eng. Giuseppe Rao are acknowledged.

REFERENCES

[1] C.A. Clausen, Chapter 14 - Biodeterioration of Wood, Wood Handb. - Wood as an Eng. Mater. USDA - Gen. Tech. Rep. FPL-GTR-190. (2010) 1–16.

[2] EN 350:2016. Durability of Wood and Wood-Based Products—Testing and Classification of the Durability to Biological Agents of Wood and Wood-Based Materials. European Committee for Standardization, Brussels, Belgium (2016)

[3] S. Ayanleye, K. Udele, V. Nasir, X. Zhang, H. Militz, Durability and protection of mass timber structures: A review, J. Build. Eng. 46 (2022) 103731.

[4] K. Candelier, M.F. Thevenon, A. Petrissans, S. Dumarcay, P. Gerardin, M. Petrissans, Control of wood thermal treatment and its effects on decay resistance: a review, Ann. For. Sci. 73 (2016) 571–583.

[5] M.J. Spear, S.F. Curling, A. Dimitriou, G.A. Ormondroyd, Review of functional treatments for modified wood, Coatings. 11 (2021).

[6] EN 335:2013. Durability of Wood and Wood-Based Products – Use Classes: Definitions, Application to Solid Wood and Wood-Based Products. European Committee for Standardization, Brussels, Belgium (2013).

[7] EN 460:1994. Durability of wood and wood-based products. Natural durability of solid wood. Guide to the durability of requirements for wood to be used in hazard classes. European Committee for Standardization, Brussels, Belgium (1994)

[8] EN 351-1 Durability of wood and wood-based products – Preservative treated solid wood – Part 1: Classification of preservative penetration and retention. European Committee for Standardization, Brussels, Belgium (2007)

[9] EN 599-1/2 (1996/1995) Durability of wood and derived material – Performances of wood preservatives as determined by biological tests – Part 1: Specification according to hazard classes – Part 2: Classification and labelling. European Committee for Standardisation, Brussels, Belgium (1996-1995)

[10] H. Cruz, D. Yeomans, E. Tsakanika, N. Macchioni, A. Jorissen, M. Touza, M. Mannucci, P.B. Lourenço, Guidelines for on-site assessment of historic timber structures, Int. J. Archit. Herit. 9 (2015) 277–289.

[11] T. Toratti, Proposal for a failure assessment template, Eng. Struct. 33 (2011) 2958–2961.

[12] A. Serafini, M. Riggio, C. González-Longo, A database model for the analysis and assessment of historic timber roof structures, Int. Wood Prod. J. 8 (2017) 3–8.

[13] M. Riggio, D. D'Ayala, M.A. Parisi, C. Tardini, Assessment of heritage timber structures: Review of standards, guidelines and procedures, J. Cult. Herit. 31 (2018) 220–235.

[14] M. Riggio, M.A. Parisi, C. Tardini, E. Tsakanika, D. D'Ayala, N. Ruggieri, G. Tampone, F. Augelli, Existing timber structures: proposal for an assessment template, in: 3rd International Conference on Structural Health Assessment of Timber Structures. Wroclaw, September 9–11, 2015, 2015.

[15] B. Faggiano, G. Iovane, A. Gaspari, E. Fournely, A. Bouchair, R. Landolfo, M. Piazza, The Cartis form for the seismic vulnerability assessment of timber large-span structures, Buildings. 11 (2021) 1–40.

[16] Á.T. Martínez, M. Speranza, F.J. Ruiz-Dueñas, P. Ferreira, S. Camarero, F. Guillén, M.J. Martínez, A. Gutiérrez, J.C. Del Río, Biodegradation of lignocellulosics: Microbial, chemical, and enzymatic aspects of the fungal attack of lignin, Int. Microbiol. 8 (2005) 195–204.

[17] A.F. Bravery, R.W. Berry, J.K. Carey, D.E. Cooper, Recognising wood rot and insect damage in buildings, Int. Biodeterior. 23 (1987) 191–192.

STRUCTURAL ASSESSMENT OF THE ROOF STRUCTURE ABOVE THE DOME HALL OF THE AUSTRIAN NATIONAL LIBRARY

GRÄF LUKAS[1], HOCHREINER GEORG[1]

[1] TU Wien

ABSTRACT

This part of the roof structure of the Austrian National Library, which was built in 1848, is a quite extraordinary example for its mix of traditional carpentry and innovations based on engineering methods of the 19th century. Following the architectural demand of a Turkish tent style roof shape, the basic structure of a purlin roof system, complemented by a grid of truss-like subsystems, form the upper storey. The truss-like king post systems had to be adopted due to intersection with the masonry dome structure. Therefore the mid-span elevated tie beam is supported by an innovative connection, which seems to be a consequent development of a traditional rectangular block shear connection type. The upper storey is placed on a set of traditional two-hinge frame systems and masonry headers surrounding the window openings of the dome.
3D-modelling using structural engineering software strengthened assumptions on load distribution through the existing sub-structures for various load combinations. By identifying vulnerable parts of the building, potential failure scenarios of the structure could be evaluated by only use of numerical methods. This could be helpful for the design of structural interventions to strengthen the existing roof. Furthermore, assumptions about the process of assembly could be validated by optional reconfiguration of the structure to its possibly initial stage.
In the framework of an ongoing master's thesis, the interaction of the timber and masonry substructures will be discussed in the context of robustness and efficient monitoring activities.

KEYWORDS: historical timber structures, masonry dome, structural modelling, robustness

INTRODUCTION

Fundamental steps of structural modelling the timber roof structure have been investigated in the framework of a bachelor's thesis. The multitude of assumptions on the *interaction of the timber roof structure and masonry dome* in combination with significant *crack formations* in essential structural timber elements and essential connections were the motivation for a continuation as master's thesis. Included in that thesis will be a more *holistic structural approach* which should reveal both mechanical transparency as well as the efficiency of concepts for the conservation of the monument in the past.

CHARACTERISATION OF THE ROOF STRUCTURE

Global dimensions and building materials

The *main dimensions* of the roof's respective dome structure seen in Fig. 1b, is dominated by the elliptic geometry of the ground plan. The top of the roof is elevated about 50m above ground.

The *roof covering* according to Fig. 1a consists of oxidized copper sheets in the moderate roof slope area as well as tiles named *Wiener Tasche*, arranged in two layers in the steep slope area.
The *substructure of the roof covering* consists of elements made of softwood trusses with a maximum length of about 10m and cross sections with dimensions of up to 26cmx20cm.
The *dome*, which has a varying thickness from 0,7m to 1,0m, is composed of a masonry structure with solid bricks.

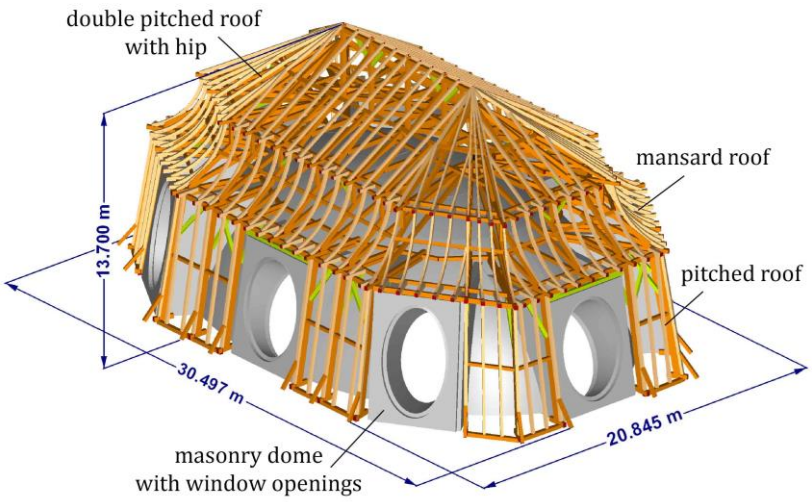

(a) Exterior view [13] *(b) Masonry dome and timber structure*

Figure 1: Overview

Conceptional evolution of the roof structure

Based on the historical structural drawing, seen in Fig. 2a, the timber roof structure should have surrounded the masonry dome structure with a different architectural shape and openings were included for lightening. In the first visualization of the architectural concept, it was certainly not clear if the roof structure would interact with the masonry dome structure regarding support forces at any level of the dome. Even the wall thickness of the dome was intended to be quite narrow to save dead load and minimize horizontal reaction forces. In addition, the options of building sequence, constructing the roof structure either before or after the masonry structure might have been discussed among experts at that time.

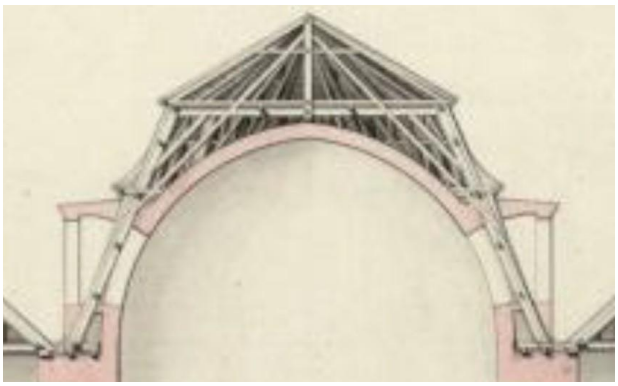

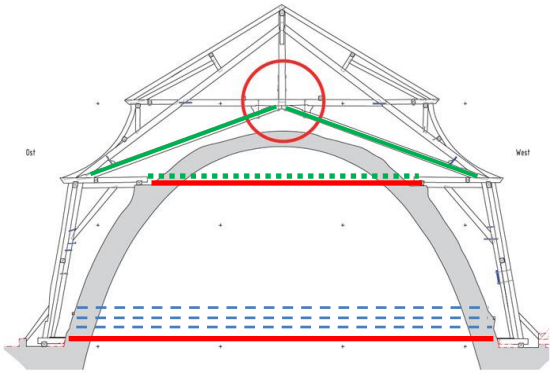

(a) Historical draft of the structure *(b) Finals concept with adoptions*

Figure 2: Initial concept and final realization with adoptions

The result of this discussion is illustrated in Fig. 2b. It can be concluded from structural realizations on site and validations by modelling the structural system at the first building stage, that the roof structure must have been built still before the implementation of the dome structure, which then could be

installed afterwards under safe weather conditions. Therefore, the horizontal elements in terms of conventional tie beams and compressive studs (Fig. 2b, read lines) might have also existed in the first stage of installation according to traditional methods for two hinge frame systems. Due to collision with the masonry dome, the initially intended horizontal tie beam of the king post system of the upper storey (Fig. 2b, green dotted line) might never have been installed in full length. Instead it was substituted as a proactive installation by an additional kinked tie beam with elevation at mid-span up to the level of the collar beam (Fig. 2b, green lines). It can be demonstrated, that the horizontal displacement of the two-hinge system without truncation under wind load is much higher than acceptable displacements of the masonry dome structure. Furthermore, investigations on site still must clarify, if the remaining horizontal elements are structurally connected to the masonry by anchorage devices. Such uncertainty about the structural consequences due to subsequent removal of colliding tie beams might have been the reason that larger wall thickness of the masonry structure was chosen. Fitting the geometry of the dome to the space within the two-hinge systems of the first storey might have simplified the building process. Nevertheless, the neighbouring buildings were realized following the traditional approach with lower absolute height of the eaves and with the top of the vaults still beneath the lowest tie beam without any collision.

It should be mentioned, that due to observed cracks in the vertical masonry walls beneath the cupola, the dome structure had been reinforced later on by several heavy rings made of flat iron tie rods near the base line of the cupola (Fig. 2b, blue dashed lines).

Global segmentation and characterisation of structural elements

The whole structure may be segmented as follows:

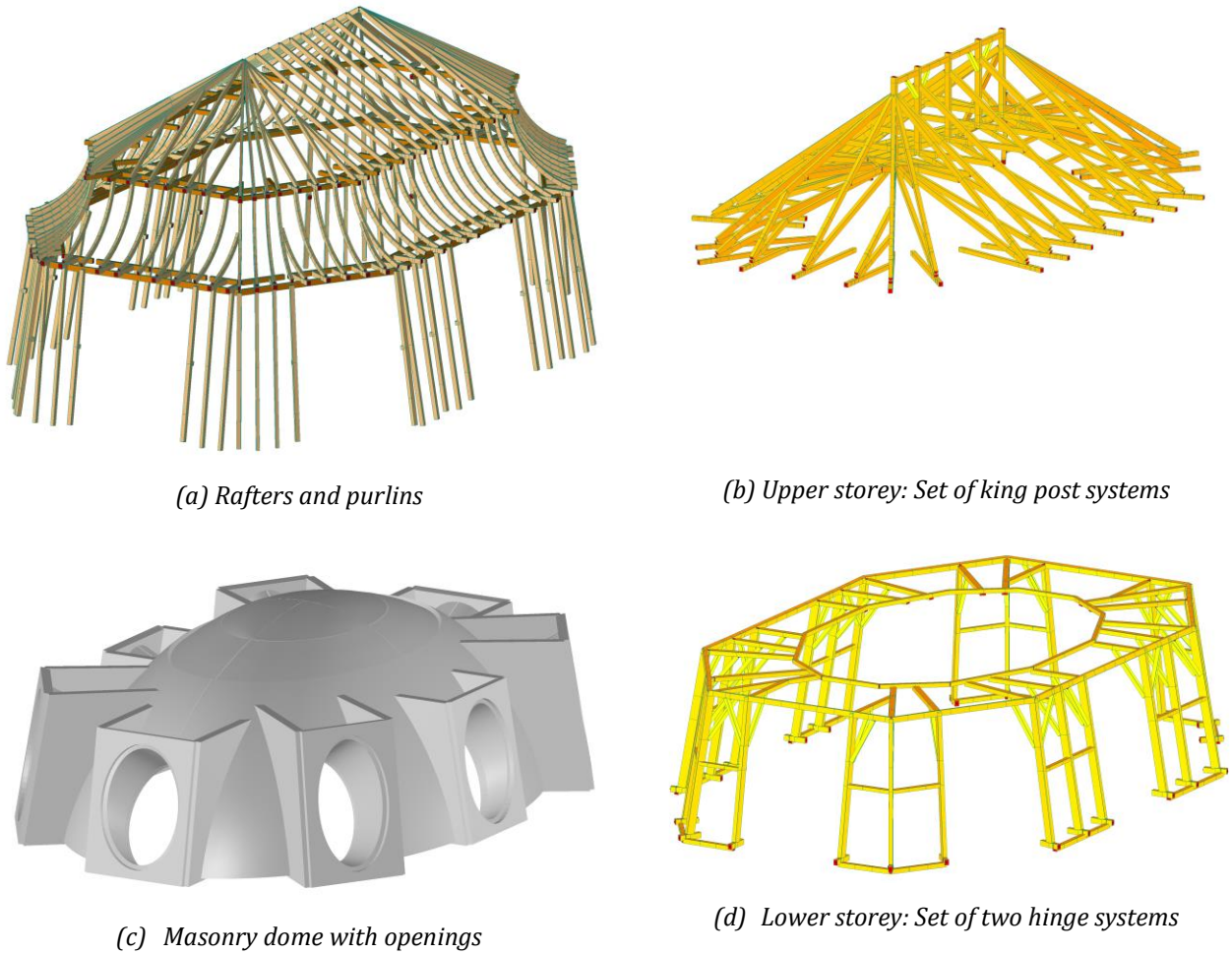

(a) Rafters and purlins

(b) Upper storey: Set of king post systems

(c) Masonry dome with openings

(d) Lower storey: Set of two hinge systems

Figure 3: Global segmentation of structural elements

- According to Fig. 3a, the first entity contains all straight and curved rafters with a distance of about 0,90m, supported by purlins. It should be mentioned, that the purlin systems at any level are not designed to take tensile forces and therefore are not acting as peripheral anchorage system.
- According to Fig. 3b, the second entity contains all supporting structural elements of the upper storey and consists of several *king post systems reinforced by collar beams* which are allocated parallel to each other at a distance of about three times the distance between the rafters or in radial directions constituting the two apses. At midspan the tie beams had been lifted up to the level of the collar beam (see Fig. 2b, green lines) to proactively avoid collision with the masonry structure. Therefore, the collar beam is locally acting as a link between the two segments of the tie beam (see Fig. 7c, Joint A). The collar beam also acts as a support for the purlins and is therefore essential for the special architectural shape of the roof.
- According to Fig. 3d, the third entity represents the lower storey and should be characterized as a *two hinge system* aligned with the geometry of the plane substructures of the upper storey. It was helpful as a platform for the installation of the second storey, but also represents the main load carrying structure of the first storey.

  The single elements with steep slope follow the contour of the elliptic geometry of the groundplan, interrupted only by elliptic openings for lighting. The structural entities between the openings could be interpreted as *early versions of wooden racking walls* made of multifunctionally used studs, interlocked purlins at half height and knee bracing elements parallel to the plane forming the roof.

  Therefore, the loads of the structural elements of the upper storey are transferred downwards either by the columns of the two hinge timber frames beneath or masonry headers surrounding the sections with openings for the windows. Only in areas with direct load from the king post systems, these headers are additionally reinforced by supplementary king post systems without post and very small structural height.
- According to Fig. 3c, the fourth entity represents the *masonry dome structures*, intersecting essential structural elements like tie beams or compressive struts of the surrounding roof structure.

In the apses, the *two hinge systems* of the first storey and the *king post systems* of the second storey both were constructed following the elliptic shape of the dome by cutting main systems at half span and rotating them neglecting all needs for regular structural performance in the context of tie beams and balancing compressive members. Due to the lack of structural truss elements like bottom chord and diagonals between the two spatial grid systems at each apsis (see Fig. 3b), the overall structural interaction becomes complicated regarding wind loads.

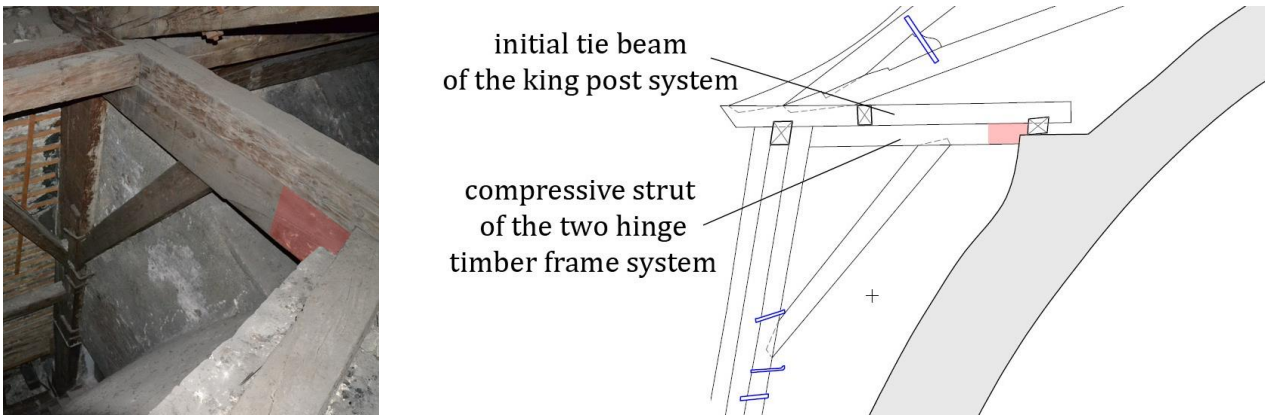

(a) View on site *(b) Drawing*

Figure 4: Intersection and interaction of the timber frame system with the dome structure

According to Fig. 4, the timber structure and the masonry dome are interacting at the level of intersection. At approximately two thirds of the height of the masonry dome, wall beams were installed at the ends of the remaining compressive struts of the two-hinge systems. They are linearly segmented following the elliptic shape of the cupola. It is not yet clear, to which extent horizontal and vertical forces can be introduced from the timber trusses into the masonry substructure via this type of detailing.
Only at the bottom end of the inclined columns of the two-hinge system, horizontal and vertical normal forces are transferred to the initially existing long tie beam, which had to be truncated after finalization of the cupola. The mechanical characterization of the embedment in the masonry structure is still undefined. Today, the horizontal load transfer seems to be primary based on friction.

Innovative connection in terms of the triangular shear block connectors made of oak

Most connections of the roof structure are in line with traditional carpentry joints like mortice and tenons, step joints and cruciform cogs, which were widely used in the 19th century.
Nevertheless, a quite extraordinary innovation for this period is the use of triangular block shear connectors made of oak (see Fig. 5a.) acting as gussets within truss systems. These elements are similar to the practice with rectangular shear block connectors, used to enlarge the moment carrying capacity of two or three mechanically doweled beams made of solid wood. Unfortunately many of these oak connectors are weakened by substantial cracking due to shrinkage.

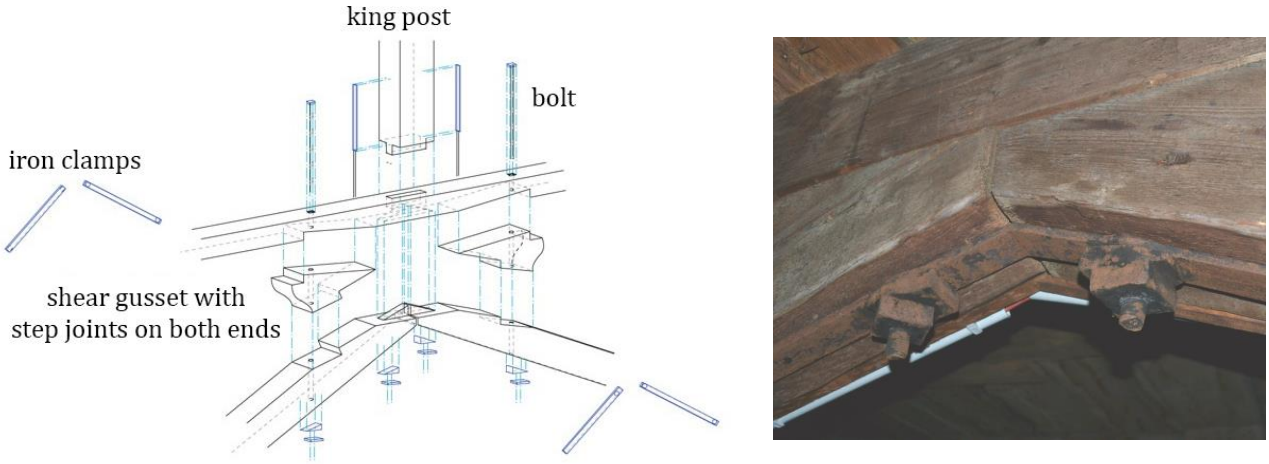

(a) Allocation of block shear connectors made of oak [3] *(b) Flat iron elements at the bottom side*

Figure 5: Connection on top of the elevated tie beam

The normal forces of the main elements of the king post system are transferred via shear and contact at varying grain directions, comparable to connections with scarphs. The induced tilting moment due to the eccentricity of the load introduction is taken by clamping bolts similar to block shear connectors according to EC5 [7]. Additionally implemented bolts (see Fig. 5a) are designed to take the vertical deviating force components induced by kinking of the tie beams and connect them to the king posts.
Uncertainty on the reliability of the triangular shear block connector might have triggered the implementation of additional connecting devices in terms of flat iron elements (see Fig. 5b) in order to take tensile loads in the case of shear failure in the timber elements made of hard wood. The present kinked shape demonstrates, thus far, none of them have ever been stressed. In comparison to modern design regulations, the size of the taper washers seems to have been underestimated at that time.

METHODOLOGY OF STRUCTURAL MODELLING

Structural system

Currently, the timber structure was modeled with 1D elements. For now, the masonry dome is just represented by surfaces without any structural effects in order to represent the geometrical context.
In the ongoing master thesis, the masonry will be modelled as a 3D object for assessment of the volumetric stress components.
Dead, snow and wind loads and equivalent imperfections have been taken from current Austrian standards [4-12].

Connections

At intersections or T-connections of structural members, hinges with special settings are directly allocated at the place of the load transfer, usually in the vicinity of side faces of a cross section. The gap between the hinge and the corresponding beam axis is bridged by rigid elements. This type of modelling allows for direct pickup of internal forces from the calculation to be used for the verification of each connection.
Joints with *tenons and/or scarf joints* are realized by hinges without any capacity to take tensile loads. In the case of compressive normal forces parallel to the beam axis, the hinges are switching to rigid.

(a) Triangular block of oak: Grain direction (yellow) and compressive force (blue)

(b) Corresponding structural modelling (1D elements): Beam axis (white), eccentricities to points of load transfer (yellow), angled rigid element reflecting fibre orientation (green) and clamping element (red)

Figure 6: Modelling of the shear force passing triangular block

In opposition, the *triangular shear block connectors* with horizontal fiber direction (see Fig. 6a) were modeled as plane subsystem with 1D-elements according to Fig. 6b. The subsystem consists of an *angled rigid beam element* (green line) between the scarph-like contact surfaces, taking compression forces and shear stress due to friction, and a vertical member (red line), which presents the centrally allocated clamping bolt. The distance between the contact zone and the beam axis of the corresponding structural elements again is bridged by rigid elements.
The special L- shape representing the oak gusset supports the direct access of force components parallel and perpendicular to the grain.

DISCUSSION

Structural performance with vertical loads only

Under predominant vertical load, the majority of the members are stressed by *compressive normal forces*. The components stressed by tensile forces as depicted in Fig. 7a and Fig. 7c are the tie beams of

the king post systems, the king posts at the center and the hanging trusses locally strengthening the masonry headers above the window openings. The king posts near the apses exhibit higher tensile normal forces in line with the multifunctional use as king post for several radially allocated sub systems. Nevertheless, the collar beams are also locally stressed by tensile loads according to Fig. 7c due to the special type of connection according to Fig. 5a. Outside of J*oint A,* these collar beams are compressed.

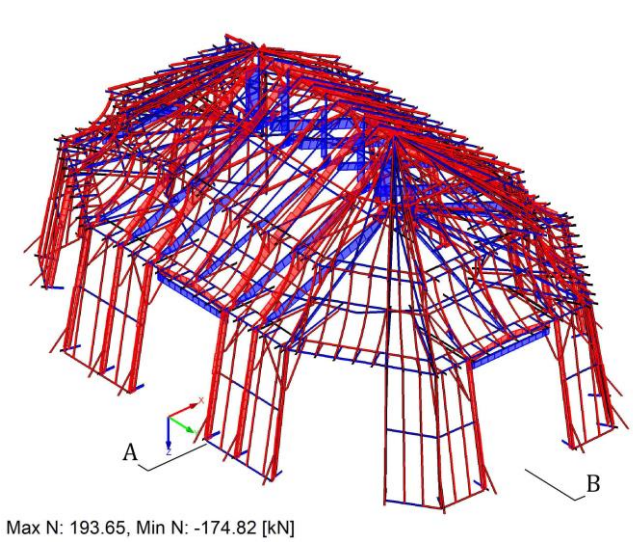

(a) Overview of normal forces: Compression (red) and tension (blue)

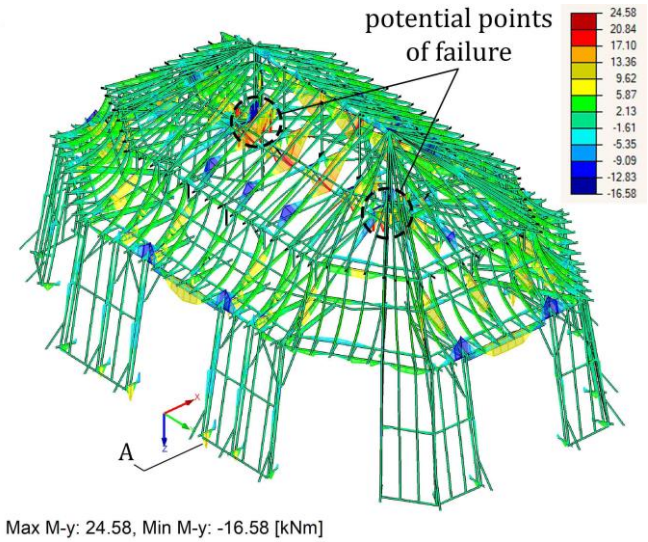

(b) Overview of moments

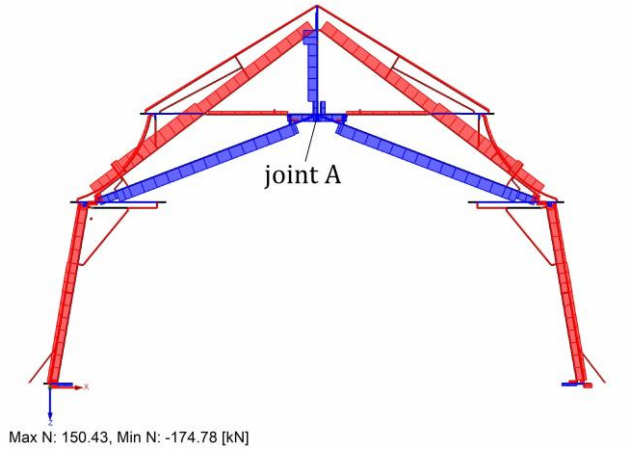

(c) Normal forces at section A-A

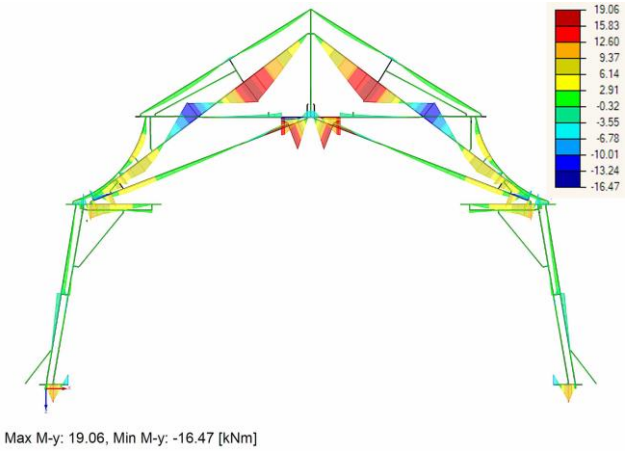

(d) Moments at section A-A

Figure 7: Distribution of normal forces and moments under vertical loading

The highest *bending stress components* according to Fig. 7b and Fig. 7d are evident in the compressive struts of the king post system due to large spans and concentrated loads in opposition to the structural elements like tie beams or collar beams which are not directly loaded by rafters or purlins. Nevertheless, bending moments of curved rafters are amplified by compressive forces.

According to Fig. 8, only a small ratio of the *vertical support forces* from the timber roof structure affects the masonry dome at unfavorable locations. Most of the vertical load is directly transferred to the vertical walls beneath the cupola, which were obviously not designed to take tangential forces induced by radial forces both from the inclined studs and effects from arching. Further investigations are still needed to assess the effectiveness of the reinforcement in terms of heavy rings made of iron bars (Fig. 2b, blue dashed lines).

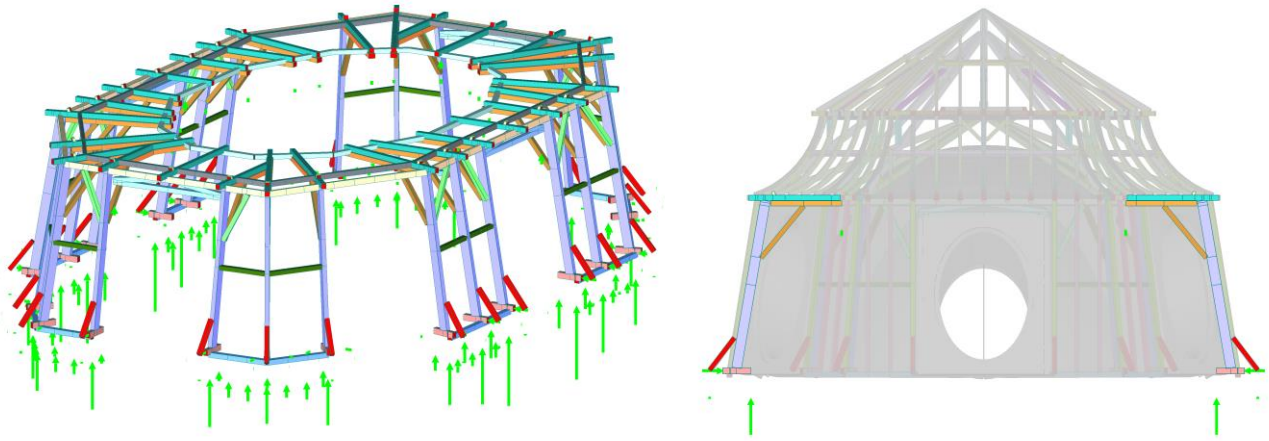

(a) Overview of support forces *(b) Interaction at section A-A*

Figure 8: Reaction and interaction forces under vertical loading

It should be mentioned, that due to wind loads the reaction forces at intersections according to Fig. 4 are much higher due to kinematic compatibility of the timber and masonry structure.

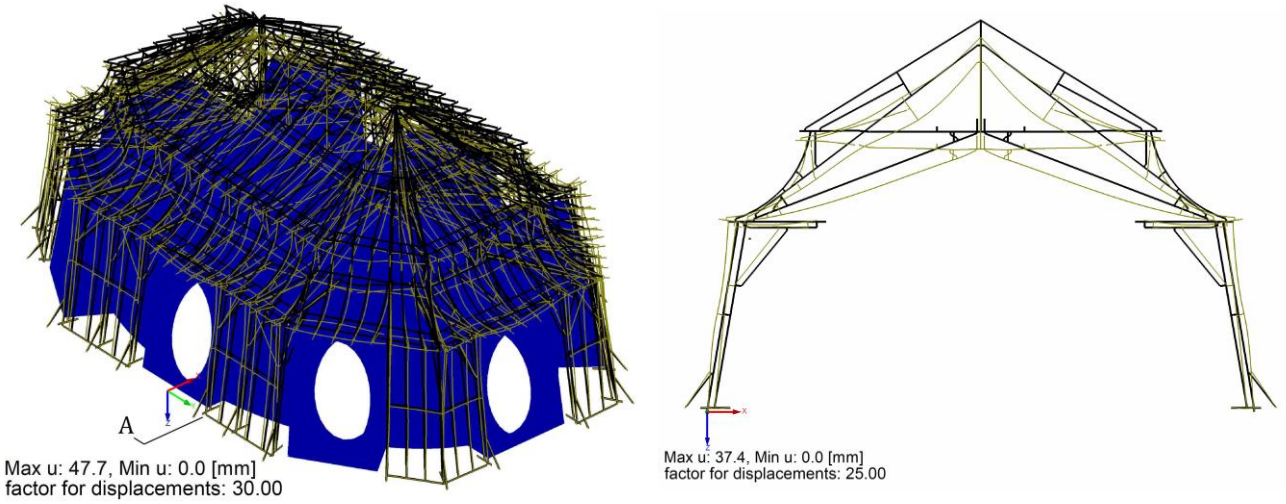

(a) Overview of displacements *(b) Displacements at section A-A*

Figure 9: Displacements under vertical loading

Solely due to vertical loads, the whole structure is characterized by *displacements* in vertical direction without any uplift due to rocking subsystems as depicted in Fig. 9. Quasi rigid body rotation can only be observed in the context of the racking walls of the lower storey.
In general, deformations due to bending are dominating and typical for rafters, purlins and the inclined studs of the kink post system due to coupling with purlins by short struts.

CONCLUSION

From the perspective of the current stage of modelling, the majority of structural members are stressed only up to 70% of their design load carrying capacity. Therefore, weakening of cross sections of up to 30% would be balanced. High grades of utilization still have to be checked and eliminated by refined structural modelling.

In the ongoing master's thesis additional investigations will focus on a *detailed assessment of connections* accounting for observable crack formations, *tangential stress components in the masonry dome* and the still unclear *interaction between the timber structure and the cupola*.
Subsequently, the issue of *robustness* and consequences of local failure of connections respective to single structural members will be discussed and will certainly have an impact on the configuration of the *monitoring system* for this monument.

REFERENCES

[1] Hilber und Schwarz. Kuppel Nationalbibliothek, Querschnitt der Dachkonstruktion, Dokumentation Ringanker. Forschungsber. E251 Institut für Kunstgeschichte, Bauforschung und Denkmalpflege, Technische Universität Wien, 2017. 83 S.

[2] Hohenrieder Johann. Dachwerke am Josephsplatz. Historische Stadtpläne der Stadt Wien, 1849

[3] Libardi, Manolova und Kampik. Die Dächer der Wiener Hofburg, Hofbibliothek_Augustinertrakt. Forschungsber. E251 Institut für Kunstgeschichte, Bauforschung und Denkmalpflege, Technische Universität Wien, 2017. 35 S.

[4] ÖNORM B 1991-1-1:2017 02 01: Einwirkungen auf Tragwerke – Teil 1-1: Allgemeine Einwirkungen – Wichten, Eigengewicht und Nutzlasten im Hochbau – Nationale Festlegungen zu ÖNORM EN 1991-1-1 und nationale Ergänzungen (konsolidierte Fassung). Wien: Austrian Standards, Feb. 2017.

[5] ÖNORM B 1991-1-3:2013 05 01: Einwirkungen auf Tragwerke – Teil 1-3: Allgemeine Einwirkungen - Schneelasten – Nationale Festlegungen zur ÖNORM EN 1991-1-3, nationale Erläuterungen und nationale Ergänzungen (konsolidierte Fassung). Wien: Austrian Standards, Mai 2013.

[6] ÖNORM B 1991-1-4:2019 07 15: Einwirkungen auf Tragwerke – Teil 1-4: Allgemeine Einwirkungen - Windlasten - Nationale Festlegungen zu ÖNORM EN 1991-1-4 und nationale Ergänzungen (konsolidierte Fassung). Wien: Austrian Standards, Juli 2019.

[7] ÖNORM B 1995-1-1:2014 11 15: Bemessung und Konstruktion von Holzbauten - Teil 1-1: Allgemeines - Allgemeine Regeln und Regeln für den Hochbau - Nationale Festlegungen zur ÖNORM EN 1995-1-1 und nationale Erläuterungen (konsolidierte Fassung). Wien: Austrian Standards, Mai 2011.

[8] ÖNORM DIN 4074-1:2012 09 01: Sortierung von Holz nach der Tragfähigkeit - Teil 1: Nadelschnittholz. Wien: Austrian Standards, Sep. 2012.

[9] ÖNORM EN 1990-0-0:2013 03 15: Grundlagen der Tragwerksplanung (konsolidierte Fassung). Wien: Austrian Standards, März 2013.

[10] ÖNORM EN 1991-1-1:2011 09 01: Einwirkungen auf Tragwerke – Teil 1-1: Allgemeine Einwirkungen – Wichten, Eigengewicht und Nutzlasten im Hochbau (konsolidierte Fassung). Wien: Austrian Standards, Sep. 2011.

[11] ÖNORM EN 1991-1-3:2016 01 15: Einwirkungen auf Tragwerke – Teil 1-3: Allgemeine Einwirkungen - Schneelasten (konsolidierte Fassung). Wien: Austrian Standards, Jan. 2016.

[12] ÖNORM EN 1991-1-4:2011 05 15: Einwirkungen auf Tragwerke – Teil 1-4: Allgemeine Einwirkungen - Windlasten (konsolidierte Fassung). Wien: Austrian Standards, Mai 2011.

[13] https://de-academic.com/pictures/dewiki/104/hofbibliothek_vienna_sept_2006.jpg, accessed 23.06.2022

NEW LOW-COST SENSOR FOR TIMBER STRUCTURAL HEALTH MONITORING

Juan J. VILLACORTA[1], Gamaliel LOPEZ[2], Roberto D. MARTINEZ[2], Antolín LORENZANA[3], Alberto IZQUIERDO[1], José-Antonio BALMORI[2], Lara DEL VAL[1], Álvaro MAGDALENO[3], Luis ACUÑA[2], Milagros CASADO[2], Luis-Alfonso BASTERRA[2]

[1] Signal Theory and Communications Department, University of Valladolid Campus Miguel Delibes, 47011 Valladolid, Spain (larval, juavil, alberto.izquierdo)@tel.uva.es

[2] Research Group of Timber Structures and Wood Technology, University of Valladolid Avenida de Salamanca, 18, 47014 Valladolid, Spain (robertomartinez, balmori, basterra)@arq.uva.es

[3] ITAP. Universidad de Valladolid Paseo del Cauce, 59, 47011 Valladolid, Spain alvaro.magdaleno@uva.es, ali@eii.uva.es

ABSTRACT

This paper presents the design of a new device to be implemented in Structural Health Monitoring for timber structures. This device is of small dimensions and uses MEMS sensors, which simultaneously acquire acceleration data in three axes, temperature, environmental relative humidity and moisture content of the wood.

Moisture is an agent that in excess deteriorates structures of any material very quickly, especially timber structures. This new device makes possible not only read the moisture content in real time, but also to correct the acceleration readings as it records, a parameter influenced by moisture content, mainly in timber elements.

These devices are inexpensive, unlike analog accelerometers, and allows to increase the number of monitoring units. The presence of more reading points facilitates the early detection of pathologies, as well as obtaining more accurate FRFs.

This device can also be used for structural wood grading and is part of a mayor monitoring system developed by this research team.

The paper discusses the design of the sensor device, detailing both the electronic components that compose it and the structural design of the casing and the external connector. Various scenarios of used sensor are also shown depending on the placement on the timber structure to be measured, ensuring the correct reading of moisture content.

KEYWORDS: MEM, Structural Health Monitoring, Timber, Moisture, Acceleration

INTRODUCTION

The diagnosis, restoration and conservation of architectural heritage structures require a thorough knowledge of the characteristics of the structure and the materials they are made of, as well as their response throughout their span life. The number of old exiting buildings and civil structures (i.e., resident buildings, hospitals, bridges, . . .) that need an adequate control and maintenance to guarantee their structural operation and safety is currently huge [1].

The evolution of these properties over time can be helpful to assess the actual state of a structure and locate the potential damage it may suffer [2,3]. In addition, monitoring the ambient properties like temperature or humidity can be of great importance in order to correlate the estimated properties with them and separate the deviations due to atmospheric phenomena from true damage [1].

In the case of wooden structures, as a hygroscopic material, wood can adsorb or desorb water in response to temperature and relative humidity of the atmosphere surrounding it. This affinity of wood for water is caused by hydroxyl groups accessible in the cell walls of wood. Consequently, the moisture content of wood is one of the most important variables affecting its physical and mechanical properties [4]. As an example, below fiber saturation point (FSP) the first natural mode of vibration of wood increases and dumping decreases with the loss in moisture content of wood [5]. The speed of sound and de young´s modulus decrease with increasing temperature and moisture content [6]. For these reasons it is essential to know the moisture content of the monitored structural timber components.

However, for these techniques to be truly effective, the sensors need to be permanently installed on the structure, continuously recording the structural response, transferring the recorded data to a remote server, and providing trustfully information about its current state [7-10].

Unfortunately, currently, this is a hard challenge that commercial structural health monitoring (SHM) systems are not fully prepared to undertake. There are many monitoring systems intended to identify the structural properties, some permit to incorporate ambient properties measurement, but few are conceived to work continuously. Finally, none of the commercially available SHM systems satisfy another important restraint: its cost [1].

This contribution presents the design of a prototype measurement sensor using an array of distributed MEMS sensors for the analysis of the vibration modes of a timber structure corrected for its moisture content.

SENSOR AND ACQUISITION SYSTEM

For the analysis of vibration modes, a low-cost data acquisition system has been designed with the - Use of digital MEMS sensors, integrating the analog sensor, the digital converter and the communication interface (Figure 1).

- Use of digital MEMS sensors, integrating the analog sensor, the digital converter and the communication interface.

- Multisensor, allowing the control and reading of up to 6 accelerometers simultaneously.

- Two analog input channels, valid for simultaneous acquisition of data from analog accelerometers or load cells.

- Two analog output channels, for the generation of excitation signals with the possibility of choosing different operating modes, single frequency sine tone, band-limited white noise, pink noise, etc.

- Stand-alone control system, with wireless connection via WIFI between the acquisition system and the computer where the captured data will be stored.

- Automatic power saving mode when the system is no longer in use.

The accelerometer chosen to implement the acquisition system is the Analog Devices model ADXL355. It is a low-power triaxial accelerometer, with a 20-bit digital output and a configurable dynamic range between ±2g and ±8g, which provides a sensitivity of up to 3.9 µg/bit. It allows the use of SPI and I2C interfaces for data reading at a maximum rate of 4000 Hz. In the case of the chosen Humidity and Temperature Sensor was Sensirion model SHT35, fully calibrated, linearized, and temperature compensated 16-bit digital output, with a typical accuracy of ± 1.5 % RH and ± 0.1 °C

Both sensors are incorporated on a 12 x 17 mm circuit board with a mini HDMI connector. This board is encapsulated in a 14x22x9mm plastic housing with different configurations depending on the type and material of the element to be monitored, as well as the duration of the monitoring.

The myRIO platform has been selected to read and control the sensors. It is an embedded hardware, developed by National Instruments and based on the Zynq 7010 chip from Xilinx, which integrates an ARM Cortex A9 dual Core processor and an FPGA. It has 40 digital I/O lines, 2 input channels and 2 analog output channels. The myRIO platform runs a real-time OS (Operating System) that allows the execution of programs created with the LabVIEW graphical language. The communication between the accelerometers and the myRIO is done through digital lines. The SPI protocol has been implemented in the FPGA to access the acceleration data of each sensor and the control program. The ARM processor is in charge of reading the data from all the connected accelerometers and sending them to the central system through the WIFI connection [11].

For the physical interconnection between the sensors and myRIO's digital connectors, mini HDMI connectors have been chosen. The interference protection of this type of wiring allows a greater distance between the sensor and the control system, with cables of up to 10 m having been successfully used.

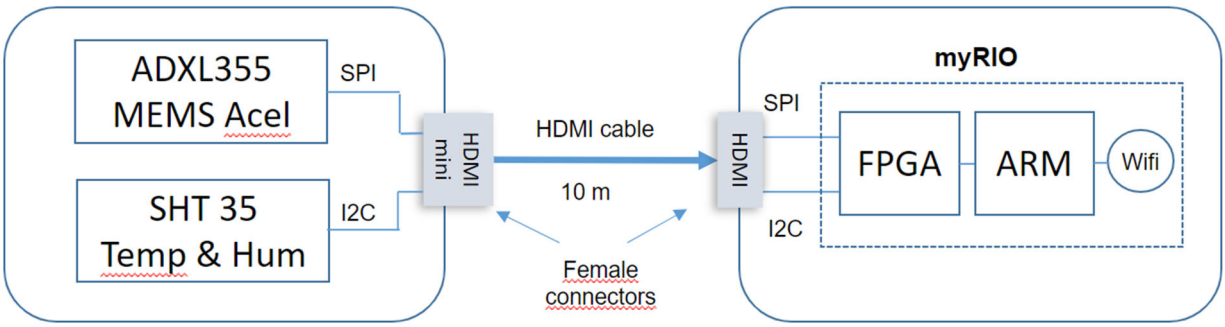

Figure 1: Proposed system architecture.

As for the way to fix the sensors to the structure to be analyzed, different external casings have been designed to adapt the circuit to different measurement scenarios (Figure 2).

A. Rectangular prismatic box to be attached to the surface to be monitored. Preferably for use in long-term monitoring where the sensor is left installed for periods longer than one year. To check the annual cyclic behavior of a structure.
B. Rectangular prismatic box with holes for screws or magnets. This design allows the installation and removal of the sensor. For wooden or masonry elements it is fixed with screws and for metallic elements neodymium magnets are placed in the holes.
C. Casing with cylindrical design, which allows it to be inserted inside the wood elements and to monitor both their dynamic behavior and their moisture content. The hole to house the sensor is drilled through a borehole. This must be at least 5 mm deeper than the length of the sensor, creating a chamber where it is possible to monitor the temperature and relative humidity of the indoor air, which is in hygroscopic equilibrium with the moisture content of the wood. This type of design is intended for constant monitoring of wooden structures.

Finally, thanks to advances in 3D printing, it is possible to design and manufacture the outer casing ad hoc for almost any monitoring scenario.

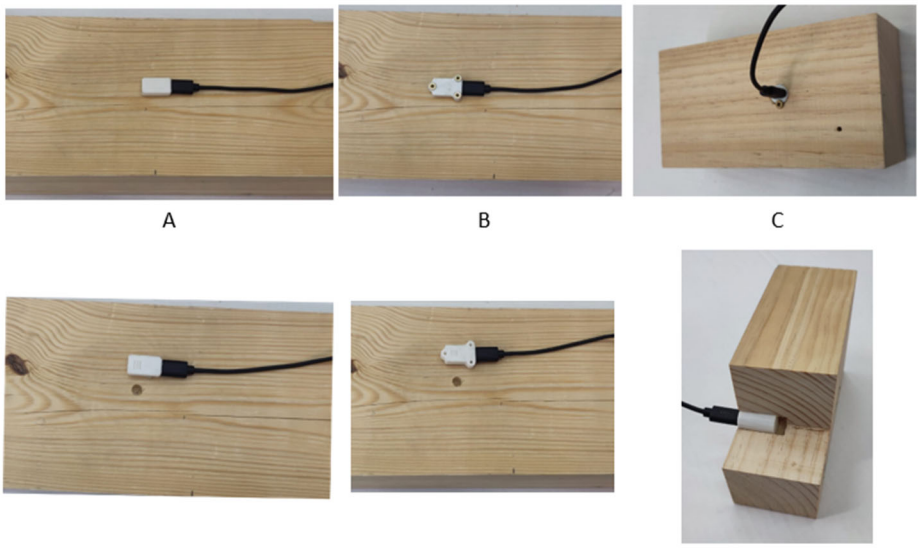

Figure 2: Different external sensor casing. A: Rectangular prismatic; B: Rectangular prismatic with holes for screws and C: Cylindrical. Top figures: installation; Bottom figures: Detail of the internal air chamber.

CONCLUSIONS

A small, versatile, and inexpensive sensor has been developed to enable Structural Health Monitoring for timber structures. This sensor can detect increases in moisture content in structural elements for any reason, as well as read the environmental data, so acceleration readings can be corrected as it records, a parameter heavily influenced by moisture content.

Funding:
This research was funded by the Junta de Castilla y León, co-financed by the European Union through the European Regional Development Fund (ref. VA228P20).

REFERENCES

[1] Magdaleno, A.; Villacorta, J.J.; del-Val, L.; Izquierdo, A.; Lorenzana, A. Measurement of Acceleration Response Functions with Scalable Low-Cost Devices. An Application to the Experimental Modal Analysis. Sensors 2021, 21, 6637. https://doi.org/10.3390/s21196637

[2] Farrar, C.R.; Doebling, S.W.; Nix, D.A. Vibration–based structural damage identification. Philos. Trans. R. Soc. A: Math. Phys. Eng. Sci. 2001, 359, 131–149.

[3] Mahammad, A.H.; Kamrul, H.; Ker, P.J. A review on sensors and systems in structural health monitoring: Current issues and challenges. Smart Struct. Syst. 2018, 2, 509–525.

[4] Hartley I., and Hamza M.F., Wood: Moisture Content, Hygroscopicity, and Sorption. In: Saleem Hashmi (editor-inchief), Reference Module in Materials Science and Materials Engineering. Oxford: Elsevier; 2016. pp. 1-7

[5] Jianget al.(2012). "Wood properties &moisture sorption,"BioResources7(3), 3585-3596.
Yang, H., Yu, L., & Wang, L. (2015). Effect of moisture content on the ultrasonic acoustic properties of wood. Journal of forestry research, 26(3), 753-757.

[6] James, W. L. (1961). Internal friction and speed of sound in Douglas-fir. For Prod J, 11, 383-390.

[7] Ye, X.W.; Jin, T.; Yun, C.B. A review on deep learning-based structural health monitoring of civil infrastructures. Smart Struct. Syst. 2019, 24, 567–585.

[8] Farrar, C.;Worden, K. An introduction to structural health monitoring. Philos. Trans. R. Soc. A: Math. Phys. Eng. Sci. 2006, 365, 303–315.

[9] Matos, J.C.E.; García, O.; Henriques, A.A.; Casas, J.R.; Vehí, J. Health Monitoring System (HMS) for structural assessment. Smart Struct. Syst. 2009, 5, 223–240.

[10] Soria, J.M.; Diaz, I.M.; Garcia-Palacios, J.H.; Iban, N. Vibration monitoring of a steel-plated stress-ribbon footbridge: Uncer-tainties in the modal estimation. J. Bridge Eng. 2016, 21, C5015002.

[11] Villacorta, J.J.; del-Val, L.; Martínez, R.D.; Balmori, J.-A.; Magdaleno, Á.; López, G.; Izquierdo, A.; Lorenzana, A.; Basterra, L.-A. Design and Validation of a Scalable, Reconfigurable and Low-Cost Structural Health Monitoring System. Sensors 2021, 21, 648. https:// doi.org/10.3390/s21020648

LONG TERM OPTICAL MONITORING TECHNIQUE OF DISPLACEMENT FIELDS BASED ON ARUCO MARKERS

J. KUNECKÝ[1]

[1] Institute of Theoretical and Applied Mechanics, Czech Academy of Sciences, v.v.i., Prosecká 76,

Praha 9, Czech Republic

ABSTRACT

In structural engineering it is often needed to measure tiny displacements of parts of the structure extremely precisely. For such a purpose it is often needed to use some type of sensor attached to the surface of the structure. This paper presents a new technique which simply uses computer vision libraries to measure displacement of markers originally developed for robotics. Such analysis can be under specific circumstances (2D planar movement) valid if we compare two images taken at different times with the same camera. Main advantage of this method is simplicity of use and low cost of markers, which can be printed in a standard office laser printer. The resolution (error) can be for standard cameras around 0.1 pixel. The method is especially developed for research of timber frames/joints behavior in real structures, because displacements of joints in creep or under load can reach an amplitude which is perfectly detectable by this method.

KEYWORDS: displacement measurement, long-term monitoring, ArUco markers

INTRODUCTION

Very often in the field of civil or structural engineering, and especially in research, we face the problems related to monitoring of an object shape or spatial changes over relatively long period. Although the structural problems are very often visible by human eye (cracks, notches etc.), the quantification of displacements or rigid body motions over time is relatively costly if we use advanced methods or relatively not precise if we use standard naked eye-based tools for measurement.

For research of historic timber structures, repair techniques and strategies we can see a lot of data from surveys and from the laboratory, however, there is not much feedback in publications from post-repair period. Such a gap can be filled with a super cheap method, which uses a camera and a set of fiducial markers to detect displacements of the markers and interpolates the displacement field. Especially in timber structures, where relatively big movements (due to creep or settling/embedment) in the order of a millimeter or so can be often found, such a method would be worth developing.

Luckily this paper comes with a solution sketched out lower. The solution is not tuned to the very end and there is a lot of room to improve it. The method stands somewhere between other methods of measurement, however, it is aimed at simplicity and usability with a particular focus on low price. There are many methods having much better precision (laser-based methods, induction-based LVDTs etc.) or full-field methods (digital image correlation, digital speckle pattern interferometry), nevertheless all of them are not usable without advanced equipment.

METHODS

The principle is based on recognition of fiducial ArUco markers [1] using standard computer vision methods [2,3]. ArUco markers are something similar to the widespread QR code, they have an intrinsic unique ID pattern. They are at the same time much less complicated and the geometry is simple (see Fig. 1).

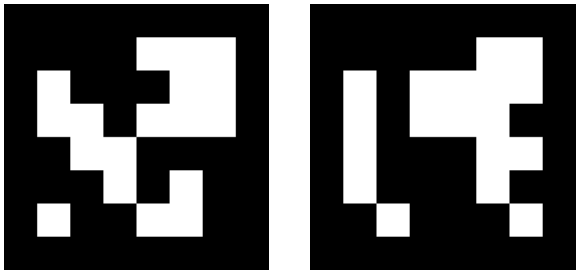

Figure 1: Example of ArUco markers

The corners of the markers are recognized using subpixel precision and thus the position of centre of gravity of the markers is very precise. We can have arbitrary number of points (markers) which we want to track. Nevertheless, among the points we choose four of them which are considered as reference and rigid, they should be chosen as not moving in time relatively to each other. But if we have them, we can remove the camera and take another picture later. We try to take the next picture nearly from the same or similar point from where the original picture (let's call it picture A) was taken, but not an absolute precision is needed, since the error of small camera movements is small enough. The second picture in time lets be called B. Based on the reference markers positions we can fit two pairs (from A and B) of four reference points (IDs are automatically recognized) to align the pictures using homography (projective transformation) [4]. From this pair of already aligned pictures (how they are taken from the same position relative to the four reference points) we can read the difference in displacements from center of gravity of each marker. Now we have the displacements of markers and the displacement field can be interpolated.

Of course, such an approach is valid only if we assume only 2D planar displacement of points, since the homography which we use is valid only for such case. Another problem which we have to solve and can be hard to determine is the fact that we need four reference points, which should be considered as rigid and not moving at all. In reality we can meet very often not ideal state: even the four points which should not move are on a slightly bent beam or so. Nevertheless, the problem depends always on the precision which we want to attain. And because precision of displacement of rigid body motion is usually a few orders higher than the one made by strain in a deformed e.g. timber, we can (of course with this idealization taken into account) still reach very good results.

Let's summarize the work needed for successful analysis:

1. Generate ArUco markers of given size and IDs
2. Print the markers having appropriate size and resolution, glue or attach the marker to the object
4. Camera calibration. The camera together with the lens has to be calibrated using standard method available, e.g. [5]. This step is crucial since lens distortion is a crucial problem in nearly any optics-based measurement.
5. Take the pictures. One in not deformed, second in deformed state. (simulation of real measurement - the pictures should be taken in some intervals)
6. Undistort the images.
7. Align the images using two sets of four reference points.
8. Find the respective marker's positions in the aligned pictures and compute displacements.

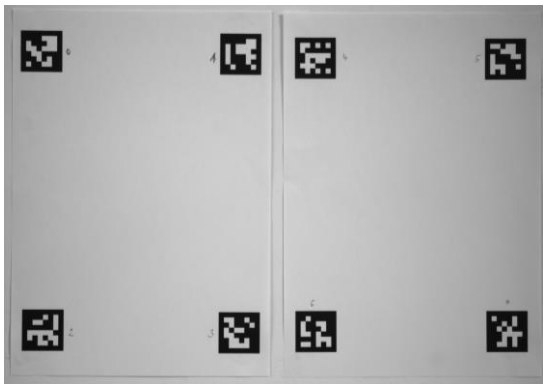

Figure 2: Test conditions, four markers in the left are considered rigid and the both papers do not move at all

To test such an approach we have done one test, which shows in practice the precision of the method. We decided to print out eight markers (a very typical setup for this kind of measurement) on two A4 size papers with marker size of 33 mm, numbers 0-3 on the left side, 4-7 on the right side (see Fig. 2). The idea is to take two pictures, one original and then go out of the office and come back and take from some similar point (but not precisely) another (second) image. For taking the pictures was used Basler Aca 2440-20gm camera with lens of focal length 25 mm. We performed first the camera lens calibration as described in [5]. Second, we took the two images, the position was not absolutely precise, but with a 10 cm tolerance. The results are shown in Fig. 3.

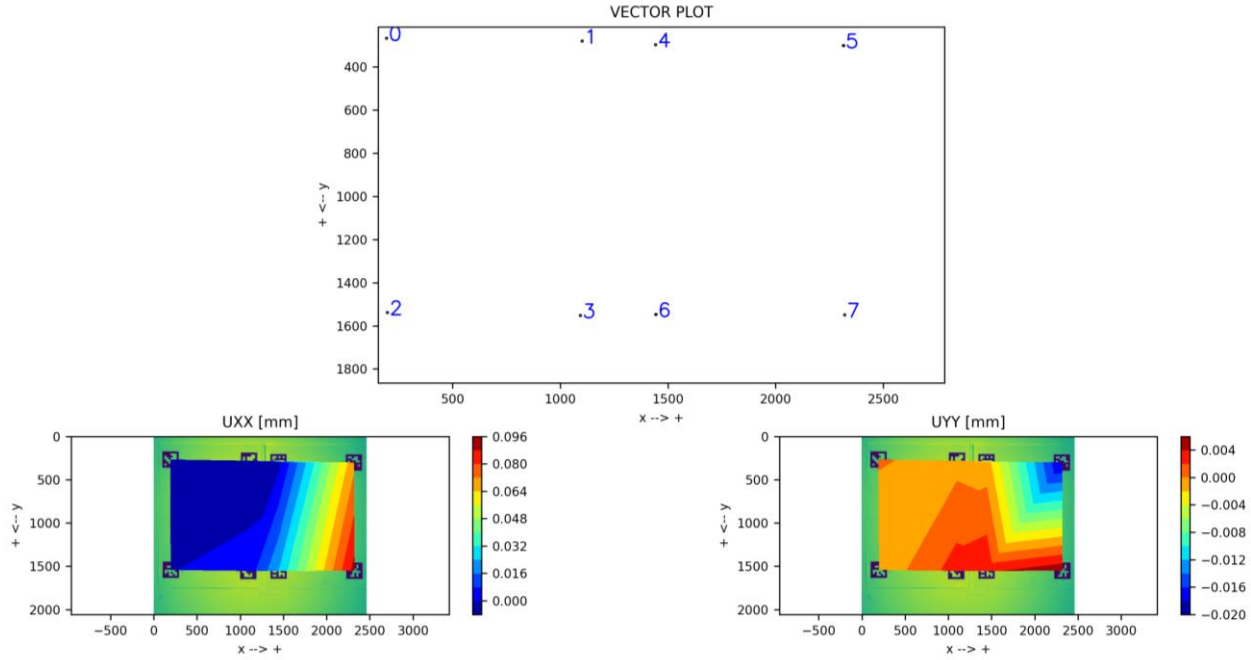

Figure 3: Test results: vector plot (infinitesimal, not visible here), contour plot (bottom) of the displacement field

As could be concluded from this preliminary test, the precision of the method, if we consider an area of A3, a standard commercial industrial camera having resolution of say 5 MP in grayscale and a standard lens, we can reach the precision of measurement about 0.1 mm.

This approach can be, of course, used to long term monitoring of timber joints, where we can deal with displacements due to creep or embedment in the order of one millimeter or also more.

To show the usability in practice we decided to perform another laboratory test with a real displacement magnitude. Se selected for the purpose a 50 mm height half lap joint with equipped with one pin, printed out ArUco markers of size 8 mm and glued them in a similar manner as in the first experiment (compare Fig. 4 to Fig. 2).

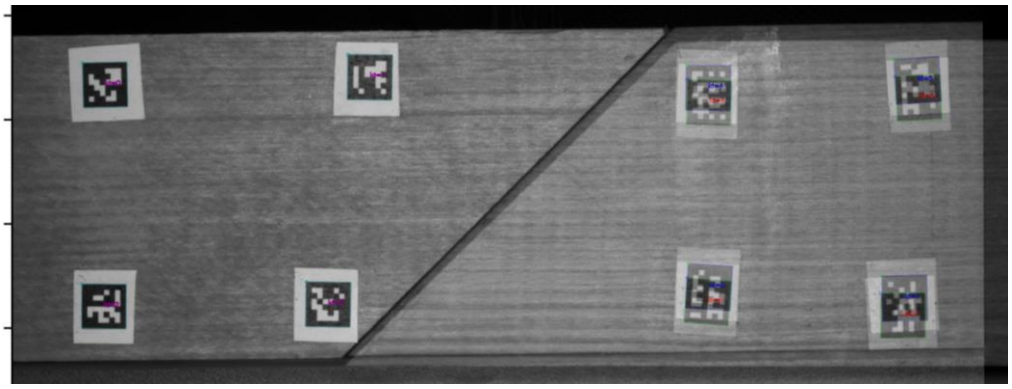

Figure 4: Simulated joint displacement. Height of the beam h=50 mm, in the image are shown two states (before and after) move glued in one

For analysis we used the same camera. Such a calibrated setup (camera and lens) was used to take one picture before we moved the joint and took another picture again. Here we do not want to address precision, more we want to show a possible use in monitoring of real structures. Results are shown in Fig. 5.

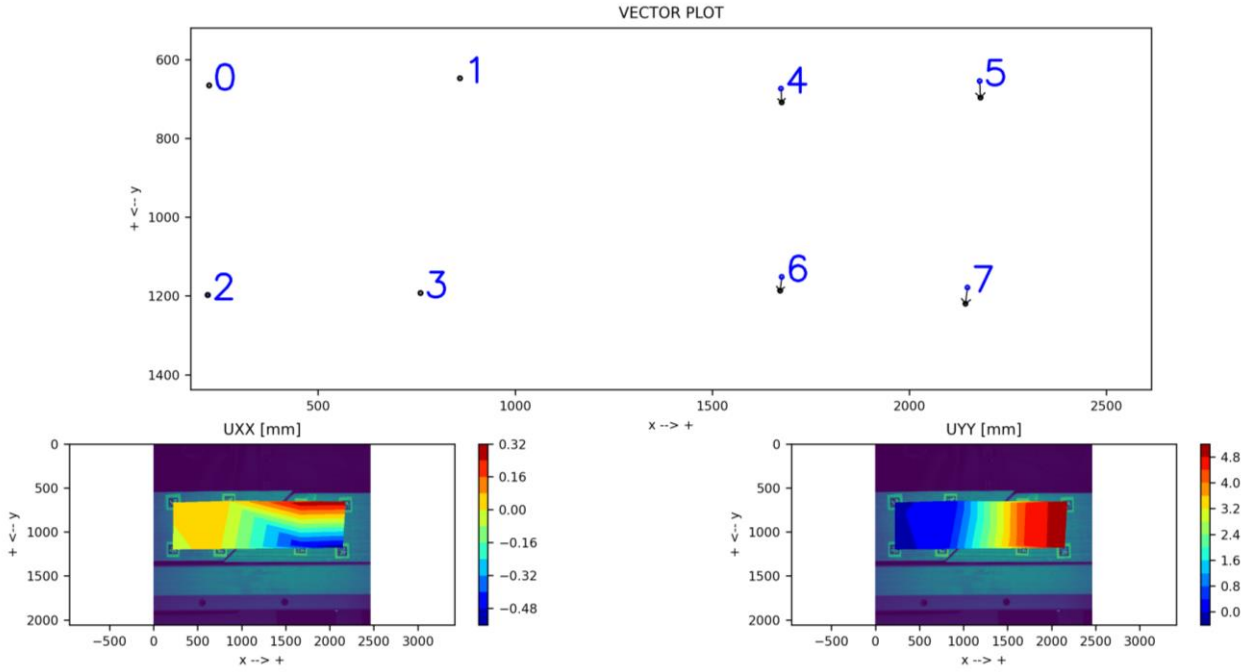

Figure 5: Test results: vector plot (see arrows), contour plot (bottom) of the displacement field

RESULTS AND DISCUSSION

To keep the flow of the article the author decided to show the results along with the description of the method. However, in this part, the method can be critically reviewed. First, the precision of the method should be set on mathematical basis, not experimental. Nevertheless, in such a practice-oriented conference the author decided to show rather possible use than matrix-based computation. This is planned in another more theoretical publication. Nevertheless, it should be said, that relatively low error has been encountered if we think about 420 mm width and 0.1 mm error in the field. This error, can be further removed using other methods: automatic alignment in real-time using an application, when the appropriate position would be specified. That would minimize alignment (reprojection) errors, help the right positioning of the camera after time etc. Another improvement can be some noise removal technique for more robust subpixel alignment.

The method has important advantages over other methods. It is cheap, can be programmed in an App in a mobile device allowing the user to do monitoring quickly and effectively. For the cultural heritage sites it is advantageous that the markers can be easily removed. If one doubts about paper stability in a changing environment, there are definitely other media materials we can use, e.g. PVC sheets etc., which ensure we do not measure changing markers. There are some improvements of the marker to be more precise, e.g. [6].

CONCLUSION

The method shown in the article deals with possible use of ArUco markers. The author shows, that such a method, based on comparison of more consecutive images taken in different times allows for relatively precise assessment of rigid body motions present in a typical long term monitoring of timber joints. The method is based on computer vision algorithms and allows for fast quantification of displacements field in 2D planar problems, often found in civil and especially structural engineering (walls, cracks, beams). The author does not present the research as an already-developed tool, but comes to the conference with an idea which should be discussed more in depth.

ACKNOWLEDGEMENT

The work is further developed with financial help of Grant of the Grant Agency of the Czech Republic GACR #21-29389S entitled “Experimental and numerical assessment of the bearing capacity of notches in timber beams at arbitrary locations using LEFM”.

REFERENCES

[1] S. Garrido-Jurado, R. Muñoz-Salinas, F. J. Madrid-Cuevas, and M. J. Marín-Jiménez. 2014. "Automatic generation and detection of highly reliable fiducial markers under occlusion". Pattern Recogn. 47, 6 (June 2014), 2280-2292. DOI=10.1016/j.patcog.2014.01.005.

[2] Aruco markers. URL: https://docs.opencv.org/master/d5/dae/tutorial_aruco_detection.html, accessed 30.6.2022.

[3] OpenCV camera library, www.opencv.org, accessed 20.6.2022.

[4] Homography. https://en.wikipedia.org/wiki/Homography, accessed 20.6.2022.

[5] OpenCV camera calibration. https://docs.opencv.org/master/dc/dbb/tutorial_py_calibration.html, accessed 20.6.2022.

[6] Y. Wang, Z. Zheng, Z. Su, G. Yang, Z. Wang and Y. Luo, "An Improved ArUco Marker for Monocular Vision Ranging," *2020 Chinese Control And Decision Conference (CCDC)*, 2020, pp. 2915-2919, doi: 10.1109/CCDC49329.2020.9164176.

COUPLING OF WEATHER DATA TO MOISTURE CONTENT IN A TIMBER BUILDING

Michael DORN[1], Carl LARSSON[1], and Osama ABDELJABER[1]

[1] Linnaeus University, Department of Building Technology

ABSTRACT

Wood and wood-based products interact with the surrounding environment. The interaction with moisture is particularly interesting since it influences the structural properties and may lead to degradation. A structural health monitoring system was established in House Charlie, a four-story office building in Växjö, Sweden, made from timber. It has been running since summer 2018, collecting vibration data and information on temperature and humidity at multiple positions within the façade and the slab. The present work shows that the moisture content within a slab of the building varies throughout the years, attributed to an ongoing dry-out and seasonal changes. Furthermore, the variation is directly coupled with the weather data from a public weather station in Växjö.

KEYWORDS: structural health monitoring, moisture content, seasonal changes, dry-out.

INTRODUCTION

Wood-moisture interaction is an ever-lasting topic within structural timber engineering and wood technology. Wood tends to be in equilibrium with the surrounding environment. Water from the surrounding air is taken up in a moist environment – and expelled in case of a dry environment. The so-called *equilibrium moisture content* (EMC) describes the moisture content achieved under constant conditions.

Under real-life conditions, the environment is continuously changing due to different effects. The weather conditions as well as the more long-term seasonal conditions control moisture content in a major way. Additionally, human influence affects the wood-moisture relationship. It is very common to control temperature by heating and cooling systems. In some cases, the indoor humidity is also actively controlled. Due to these effects, the moisture content in wood cannot be assumed to be constant over time.

Moisture content in natural materials such as wood has significant consequences on its physical properties (with increased moisture content, density and hence weight increases and timber swells), and its mechanical properties (mainly a decrease of stiffness and strength is of interest). In addition, degradation is increased above certain moisture content levels, which may lead to loss of durability and potentially negative health consequences [1].

The orthotropy and the natural heritage of wood add to the complexity of wood-moisture since the material properties in the three main directions show different correlations with moisture content. These effects can be seen directly when bowing, cupping, or warping occur. In engineered wood products, these effects can partially be overcome since multiple boards are glued together in a particular manner. In glulam (GLT), multiple lamellas of structural timber are stacked on top of each other. In cross-laminated timber (CLT) individual layers are orientated at 90° to each other. Consequently,

restrained movement of the individual boards due to moisture changes leads to internal stresses in some form. Beams, columns, shear walls and floor slabs made from CLT and GLT hence are long and thick structural elements where moisture content needs to be considered inhomogeneous in its directions [3].

Structural health monitoring (SHM) of buildings and structural elements is an ever-growing field, dealing with different materials and usage scenarios. In timber structures, SHM is of particular interest due to the sensitivity of many properties to moisture changes. SHM systems are responsible for acquiring data, translating the measurements into meaningful information, and then summarizing and reporting the information to the owners and users. Examples for applications are found worldwide, e.g., in Sweden [4], Switzerland [5], Slovenia [6] or the US [8].

In House Charlie, a four-story office building in Växjö, Sweden, such an SHM system has been implemented during construction. The building consists of a beam-column system in glulam with floor slabs made from CLT. The elevator shaft in concrete, as well as the steel bracings, take over horizontal stabilization. The building was opened in August 2019, measurements were started in July 2019, and the SHM system has been running since then with a few interruptions.

The monitoring system consists of a variety of sensors: combined humidity and temperature sensors placed in the outer light-frame timber walls; combined humidity and temperature sensors placed in a CLT slab at one position at different depths; displacement transducers used for checking compression perpendicular at certain beam-column connections; 12 uniaxial geophones and one triaxial accelerometer placed at corner points of the building; finally, an external weather station placed on top of the building for ambient data collection.

In the following, the moisture content measured in the CLT-slab during three years of monitoring will be reported and analysed. More detailed information on House Charlie is available at [9]. The data used in this paper is from the period between August 1st, 2018, and August 31st, 2021. The building itself was opened in September 2018 when the office spaces were occupied.

METHODOLOGY

Measurement data from Charlie from a total of four different sources are used: the CLT slab (from the built-in combined humidity-temperature sensors); the indoor climate (the combined sensors right behind the inner gypsum of the light-weight timber frame outer walls); from the weather station on top of House Charlie (temperature and humidity); as well as from a weather station close by (run by the Swedish Meteorological and Hydrological Institute, SHMI, about 1.2 km away).

Equilibrium moisture content (in percentage notation) in wood is calculated according to [10] for spruce from measurement data of temperature (T, in °C) and relative humidity (RH, in decimal notation):

$$\%EMC = \frac{1\,800}{W}\left(\frac{K * RH}{1 - K * RH} + \frac{K_1 K * RH + 2\,K_1\,K_2\,K^2 * RH^2}{1 + K_1\,K * RH + K_1\,K_2\,K^2 * RH^2}\right) \quad (1)$$

Hereby, the parameters $W = 349 + 1.29\,T + 0.013\,5\,T^2$, $K = 0.805 + 0.000\,736\,T - 0.000\,002\,73\,T^2$, $K_1 = 6.27 - 0.009\,38\,T - 0.000\,303\,T^2$, and $K_2 = 1.91 + 0.040\,7\,T - 0.000\,293\,T^2$ are used. Other methods for determining moisture content in wood are also frequently used, an overview of different methods can be found in [11].

Absolute humidity (AH) according to [12] is calculated from the measurement data of temperature (in either Celsius, T_C, or Kelvin, T_K) and relative humidity (in percentage, $\%RH$):

$$AH\ \left(\frac{\mathrm{g}}{\mathrm{cm}^3}\right) = \frac{e_a * MW}{R * T_K} * 1000 \quad (2)$$

Hereby, the vapor pressure is defined as $e_a(\mathrm{kPa}) = \frac{\%RH}{100} * e_s$; and the saturated vapor pressure is defined as $e_s\ (\mathrm{kPa}) = a * \exp\left(\frac{b * T_C}{c + T_C}\right)$. The following constants are used: $MW = 18.02$ g/mol (molecular

weight of water); $R = 8.31$ J/mol/K (universal gas constant); $a = 0.611$ kPa; $b = 17.502$; $c = 240.97$ K.

Finally, the curve-fitting of the properties is done according to a function that considers three terms: a mean value, an exponential decay, and a sine-function.

$$X(t) = X_a + \Delta X_b * \exp(-k_b * t) + \Delta X_c * \sin\left[\frac{2\pi}{365\ d}(t - t_c)\right] \quad (3)$$

The parameter X_a describes the long-term average; the parameter ΔX_b is the initial dry-out with k_b the decay constant; and ΔX_c the amplitude of annual changes of the sine function with a period of 365 days, i.e., a full year, and a phase offset of t_c.

The same curve-fitting function is used in all parts, X is to be exchanged for temperature, relative humidity, absolute humidity, and moisture content, respectively. The term for dry-out is only used for the humidity in the CLT-slab where excessive moisture from during the building phase is to be expected. Three full years of measurements allow for assumptions of the annual cyclic behaviour as well as the dry-out processes to be seen properly.

RESULTS

Temperature and relative humidity

The original measurement data is presented in Figure 1 where temperature and relative humidity are shown from the SMHI weather station, the weather station on top of House Charlie, as well as the indoor at an office in the bottom floor. As there are multiple sensors placed throughout the façade, the innermost sensor is chosen which sits inside a blind box.

Both weather stations clearly show identical trends throughout the three years. The seasonal changes are obvious and each local peak and valley in temperature and relative humidity is found in both diagrams. The seasonal variations between temperature and humidity are not totally synced; the highest temperatures are found in July/August and the coldest in January/February, while the highest relative humidity is measured in November/December and the lowest in April.

Indoors, the variation in relative humidity over the year is clearly seen as well, peaking in late summer, and hitting bottom in spring. For temperature, the annual variation is far smaller in contrast and rather constant due to the climatization of House Charlie.

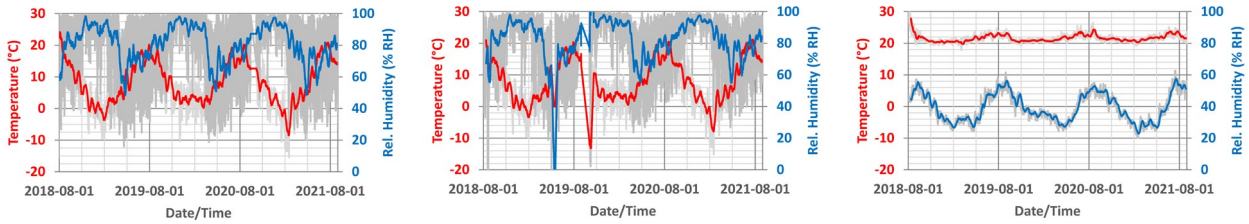

Figure 1: Data for temperature and relative humidity from the SMHI weather station (left), from the weather station on top of House Charlie (centre), and the indoor of an office in House Charlie. The original data is shown in grey, moving averages in colours

The data at the three positions within the CLT slab is plotted in Figure 2 for all three depths. Temperature is rather constant at 21-22 °C except for the beginning in August 2018 when readings where partially above 27 °C before the cooling system took effect. Relative humidity values show a downwards trend for all three positions, starting as high as 72% in the two upper positions whilst the bottom position peaks at 61%. Annual cycles are visible; peaks occur around September/October and lows around May/June. Particularly for the upper positions, the curves for relative humidity are far smoother than for the other sources shown above, exhibiting a clear damping effect.

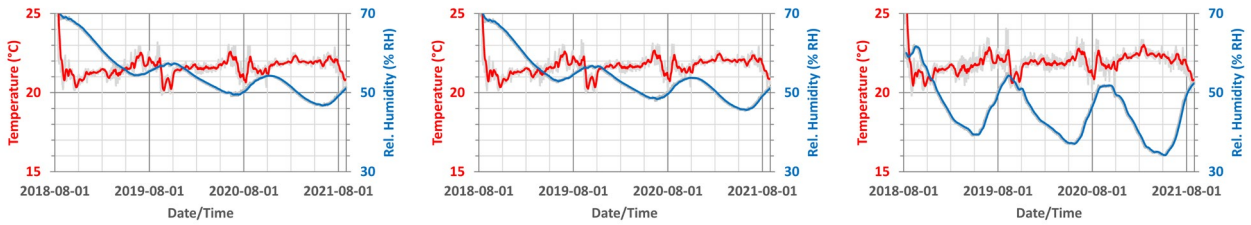

Figure 2: Data for temperature and relative humidity from the measurement points in the CLT slab: position 1 (left), position 2 (centre), and position 3 (right). The original data is shown in grey, moving averages in colours

Moisture Content

Moisture content is calculated according to Equation 1 above from the measurement of temperature and relative humidity for the three positions. In Figure 3 (left), the data for the three years is shown. The same cyclic behaviour as the relative humidity itself is visible. Since temperature in the CLT is barely varying over time, it is not expected to play a major role either.

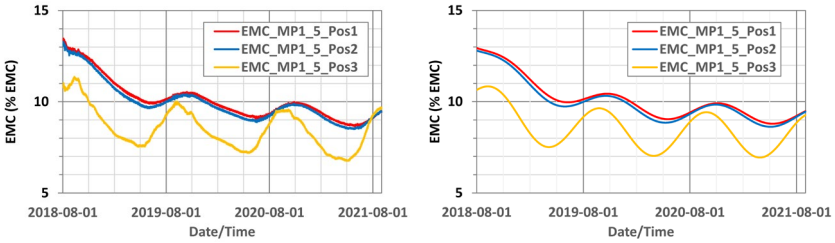

Figure 3: Moisture content in the CLT-slab at the three positions: measured/calculated data (left), fitted curve (right)

Additionally, the curve-fitting of moisture content with time is carried out according to Equation 3 taking all terms into account: long-term average, initial dry-out, and seasonal variations. The parameters are found in Table 1. The excellent R^2-values show the appropriateness of the model assumption.
Throughout the time interval observed, the moisture content is significantly higher in positions 1 and 2, on top of the CLT-slab, as compared to position 3 on the bottom. The differences are getting smaller with time since dry-out is more pronounced on positions 1 and 2, which results in a drop of almost 3.8%. Dry-out is also happening slower for those positions, seen by parameter k_B.
The amplitude of seasonal variations (ΔMC_c) at position 3 is more than twice as large as the upper positions. There is also a time-delay between the three positions, seen by the parameter t_c.

Table 1: Parameters for curve-fitting function of the moisture content in the CLT-slab

Parameter	Unit	Position 1	Position 2	Position 3	Description
MC_a	%MC	9.22	9.12	8.15	Long-term mean
ΔMC_b	%MC	3.79	3.68	1.83	Dry-out
k_B	$1/d$	-1/271	-1/254	-1/217	Dry-out
ΔMC_c	%MC	0.517	0.572	1.23	Seasonal variation
t_c	d	7.77	0.928	-33.9	Seasonal variation
R^2	–	0.993	0.998	0.947	Goodness of fit

Absolute Humidity

Finally, the absolute humidity is calculated, using Equation 2 (see Figure 3, left). Not surprisingly, the two weather stations show almost identical values. Absolute humidity indoors is also identical to the ones from outdoor. There is obviously a direct coupling between the indoor and outdoor environment regarding humidity since changes in temperature do not affect the absolute water in the air.
Annual periodic cycles are clearly visible with the highest absolute humidity occurring during summer (July/August) and the lowest values observed during late winter/early spring (February/March/April).

The highs and lows are not in full sync with neither temperature nor relative humidity, the interaction of the two parameters leads to a shift of the highs/lows.
At the three measurement points in the CLT-slab, the absolute humidity again shows both a downward trend as well as cyclic behaviour. Similar conclusions as for the moisture content in the slab can be drawn. (Note: absolute humidity in the slab shown in Figure 3 is not to be mixed with the water content of the timber in g/m^3 of timber. The values presented correspond to the air at the measurement points.) Using the curve fitting approach from Equation 3, the absolute humidity in the CLT-slab is approximated (see Figure 3, right, and Table 2 for the parameters). Similarly to moisture content, the basic features of dry-out and annual variation are captured. Nevertheless, for position 3, the R^2-value clearly is lower for position 3 than for the other position and for EMC (Table 1), respectively.

Table 2: Parameters for curve-fitting function of absolute humidity in the CLT-slab

Parameter	Unit	Position 1	Position 2	Position 3	Description
AH	g/m^3	9.77	9.78	8.65	Long-term mean
ΔAH_b	g/m^3	3.29	3.39	5.16	Dry-out
k_B	$1/d$	-1/260	-1/207	-1/34.0	Dry-out
ΔAH_c	g/m^3	0.418	0.461	1.31	Seasonal variation
t_C	d	16.7	9.85	-26.7	Seasonal variation
R^2	–	0.942	0.978	0.604	Goodness of fit

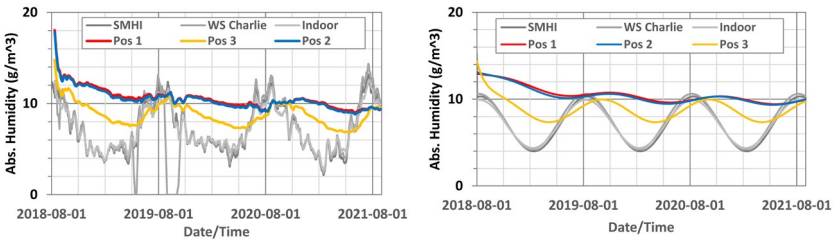

Figure 3: Absolute humidity at all points: weather stations and indoor in grey; in the CLT-slab coloured: measured/calculated data (left), fitted curves (right)

CONCLUSION

Water content in the slab at three positions is presented in different terms: as raw-data readings with relative humidity and temperature; as moisture content; and as absolute humidity at the sensor. It is compared to the absolute humidity measured in the surrounding, both inside the building but also from weather stations outside the building.
The maximum absolute humidity during a year outside the timber is slightly higher after the dry-out has mostly happened (see Figure 3). The minimum values outside, though, are far lower than the lowest readings in the timber. As seen from the fitted curves (Figure 3, right), there is also a clear time delay between the valleys. The minimum values occur in February outside, in April in the bottom point in the CLT and in June in the uppermost points, respectively; the maximum values a half year later.
The data from the first three years together with the proposed three-term fitting function allow for predicting the future changes in relative humidity, absolute humidity, and moisture content. It remains to be seen how accurate these predictions are. Nevertheless, this approach is part of a typical structural health monitoring system where the baseline, i.e., the expectation, is defined by the history data.
The connection between the environment data from an external weather station, independent from the measurements at House Charlie , has been done. A next step will be to map the outdoor data to the moisture in the CLT-slab by correlation, as is outlined in Figure 4. In the long run, it may be possible to predict moisture content directly from environment data so that no internal sensors are needed.
Dynamic measurements are also done at House Charlie so that the eigenfrequencies can be determined [13]. Evaluations have shown that also those vary with time and follow the behaviour that is observed

for the moisture content in the CLT slab (annual variation and dry-out). A direct connection between outdoor humidity and the eigenfrequencies could possibly be established. An additional application could be to see how changes in the outdoor climate affect the timber parts, e.g., how future changes to the annual rain and temperature cycles influence timber buildings.

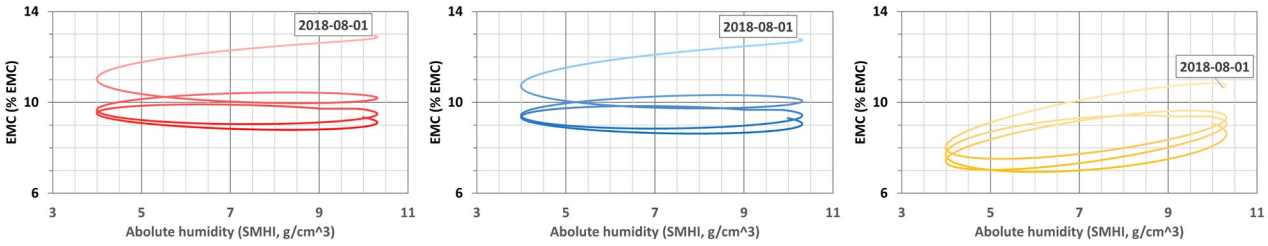

Figure 4: Absolute humidity from the SMHI-weather station as compared to the moisture content in the CLT for the three positions for the period 2018-08-01 – 2021-08-31 with the starting point marked

REFERENCES

[1] J. Cappellazzi, M. J. Konkler, A. Sinha, and J. J. Morrell, "Potential for decay in mass timber elements: A review of the risks and identifying possible solutions," *Wood Material Science and Engineering*, vol. 15, no. 6, pp. 351–360, 2020.

[2] E. L. Schmidt, M. Riggio, A. R. Barbosa, and I. Mugabo, "Environmental response of a CLT floor panel: Lessons for moisture management and monitoring of mass timber buildings," *Building and Environment*, vol. 148, pp. 609–622, 2019.

[3] P. Dietsch, A. Gamper, M. Merk, and S. Winter, "Monitoring building climate and timber moisture gradient in large-span timber structures," *Journal of Civil Structural Health Monitoring*, vol. 5, no. 2, pp. 153–165, 2015.

[4] E. Serrano, B. Enquist, and J. Vessby, "Long term in-situ measurements of displacement, temperature and relative humidity in a multi-storey residential CLT building," in *WCTE 2014 - World Conference on Timber Engineering*, 2014.

[5] M. Schiere, B. Franke, S. Franke, and A. Müller, "Comparison between Predicted and Measured Moisture Content and Climate in 12 Monitored Timber Structures in Switzerland," *Buildings*, vol. 11, no. 5, 2021.

[6] M. Humar, D. Kržišnik, B. Lesar, and B. Dujič, "Monitoring a building made of CLT in Ljubljana," *Wood Material Science and Engineering*, vol. 15, no. 6, pp. 335–342, 2020.

[7] S. Kordziel, S. Pei, S. V. Glass, S. Zelinka, and P. C. Tabares-Velasco, "Structure Moisture Monitoring of an 8-Story Mass Timber Building in the Pacific Northwest," *Journal of Architectural Engineering*, vol. 25, no. 4, 2019.

[8] E. J. Baas, M. Riggio, and A. R. Barbosa, "A methodological approach for structural health monitoring of mass-timber buildings under construction," *Construction and Building Materials*, vol. 268, 2021.

[9] M. Dorn, O. Abdeljaber, and J. Klaeson, "Structural Health Monitoring of House Charlie." Department of Building Technology, Linnaeus University, 2019.

[10] R. Bergman, Z. Cai, C. G. Carll, C. A. Clausen, M. A. Dietenberger, R. H. Falk, C. R. Frihart, S. V. Glass, C. G. Hunt, R. E. Ibach, D. E. Kretschmann, D. R. Rammer, R. J. Ross, N. Stark, J. P. Wacker, X. Wang, A. C. Wiedenhoeft, M. C. Wiemann, and S. L. Zelinka, *Wood handbook – Wood as an engineering material*. Forest Products Laboratory, 2010.

[11] P. Dietsch, S. Franke, B. Franke, A. Gamper, and S. Winter, "Methods to determine wood moisture content and their applicability in monitoring concepts," *Journal of Civil Structural Health Monitoring*, vol. 5, no. 2, pp. 115–127, 2015.

[12] D. Bolton, "The computation of equivalent potential temperature," vol. 108, no. 7, pp. 1046–1053, 1980.

[13] C. Larsson, O. Abdeljaber, Bolmsvik, and M. Dorn, "Long-term analysis of the environmental effects on the global dynamic properties of a hybrid timber-concrete building," vol. 268, no. 114726, 2022.

STRUCTURAL REINFORCEMENT FOR WOODEN BUILDINGS IN PRE-MODERN JAPAN FOCUSING ON PENETRATING TIE BEAM

Satoshi UNNO[1]

[1] The University of Tokyo, Department of Architecture, Graduate school of Engineering

ABSTRACT

This study examines the structural reinforcement of Japanese historical buildings in the pre-modern era. In Japan, it was thought that the technology of penetrating tie beam was newly introduced from China in the late 12th century and prior to the Middle Ages, there was no horizonal member between pillars like penetrating tie beam. But the authors' investigation of the East Pagoda of *Yakushi-ji* Temple revealed that horizontal members look like penetration tie beam were also used in ancient architecture. In addition, when focusing on penetrating tie beam of medieval structural reinforcement, it became clear that penetrating tie beam penetrate thick pillars in one direction. Based on these facts, when I review the penetrating tie beam based on the existing building and repair work reports, it became clear that there are four methods of penetration as below. Type 1 is that penetrating tie beams are in one direction, Type 2 is that they are at different level, Type 3 is that they are at same level and Type 4 is that they are separate members.

KEYWORDS: Reinforcement, Penetrating Tie Beam, Conservation technique, Philosophy of repair method,

INTRODUCTION

In this paper, I will analyse historical buildings in Japan and examine techniques related to penetration tie beam. Many wooden buildings remain in Japan. However, these wooden buildings cannot have existed without structural reinforce since the beginning of construction, but structural reinforcement in the Middle Ages and early modern times plays a major role in the preservation of buildings. The addition of the support pillars in each corner and the insertion of the penetrating tie beams are typical examples. In 1180, there was a major inner war in Nara, and almost all the buildings such as *Todai-ji* and *Kofuku-ji* temple were burned down. *Todai-ji* temple and Kofuku-ji temple were built in the 8th century when the capital was located in Nara. *Tōdai-ji* temple is a famous Buddhist temple complex located in Nara and its main hall is the Great Buddha Hall which is one of the largest buildings made of wooden framework structure. The Great Buddha Hall of *Todai-ji* temple was immense at 86 m long by 50 m deep and its size was too huge to build [1]. Therefore, the buildings built in the 8th century had many structural defects. In fact, the literature states that about 50 years after construction, reinforcement pillars were added, and behind the Great Buddha, a mountain was built with soil to support the Great Buddha.

So the Great Buddha Hall was rebuilt in the end of 12th century with Chinese techniques, newly brought to Japan owing to the difficulty of this construction. The feature of this technique is penetrating tie beam are inserted into pillars. To penetrate the pillars, it is necessary to process the wood accurately. In addition, when assembling, it is very difficult in terms of the construction method because the members

from four directions are combined. It can be confirmed from existing buildings that this technology was used not only as a newly built building but also as an effective reinforcement method in repair work. Especially, to insert the penetrating tie beam without dismantling of building, it needs ingenuity in construction. By changing the height of the penetrating tie beams in the girder line direction and the beam-to-beam direction, the penetrating tie beams in both axial directions are devised so as not to interfere with each other.

METHODOLOGY

I analyse the presence or absence of penetrating tie beam and the ingenuity of construction methods for ancient buildings existing in Japan. In Japan, detailed investigations are conducted during preservation work. The content extends to the procedure of dismantling, the method of assembling up the building, and the position of the nail hole. The contents of these detailed investigations have been compiled and published as repair work reports. So, from this repair work report, it is possible to know the construction method of the building and the history of repair. Therefore, based on the field survey of historical buildings and the analysis of repair work reports, I will clear out the construction method and the timing when penetrating tie beams and horizontal materials were used. Focusing on the construction accuracy, the classification of penetrating tie beam types is carried out from the difficulty of the construction method.

I will extract the use of penetrating tie beams and horizontal materials from buildings built in ancient age. As specific examples, the East Pagoda of *Yakushi-ji* temple, the East Gate of *Todai–ji* temple, and the *Byodo-in* Phoenix Hall are the subjects of my analysis. In addition to these existing buildings, cases of excavated building members will be analysed.

CASE 1

At the East Pagoda of *Yakushi-ji* temple is built in 730, in addition to the horizontal member dropped from the above of the pillar on the head of the pillar, horizontal member is also used under it. The use and construction method of this member were newly confirmed in a repair project I participated in in 2013. These members were hidden under the roof tiles by later modifications, so their existence was not known before this repair project. The use of this horizontal member similar to the members of *Yakushi-ji* Temple Pagoda was confirmed on some paintings in contemporary Chinese Tang Dynasty architecture as Fig.1, but in Japan it was not confirmed until after the Middle Ages before this conservation work. To see details of these horizontal members, the upper horizontal member

The Mural of Qianling Mausoleum

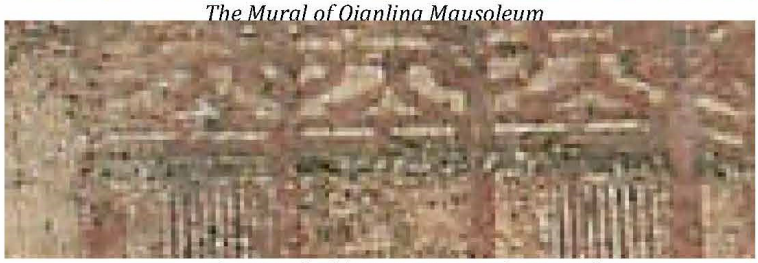

The Mural of Crown Prince Yide Mausoleum

Figure 1: Two horizontal members depicted on a tomb mural (quoted from[2])

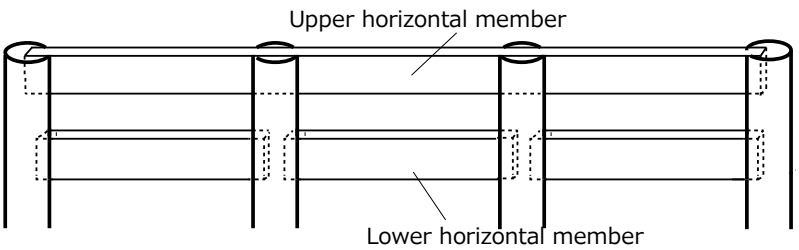

Figure 2: Schematic figure of horizontal member of Yakushi-ji East Pagoda (created by author)

penetrates the pillars. On the other hand, the lower horizontal member is separated for each pillar. The structure of these horizontal members and pillars is like Fig.2. Although this lower horizontal member is often used for Tang Dynasty architecture in China, it is rare for this member to be used in Japan.

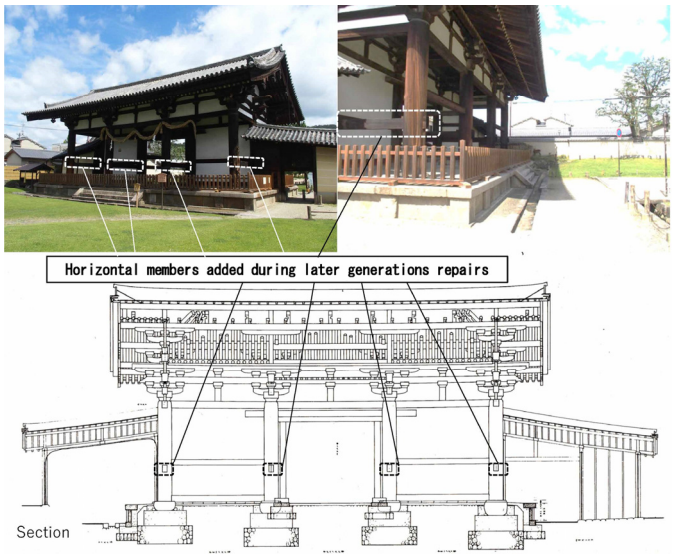

Figure 3: Penetrating tie beam of Todai-ji Temple Tegaimon gate added to in medieval repairs (Lower figure is created by author based on reference [3] and photos taken by the author)

CASE 2

In the case of the *Tegai-mon* gate of *Todai-ji* temple built in the 8th century, penetrating tie beams were added to thick pillar in the Middle Ages as Fig.3[3]. This is a case pillars of ancient architecture are thick enough to penetrate additional member. In this case, penetrating tie beams were added only in the beam direction to the existing gate in 1185. Generally speaking, after the latter half of the Middle Ages, the pillars became thinner and it became difficult to insert penetrating tie beam after construction. But ancient architecture was characterized by thick pillars, so penetrating tie beams could be added later. Previous studies have considered it to be the oldest case of penetrating tie beam.

CASE 3

In the corridors on both sides of the *Byodo-in* Phoenix Hall built in 1053, penetrating tie beams can be seen in this buildings. In previous studies, these horizontal members were thought to have been added during medieval modifications[4]. However, when I conducted a field survey in 2019, the following things were revealed. Depending on the difference in height of penetrating tie beam, there are two way of penetrating tie beams as Fig.4. The transition of the upper and the lower penetrating tie beam is different.

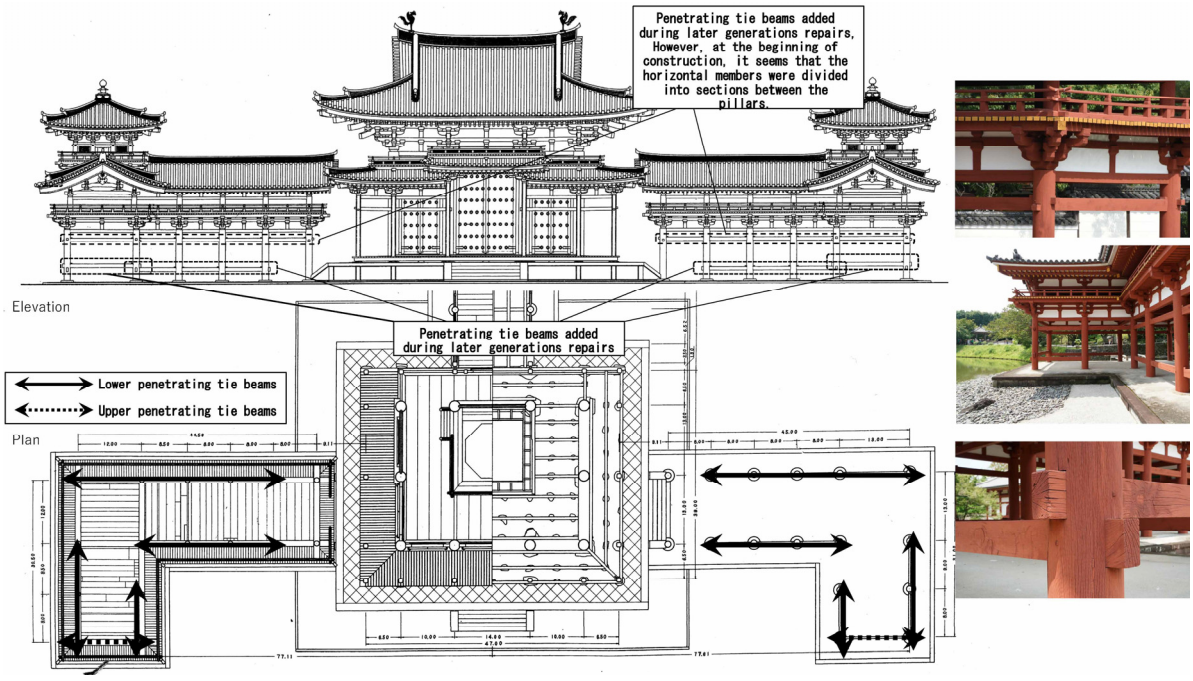

Figure 4: Penetrating tie beam of the Corridors on both sides of the Byodo-in Phenix Hall (Lower figure is created by author based on reference [4] and photos taken by the author)

Currently, the horizontal member near the top of pillar penetrates the multiple pillars, but judging from the traces of original pillars dismantled at the time of repair, it reveals that these upper horizontal members were added at the same time as the insertion of the lower penetrating tie beams. Moreover at the time of initial construction, the horizontal members were separated between each pillar, just like the *Yakushi-ji* temple East Pagoda. From these two cases, it becomes clear that there was a method of construction with non-penetrating horizontal members even before the 12th century.

In addition, penetrating tie beam in two directions of different heights can be confirmed in the corridors on both sides of the *Byodo-in* Phoenix Hall. Furthermore, the penetrating tie beam with different heights was added in later repairs. The difference in height seems to be a contrivance to insert the penetrating tie beam into the pillars later without dismantling.

CASE 4

From the Unehara Tanaka Historical Site in the 2nd century located at the north of Chikusa River, pillars of stilt building have been excavated. These members have some holes, and it seems that horizontal members penetrated through these holes. When comparing the height and the side of these holes in these members, the direction of the holes is drilled alternately according to the height as Fig. 5. This feature is the same configuration as the penetrating tie beam of the corridors on both sides of the *Byodo-in* Phoenix Hall.

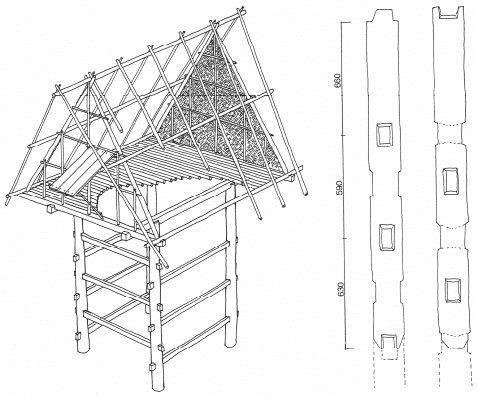

Figure 5: Unearthed building members in the Unehara Tanaka Historical Site (Quated from reference [5])

RESULTS

As a result of analysis of repair work reports and on-site investigations, it was confirmed that penetrating tie beam which was the new technology of the Middle Ages, was used not only for newly built architecture but also for reinforcement of ancient architecture. Furthermore it has become clear that there was a method of horizontal members used between pillars outside the top and bottom of pillar existed in ancient time, although historical member don't penetrate multiple pillars.

When I investigated existing historical architecture and excavated members in ancient age, it became clear that there are four ways of penetrating tie beam as Fig.6. Type 1 is a method to insert penetrating tie beam only in one direction. Type 2 is a method to insert penetrating tie beam at different heights from two directions. Type 3 is a method to insert penetrating tie beam at same height from two direction. Type 4 is a method that horizontal member are at the same height, but this member doesn't penetrate columns.

There are also significant differences in assembly methods and construction accuracy for each Type. These differences not only indicate the difference of construction age, but also lead to the difference in whether it is a method that can be used for repair after initial construction.

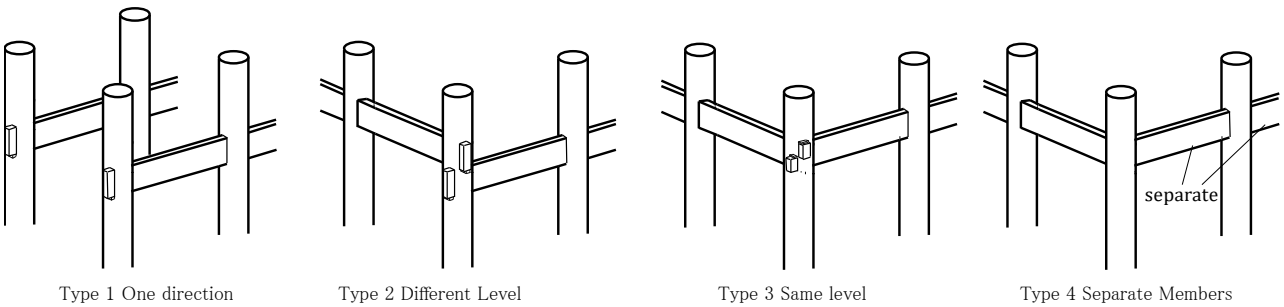

Figure 6: 4 types of penetrating tie beam (Created by author)

The excavated building components of Type 1 revealed that this structure existed in Japan even before the 12th century, when it was thought new technique were brought from China. Prior to the discovery of this site, it was considered that this construction method had been developed after the 12th century, so this discovery was a very shocking study. In this way, construction accuracy is comparatively not required with penetration tie beam. Therefore, construction was possible even in the era when the construction accuracy was low. In addition, it is a useful repair method to insert penetrating tie beam without dismantling. However, it is structurally reinforced in only one direction, and it is a limited effect as a reinforcement method.

Compared to Type 1, Type 2 requires higher construction accuracy, but using this method, it is also able to insert penetrating tie beam to pillars without dismantling in repair work. Since it is a two-direction structural reinforcement, it is a relatively effective method of structural reinforcement.

Type 3 is a method commonly used from the late 12th century onwards. It is necessary to make a hole for penetrating tie beam from four directions, and in the pillar, joint processing is performed with difficulty on the penetrating tie beam from each direction. Therefore, high processing technology and construction accuracy are required, and it is also effective in terms of structural reinforcement. In addition, since the penetrating tie beam penetrates from all sides with complexity and tightness, once assembled, it is difficult to dismantle. Hence it is difficult to add this member later without dismantling repairs.

Type 4 is a very different method from Type 1,2 and 3. This method was used extensively in the Chinese Tang Dynasty, but was not confirmed to exist in ancient Japanese architecture. I confirmed that it was used in the dismantling repair work of the East Pagoda of *Yakushi-ji* temple bult in the 8th century. Before the dismantling of this Pagodas in the 21st century, this part was covered with roof tiles, so it could not be confirmed. But our dismantling repair revealed that this horizontal member below the top of pillar was used between pillars. The construction method of inserting this member is as shown in the following Fig.7. First step is to make pillar hole deep and to insert this horizontal member into one side hole. Then second step is to insert a member between the pillars. Thereafter, third step is to insert this member into the opposite hole. Therefore, in this method, the horizontal material does not penetrate the pillars.

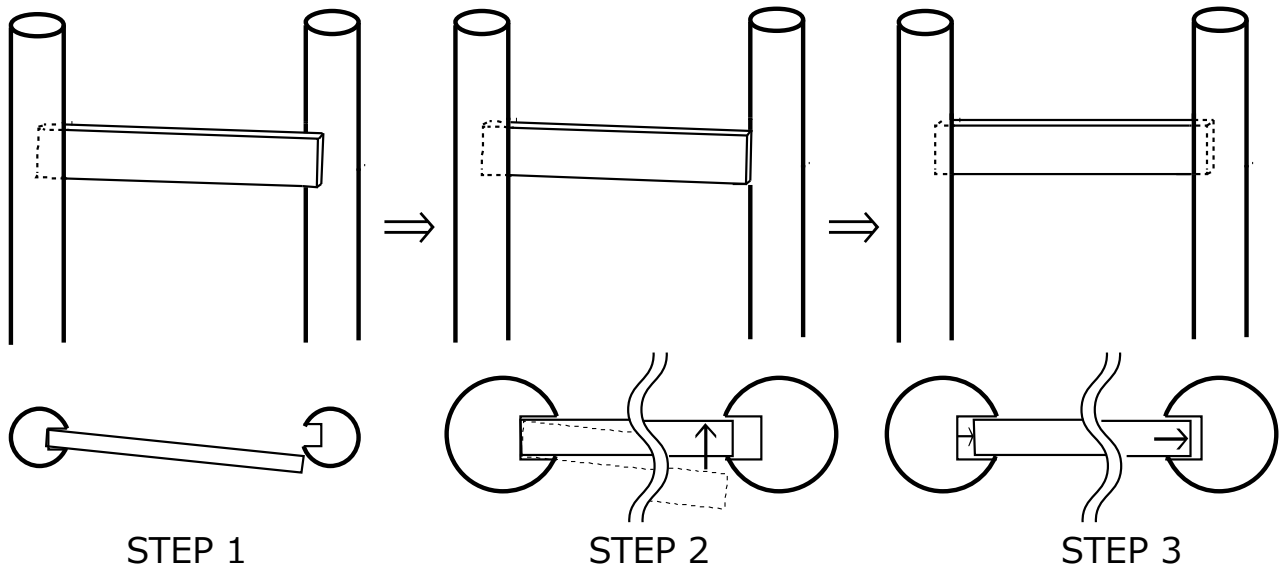

Figure 7: Construction method of horizontal member (Created by author)

CONCLUSION

It is generally said that penetrating tie beam is structurally advantageous members and this structure method was brought from China in the late 12th century. Due to the high construction accuracy required for penetrating tie beam, it could not be used in ancient age. Since construction accuracy was low in ancient times, it has been thought that horizontal members were not used except for horizontal materials at the top and bottom of the pillars in past research.

This study revealed three points about penetrating tie beam, the construction method, the age of occurrence and the usage for repairs. When I carefully classify the horizontal member and the penetrating tie beam method, I was able to divide it into 4 types. Among them, it became clear that horizontal members with non-penetrating or in one-way penetration, do not require such high construction precision and this method have existed since the 2nd century from excavated building members.

In particular, the discovery of non-penetrating structure in the East Pagoda of *Yakushi-ji* temple led to a re-examination of the horizontal members of the corridors on both sides of the *Byodo-in* Phoenix Hall. As a result of these field surveys and analyses of repair work reports, this method of non-penetrating horizontal members was able to be positioned as a method used in ancient times. In addition to this, there is a possibility to use the method of penetrating tie beam Type1 or Type 2 in ancient times.

After the Middle Ages, it has been used not only for new construction but also for structural reinforcement of old buildings. Even if it is a one-direction penetrating tie beam or two directions by changing the height of the penetrating tie beam, the addition of penetrating tie beam was effective structural reinforcement without dismantling. That is to say, new technology was also applied to repairs while partially improving and devising to reinforce the structure even in premodern times.

Structural reinforcement in these premodern repair shows that it is not appreciated only by inheriting the original, but introducing new effective technologies. This is also an important viewpoint for considering the philosophy of preservation for the introduction of new technology in contemporary preservation.

REFERENCES

[1] UNNO Satoshi, “Securing system of wooden materials for preservation in Japan” ”22th IIWC International Symposium Wooden Heritage Conservation: beyond disciplines” 2020. ISBN 978-0-6485799-1-5

[2] TANAKA Tan, “Sekai Bijutsu Zenshu （世界美術全集）” Tokyo, Shogakkan, 1997,ISBN 4-09-601054-5

[3] Nara National Research Institute for Cultural Properties,”Survey Report of national treasure Todai-ji temple Tegaimon gate（国宝東大寺転害門調査報告書）”Nara, Nara National Research Institute for Cultural Properties, 2003. ISBN 4902010119

[4] SUZUKI Kakichi, “Byodo-in Taikan（平等院大観）” Tokyo, Iwanami-shoten, 1998, ISBN 4000080369

[5] MIYAMOTO Nagajiro, ”Nihon Genshi Kodai no Jukyo Kenchiku（日本原始古代の住居建築）” Tokyo, Chuokoron Bijutsu shuppan, 1996. ISBN 4805502835

MOISTURE MONITORING TECHNIQUES FOR THE PROTECTION OF TIMBER STRUCTURES

N. FLEXEDER[1,2], M. SCHENK[1] and P. AONDIO[1]

[1] Technical University of Munich, Chair of Timber Structures and Building Construction

[2] Contact: nina.flexeder@tum.de

ABSTRACT

Moisture protection of timber structures is of high importance for a sustainable built environment. This paper provides an insight into moisture protection concepts and international regulations for moisture monitoring with permanently installed sensors. Comparative experiments for the method of long-term electrical resistance measurements and the sorptive method are conducted in both, in-vitro and in-situ measurement campaigns in CLT. Based on oven-dried samples, electrical resistivity conversion seems to tend to give too low values for wood moisture content, while results after conversion from sorption isotherms tend to be too high, depending on the equation used. Thus, the investigations show significant discrepancies and the need for further laboratory measurements. Finally, the paper outlines the further potential of moisture monitoring concepts based on European standardization work.

KEYWORDS: moisture protection, wood moisture monitoring, standardization, electrical resistance measurements, sorption method, temperature gradient, cross-laminated timber

INTRODUCTION

Moisture monitoring systems might constitute a decisive part in future holistic concepts for the protection of multi-storey timber buildings. Moisture variations can lead to constraints within built structures. Furthermore, moisture affects the mechanical properties of building materials such as strength and stiffness. In unfavourable temperature ranges, a certain moisture content can lead to deterioration by wood-destroying fungi. As a consequence, concepts for the moisture protection of timber structures have existed for centuries. Moisture monitoring is considered a part of structural health monitoring and could be described as a preventive concept based on permanent technical equipment within building structures [1]. Moisture monitoring is usually conducted to acquire information when progressive phenomena are suspected, to prevent or reduce the cost of interventions during maintenance or renovations and to evaluate long-term effects [2]. Especially structural changes in existing buildings or changes in use have an influence on the ambient conditions. Those changes mainly influence safety, serviceability and durability of timber structures but similar problems also arise with wooden objects, e.g. cultural heritage or art.

MOISTURE MEASUREMENTS AND FUTURE EUROPEAN REGULATIONS FOR TIMBER STRUCTURES

According to mandate M/515, issued by the European Commission, the second generation of European structural design standards – the Eurocodes – is currently under preparation [3,4]. Future Eurocode 0 categorises moisture and temperature variations among the so-called indirect actions [5]. The effects of those actions can be verified e.g. according to the timber design rules for buildings in EN 1995, see Fig. 1. Design values of resistance of timber structures in [6] depend on several conversion factors, such as k_{mod} and k_{def} which include effects of moisture. The completely new draft of EN 1995-3 *Execution rules* for

the design of timber structures (see Tab. 1) contains minimum requirements for moisture control [7]. It recommends the designer a documentation of (i) expected moisture content in service, (ii) permitted moisture content range during execution, (iii) assumptions about protection during execution and (iv) information whether a moisture control plan is required. This plan comprises, among other things, information on (1) how moisture content gets measured, (2) whether it gets measured at depth, (3) when it gets measured and (4) how the measurements are assessed. Moisture content measurements should be taken (5) at locations at risk of high moisture and where the moisture level is critical for the structure (6) in accordance with the relevant product standard. Additionally, it should be documented (7) how temperature and relative surrounding humidity of the surrounding air get measured in parallel. In certain cases, it seems possible to obtain additionally needed average air temperate and relative air humidity over the relevant period from local weather data [7]. If required, EN 1995-3 proposes the inspection of moisture content at delivery, during execution and on completion of the structure. Besides the rules for new structures, the pre-normative CEN/TS 17440 for the assessment and retrofitting of existing structures states that testing and monitoring may be used to verify and improve the assumptions of the structural analysis for existing structures [8]. Based on such information, the basic variables of the materials may be updated. This leads to the conclusion that whether in existing structures or new buildings, moisture measurement plays a crucial role in European timber design. It thus supplements, e.g. structural wood preservation by the assessment of sensitive parts of built structures and in execution. However, the assessment of technical methods suitable for such moisture monitoring is beyond the scope of current standardization.

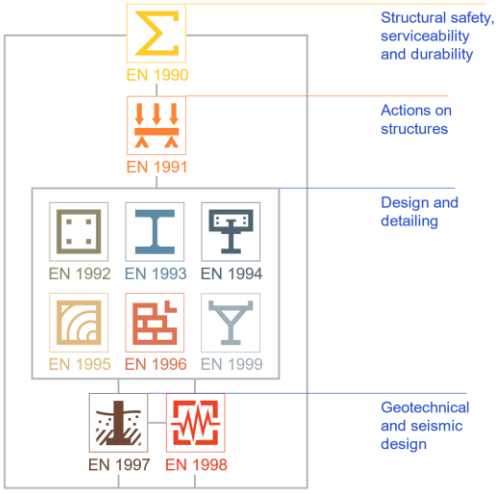

Figure 1 – Structural Eurocodes at a glance (© European Commission)

Table 1 - Overview of the Eurocode 5 series

Standard	Title
EN 1995-1-1	General rules and rules for buildings
EN 1995-1-2	Structural fire design
EN 1995-2	Timber bridges
EN 1995-3	Execution rules

PREVIOUS FINDINGS ON DIFFERENT WOOD MOISTURE MONITORING TECHNIQUES

A number of techniques and instruments are used in practice to determine the moisture content of timber. Three of them are standardized in EN 13183: Part 1 - *Determination by oven dry method*, Part 2 - *Estimation by* electrical resistance method and Part 3 - Estimation by capacitance method. It is noted that EN 13183 generally does not provide guidance on moisture monitoring. For direct wood moisture measurement, only the oven dry method [9] is used in the timber engineering practice. All other measuring methods are considered indirect [10]. Two of them are discussed in the investigation on hand with regard to their suitability for monitoring projects: The repeated measurement of electrical resistances (here method b) is based on the standardized method for estimating the moisture content of a piece of sawn timber [11]. However, there are no regulations how to conduct the same measurements over a long period with built-in electrodes. Furthermore, there is still no widespread technical solution for the monitoring of moisture gradients in timber elements, especially when influenced by thermal fluctuations. Tilleke & Fouad show measurement series with electrical resistance measurements used on a single spruce beam for experimental long-term observation over 25 years [12]. They proof their results in comparison with simulated expected values. Consequently, in the last two decades, numerous monitoring projects have been undertaken with the electrical resistance measurement of engineered timber

components, for examples see [13–16]. Even if the individual research projects differ slightly in the design of the electrodes, they all have in common that the temperatures in the components examined were always sufficiently balanced.

The sorptive method (here method a, also *sorption method* or *bore hole method* or *hygrometric method*), could be a possible alternative for monitoring in the future. In order to improve techniques for the preservation of wooden objects, [17] compare both, the sorptive method and electrical resistance measurements with expected results by a Fickian model for moisture diffusion. They only obtained very inconsistent results from the comparative laboratory measurements on *Scots Pine* for the electrical resistance measurements. It could therefore be suggested that the electrical resistance method is not suitable for examining cultural heritage. Regarding the investigation of engineered timber products, Schiere et al. [18,19] compared these two methods in terms of their suitability for in-situ monitoring. In their literature review they state that the sorptive method is more suitable for the lower hygroscopic range, while the electrical resistance method can also be used above the hygroscopic range with larger uncertainties. However, for monitoring projects on beech LVL they achieved similar results with either method. Even if the authors mentioned above obtain different results, they have in common that their monitoring techniques are mainly used for wooden elements surrounded by a similar ambient climate. But how do the two methods compare under thermal gradients such as those found in exterior cross-laminated timber (CLT) walls?

METHODOLOGY OF THE EXPERIMENTAL INVESTIGATIONS (IN-VITRO AND IN-SITU)

The moisture gradients in CLT differ significantly from simple solid wood due to the different fiber directions and the diffusion-retarding effect of the glue lines [20, 21]. Still, the moisture content of CLT walls could be estimated by periodic measurements in the individual lamellas based on the electrical resistance method according to EN 13183-2:2002 [11]. Pairs of electrodes (galvanized steel, completely insulated except for the tips, see Fig. 2b, are drilled in at a distance of 30 mm each and with the measuring direction transverse to the grain. The method used for electrical resistance measurement in this paper corresponds to that described in detail in [2]. The further processing of the raw resistance values is carried out by means of a wood-specific calibration curve and a generic temperature compensation, both as specified by the manufacturer. The temperature values of the different depths for this are taken from the combi-sensors, which are also used for the sorptive method.

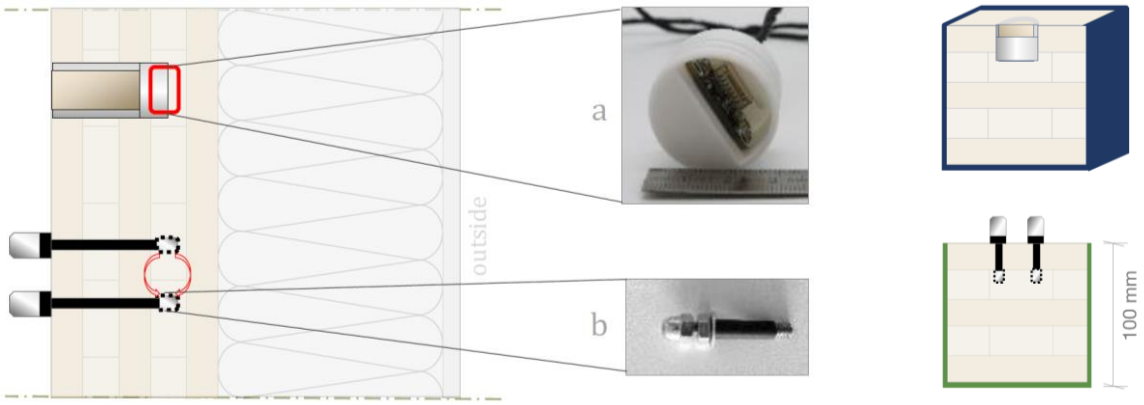

Figure 2 –Two measurement techniques in comparison in-situ in an exterior CLT wall (left) and in-vitro in lab experiments with test specimens of five-layer CLT and five sides covered with a vapor barrier film (right)

For the alternative sorptive method (see Fig. 2a) a small, closed air chamber is drilled into the material at a defined layer depth and tightly sealed by specially designed sensor casings and additional aluminium tape [22, 23]. Here, the relative water vapor partial pressure and the temperature of the enclosed air are measured. Then the corresponding equilibrium moisture content is inferred. The conversion of the input variables relative humidity h and air temperature T to an equilibrium moisture content EMC

could be performed using various equations [24]. In the context of this paper, two approaches are used, both of which are based on the sorption model by Hailwood and Horrobin [25] and the sorption data for *Sitka Spruce*. With equation (1) *EMC* is derived according to the formula of [25, 26], herein referred to as a1 (see Fig. 3). Equation (2) is a more simplified approach based on the findings by [27, 28], results are marked as a2 (see Fig. 3). In both equations, the inputs are relative humidity h as a decimal ($0 \leq h \leq 1$) and air temperature T [°C]. The individual values of the parameters W, K, K_1, K_2 and A, B, C, D fitted for *Sitka Spruce* can be found in [28, 29].

$$EMC\ [m.-\%] = \frac{1800}{W}\left(\frac{Kh}{1-Kh} + \frac{K_1Kh+2K_1K_2K^2h^2}{1+K_1Kh+K_1K_2K^2h^2}\right) \quad (1)$$

$$EMC\ [m.-\%] = 100\left[A(T+273{,}15)\left(1-\frac{T+273{,}15}{647{,}1}\right)^B \ln(1-h)\right]^{C(T+273{,}15)^D} \quad (2)$$

For the preliminary tests in-vitro, five test specimens with sorptive sensors (a) and four test specimens with electrical resistance measurements (b) in different depths were compared. Before mounting the sensors, the CLT blocks were first pre-conditioned to mass consistency in the laboratory and weighed regularly with a precision scale to determine the equilibrium moisture content. After sensor insertion they were then subjected to several isothermal humidity jumps over a period of several months. During this period, both monitoring systems ran in parallel with a time increment of 10 minutes. Oven drying the test specimens [9]concluded the test and retrospectively determined the respective actual wood moisture contents (distributed over the entire test piece). In addition to the laboratory tests, both measuring systems were compared with regard to their long-term behavior (see Fig. 2, left). For this purpose, they were installed in a measuring cube in CLT construction in the exterior wall, i.e. with a temperature gradient, over several months and then compared. For better clarity, only the conversions according to method a1, based on equation (1), are shown when evaluating the results from the outer wall.

RESULTS AND DISCUSSION

When comparing the resulting wood moisture values, it is noticeable that those according to the sorptive method (a) are always higher than those according to the electrical resistance method (b). The results from equation 2 (a2) are again slightly higher than the results from equation 1 (a1), but they both show much more pronounced amplitudes then results from method b after the isothermal moisture jumps in the laboratory, see Figure 3. The moisture contents determined according to oven drying and thus with the only direct measurement method refer in each case to the entire test specimen, but without the weight of the sensors and the adhesive film. From these values, it can be estimated which actual wood moisture contents should have set in at the various depths at the time of measurement.

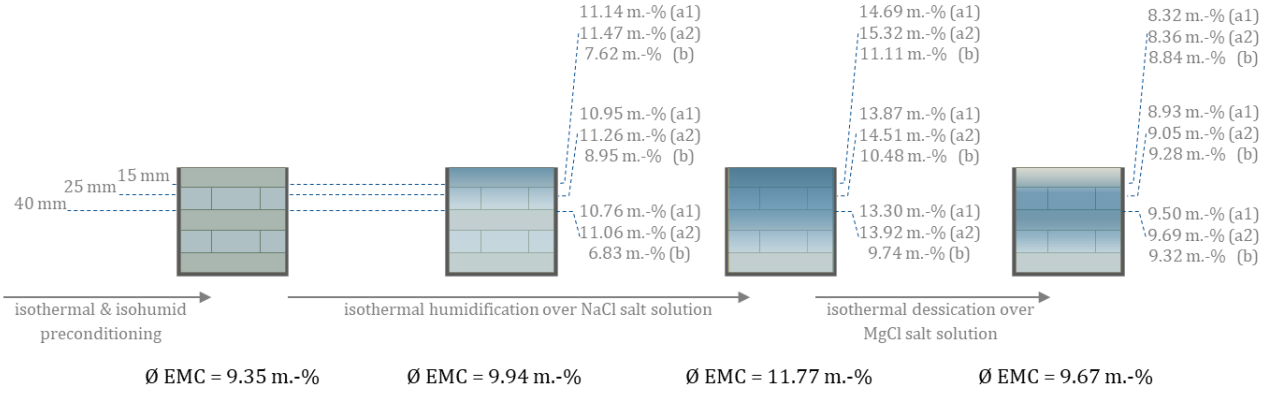

Figure 3: Results from different wood moisture monitoring techniques, obtained at three different measurement depths (15, 25, 40 mm). Sorptive measurements a1, calculated to EMC-Values acc. to equation 1 by [26]. Sorptive measurements a2, calculated to EMC-Values acc. to equation 2 by [27]. Results by electrical resistance measurements b. The average equilibrium moisture contents Ø EMC were derived by oven dry method.

Due to the lack of consideration of known phenomena such as sorption hysteresis, the available equations of the sorptive measurements are considered not suitable for in-depth scientific investigations but rather for a rough estimation [28]. However, the results according to a1 and a2 seem to depict the expected moisture distribution still more realistically than those by method b. Since the sensors used (Texas Instruments, HDC1080) can be subject to drift after prolonged exposure to high relative humidities, they were repeatedly checked for accuracy after removal from the test specimens. After completion of the lab measurement series, the deviations were still within ±2 % relative humidity.
Both measuring systems were employed simultaneously in a test cube with an exterior wall of CLT in four different depths: 15, 25, 40 and 70 mm from the inner surface. They were therefore also exposed to a thermal gradient over several months. Similar to the laboratory experiments, pronounced differences between the two monitoring techniques can be seen, see Fig. 3. Nevertheless, commonalities can also be identified: the deeper layers (70 mm) of the CLT wall seem to become more humid in the course of winter and spring, although the actual moisture content is still unclear. The wood moisture content calculated with the sorptive method (a1) according to [25, 26, 29] seems to be around three to four percentage points higher than what would result from the electrical resistance measurement according to the calibration curves (b).

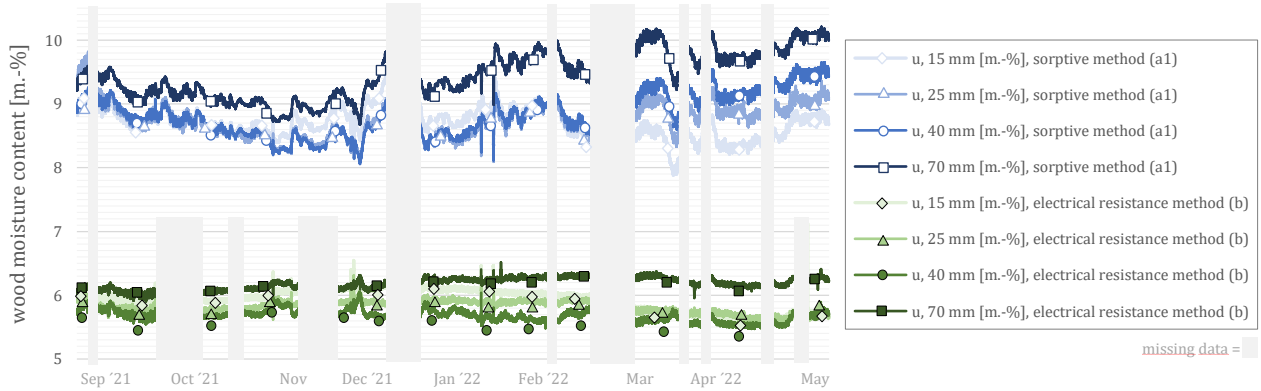

Figure 4 – Results from six months of measurements in a test cube

CONCLUSION AND OUTLOOK

The series of measurements presented here provide an insight into why it is necessary to investigate the methods of moisture monitoring in more detail. The following insights for future measurement series can be derived from the results obtained so far: It is not possible at this point to make a clear statement about the actual moisture distribution of the test specimens using the oven dry method. Due to their thickness the relatively large sample pieces (100 x 100 x 100 mm³) would require significantly more time to achieve constant equilibrium moisture content throughout (1). Furthermore, the sample size of this preliminary test is too small (2). In addition, for clearer results, extended series of measurements with a larger number of samples as well as greatly reduced specimen thickness (20 mm) are planned for the future. Especially in the case of strong temperature gradients, a mathematical falsification of the measured values by electrical resistance measurements is suspected (3). Laboratory measurements are expected to provide a strongly improved curve fitting of the formula for temperature compensation. Typical wood characteristics such as anisotropy or sorption hysteresis could have an influence on the measurement results, which have not yet been taken into account (4).
Furthermore, it is explicitly pointed out that the two indirect methods investigated are both only estimation methods. Nevertheless, it is important for the engineering practice that the methods provide at least sufficient accuracy. Future European standards refer to moisture measurements in a multitude of application cases, either during execution or in existing structures. Hence, further information and

guidelines on how to adequately conduct this monitoring on site are in heavy need. The investigations on hand and the described work in European standardisation are small but important parts in the big picture of further achieving holistic sustainability for our built environment.

ACKNOWLEDGEMENTS

Parts of the research activities were made possible by the German Federal Institute for Research on Building, Urban Affairs and Spatial Development (BBSR) as part of the research initiative "Zukunft Bau" SWD-10.08.18.7-18.46. Other parts were funded by the German Federal Ministry for Economic Affairs and Energy as part of the "Central Innovation Program for SMEs (ZIM)" ZF4777401SA9.

REFERENCES

[1] M. Riggio, M. Dilmaghani, Structural health monitoring of timber buildings: a literature survey, Building Research & Information, vol. 48, no. 8, pp. 817–837, 2020, doi: 10.1080/09613218.2019.1681253.

[2] D. D´Ayala, J. M. Branco, M. Riggio, A. Harte, J. Kurz, T. Descamps, Assessment, Reinforcement and Monitoring of Timber Structures: FPS COST Action FP1101, Proceedings of the World Conference on Timber Engineering, WCTE Quebec City, 2014.

[3] CEN/TC 250 (ed.): N 993 - Response to Mandate M/515 EN 'Towards a second generation of EN Eurocodes'. Brussels, Belgium, 2013 - unpublished.

[4] M. Kleinhenz, S. Winter, P. Dietsch, Eurocode 5 - A halftime Summary of the Revision Process, Proceedings of the World Conference on Timber Engineering, WCTE Vienna, 2016.

[5] CEN/TC 250/SC 10 (ed.): prEN 1990: EN 1990 Basis of structural design, Brussels, Belgium, 2022 - unpublished.

[6] CEN/TC 250/SC 5 (ed.): prEN 1995-1-1: Eurocode 5: Design of timber structures — Common rules and rules for buildings — Part 1-1: General, Brussels, Belgium, 2021 - unpublished.

[7] CEN/TC 250/SC5/WG9 (ed.): prEN 1995-3: Eurocode 5: Design of timber structures — Execution rules, Brussels, Belgium, 2022 - unpublished.

[8] CEN-CENELEC (ed.): CEN/TS 17440: Assessment and retrofitting of existing structures, Brussels, Belgium, 2020.

[9] CEN-CENELEC (ed.): EN 13183-1: Moisture content of a piece of sawn timber - Part 1: Determination by oven dry method, Brussels, Belgium, 2002.

[10] P. Dietsch, S. Franke, B. Franke, A. Gamper, S. Winter, Methods to determine wood moisture content and their applicability in monitoring concepts, J Civil Struct Health Monit, vol. 5, no. 2, pp. 115–127, 2015, doi: 10.1007/s13349-014-0082-7.

[11] CEN-CENELEC (ed.): EN 13183-2: Moisture content of a piece of sawn timber - Part 2: Estimation by electrical resistance method, Brussels, Belgium, 2002.

[12] S. Tilleke, N. A. Fouad, Rechnerische Simulation zeitlicher Holzfeuchteverläufe im Vergleich zu langjährigen Messreihen, Bauphysik-Kalender, 2022, pp. 251–273.

[13] A. Gamper, P. Dietsch, M. Merk, S. Winter, Gebäudeklima - Langzeitmessung zur Bestimmung der Auswirkungen auf Feuchtegradienten in Holzbauteilen: Final Report, Technical University of Munich, 2013.

[14] M. Fredriksson, L. Wadsö, P. Johansson, Small resistive wood moisture sensors: a method for moisture content determination in wood structures, Eur. J. Wood Prod., vol. 71, no. 4, pp. 515–524, 2013, doi: 10.1007/s00107-013-0709-0.

[15] L. Emmerich, C. Brischke, Electrical moisture content measurements of modified wood: Determination of resistance characteristics and outdoor monitoring, holztechnologie, vol. 62, no. 2, pp. 11 - 22, 2021.

[16] C. Brischke, A. O. Rapp, R. Bayerbach, Measurement system for long-term recording of wood moisture content with internal conductively glued electrodes, Building and Environment, vol. 43, no. 10, pp. 1566–1574, 2008, doi: 10.1016/j.buildenv.2007.10.002.

[17] C. B. Melin, T. Gebäck, A. Geynts, J. Bjurman, Monitoring Dynamic Moisture Gradients in Wood using Inserted Relative Humidity and Temperature Sensors, 2016.

[18] M. Schiere, B. Franke, S. Franke, A. Müller, Calibration and comparison of two moisture content measurement methods for in situ monitoring of beech laminated veneer lumber, Wood Material Science & Engineering, pp. 1–12, 2021, doi: 10.1080/17480272.2021.1958918.

[19] M. Schiere, B. Franke, S. Franke, A. Müller, Comparison between Predicted and Measured Moisture Content and Climate in 12 Monitored Timber Structures in Switzerland, Buildings, vol. 11, no. 5, p. 181, 2021, doi: 10.3390/buildings11050181.

[20] S. Bora, A. Sinha, A. R. Barbosa, Effect of Short-Term Simulated Rain Exposure on the Performance of Cross-Laminated Timber Angle Bracket Connections, J. Archit. Eng., vol. 28, no. 4, 2022, doi: 10.1061/(ASCE)AE.1943-5568.0000560.

[21] T. Gereke, Moisture-induced Stresses in cross-laminated Wood Panels, Dissertation, ETH Zurich, 2009.

[22] N. Flexeder, N. Schumacher, C. Hepf, A.S. Nouman et al., PhyTAB – Potenziale hygrothermisch aktivierter Bauteile: Energieeffiziente Raumkonditionierung mittels luftdurchströmter Massivholzelemente und hygroskopisch optimierter Oberflächen, Bonn: BBSR-Online Publikation, 2022 - in press.

[23] N. Flexeder, Geometry data of a sensor envelope for the hygrometric method to determine material moisture content, data, Technical University of Munich, 2022, doi:10.14459/2022mp1651104.

[24] St. Avramidis, Evaluation of "three-variable" models for the prediction of equilibrium moisture content in wood, Wood Science Technology, vol. 23, pp. 251–258, 1989.

[25] A. J. Hailwood, S. Horrobin, Absorption of water by polymers: analysis in terms of a simple model, Trans. Faraday Soc., vol. 42, no. 0, B084-B092, 1946, doi: 10.1039/TF946420B084.

[26] T. W. Simpson, Predicting Equilibrium moisture content of wood by mathematical models, Wood and Fiber, vol. 5, no. 1, pp. 41–49, 1973.

[27] C. Zuritz, R. P. Singh, Moini, S. M., Henderson, S. M., Desorption isotherms of rough rice from 10 °C to 40 °C, Trans. ASAE, pp. 433–440, 1979.

[28] S. V. Glass, Investigation of Historic Equilibrium Moisture Content Data from the Forest Products Laboratory, USDA Forest Service, 2014, https://doi.org/10.2737/FPL-GTR-229.

[29] Forest Products Laboratory, Wood handbook—wood as an engineering material: General Technical Report FPL-GTR-282. Madison, WI, 2021.

STRUCTURAL INTERVENTIONS

ANALYTICAL MODEL OF JOINT LOADED PERPENDICULAR TO WOODEN GRAIN

M. HATAJ[1], J. POŠTA[1], H. HASNÍKOVÁ[2], J. KUNECKÝ[2]

[1] Czech Technical University in Prague, University Centre for Energy Efficient Building, Třinecká 1024, 27343, Bustehrad, Czech Republic

[2] Institute of Theoretical and Applied Mechanics of the Czech Academy of Sciences, Prosecká 809/76, 190 00 Prague 9, Czech Republic

ABSTRACT

Computing models for structural behaviour and determination of traditional timber butt joints using analytical relations are presented in this paper. A component method is the base of the computing technique introduced herein. This method is usually used for steel joint design. The component method is based on dividing a joint into individual components. These are defined by partial joint component stiffness. An analytical solution includes a subsidence effect of wooden material close to compressive loading. Analytical computation results are compared with the experimental outputs. A design procedure according to Eurocode 5 for a load capacity determination of perpendicularly loaded structural elements is stated in the paper.

KEYWORDS: analytical models, load capacity, butt joint, carpentry, timber structures

INTRODUCTION

A perpendicular butt joint represents an elementary perpendicular carpentry joint. The joint transmits compression load from an ending structural element into a continuous element through a contact area of both the elements jointed together. This joint is usually fixed by carpentry iron cramps to prevent the elements from dislocation. There is an extensive difference between wooden material properties in longitudinal and transversal directions due to the orthotropic behaviour of wood. The modulus of elasticity and load capacity of wood in the transversal direction is lower than the capacity in the longitudinal direction. This is a reason for the continuous element being deformed when compressed.

EXPERIMENT

A set of five specimens, with the continuous element 500 mm long, was tested experimentally. Geometry parameters are depicted in figure 1. The moisture content of all wooden parts was between 11.2 and 13.1 %. The experiment was vertical displacement-controlled with a speed of 1.5 mm/min and was performed at an ambient temperature of 20.5 °C.

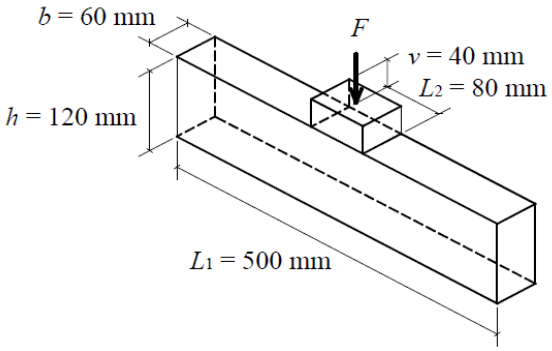

Figure 1: Geometry of tested joint

EUROCODE 5 DESIGN PROCEDURE

The design procedure according to Eurocode 5 (ČSN EN 1995–1–1, 2006) listed below determines the load capacity of timber structural elements exposed to the actions of loading in the direction perpendicular to the grain. The standard calculation does not include a deformation extent therefore it is not possible to define force-displacement dependence, in a respectively stress-strain diagram. This dependence can be an input for more precise modelling of the whole structure, for example, a roof structure.

$$\sigma_{c,90,d} \leq k_{c,90}\ f_{c,90,d} \tag{1}$$

$$\sigma_{c,90,d} = \frac{F_{c,90,d}}{A_{ef}} \tag{2}$$

where:

$\sigma_{c,90,d}$ is the design compressive stress in the contact area perpendicular to the grain;

$F_{c,90,d}$ the design compressive force perpendicular to the grain;

A_{ef} the effective contact area perpendicular to the grain;

$f_{c,90,d}$ the design compressive strength perpendicular to the grain, for the most common strength class in the Czech Republic – C24 – according to ČSN EN 338 (2016) – the characteristic value of strength is $f_{c,90,k} = 2,5$ MPa ;

$k_{c,90}$ factor considering the load configuration, possibility of splitting and degree of compressive deformation.

The effective contact area perpendicular to the grain, A_{ef}, should be considered as the effective contact length along the grain, where the real contact length l is increased by 30 mm in both directions, however, no more than a, l or $l_1/2$, see figure 2. The value $k_{c,90}$ should be considered as being equal to 1.0, unless the members´ arrangement, seen in the following paragraph, applies. For an element resting on continuous supports, provided that $l_1 \geq 2h$, the factor $k_{c,90}$ is given by:

$k_{c,90}$ = 1,25 for solid softwood

where h is the height of an element and l is the contact length.

ADDITIONAL LENGTH EFFECT

A specific phenomenon occurs when a timber element is a compressed perpendicular to the grain flow. The effect is called “subsidence trough” in the soil mechanics. Japanese scientists (Kitamori et al., 2009)

dealt with this effect in the timber structures context. They determined logarithmic function $f_{(x)}$ that approximates subsidence curve - equation (3) and equivalent factor a that depends on the height of compacting element Z_0, its boundary conditions - equation (5). It is possible to calculate an effective length of subsidence effect L_{ef} – equation (6) – by the quotient of the area under the curve $A_{(x)}$ divide line of compacting δ. Figure 2 describes important parameters for the analytical calculation.

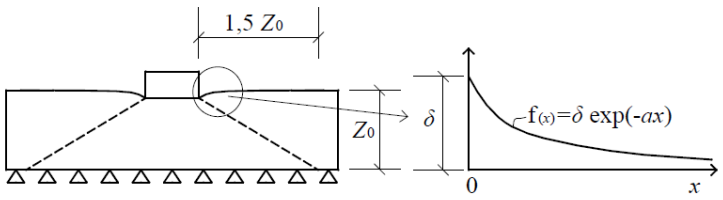

Figure 2: Additional length effect

$$f_{(x)} \leq \delta \, e^{-a\,x} \tag{3}$$

$$A_{(x)} = \int \delta \, e^{-a\,x} dx = \frac{\delta}{a}(1 - e^{-a\,x}) \tag{4}$$

$$a = \frac{2,5}{Z_0} \tag{5}$$

$$L_{ef} = \frac{A_{(x)}}{\delta} = \frac{(1 - e^{-a\,x})}{a} \tag{6}$$

ANALYTICAL MODEL

An analytical model is based on dividing a joint into individual components. These are defined by partial joint component stiffness. In this model, an important function holds the subsidence effect, listed above, that increases the complete stiffness of the continuous element.

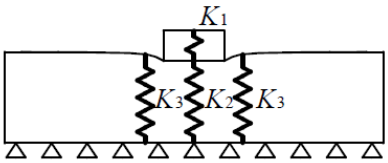

Figure 3: Stiffness model

The component stiffness is specified by the following relations (geometrical parameters correspond to figure 1):

$$K_1 = \frac{E_{0,mean}\, b\, L_2}{v}\,,\; K_2 = \frac{E_{90,mean}\, b\, L_2}{h}\,,\; K_3 = \frac{E_{90,mean}\, b\, L_{ef}}{h} \tag{7}$$

Mean values of modulus of elasticity for timber strength class C24 according to ČSN EN 338 (2016):

$$E_{0,mean} = 11\,000 \text{ MPa}\,,\; E_{90,mean} = 370 \text{ MPa} \tag{8}$$

Complete stiffness of a joint considers parallel impact of K_2 and K_3 and serial impact of these two stiffnesses with stiffness K_1:

$$K = \frac{K_1\,(K_2 + 2K_3)}{K_1 + K_2 + 2K_3} \tag{9}$$

A maximal compression load with consideration of the design compressive strength perpendicular to the grain $f_{c,90,d}$ and factor considering the load configuration, possibility of splitting and degree of compressive deformation $k_{c,90}$:

$$F_{max,d} = k_{c,90}\; f_{c,90,d}\; b\,(L_2 + 2L_{ef}) \tag{10}$$

COMPARISON

Figure 4 describes the experimental average values curve of force-displacement function, calculated analytical model curve according to chapter 5 and load capacity according to Eurocode 5 – chapter 3. The characteristic compressive strength perpendicular to grain $f_{c,90,k}$ and factor $k_{c,90}$ being equal to 1.25 are applied in calculations. Real contact length was increased by 30 mm in both directions in a Eurocode 5 based calculation. Defining the design compressive strength perpendicular to the grain $f_{c,90,d}$ includes the partial safety factor γ_M and modification factor k_{mod} taking the effect of loading duration and moisture content into account.

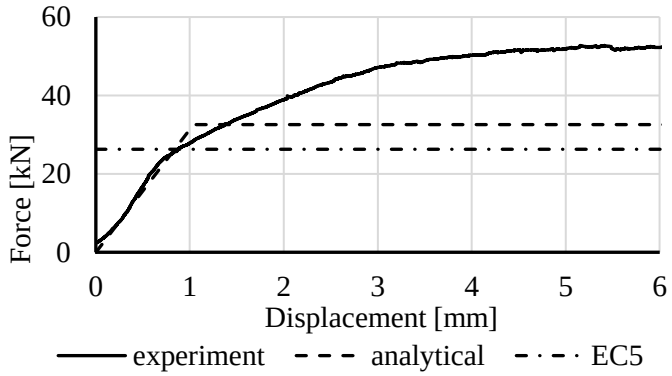

Figure 4: Force – displacement diagram

APPLICATION OF ANALYTICAL MODEL FOR MORTISE AND TENON JOINTS

The presented analytical model can also be applied to technologically more complex carpentry joints. This chapter is devoted to the model of mortise and tenon joints. In contrast to the perpendicular butt joint, the perpendicular mortise and tenon connection is provided with a tenon on the end of one connecting element and a mortise on the side of the other element. The mortise and tenon connection is usually provided with additional connecting fasteners - a bolt or a pin. The author presents models without the use of these connecting fasteners. This leads to conservative results.

The height of the tenon is 5 - 10 mm shorter than the depth of the mortise. This difference is due to the technology of production of mortise and tenon joints, where the end of the tenon must not touch the bottom of the mortise. If this measure is not met, excessive stress will be concentrated in the tenon and at the bottom of the mortise and the full contact of the joint contacting surfaces will not be ensured. The thickness of the tenon is based on the empirics used to date as a third of the width of the element with mortise.

Components approximating the behaviour of parts of the associated element with mortise have a proportionally reduced stiffness compared to previous cases. The additional length effect in the transverse direction of the element with mortise is neglected. This assumption leads to conservative results.

Components with proportionally reduced stiffness (other components are identical to the relationships given in the chapter Analytical model):

$$K_2' = \frac{E_{90,mean}\,\frac{b-b_1}{b}\,L_2}{h}, \qquad K_3' = \frac{E_{90,mean}\,\frac{b-b_1}{b}\,L_{ef}}{h} \tag{11}$$

where: b_1 is thickness of the tenon.

CONCLUSIONS

A methodology defining the structural behaviour and load capacity of a traditional perpendicular butt joint is presented in this paper. The analytical model corresponds with the experimental force-deflection dependence in the elastic phase. The effective contact length, as well as load capacity according to analytical calculation, exceeds the contact length and load capacity according to Eurocode 5. The real load capacity given by the experiment is higher than a calculated one. This fact is influenced by characteristic compressive strength $f_{c,90,k}$ which is higher in reality. Elastic strength is considered in Eurocode 5. The model with nonlinear – for example, bilinear – the behaviour of stiffness and plastic strength may express the real behaviour of such a joint better.

ACKNOWLEDGEMENT

This work has been supported by The Czech Science Foundation (GACR), project GA21-29389S: Experimental and numerical assessment of the bearing capacity of notches in timber beams at arbitrary locations using LEFM.

REFERENCES

[1] ČSN EN 1995-1-1: Eurokód 5: Navrhování dřevěných konstrukcí – Část 1-1: Obecná pravidla – Společná pravidla a pravidla pro pozemní stavby + Změna A1 + Změna A2. (2006) Český normalizační institut, Praha..

[2] ČSN EN 338: Konstrukční dřevo – Třídy pevnosti. (2016) Úřad pro technickou normalizaci, metrologii a státní zkušebnictví, Praha.

[3] Kitamori, A.; Mori, T.; Kataoka, Y. and Komatsu, K. (2009) Effect of Additional Length on Partial Compression Perpendicular to the Grain of Wood. Journal of Structural and Construction Engineering, 74, 642, pp. 1477-1485.

DYNAMIC CHARACTERIZATION OF A SIX-STORY LIGHT-WEIGHT TIMBER-FRAME BUILDING

Carmen AMADDEO[1] and Michael DORN[1]

[1] Department of Building Technology, Linnaeus University, Sweden.

ABSTRACT

Multi-story residential and commercial timber buildings are an efficient solution for sustainable cities. Numerous projects have been and are expected to be realized in Sweden. In-situ wind-induced ambient vibrations tests have been conducted on a six-story light-weight timber-frame building in Varberg (Sweden). The load-bearing structure is composed of outer walls and some interior walls. For horizontal stabilization, the walls are supported by a bracings system realized with steel rods. To perform the in-situ measurements, multiple battery-driven data acquisition units, with uni-axial accelerometers have been used. Repeated measurements at different positions have been performed to be able to collect data at each floor and along both directions (longitudinal and transversal). Two different Operational Modal Analysis (OMA) methods have been used to evaluate the modal parameters: frequency, damping and mode shapes. The in-situ dynamics properties have been compared with the dynamic properties obtained from the Finite Element (FE) model of the structure.

KEYWORDS: operational modal analysis, light-weight timber-frame building, finite element modelling

INTRODUCTION

Light-weight timber-frame (TF) construction has been increasingly used in multi-story residential and commercial buildings. Such types of structures can be realized quickly due to the high-level of prefabrication. In order to be able to realize taller structures with this construction system, it is important to understand their dynamic behaviour. Vibrations in multi-story light-weight TF structures can cause discomfort on the building occupants. Such vibrations are related to the non-linear behaviour of the building connections as well as the rotation of the panels [1]. Dynamic tests on light-weight TF multi-story buildings have not been extensively conducted with exception of some few cases [2], such as the six-story stud-and-rail Timber Frame 2000 building by Ellis and Bougard [3].

This study identifies the modal parameters of a six-story light-weight TF building using ambient vibration measurements. The modal parameters of the building are identified using two Operational Modal Analysis (OMA) methods: Enhanced Frequency Domain Decomposition (EFDD) [4], and Stochastic Subspace Identification (SSI) [5]. This type of test allows us to understand the behaviour of the building as built.

These are the preliminary results that will be used as a benchmark for a more extensive test campaign that will be conducted on three other TF buildings realized in Varberg (Sweden) with the exact same design. The modal parameters obtained from the field test are compared with the one obtained from the FE model of the building.

DESCRIPTION OF THE BUILDING

The Pilgatan building is a six-story residential building with four apartments on each floor. Its load bearing system is composed of light-weight TF. The TF external wall panels are made with 45 mm x 170 mm solid timber studs and Oriented Strand Board (OSB) sheeting panels, 11 mm thick (see Figure 1), on both sides of the walls to provide horizontal stability. The TF internal wall panels are made with 45 mm x 220 mm and 45 mm x 95 mm solid timber studs and particle board sheeting panels, 38 mm thick, between the studs for horizontal stability. Also, the shaft with the elevator and staircase is made the same way. The load-bearing wall elements are prefabricated and assembled on-site. For horizontal stabilization, diagonal steel rods have been used on the stairwell walls.

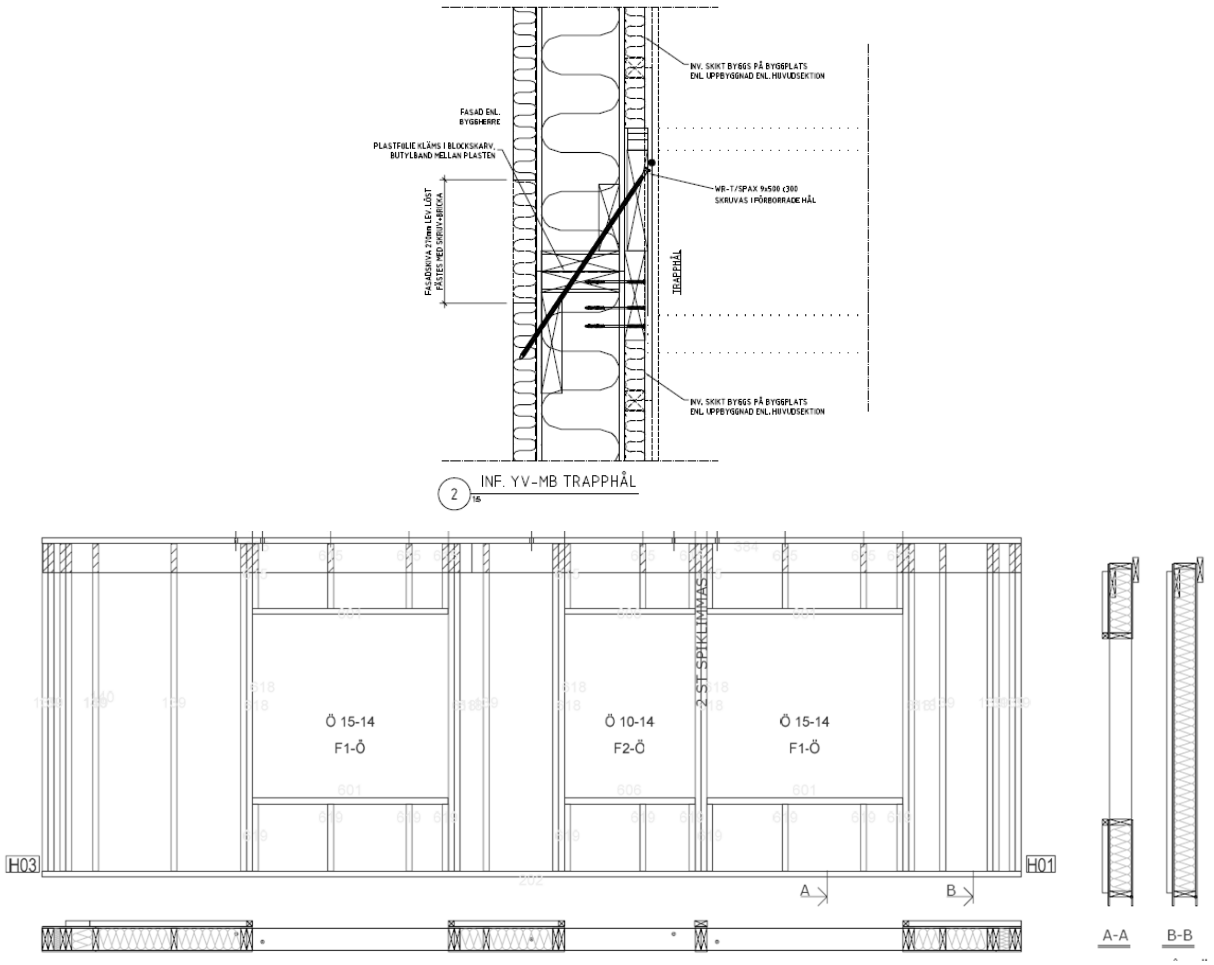

Figure 1: Detail of the TF wall panel for one of the external walls.

TESTING DESCRIPTION

To avoid any interference during the test, the testing campaign on the Pilgatan building was performed right after the construction of the building was finished and before the occupants moved into the apartments. The building was tested with the assumption that it would be excited by only ambient vibrations such as wind. For the ambient vibration tests, a wireless data-acquisition system with 4 uni-axial accelerometers were used (see Figure 2). The uni-axial accelerometers used were the PCB model 393B12.

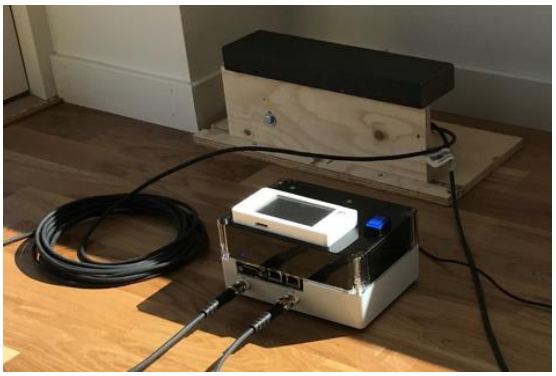

Figure 2: Test setup: 2 uni-axial accelerometers and portable data acquisition system

Due to the limited number of accelerometers, nine different tests were performed on the building to record the accelerations at each level while keeping fixed the reference system at the level 1. Figure3 from (a) to (d) shows the different test setups for each measurement, showing the X and Y positive direction. For each test setup, the ambient accelerations were collected for approximately 30 min. with a sampling frequency of 120 Hz. The sensor layout was selected based on a preliminary numerical analysis of the building in order to be able to identify the torsional mode shapes.

Figure 3: Floor plans with sensor locations: (a) Reference sensor location for all tests; (b) Test setup #1 Floor 1; (c) Test setup #2, #4, #6, #8 Floor 1 to 5; (d) Test setup #3, #5, #7, #9 Floor 1 to 5

OPERATIONAL MODAL ANALYSIS (OMA)

The collected accelerations were analyzed using Operational Modal Analysis (OMA) techniques. The methods used for the estimation of the modal parameters are EFDD and SSI. Both methods are already implemented into the used software ARTeMIS [6]. A similar approach has been used by Mugabo et al. [7], Magalhases et al. [8], and Moaveni et al. [9].

The data has been post-processed in order to better identify the first natural frequencies. In particular, a filter between 0 and 6 Hz has been performed using ARTeMIS. The algorithm used in the software ARTeMIS to perform the peak reduction is described by Gres et al. [10].
For the EFDD method, Figure 4 shows the Singular Value Decomposition (SVD) obtained for the test setup #9. Two well defined peaks can be observed at the frequency range between 2 - 4.0 Hz.

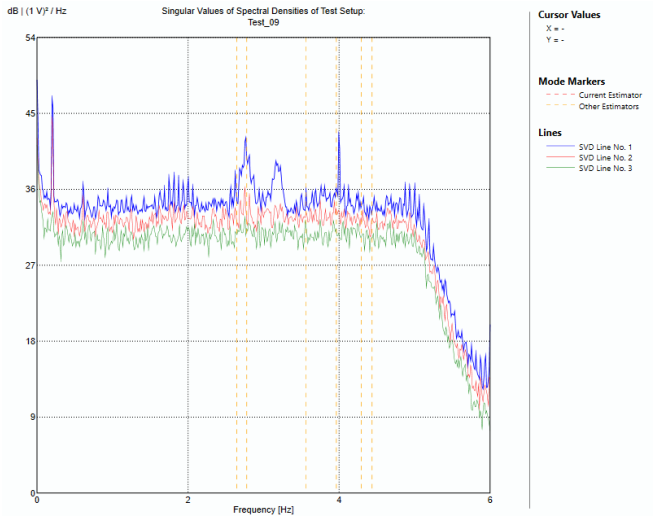

Figure 4: Singular Value Decomposition (SVD) plots for the Test Setup #9 used for the EFDD method.

For the SSI method, Figure 5 shows the state space stabilization model for the test setup #9. A maximum order of 55 was selected. The vertical red dots are indicating the stable modes for five different frequencies between 0 and 6 Hz.

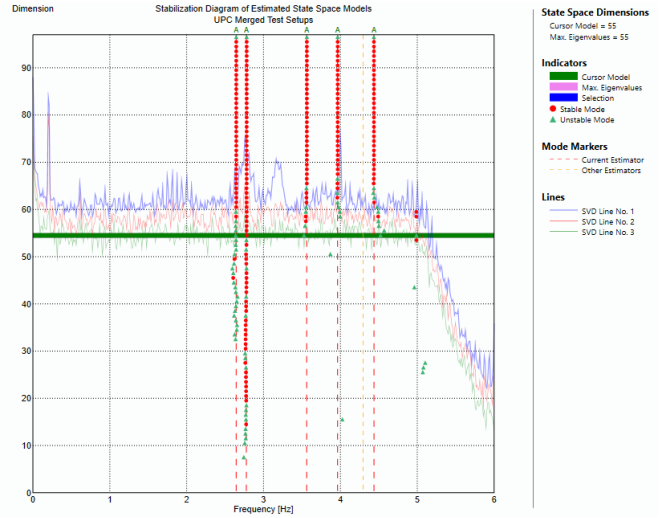

Figure 5: State space model for the Test Setup #9.

The obtained natural frequencies and damping ratios for the two OMA methods are summarized in Table 1.

Table 1: Identified natural frequencies and damping ratios for the EFDD and SSI methods.

1st Mode Torsional		**2nd Mode Y direction**		**3rd Mode Torsional**	
EFDD	**SSI**	**EFDD**	**SSI**	**EFDD**	**SSI**
f_1 = 2.75 Hz	f_1 = 2.77 Hz	f_2 = 3.17 Hz	f_2 = 3.96 Hz	-	f_3 = 4.43 Hz
ζ_1 = 0.60%	ζ_1 = 2.73%	ζ_2 = 0.60%	ζ_2 = 8.3%	-	ζ_3 = 9.16%

Two modes of vibration were identified using the EFDD method and three using the SSI method. In particular, the first torsional mode and the first translational mode were clearly identified by both

methods while the second rotational mode was identified only with the SSI method. This difference can be due to the fact that the peak-picking technique is more effective when the system's modes are well separated and it is less suitable in case of close modes [11], [12].
Figure 6 shows the identified mode shapes. The variations in terms of frequency and damping for closely spaced modes can be attributed to some factors such as length of the recorded data, excitation amplitude and noise level [7], [8] and [9].

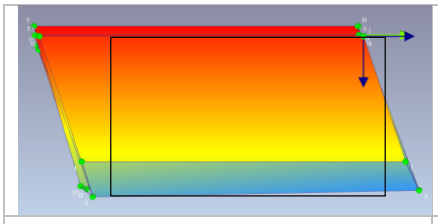

EFDD – f_1 = 2.75 Hz; z_1 = 0.60%

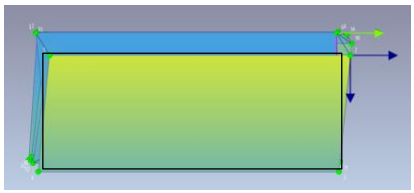

EFDD – f_2 = 3.17 Hz; z_2 =0.60%

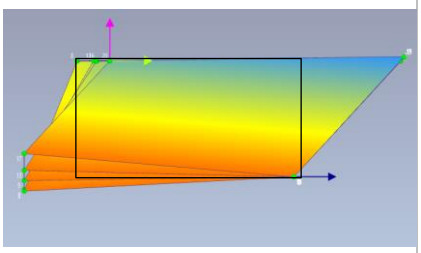

SSI – f_1 = 2.77 Hz; ζ_1 = 2.73%

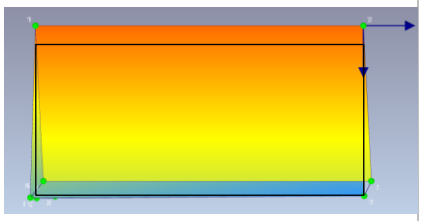

SSI – f_2 = 3.96 Hz; z_2 = 8.3%

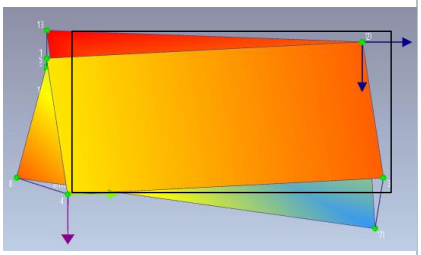

SSI – f_3 = 4.43 Hz; z_3 = 9.16%

Figure 6: Identified mode shapes for the EFDD and the SSI method.

FINITE ELEMT MODAL ANALYSIS

The FE model of the building was developed using SAP2000 [13]. The model was realized using beam elements to model the frame and shell elements for the OBS panels and particle boards. A detailed model was necessary to validate the identified modal parameters.
Table 2 shows the material properties used for the FE model for the different elements. Figure 7 shows the FE model with the studs and shell elements. The connections between the walls were modelled as spring elements. The mass of the floor was applied as distributed masses at each level.

Table 2: Material stiffness properties used for the FE model

Material	**Elastic Modulus (MPa)**	**Shear Modulus (MPa)**
Timber C24	10800	690
OSB panel	6000	1574
Particle board panel	2700	900

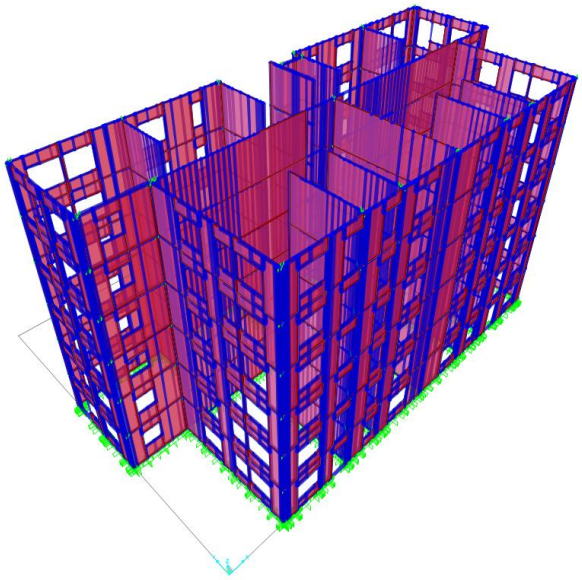

Figure 7: FE model of the Pilgatan building.

The first three modes of the building were taken into account (see Figure 8). The first and third mode of the building are torsional modes while the second mode is predominantly translational along the Y direction (short direction).

The frequencies obtained with the modal analysis are very close to the one identified experimentally. The differences in terms of frequencies observed between the test results and FE model may be due the mass and/or stiffness characteristics of the elements used to construct the model including the stiffness of the connectors.

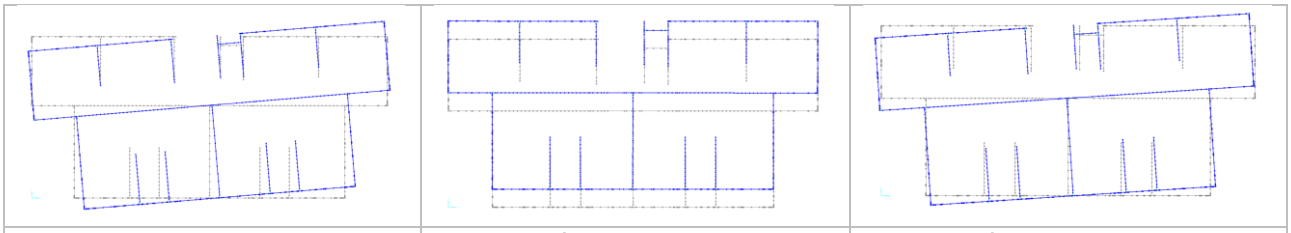

(a) 1st Mode: f_1=2.598 Hz	(a) 2nd Mode f_2=3.997 Hz	(c) 3rd Mode: f_3=4.732 Hz

Figure 8: Mode shapes obtained with the FE model of the building: (a) 1st Mode: f_1=2.598 Hz; (b) 2nd Mode: f_2=3.997 Hz; (c) 3rd Mode: f_3=4.732 Hz.

CONCLUSIONS

Ambient vibration tests were performed on a six-story light-weight TF residential building. The structural modes identified with the two OMA methods are the first two rotational modes and the first translational mode. The second rotational mode was identified only using the SSI method since the frequencies were very close. It was not possible to identify any of the higher modes due to the limited number of sensors, noise level in the recorded data, as well as the limited level of excitation. It is well known that these factors can influence the modal identification especially for such a typology of buildings.

The accuracy of the results can be improved by using a larger number of sensors. This way, it will be possible to measure the accelerations at each floor in two different locations for each test setup instead of having two different tests. This will improve the accuracy of the mode shape results.

The deformability of the sheathing-to-framing connections was not taken into account in the FE model. A more detailed model is necessary in order to take into account the connections deformability and to understand how this parameter can influence changes in the modal parameters of the building.

The use of light-weight TF system for the construction of multi-story buildings is rapidly increasing. Further experimental research is required in order to better understand the dynamic behaviour of such structures, in particular, to evaluate the damping ratio in multi-storey TF buildings.
This study can be considered a benchmark for further investigations that will focus on influence of the environmental conditions in the dynamic response of light-weight TF multi-storey buildings, as well as how the realization process can influence the modal parameters.

REFERENCES

[1] T. Reynolds, D. Casagrande, R. Tomasi, Comparison of multi-storey cross-laminated timber and timber frame buildings by in situ modal analysis, Construction and Building Materials, vol. 102, part. 2 (2016), pp 1009-1017.

[2] T. Reynolds, A. Bolmsvik, J. Vessby, W.-S. Chang, R. Harris, J. Bawcombe, J. Bregulla, Ambient vibration testing and modal analysis of multi-storey cross-laminated timber buildings, World Conference on Timber Engineering, 2014.

[3] B.R. Ellis, A.J. Bougard, Dynamic testing and stiffness evaluation of a six-storey timber framed building during construction, Eng. Struct, 23 (10) (2001), pp. 1232-1242.

[4] R. Brincker, L. Zhang, P. Andersen, Modal identification of output only systems using frequency domain decomposition, Smart Mater. Struct. 10 (2001), pp. 441–445.

[5] R. Brincker, P. Andersen, Understanding stochastic subspace identification, Proceedings of the 24th International Modal Analysis Conference, St. Louis, (MO) (2006), pp. 461–466.

[6] ARTeMIS Modal (2017). Available online at: http://www.svibs.com/products/ ARTeMIS_Modal.aspx.

[7] I. Mugabo, A. R. Barbosa, M. Riggio, Dynamic characterization and vibration analysis of a four-story mass timber building, *Front. Built Environ*. 5:86 (2019).

[8] F. Magalhães, R. Brincker, Á. Cunha, E. Caetano, R. Brincker, Damping estimation using free decays and ambient vibration tests, Proceedings of the 2nd International Operational Modal Analysis Conference (Copenhagen) (2007), pp. 513–521.

[9] B. Moaveni, A. R. Barbosa, J. P. Conte, F. M. Hemez, Uncertainty analysis of system identification results obtained for a seven-story building slice tested on the UCSD-NEES shake table. Struct. Control Heal. Monit. 21 (2014), pp. 466–483.

[10] S. Gres, P. Andersen, C. Hoen, L. Damkilde, Orthogonal projection-based harmonic signal removal for operational modal analysis, Structural Health Monitoring, Photogrammetry and DIC, Volume 6. Conference Proceedings of the Society for Experimental Mechanics Series, eds. C. Niezrecki and J. Baqersad (Cham: Springer) (2019).

[11] M. H. Masjedian, M. Keshmiri, A review on operational modal analysis researches: classification of methods and applications, Proceedings of 3rd International Operational Modal Analysis Conference (IOMAC'09), Portonovo, Italy, (2009). pp. 707–718

[12] L. Zhang, T. Wang, Y. Tamura, A frequency-spatial domain decomposition (FSDD) method for operational modal analysis, Mechanical Systems and Signal Processing, vol. 24, no. 5, (2010), pp. 1227–1239.

[13] CSI (Computers and Structures, Inc). SAP2000: Integrated Software for Structural Analysis and Design, Ver. 19. Berkeley, CA: CSI, (2017).

ASSESSMENT OF THE CENTER OF ROTATION OF MOMENT-RESISTING TIMBER JOINTS

Caroline D. AQUINO[1], Amirmahdi ZARGHAMI[2], Leonardo G. RODRIGUES[1], and Jorge M. BRANCO[1]

[1] Department of Civil Engineering, University of Minho, ISISE, 4800-058, Guimarães, Portugal

[2] ALMA MATER STUDIORUM – University of Bologna

ABSTRACT

This work presents an investigation of moment-resisting timber joints. Digital image correlation was used to determine the centre of rotation of the connection. In addition, an analytical model is proposed to optimize the design of joints, while exploiting an iterative process. From the experimental and analytical results obtained, it is possible to conclude that the estimation of the centre of rotation plays a crucial role on the design of moment-resisting joints.

KEYWORDS: timber structures, moment-resisting joints, centre of rotation, digital image correlation

INTRODUCTION

The capacity of connections to deform without rupture is essential to fulfilling timber buildings' safety requirements regions [1]. Timber elements must be considered elastic, while all nonlinear responses must be concentrated on the joints [2]. The structural design might promote energy dissipation through ductile connections that must present adequate strength and stiffness [3]. Consequently, the structural design may include optimization procedures to fulfil performance-based criteria while considering the materials' specific properties [4].

Dowel-type connections are commonly used in timber engineering for an extensive range of structural applications, where loads are transferred through wood embedment stresses and dowels' bending. The so-called dowelled moment-resisting joints result from specific geometrical dispositions of dowels that provide the capacity to bear moment forces [5]. According to different limit states and respective unfavourable design scenarios, practitioners commonly consider connections as rigid or pinned [6]. However, their response in service exhibits a semi-rigid behaviour, which must be accounted for material optimization, especially for resilient structures. Furthermore, the analytical design approach considers that the dowels have the same stiffness independently from the load direction. This assumption results in an equal loading distribution among the dowels, where the load applied on each dowel is dependent on its position [7,8]. An inappropriate joint detailing can lead to brittle failures due to shear and perpendicular to the grain tensile stresses [9].

International standards have set ground rules to prevent splitting by limiting the minimum fastener spacing, end-distances, and edge-distances. Nonetheless, recent studies have shown that moment-resisting joints, designed according to Eurocode 5 provisions, present brittle failures, and low ductility [1,5]. Besides, load-to-grain angle caused differences in single dowel connections' slip curves, leading to a non-uniformly distributed load among dowels [10]. Thus, it is paramount to evaluate the existing analytical models and perform research towards their update to include brittle failure modes while ensuring a ductile response of connections.

The design of dowelled moment-resisting joints depends considerably on the position assumed for the centre of rotation (CR). Digital image correlation (DIC) can be used to assess the displacement field and estimate the CR of experimental tests, which allows to better characterize the strength and stiffness of

moment-resisting connections. The present paper introduces an analytical model along with an iterative process to determine the CR, as well as the internal forces applied on dowels. Its results are compared with the experimental measurements obtained from DIC.

EXPERIMENTAL CAMPAIGN

Monotonic tests were performed at the structural laboratory of the University of Minho, aiming to simulate a beam-column connection, as presented in **Erro! Fonte de referência não encontrada.**. The setup configuration was based on the experimental campaign performed in Shu et al [5].

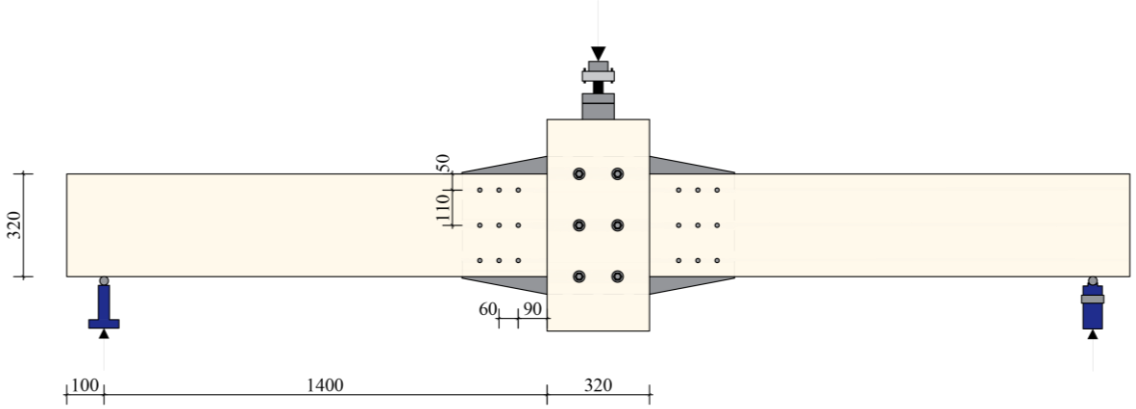

Figure 1: *Scheme of the connection (dimensions in mm)*

The geometrical dimension for the two glulam beams were 140 x 320 x 1500 mm^3, while the column was of 160 x 320 x 660 mm^3. A 12 mm thick steel plate from S275 grade, along with M27 bolts from grade 10.9, was used to transfer the load. Consequently, the damage shall be concentrated at the beams, which are connected to the plate through 12 mm smooth dowels from S235 grade. Based on the results of the first set of tests, a reinforced connection was tested. The reinforcement consisted on the use of VGZ self-tapping screws, 5 VGZ 7 x 140 on each side of the plate for the top part of the beam, and of 4 VGZ 5 x 80 and 4 VGZ 7 x 100 on each side of the plate for the bottom part of the beam, as shown in Figure 2. Two tests without reinforcement and one test with reinforcement were performed and will be referred in the text as test 1, 2, and 3, respectively.

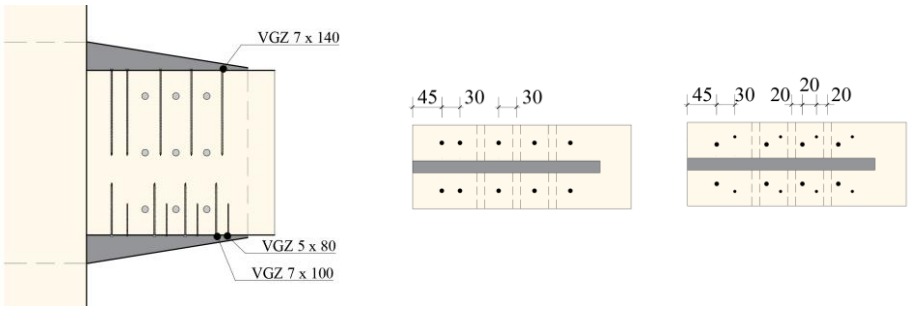

(a) side view *(b) top view* *(c) bottom view*

Figure 2: *Details of reinforcement*

DIC MODEL

Digital Image Correlation (DIC) is an innovative non-contact optical technique for measuring strains and displacements [11]. In this work, INSTRA 4D V4.4.7 x64 was used along with two cameras of 2.0 megapixels positioned at 190 cm from the specimens and 100 cm between each other. The acquisition frequency to obtain the frames was 1 Hz. DIC is used to track the displacement fields.

The displacement field of the connection of each step (every 1s) was obtained from DIC. The rotation of each point per step was computed as the difference between initial and final position, both in the vertical

and horizontal direction. To evaluate the rotation of beam related to the column, the displacement field of the column was discounted from the beam one. This was done considering a range of points of same vertical coordinates.

ANALYTICAL MODEL

The analytical model considers compression stresses and friction forces at the contact of the beam with the column, as well as the forces associated to dowel wedging into wood. A compression strength perpendicular to grain (σ_c) is assumed as equal to 4.3 MPa and a friction coefficient (ν) of 0.4 [12]. The forces applied on dowels are determined according to the provisions of Eurocode 5. The iteration process consists of simulating several positions of the CR and choosing the one that best equilibrate the internal and external forces. The flowchart of steps to determine CR is presented in Figure 3, and a scheme of the forces considered are presented in Figure 4.

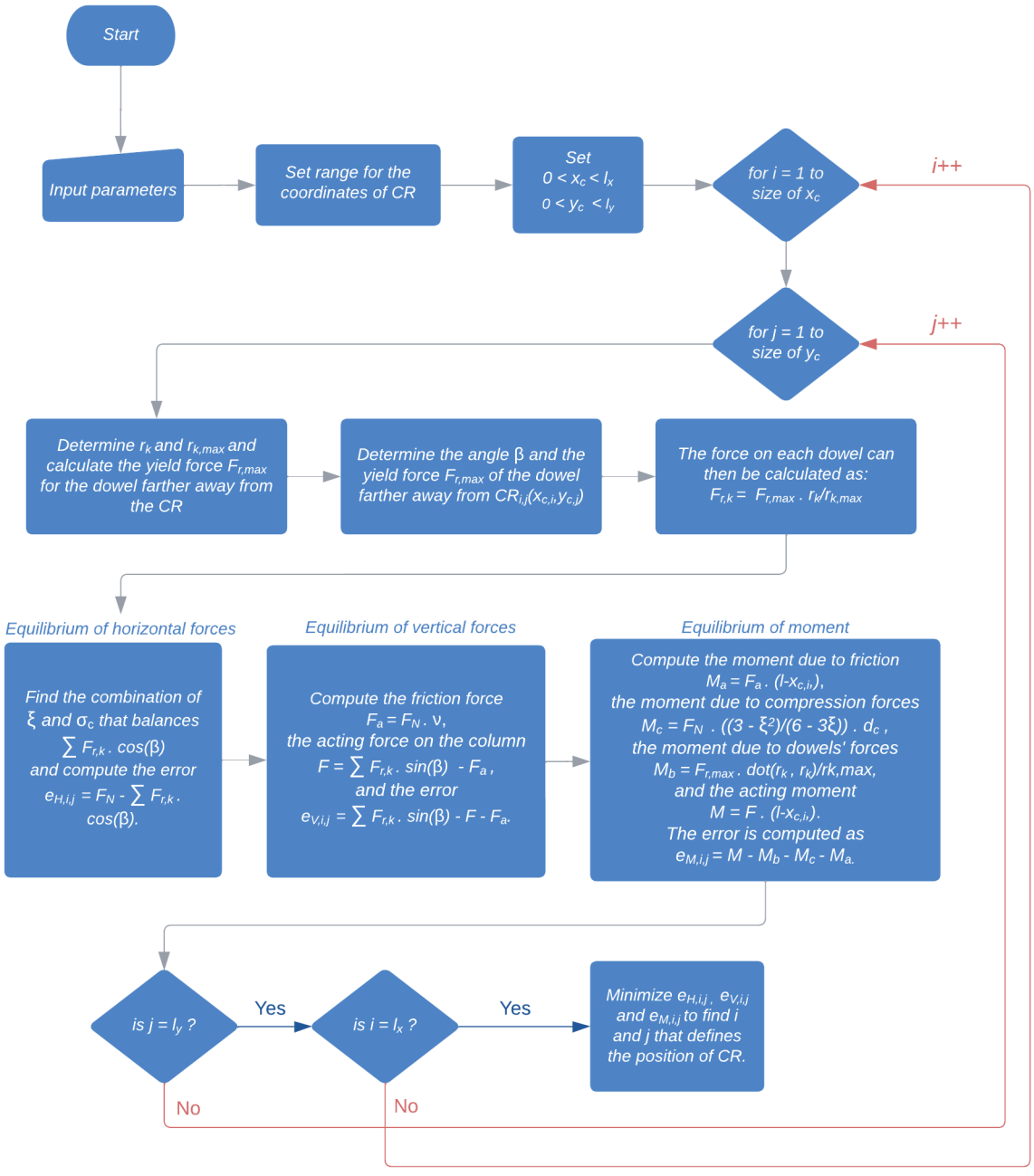

Figure 3: *Flowchart to determine CR*

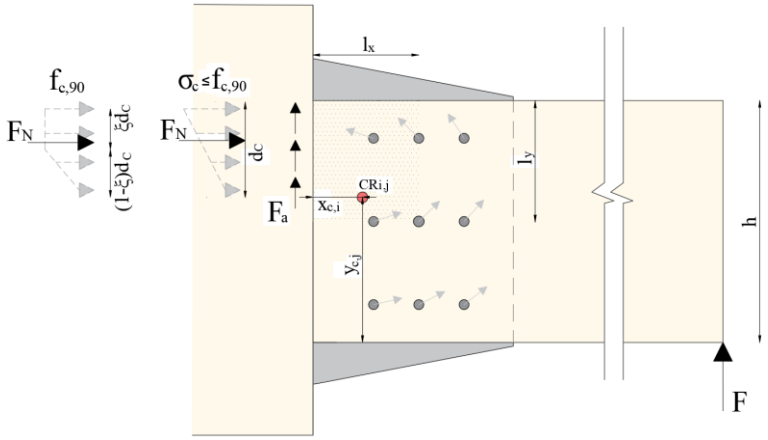

Figure 4: *Scheme of the forces acting on the connection*

RESULTS

Fig. (5) presents the moment-rotation curves for the experimental tests, as well as the specimen deformation with and without reinforcement. The rotation of the beams was obtained via DIC results.

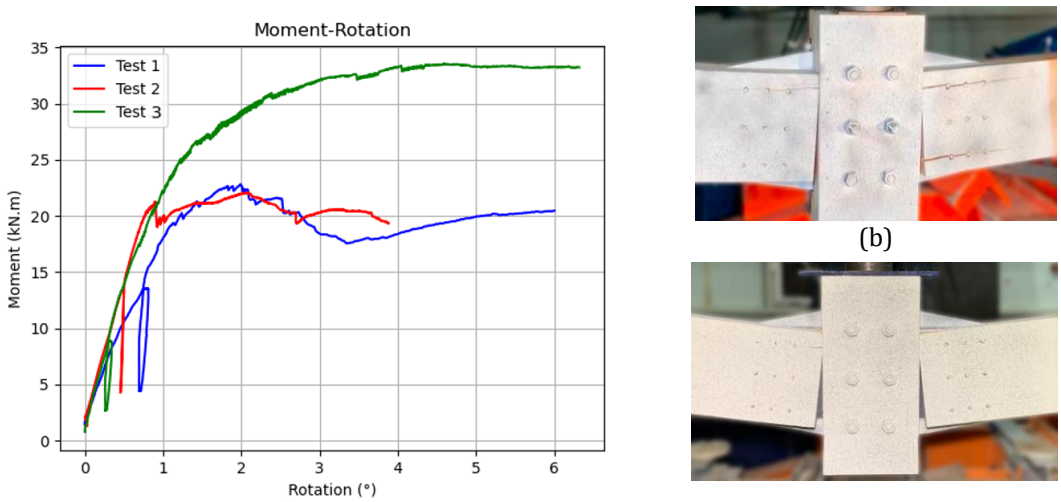

Figure 5: (a) *Moment-rotation curves and specimen deformation for b) without reinforcement, and c) with reinforcement*

The locations of the CR for each test are presented in Figures 6, 7, and 8. The position of CR is expressed in terms of time steps measured in seconds, and the correspondent elastic range is highlighted. The DIC estimations for the final step were compared with the specimen marks after test stopped, reaching approximate locations for the CR. This allowed to validate the DIC measurements obtained.

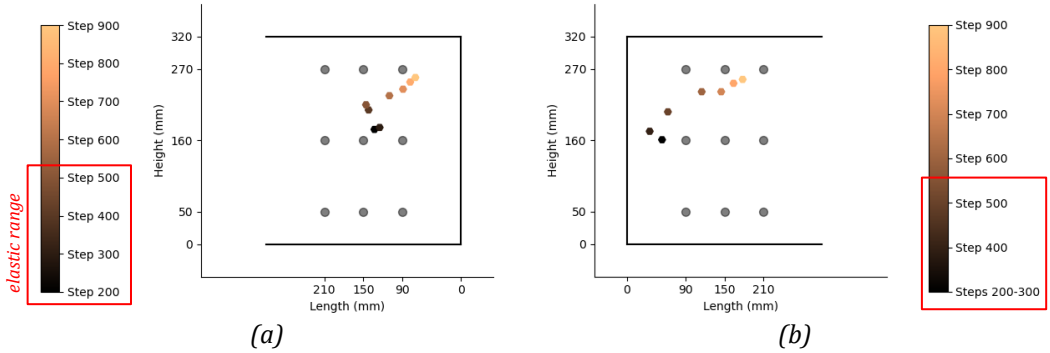

Figure 6: *Experimental centre of rotation for unreinforced connection (Test 1): a) left beam, and b) right beam*

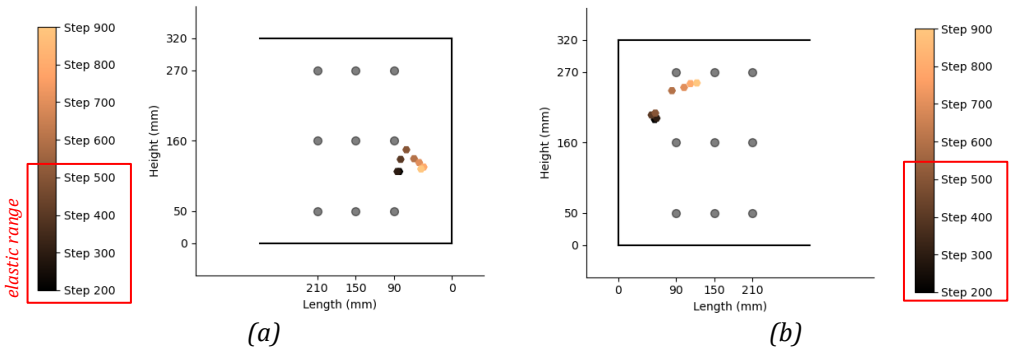

Figure 7: *Experimental centre of rotation for unreinforced connection (Test 2): a) left beam, and b) right beam*

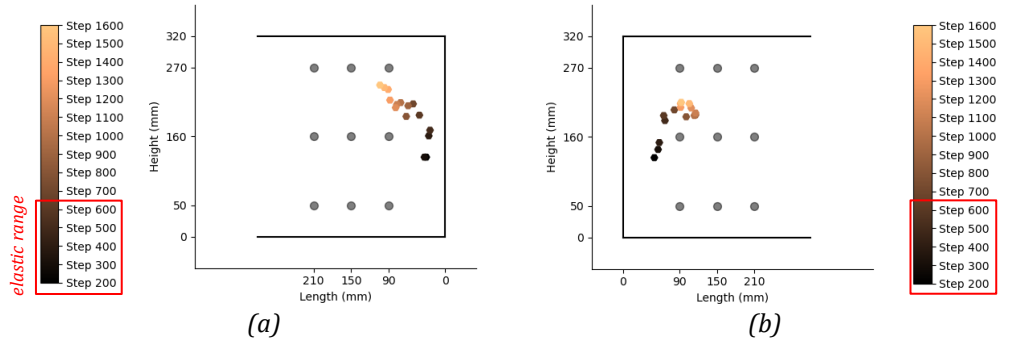

Figure 8: *Experimental centre of rotation for reinforced connection (Test 3): a) left beam, and b) right beam*

Finally, Figure 9 presents the centre of rotation found analytically via the iteration algorithm presented in Figure 3. The equilibrium of forces led to a resisting moment of 17.8 kNm. Since the analytical model does not consider splitting, and the position of the CR is determined based on the premise that the dowel farther away from the CR yielded, the result found shall be strictly compared with the elastic range of the experimental results. Comparing Steps 500 of tests 1 and 2, and Step 600 of test 3 (limit of the elastic range) with the analytical CR, one can conclude the analytical model gets close to the experimental position for test 1 and 3. The analytical model did not approximate well the results for test 2, especially for left beam. This is related to the deformation and failure mode of the test, the column suffered rotation and only the right beam experienced splitting.

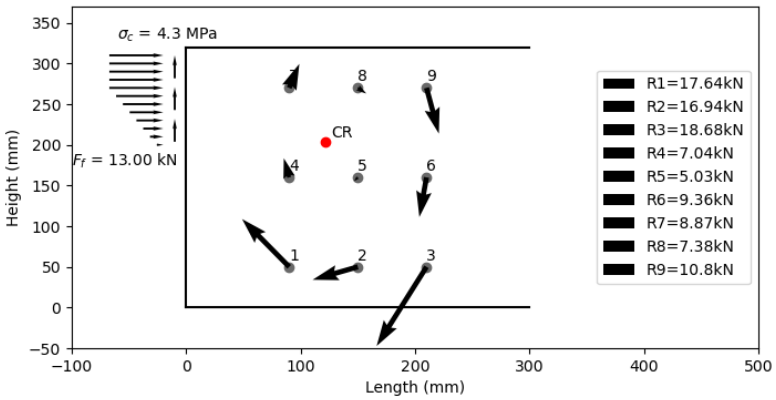

Figure 9: *Analytical centre of rotation and internal forces*

CONCLUSION

The problem related to the determination of the CR position was investigated using DIC and through an analytical model proposed herein. In the investigation conducted, no gap was considered between column and beam since the gap defined in the design phase is often not fulfilled on the construction site. This arrangement of the structure results in compression and friction forces in the contact of elements.

The analytical model presented shows good agreement with experimental results both in terms of the yield moment and position of the CR. A coherent assessment of the CR can allow a proper estimation of the perpendicular to grain forces that caused splitting, as well as an optimized reinforcement design. Despite the fulfilment of all the provisions of Eurocode 5, in terms of dowel spacing, end distances, and edge distances, brittle failures were observed. Thus, a reinforcement scheme was proposed aiming to refrain timber splitting, while allowing the development of higher embedment deformations beneath dowels that reached yielding.

ACKNOWLEDGMENTS

This work was financed by FCT – Foundation for Science and Technology within the scope of the Timquake project POCI-01-0145-FEDER-032031 and through a PhD grant 2021.07308.BD conceded to the first author.

REFERENCES

[1] Zhang, C., Guo, H., Jung, K., Harris, R., & Chang, W. S. Screw reinforcement on dowel-type moment-resisting connections with cracks. Construction and Building Materials 215 (2019) 59-72. https://doi.org/10.1016/j.conbuildmat.2019.04.160

[2] Jorissen, A., & Fragiacomo, M. General notes on ductility in timber structures. Engineering Structures, 33(11) (2011) 2987–2997. https://doi:10.1016/j.engstruct.2011.07.02.

[3] Rodrigues, L. G., Branco, J. M., Neves, L. A. C., & Barbosa, A. R. Seismic assessment of a heavy-timber frame structure with ring-doweled moment-resisting connections. Bulletin of Earthquake Engineering 16(3) (2017) 1341–1371. https://doi:10.1007/s10518-017-0247-y

[4] Mam, K., Douthe, C., Le Roy, R., and Consigny, F. Shape optimization of braced frames for tall timber buildings: Influence of semi-rigid connections on design and optimization process. Engineering Structures 216 (2020) 110692. https://doi.org/10.1016/j.engstruct.2020.110692.

[5] Shu, Z., Li, Z., Yu, X., Zhang, J., and He, M. Rotational performance of glulam bolted joints: Experimental investigation and analytical approach. Construction and Building Materials 213 (2019) 675-695. https://doi.org/10.1016/j.conbuildmat.2019.03.002.

[6] Porteous, J., & Kermani, A. Structural timber design to Eurocode 5. John Wiley & Sons (2013).

[7] Bouchaïr, A., P. Racher, and J. F. Bocquet. Analysis of dowelled timber to timber moment-resisting joints. Materials and Structures 40(10) (2007) 1127-1141. https://doi.org/10.1617/s11527-006-9210-0.

[8] Xu, B. H., Bouchaïr, A., and Racher, P. Mechanical behavior and modeling of dowelled steel-to-timber moment-resisting connections. Journal of Structural Engineering 141(6) (2015) 04014165. https://doi.org/10.1061/(ASCE)ST.1943-541X.0001119.

[9] Lam, F., Gehloff, M., and Closen, M. Moment-resisting bolted timber connections. Proceedings of the Institution of Civil Engineers-Structures and Buildings 163(4) (2010) 267-274. https://doi.org/10.1680/stbu.2010.163.4.267.

[10] Bader, T. K., Schweigler, M., Hochreiner, G., and Eberhardsteiner, J. Load Distribution in Multi-dowel Timber Connections under Moment Loading-Integrative Evaluation of Multiscale Experiments. Proceedings of the World Conference On Timber Engineering (WCTE) (2016) Vienna, Austria.

[11] N. McCormick and J. Lord, Digital Image Correlation, Materials Today 13 – 12 (2010) 52–54.

[12] Sandhaas, C., Sarnaghi, A.K. and van de Kuilen, JW. Numerical modelling of timber and timber joints: computational aspects. Wood Science Technology 54 (2020) 31–61.

Experimental assessment of the dynamic behavior of timber trusses: a not so straightforward task

S. CASTELLARO[1], D. PRATI[2], S. ISANI[3], L. GUARDIGLI[2],

[1] Alma Mater Studiorum Università di Bologna – Dipartimento di Fisica e Astronomia, viale C. Berti Pichat 8, 40126 Bologna (Italy)

[2] Alma Mater Studiorum Università di Bologna – Dipartimento di Architettura, viale Risorgimento 2, 40136 Bologna (Italy)

[3] Senior bridge designer – Matildi+Partners, vicolo Sant'Arcangelo 2, 40123 Bologna (Italy)

ABSTRACT

Several FE models of timber trusses can be found in the scientific literature aiming to predict their static and dynamic behaviors. On the contrary, surveys aimed at experimentally assessing those behaviors and tuning the models are far rarer. We present the operational modal analysis of 18 XVII century timber trusses, acknowledged among the longest in Europe, from the San Pietro Cathedral in Bologna (Italy). We show that the experimental assessment of their natural modes is not straightforward due to the forcing vibrations induced by directly linked (the cathedral walls) and indirectly linked (the vault, the belltower, the ground) elements. We show how to separate the different contributions and discuss the extent to which the tie beams' dynamic properties can be used to assess their tension level.

KEYWORDS: operational modal analysis, timber truss, natural eigen-modes, dynamic characterization

INTRODUCTION

Musicians know that the way in which strings vibrate, and the sound they produce, mainly depend on their length and the tension applied to them. Bridge engineering also exploits this principle and measures the modal properties of suspension cables to check and tune their tension level.
As long as the elements of interest are monodimensional, classical physics provides all the analytical solutions [1]. However, when the elements of interest cannot be idealized as 1D elements, thus moving from strings and cables to beams and trusses, then their vibration modes are ruled by their constraints, their geometric (length and moment of inertia) and mechanical (density and elastic moduli) properties and by the applied tension.
Here we focus on the 18 timber trusses of the San Pietro cathedral in Bologna (Northern Italy). These may be deemed the longest and still original (1616-1622) church trusses in Europe [2] and are interesting for two reasons: 1) their number allows performing a statistical study on the stability of the experimentally assessed dynamic properties and their constraints, 2) to check whether possible differences in the dynamic properties of the investigated trusses can be traced back to different tension levels applied to them.

METHODOLOGY

The pitched (22°) roof of San Pietro Cathedral stands 42 m high and covers a rectangular shape measuring 27x60 m. By means of purlins, the tiled roof rests on 18 timber trusses and is not visible from inside the Cathedral as it is cloaked by a barrel vault that runs throughout the nave (Figure 1a). The trusses are spaced 2.8-3.1 m apart and are all coeval (Figure 1b), except for the two that were added in 1748, when the main façade was advanced, according to Alfonso Torreggiani's project [3].

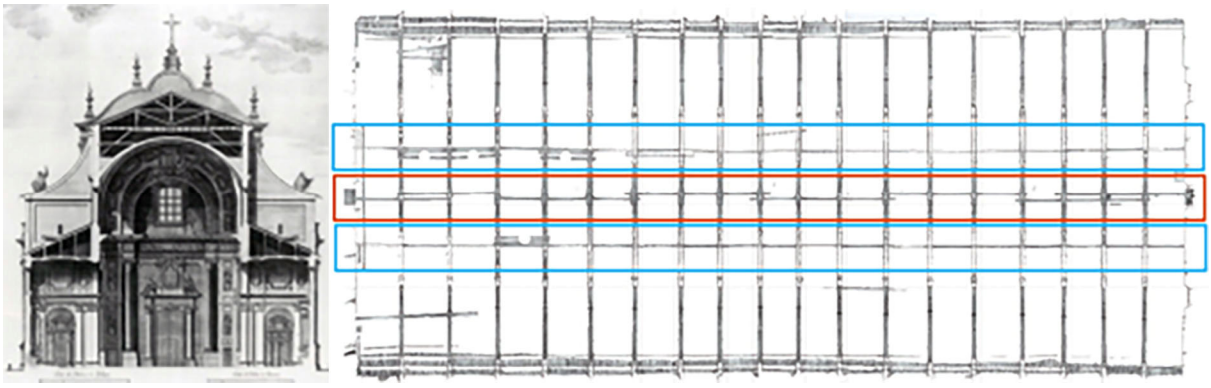

Figures 1: a - section of the Cathedral 1700 ca. [3]; b - Plan of the roof from laser scanner survey showing the longitudinal bracing connections between the 18 trusses; @Prati, 2019

The geometry of the red spruce timber trusses does not follow a classical queen-post truss scheme (tie beam, principal rafters, posts, and struts). In fact, that scheme is doubled on two levels (Figure 2). Timber cross-sections range from 30x30 cm^2 of single members to 90x30 cm^2 of assembled ones. The average span is about 27 m with a ridge height of 6 m. Each truss weighs approx. 10 tons [4].

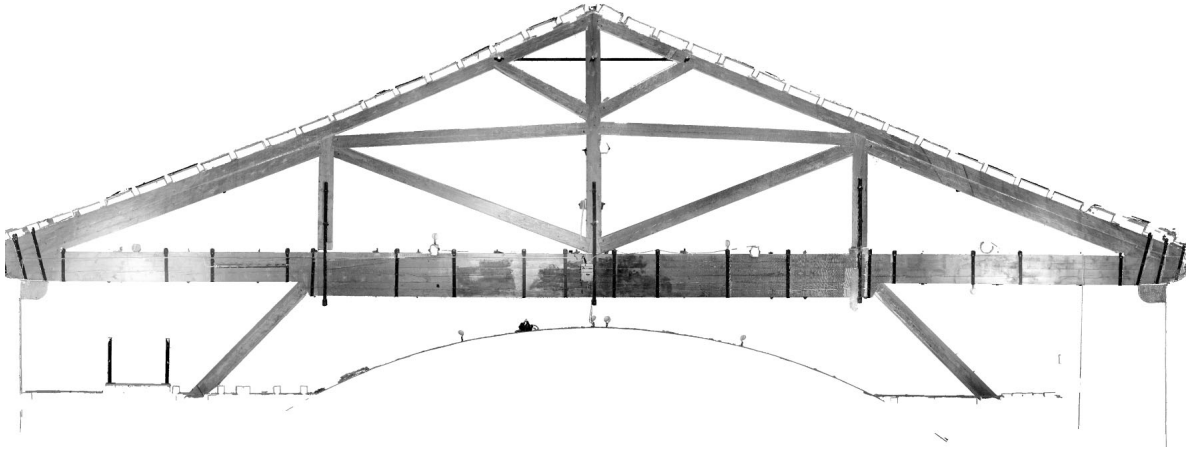

Figure 2. Orthophoto of a truss from laser scanner survey. The size of the members, the metal straps, the profile of the vault, and the planking on both sides are clearly recognizable. @Prati, 2019

The truss assembly and the junctions are fascinating. In particular, each tie beam consists of two overlapping double-length elements, joined head-to-head without particular scarfing. The joint is placed alternatively once to the right and once to the left of the centerline. The use of a lower supporting trestle (this one is a single-length element, being "only" 14 m long) further increases the cross-section of the tie beam in the center part.

EXPERIMENTAL SURVEY

We performed:

- 40 single-station ambient vibration acquisitions on the perimeter walls of the Cathedral. We set the seismometers within niches on the walls and in the centerline of the tie beam of each truss,
- one multichannel seismic acquisition along the tie beam longitudinal axis of truss number 2 (Figure 3),

- two acquisitions on the vault, one in the center and one at a quarter of its span.

Single-station and multichannel triaxial portable seismometers were used (Tromino® and SoilSpy from MoHo Ltd., respectively).

Figure 3: One of the 18 inspected timber trusses of the San Pietro cathedral in Bologna. Placement of vertically polarized geophones connected to a SoilSpy digitizing system. @Prati, Isani, 2019

RESULTS

The collected data were processed according to the operational modal analysis and Frequency Domain Decomposition (FDD) principles to extract the modal frequencies, shapes, and damping.

However, a set of problems emerged during the survey. Depending on the position of the measurements, several alternative vibration modes affected the eigen-modes of the trusses, to the point that these latter were hardly acknowledgeable at some sites. This uncertainty imposed a more in-depth study of the "disturbances" affecting the trusses natural vibrations.

We thus performed the dynamic characterization of the main structural elements of the Cathedral, i.e., its magnificent belltower, the vault, the perimetral walls, and the foundation subsoil. We found that the timber trusses eigen-modes emerge and become understandable only after removing all these elements from the recordings acquired on them (Figure 4).

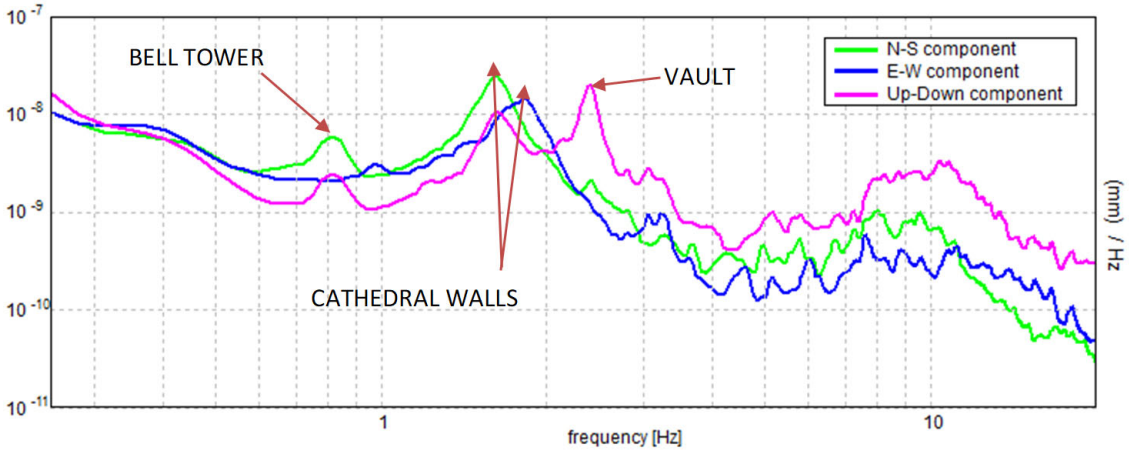

Figure 4: Amplitude displacement spectra recorded at the center of the vault. @Castellaro, 2019

Thus, we first analyzed the displacement spectra acquired within the niches of the perimeter walls. These show that the first mode of the Cathedral in transversal (in the plane of the trusses) and longitudinal (outside the plane of the trusses) directions are 1.7 and 1.8 Hz, respectively.

A clear forcing vibration is observed at 0.8-0.9 Hz in the measurements acquired near the belltower. Measurements made *ad hoc* on the belltower highlighted that this is a side effect of the first eigen-mode of the belltower itself.

On the other hand, the barrel vault shows its first eigen-mode at 2.3-2.5 Hz in the vertical direction. This modal amplitude is very relevant, and its effect on the walls and trusses is evident. The spectra, analyzed in the same way, gave a frequency of 2.5 Hz for this mode in July and 2.3 Hz in September. Thermal variations in the modal frequencies of the structures (by a few %) are well documented and within the normal range.

The spectral ratio of homologous components was carried out to remove the wall natural-modes from the records on the truss tie beam. Figure 5 shows how the peaks related to the walls disappear in all spectral ratios. The remaining diagrams emphasize only the modes of the elements that do not belong to the perimeter walls.

In the plane orthogonal to the truss, the first horizontal flexural mode appears at 4.1 Hz for trusses 1 to 9 and 3.7 Hz for trusses 10 to 18. Interestingly, the behavior is different between the two truss groups (1-9, 10-18) but identical within the groups. This result indicates that trusses 10 to 18 are stiffer overall. The peaks at 2.3-2.5 Hz, due to the underlying vault, are still recognizable in the spectral ratios between trusses and walls. Predictably, given the lower deformability and higher inertia in the truss plane, no eigen-modes related to the truss are recognizable but only eigen-modes related to adjacent structures.

The main modal frequencies identified for the main elements of the Cathedral are given in Table 1.

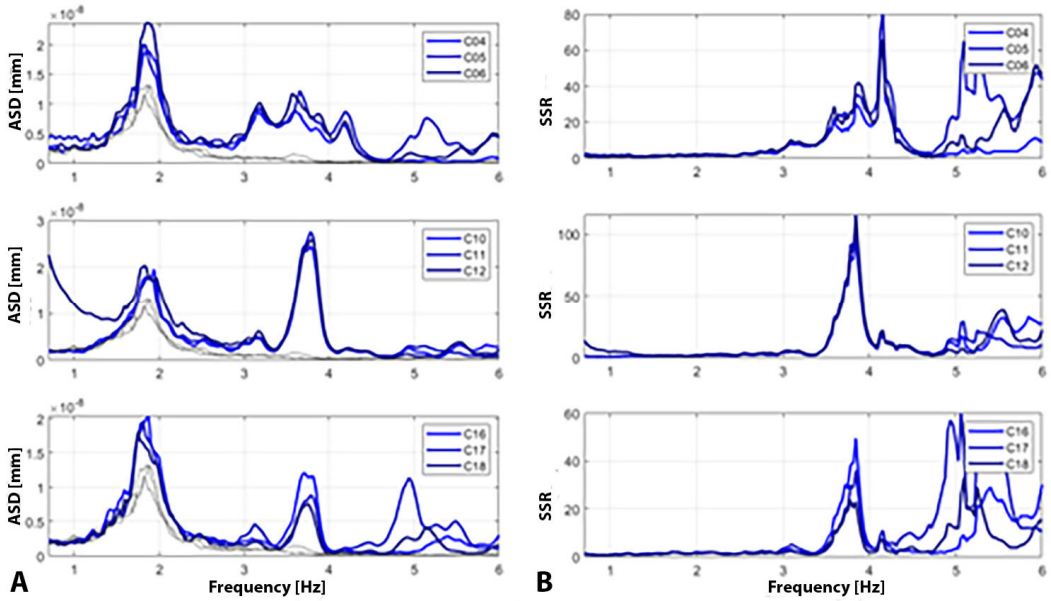

Figure 5: a – Amplitude displacement spectra of a selection of tie beams along the longitudinal axis of the Cathedral. b – Amplitude displacement spectra of the same selection of tie beams normalized versus the homologous component of walls. @Castellaro, 2019

Table 1: Main identified modal frequencies (stand for thermal variations)*

Element	Mode type	Longitudinal [Hz]	Transversal [Hz]	Vertical [Hz]
Belltower	Bending	0.95	0.8	
Walls	Bending	1.8	1.7	
Vault	Arch bending			2.3-2.5*
Timber-trusses (tie-beam)	Bending		3.7	3.1

DISCUSSION

It can be inferred from Table 1 that the transverse modes of the truss tie beams occur at a slightly higher frequency than the vertical ones. Since the cross-section of the tie beams offers 30 times greater inertia in the vertical direction than in the transversal one, and since the constraint level of each tie beam on the supports can be considered equal in both directions, this behavior cannot be explained by geometrical means only. Halfway between the central king-post and the queen-posts, two rows of

transversal beams rigidly connect all the tie beams, acting as bracing along the longitudinal axis of the Cathedral (Figures 1). These beams act as a constraint, so the actual transversal deflection length of tie beams is less than the distance between the queen-posts (≈15 m).
Even in the vertical direction, we can consider the lateral struts of the three voussoir timber arch as supports, and thus the effective length in the vertical direction is still about 15 m. This assumption was verified experimentally, as witnessed by the modal shapes (Figures 6).

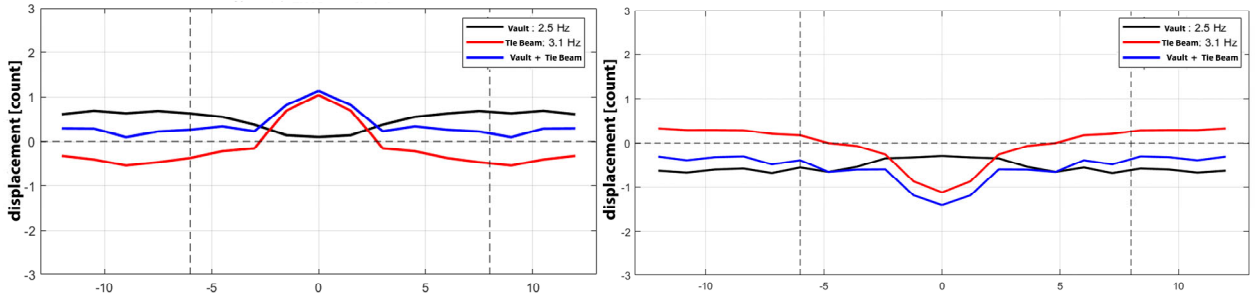

Figure 6: Modal deformations snapshots of the vault (black line, 2.5 Hz), tie beam (red line, 3.1 Hz), and the combination of both (blue line). @Castellaro, 2019

The modal frequencies (n) of vibration of simply supported beams depend (1) on their length (L), the specific weight (γ), Young's modulus (E), moment of inertia (J), and finally tensile stress (P)

$$f'_n = \frac{1}{2\pi}\sqrt{\frac{n^4\pi^4}{L^4}\frac{EJg}{A\gamma}\left(1+\frac{P}{\frac{n^2\pi^2EJ}{L^2}}\right)} \quad (1)$$

To study the expected eigen-modes for the tie beams of San Pietro Cathedral, we imposed a beam cross-section of A = a x b = 60x30 cm^2, the specific weight for spruce γ=450x9.8 N/m^3, and the elastic modulus E = 10 GPa. Letting only one parameter vary at a time among L, γ, E, and J, we obtained the graphs in Figure 7, from which we can observe that:

- Graph γ. The variation of modal frequencies as a function of γ is minimal.
- Graph E. Estimation errors of E also have a minor effect on the estimation of the eigen-frequencies of the tie beams. However, low E brings the model closer to the experimental data. This observation would confirm that 10 GPa overestimates the actual value in the dynamic case.
- Graph J. The moment of inertia of the cross-section significantly influences the eigen-frequencies. The cross-section of the tie beams under consideration is not homogeneous varying throughout its length from 60 to 90 cm height. This variation cannot be analytically modeled in a simplified way. However, in order to reproduce the experimentally measured natural frequencies (3.1 Hz), we must impose low values of J. Given the base a = 30 cm, a parameter about which there is little doubt, the model would also require a height b = 30 cm for the imposed free inflection length (14 m).
- Graph L. The span of the tie beam clearly has a first-order effect in determining the flexural eigen-modes. Holding the other parameters fixed at the imposed values, we see that the free length that allows the experimental data to be explained would be 20 m.

So far, we have not considered the tensile stress on the tie beam, i.e., the parameter P in (1). Calculations show that the tensile stresses acting on the tie beams, in the absence of snow, are about 200 kN, i.e., very small. The effect of these actions on the eigen-modes of the tie bean can then be considered a second-order effect.

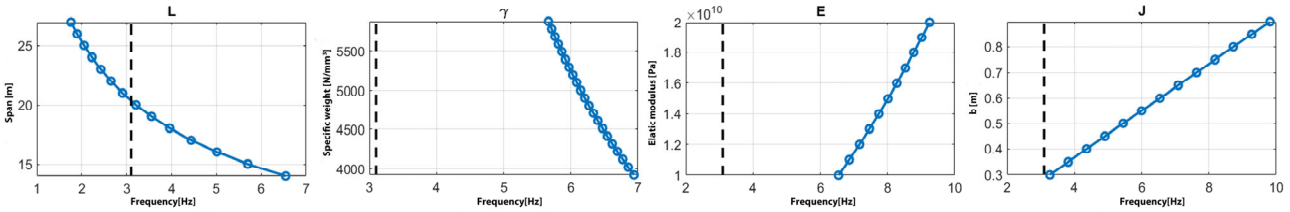

Figure 7: Variation of the first eigen-mode of a beam as a function of the span (L), the specific weight (γ), Young's modulus (E), and moment of inertia (J). The black dotted line marks the experimentally measured eigen-mode. @Castellaro, 2019

CONCLUSION

We wanted to apply the theory of oscillatory motion of strings, extended to elements with a non-zero moment of inertia, to structural elements endowed with two non-negligible spatial dimensions, such as beams. We focused on the tie beams of the timber trusses of San Pietro Cathedral in Bologna. These 18 trusses allow a statistical study to verify whether the inevitable construction differences (also related to the impossibility of using the same wood) reflect in their dynamic behavior. Knowing the geometry of the elements, the types of constraints, and the mechanical parameters, the goal is to analytically estimate the eigen-modes of the tensioned tie beam. These values can be measured experimentally, and their critical analysis would eventually suggest corrections to the model.

We show that the free and forced modes of the inspected timber trusses depend not only on their tensional state but also on the dynamics of other external elements (walls, vault, belltower, ground). The dependence of tie-beam eigen-modes on their tensional state appears to be modest compared to the other interfering variables. This outcome makes the experimental modal surveys very delicate but still fundamental to tuning numerical models.

The experimental analyses showed that:

- The belltower acts as a forcer at 0.9 Hz for the Cathedral and all its structural elements;
- The main eigen-mode of the Cathedral in its transverse direction is 1.8 Hz. This mode of vibration also constitutes a forcing vibration for the trusses;
- The natural vertical eigen-mode of the vault at 2.5 Hz forces both the side walls and the trusses. This is the most significant movement in amplitude recorded on the vertical component, larger even than the flexural eigen-modes of the truss tie beams;

Therefore, to highlight the bending eigen-modes of the trusses, it is necessary to purify them from the belltower, wall, and vault forcings. Once this is done, the transverse flexural eigen-frequencies of the trusses appear at 3.7 - 4.1 Hz.

In the horizontal direction, the trusses are braced by beams arranged along the entire length of the Cathedral. In the microtremor regime, they create an efficient constraint for the truss tie beams, with the result that the effective length of out-of-plane deflection is not 27 m but only 15 m and the eigenfrequency higher. In the vertical direction, the tie beams rest on a three voussoir timber arch with 2 struts that thrust onto the side walls and are also a cause of the transmission of the vault eigen-modes to the trusses themselves. This additional support reduces the effective length of vertical deflection to the distance between the struts of the external timber support.

Thermal fluctuations significantly impact on dynamic behavior. In July 2019, the vertical oscillation of the truss was 2.5 Hz, while in September 2.3 Hz. This 8% fluctuation is important, and it is mandatory to consider it before invoking structural changes.

The analysis of the experimental data proved particularly complex given the strong dynamic interaction between the elements, which required repeated normalizations of the effects of one to understand the dynamics of the others.

The combination of parameters that best approximates the experimental behavior identified for the tie beams in the horizontal direction is given in Table 2.

Table 2: Parameters to describe the dynamic behavior of the analyzed tie beams.

Effective Length	**Moment of Inertia**	**Specific Weight**	**Young's Modulus**	**Tensile Stress**
L [m]	J [m^3]	ρ [kg/m^3]	E [GPa]	P [kN]
14	0.0013	450	10	≈ 130

Countless finite element models can be found in the literature to predict the static and dynamic behavior of timber trusses [5, 6], yet we could not find any modeling that was validated by experimental data. Indeed, timber trusses, given their use for covering wide spans, are not easily accessible, and the instruments to be installed must be small compared to the elements to be measured. However, the number of "contingencies" that emerge during experimental investigations practically forces the assumptions made on the models to be revised and must be considered.
Measuring the eigen-modes of the elements of a truss is possible. When dealing with ancient structures, the complexity of interaction that emerges between structural elements may discourage using models that have no chance of being validated with experimental data. As emerged in the present case, structural elements usually modeled as stand-alone entities are actually excited by forcings related to proximity structural elements to a much greater degree than their eigen-mode. Not taking this into account makes the models unrealistic.
Last, though it is true that the eigen-modes of structural elements also depend on their tensional state, this dependence may be modest compared to other physiological elements that cause the eigen-modes to vary, first and foremost thermal effects. This must be carefully considered nowadays when experimental measurements are easier to perform than in the past, and there is the willingness to predict many structural problems through dynamic monitoring.

REFERENCES

[1] J.L.R. d'Alembert, Recherches sur la courbe que forme une corde tenduë mise en vibration, *Memoire de l'académie royale des sciences et belles lettres de Berlin*, 3, (1747) 214-219.

[2] G.B. Natali, Manuscript, Archivio Generale Arcivescovile di Bologna, *Fabbrica di S. Pietro in Bologna* (1616).

[3] A. Torreggiani, Drawing, Archivio Arcivescovile di Bologna, raccolta Breventani, scansia E, cartella X, fascicolo 1, n. 29 (1700).

[4] D. Prati, G. Zuppella, G. Mochi, L. Guardigli, and R. Gulli, Wooden trusses reconstruction and analysis through parametric 3D modeling, *Int. Arch. Photogramm. Remote Sens. Spatial Inf. Sci.*, XLII-2/W9, 623-629, (2019) https://doi.org/10.5194/isprs-archives-XLII-2-W9-623-2019.

[5] M.P. Piazza, M.R. Riggio, G.B. Brentari, Strengthening and control methods for old timber trusses: the queen-post truss of the Trento theatre, in *Structural Analysis of Historical Constructions*, Modena, Lourenço & Roca (eds.), Taylor & Francis Group, London, (2005) 956-965, ISBN 04 1536 3& 79 9.

[6] C. Menichelli, C. Modena, M.R. Valluzzi, E. Garbin, F. Da Porto, Timber roof structures of the "Arsenale" of Venice, in *Structural Analysis of Historical Constructions*, Modena, Lourenço & Roca (eds.), Taylor & Francis Group, London, 967-975, ISBN 04 1536 3& 79 9.

MODAL ANALYSIS AND FINITE ELEMENT MODEL UPDATING OF A TIMBER-CONCRETE HYBRID BUILDING

Carl Larsson[1], Osama Abdeljaber[1], Thomas Bader[1], and Michael Dorn[1]

[1] Linnaeus University, Department of Building Technology

ABSTRACT

In recent years, there has been a rapid development of new timber products, such as cross-laminated timber, leading to an increase in buildings using timber as a structural material. House Charlie, a 4-story office building in Växjö, Sweden, is a typical example of a hybrid building that uses glulam timber for the post-beam system combined with slabs in cross-laminated timber and shear walls in concrete. A structural health monitoring system has been installed, collecting data ever since its completion in 2018. This work presents the building's modal performance collected by geophones under ambient vibrations over three years, which are used to calibrate a finite element model. The effects of changes in different material properties and model assumptions on the overall dynamic behavior of the building are shown. The aim is to establish a structural model that captures the actual behavior of the built structure that uses both timber and concrete as structural materials.

KEYWORDS: Structural health monitoring, Ambient vibration monitoring, Finite Element Model Updating, Timber-concrete hybrid building.

INTRODUCTION

There is an increasing interest in using timber as a structural material in modern buildings. Due to the beneficial carbon footprint of the material in comparison to steel and concrete, the market for timber buildings has grown rapidly. Simultaneously, the timber industry has heavily increased the production capacity, both for products like glued laminated timber (GLT) and cross-laminated timber (CLT), the latest example of the rapid product development in the timber industry. However, due to several reasons, such as lack of self-weight, connection capacity, acoustics, or fire, timber is not suitable for all types of constructions. One solution to implementing more timber in the construction industry is to use structural elements in timber in addition to elements in other materials such as concrete and to some extent, steel, introducing timber-concrete hybrid buildings.

Due to the lack of self-weight in timber elements, the dynamic properties must be considered during design, even for relatively low buildings compared to buildings using steel and concrete elements. There are several research papers in this field, including measurements to characterize the dynamics of a timber building [1], [2]. Model updating using dynamic measurements of timber building has been performed in [3] and [4].

This paper presents the results from dynamic measurements taken place by the structural health monitoring system (SHM) installed in House Charlie, a 4-story office building in Växjö, Sweden. In addition, a finite element (FE) model is presented with the aim of reproducing the measurement results in the model analysis.

HOUSE CHARLIE

House Charlie is a four-story timber-concrete hybrid building in Växjö, Sweden. The building houses the reception and office spaces and was completed in 2018, as shown in Figure 1.

Figure 1: Photo of House Charlie in 2022

The structural system consists of a post-beam system in GLT along with slabs in CLT. The shear walls are in precast concrete, and the bracings are steel. At some locations, such as external columns, timber columns are replaced with concrete-filled steel columns. The structural system is shown in Figure 2.

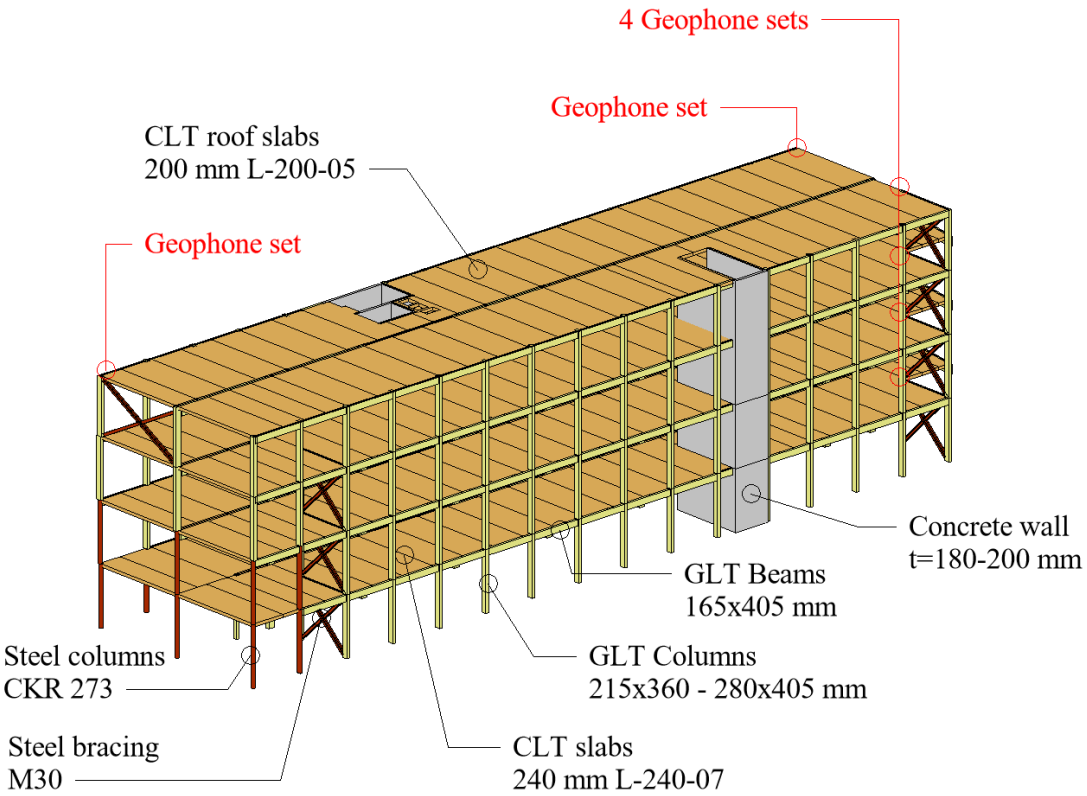

Figure 2: Structural system of House Charlie.

Additional walls, such as exterior and interior, are considered non-structural. These walls, seen in Figure 3, are built like light-frame timber walls that include installations and insulation. Fire insulation and a 40 mm putty are put on top of the CLT slab elements to increase the acoustic performance of the slabs.

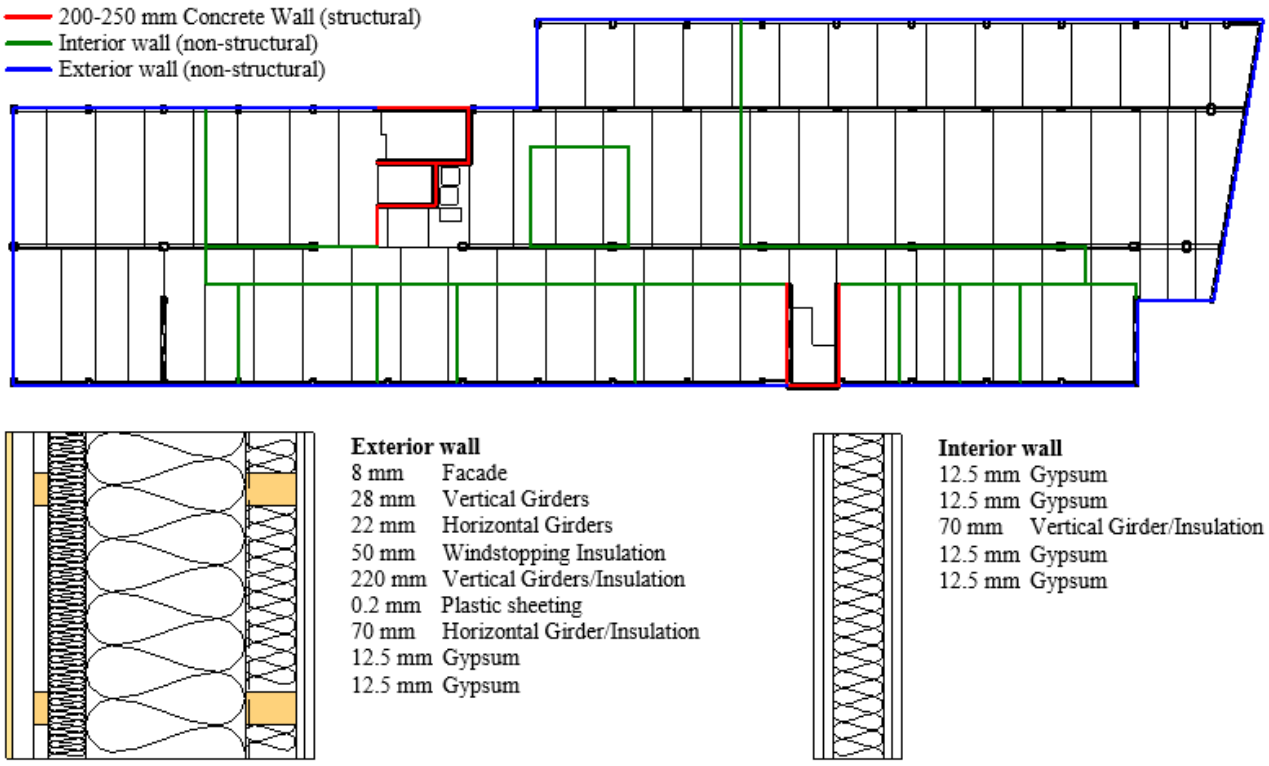

Figure 3: Wall section details shown on a floor layout of the 3rd floor in House Charlie.

During construction work, a SHM system was installed, including six sets of geophones to measure ambient vibrations in the building over time. Ambient vibration measurements are suitable in this type of system because they don't require any external excitation of vibrations other than natural forces like wind or traffic load. In one corner of the building, four sets of geophones were placed at each story. These were complemented by two additional sets in different corners on the roof slab. All locations of the sets of geophones can be seen in Figure 2.

Each geophone set consists of two geophones, measuring the x and y directions separately. A weather station is installed on the roof, triggering the geophones to collect data if the mean wind speed exceeds 5 m/s. In addition, the geophones are triggered twice a day at fixed times. Each measurement collects data for 90 minutes. More information about the measurement system can be found in [5]. The construction work was finished during the summer of 2018, and the SHM system has been collecting data ever since.

MEASUREMENT DATA

A data processing on a single data set was performed to identify the first three natural frequencies (NF) of House Charlie. After the initial identification, each frequency from each data set was analyzed and sorted for the entire measurement period. The results of this analysis can be seen in Figure 4, showing that the observed natural frequencies change over time. A yearly pattern can be observed where the highest natural frequencies are recorded in the late summer and the lowest NF in the spring. The variation around the mean NF over time is approx. +/-6 % for each of the first three observed NFs.

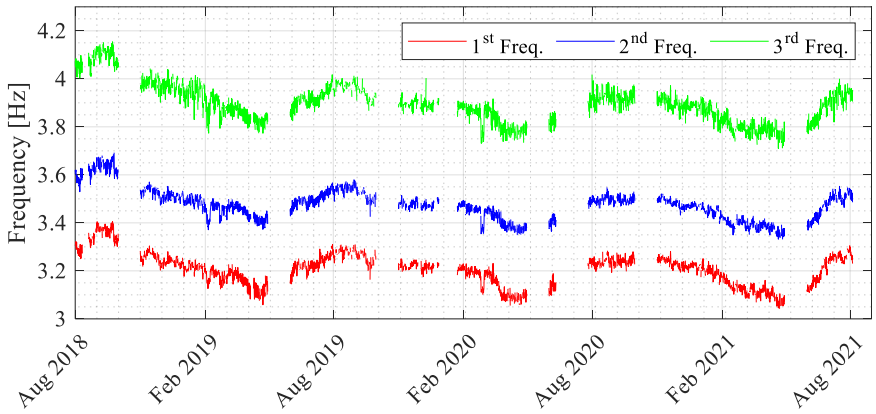

Figure 4: The recorded natural frequencies for House Charlie during the period from August 2018 to August 2021.

MODEL UPDATING

The dynamic analysis of House Charlie is performed for four different FE models using the commercial FE software Dlubal RFEM 5.25. A brief description of each model is given in this section.

The first model is based on the geometry given in the structural drawings of the project. Boundary conditions for the foundations are fixed [4], [6]. Material properties are according to the Eurocode standards and the timber manufacturer for the project. The CLT plates are simplified to shell elements using the Mindlin-Reissner plate theory [7]. The reduction factors k_{33} and k_{88} for non-edged glued lamellas is calculated according to the Austrian guidelines [8]. No additional loads except the dead load for the structural elements are included.

Model 2 adds the dead load for non-structural elements into the model. This information is gathered from both structural and architectural drawings and documents regarding the acoustic study of the building. These additional loads include exterior walls, interior walls, and the additional load on the CLT slabs, including putty and fire insulation. An additional service load of 0.25 kN/m^2 is added to consider the in-service load [4].

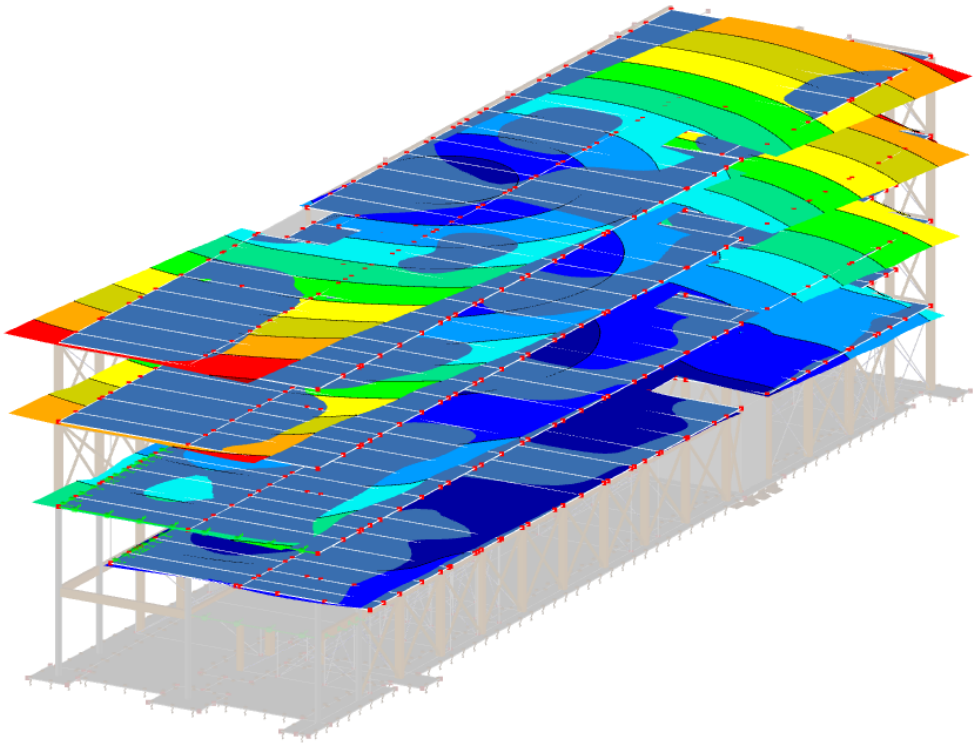

Figure 5: Mode shape for the 1st natural frequency at 3.11 Hz from the FE analysis of Model 4 with 8 % MC.

Model 3 considers the additional stiffness provided by non-structural walls. It is known that these walls have a significant effect on the dynamic properties of a building [9]. These were modeled as bracings, using C18 timber 95x95 mm tension members. The foundation of the shear walls is considered stiff, but a spring stiffness is used for the columns considering the shallow foundations. The assumptions of the stiffness of the non-structural walls and the foundation spring stiffness can be seen in [10].

The observed NFs show a variation over time, suggesting introducing a time-dependent variable for the model updating. Moisture content (MC) is known to affect timber properties such as density and E-modulus. It is also known to change due to the variation of the relative humidity in the environment and is thereby introduced as a time-dependent variable. Model 4 considers the different density and strength properties of the timber material at varying levels of MC. Otherwise, it is identical to Model 3. Timber elements are generally delivered with a MC of 12 % at maximum, and this is the MC that is the basis for the tabled strength values. In model 4, the MC is considered to be in the range of 8 %, for a typical indoor climate, to 16 % for an extreme event such as major water damage. These values are used to calibrate the density and strength properties according to the equations given in [11], where the density increase while stiffness and strength properties decrease with an increased MC. The implementation of MC dependent variables in the analysis performed in model 4 aims to investigate if the variance in the measured NF can be seen in an FE analysis as well.

RESULTS

Table 1 shows the dynamic analysis results for each of the models, along with the mean NF for each frequency that was measured, presented in Figure 4.

Table 1: Measurement and FE analysis results of the first three NF of House Charlie (differences are given in relation to the measured values)

	1st NF		2nd NF		3rd NF	
	Freq.	**Diff.**	**Freq.**	**Diff.**	**Freq.**	**Diff.**
Measurement (mean)	3.21 Hz	---	3.48 Hz	---	3.90 Hz	---
Model 1	3.62 Hz	+13 %	4.89 Hz	+41 %	5.89 Hz	+51 %
Model 2	2.51 Hz	-22 %	3.34 Hz	-4.0 %	4.23 Hz	+8.5 %
Model 3	3.09 Hz	-3.7 %	3.42 Hz	-1.7 %	3.95 Hz	+1.3 %
Model 4 – MC 8 %	3.11 Hz	-3.1 %	3.44 Hz	-1.1 %	3.97 Hz	+1.8 %
Model 4 – MC 16 %	3.08 Hz	-4.0 %	3.40 Hz	-2.3 %	3.93 Hz	+0.8 %

The observations of varying NFs with time make it challenging to do a model update of a FE model that is accurate over time. The recorded variations of the NFs are in the same range as the differences in different model updates performed. This clearly shows the difficulties of producing a FE model that will give reliable results that can be confirmed in situ measurements over time.

The amplitude of the variation in the observed NFs differs from the analysis performed in Model 4. Changing the density and strength parameters in the timber material for a MC of 8 % and 16 % gives a difference in the NFs of only about 1 %. The measured variance in frequency over the three years is significantly higher and in the range of 10 % to 12 %, according to Figure 4. This suggests that the MC-dependent variables in timber's density and stiffness properties alone cannot explain this variation.

CONCLUSION

The present work complements previous studies in model updating of timber buildings by presenting results from a timber-concrete hybrid building. The results from model 3 are very close to the measurements for all three NFs considered. This supports findings in previous studies that non-structural walls significantly affect the dynamic response of a building using a post-beam system and non-structural walls.

Considering the model updating, a more detailed investigation can be performed but is not covered in this paper. For example, forced vibration tests on the building can give the scaled mode shapes. This additional information can later be used in the model updating as this paper only performs the model update on the natural frequencies. Further analysis could include the recorded mode shapes using the modal assurance criteria to verify the model to the measured dynamic properties.

However, the long-term monitoring shows a significant variation of the NFs over time, implying a time-dependent variable in the model updating. In this work, MC was investigated as the time-dependent variable, changing the density and E-modulus of the timber material. The results clearly showed that the observed variation in NF is significantly higher than the results from the model. These findings highlight the importance of continuous monitoring of the dynamic properties in timber-concrete hybrid buildings, encouraging further analysis of the time-dependent factors affecting the dynamic properties in these types of buildings.

REFERENCES

[1] Reynolds T, Bolmsvik Å, Vessby J, Chang W-S, Harris R, Jonathan B, et al. Ambient vibration testing and modal analysis of multi-storey cross-laminated timber buildings. World Conf. Timber Eng. Oslo, 2014.

[2] Ellis BR, Bougard AJ. Dynamic testing and stiffness evaluation of a six-storey timber framed building during construction. Eng Struct 2001;23:1232–42. https://doi.org/10.1016/S0141-0296(01)00033-5.

[3] Aloisio A, Pasca D, Tomasi R, Fragiacomo M. Dynamic identification and model updating of an eight-storey CLT building. Eng Struct 2020;213:110593. https://doi.org/10.1016/j.engstruct.2020.110593.

[4] Kurent B, Brank B, Ao WK. Model updating of seven-storey cross-laminated timber building designed on frequency-response-functions-based modal testing. Struct Infrastruct Eng 2021;0:1–19. https://doi.org/10.1080/15732479.2021.1931893.

[5] Dorn M, Abdeljaber O, Klaeson J. Structural Health Monitoring of House Charlie. 2019.

[6] Castellaro S, Perricone L, Bartolomei M, Isani S. Dynamic characterization of the Eiffel tower. Eng Struct 2016;126:628–40. https://doi.org/10.1016/j.engstruct.2016.08.023.

[7] Mindlin RD. Influence of Rotatory Inertia and Shear on Flexural Motions of Isotropic, Elastic Plates. ASME J Appl Mech 1951;18:31–8.

[8] Austrian Standards Institute. Eurocode 5: Bemessung und Konstruktion von Holzbauten Teil 1-1: Allgemeines — Allgemeine Regeln und Regeln für den Hochbau. 2014.

[9] Devin A, Fanning PJ. Non-structural elements and the dynamic response of buildings: A review. Eng Struct 2019;187:242–50. https://doi.org/10.1016/j.engstruct.2019.02.044.

[10] Svanberg A, Petersson V. Operational modal analysis and finite element modeling of a low-rise timber building. 2021.

[11] European committee for standardization. EN 384 - Structural timber - Determination of characteristic values of mechanical properties and density. 2016.

ANALYSIS OF THE STOP-SPLAYED SCARF CARPENTRY JOINT

Anna KAROLAK[1], Jerzy JASIEŃKO[1], Krzysztof RASZCZUK[1] and Piotr RAPP[2]

[1] Wroclaw University of Science and Technology, Wybrzeże Wyspiańskiego 27, 50-370 Wrocław, Poland

[2] Łukasiewicz Research Network - Wood Technology Institute, Winiarska Str. 1, 60-654 Poznan, Poland

ABSTRACT

The paper presents a description of the static behaviour of the stop-splayed scarf joints (so-called 'bolts of lightning') in bending. The joints with geometry based on the historical joints strengthened with two metal bolts were analysed. The results of experimental research (four-point bending tests) that were performed on technical scale beams, along with the interpretation and the simplified analytical model of the joint behaviour, are presented. Based on the observation of the failure mechanism, an addition of reinforcing bolt was proposed to obtain a greater load-bearing capacity of the joint. The comparative analysis of the beam with stop – splayed scarf joint and continuous reference beam was carried out in a theoretical (computational) and a practical (test) way. The analysis revealed that the stop-splayed scarf joint with two bolts can reach about 30% of the load-bearing capacity compared to a continuous beam, which was confirmed in the tests. By calculation, it is possible that with the appropriate bolt arrangement, the joint can reach about 60% in relation to the capacity of the continuous beam.

KEYWORDS: carpentry joints, stop-splayed scarf joints, 'bolt of lightning', static behaviour

INTRODUCTION

Historical carpentry joints, developed over the ages, took various forms depending on their function, as well as the time and place of their formation. Stop-splayed scarf joints (sometimes also described as scarf joints of 'lightning sing', 'Bolts of lightning' or 'Trait-de-Jupiter' [1-3] are the developed forms of carpentry joints created lengthwise of the wooden elements or to create so called 'built-up beams' (composite beams with a teethed joint – elements connected along their whole length with the scarf joints of the lightning sign), described i.a. in [4-6]. They were designed and used in the times of antiquity (e.g. in the constructions of Roman bridges) and the time of the renaissance (e.g. in Italy by Leonardo da Vinci). An example is presented in Fig. 1.

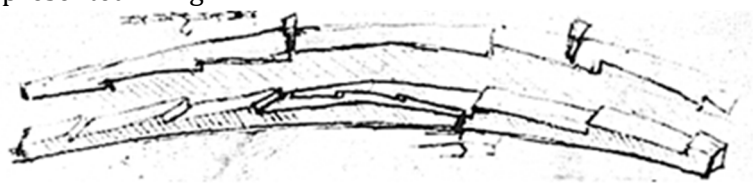

Fig. 1. Drawing of the scarf joint of 'lightning sign' in a composed beam with imposed curvature according to Leonardo da Vinci [4]

There are few available descriptions of typical scarf joints in flexural elements presented in the literature so far [4-9] and in Fig. 2.

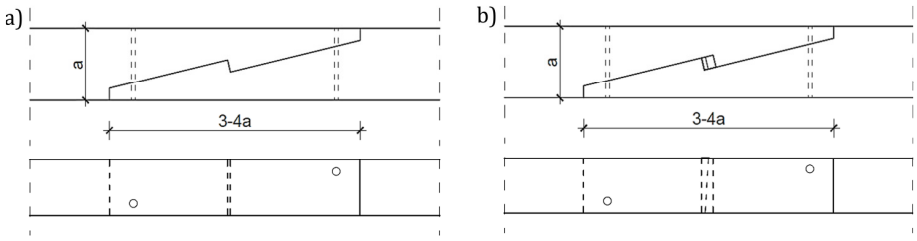

Fig. 2. Scarf joints: a) stop – splayed scarf joint, b) stop – splayed and tabled scarf joint with a key

Moreover, most of the researchers dealing with the issue of the static behaviour of the carpentry joints in bending (among others, Rug et al. in [5,6], Hirst et al. in [8], Kunecký et al. in [10-14] and Fajman et al. in [15-18] as well as) agree that research on this subject should be continued in order to obtain a full description of the static behaviour of these joints and hence to help in designing the most beneficial methods for strengthening and repairing.

Nowadays, scarf carpentry joints are used mainly to restore historical joints or to replenish the material in the historical elements. Because of the complex geometry of this kind of joints, it is worth to include the results of laboratory investigations and numerical simulations, before any decision about technical, restoration solutions. The research project, financed by Polish National Science Centre, on these types of joints was conducted to investigate their static behaviour.

LABORATORY INVESTIGATIONS

In the experimental investigations, beam models were prepared in technical scale with the dimensions as follows: 360 cm of length and a cross-section of 12 cm x 18 cm, from pine wood (*Pinus sylvestris L.*). The stop-splayed scarf joints geometry was created on the basis of the geometry of the historical joints described in the literature and found in the existing structures. The prepared models were subjected to four-point bending according to the standard procedure presented in EN 408 [20]. Presented tests involved 2 series (A and E, as a part of extensive research programme that include more series) with 3 beam models each. Series A included continuous beams as references and series E included beams with stop-splayed scarf joints. The joints were strengthened with metal bolts (M12) and double-sided tooth plate connectors type C10 (Geka). The geometry of the joints was based on the data from the literature and the real structures. Beam model from series E with the joint in details and dimensions is presented in Fig. 3.

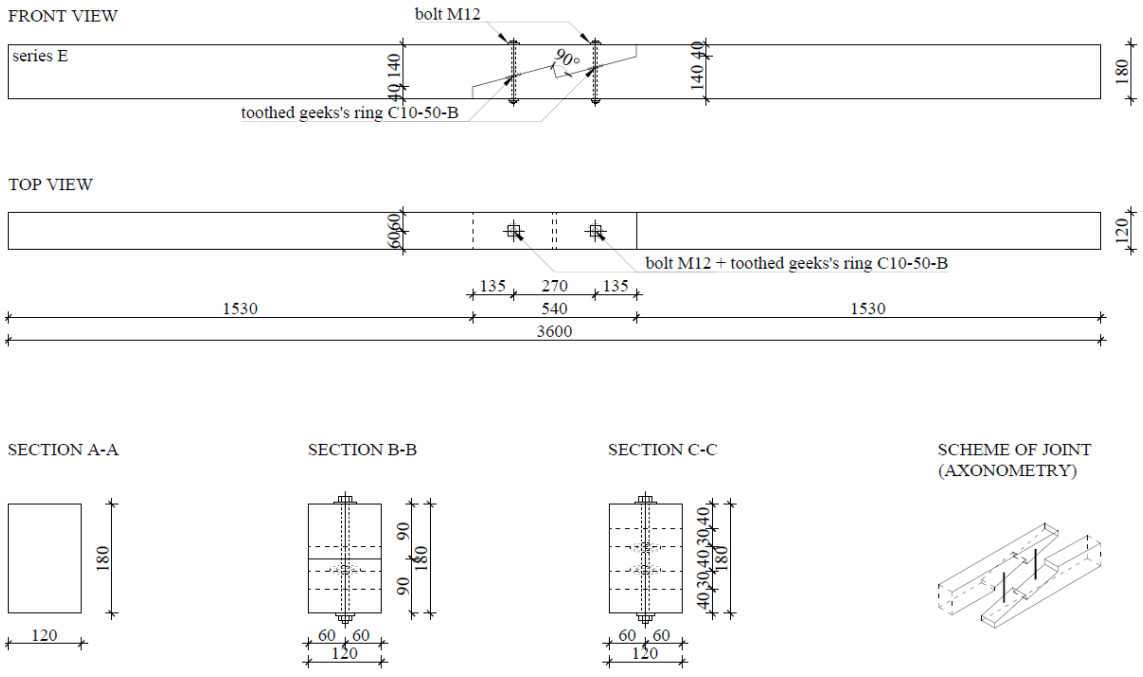

Fig. 3. The model of the beam with the stop-splayed scarf joint.

The experimental testing was conducted at the Building Construction Laboratory of the Faculty of Civil Engineering at Wroclaw University of Science and Technology. An electronically controlled linear hydraulic jack - Instron 500 was used for the load application. The results were registered using the MGC plus measurement system made by the Hottinger Baldwin Messtechnik. The measurement equipment used in the experimental testing was calibrated to at least class 1 accuracy. To determine the load-bearing capacity, the beams were subjected to 4-point bending tests according to the standard procedure [19,20]. The beams with the span 3.24 m were simply supported with a fork support at both ends and protected against lateral buckling. The load was applied symmetrically at 2 points, to obtain pure bending moment in the middle. The load was applied with the speed of 5 mm/min according to the standard procedure up to destruction of the tested models. Fig. 4 presents the scheme of 4-point bending test according to the standard procedure (4 a) and the view of one of the models (4 b).

a)

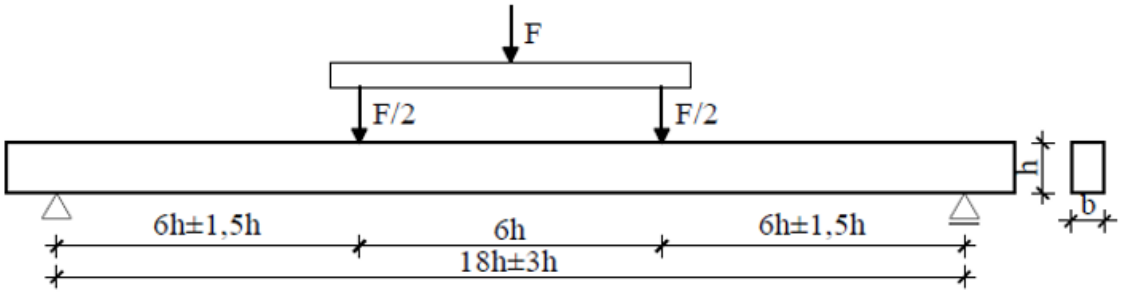

b)

Fig. 4. The beam E02 during investigation

Additionally, during tests, the wood moisture was determined by the use of a resistance hygrometer (FMW moisture meter) to take measurements in several locations on each tested beam. The moisture content of the elements was kept close to the required standard of 12%.

As can be seen from laboratory tests, the joint in the bending beam works asymmetrically. Destruction takes place in the left part of the joint by breaking the top element in the section AB. The location of the theoretical destruction cross-section PZ is between points A and B and depends, among other things, on the location of the bolt and the mutual pressure of the upper and lower elements on the section AB (Fig. 5.).

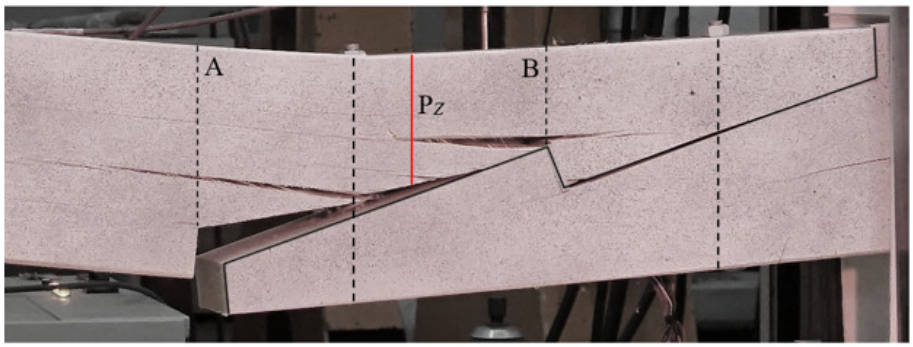

Fig. 5. The failure mechanism: destruction section (PZ) and its location between points A and B

SIMPLIFIED CALCULATION MODEL

In the next step, a simplified calculation model of the joint was created by interpreting the results of the experimental tests and based on the images of destruction (failure modes). It was a basic model representing, in a simplified way, the work of the analysed joint, created for engineering purposes. The theoretical load-bearing capacity of the beam with the joint was calculated according to that model.
For each location of the failure cross-section, the joint load-bearing capacity factor χ_Z, (ratio of the load-bearing capacity of beam with the joint to the load-bearing capacity of the continuous beam) can be calculated according to the formula:

$$\chi_Z = \frac{h_z^2}{h^2} \tag{1}$$

where,
h_z – cross-section failure depth of the beam with a joint,
h – cross-section failure depth of the continuous beam.

$$\chi_{Z,E} = \frac{h_{z,E}^2}{h^2} = 0.275 \tag{2}$$

For the data h_A = 140 mm and h_B = 70 mm, the respective load-bearing capacity factors of the joint are: $\chi_A = 0.605$ and $\chi_B = 0.151$.
This means that the maximum theoretical load-bearing capacity factor of the beam with the joint cannot exceed $\chi A = 0.605$.The main factors determining the load-bearing capacity of the beam with the joint are the location of the bolt and the amount of mutual pressure between the elements on the left side of the joint on the AB section.

RESULTS

The results of experimental testing: ultimate force and load-bearing capacities for bending for each series were calculated and presented in Table 1.

Table 1: Results for the tested beams

	Reference beam (series A)	**Beam with the joint (series E)**
Ultimate force [kN]	44.95	13.21
	37.52	13.79
	55.74	11.00
Mean ultimate force [kN]	46.07	12.67
Mean load-bearing capacity for bending [kNm]	24.88	6.84

The theoretical load-bearing capacity of the beam with the joint (beam E) was calculated according to the proposed simplified model (Fig. 6. a). Then, a modification of joint with additional bolts (beam E') in asymmetrical arrangement was proposed in order to obtain higher load-bearing capacity (Fig. 6. b).

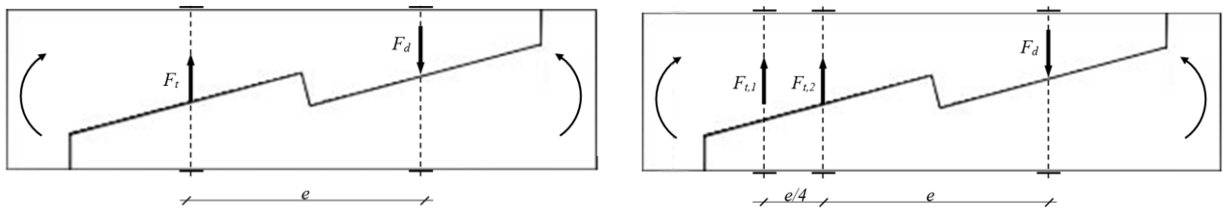

a) b)

Fig. 6. Model of the joint a) with two bolts – beam E, b) with the reinforcement in the form of an additional bolt– beam E'

Based on the forces distribution, the theoretical load-bearing capacity of the joint was determined. The load-bearing capacity is the lower of the calculated values: $M_{R,E,1}$ – bending moment transmitted by the tensile force in the bolt in the left part of the joint, $M_{R,E,2}$ – bending moment transmitted by the resultant force of compressive stresses between the elements in the right part of the joint.

$$M_{R,E,1} = F_t \cdot e = 30.35\ kN \cdot 0.27\ m = 8.19\ kNm \quad (3)$$

$$M_{R,E,2} = F_d \cdot e = b \cdot l_Z \cdot f_{c,\alpha} \cdot e = 0.12\ m \cdot 0.27\ m \cdot 3710\ kPa \cdot 0.27\ m = 32{,}45\ kNm \quad (4)$$

where:

F_t – tensile force in the bolt,

e – spacing between bolts,

F_d – compression force in the joint,

b – width of the beam,

l_z – length of half of the joint,

$f_{c,\alpha}$ – compressive strength at an angle to the fibers.

Even assuming the compressive strength at an angle to the fibers $f_{c,\alpha}$ as the minimally extreme value equal to $f_{c,90}$ the obtained result is $M_{R,E,2} > M_{R,E,1}$, therefore the load-bearing capacity of the beam with the joint with two bolts (beam E) should be assumed equal to $M_{R,E}$ = 8.19 kNm.

The theoretical coefficient of the load-bearing capacity of the joint with two bolts of the beam E, χ_E is:

$$\chi_E = \frac{M_{R,E}}{M_{R,A}} = \frac{8.19\ kNm}{25.92\ kNm} = 0.316 \quad (5)$$

The theoretical load-bearing capacity for the beam with two-bolt joint (beam E) is 8.19 kNm, and the test load-bearing capacity is 6.84 kNm. The theoretically calculated joint load-bearing capacity factor is 0.316, and the joint load-bearing capacity factor is 0.275.

A model was proposed to increase the number of bolts in an unsymmetrical configuration, for which the theoretical load-bearing capacity may be higher.

Proportion of the tensile force distribution in the bolts in the left part ($F_{t,2}$) of the joint resulting from the geometry of the bolt arrangement in the joint ($F_{t,1}$):

$$F_{t,2} = \frac{2}{3} F_{t,1} \quad (6)$$

$$M_{R,E',1} = F_{t,1} \cdot \frac{5}{4} e + F_{t,2} \cdot e = 30.35\ kN \cdot 0.3375\ m + 20.23\ kN \cdot 0.27\ m = 15.70\ kNm \quad (7)$$

$$M_{R,E',2} = F_d \cdot e = b \cdot l \cdot f_{c,\alpha} \cdot e = 0.12\ m \cdot 0.27\ m \cdot 3710\ kPa \cdot 0.27\ m = 32.45\ kNm \quad (8)$$

$M_{R,E',2} > M_{R,E',1}$, therefore, the load-bearing capacity of the beam with the four-bolt joint E' should be taken equal to $M_{R,E'}$ = 15.70 kNm.

The theoretical coefficient of the load capacity of the joint with three bolts in the asymmetric configuration is:

$$\chi_{E'} = \frac{M_{R,E'}}{M_{R,A}} = \frac{15.70\ kNm}{25.92\ kNm} = 0.606 \quad (9)$$

The results are summarised in the Table 2. The load-bearing capacity of the joint with two bolts compared to the continuous reference beam and the load-bearing capacity factor of the joint were determined in theoretical (computational) and practical (test) way. The load-bearing capacity of the

joint with four bolts compared to the continuous reference beam and the load-bearing capacity factor of the joint were determined in theoretical (computational) way based on a proposed model.

Table 2. Comparison of results

Type of beam	Continuous	Two-bolts joint	Four–bolts joint
Series	A	E	E'
M_R theoretically [kNm]	25.92	8.19	15.70
M_R from the test [kNm]	24.88	6.84	-
χ [-]	1.000	0.316	0.606

CONCLUSIONS

1) As can be seen, the difference in the load capacity obtained from the tests and from the proposed calculation model is only a dozen or so percent. As the authors emphasize, the presented model is a simplified and presents the static work of the joint for quick calculations for engineering purposes. In this case, creating a comprehensive model with a detailed description of the static work of the joint is a difficult challenge, taking into account the complex nature of the material, which is wood.
2) The analysis revealed that the stop-splayed scarf joint with two bolts can reach about 30% of the load-bearing capacity compared to a continuous beam, which was confirmed in the experimental tests.
3) By simple calculation, it is possible to assume that with the appropriate bolt arrangement, the joint can reach higher load-bearing capacity, in the discussed case– even about 60% in relation to the capacity of a continuous beam.
4) The location of the theoretical destruction depends on the location of the bolt and the mutual pressure of the upper and lower elements in the joint.
5) Because of the complex geometry of stop- splayed scarf carpentry joints, as well as the characteristic of wood, it is worth to include the results from laboratory investigations before any application on – site.

REFERENCES

[1] Tampone G., Semplici M. (2006). *Rescuing the Hidden European Wooden Churches Heritage*, An International Methodology for Implementing a Data Base for Restoration Projects. In cooperation with Fly Events and Alter Ego Ing Arch S.r.l. (a Subsidiary Company of the Collegio degli Ingegneri della Toscana), Città di Castello.

[2] Parisi M. A., Piazza M. (2008). Seismic strengthening of traditional carpentry joints. In: *Proceedings of the 14th World Conference on Earthquake Engineering*, Beijing, China, 12-17 October 2008.

[3] Perria E. (2017). Characterization of halved undersquinted scarf joint and stop-splayed undersquinted & tabled scarf joint with key (Jupiter joint). *PhD dissertation*. University of Braunschweig – Institute of Technology, Department of Architecture and University of Florence, Department of Civil and Enviromental Engineering.

[4] Mirabella-Roberti G., Bondanelli M. (2013). Study and analysis of XIV century timber built-up beams in Verona. *Advanced Materials Research*, 778, 511-516.

[5] Rug W., Thoms F., Grimm U., Eichbaum G., Abel S. (2012). Untersuchungen zur Biegetragfähigkeit von verzahnten Balken. *Bautechnik* 89, 26-36.

[6] Rug W., Linke G. (2015). Study on the load bearing capacity and the load- deferral behavior of wooden composite beams with a teethed joint. In: *Proceedings of the 3rd International Conference on Structural Health Assessment of Timber Structures – SHATIS'15*, Wrocław, Poland, 9-11 September 2015.

[7] Hirst E., Brett A., Thomson A., Walker P., Harris R. (2008). The structural performance of traditional oak tension & scarf joints. In: *Proceedings of the 10th World Conference on Timber Engineering*, Miyazaki, Japan, 2-5 June 2008.

[8] Sangree R. H., Schafer B. W. (2009). Experimental and numerical analysis of a stop-splayed traditional scarf joint with key. *Construction and Building Materials*, 23, 376-385.

[9] Ceraldi C., Costa A., Lippiello M. (2019). Stop-Splayed Scarf-Joint Reinforcement with Timber Pegs Behaviour. In: Aguilar R., Torrealva D., Moreira S., Pando M., Ramos L.F. (Eds.). *Structural Analysis of Historical Constructions*. Springer, Cham., 360-369.
[10] Kunecký J., Sebera V., Tippner J., Kloiber M. (2014). Numerical assessment of behavior of a historical central European wooden joint with a dowel subjected to bending. In: *Proceedings of the 9th International Conference on Structural Analysis of Historical Constructions*, Mexico City, Mexico, 15-17 October 2014.
[11] Kunecký J., Sebera V., Hasníková H., Arciszewska-Kędzior A., Tippner J., Kloiber M. (2015). Experimental assessment of full-scale lap scarf timber joint accompanied by a finite element analysis and digital correlation. *Construction and Building Materials*, 76, 24-33.
[12] Kunecký J., Hasníková H., Kloiber M., Milch J., Sebera V., Tippner J. (2018). Structural assessment of a lapped scarf joint applied to historical timber constructions in central Europe. *International Journal of Architectural Heritage*, 12.4, 666-682.
[13] Arciszewska- Kędzior A., Kunecký J., Hasníková H. (2015). Mechanical response of a lap scarf joint with inclined faces and wooden dowels under combined loading. In: *Proceedings of the 3rd International Conference on Structural Health Assessment of Timber Structures – SHATIS'15*, Wrocław, Poland, 9-11 September 2015.
[14] Arciszewska-Kędzior A., Kunecký J., Hasníková H., Sebera V. (2015). Lapped scarf joint with inclined faces and wooden dowels: Experimental and numerical analysis. *Engineering Structures*, 94, 1-8.
[15] Šobra K., Fajman P. (2013). Utilization of splice skew joint with a key in the reconstruction of historical trusses. *Advanced Materials Research*, 668, 207-212.
[16] Fajman P., Máca J. (2015). Scarf joints with pins or keys and dovetails. In: *Proceedings of the 3rd International Conference on Structural Health Assessment of Timber Structures – SHATIS'15*, Wrocław, Poland, 9-11 September 2015.
[17] Fajman P. (2015). A scarf joint for reconstructions of historical structures. *Advanced Materials Research*, 969, 9-15.
[18] Fajman P., Máca J. (2018). The effect of inclination of scarf joints with four pins. *International Journal of Architectural Heritage*, 12(4), 599-606.
[19] Structural Timber—Determination of Characteristic Values of Mechanical Properties and Density; PN-EN 384: 2016-10. PKN: Polish Committee for Standardization, Warsaw, Poland, 2016.
[20] Timber Structures. Structural Timber and Glued Laminated Timber. Determination of Some Physical and Mechanical Properties. PN-EN 408+A1: 2012; PKN: Polish Committee for Standardization, Warsaw, Poland, 2012.

PAŁAC SZTYNORT, Republic of Poland
New technology for strengthening wide-span wooden beam ceilings

Wolfram Jäger[1], Fabian Meyer[2]

[1] Wolfram Jäger, Prof. Dr.-Ing.; 1998-2019 Chair of Structural Design, Technical University of Dresden

[2] Fabian Meyer, Dipl.-Ing., M.Sc. Planungs- und Ingenieurbüro für Bauwesen, Prof. Dr.-Ing. Wolfram Jäger, Radebeul

ABSTRACT

When preserving historic buildings, repairing and strengthening wooden beam ceilings is usually an essential part of the measures to be planned. In contrast to the typical spans of 5 to 8 metres, there are also a large number of wide-span wooden beam ceilings that need particular strengthening to meet the standards of modern usages. In addition to load-bearing capacity and serviceability, other aspects that have to be considered are technical feasibility, economic viability and compatibility with heritage requirements. The baroque wooden beam ceilings in the cultural monument Pałac Sztynort are characterized by their unusually large span and unique polychrome painting. The preservation of Pałac Sztynort is a special measure of public interest due to the cultural monument's historical value and its important place in international history as a site of resistance to National Socialism. In order to meet new requirements for public use and guarantee the preservation of the historic building structure, a methodology suitable for historic monuments was developed at the Chair of Structural Design at TU Dresden for strengthening wide-span wooden beam ceilings using a wooden cross-sectional expansion piece. To achieve the highest possible load-bearing capacity, a load-bearing connection is glued between the original beam and the addition.
The preservation and strengthening of the wooden beam ceilings at Pałac Sztynort follow an innovative approach combining new, sustainable engineering methods with high standards of modern monument preservation in a manner that helps maintain cultural heritage.

KEYWORDS: timber structures, ceiling, heritage preservation, strengthening, structural bonding

INTRODUCTION

Palace Sztynort, a manor house once belonging to the von Lehndorff family, is a cultural monument with an important place in Polish-German history. The baroque core building was constructed between 1689 and 1693 [1]. Polychrome painted ceiling beams reflecting traditional Masurian craftmanship have survived from the time of its construction (Fig.1). The preservation of the polychrome wooden beam ceilings with span of 10,00 m and the plans for the public use of Pałac Sztynort require a careful structural solution. The existing structure must be strengthened for public use as a museum or exhibition space with an allowable imposed load of 5 kN/m^2 [3]. For strengthening, it is important that the basic load situation should not be changed if the existing foundations are to be retained.
Furthermore, from the point of view of heritage preservation, the strengthening should be carried out in a way that preserves the building structure without changing the ceiling heights.

Figure 1: View of a polychrome painted ceiling, 2004 Source: private archive of B. Kulczynska Nowak

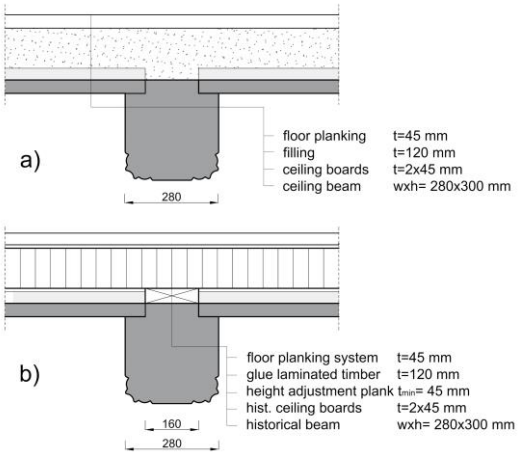

Figure 2: comparison of ceiling construction [2]
a) historical ceiling
b) new ceiling incl. strengthening

METHODOLOGY

To meet the structural requirements for public use and the conditions for the preservation of historical monuments, the idea for strengthening the ceiling beams is based on transforming the rectangular cross-section into a T-beam (Fig. 3). The geometry allows the ceiling beam to be made into a T-beam as the ceiling used to have a floor construction above the beams that was about 15 cm thick (Fig.2). The former filler made of loose organic material is replaced with a glue-laminated timber element, so that the pre-existing fixed geometrical points (e.g.doorsteps) can be retained.

In this cross-section expansion, the individual cross-sections are not connected by conventional, metal fasteners, but are joined together by structural bonding to form a high-performance composite cross-section. This means the historical wooden beams retain their load-bearing function, the wooden expansion increases their load-bearing capacity.

By placing a wooden height adjustment element between the existing beam and the glue-laminated timber element, it is possible to return the historically painted ceiling boards to their original position after restoration (Fig. 8). In addition to the geometrical requirements, the connection between the beam and the height adjustment plank levels out deformations on the historic beam and ensure a load bearing bonding with a thickness of $t_{f,max} \leq 1{,}5$mm.

The technological feasibility of the method developed here was verified with test beams on a scale of 1:2. Their load-bearing capacity and serviceability under the new usage requirements were tested in the Otto-Mohr Laboratory at TU Dresden (Fig. 4).

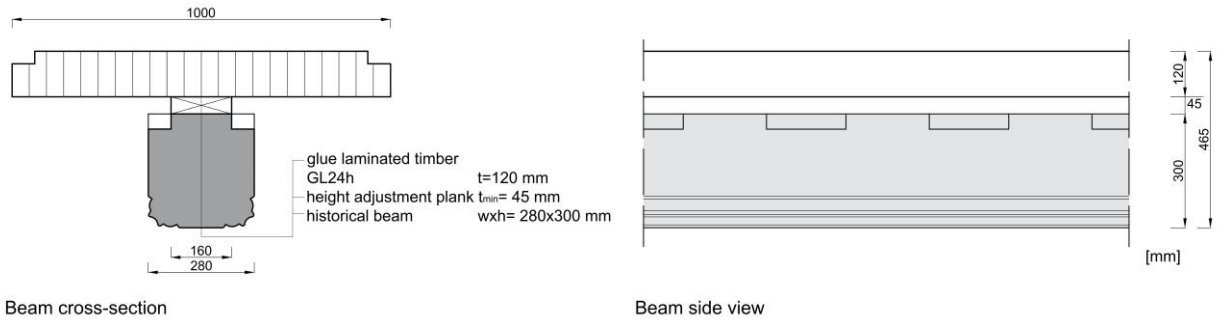

Figure 3: T-beam cross-section and beam side view

RESULTS

The feasibility of using structural bonding to strengthen timber components, in this case historic beams, is mainly influenced by the environmental conditions at the site. Those conditions affect the reliability of the adhesive bond and the processing time when applying the adhesive. The processing time is the time required to apply the adhesive, assemble the parts and apply the compressive pressure. The key environmental factors affecting the use of melamine-urea resin adhesive are the room temperature (T_{min}=20 °C), relative humidity (RH=65%) and, importantly, the wood moisture content (u ≤ 15%). Using bonding on the construction site requires prior monitoring of the room climate and the wood moisture content. Depending on the building situation (e.g. in unheated rooms), increased wood moisture content is to be expected and must be regulated with the room climate over a longer period of time [4].

A further requirement for structural bonding is compressive pressure. The compressive pressure of 0.6 N/mm^2 for melamine-urea resin adhesive was generated using screw-press-bonding. The use of screw-press-bonding was investigated for this special application by selecting special screw and screw spacing. The screws used were partially threaded screws with a large head (washer head) according to the specifications. Screw press bonding has the advantage that access is only required to the unpainted top side of the beams when generating the compressive pressure.

The experimental investigations on a scale of 1:2 included examinations of the load-bearing behaviour and the vibration behaviour of the strengthened beams. The load-bearing behaviour was tested using a 4-point bending test arrangement in the Otto Mohr Laboratory at TU Dresden. The test was carried out on two test beams (Fig. 5) under a path-controlled load until failure. The clear fracture in the tensile zone of the composite section and the achieved average fracture load of 96,2 kN at an average deflection of 65.3 mm prove the load-bearing capacity of the strengthened beam and show that the new technology can be used to produce a load-bearing, structural bonding.

Figure 4: 4-point bending test, beam- scale 1:2

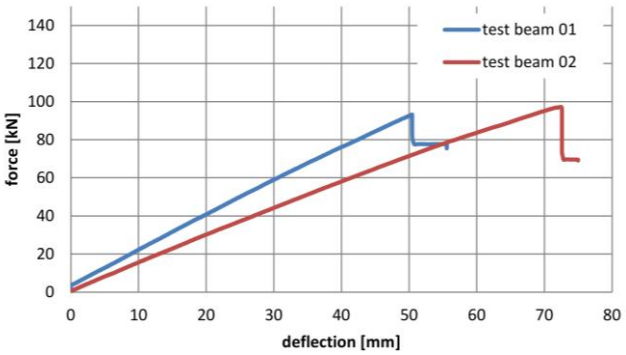

Figure 5: Results – 4-point bending test

Based on the experiences and the results from the theoretical and experimental investigation, a special case in Pałac Sztynort with a collapsed ceiling allows to transfer this method into practice.

This situation, means that the beams can be prepared while removed. Repairing them in the factory has the advantage that finger jointing can be used between the historical beam pieces and the new wooden additions. The disadvantage of conventional joints is that most use metal fasteners with joint slip and a large transition area between the components to be connected. A finger joint is a load-bearing connection without any slip and requires only a small connecting area of 5 cm, so the polychrome painting is still preserved.

The repair of the historic ceiling beams was completed by extending the shaping to the new beam sections (Fig. 6; Fig. 7).

Figure 6: Detail with a finger joint

Figure 7: View of the beams - shaped surface at the top (Photo taken with a fisheye)

The strengthening measures that follow involve preparing an adhesive surface on the top of the beams, including levelling out the deformations on the repaired rectangular beams. The height of the adjustment planks is individually adapted to the specific beam, so that the glue-laminated timber elements are at the same height and the ceiling boards between the beams can be integrated into the ceiling after the restoration (Fig. 8). The bonding is carried out in line with the results of the preliminary investigation using screw-press bonding. When the strengthening work is completed, vibration tests are to be carried out directly in the factory hall and compared with the requirements and the experimental test. The knowledge and experience gained in repairing and strengthening the beams will be applied to the other ceilings in Pałac Sztynort.

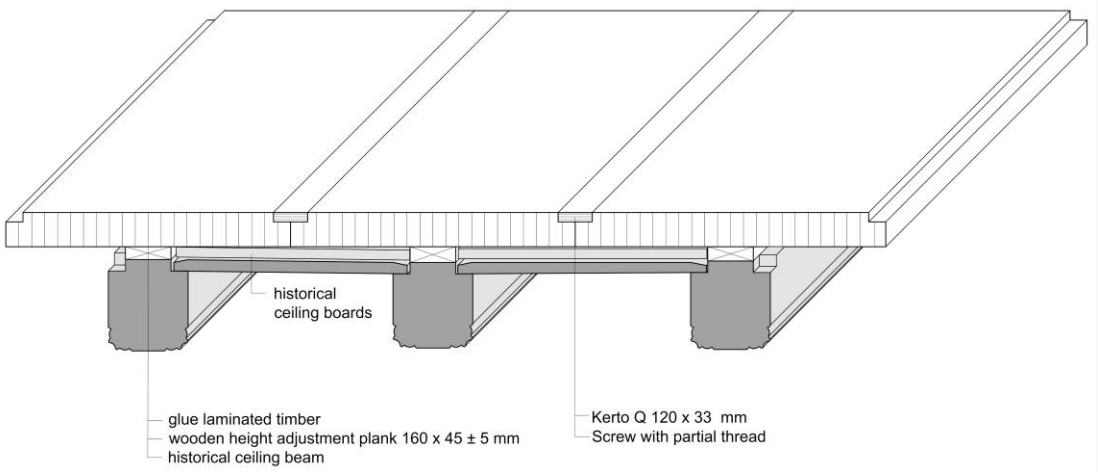

Figure 8: Structural solution with integrated ceiling board

DISCUSSION

The presented method for material-appropriate strengthening enables the wide-span wooden beam ceilings to be used by the public in a way that traditional solutions cannot achieve. The use of load-bearing glued connections draws on decades of experience in the manufacture of glued laminated timber [5]. Based on building research, this method is suitable for historic buildings, such as Pałac Sztynort, taken into consideration international principles of monument conservation [6]. Alternatives to this method are a wooden cross-section extension using metal fasteners, a timber-concrete composite ceiling and a reinforced concrete ceiling. The alternatives listed here are already established in construction practice, but they have the disadvantage of joint slip or a significantly

higher dead weight, which requires extensive work on the foundations. The effort and expense of strengthening using structural bonding are justified by the great historical and architectural significance of Pałac Sztynort.

CONCLUSION

The preservation and strengthening of the wooden beam ceilings at Pałac Sztynort combine of new sustainable engineering, innovative constructional approaches and high public standard for modern monument preservation in a manner that helps maintain cultural heritage.

The safeguarding measures at Pałac Sztynort are financially supported by the Federal Government Commissioner for Culture and Media (BKM) - Federal Republic of Germany. The practical work described here was carried out by Burgbacher Holztechnologie GmbH Trossingen, Germany. The authors thank their company for their support and in particular for contributing their own experience.

Figure 9: Pałac Sztynort in Sztynort, Republic of Poland *Photograph: Weichelt 2016*

REFERENCES

[1] Lorck, C. von: Groß Steinort – Der Bauvorgang eines Barockschlosses im deutschen Osten. Boettcher, Pillkallen, 1937.

[2] Meyer, F.: Increasing the load bearing capacity of historically valuable wooden beam ceilings. Dresden, Technische Universität Dresden, Chair of timber engineering and construction design, Prof. Dr.-Ing. Peer Haller and Chair of structural design, Prof. Dr.-Ing. Wolfram Jäger, diploma thesis, 2017.

[3] EN 1991-1-1:2010/ PN EN 1991-1-1/NA 2010 Eurocode 1: Actions on structures - Part 1-1: General actions - Densities, self-weight, imposed loads for buildings; Polish version EN 1991-1-1:2002 +AC:2009 /Polish National Annex 2010

[4] EN 1995-1-1:2010 / PN EN 1995-1-1/NA:2010; Eurocode 5: Design of timber structures – Part 1-1: General- Common rules and rules for buildings; Polish version EN 1995-1-1:2010 /Polish National Annex 2010

[5] Lißner, K.; Rug, W.: Holzbausanierung beim Bauen im Bestand. Springer Berlin Heidelberg, Berlin, Heidelberg, 2018; S. 351

[6] Principles of Monument Conservation: Venice Charter – Intern. Charter for the Conversation and Restoration of Monuments and Sites, ICOMOS 1964; Burra Charter – Charter for Places of Cultural Significance, ICOMOS 1979

CASE STUDIES
RESEARCH & PRACTICE

INSPECTION AND DIAGNOSIS OF TIMBER STRUCTURES OF THE BIRTHHOUSE OF JORGE JUAN Y SANTACILIA

JOSÉ RAMÓN AIRA-ZUNZUNEGUI[1], LAURA GONZALO-CALDERÓN[1], MARIANO GONZÁLEZ-SANZ[2], ESTHER MORENO-FERNÁNDEZ[1], FRANCISCO GONZÁLEZ-YUNTA[3]

[1] Universidad Politécnica de Madrid, ETS Arquitectura.

[2] Universidad Politécnica de Madrid, ETSI Montes.

[3] Universidad Politécnica de Madrid, ETS Edificación.

ABSTRACT

A case study is presented on the inspection and diagnosis of the timber structure of the house where Jorge Juan y Santacilia was born. The house dates from the 17th century and has 3 floors with a total constructed area of 1553 m^2. The tasks of the inspection and diagnosis of the timber elements with recommendations for intervention, including determination of wood species in laboratory, strength grading by means of non-destructive testing and identification of xylophagous organisms by microscopy were carried out. Among other pathogens, structure shows a very important generalised attack of woodworms that reduces the effective cross-section in most of the timber elements.

KEYWORDS: pathology, timber structure, NDT, inspection and diagnosis, case study.

INTRODUCTION

The building under study is located in El Fondonet (Novelda, Alicante). The naval engineer and scientist Jorge Juan y Santacilia was born there on January 5, 1713. He was an illustrious personage who stood out for measuring the longitude of the Earth's meridian, demonstrating that the Earth is flattened at the poles, and for reforming the Spanish naval model. It is a single-family house recently acquired by the local government with the aim of restoring and converting it into a house-museum.

The property has three floors (ground, first and second) with a total constructed area of 1553 m^2. The floors are connected by a staircase with three flights located in the central part. The ground floor has 21 rooms and a constructed area of 671 m^2, the first floor has 21 rooms and a constructed area of 441 m^2, and the second floor has 14 rooms and a constructed area of 441 m^2. Some of the rooms correspond to old bathrooms, or kitchens or laundry rooms where there was a risk of attacks by xylophagous agents associated with high moisture content.

From the north façade, the main floor of the house (first floor) is accessed directly from the garden via a monumental staircase, figure 1. From the south façade there is access to the ground floor, where the service personnel were housed, and to the stables.

Figure 1: North façade (left) and ground floor (right) of the building

In recent decades, several research projects have been carried out with the aim of developing and standardising procedures for the assessment of existing timber structures of historic buildings. One of the most outstanding works is the one developed within the framework of the COST action IE0601 "Wood Science for Conservation of Wooden Cultural Heritage", which resulted in the publication of guidelines for the on-site assessment of historic timber structures [1], and subsequently led to the drafting of the EN 17121 standard [2].

This standard divides the procedure into two phases, a preliminary assessment phase and a detailed study phase. In the preliminary assessment, a documentary study is carried out to provide information on the history of the structure and the intentions of the owner of the building with regard to its final use, a preliminary visual inspection to get a first approximation of the state of the structure and identify the auxiliary means necessary for its in-depth inspection, and a geometric survey of the structure with an indication of the lengths and sections of the elements. The preliminary assessment concludes with a preliminary report which includes a general description of the structure with the most worrying areas. In the detailed study phase, a more detailed inspection is carried out where the damaged areas are measured, the results of non-destructive tests are shown, the quality of the wood and the validity of the joints are established. This second phase concludes with the drafting of the diagnostic report on the state of the structure, causes of exhaustion and proposals for intervention.

In this work, the preliminary assessment was contracted by the company Proiescon S.L., which would later carry out all the intervention works in the building. The preliminary report concluded that wooden beams and joists show obvious symptoms of xylophagous attacks of different intensities, so it was necessary to carry out a detailed study of the whole timber structure by examining each of the individual elements. It also indicates that during the life of the building numerous interventions have been carried out on the structure. All that remains of the original timber structure are the large-square beams that divide the rooms, and the round rafters of some parts of the roof. The other timber elements have been replaced at some point by other new wooden elements and sometimes even by metal and concrete beams.

The preliminary report established the inspection tasks to be carried out in the second phase indicating that the work was to be done by specialists with recognized experience in the sector. Thus, the case study presented in this paper corresponds to the second phase of the procedure. The objective of this work was the inspection and diagnosis of the timber elements with recommendations for intervention, including determination of wood species in laboratory, strength grading and identification of xylophagous organisms by microscopy.

METHODOLOGY (INSPECTION)

In order to determine the species, two wooden blocks were taken, one from the ground floor slab and the other from the roof. The samples were analysed in the laboratory. In addition, the density of these specimens was obtained in accordance with the standard EN 408+A1 [3] to verify the density obtained by non-destructive testing.

According to EN 338 [4] there are three fundamental properties for assigning a strength class to a structural timber element. These are the characteristic values of stiffness (Modulus of Elasticity, $MOE_{average}$), strength (Modulus of Rupture, $MOR_{characteristic}$) and density ($density_{characteristic}$). A timber element can be assigned to a strength class if the characteristic values are higher than those given in EN 338 standard [4]. Furthermore, using the equations shown in EN 384 standard [5] it is possible to obtain other physical and mechanical properties from these three fundamental properties.

The strength grading was carried out following the scheme shown in figure 2. In this particular case, the visual grading was really complicated by the fact that most of the timber elements were covered with white paint which made it difficult to measure the knots or the slope of grain. Therefore, the aim was to determine the three fundamental properties ($MOE_{average}$, $MOR_{characteristic}$ and $density_{characteristic}$) by means of non-destructive techniques. This procedure has been used by other researchers in Spain previously with satisfactory results [6-8].

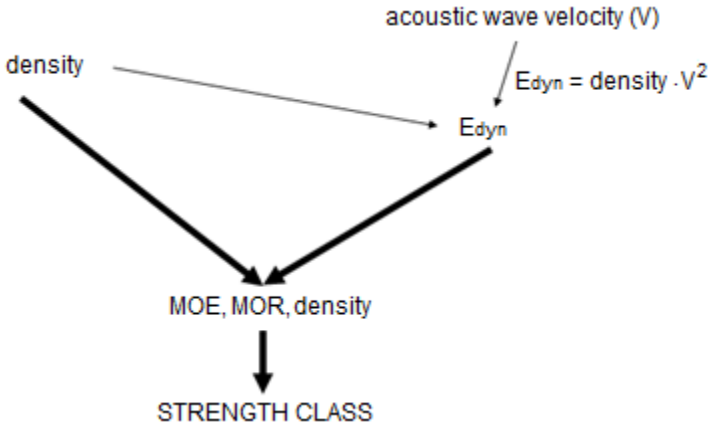

Figure 2: Strength grading process

To obtain the values corresponding to the pieces of the whole structure, 10 pieces of each floor were analysed without xylophagous attacks (a total of 30 pieces), taking 3 measurements in each piece and at different points. Moisture content was measured with a resistive xylohygrometer, figure 3.

Figure 3: Resistive xylohygrometer (left), Pilodyn (centre), MST (right)

Density was measured with a specific penetrometer for wood (Pilodyn) applying the equation (1) from Llana *et al.* [9].

$$\delta = 689.73 - 10.32 \cdot D_{12} - 86.42 \cdot Z_{rad} - 28.69 \cdot Z_{sco} + 43.02 \cdot Z_{sal} + 0 \cdot Z_{mar} \quad (1)$$

where δ is the density in $kg \cdot m^{-3}$, D_{12} is the penetration depth of Polidyn in mm corrected to 12% moisture content; and Z_{rad}, Z_{sco}, Z_{sal} and Z_{mar} are the constants for Radiata, Scots, Salzmann and Maritime pine, respectively, which are only equal to 1 for this species and equal to 0 for other species.

A correction for moisture content was previously applied to the penetration depth of Pilodyn according with equation (2) from Llana *et al.* [9].

$$D_{12} = \frac{D_{MC}}{[1+k_{DMC} \cdot (MC-12)]} \quad (2)$$

where D_{12} is the penetration depth of Polidyn in mm corrected to 12% moisture content, D_{MC} is the penetration depth of Polidyn in mm at MC% moisture content, and k_{DMC} is the per unit adjustment factor taking the values of 2.2, 1.6, 1.7 and 2.0 for Radiata, Scots, Salzmann and Maritime pine, respectively.

The average density ($density_{average}$) was calculated as the average value of the 30 measurements taken. The characteristic density ($density_{characteristic}$) was taken as the lowest value of those 30 measurements.

The MOE and MOR were obtained by acoustic methods (Fakopp Microsecond Timer or MST) applying the equations (3) and (4) from Llana *et al*. [9].

$$MOE = -1662 + 0.78 \cdot E_{dyn} - 428.70 \cdot Z_{rad} + 958.05 \cdot Z_{sco} + 232.23 \cdot Z_{sal} + 0 \cdot Z_{mar} \quad (3)$$

$$MOR = -38.09 + 0.0075 \cdot E_{dyn} - 11.92 \cdot Z_{rad} - 2.71 \cdot Z_{sco} - 12.17 \cdot Z_{sal} + 0 \cdot Z_{mar} \quad (4)$$

where MOE is the Modulus of Elasticity in MPa, MOR is the Modulus of Rupture in MPa, E_{dyn} is the Dynamic Modulus of Elasticity in MPa; and Z_{rad}, Z_{sco}, Z_{sal} and Z_{mar} are the constants for Radiata, Scots, Salzmann and Maritime pine, respectively, which are only equal to 1 for this species and equal to 0 for other species.

The Dynamic Modulus of Elasticity was obtained by the well-known equation (5).

$$E_{dyn} = \delta \cdot V_{12-end-to-end}^2 \quad (5)$$

where E_{dyn} is the Dynamic Modulus of Elasticity in $N \cdot m^{-2}$, δ is the density in $kg \cdot m^{-3}$, and $V_{12\text{-}end\text{-}to\text{-}end}$ is the velocity of MST in $m \cdot s^{-1}$ corrected first for position and then for moisture content.

The MST velocity was firstly corrected for position from indirect (face-to-face) to direct (end-to-end) measurements according to equation (6) from Arriaga *et al.* [10].

$$V_{end-to-end} = \frac{V_{face-to-face}}{0.994} \quad (6)$$

where $V_{end\text{-}to\text{-}end}$ is the velocity corrected for position in $m \cdot s^{-1}$, and $V_{face\text{-}to\text{-}face}$ is the velocity measured by placing the transmitting and receiving sensors on the same beam face in $m \cdot s^{-1}$.

Subsequently, velocity was corrected for moisture content by equation (7) from Llana *et al*. [9].

$$V_{12} = \frac{V_{MC}}{[1-k_{VMC}\cdot(MC-12)]} \quad (7)$$

where V_{12} is the velocity of MST in $m \cdot s^{-1}$ corrected to 12% moisture content, V_{MC} is the velocity of MST in $m \cdot s^{-1}$ at MC% moisture content, and k_{VMC} is the per unit adjustment factor taking the values of 0.62, 0.61, 0.72 and 0.76 for Radiata, Scots, Salzmann and Maritime pine, respectively.

The average values of MOE and MOR ($MOE_{average}$ and $MOR_{average}$) were calculated as the average of the 30 measurements taken. The characteristic MOR ($MOR_{characteristic}$) was obtained by equation (8) from Aira [11].

$$MOR_{characteristic} = 0.75 \cdot MOR_{average} \quad (8)$$

A visual inspection of all the pieces was carried out using a punch, screwdriver, wood chisel and plastic hammer, figure 4. In addition, samples were taken of the detritus present inside the attacked pieces for identification of xylophagous agent in laboratory by microscopy. Specifically, 18 samples were taken from 18 different pieces, 6 from each plant.

The identification of the agents of wood degradation is important for several reasons. On the one hand, it allows a more accurate assessment of the damage caused by knowing more precisely the size of the causal agent. Furthermore, by knowing the biological cycle of the causal agent, it is possible to design a more effective method for its extinction. Finally, this information is very useful to estimate the effective cross-section of the timber elements for structural calculations.

Figure 4: Punch and screwdriver inspection

There was a special interest in knowing exactly the condition of the larger pieces because it is difficult to find dry sawn timber of these dimensions. Moreover, these pieces were part of the original timber structure, so, as far as possible, an attempt would be made to reinforce them rather than replace them with new ones. Consequently, the following specific checks were carried out on the larger pieces with structural responsibility (widths greater than 25 cm): moisture content measurement with resistive xylohygrometer, verification of the depth of attack with Pilodyn, analysis of the inside of the piece with a resistograph, and verification of the activity of xylophagous insects with an acoustic detector (Audiotermes) and a thermographic camera, figure 5.

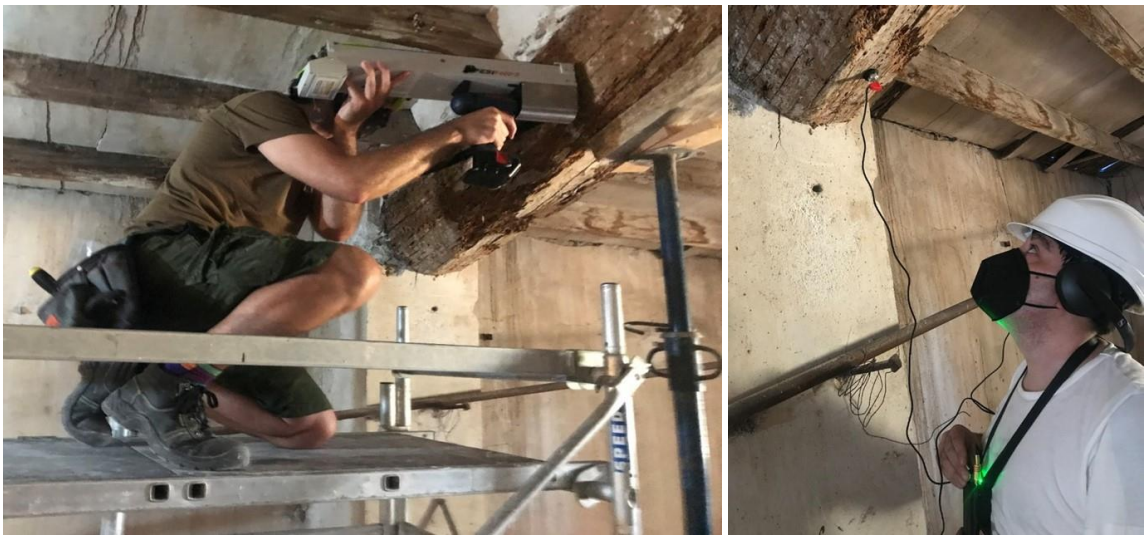

Figure 5: Inspection of larger pieces with resistograph and Audiotermes

RESULTS (DIAGNOSIS)

It was determined that wood of timber slabs between floors was *Pinus sylvestris* L. (Scots pine) or *Pinus nigra* Arn. (Salzmann pine), and wood of the roof was *Pinus pinaster* Ait. (Maritime pine) or *Pinus radiata* D. Don (Radiata pine), figure 6. In addition, the characterising variables were obtained: $MOR_{characteristic}$, $MOE_{average}$ and $density_{characteristic}$, which were used to assign a strength class C14 to the whole structure following the classification of strength classes defined in EN 338 standard [4]. As usual in wooden elements, the most limiting value when strength grading was the stiffness ($MOE_{average}$) while density ($density_{characteristic}$) and strength ($MOR_{characteristic}$) values would have allowed a much higher strength class to be assigned.

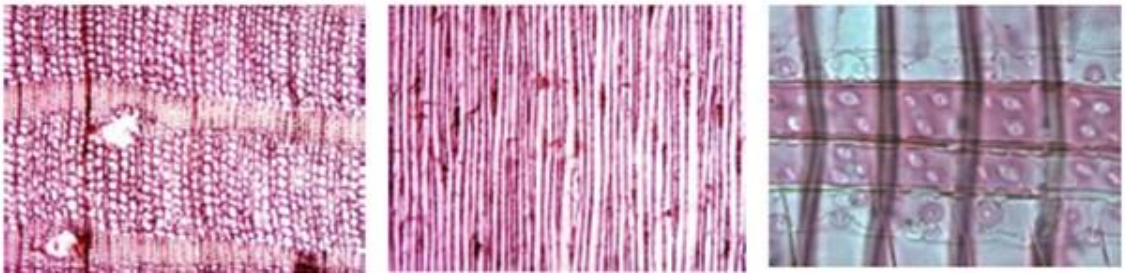

Figure 6: Identification of species in the laboratory: "Pinus pinaster Ait. or Pinus radiata D. Don". Transverse section (left), tangential section (centre) and radial section (right).

In general, the building is well ventilated with moisture content levels of around 11%, reaching 16% in some areas. There are some chromogenic fungi that discolour the wood, indicating the temporary presence of humidity, but of no structural importance as long as the structure is properly ventilated. Brown rot and white rot also appear on heads of some joists at supports with exterior wall, and at intermediate points of moisture accumulation due to downpipes or water filtrations, figure 7. The structure is completely attacked by large woodworm (*Hylotrupes bajulus* L.) and common woodworm (*Anobium punctatum* De Geer) that have been in activity for many larval cycles, figures 8 and 9. Woodworm attack remains active, being moderate on the ground and first floors, and more intense on the second floor (roof). Subterranean termite (*Reticulitermes lucifugus* Rossi) and drywood termite (*Criptotermes brevis* Walker) were also found in localised areas, figure 10, but their attack is currently inactive.

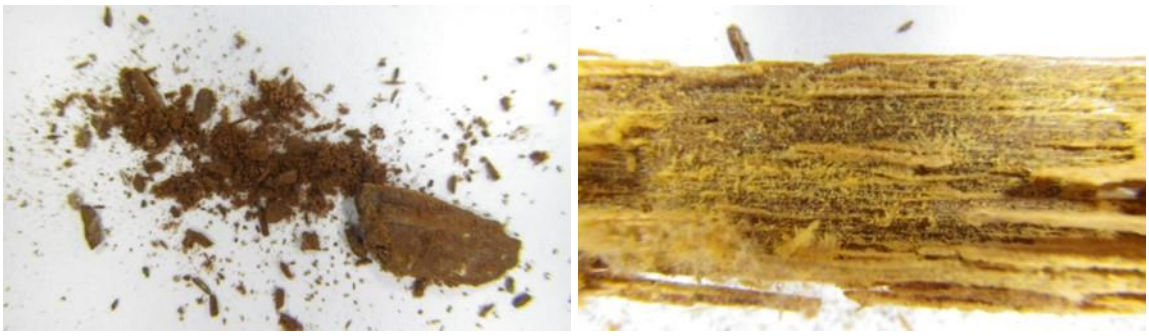

Figure 7: Brown rot (left) and white rot (right).

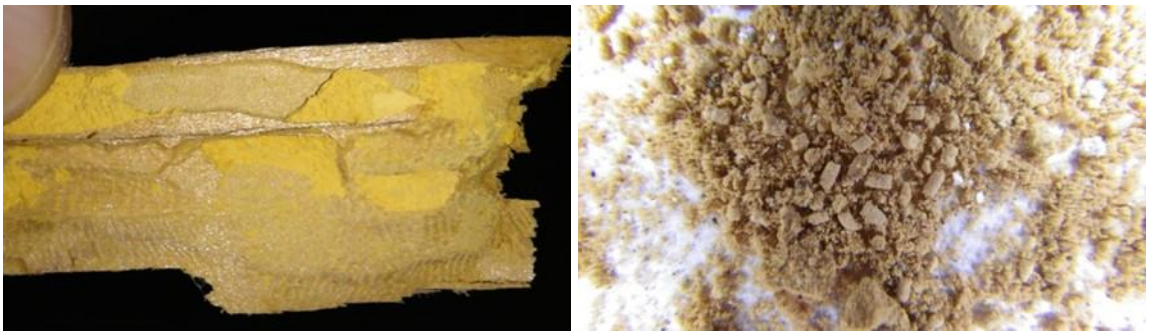

Figure 8: Soft undulations in the galleries (left) and detritus (right) of Hylotrupes bajulus L.

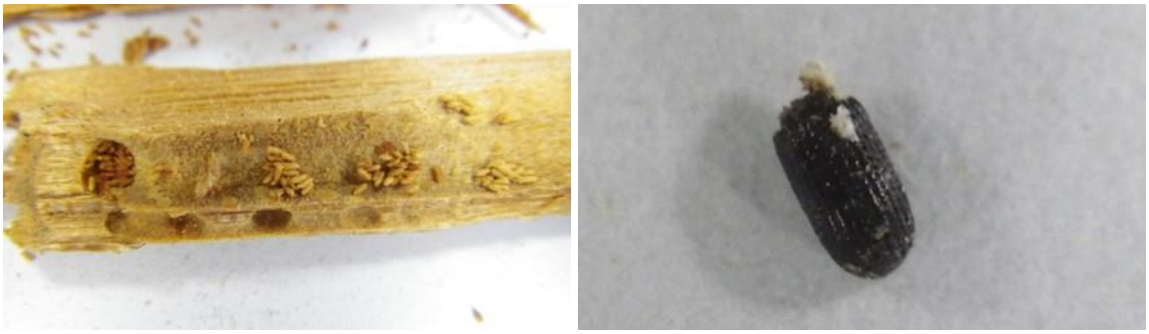

Figure 9: Detritus (left) and elytra (right) of Anobium punctatum De Geer.

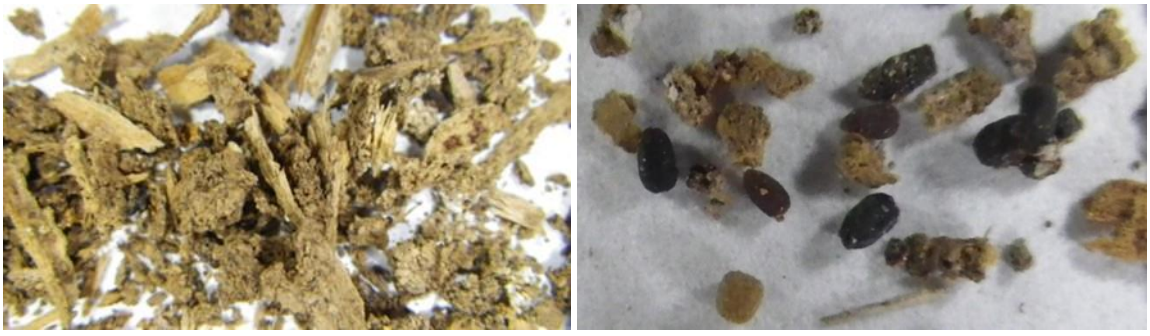

Figure 10: Mud in galleries of Reticulitermes lucifugus Rossi (left) and detritus of Criptotermes brevis Walker (right).

In the larger pieces where resistographic profiles were made, it was found that some had been deeply attacked with the presence of xylophagous galleries in internal areas, and others had received milder attacks with the presence of galleries only in the perimeter areas. It was also found that there was a significant difference in density from one piece to another, figure 11.

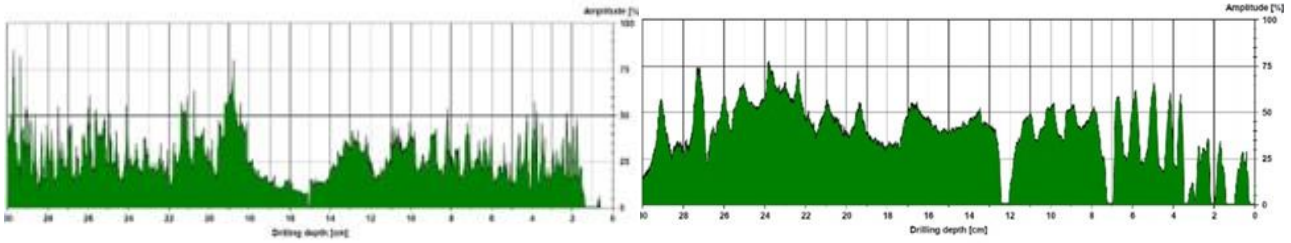

Figure 11: Resistographic profile of a piece with little attack with the presence of pith, juvenile wood and low density (left), and another piece with considerable attack in the first 13 cm and higher density (right).

From a constructive point of view, the following recommendations were made:

- Maintain correct ventilation of the structure throughout its useful life, for which it is necessary to carry out an adequate design of the water evacuation routes.
- Special attention should be paid to the risk areas detected during the inspection: support of joists in walls where capillary water rises, floor slabs in damp areas (bathrooms, kitchens, laundry rooms, etc.) and roof downpipes.

Considering the bearing capacity of the structure the following was recommended:

- All parts remaining on site should be recalculated to check their bearing capacity considering the effective cross-section. The strength class to be considered for the calculation will be C14.
- In the event that the joists of the floor slabs or roof rafters do not verify the bearing capacity, the pieces must be replaced. In the event that the larger pieces (main beams) do not meet the bearing capacity, they must be replaced or they may also be reinforced to ensure the required strength.
- In cases where any of the pieces verify the bearing capacity but have localized rotting at the heads of support in walls, the pieces can be restored by removing the damaged part and placing wood or epoxy mortar prosthesis with fiberglass reinforced polyester rods (or plates).
- New parts should also be calculated to check their bearing capacity. It is recommended to use sawn timber of Salzmann pine or Scots pine of strength class C22. This strength class is recommended because it is the one established by the Spanish visual grading standard for large-square timber of these species, UNE 56544 standard [12]. Glued laminated timber may be used, in which case it is recommended to use glued laminated timber of Scots pine of strength class GL24h or GL24c.

Finally, the following suggestions were made regarding curative protective treatment:

- Woodworm (active generalised attack): all the timber elements remaining on site, without exception, should receive an anti-worm curative treatment. It will consist of a deep treatment by means of injections with fungicide and insecticide products followed by a superficial treatment by spraying with the same products. The injections will be placed in a 60-degree staggered pattern to cover the surface more effectively.
- Rot (inactive isolated attacks): replacement of the affected parts and fitting of glued-in-place wooden prosthesis or epoxy mortar prosthesis.
- Termite (inactive isolated attacks): replacement of the affected parts. In addition, surrounding the building by injections with insecticide product and bait system with hexafluomuron impregnated cellulose.
- New timber elements will have a deep autoclave treatment with fungicide and insecticide product.

CONCLUSION

In this work, an inspection and diagnosis of a timber structure of historical relevance has been carried out. Several portable non-destructive devices were used for this purpose. The in-situ work was complemented by microscopic analysis in the laboratory to identify the wood species and pathogens.

The entire structure is made of pine wood, which has been assigned strength class C14. There is a very serious generalised attack by woodworm, especially large woodworm, which due to the passage of numerous larval cycles has substantially reduced the effective cross-section of most of the pieces. In addition, occasional attacks of brown rot, white rot, subterranean termite and drywood termite have been found.

REFERENCES

[1] Cruz H., Yeomans D., Tsakanika E., Macchioni N., Jorissen A., Touza M., Mannucci M., Lourenço P.B. Guidelines for on-site assessment of historic timber structures. Int. J. Archit. Herit. 9 (3) 277–289. DOI: 10.1080/15583058.2013.774070.

[2] EN 17121:2019. Conservation of cultural heritage. Historic timber structures. Guidelines for the on-site assessment of load bearing timber structures. European Committee for Standardization (CEN).

[3] EN 408:2010+A1:2012. Timber structures - Structural timber and glued laminated timber - Determination of some physical and mechanical properties. European Committee for Standardization (CEN), Brussels, Belgium.

[4] EN 338:2016. Structural timber - Strength classes. European Committee for Standardization (CEN).

[5] EN 384:2016. Structural timber. Determination of characteristic values of mechanical properties and density. European Committee for Standardization (CEN).

[6] Íñiguez G. 2007. Grading by non-destructive techniques and assessment of the mechanical properties of large cross section coniferous sawn timber for structural use. Doctoral thesis. Universidad Politécnica de Madrid.

[7] Arriaga F., Osuna-Sequera C., Esteban M., Íñiguez-González G. Bobadilla I. 2021. In situ assessment of the timber structure of an 18th century building in Madrid, Spain. Construction and Building Materials, 304, 124466. DOI: 10.1016/j.conbuildmat.2021.124466.

[8] Arriaga F., Osuna-Sequera C., Bobadilla I., Esteban M. 2022. Prediction of the mechanical properties of timber members in existing structures using the dynamic modulus of elasticity and visual grading parameters. Construction and Building Materials, 322, 126512. DOI: 10.1016/j.conbuildmat.2022.126512.

[9] Llana D.F., Íñiguez-González G., Díez M.R., Arriaga F. 2020. Nondestructive testing used on timber in Spain: a literature review. Maderas Ciencia y Tecnología, 22 (2) 133-156. DOI: 10.4067/S0718-221X2020005000201.

[10] Arriaga F., Llana D.F., Esteban M., Aira J.R., Íñiguez-González G. 2016. Time lag determination on ultrasound wave measurement using different sensors positioning. World Conference on Timber Engineering (WCTE2016). Vienna, Austria.

[11] Aira, J.R. 2013. Experimental and finite element analysis of the stress state in carpentry scarf joints. Doctoral thesis. Universidad Politécnica de Madrid.

[12] UNE 56544:2011. Visual grading of structural sawn timber. Softwood lumber. Asociación Española de Normalización (AEN).

WOODEN CONSTRUCTION OF THE MOVABLE ROOF OF THE GARDEN PAVILION IN ČESKÝ KRUMLOV CASTLE

Jiří BLÁHA, Michal KLOIBER

Institute of Theoretical and Applied Mechanics of the Academy of Sciences of the Czech Republic

ABSTRACT

A remarkable technical monument is situated on one of the garden terraces belonging to the state castle and chateau in Český Krumlov. The umbrella-shaped roof of the lookout pavilion can be lifted about a meter above the masoned parapet allowing the visitor a beautiful view of the World Heritage town panorama when the weather is fine. In windy conditions or in case of heavy rain the roof could be lowered and the pavilion thus closed. The lifting is operated by means of a wooden lever mechanism with a counterweight box hidden in the basement level of the building. The unique construction was built in 1823 and needed to be partially altered in 1830-1835. However, since then it has been preserved in a surprisingly authentic state even allowing practical demonstrations of its original function.

Prior to recent repairs in 2016, a comprehensive non-destructive survey was conducted. The extent of the damage discovered was determined by measuring the speed of elastic wave propagation using stress waves (Fakkop 2D) and measuring the mechanical resistance when drilling with a thin bit using resistance micro-drilling (Resistograph). Another method based on loading timber by means of a miniature loading jack inserted into a drilled hole was selected to determine the current mechanical properties.

KEYWORDS: Lookout pavilion, gazebo, non-destructive testing, roof, timber, wood

INTRODUCTION

Český Krumlov is a charming historical town included in the UNESCO World Heritage List. The combination of rocky spurs, steep slopes and a meandering river gave rise to a medieval castle, which gradually grew into a comfortable chateau closely connected to the town. Already in the 16th century, modifications enhancing the natural and landscape environs of the noble residence became part of the courtly representation related to the lifestyle and political ambitions of the lords of Rosenberg. In the floodplain of the Vltava River and its tributary Polečnice, a game reserve with a pond and an artificial island was created, and in the neighbourhood of the originally medieval Franciscan monastery a Renaissance garden with ornamental plants and bird aviaries appeared. At the opposite end, a formal garden with fountains, rectangular pond and an orangery was created on the terrace in the highest position of the surrounding terrain west of the castle grounds [1]. Inspired by Tuscan Florence, the upper and lower gardens were connected to the castle apartments by covered bridges and corridors passing through the roof spaces of the houses. Such linking allowed for easy and convenient access while offering numerous impressive views of the city and the surrounding hilly countryside [2].

During the construction of the covered connecting bridges, as well as the Baroque theatre building with its still-preserved and functional scenic machinery, atypical wooden structures designed for specific purposes were used, often with innovative structural or functional details. For example, the four-level covered bridge connecting the wing hiding the Masquerade Hall, i.e. the ballroom, with the Chateau Theatre and the Upper Garden gives the impression of another castle wing from the outside, but in fact it is a wooden structure covered with planks and rendered with painted lime plasters. Similarly, a technical mezzanine floor hidden between the two main communication corridors of the bridge enables the condition of the load-bearing wooden elements to be regularly checked [3].

Most of the buildings of the Český Krumlov castle complex are now accessible to its visitors. However, some parts are still waiting to be rediscovered, such as the former Mountain Garden established on a steep slope above the Vltava River around 1800. Here, near the gardener's house, orangery and supply garden, there are two gazebos, both of early 19th-century origin [4]. One of them is the so-called Rindenhaus, a light shelter made of round fir poles and originally covered with sheets of bark. It offered an intimate meeting place, framed by natural scenery, with a wonderful view of the city, the castle and the surrounding countryside. The second lookout place is located 140 m south from there and adjoins a stone masoned storage building partially nestled into the sloping terrain. This gazebo offered impressive views of the town as well. However, unlike the bark house, it could also be used for larger social gatherings. The structure has the form of a large parasol, with a shingle roof supported by a massive central post of octagonal cross-section. Its traditional name Paraplíčko is a Czech diminutive derived from the French word parapluie, meaning literally "a tiny umbrella". The gazebo is notable primarily for its ingenious rocker mechanism, hidden in the basement space, that allowed the entire roof to be raised in a few minutes in good weather and quickly lowered again if necessary, for example during rain. In wintertime, it was possible to leave the roof completely dropped down to the parapet wall height (Fig. 1).

Figure 1: A view of the gazebo with its roof fully lowered, photo Jiří Bláha, 2022.

HISTORICAL CONTEXT

At the beginning of the 19th century the idea of a wooden structure with a vertically sliding roof was not as unusual as it might seem at first glance. Since the Middle Ages, hay or straw barracks with height-adjustable roofs had spread throughout most of Europe and were later also adopted in the USA and Canada [4]. One of the oldest known depictions of such a movable, so-called Dutch, roof comes from the Czech lands (Fig. 2), and is found in the richly illustrated Velislaus Bible from 1325-1349 [5].

Figure 2: Hay barrack with adjustable roof in the Velislaus Bible from 1325-1349, Czech National Library.

A specific group among modifiable shelters facilitating the drying of hay consists of light umbrella-shaped constructions with a single central post. They are still popular mainly in the Netherlands, the supposed country of their origin, where their replicas are still produced both for economic purposes and as garden gazebos (e.g. Pape Hooiberg or Wigink Hooibergen & Gebinten BV). When the plan for the Paraplíčko in Český Krumlov was created two hundred years ago, the author may have possibly been inspired by period study books. A depiction of such a structure (Fig. 3) was available, for example, in the carpentry textbook published by Leopold Leideritz in Dessau in 1801 [6].

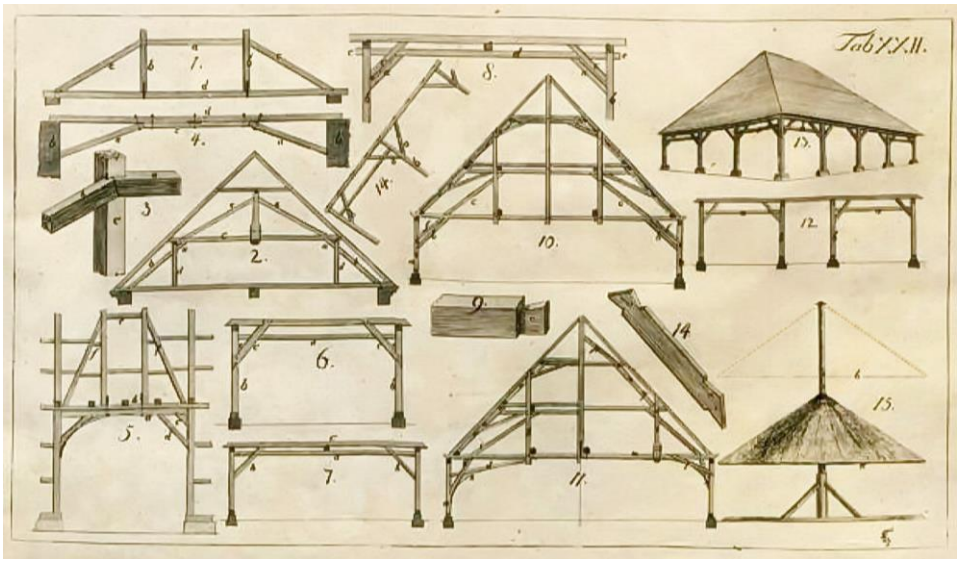

Figure 3: Single pole hay barrack (lower right) in the book by Leopold Leideritz, 1801.

In contrast with the hay barracks, the gazebo roof in Krumlov had to be modified so as to make the process of its extension in the vertical direction smooth and at the same time as fast as possible. For this purpose, a well-balanced rocker-beam system was designed, probably inspired by structures that had sometimes been used to operate large candle chandeliers in churches and palace buildings. The main difference being, that in such cases the rocker structures were located in the roof spaces above the ceilings or vaults. A heavy chandelier would be suspended by a chain to the end of the longer arm of the rocker beam. Then a counterweight, made from a wooden box filled with stones, had to precisely equilibrate the weight of the chandelier, which could then be easily pulled down from below using a wooden rod with hook. After all the candles were lit and it was released again, the chandelier would automatically return to the position above the heads of those present.

According to preserved accounting documents, the roof mechanism of the Paraplíčko gazebo was already in operation in 1824. Six years later, in the fall of 1830, an improvement was proposed, and the lifting mechanism was modified to its present form. Written sources [7] report in detail about this intention. In 1835 at the latest, as evidenced by the date inscribed directly on the structure, the new mechanism was ready to use. At that time, the beams of the rocker arm were shortened and ended with segmental elements integrating a chain system to facilitate the manipulation of the column. The cross profile of the main post supporting the umbrella-shaped roof was modified from the original roughly square one to a hexagonal one, and set to fit into the guiding notch in the securing cross beam. In 2015, when a detailed survey of the condition of the wooden structure was conducted [8], the movable substructure was still almost completely authentic, only the roof of the gazebo and the upper part of the main post had come from a repair carried out in the late 1980s.

Figure 4: Lifting mechanism in lowered position. Hinge of the principal post in foreground, counterweight box in the background, photo Jiří Bláha, 2022.

SURVEY RESULTS

The gazebo is located in the southern part of the storage area of the supply garden. The diameter of the roof is 6.8 m, the total height of the umbrella is approx. 9 m, and the lifting height is 0.8 m. The roof is conical with a covering of wooden shingles. The timber structure of the umbrella consists of a central post and rafters anchored at the top. The rafters are supported by struts leaning into the main post, which passes through the floor of the gazebo to the lower floor, where the entire lifting device is located.

The lifting is enabled by a lever mechanism consisting of a rocker with a counterweight (Fig. 4) hidden in a vaulted room situated partially below ground level. The lever mechanism of the rocker consists of two beams 6.6 m long: the southern beam with a cross-section of 160×210 mm and the northern beam 160×200 mm. The pivot point of the rocker arm is at approximately 1/4 of the length of the beams. It is fitted with metal pins which are placed in metal beds fixed to the vertical posts of the main supporting frame, thus eliminating friction in the lever mechanism. The posts of the frame have a cross-section of 210×240 mm and are tenoned into a transverse threshold beam. Their upper ends were originally connected with the vaulted arch using saddles made of massive wooden beams. At the time of the survey, the entire frame had dropped by several centimetres, and the cross bars had lost their function, thus rendering the lifting mechanism unstable.

Attached to the longer arm of the rocker there is a massive wooden box, into which stones are put. Near the rear end of the rocker beams there is a guiding frame which consists of two oak posts used to lock the lever mechanism in position. At the opposite end there is a circular pit into which the main post of the gazebo roof is lowered. There the transmission of force between the rocker and the post is secured by segmentally shaped guiding elements and chain hinges that help to keep the post in an upright position (Fig. 4 and 5). Maintenance of the vertical orientation during lifting is also aided by a notch in the beam set transversely on the upper edge of the circular pit. Another guiding point is the hole through which the main post passes through the gazebo floor.

Figure 5: Bottom view of hinge at the lower end of the main post guided by the notch in the transverse beam, photo Jiří Bláha, 2015.

The assessment of the actual condition of the roof lifting mechanism was focused on evaluating the condition of the individual wooden elements by direct and indirect visual observation using an endoscope and, above all, on measurements using a drilling resistance tool (Resistograph). In order to determine the mechanical properties of the wood, two instruments developed at ITAM for the needs of on-site surveys were used [8], [9]. They enable the measuring of material resistance along the grain in a drilled hole (Loading Jack) and against the grain when pushing in a calibrated pin (Pin Pushing). For selected elements, the survey was supplemented by measuring the speed of propagation of elastic waves through the material (Stress Wave).

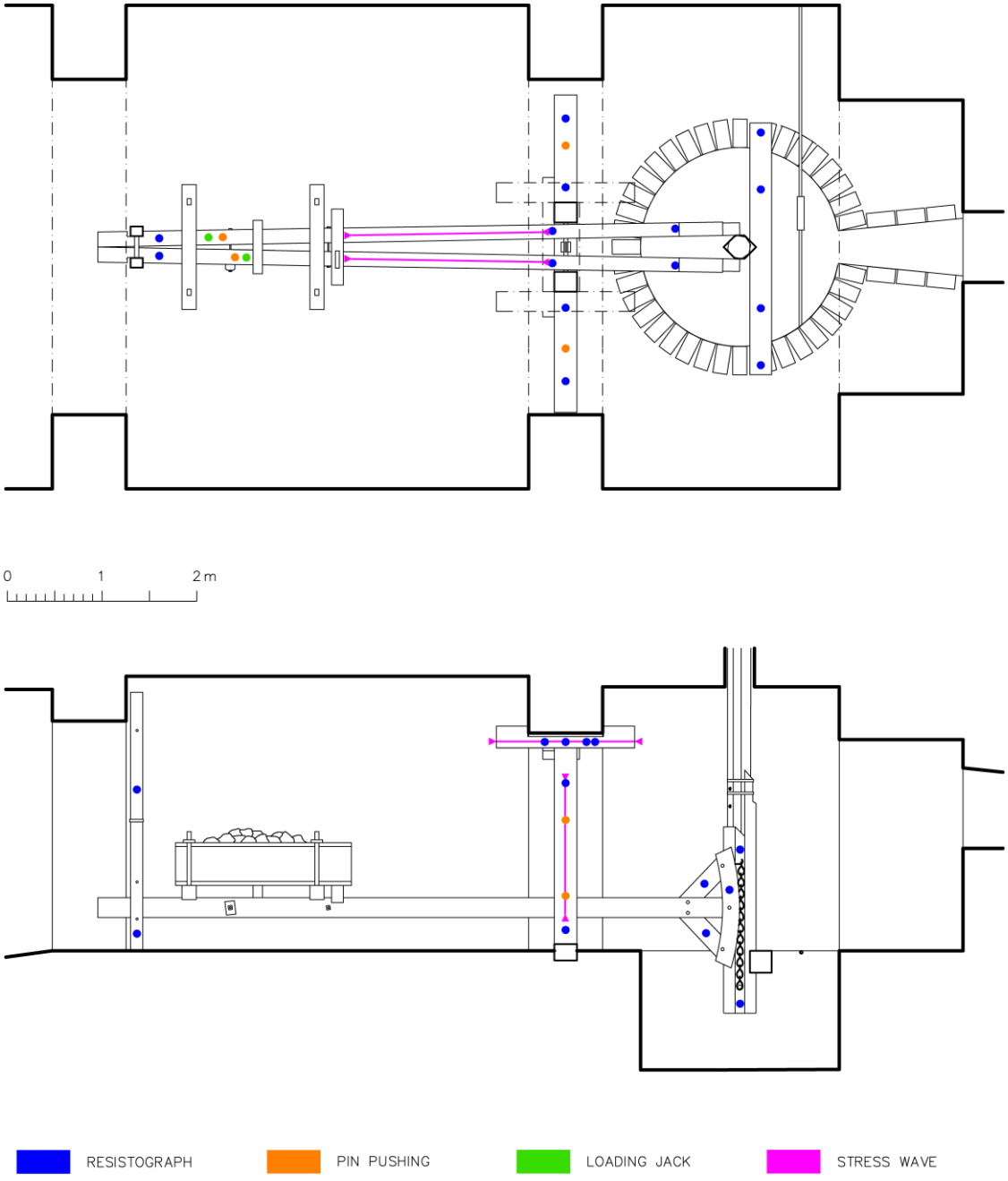

Figure 6: Layout and side view with localisation of the testing methods used, Michal Kloiber, Jaroslav Buzek.

Based on the results of the survey, it was deemed that operating the roof lifting mechanism is possible, consistent with the purpose for which the structure was designed. However, when raising and lowering the roof, the presence of people in the upper space of the gazebo should be avoided. In both extreme positions of the roof, supporting the main post with a wooden block (as can be seen in Fig. 5) could limit the long-term adverse stress to the hinge and lever arms. A new threshold beam made of oak wood without sapwood was proposed in order to ensure the durability of this element placed in direct contact with the floor, i.e. in an environment with increased humidity. Replacing both saddles in the heads of the main stabilization frame posts was also recommended, which would allow for a restoration of the original interaction with the vaulted ceiling.

CONCLUSION

Experiences gained in the case of the Český Krumlov gazebo survey can perhaps be generalized. The uniqueness and significance of the investigated technical monument, as well as its relatively small size, allowed for the utilization of state-of-the-art semi-invasive diagnostic instruments which enabled the assessment of almost all the preserved structural elements. Convenient access to all of the elements facilitated testing, and will enable monitoring of the technical condition of the lifting mechanism in the future. The logical intention to maintain and guarantee its safe functionality, however, requires the replacement of some particular components, as reflected in the range of recommended interventions. Though, in order to conserve their historical source value, it is advantageous to deposit any original dismantled elements directly in the restored building, as this allows them to be used in further research, e.g. in traceological analyses, as well as to serve as models for future faithful copies.

REFERENCES

[1] J. Olšan, Zahrady v obrazu města a krajiny Českého Krumlova, in: M. Gaži (Ed.), Český Krumlov: Od rezidenčního města k památce světového kulturního dědictví, NPÚ ÚOP, České Budějovice 2010, pp. 231–290.
[2] J. Bláha, Českokrumlovské kryté chodby, Spojení rezidence, zahrad, Latránu a Nového Města, in: M. Gaži (Ed.), Český Krumlov: Od rezidenčního města k památce světového kulturního dědictví, NPÚ ÚOP, České Budějovice 2010, pp. 191–216.
[3] J. Bláha, The Cloak Bridge in Český Krumlov – construction history research, in: Conference Proceedings, ICTB 3rd International Conference on Timber Bridges, Skellefteå 2017, pp. 296–301.
[4] J. Špulerová et al., Past, Present and Future of Hay-making Structures in Europe, Sustainability 2019, 11(20), 5581.
[5] Velislaus Bible, Czech National Library, sign. XXIII.C.124 (Facsimile Praha : Archa 90, 2007), fol. 43v
[6] L. Leideritz, Ausführliche Anleitung zur Zimmerkunst in allen ihren Theilen, Dessau 1801, Table XXII, Fig. 15.
[7] State Regional Archive Třeboň, Dept. Č. Krumlov, Č. Krumlov Estate, sign. I^{A} 6G.$^{\alpha}$ 3a, pp. 371–388.
[8] M. Kloiber, J. Bláha, J. Buzek, Posouzení stavu a měření mechanických vlastností dřevěné konstrukce zdvihu Paraplíčka, zámek Český Krumlov, p. č. 654/1 v k. ú. Český Krumlov, Scientific report ITAM AS CR Telč 2015, 51 p.
[9] M. Drdácký, M. Kloiber, In-situ compression stress-deformation measurements along the timber depth profile, Advanced Materials Research 778, 2013, pp. 209–216.
[10] M. Kloiber, M., Drdácký, M., Tippner, J. Hrivnák, Conventional compressive strength parallel to the grain and mechanical resistance of wood against pin penetration and microdrilling established by in-situ semidestructive devices, Materials and Structures 48 (10), 2015, pp. 3217–3229.

THE TIMBER ROOF OF THE CHURCH OF SANT'AGOSTINO IN CREMONA

Angelo G. LANDI[1] and Emanuele ZAMPERINI[2]

[1] DAStU, Politecnico di Milano, Milan, Italy

[2] DIDA, Università di Firenze, Florence, Italy

ABSTRACT

The current church of Sant'Agostino dates back almost entirely to the 14th century (1340-1370 ca.) and has a three-aisles structure built in two distinct construction phases. Originally it had vaults covering the presbytery alone, while the aisles had an exposed wooden roof; between 1553 and 1559 the interior of the church was renovated, creating the vaults to cover the three aisles, thus hiding the timber roof from sight. The original roof was intended to be seen from inside the church and it is still well preserved in the nave and southern aisle; it presented interesting construction features and some simple polychrome decorations, still preserved in a few elements. On the basis of a careful dimensional, geometric, material and constructional survey, the article will describe in detail the constructive characteristics of the interesting fourteenth-century structure.

KEYWORDS: Church of Sant'Agostino in Cremona, medieval timber roofs, timber trusses, closed-joint trusses, painted timber structures.

INTRODUCTION

The presence of a group of Hermit friars in Cremona has been documented since 1249, and from 1260 they began some targeted purchases of buildings in the city, in order to have an area for the construction of a convent [1, 2]. Thus, a first church dedicated to Saint Augustine was built in Cremona by the Hermit friars in the second half of the 13th century (1262-1270 ca.) [3-4]. Having increased the number of friars and the needs of preaching, after less than a century, the Hermit friars decided to expand the church [3]. Therefore, the church was rebuilt in the 14th century (1340-1370 ca.) with a three-aisles structure [4] in two distinct construction phases, as can be seen from the external cornices and from some details of the roof structures, as well as from the construction joint in the walls. Originally the new church had vaults covering the presbytery alone, while the nave and the aisles had an exposed wooden roof. Starting from the late 14th century various chapels were attached to the southern aisle of the church [1, 5]. Between 1553 and 1559 the interior of the church was renovated, covering the three aisles with vaults and hiding the timber roof from sight [3-4]. In the following centuries the roof of the church was subject to numerous modifications, however, the timber structure of the nave and of the southern aisle is still almost entirely preserved. The construction and the building reforms of the church reveal a period of economic prosperity in the city, where mercantile activity with other European regions ensured prosperity and cultural exchanges. The rich medieval heritage – above all churches and palaces – is fixed graphically in the plan by A. Campi [6]: the refined construction techniques (i.e. wooden or masonry structures) and the artistic works still constitute a precious testimony, only partially investigated, despite being widely preserved.

METHODOLOGY

During the study of the church, a careful bibliographic research and the examination of archival documents relating to the two most recent centuries were carried out. A careful geometric and dimensional survey of the timber roof and of the masonry structure in the attic, compared with the traditional units of measurement of the Cremona area (the Cremonese arm – *braccio* – is 48,353 cm, and it's divided into twelve ounces about 4,04 cm each), made it possible to hypothesize some geometric-proportional rules for the definition of the dimensions and distances between the construction elements. This survey made it possible also to identify the presence of two distinct construction phases, a fact that wasn't clear in the archival documentation cited in the historical studies on the church.

RESULTS AND DISCUSSION

The original timber roof was intended to be seen from inside the church and presented interesting construction features and some simple polychrome decorations, still preserved in a few elements. The wood species used in the roof are oak for trusses, rafters, and purlins, fir or spruce for the boards, and probably poplar for the laths.

Figure 1: Aerial photo of the church (source: AEGEA 2015, www.geoportale.regione.lombardia.it).

Figure 2: Photomosaic of the southern side of the church.

The roof of the nave has twenty-three king post closed-joint trusses [7], fourteen belonging to the first phase, nine to the second, whose span is quite irregular 10-10.15 m. The centre-to-centre distance of the trusses of the first phase (T04-T17) is rather irregular, since it varies between about 220 and about 236 cm, without an apparent connection with the ancient local measures; instead the net distance between the trusses corresponds almost exactly to regular measures (four Cremonese arms plus 1 to 4 ounces). The trusses of the second phase (T18-T26) are instead arranged at a much more regular distance, equal to about 240 cm (i.e. five Cremonese arms). From the point of view of the relationship with the wall structure, it can be noted that the first construction phase corresponds to four spans of the underlying arches; in correspondence with the second and fourth pair of pillars there are trusses and in the intermediate spaces the other trusses are arranged in a regular way, so that it can be said that the structure can be substantially divided into two modules with two spans each. In the second construction phase, three spans of arches were built, and the position of the trusses has no relationship with the position of the pillars.

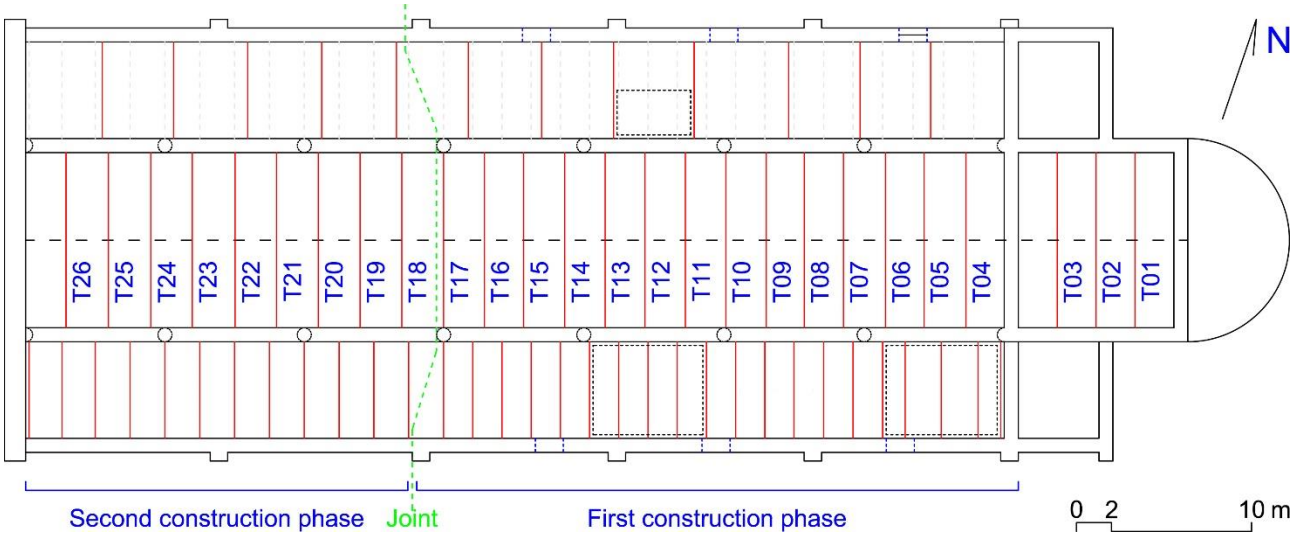

Figure 3: Planimetric scheme of the principal frame of the roof.

The trusses support a pentagonal ridge beam and six closely spaced purlins for each pitch. The centre to centre distance of the purlins is particularly precise: about 96÷97 cm (i.e. two Cremonese arms) between the first and the second purlin from the eaves and between the sixth and the ridge beam; about 84÷86 cm (i.e. one Cremonese arms and nine ounces, that is one arm and ¾) between all the other. Almost all the purlins are original and still have the notches for housing of the laths intended to hide the joints between the large boards (ca. 40 cm, ten ounces) of the roof.

The boards are still largely preserved, although partly repositioned during a past renovation; very few are the laths preserved, however the interest in them is considerable, since they retain the original polychrome decoration, giving us a hint as to what the roof might look like originally.

The arrangement of the purlins is particularly interesting; if we exclude some isolated cases, the purlins are arranged with a very clear pattern, different between the first and second phase, suggesting that in the two phases the builders focused their attention on different technical and construction problems.

In the first phase starting from the presbytery there is a first set of purlins which develops continuously over two spans; subsequently there are four more set of purlins that develop over three spans each. The arrangement of the ridge beams is different: starting from the presbytery there are four beams on three spans each, ending with one beam on two spans; in this way the joints of the purlins and those of the ridge beams do not fall on the same truss. In the second construction phase, instead, all the purlins and the ridge beams are developed on two spans; in this way the discontinuities are all aligned and there are trusses that support only intermediate joints alternating with trusses that support only end joints. The structure is less stable and less interlinked, but easier to build.

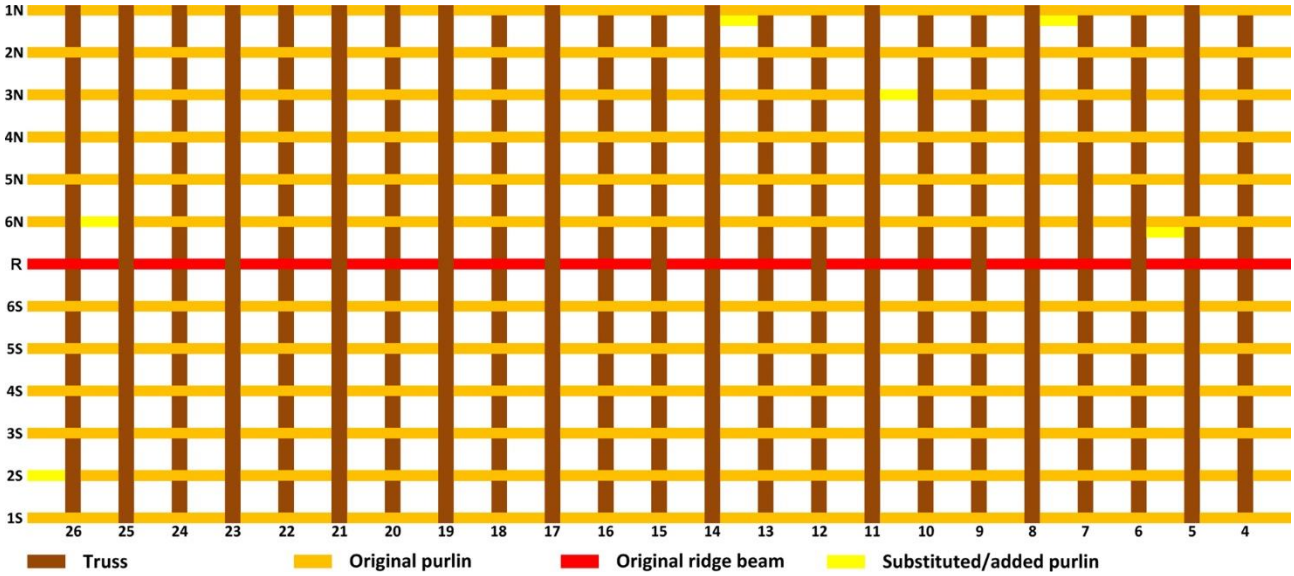

Figure 4: Planimetric scheme of the purlins of the roof of the nave.

Other differences between the first and second construction phases can be found in the relationship between trusses and masonry. All the trusses of the nave rest on brick masonry corbels. In the first phase, immediately below the tie-beams of the trusses there is a plate beam, placed at the internal edge of the masonry, which interrupts the continuity between the wall and the corbel; due to this lack of connection, many corbels are damaged. In the second phase no plate beam is visible and perhaps they are moved inwards in the masonry to prevent the strength reduction in the corbels. On the other hand, there don't seem to be obvious constructive differences between the trusses of the two phases.
The trusses of both phases have peculiar constructive characteristics: the rafters – inclined about 23.5° on the horizontal – have a rectangular section, with the longer side arranged horizontally (ca. 24 cm × 18 cm), as well as the struts, which are substantially thick boards, large as the rafters (ca. 24 cm × 12 cm), to which they are connected with a deep notch. As for the king post, the closed joint with the tie beam does not present specific particularities with respect to the construction context of the low Po Valley: the king post has half-dovetail tenon which enter the mortise made in the tie beam to which it's fixed with a wooden wedge. The most characteristic aspect, instead, is that – in the part between its connection to the rafters and to the struts – the king post keeps the section reduced by the connection (ca. 24 cm × 14 cm).

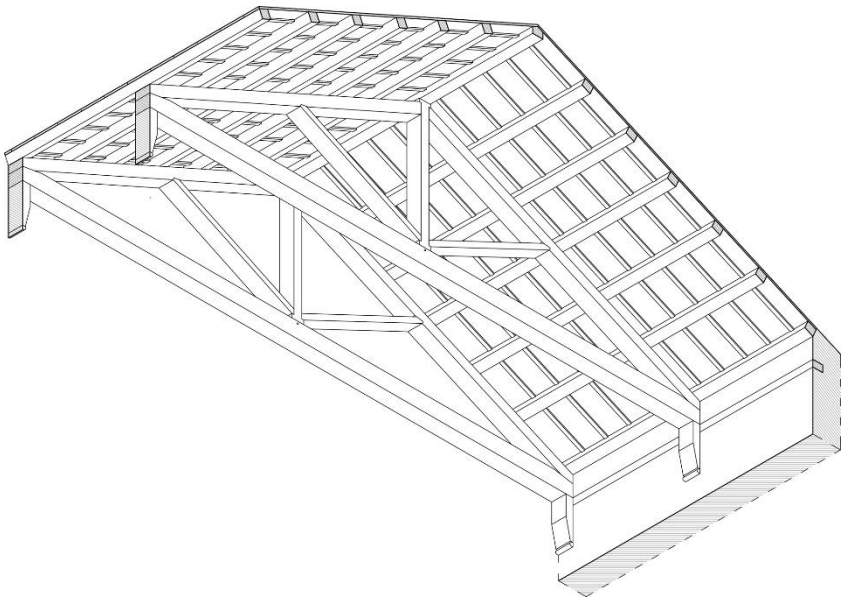

Figure 5: Hypothetical reconstruction of the roof of the church in the 14th century and photo of a painted lath.

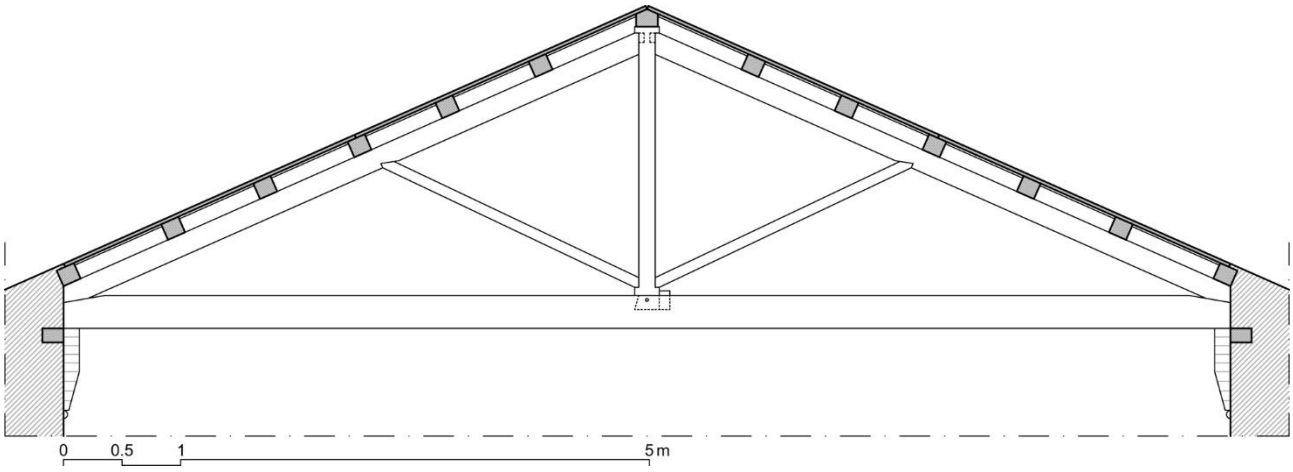

Figure 6: Geometric scheme of trusses of T17.

Figure 7: On the left, roof of the nave; on the right view of the southern aisle attic.

The roof of the southern aisle has thirty-two rafters placed at a small distance (ca. 170 cm, three Cremonese arms and a half, in the first construction phase; 195 cm, four Cremonese arms, in the second), supporting six rows of purlins with notches for the polychrome laths, also in this case still preserved in some specimens. In two areas, the roof of the south aisle was lowered when the vaults were built, to allow light to enter the nave through large semi-circular windows specially opened in the wall that separate the nave from the aisle. As for the rafters of the southern aisle, the relationship with the masonry in the first and second construction phases is different from that of the trusses of the nave. The rafters of the first phase were arranged at an almost uniform spacing, but completely indifferent to the position of the pillars of the nave; instead in the second phase there is a rafter in correspondence of each pillar and three intermediate rafters.

The roof of the northern aisle has been completely renovated in 1938 [8]. The new rafters are twelve, more spaced (ca. 420 cm) and bigger than in the original roof, they support a single central purlin, on which the joists rest; a layer of hollow flat bricks – "Excelsior" model of the Frazzi brick production industries of Cremona (60 cm × 25 cm × 4 cm) – is supported by the joists [8]. However, the traces left in the masonry by the original rafters after their removal allow to reconstruct the scheme of the original roof that was similar to that of the southern aisle.
A careful analysis of the construction details and the assembly marks of the trusses – the description of which is deferred to other forthcoming publications – can allow to draw some interesting conclusions on the teams of carpenters active in the construction of the roof in question and – in a comparative way – of other contemporary roofs in the city of Cremona (e.g. the church of San Luca).

CONCLUSION

The detailed and careful dimensional, geometric, and constructional survey of the roof of the church of Sant'Agostino allowed to recognize a series of metric and modular rules used by the builders of the interesting fourteenth-century structure, as well as to describe in detail its constructive characteristics. From these analyses the presence of two distinct construction phases – not previously described in the bibliographical references relating to the church – clearly emerges.
Another aspect that emerges clearly is the fact that the builders active in the second phase – while keeping the concept and above all the general appearance of the roof unchanged – have modified some aspects of the structural organization (especially as regards the purlins) and above all adopted a different and more regular metric organization of the wooden members.
The research presented in this paper demonstrates that a careful constructive and metric study of the roof structures allows to identify significant changes in the conception of an architectural work, also with reference to the workers active in the construction of the building. The data collected in the church of Sant'Agostino will also allow to develop further insights into construction techniques and workers specialized in the construction of large-spans roofs, between the 13th and 15th centuries in Cremona and, more generally, in the territory of the Po Valley.

REFERENCES

[1] E. Filippini, Gli ordini religiosi tra vita ecclesiastica e impegno caritativo nel secolo XIV, in: G. Andenna, G. Chittolini (Eds.), Storia di Cremona. Il Trecento, chiesa e cultura (VIII – XIV secolo), Bolis edizioni, Azzano San Paolo, 2007, pp. 170-195.

[2] E. Chittò, Note per la storia del convento di Sant'Agostino di Cremona e i rapporti con l'Osservanza di Lombardia, Insula Fulcheria 43 (2013) 163-182.

[3] P. Merula, Santuario di Cremona, Bartolomeo, & Heredi di Baruccino Zanni, Cremona, 1627.

[4] G. Voltini, L'architettura: spazi geometrizzanti e paramenti murari policromi, in: G. Andenna, G. Chittolini (Eds.), Storia di Cremona. Il Trecento, chiesa e cultura (VIII – XIV secolo), Bolis edizioni, Azzano San Paolo, 2007, pp. 394-415.

[5] G. Picenardi, Nuova guida di Cremona per gli amatori dell'arti del disegno, Giuseppe Feraboli, Cremona, 1820.

[6] A. Campi, Cremona fedelissima città et nobilissima colonia de Romani [...], in casa dell'auttore, per Hippolito Tromba, & Hercoliano Bartoli, Cremona, 1585.

[7] E. Zamperini, Timber trusses in Italy: the progressive prevailing of open-joint over closed-joint trusses, in: B. Bowen, D. Friedman, T. Leslie, J. Ochsendorf (Eds.) Proceedings of the fifth International Congress on Construction History. Volume 3, Construction History Society of America, Chicago, pp. 629-636.

[8] Archivio Storico Diocesano Cremona, Archivio Parrocchiale di Sant'Agostino, Consuntivi, 1939.

SHATIS 22

6th International Conference on Structural
Health Assessment of Timber Structures
7-9 September 2022, Prague

EARLY MODERN CARPENTRY IN POLAND. A CASE STUDY OF THE ROOF STRUCTURES OVER THE BURGHER HOUSE AT 6 MOSTOWA STREET IN TORUŃ

ULRICH SCHAAF[1] and MACIEJ PRARAT[1]

[1]Faculty of Fine Arts, Nicolaus Copernicus University in Toruń

ABSTRACT

Toruń is a city in Poland where most of the medieval and early modern roof structures, so far only initially examined, have survived. This case study focuses on the architectural research of two selected structures over the building complex at 6 Mostowa Street. At the centre of the analysis are questions about their original construction and later transformations. The research shows that one of them is a king strut structure, while the other is a collar beam structure, both of similar dimensions. They come from the mid-16th century, but were repaired in the 17th century. They are constructed with the use of cogged, tenon, and lap joints, with the latter being dominant. During their framing, simple carpenter's bar marks, triangular and round marks, made with sanguine, styluses, or chisels and axes were used. The structures were made of pine wood, transported by rafts from a distance of about 200 km. Whole trees worked with an axe and an adze were mostly used, and to a lesser extent, quarter-trees obtained by further dividing them with a handsaw. According to the current state of research, these structures do not stand out against the background of the development of roof structures in Toruń. The only exception is assembly marks made with sanguine and partially fulfilling the function of matchmarks. Their analysis and dating have significantly clarified the history of the house itself.

KEYWORDS: Toruń, roof construction, carpentry art, architectural investigation

INTRODUCTION

Toruń, a city inscribed on the UNESCO World Heritage List, is the place where the largest number of historic roof structures over town houses in Poland has survived. They come from the Middle Ages (14th-15th centuries) and the modern period (16th-18th centuries). So far, they have only been studied typologically [1]. The purpose of this text is to present the results of the architectural research on two previously unrecognised structures in the building complex at 6 Mostowa Street (Fig.1). It is one of the most interesting examples of bourgeois architecture in Toruń [2]. The results of the analysis of these structures, taking into account the carpentry workshop, will be contrasted both with the history of the buildings themselves and against the broader background of the development of mediaeval and modern city roof structures in Toruń.

METHODOLOGY

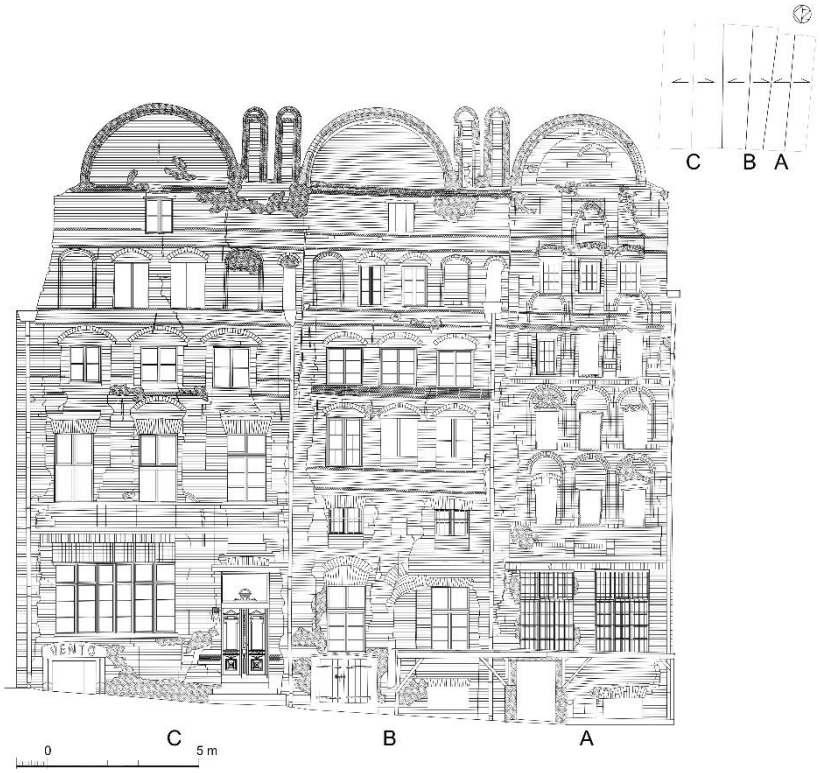

Fig. 1. Toruń, 6 Mostowa Street. The front elevation of buildings A, B and C (compiled by U. Schaaf, M. Prarat).

Before commencing comprehensive research on the entire complex, a detailed measurement and drawing inventory was made with the use of geodetic devices [3]. The roof structures are presented in top views as well as in transverse and longitudinal cross-sections. Architectural research was performed on this basis. The analysis consisted in the characteristics of the construction system, the side of the timber framing, the system of carpentry assembly marks and joints, and the size of the building material and its processing. The relationship of the outer trusses with brick gables was also analysed. On the basis of this diagnosis, complexes were qualified for dendrochronological examinations, which were performed by Tomasz Ważny. At the same time, a source query was conducted to supplement the information on the transformations of this complex.

RESULTS

The structure above the C burgher house – northern

The roof structure over the C burgher house is a king post structure with a king strut appearing only in every second or third truss. It consists entirely of 16 trusses (Fig. 2). It is 17.3 m long, has a span of 7.85 m and an angle of inclination of 60°. The king strut itself extends to the ridge, but does not bind to the rafters. It is hung from only two collars and one pair of braces. An additional transverse stiffener was originally a pair of down braces, the existence of which is evidenced by recesses for lap joints in each king strut. The frame, which stiffens the structure in the longitudinal direction, consists of king struts, spandrel beams stretched between them, and braces on two levels.

The lack of the original tie beams prevented the recognition of their connection to rafters, but it can be assumed that it was a tenon joint. The following elements were used to connect the remaining structural elements with each other: a straight pegged lap joint to connect rafters in the ridge and collars with king strut, a stopped single dovetail lap joint at the connection of: collars with rafters, braces with king struts, collars with spandrel beams, and tenon joints at the connection of spandrel beams with king struts.

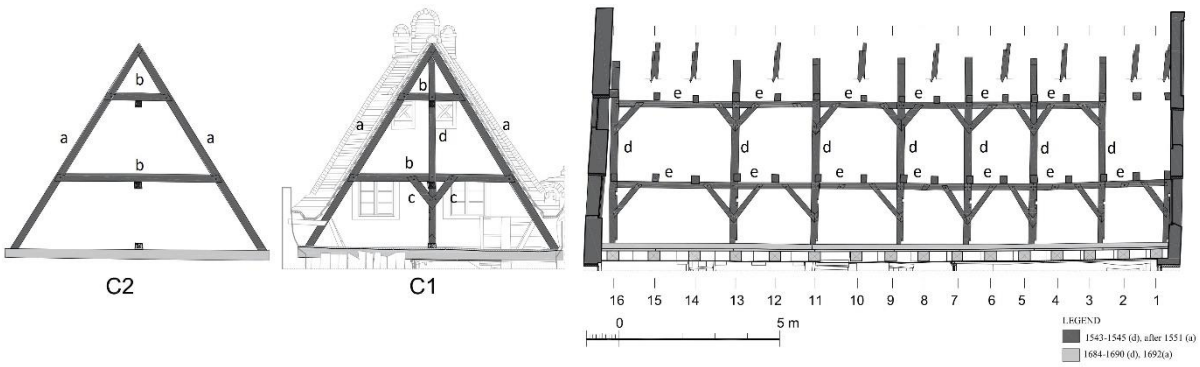

Fig. 2. Toruń, 6 Mostowa Street. Roof structure of building C. Longitudinal and transverse cross-sections: C - principal rafter trusses; C1 - paired common rafter; a – rafter, b – collar, c – brace; d – king struts; e – spanderal beam (compiled by U. Schaaf, M. Prarat).

Carpentry assembly marks were made with either a carpenter's adze or sanguine. Owing to the repeated whitewashing of the construction, the last characters were only partially recognised in a fragmented manner. Nevertheless, the whole system can be generally characterized: the individual trusses are generally marked with sanguine from west to east, from 1 to 16. On the left rafters, round marks were used, and on the right rafters - bar marks. The latter extend partially through the whole joint (Fig. 3), so they simultaneously fulfil the function of so-called matchmarks (in German "Passzeichen"). The king struts from west to east were marked separately, from 1 to 8, with an increasing number of Xs, made with either a carpenter's adze or sanguine.

Fig. 3. Toruń, 6 Mostowa Street. Roof structure of building C. A carpenter's assembly mark made with a sanguine (Photo by U. Schaaf).

Pine wood was used for the construction of the structure. The individual types of elements have similar cross-sections and are made of a whole tree, pre-treated with an axe and then smoothed with an adze. Only the lower braces of the longitudinal frame have a smaller cross-section and are made of cross wood obtained by dividing the entire material with a handsaw. Typical traces of transporting the logs by raft (Fig. 4) prove that timber was transported by water. This conclusion is confirmed by dendrochronological studies, according to which the timber was floated down the Drwęca River from Warmia to Toruń, i.e. at a distance of approximately 200 kilometres.

Fig. 4. Toruń, 6 Mostowa Street. Roof structure of building C. Traces of raft floating of the building material (Photo by U. Schaaf).

Architectural research has shown that the roof structure has largely survived to modern times, but not without changes. The secondary origin of the beams is indicated only by the butted connection of the rafters with the tie beams secured with nails and the lack of mortises from down braces in those beams. Together with the replacement of the tie beams, the ground plate was also inserted into the king strut frame. In addition, some braces and the upper fragment of the king strut in the full truss were removed, as evidenced by the empty joint mortises and recesses for laps.

Dendrochronological research has made it possible to determine the date of the felling of trees for the construction of the roof structure in the years 1543-1545. The historical study shows, however, that the structure was not made until 1551, when all the buildings were purchased by one owner. Only then were semi-circular gables made over the buildings. The replacement of the tie beams and the introduction of the ground plate took place only at the end of the 17th century.

Fig. 5. Toruń, 6 Mostowa Street. Roof structure of building B. Longitudinal and transverse cross-sections (compiled by U. Schaaf, M. Prarat).

The roof structure above the B burgher house – central

The roof construction over burgher house B is a two-collar beam roof consisting of 15 identical trusses (Fig. 5). It is 18.2 m long, has a span of 7.46 m and an angle of inclination of 60°. The tie beams rest on the wall plates. The longitudinal stiffening of the roof structure is provided only by wind braces in both roof hips, which run diagonally each time through several rafters. The following carpentry joints were used to connect the individual elements to each other: a middle

notch when connecting the wall plate with the tie beams, a barefaced tenon joint when joining the rafters with the tie beams, a straight lap joint when connecting the rafters in the ridge, and a stopped single dovetail lap joint when connecting collar beams with rafters (Fig. 6).
During timber framing, the structural elements of individual trusses were marked with triangular cuts on the left and simple bar marks on the right (Fig. 6). Their number increases from west to east from 1 to 15. In this way, each element was assigned a specific place in the spatial structural system. The triangular signs were made with a stylus and a chisel, and the bar marks were made with a stylus and a hand adze.

Fig. 6. Toruń, 6 Mostowa Street. Roof structure of building B. The connection of the rafter with a collar by means of a single dovetail lap joint (Photo by U. Schaaf).

Despite some differences in cross-sections between individual types of elements, only the whole pine tree was used to build a collar beam roof. Such a tree was obtained by pre-treating the logs with an axe, and then smoothing them with an adze. The typical traces of log transport by the raft prove that the wood was transported by water, and the dendrochronological research shows again that the wood comes from Warmia. The analysis of the structure has made it possible to recognise, not only the primary, but also secondary elements: introducing an additional reinforcing beam next to most of the tie beams; some ends of the rafters on the southern side were replaced and all the trusses on this side were reinforced with a down brace.
Dendrochronological research has proved that the timber for its construction was felled in the winter of 1546/1547. The historical study shows, however, that the structure was made only after 1551 together with the C structure over the northern burgher house. Only then were semicircular gables made over the entirety. Strengthening with additional down braces took place only in the 1640s, and with additional ceiling beams in the 1660s.

CONCLUSIONS AND OUTLOOK

Architectural research has made it possible to determine the building technique used both for the construction of both examined roof structures and their subsequent transformations.
The types of roof structures used are not innovative compared to the secular architecture of Toruń. Collar beam roofs, including two-collar ones, have been known since the Middle Ages and have been common throughout the modern period. King strut structures distinguishing between principal rafter trusses and paired common rafters have been present in church architecture since the beginning of the 14th century [4], and the oldest known examples in the secular architecture of Toruń come from the end of the 15th or the beginning of the 16th centuries [1]. Also, the

carpentry joints used do not differ from those used in older or simultaneously erected roof structures. It was only later that lap joints were replaced with lap tenon joints. The system of carpentry assembly marks consisting in adding simple bar, triangular or other marks is typical. On the other hand, marking them with a sanguine and drawing them partially through the entire joint as matchmarks is a solution unknown to date in the wooden constructions of Toruń of that period. The use of a whole pine tree, processed with an axe and an adze, and partially divided with a handsaw, is part of the traditional construction technique [5].
To sum up, it should be stated that in the roof structures used in the construction of 6 Mostowa Street, technical solutions are in the canon of medieval and early modern carpentry art in Toruń - with the exception of carpentry assembly signs. Their analysis was very important in the context of the history of the building itself.

ACKNOWLEDGEMENT

Initial examinations of the roof structures at 6 Mostowa Street in Toruń were made during student practice. The authors of the article thank the following students: N. Czaplicka, J. Hrycalik, A. Lipińska, M. Rogalewska, Ł. Szplit, and K. Śmiejczak. The deepening of the research and its presentation on a wider background was possible thanks to the grant from the National Science Centre of the OPUS 2018 competition, grant numbers: 2019/35/B/HS2/02302, project: Carpentry craft and the development of secular construction in the Old and New Town of Toruń from the Middle Ages until the end of the 18th century in the light of interdisciplinary research on roof trusses.

REFERENCES

[1] Tajchman J, Ze studiów nad więźbami storczykowymi Torunia. Acta Universitatis Nicolai Copernici, Zabytkoznawstwo i Konserwatorstwo 1989;176:191-206.

[2] Prarat M, Średniowieczne przekształcenia zespołu trzech budynków przy ul. Mostowej 6 w Toruniu. Ochrona Zabytków 2018;2:9-33.

[3] Prarat M, Wykorzystanie tachimetrii i fotogrametrii w dokumentacji zabytków architektury na przykładzie inwentaryzacji pomiarowo-rysunkowej wybranych kamienic toruńskich. Acta Universitatis Nicolai Copernici. Zabytkoznawstwo i Konserwatorstwo 2015; 46: 509-531.

[4] Schaaf U, Prarat M, Badania architektoniczne więźby nad nawą środkową kościoła Świętojańskiego w Toruniu oraz ich znaczenie dla historii budowlanej i średniowiecznego warsztatu ciesielskiego świątyni. In: Katarzyna Kluczwajd editor. Kościół Świętojański w Toruniu – nowe rozpoznanie. Toruń: Stowarzyszenie Historyków Sztuki; 2015: 125-153.

[5] Schaaf U, Prarat M, Wood as a building material in Toruń. A contribution to research on medieval carpentry art of Northern Poland. In: Mascarenhas-Mateus J, Paula-Pires A, editors. *History of construction cultures*, London: Taylor&Francis Group; 2021; 1: 643-649.

FOLLOWING THE STANDARDS, FOLLOWING THE STRUCTURES – THE CASE OF LOUHISAARI CASTLE MID 17TH CENTURY ROOF STRUCTURES

P. SAARINEN[1], M. HUTTUNEN[1], L. LAINE[1] and P. SAVOLAINEN[1]

[1] Aalto University, Helsinki

Figure 1: Timber roof structures of Louhisaari Castle. Photo: Panu Savolainen.

ABSTRACT

This article examines the assessment of Louhisaari Castle roof structures in southwestern Finland. We examine the practical implementation of an EU Standard [1] of the assessment of historical timber structures that was used in the research of the structures from 2017 to 2021, and also widely tested in university fieldwork courses organized in 2017 and 2021 [2].

Our article engages the assessment carried on and remarks on the fieldworks when the standard is used in practice. We conclude with critical remarks of the relevance of the standard in the fieldworks of the assessment of historical timber structures. Furthermore, we explore in brief the results of the assessment.

Our article examines the methods used in the study of the roof structure of Louhisaari Castle, the utilization of interdisciplinary university cooperation, and the experience we have gained in using the EU standard as a guideline for such research and cooperation. Finally, we briefly evaluate the project as a whole: what significance it has for the preservation and restoration of the roof structure and for the training of emerging professionals.

KEYWORDS: on-site assessment, timber roof structure, restoration, architectural conservation, training, 17th century, Finland

Figure 2: Louhisaari Castle (built 1654–1658).

INTRODUCTION AND BACKGROUND

Louhisaari Castle is one of the rare 17th century high nobility manors in Finland. The builder of the castle, Herman Fleming, was one of the most important political figures of the 17th century Sweden, who commissioned the building of the castle according to examples from Stockholm. Construction of the castle began in 1654 and the building was completed in 1658. [3] In the 17th century, Finland belonged to the Kingdom of Sweden.

The value of the building in Finland stems from its architectural exceptionality and historical importance, but also from its roof structure. The structure is exceptional of its constructional principles compared to trussed rafter roof that have been in use in large roof structures in Finland from the Middle Ages to the 20th century. Compared to the prevailing rafter structure the roof structure of Louhisaari Castle is remarkably rigid and the method and order of construction is rare in Finland. Besides Louhisaari Castle, only two other roof structures of the same principle are known to exist in Finland, both in churches in the surrounding area of Louhisaari.

Today, the roof structures of the castle, preserved in their original state over 360 years, form the one of the most valuable entirely preserved timber structures from the 17th century Sweden. The castle's original top of wall and wooden eave structure is probably the only or one of the only ones that have survived in its original state from the era in Sweden. The castle is a state-owned museum since 1961.

The roof structure has never been studied in detail before the work carried out by the current project running from 2017 by Livady Architects and university courses. The goal of the on-going study and courses is to find the optimal way to preserve the full authenticity and load-bearing function of the structure. [2] The only previous studies were dendrochronological datings from late 1990s, which were done to date the construction of the castle accurately.

A special course on architectural conservation *Traditional roof structures in Finland* was organized jointly by *Senate* Properties (The largest property and real estate owner of the state of Finland), the Finnish Heritage Agency and Aalto University (Helsinki) in 2017 and 2021. In 2017, the assignment of the course was restoration of the roof structure of the south-eastern annex of the castle and partially the roof of the main building. The course piloted the EU-standard [1], which was still in the draft stage at that time.

In the following years, the study of the castle's roof structure was mainly carried out by Livady Architects, until in 2021 a new course for structural engineering and architecture students was organized. This course engaged entirely the roof structure of the main building, and the task was a

comprehensive and extensive assessment of the structure in accordance with the final EU standard. The studies revealed relevant building archaeological information and new information about the structural resilience of the complex structure.

METHODOLOGY AND IMPLEMENTATION

Two international declarations and one EU standard were used to guide the research and restoration tasks of the course: *Principles for the Analysis, Conservation and Structural Restoration of Architectural Heritage* (ICOMOS 2003), *Principles for the Conservation of Wooden Built Heritage* (ICOMOS 2017) and *Historic Timber Structures - Guidelines for the On-Site Assessment* (EN 17121: 2019), which were tested to practice in both the research of Livady architects and the university courses.

The complex history of the structure requires studies and proposals in precise steps to gain understanding for individuation of the causes of damage and decay. The goal is to find correct choice of the restoring measures and to control the efficiency of the interventions. In order to cause minimal impact on the structure and preserve its heritage values it is necessary that the study repeats these steps in an iterative process. [4]

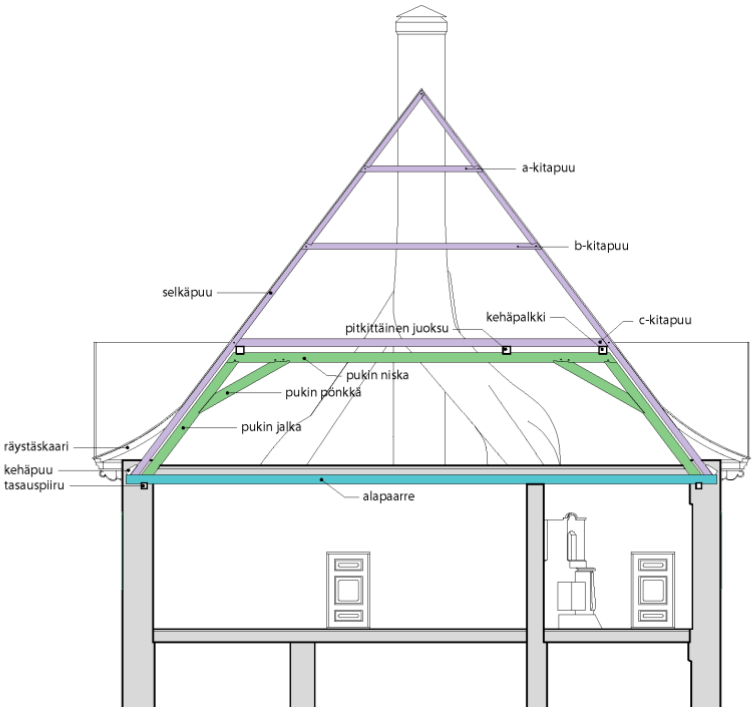

Figure 3: Cross-section of the roof structure. Livady Architects.

For research and monitoring of the roof structure, a coding system was created for the identification of structural member types. The system made it possible to identify each structural element and joint of the roof structure as well as the larger structure ensemble. In addition, Finnish names illustrating the structure or its function were developed for the gable roof structure and its structural member types.

The main purpose of the preliminary assessment is to determine whether the structure as such will be able to carry the loads and whether it will function properly in the future. The load-bearing capacity of structures is often difficult or impossible to calculate, so analyses are largely based on estimates. Understanding a structure and its loads requires an interdisciplinary approach and structural engineers must work in collaboration with architects, historians and conservation specialists. For this reason, the students of the course were chosen from different disciplines including mainly conservation architecture and structural engineering but also building archaeology.

In 2018–2019 the entire roof structure was modelled using the Rhinoceros 3D Cad program by Livady Architects. The model did not depict the current state of the roof structure, with its damage and deformation, but provided an ideal model for the roof structure as it was initially planned to be built. In addition to the original construction plan, historical information was added to the model as research progressed, for example on moisture damage affecting roof structures and observed changes during initial construction and later interventions.

In addition to the above-mentioned building information model, a photogrammetric model was used to document the current state of the roof structure, both outside and inside. The photogrammetric model is an excellent tool for observing the condition and structure of the roof and its overhead parts, as well as their changes. Besides these methods, also micro-drilling and surface radar were used to probe and monitor the actual state of the timber material and structures inside masonry structures.

In pedagogical terms, our central methodologies are Problem Based Learning (PBL) and Object Based Learning (OBL), which were used in the courses to implement the use of the standards in an authentic learning environment. In addition to the fieldworks the courses engaged historical roof structures and their restoration through literature, lectures, excursions, course publications and final exhibition at the site (2022).

At the beginning of the course, students prepared translation summaries of the EU Standard and the ICOMOS guidelines. Seminars and field research were organized during one week intensive period at Louhisaari Castle. Work on the assignments continued with seminars and culminated in an exhibition at Louhisaari in summer 2022.

The courses were attended by 20 graduate engineering and architecture students both in 2017 and 2021. The learning objectives of the course were that after the course, students will have basic skills in assessing and researching historic wooden structures, an understanding of the varying operating principles of traditional roof structures, restoration planning skills in accordance with internationally accepted principles and a preliminary ability to grasp a restoration project.

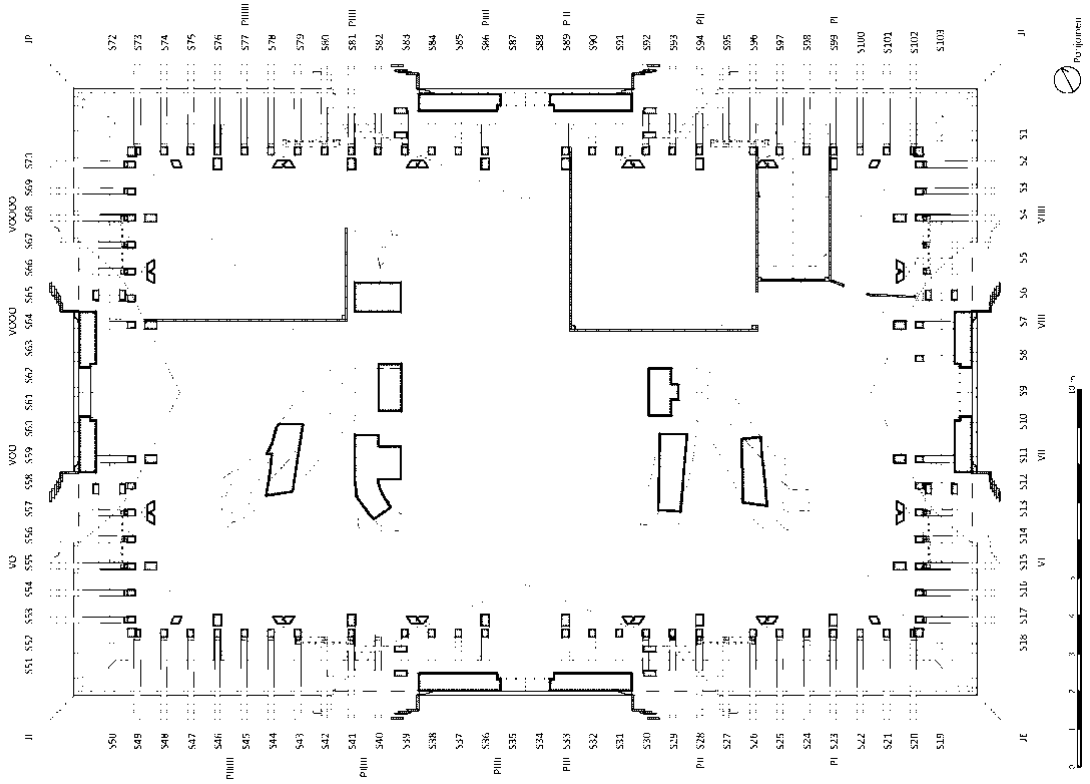

Figure 4: Floor plan of the attic, inscribed with the coding of the rafters and posts. Livady Architects.

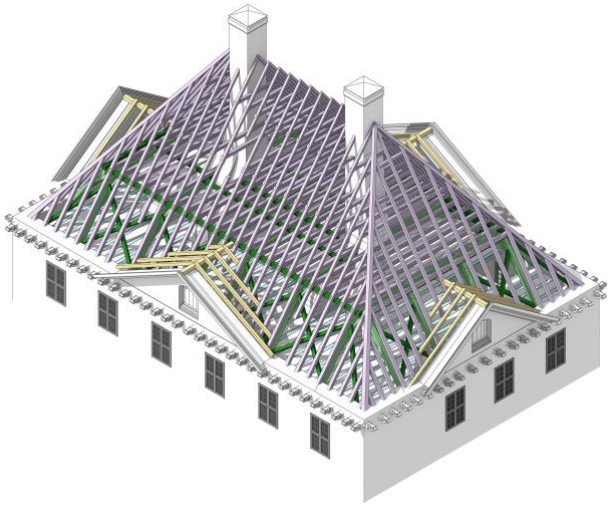

Figure 5: Axonometry of the roof structure. Livady Architects.
Figure 6: Wooden Corniche from the 1650s is preserved entirely. ´Photo: Finnish National Board of Antiquities.

RESULTS AND DISCUSSION

The results of the research are twofold. Firstly, our research unveiled how the EU standard can be implemented in practice by professionals, but also within groups of students performing their first conservational survey of a historical timber structure. Secondly, the research made both by Livady Architects and also the students revealed a lot of new information about the structure and its structural performance.

The practical results of the study, both by Livady Architects and the students, were the description of the history of the structure, the mapping and the mechanisms of damage, the modelling of the structural principles and the clarification of the causes of changes in the functioning of the structure. One of the results of the course was the comments sent to the Finnish representatives of the EU standards group about the functionality of the standard.

To understand the roof structure of Louhisaari castle, we compared it to other similar structures through field and archival studies. The most similar roof structure with Louhisaari Castle is the Skokloster castle in Uppsala County, Sweden, built between 1654 and 1668.

The only buildings in Finland known to have similar roof structures as Louhisaari castle are the Askainen church (1653) and the old church of Uusikaupunki (1629). In addition to the roof structures, what is also common to these three buildings is that designers and builders are known to have come from other parts of Europe. The building of Askainen Church was also financed by Herman Fleming, owner of Louhisaari Castle.

One of the historically most interesting observations was, achieved by combining the results of desk study and field work, that during the Great Northern War (1700–1721), the Russian forces looted, among other things, the iron tie beams of the eaves structure. This changed the principles of functioning of the structure.

The field study confirmed that the roof structure is original and has undergone little repair or modification. Furthermore, the field study found a feature of the structure that had previously gone unnoticed: the painted ceiling joists in the top floor are an integral part of the roof structure. Previously these parts, covered by exceptionally well-preserved paintings from the 1660s were conceived as an independent structure of the roof constructions. The conservation and preservation of the most valuable and well-preserved ceiling paintings in Nordic countries became therefore one of the key objectives also in the restoration of the roof structure.

In monitoring the student assignments, we identified several strong and useful aspects of the standard. These were firstly the processual nature of the standard, which enables learning step by step from basic tasks to more complex surveying and understanding the structural performance. The standard was also proved easily understandable and students were able to follow it with relatively short amount of time after reading it. The key weaknesses, however minor ones, we identified in the implementation of the standard by the students, were first of all the relatively structural and technical nature of the standard. It seems that more emphasis on the importance of desk survey and archival work, as well as familiarization with similar sites and structures, might be relevant prior to the fieldwork. We also observed, that the standard should give more detailed guidelines for the publication and accessibility (OA policies) of the results and reports. Furthermore, the standard relies very much on national legislations, which may cause problems with flexible international mobility of future professionals using it in different countries.

CONCLUSIONS

The research showed that the EN 17121:2019 works well in practice when applied to complex architectural conservation prtojects including also training and students. The different stages and the processual nature of the standard, proceeding from preliminary to more detailed observations and surveys, offer a precise but flexible framework in different situations in long-lasting projects. The standard also proved to be easily understandable and possible to adopt also by students doing their first heritage survey.

Furthermore, we conclude, that an in-depth understanding of the structure is crucial for limiting the invasive actions to minimum. The operation of traditional roof structures relies on the combined effect of different parts of the structure, the understanding of which requires a holistic approach. Instead of focusing on individual parts, the whole structure should be followed, and the standard also guides the research and surveys to this direction. Although weak and damaged structural parts and joints are found in the structure, their reduced capacity is compensated by intact and functional structural parts. The load distribution follows the stiffest path principle.

REFERENCES

[1] EN 17121:2019 ”Conservation of cultural heritage. Historic timber structures. Guidelines for the on-site assessment of load-bearing timber structures”.
[2] Huttunen, Marko & al.: *Ruotsin suurvalta-ajan vesikattorakenteet Suomessa*, Senaatti-kiinteistöt, Helsinki, (2018).
[3] Lounatvuori Irma, Knapas Marja Terttu (toim.): Louhisaaren kartano, suku ja rälssi – säteri ja kirkko, Museovirasto, Helsinki, (2005).
[4] Principles for the analysis, conservation and structural restoration of architectural heritage (ICOMOS, 2003)

DIAGNOSIS AND PROPOSAL FOR THE RESTORATION OF A TIMBER-FRAMED BUILDING AND ITS RESULTS APPLYING STATIC AND DYNAMIC TESTS

Luis-Alfonso BASTERRA[2], Gamaliel LOPEZ[2], Roberto D. MARTINEZ[2], José-Antonio BALMORI[2], Antolín LORENZANA[3], Álvaro MAGDALENO[3], Alberto IZQUIERDO[1], Juan J. VILLACORTA[1], Lara DEL VAL[1], Luis ACUÑA[2], Milagros CASADO[2].

[1] Signal Theory and Communications Department, University of Valladolid Campus Miguel Delibes, 47011 Valladolid, Spain (alberto.izquierdo, juavil, larval)@tel.uva.es

[2] Research Group of Timber Structures and Wood Technology, University of Valladolid Avenida de Salamanca, 18, 47014 Valladolid, Spain (basterra, gama, robertomartinez, balmori)@arq.uva.es, maderas@iaf.uva.es, mmcasado@uva.es

[3] ITAP. Universidad de Valladolid Paseo del Cauce, 59, 47011 Valladolid, Spain ali@eii.uva.es, alvaro.magdaleno@uva.es.

KEYWORDS: assessment, NDT, restoration, load test, dynamic behaviour

ABSTRACT

This communication presents the results of the tests carried out on a newly assessed and subsequently restored timber structure of a residential building in the city of Valladolid (Spain).
Initially, a diagnosis of the structural timber condition, applying non-destructive testing techniques and visual recognition was performed. Also, a dynamic test was carried out, monitoring the slab with a self-developed measurement chain (AMEMOME) and exciting the structure with a shaker.
Based on the previous results, constructive actions were planned based on specific local interventions and on the general reinforcement of the floor slabs with a mixed solution, wood and concrete with mechanical connections.
After the works carried out, the suitability of the works performed was checked by means of static load tests.

INTRODUCTION

The building, which is approximately 100 years old, is located between party walls, in the historic center of the city of Valladolid. It has been used for residential purpose, but for several years it was abandoned and in a state of serious decay until it was finally acquired in 2019 by a real estate company with the aim of refurbishing it and putting it back on sale. (Figure 1:).

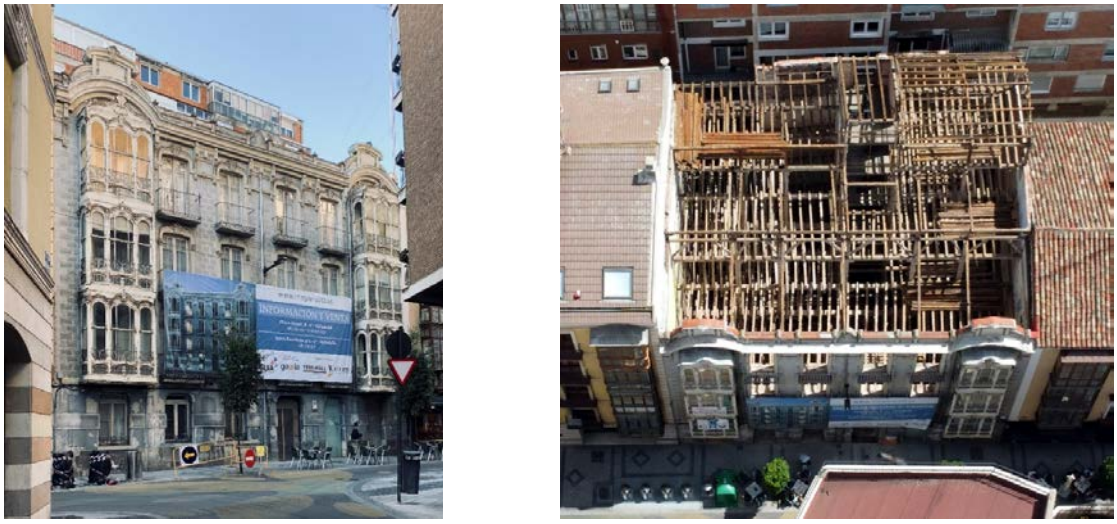

Figure 1: Previous state of the buiding (2019).

The building has a ground floor plus three complete floors, one more under the roof -with a smaller surface area- and a partial underground area- located at the back. Each floor has an approximate surface area of 250 m^2. The vertical and horizontal structure is entirely made of wood and, initially, the owner company was asked to demolish all the supported construction systems, keeping only the wooden load-bearing structure, in order to study it. (Figure 2:).

Figure 2: Timber structure (initial state).

METHODOLOGY

Macroscopically, it was determined that the wood corresponds to a conifer, most probably a pine. Previous studies of buildings in this region show that the species most commonly used for their construction have been Scots pine and, to a lesser extent, *Pinus pinaster*. Given the great inter-species similarity, it was not considered necessary for the purposes of this work to investigate further.
As a preliminary assessment, a visual classification of the wood was carried out, based on the European standard UNE EN 56.544 for conifers [1], which specifies the methodology to measure the different defects and singularities in the wood of these species and to be able to assign a specific quality based on them.

The following non-destructive tests were carried out on a selection of pieces:

- Determination of the humidity with a resistance xylohygrometer, mod. GANN-Hydromette BL A plus.
- Density estimation by means of a test specimen piece, extracting samples on site.
- Ultrasonic wave propagation tests (9 tests) with a FAKOPP Microsecond Timer© model.
- Tests with a resistograph, model RINN-TECH RESISTOGRAPH® SC-650.

Secondly, a dynamic test was carried out on one of the floor slabs, applying vibrations by means of a long stroke shaker with ball bearing SPA-APS 113. The data was collected by means of a series of digital MEMS accelerometers. forming part of an original measurement chain (AMEMOME) developed and fine-tuned by our research team as an alternative to the usual vibration monitoring systems in the industry, which are much more expensive [7].

Regarding the state of the structure and the technical and economic feasibility of its rehabilitation, it was recommended to carry out local repair operations of the parts with damages and constructive problems, and a generalized reinforcement of the floors with a concrete slab, lightly steel reinforced and mechanically connected to the timber structure (Figure 3: and Figure 4:).

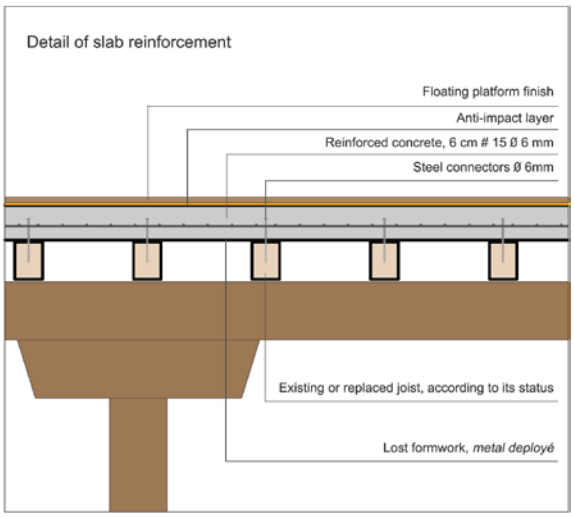

Figure 3: Detail of the reinforcement of the floors.

Figure 4: Laying of the mixed floor slab.

Finally, once the repair and reinforcement work on the timber structure was completed, EPTISA carried out a static load test on two specific zones of the floors, in order to verify that the strain under load was within the expected range [5]. For the loading, pools of water were used, up to a maximum depth of 55 cm, equivalent to 100% of the total load expected in the project, which was applied in 5 steps. And for strain measurement, 5 MITUTOYO analog micrometers with a precision of 0.01 mm were used.

RESULTS

The results of visual inspection and non-destructive testing were included in a complete report and were plotted on the drawings provided by the client, following the Spanish UNE 41808 standard [4]. As an example, one of the floors of the building is shown below. (Figure 5:):

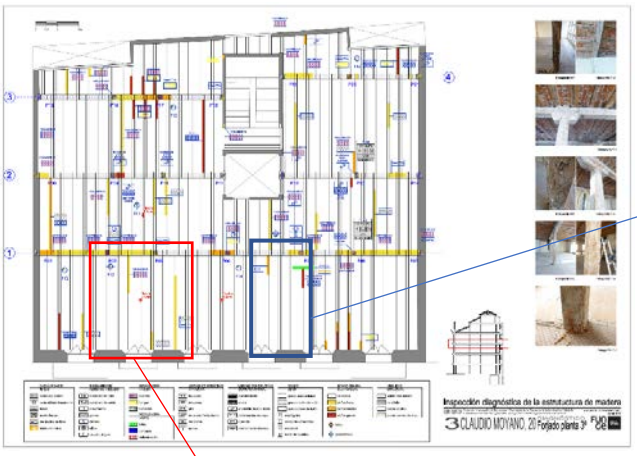

Figure 5: Diagnosis of pathology and test areas.

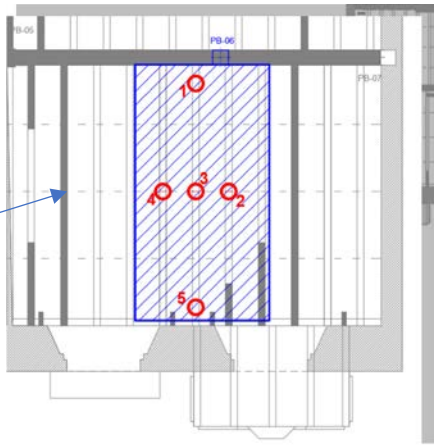

Figure 6: Static load test area.

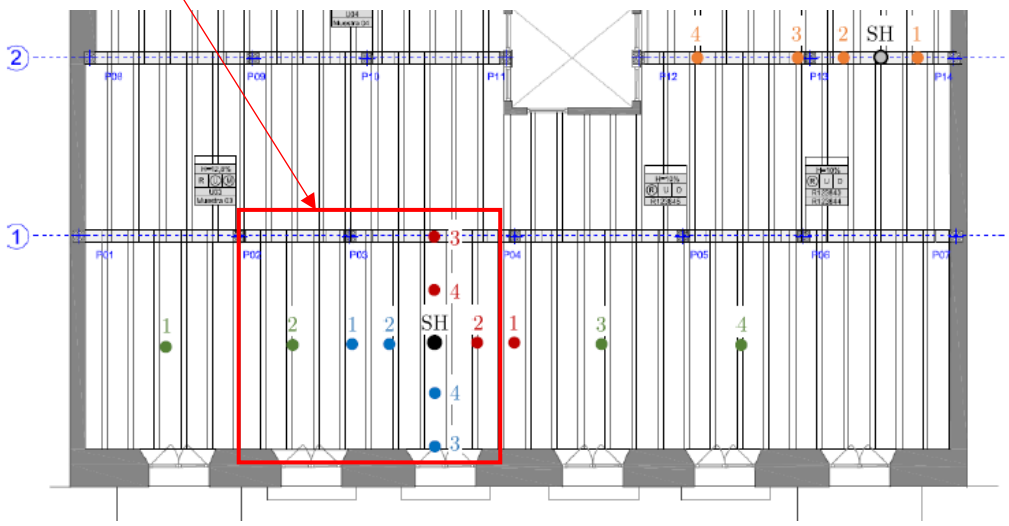

Figure 7: Dynamic test area.

The area shown in Figure 7: was instrumented with accelerometers distributed in 12 points throughout the span in 3 set-ups, adding 2 more common accelerometers located in the fixed and mobile part of the shaker. After an upward sweep from 1 Hz to 20 Hz, lasting 120 s, and the corresponding downward sweep, all recorded at 400 S/s, the frequency response functions were calculated and the modal parameters (including modal shapes, eigenfrequencies and modal damping) were extracted. As a result, after the modal identification, it was estimated that the liveliest and most relevant mode of the timber floor was the bending vertical one, at 8.97 Hz, with a damping ratio of 4.6%. This is valuable information from which derive an updated computational model.

The results of the static load test were summarized as follows:

Table 1: Absolute strain at each instrumented point.

STRAIN (mm)						
Stage	Date/time	Micrometers				
		1	2	3	4	5
Unloaded	11/01/2022 – 09:40h	0.00	0.00	0.00	0.00	0.00
1º load step (1kPa)	11/01/2022 – 10:05h	0.04	0.19	0.19	0.15	0.05
2º load step (2kPa)	11/01/2022 – 10:25h	0.14	0.42	0.42	0.34	0.06
3º load step (3kPa)	11/01/2022 – 10:50h	0.25	0.66	0.68	0.57	0.11
4 º load step (4.5kPa)	11/01/2022 – 11:30h	0.49	0.98	1.11	0.96	0.25
5 º load step - full load (5.5kPa)	11/01/2022 – 11:55h	0.58	1.32	1.35	1.16	0.36
5 º load step - full load (5.3kPa)	12/01/2022 – 12:00h	0.50	0.78	0.90	0.86	0.36
1º load step (2.7kPa)	12/01/2022 – 12:35	0.24	0.18	0.30	0.32	0.11
Unloaded	12/01/2022 – 12:55h	-0.07	-0.49	-0.35	-0.24	-0.22
Unloaded	12/01/2022 – 13:10h	-0.07	-0.59	-0.40	-0.24	-0.26

DISCUSSION

The combined study of the wood species, visual grading and nondestructive testing results led to the following timber grading proposal:

Table 2: Resistant class proposal for solid wood.

RESISTANCE CLASS	MOR f_m (N/mm²)	MOE $E_{0,med}$ (N/mm²)	Mean density (Kg/m³)
Scots pine (*Pinus sylvestris* L.)	18 (C18)	9.000 (C18)	460 (C30)

The density is the value determined in the tests carried out with real samples, higher than the one stated in the UNE EN 338 [2] for C-18, since it is on the safety side as it is part of the permanent loads of the structure.

The maximum strain values (between 1.16 and 1.35 mm) obtained in the load test are below the limit value prescribed by the Spanish Structural Code [6] for this type of structures. In addition, the maximum strain value obtained in the test is lower than the theoretical one, which can be estimated according to the mechanical characteristics of the materials that make up the floor slab and the general theory of structures. Finally, when the structure was unloaded, recoveries above the initial situation (negative) were obtained at some points

CONCLUSION

The visual inspection, in accordance with the visual grading standards, allows to determine the quality of the structural timber of old buildings and, with it and the wood species, to assign a resistance class.

Logically, it is advisable to carry out complementary non-destructive tests, which in this case have shown values different from those specified in the standards for some properties, which must be used on the safety side.

The proposed rehabilitation of this timber structure by means of a mixed timber-concrete solution has demonstrated. In the final load tests to which it has been subjected, a structural safety and stiffness

superior to those obtained by the calculation methods of the general theory of structures, complying with the limitations of the applicable regulations.

Funding:
This research was funded by the Junta de Castilla y León, co-financed by the European Union through the European Regional Development Fund (ref. VA228P20).

REFERENCES

[1] UNE 56.544:2011. Clasificación visual de la madera aserrada para uso estructural. Madera de coníferas.

[2] UNE-EN 338:2016. Structural timber. Strength classes.

[3] UNE-EN 17121:2020. Conservation of cultural heritage. Historic timber structures. Guidelines for the on-site assessment of load-bearing timber structures.

[4] UNE 41808:2013. Estructuras de madera existentes. Sistema de representación gráfica del estado constructivo de las estructuras de madera existentes [in Spanish].

[5] Ministerio de la Vivienda. *Código Técnico de la Edificación*. DB-SE-Seguridad Estructural. REAL DECRETO 314/2006, de 17 de marzo (BOE 28/03/06) [in Spanish].

[6] Ministerio de la Presidencia. *Código estructural*. Real Decreto 470/2021, de 29 de junio (BOE, de 10 de agosto de 2021) [in Spanish].

[7] Villacorta, J.J.; del-Val, L.; Martínez, R.D.; Balmori, J.-A.; Magdaleno, Á.; López, G.; Izquierdo, A.; Lorenzana, A.; Basterra, L.-A. Design and validation of a scalable, reconfigurable and low-cost Structural Health Monitoring system. *Sensors* 2021, *21*, 648. https://doi.org/10.3390/s21020648, accessed 14.06.2022.

ZAGREB CATHEDRAL – STRUCTURAL ASSESSMENT OF TIMBER ROOF STRUCTURE

Hrvoje TURKULIN[1], Tomislav SEDLAR[1], Andrija NOVOSEL[1], Juraj POJATINA[2], and David ANĐIĆ[2]

[1] University of Zagreb, Faculty of Forestry and Wood Technology, Svetošimunska 23, 10000 Zagreb, CROATIA *h.turkulin@sumfak.hr*

[2] STUDIO-ARHING d.o.o., Ćire Truhelke 49, HR 10000 Zagreb, CROATIA, *juraj@studio.arhing.com.hr*

ABSTRACT

The roof of the Zagreb Cathedral, dating from the general reconstruction in 1890-ties, withstood the 2020 earthquake in Croatia with remarkably good resilience. However, the restructuration project after the quake initiated extensive activities on the condition survey and consideration of possible measures for ensuring the future longevity, structural stability, and seismic resistance of the structure. The assessment encompassed the determination of wood species, anatomical structure, hygrotechnical conditions, as well as physical, mechanical, and biological properties of wood and load-bearing capacity of timber. It was demonstrated that visual grading and density measurements on drill cores proved adequately chosen main inputs for determining mechanical properties. The (quasi) nondestructive testing (NDT) - stress-wave, screw withdrawal and resistance drilling - proved useful additional methods yet fully effective only in combination with microscopic evidence on cores. A newly developed method of fairly invasive but completely re-constructive sample withdrawal of 50×50×800 mm beams yielded the MOE_{stat} and standard test values on small clear samples (bending, MOE_{stat}, shear ∥ and compression ∥). NDT tests and small clear samples varied in conformity and measurement uncertainty but usefully complemented the main results and indicated the required corrections in mechanical classification.

Special attention was paid to the detailed survey and analysis of timber joints and the consequent stability of the structure in the future. Dead loads, snow loads, and wind loads were considered in structural analysis models. Also, the history of seismic responses was also analysed. Such analyses form a sound base for the technical design of reinforcements as well as necessary repair and reconstruction measures of the roof structure.

KEYWORDS: Zagreb Cathedral, timber structures, NDT, standard wood testing, structural analysis

INTRODUCTION

Zagreb Cathedral, originally dating from the 13th century, was generally re-constructed in neo-gothic style at the end of the nineteenth century. Nowadays, it presents one of the jewels of the cultural heritage in Croatia. The roof structure, consisting of five segments and reaching nearly 21 m in total height, is an excellent example of the highest standards in technical design and carpentry skills of the period. The roof has withstood the 2020 earthquakes in Croatia (5.5 Richter) surprisingly well, only with minor damages. The preliminary survey scrutinised the roof structure for indications of structural damage and its possible effects on the stability of walls and towers. However, the following extensive activities were

performed within the detailed condition survey and in consideration of possible measures for ensuring the future longevity, structural stability, and seismic resistance of the structure. The assessment, executed in an interdisciplinary approach, followed the guidelines outlined in the EN 16096, EN 17121 and related standards. The work is ongoing; the general project for remedial and reinforcement measures is briefly presented here and will be adjusted during the works accordingly. Therefore, only the most indicative findings are presented in this paper.

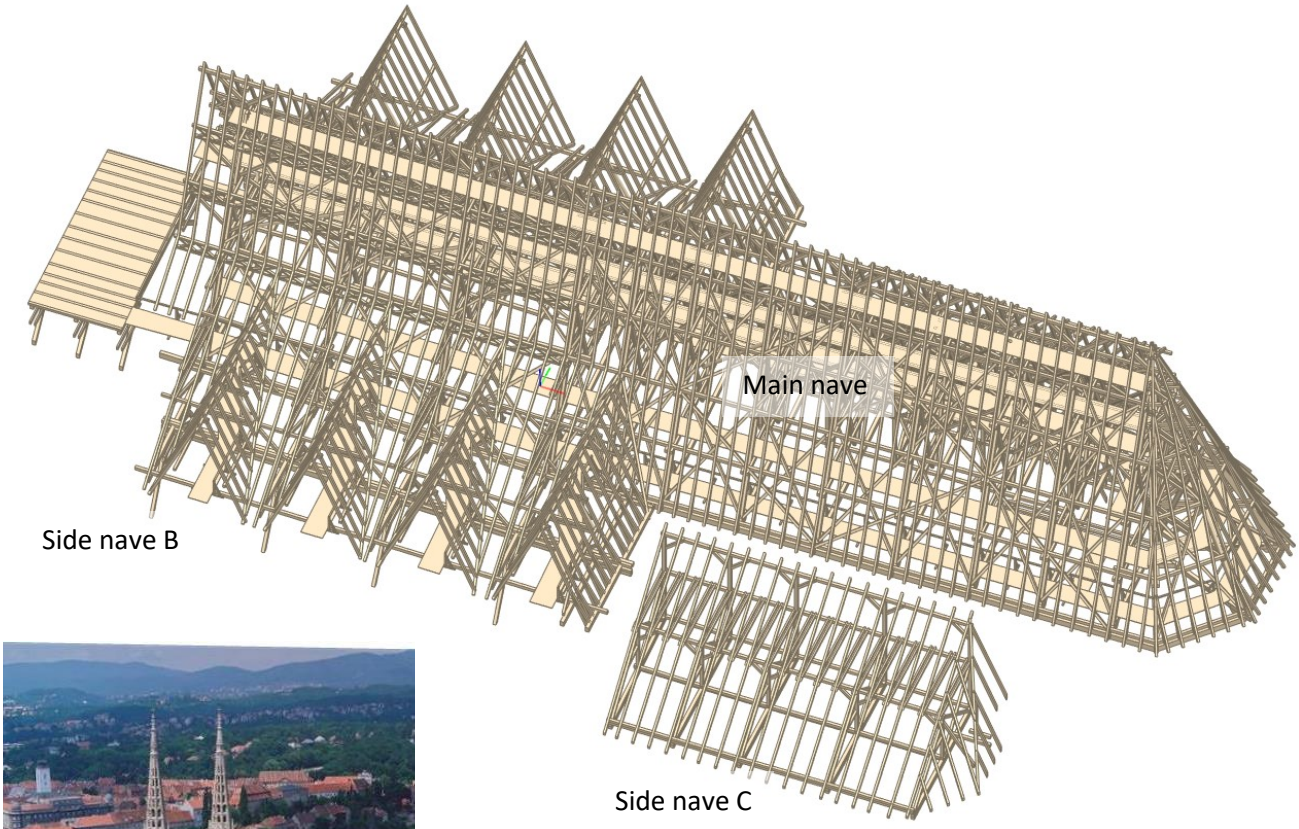

Figure 1: Zagreb cathedral – panoramic view and structural representation of the roof structure

The structure consists of five segments: the main roof over an 11-bays nave is a king-post structure with a tented roof over the apse, divided by collar ties into five ca 3 m high levels. The purlins are constructed over the first four bays as flat trusses with solid-wood webs. Lateral, four-gabled roofs over side naves (B) are two-levelled queen-post structures on trestles above vaults. Structures C covers aisles of the old church, forming mono trusses with tented ends.

The roof is made of softwoods (spruce and fir); however, the tie-beams lie on oak-wood corbels in abutments. Oak was also used for some complex joint blocks. The roof is aerated through the vents, roof cover (initially clay tiles) was replaced in the sixties of the 20th century by softwood boards and copper sheathing. Principal elements are boxed heart, sawn, and hewn timber, while collar ties, purlins and rafters are halved- or slabbed converted timber. Boxed heart timber contains no - or only small - sapwood zones at the edges.

METHODOLOGY

A total of 60 measuring sites were chosen to represent all roof areas in different structure segments, height levels or hygrotechnical/biological risk areas (ridge, wall bearings, leakages etc.) and on at least four structural members of each type. In addition, over 240 various specimens were taken for lab tests. Moisture content (MC) by electric resistance (EN 13183-2) with its gradient (2 cm / 4,5 cm/element centre) and drilling resistance profile (IML 500, further on *RESI*) were recorded at each location in the radial direction, along with wood surface temperature and climatic conditions (t [°C] and φ [%] rel. air humidity, RH). Possible intensive biological damage was detected by percussion or by RESI drills *in situ*. Pressler drill cores ϕ 6,5 or ϕ 12,5 mm were taken at each location for laboratory determination of mean density (ρ_{12} [kg/m^3] acc. to EN 13061-2) and gravimetric moisture content (EN 13183-1). Further, the cores were embedded in epoxy or aliphatic adhesive to be prepared for reflectance optical microscopy and the determination of wood structural cross-section features (species identification, ring width, latewood proportion) or evaluation of biological infestation and traces of damage.

Mechanical properties (strength class EN 338) were determined based on mean density and by visual grading (EN 1912 acc. to DIN 4074-1, -5) and a series of supplementary tests (Figure 3). Static MOE of members was determined based on a dynamic modulus by a stress-wave method (FAKOPP Microsecond timer [2]). Screw withdrawal testing (FAKOPP SWT) served for estimation of density [5], shear modulus [1], and MOR in bending [3].

Direct mechanical tests were executed on material from the medium-sized beam (50×50×800 mm) separated from the compression zone of structural elements (Fig. 2a).

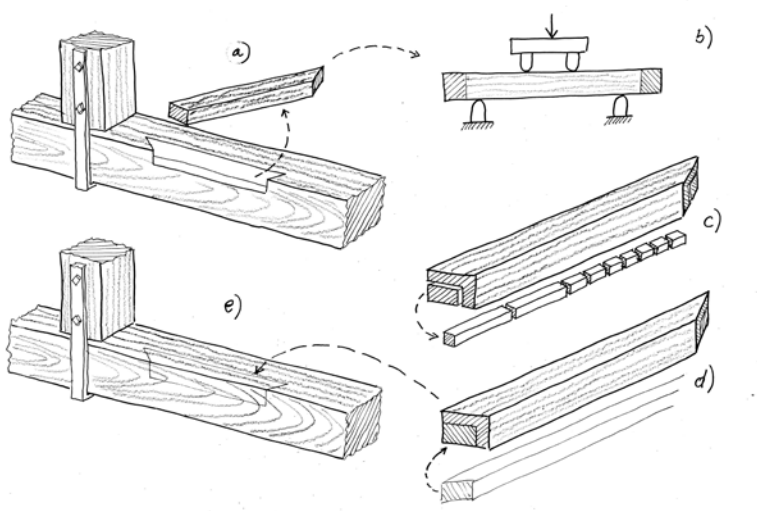

Figure 2: Schematic presentation of the procedure for direct mechanical testing

Firstly, the beams were tested in the elastic region in four-point bending acc. to EN 408 (MOE_{stat}, [GPa]) using a universal testing machine and GOM Aramis DIC (Digital Image Correlation) system, demonstrating that the recovery after the test was complete (Fig 2b). Subsequently, the inner edge of the beam was extracted to yield small clear samples (Fig 3c). The withdrawn material was replaced with a glued-in lath and 2 mm thick edge veneer strips, thus forming the beam with retained original visible surfaces. The structural member was finally reconstituted on-site by fitting the re-composed beam to its original position and gluing it with EN 15425 PU adhesive for constructive purposes (Fig 3d), thus ensuring the adequate structural and cosmetic repair.

Small clear samples served for standard bending (MOR and MOE_{stat} acc. to ISO 13061-3 and -4), compression ∥ (ISO 13061-5) and shear tests (ISO 3347). Further on, the MOE_{stat} was used to calculate

the characteristic bending strength of structural members (f_{mk}) according to [5]. All the test results were re-calculated to values at 12 % MC acc. to ISO 13061-3.
Biological health was evaluated according to the following scheme:

1. Visual examination and percussion (evidently present decay or dull echo): - if NO, then	if YES, then:	RECORDED Rejected, or:
2. resistance drill check: - if NO, then	- if YES, then:	RECORDED Rejected, or:
3. drill core inspection	- if YES, then:	RECORDED, or
4. additional microscopic or microbiological check in the laboratory		

Joints were inspected in detail for their fitness acc. to EN 17121 (c. 5.8) in their exterior appearance and tightness, while their interior design (and possible workmanship flaws or biological damage) were studied using resistance drilling. In addition, wall brickwork abutments were opened in places to enable the inspection of tie-beam ends and oak-wood corbels keyed inside wall support. Finally, the detailed mapping encompassing leakages, biological damage, displacements and deformations of structure or joints was presented for a restoration and restructuration project.

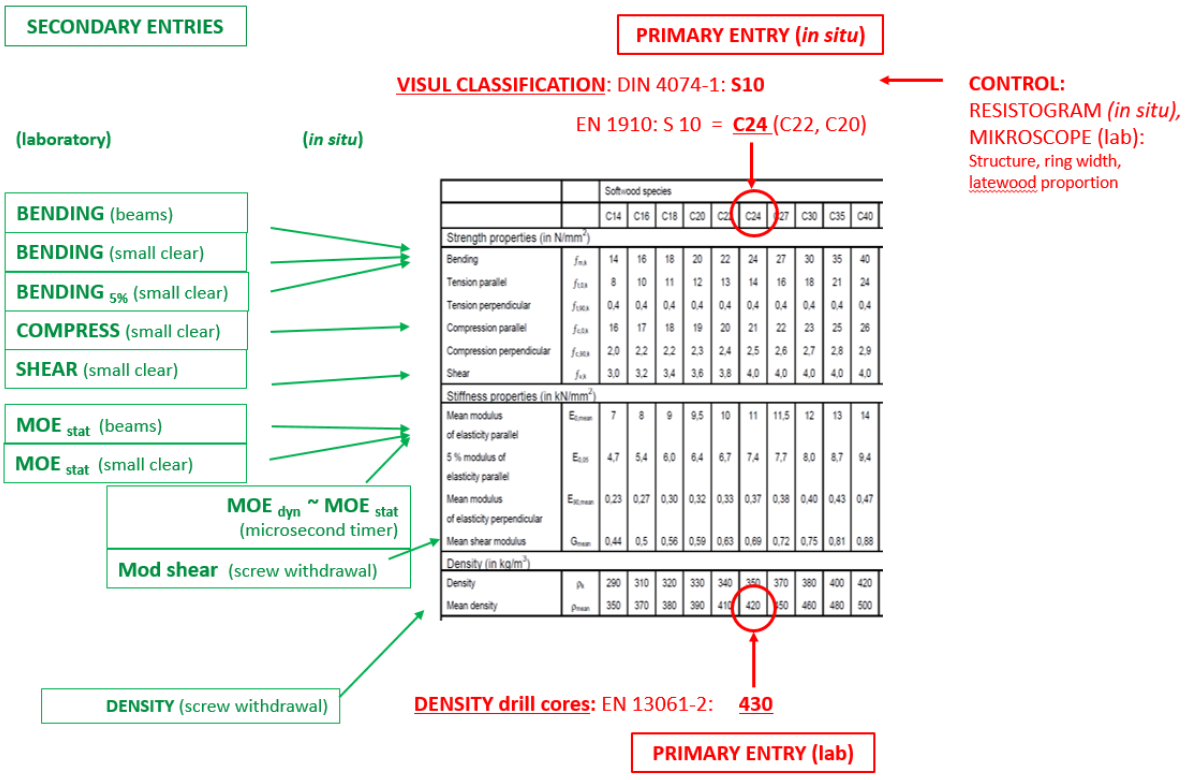

Figure 3. Representation of comparative determination of mechanical properties (strength class in EN 338) with different methods. Primary criteria (visual classification and density) were accordingly complemented with NDT and small clear sample tests (secondary entries).

For the purpose of the structural analysis of the main roof structure, a 3D structural model was made according to the measurement of elements on site (Fig.1). The measurement included the basic geometry, local dimensions of the elements, and types of joints, connections, and bearings. The basic actions were then entered into the model: dead, snow and wind loads. Using linear analysis, the model was created and analysed in the Tower - Radimpex software package.

RESULTS

Table 1. Physical and mechanical properties of wood of the main nave structural elements (10 selected amongst a total of 60 locations) with assigned strength classes and reduced active cross-sectional areas

LOCATION		ELEMENT SPECIES DIMENSIONS (cm)	MOISTURE CONTENT min/max (%)	DENSITY (mean) $\rho_{12\%}$ (kg/m^3)	DENSITY (mean) Strength class acc. to EN 388	VISUAL GRADING CLASS DIN 4074	VISUAL GRADING CLASS EN 1912	VISUAL GRADING Ring width/ latewood proportion (mm-%)	SELECTED STRENGTH CLASS EN 338	COMMENT RESI – BIO – remaining cross-section
MAIN NAVE, BASE (TIE) LEVEL	M1	**PRINCIPAL RAFTER** spruce **15-16 / 23-26**	10.8 - 12.9	407	**C20**	S13	**C30**	1,2 - **1,9** - 5,9 17 - **26** - 50	**C20**	Sound wood, **very low density in juvenile zone 15/22**
	M5	**TIE BEAM** spruce **20-22 / 28-30**	13.0 - 13.9	435	**C24**	S13	**C30**	0,9 - **2,8** - 4,5 18 - **27** - 30	**C24**	Sound wood, **low density in juvenile wood 20/28**
	M6	**TIE BEAM** spruce **20-22 / 28-30**	11.9 – 15.1	463	**C30**	S13	**C30**	1,5 - **2,0** - 3,9 20 - **35** - 42	**C30**	Sound wood, high density, **decayed in bearer zone 20/28**
	M7	**TIE BEAM** spruce **20-22 / 28-30**	12.7 – 15.6	411	**C22**	S13	**C30**	1,2 - **3,1** - 6,3 8 - **16** - 34	**C22**	Very low density and LW proportion, **decayed in the wall**
	M8	**DRAGON TIE** fir **21 / 29**	15.6 – 16.5	538	**C45**	S13	**C30**	2,0 - **5,4** - 6,9 28 - **37** - 55	**C30**	Sund wood, except. high density **20 / 28**
	M9	**PRINCIPAL RAFTER** spruce **15-16 / 23-26**	10.5 – 13.1	492	**C35**	S13	**C30**	0,4 - **1,2** - 2,9 25 - **33** - 50	**C30**	Sound wood, except. high density **15/22**
2. LEVEL	M10A	**KING POST** spruce **20-21 / 25-26**	11.6 – 13.6	596	**C50**	S13	**C30**	0,4 - **1,0** - 3,0 20 - **32** - 50	**C30**	Sound wood, except. high density **20/25**
	M11	**PRINCIPAL RAFTER** spruce **15-16 / 23-26**	11.7 – 14.4	444	**C24**	S13	**C30**	0,9 - **2,4** - 6,7 11 - **21** - 63	**C24**	Sound wood, average density **15/22**
4. LEVEL	M15	**KING POST** spruce **20-21 / 25-26**	11.8 – 17.2	405	**C20**	S13	**C30**	1,3 - **3,5** - 5,3 9 - **11** - 23	**C20**	Sound wood, very low density **20/25**
	M17	**PRINCIPAL RAFTER** spruce **15-16 / 23-26**	9.8 – 13.1	484	**C35**	S13	**C30**	0,9 - **2,4** - 4,1 22 - **29** - 32	**C30**	Sound wood, except. high density **15/22**

Table 2. Mechanical properties of selected structural elements (listed in Table 1) by various methods and finally chosen strength classes

LOCATION		ELEMENT	STRESS WAVES MOE_{stat} MOE_{dyn} (GPa)		SCREW WITHDRAWAL FORCE DENSITY $\rho_{12\%}$ (kg/m^3)		SCREW WITHDRAWAL FORCE SHEAR MODULUS (N/mm^2)		DIRECT MECHANICAL TESTS MOE (kN/mm^2) large samples		DIRECT MECHANICAL TESTS MOE (kN/mm^2) small clear		DIRECT MECHANICAL TESTS MOR_{char} (N/mm^2)/ class EN 338		ARBITRARY SELECTED STRENGTH CLASS** EN 338
METHOD/SOURCE			[2]		[1]		[2]		EN 408		ISO 13061-4		ISO 13061-3 [5]		
MAIN NAVE, BASE (TIE) LEVEL	M1	**PRIN. RAFTER**	10.1	**C22**	529	**C45**	0,71	**C24**	12.2	**C30**	12.0	**C30**	27	**C27**	**C24**
	M5	**TIE BEAM**	13.3	**C24**	500	**C40**	0,66	**C22**	12.9	**C30**	12.9	**C30**	12.8	**C30**	**C24**
	M6	**TIE BEAM**	10.8	**C22**	469	**C30**	0.62	**C20**	12.1	**C30**	12.1	**C30**	12.1	**C30**	**C30**
	M7	**TIE BEAM**	10.4	**C22**	503	**C40**	0.69	**C24**	9.8	**C20**	9.8	**C20**	11.1	**C24**	**C22**
	M8	**DRAGON TIE**	12.4	**C30**	518	**C40**	0.73	**C27**	9.3	**C18**	9.3	**C18**	9.8	**C20**	**C30**
	MM9	**PRIN. RAFTER**	12.5	**C30**	482	**C35**	0.62	**C20**	10.9	**C22**	10.9	**C22**	11.2	**C24**	**C24**
2. LEVEL	M10A	**KING POST**	15.6	**C45**	503	**C40**	0.67	**C22**	15.4	**C45**	15.4	**C45**	14.1	**C40**	**C30**
	M11	**PRIN. RAFTER**	13.8	**C35**	469	**C30**	0.61	**C20**	12.2	**C30**	12.2	**C30**	10.6	**C22**	**C24**
4. LEVEL	M15	**KING POST**	10.4	**C22**	500	**C40**	0.70	**C24**	10.8	**C22**	10.8	**C22**	10.5	**C22**	**C22**
	M17	**PRIN. RAFTER**	14.4	**C40**	466	**C30**	0.65	**C22**	7.0*	**C14**	7.0*	**C14**	8.6*	**C16**	**C30**

** Element yielded very variable results due to defects in small clear samples.*
*** A reasonable compromise between results in Table 1 and Table 2*

Table 3. Results on small clear specimens: comparison of density by standard volumetry on drill cores and screw withdrawal testing in situ*, and mechanical strength values on extracted beams.*

DETERMINATION METHOD	MEAN DENSITY ρ_{12} (n=48)				
	min	avg	max	sd	CoV %
ISO 13061-2	389	**463**	596	49,35	**10,66**
Screw withdrawal **[5]**	420	**499**	631	40,74	**8,16**
	MECHANICAL PROPERTIES, SMALL CLEAR SAMPLES (n=9*)				
	min	avg	max	sd	CoV %
Bending strength, ISO 13061-3	72.5	**77.9**	95.6	7.87	10.11
Reference values, spruce [7]	65	**71**	77		
Compression parallel, ISO 13061-6	40.2	**45.7**	51.2	3.64	7.97
Reference values, spruce [7]	40	**45**	50		
Shear parallel, ISO 3347	8.8	**11.0**	14.6	1.42	12.57
Reference values, spruce [7]	5.0	**6.3**	7.5		

*Results from one beam were discarded due to evident micro1acking and insect damage

Table 4. Strength classification by various methods and their evaluation based on comparison with structural properties of wood.

DRILL CORE embedded and polished/resistogram HOMOGENITY OF STRUCTURE, DENSITY AND LATEWOOD PROPORTION	METHOD ASSIGNED STRENGTH CLASS EN 338			
	EN 13061-2	STRESS WAVES	SCREW WITHDRAWAL	
	kg/m³	MOE_{stat} / MOE_{dyn}	SWT DENSITY	SWT SHEAR MODULUS
	596 C 50	C 45	503 C 40	C 22
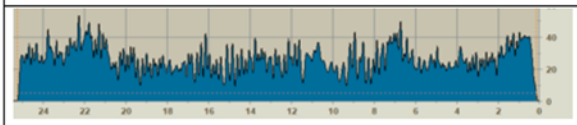	REGULAR GROWTH EXTR. HIGH DENSITY Stress wave appropriate, SWT UNDERESTIMATES strength class			
	463 C 30	C 22	469 C30	C 20
	REGULAR GROWTH AVERAGE DENSITY SWT reliable for density, stress waves and SWT shear modulus UNDERESTIMATE strength class			
	389 C 18	C 22	473 C 30	C 22
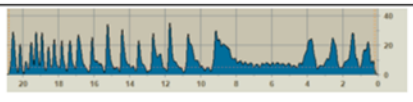	REGULAR GROWTH VERY LOW DENSITY NDT methods OVERESTSIMATE strength classes			
	467 C 30	C 40	516 C 40	C27
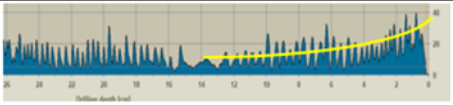	IRREGULAR GROWTH LOW PITH/JUVENILE DENSITY NDT methods UNREILABLE: OVERESTIMATE strength class			

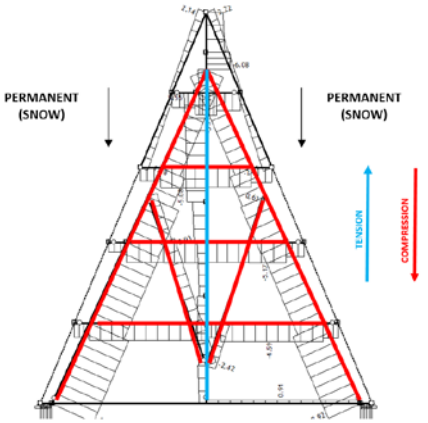

Figure 4. Forces in the main span truss for vertical loads

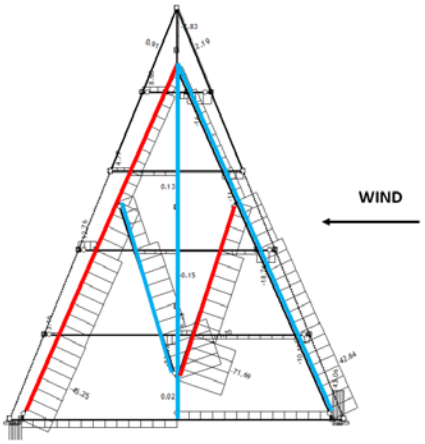

Figure 5. Forces in the main span truss for horizontal loads

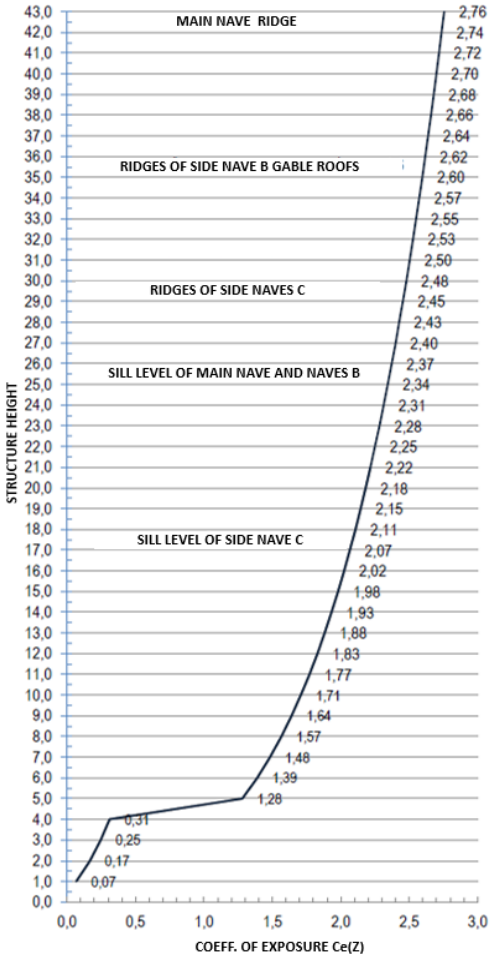

Figure 6. Values of the coefficient of exposure to lateral wind load

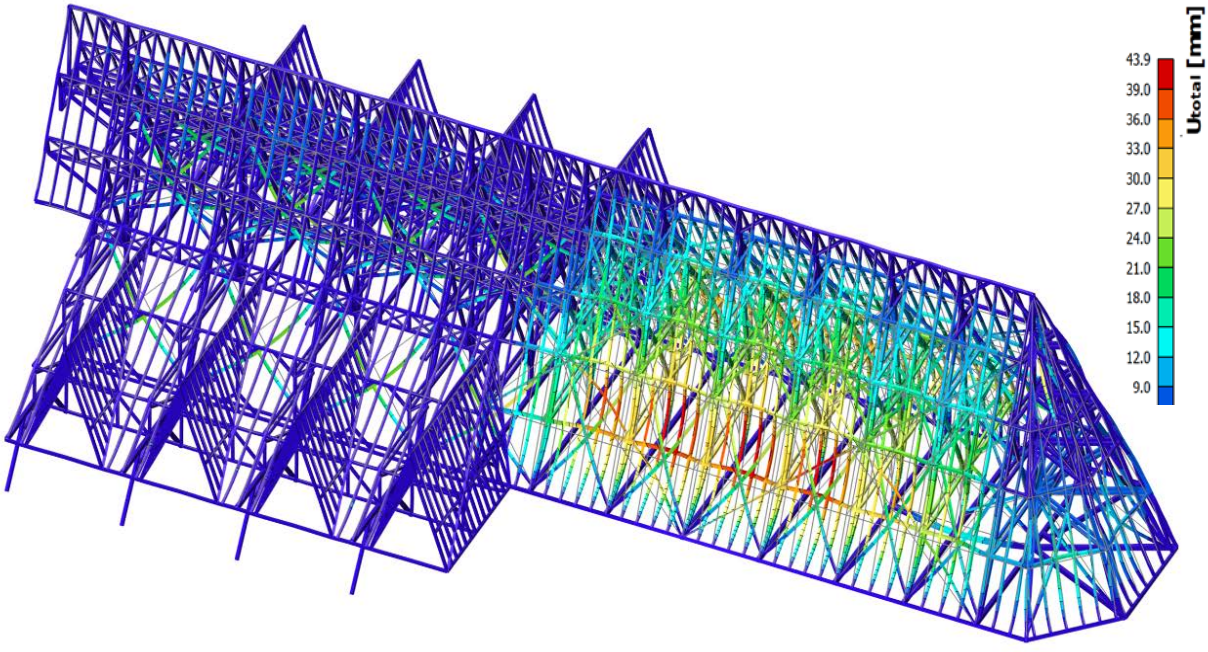

Figure 7. Graphic representation of the deflections for the governing serviceability limit state combination

DISCUSSION

The wood of the highest quality was selected to build the structure. An exquisite level of workmanship is still evident in the condition of the majority of joints, which are practically all in pristine condition, tight and completely functional. Therefore, the structural analysis may have been executed assuming that such joints are fully capable of transferring loads (EN 17121), and the calculations were based on assigned strength classes and minimum load-bearing cross-sections of the elements. Special analysis of joints (design, level of workmanship or damage) does not fit the length of this article.

The moisture content of wood (Table 1) is low in values (12-16%) and of a small gradient (<3%), which indicates that no further stresses in joints, member distortions and cracking, or development of biological damage may be expected. Accordingly, the durability of the structure was designed for a risk class 2 acc. to EN 335 and in use class 2 acc. to EN 1995-1-1 (below 85 % r.h. at 20 °C except for a few weeks a year).

Results in Tables 1 and 2 demonstrate the difficulties in determining the strength classes of timber. Visual grading is not discriminative enough: all presented elements were of S13 visual grade acc. to DIN 4074-1 (which would correspond to strength class C30 in EN 1912), yet specific measurements recorded such wood properties that would classify the timber in a range between C18 and C45. Worse than that, the appearance of the surface (the basis of visual classification) may disguise weaker layers deeper within the timber, even in healthy elements (pith and juvenile wood). In several cases, the mean density (determined on the through core drills) was, therefore, a corrective factor, and the finally selected strength class (column 10 in Table 1) was conservatively chosen to be the lower value of the two principal criteria presented in Figure 2.

The notorious discord of the results is evident from all the supportive methods applied (Table 2). The results can be evaluated only in comparison with resistograms and structural analyses of polished drill cores (cross-section); examples are presented in Table 4. One should carefully examine the possible causes for aberrations of the NDT results (e.g. ring width and latewood portion, Table 1) and take the results either as corroborative information for the strength class determination by principal criteria or reject the discriminative results based on obvious misjudgement or shortcomings of a particular technique. Table 4 presents some of such cases, where e.g. stress wave or screw withdrawal methods that probe the exterior zones of the boxed-hearted elements obviously failed to record broad rings, low latewood portion (Table 1) and other inferior properties of the central zone of the elements.

Screw withdrawal testing proved very useful in the determination of the mean density, taking that the results of SWT showed a good correlation with measurements on 12.5 mm drill cores, with the advantage of being less destructive and enabling faster testing that can be conducted on much wider areas of the structure. The results in Tables 1 and 2 (density of cores and SWT density estimation) indicate good correlation, but generally higher EN 338 strength class determined by screw withdrawal technique. The results on all 60 measurement locations (Table 3) show a bias of ca 10 % higher SWT-determined density but very similar dissipation of results, therefore a reliable estimation. The bias may originate from the incorrect formula for specific species and wood tissue [1], but more likely from the fact that SWT records the wood properties in the outer zone of the large cross-section elements, which in the centre contain the pith and less dense juvenile wood. In that sense, the SWT estimation of density may be considered reliably, with a need to conservatively denote a 10 % smaller mean value and corresponding strength class to structural elements.

Small clear samples can't be representative for evaluating the load-bearing properties of large-sized construction timber. However, the congruity of their values (variance below 15 %) and concordance with referenced wood properties (Table 3) are helpful in the general assessment of wood quality (particularly for S10 and S13 grades), indicating the absence of partial biological deterioration

(perforations and limited mass loss) and presents a useful correction factor for density-dominated strength classification.

Results indicate that the arbitrary decision about the strength class determination remains the key factor in timber classification, although subject to the evaluator's experience. Several additional methods can never be superfluous for corroboration of the overall strength class selection, no matter how limited or unreliable they may be, provided that the results of each additional method be carefully analysed and taken with caution regarding their possible misguidance in reaching the ultimate decision.

Engineers were provided with the information about strength class values either as the "dominant class" for a particular type of structural element (e.g. appearing in 80 % or more of members) or as a "minimum class ever recorded". The latter were conservatively taken for structural calculations, with reasonable confidence in mechanical properties classification and consequentially in the load-bearing capacity estimation. Additionally, the useful load-bearing cross-section was reduced for all elements exhibiting significant surface biodeterioration levels. Some of the elements of the king post structure, for example, may be loaded either in tension or compression, depending on the external loads (Figs 4 and 5), which were taken into consideration during calculations.

Ultimate limit state checks for every element were performed. Also, serviceability limit state checks (Fig. 7) were performed for dead and wind loads. Most of the elements meet the short-term deflection criteria. However, long-term criteria were exceeded in several parts of the side naves structures. It is planned to reverse these deflections with external post-tensioning of the trusses. Also, some types of elements (common rafters and purlins) exhibited insufficient stiffness and load-bearing capacity.

In general, it can be concluded that most of the elements for the given input parameters meet the criteria, i.e. have sufficient resistance to design actions according to EN standards. All joints are very neat and functional. At the same time, however, it should be emphasised that the traditional carpentry joints are conceptually unsuitable for dynamic alternating actions such as an earthquake (a rapid change of force direction with significant horizontal shifts).

Further work will focus on the design of restoration methods for the replacement of the roof parts that are totally degraded by rot and for the restructuration of the members that obviously require strengthening.

CONCLUSION

The structural analysis of the Zagreb cathedral is presented through the analysis of timber properties and consequent structural stability checks and seismic calculations. The quality of wood and its specific features were analysed by several methods, of which visual grading and density determined by core drilling proved to be the adequate principal criteria. However, other methods are needed in order to specify the load-bearing capacities of timber as a sound base for static calculations. Among those, resistance drilling proved very useful, albeit only as an indicative method, whereas other fast and indirect methods (stress-wave analysis and screw withdrawal), with their ability to estimate either density or specific mechanical properties, yielded disputable results. Therefore, a new approach to direct testing was applied on medium-sized beams and on small clear samples to corroborate the findings of NDT techniques. Only the comparative analysis of the complete body of results (although subject to the evaluator's expertise), further clarified by microscopic inspection of wood structural features, enables a complete insight into the strength classification of timber.
The conservatively chosen strength classes and reduction in cross-sections (where proven appropriate) were used for modelling the structure's load-bearing capacity and ultimate limit state checks. It was demonstrated that the roof structure of the Zagreb cathedral generally meets all the EN standardised

criteria and has sufficient resistance to design actions. However, the resistance to dynamic alternating actions (e.g. in an earthquake) should be further taken into consideration, and appropriate anti-seismic structural reinforcements shall be proposed.

REFERENCES

[1] Divos, F. 2010: *User's guide - Screw withdrawal resistance meter*. Fakopp Enterprise Bt. H-9423 Ágfalva, Fenyő u. 26. Hungary, 2010; www.fakopp.com.

[2] Divos, F.; Tanaka, T. 2005: *Relation between static and dynamic modulus of elasticity of wood*. Acta Silvatica et Lignaria Hungarica, 2005 (1), 105-110.

[3] Divos, F.; Sismándy Kiss, F.; Takats, P. 2011: *Evaluation of historical wooden structures using nondestructive methods*. Proceedings: SHATIS'11 International Conference on Structural Health Assessment of Timber Structures - Lisbon, Portugal - June 2011: LNEC.

[4] Ericsson, K; Karawajczyk, E.; Kliger, R.; Lechner, T.; Lukaszewska, E.; Misztal, W.; Nowak, T. 2018: Non-destructive testing of the historic timber roof structures of the National museum in Stockholm, Sweden. Int. J. of Herit. Archit., Vol. 2, No. 2 (2018) 218–229.

[5] Rammer, D. R. 2010: Fastenings. *Wood Handbook, Wood as an Engineering Material*, Forest Products Laboratory, U.S. Department of Agriculture, Forest Service, Madison, WI, Chapter 08.

[6] DIN 4074-1,5 (2012) Strength grading of wood - Part 1-5: Sawn timber.

[7] EN 335 (2013) Durability of wood and wood-based products -- Use classes: definitions, application to solid wood and wood-based products.

[8] EN 338 (2016) Structural timber -- Strength classes.

[9] EN 408 (2010) Timber structures -- Structural timber and glued laminated timber -- Determination of some physical and mechanical properties.

[10] EN 1912 (2012) Structural Timber -- Strength classes -- Assignment of visual grades and species.

[11] EN 1993-1-Parts 1-14 (2014): Design of steel structures (with national annexes).

[12] EN 1995-1-1 (2015): Design of timber structures (with national annexes).

[13] EN 1998-1- Parts 1-6 (2011): Design of structures for earthquake resistance with national annexes.

[14] EN 16096 (2012) Conservation of cultural property -- Condition survey and report of built cultural heritage.

[15] EN 17121 (2019) Conservation of cultural heritage -- Historic timber structures -- Guidelines for the on-site assessment of load-bearing timber structures.

[16] EN 13183-1 (2002) Moisture content of a piece of sawn timber -- Determination by oven dry method.

[17] EN 13183-2 (2002) Moisture content of a piece of sawn timber -- Estimation by electrical resistance method.

[18] EN 13061-2 (2014) Physical and mechanical properties of wood -- Test methods for small clear wood specimens -- Determination of density for physical and mechanical tests.

[19] EN 15425 (2017) Adhesives -- One component polyurethane (PUR) for load-bearing timber structures -- Classification and performance requirements.

[20] ISO 3347 (1976) Wood — Determination of ultimate shearing stress parallel to grain.

[21] ISO 13061-3 (2015) Physical and mechanical properties of wood – Test methods for small clear wood specimens – Determination of ultimate strength in static bending.

[22] ISO 13061-4 (2014) Physical and mechanical properties of wood -- Test methods for small clear wood specimens -- Determination of modulus of elasticity in static bending.

[23] ISO 13061-5 (2020) Physical and mechanical properties of wood — Test methods for small clear wood specimens — Determination of strength in compression perpendicular to grain.

STRENGTHENING OF A TOWER CARPENTRY CONSTRUCTION USING STEEL CABLE BASED ON THE EXAMPLE OF A CHURCH IN STARA KAMIENICA, POLAND

Krzysztof AŁYKOW[1] and Magdalena NAPIÓRKOWSKA-AŁYKOW[2]

[1] Team of Civil Engineers AŁYKOW, Poland

[2] Team of Civil Engineers AŁYKOW, Poland

ABSTRACT

This paper shows the example of strengthening of a church tower carpentry construction using traditional carpenter's solutions supported by a system of steel cables. The medieval church in Stara Kamienica, Lower Silesia, Poland mentioned in 1370 was rebuilt in 1677 and in 1769 the carpentry construction of the top part of the tower was changed in order to hang new bells. The changes from 1769 caused some wrong kind of working-forces of the tower carpentry construction, especially in the carpentry joins areas, caused by hard weather conditions strengthened by dynamical influence made by bells. The authors of the paper did expertise and designed a steel cable system for strengthening bearing elements by changing the static scheme of the carpentry construction. They also supervised the rescue works which were carried out successfully in 2017. The paper shows how to minimize the need to change the original elements while changing the way of working of the static system of carpentry construction.

KEYWORDS: church tower, strengthening carpenter construction, support cable system, Lower Silesia

INTRODUCTION

In 2016 was observed a lean of carpenter construction of the church tower. The expertise made by authors confirms damage of wooden members according long time working in wrong weather conditions. The effect was strengthening by influence of tower bells working. More over huge influence on kind of damage has changing of statical scheme of carpenter construction made in wrong way in 1769, by the way of building in new bells-support-construction [1, 2].

As a result of the failure, there was an uncontrolled redistribution of loads and stresses in the area of directly adjacent structural elements, increasing their effort to a degree that threatened the integrity of the object [3].

The zone of connection of the lower and upper carpentry structure of the tower truss, within the support on the crown of the brick shaft of the tower [4], required strengthening due to the progressive stress redistribution processes generated by the aging of the carpentry structure material on the one hand and the rheological processes in the steel anchoring elements subjected to constant stress on the other

The deviation from the axis of the ceiling elements above the lower carpentry structure of the tower from the axis of the columns was visible.

DESCRIPTION OF CARPENTER CONSTRUCTION

The main structural system of the tower consists of two interacting parts: the lower one located within the masonry core of the tower, which is a structural system ensuring global stability of the entire system; the upper tower, located above the masonry crown, exposed to climatic influences. At the point where both parts meet, the tower's carpentry structure is additionally supported on the crown of the walls of the masonry core of the tower.

The masonry core of the tower [5] is described on an octagon, and the wooden columns are located in its corners, additionally stiffened with a system of ceilings that also constitute the landings of communication routes. Such a system protects the entire structure against excessive torsional movements, at the same time not stiffening the structural system.

As a result of the analysis of the existing structure, it was found that the carpentry structure of the tower truss was significantly modified, most probably in 1769, when the self-supporting bell structure was built in. Additional reinforcements most probably come from the renovation period carried out in 1929. As a result, the upper part of the carpentry structure was rebuilt, increasing the spacing of the posts of the lower lantern in order to allow the supporting structure of the bells to rest on the crown of the tower walls. For this purpose [6], the columns of the lower carpentry system of the tower were most likely cut off above the level of the crown of the tower's shaft walls and suspended with steel flat bars with bolts to the newly built-in system of ceiling beams, additionally supported on the overhead crown of the tower walls. The new columns of the lower lantern of the upper structure of the carpentry structure were supported on the ceiling beams, probably connected to carpentry joints [7].

Above the lower lantern, there is a lower dome, the circles of which are additionally supported on poles, which also constitute the structure of the upper lantern; the pillars within the lower dome are stiffened with a system of braces and - between themselves - with a system of crosses of St. Andrew. The upper dome is shaped by circles supported on a conical arrangement of rafters with the king. Both the poles of the lower and the upper lantern are protected against weather conditions by a plank cladding with ventilation openings in their upper part, and copper overlays protected against birds.

The steel supporting structure of the bells rests on the crown of the tower walls and is independent of the carpentry structure of the tower truss. However, the working bells indirectly affect the technical condition of the tower's truss structure through the generated vibrations transmitted through the walls of the tower, on which, in the immediate vicinity [8], the supporting structure of the bells and the carpentry structure of the tower lanterns and helmets are based. In the case of healthy elements of carpentry structure [9], the influence of vibrations on the stability of the structural system of lanterns and domes is negligible due to the ability to absorb vibrations and the elasticity of the material, which is wood. However, in the case of technically degraded elements, the vibrations generated by the eccentric movement of the bells may lead to uncontrolled stress concentrations of the entire structural system in the zone of biological corrosion damage, where the wood has been annihilated.

DESCRIPTION OF DAMAGES OF CARPENTER CONSTRUCTION

A construction failure was found in the roof of the lower lantern of the carpentry structure, caused by the deflection of the beam of the lower lantern and its crushing by the pillar and strut of the lower dome. As a result of the failure, there was an uncontrolled redistribution of loads and stresses in the area of directly adjacent structural elements, increasing their effort to a degree that threatened the integrity of the object. The global structural system was stabilized due to the fact mentioned above.

Figure 1: Lower lantern of the tower (left). Element connecting the structure of the lantern with the masonry core of the tower (right)

Also, the area of connection of the lower and upper carpentry structure of the tower truss, within the support on the crown of the brick stem of the tower, required strengthening due to the progressing stress redistribution processes generated by aging of the carpentry structure material on the one hand and rheological processes in the steel anchoring elements subjected to constant stress on the other. The deviation from the axis of the ceiling elements above the lower carpentry structure of the tower from the axis of the columns was visible. The elements of the lower structural system showed visible traces of previous repairs and reinforcements.

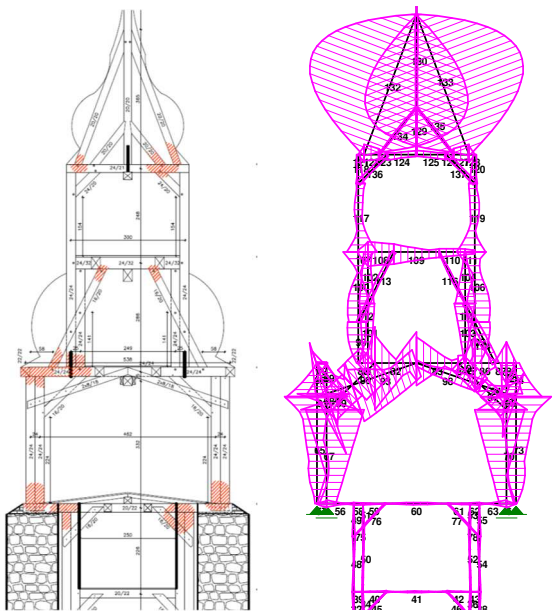

Figure 2: Main damage areas (left), original stresses (right)

METHODOLOGY

In 1769, the upper part of the carpentry structure was rebuilt, increasing the spacing of the posts of the lower lantern in order to allow the supporting structure of the bells to rest on the crown of the tower

walls. For this purpose, the columns of the lower carpentry system of the tower were cut off above the level of the crown of the tower's core walls and suspended with steel flat bars with bolts to the newly built-in system of ceiling beams, additionally supported on the tower's overbuilt crown.
After analysing the damage and the distribution of forces in the existing structure, in addition to repairing the structure using traditional carpentry methods, the authors decided to additionally strengthen it by building a system of tension members made of steel bars (cables).

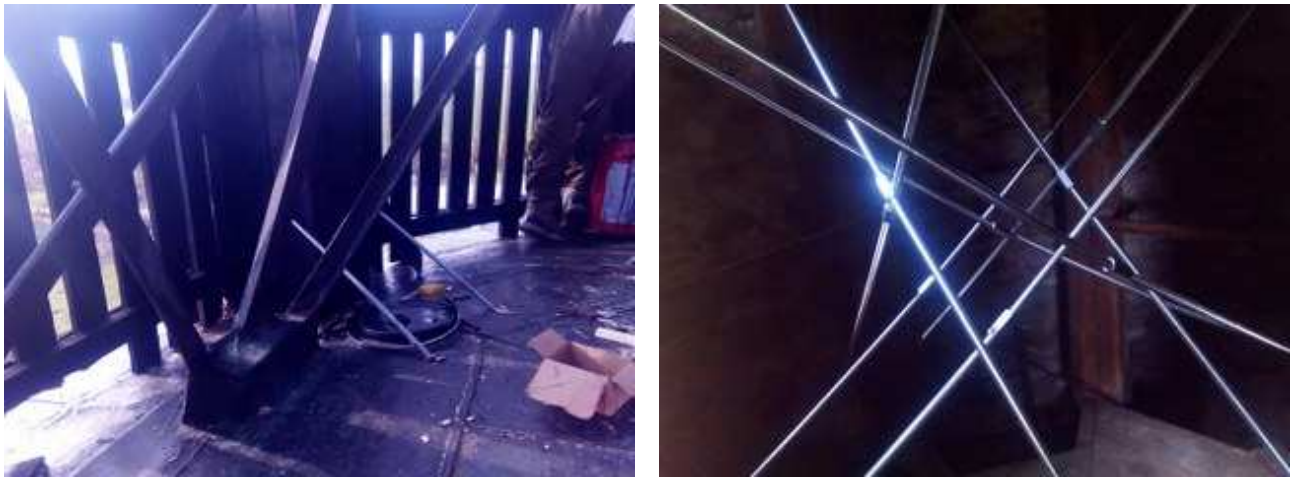

Figure 3: Example of strengthening construction outside (left) and inside (right)

This resulted in a change in the static structure of the entire tower structure and a reduction in the effort of the weakened elements.
The unusual carpentry structure of the tower, rebuilt in 1769, also made it possible to disassemble the upper dome, repair it at ground level and reassemble it using a crane. It was important for the works carried out in a short period of time in the piedmont area, due to the difficult weather conditions.

Figure 4: Removed upper dome for repair works (left) Repair of the upper dome on ground level (centre) Lifting repaired upper dome (right)

Figure 4: Repair of the upper dome on ground level (left) Connector for fixing upper dome (centre) After fixing (left)

Figure 5: Upper (left) and lower (right) lantern of the tower after works

CONCLUSION

The article presents the method of carrying out repair works with the use of modern technologies in historic buildings [10]. The authors try to combine modern solutions [11], adjusting them to the permissible scope of interference in the historical structure specified by the Historic Preservation Office.

REFERENCES

[1] K. Ałykow, M. Napiórkowska-Ałykow, The influence of the 19th century technical solution of the work oof the Baroque hall churches, in: Jasieńko (Eds.) Structural Analysis of Historical Constructions 2012, pp. 986-994

[2] K. Ałykow, M. Napiórkowska-Ałykow, The influence of faulty 19th century technical solution on work of 18th century rafter framing as exemplified by church in Nowy Kościół in Lower-Silesia, Poland - case study, in: Advanced Materials Research, Trans Tech Publications 778 (2013) pp: 903-910

[3] K. Ałykow, M. Napiórkowska-Ałykow, On the inadequate modeling of the structure of architectural heritage, in: Wiadomości Konserwatorskie – Journal of Heritage Conservation 41 (2015), pp: 59-64

[4] Ł. Bednarz, D. Bajno, Z. Matkowski, I. Skrzypczak, A. Leśniak, Elements of Pathway for Quick and Reliable Health Monitoring of Concrete Behavior, in: Materials vol. 14(6) (2021), pp: 1503-1511

[5] J. Jasieńko, K. Raszczuk, P. Frąckiewicz, K. Kleszcz, Ł. Bednarz, Strengthening of masonry rings with composite materials in: Heritage Science 9(1) (2021), pp: 1-9

[6] D. Bajno, Ł. Bednarz, T. Nowak, Problems relating to assessment, repair and restoration of wooden roof structures in historic buildings, as exemplified by two case studies in southern Poland, in: Advanced Materials Research Vol. 778 (2013), pp: 888-894

[7] A. Karolak, J. Jasieńko, T. Nowak, K. A. Raszczuk Experimental investigations of timber beams with stop-splayed scarf carpentry joints, in: Materials vol. 13 (2020), nr 6, art. 1435, pp: 1-17

[8] J. Jasieńko, T. Nowak, Ł. Bednarz, Wrocław University's Leopoldinum Auditorium–Tests of Its Ceiling and a Conservation and Strengthening Concept in: Advanced Materials Research Vol. 133 (2010), pp: 265-270

[9] P. Rapp, Methodology and examples of revalorization of wooden structures in historic buildings, in: Wiadomości Konserwatorskie – Journal of Heritage Conservation 43 (2015), pp: 92-108

[10] J. Krawczyk, Polish Monument Conservation In the Face of Changing Historical Contexts. Tradition, Identity, Dialogue, in: Heritage for future (Eds.) B. Szmygin (2016) 1(3), pp: 127-136

[11] M. Murzyn-Kupisz, Values of cultural heritage In the context of socio-ecomomics, in: Heritage value assessment systems – the problems and the state of research (Eds.) B. Szmygin (2016), pp: 147-164